GEOLOGICAL SURVEY RESEARCH 1970

Chapter C

GEOLOGICAL SURVEY PROFESSIONAL PAPER 700–C

Scientific notes and summaries of investigations in geology, hydrology, and related fields

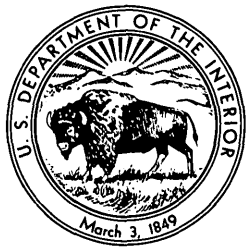

UNITED STATES GOVERNMENT PRINTING OFFICE, WASHINGTON: 1970

UNITED STATES DEPARTMENT OF THE INTERIOR

WALTER J. HICKEL, Secretary

GEOLOGICAL SURVEY

William T. Pecora, Director

For sale by the Superintendent of Documents, U.S. Government Printing Office
Washington, D.C. 20402 – Price $3.25 (paper cover)

CONTENTS

GEOLOGIC STUDIES

HYDROLOGIC STUDIES

TOPOGRAPHIC STUDY

INDEXES

GEOLOGICAL SURVEY RESEARCH 1970

This collection of 42 short papers is the second published chapter of "Geological Survey Research 1970." The papers report on scientific and economic results of current work by members of the Conservation, Geologic, Topographic, and Water Resources Divisions of the U.S. Geological Survey.

Chapter A, to be published later in the year, will present a summary of significant results of work done in fiscal year 1970, together with lists of investigations in progress, reports published, cooperating agencies, and Geological Survey offices.

"Geological Survey Research 1970" is the eleventh volume of the annual series Geological Survey Research. The ten volumes already published are listed below, with their series designations.

Geological Survey Research	*Prof. Paper*
1960	400
1961	424
1962	450
1963	475
1964	501
1965	525
1966	550
1967	575
1968	600
1969	650

SPATIAL RELATION OF MINERAL DEPOSITS TO TERTIARY VOLCANIC CENTERS IN NEVADA

By JOHN P. ALBERS and FRANK J. KLEINHAMPL,
Washington, D.C., Menlo Park, Calif.

Abstract.—About 80 major Tertiary volcanic centers have been recognized in Nevada. Some 17 are either certain or possible calderas ranging in diameter from 3 to 25 miles. Associated with 35 of the 80 centers are spatially related mineral deposits. The more important ones are in the following districts: Bullfrog (gold, silver), Daisy (fluorspar), Goldfield (gold, silver), Tonopah (silver), Silver Peak (silver), Bodie and Aurora (gold and silver), Comstock (silver, gold), and Opalite (mercury). Geologic settings typical of deposits associated with volcanic centers include: (1) rim fracture zones of calderas; (2) areas of local uplift that may reflect the intrusion of an igneous body; and (3) groups of veins, breccia pipes, and breccia zones near the heart of a volcanic center, which may dip inward toward the presumed center.

A program of geologic mapping of counties in Nevada by geologists of the U.S. Geological Survey and the Nevada Bureau of Mines, underway since the 1950's, has led to the recognition of about 80 Tertiary volcanic centers from which a large volume of rhyolitic to andesitic material has been erupted (fig. 1). These 80 centers are, for the purpose of this discussion,[1] regarded as the major ones. Their number does not include the hundreds, perhaps thousands, of small rhyolitic domes and plugs and basaltic vents. Of the major centers, about 17 are believed to be calderas ranging in diameter from 3 to 25 miles. Some of the centers have been described in the literature by geologists working at the Nevada Test Site and by other geologists. Most of the 80 centers, however, have not been described in publication. We are indebted to our colleagues, all members of the Geological Survey except where otherwise noted, for locating them in many of the counties: R. R. Coats, Elko County; Ronald Willden, R. G. Yates, and G. W. Walker, Humboldt County; Ronald Willden, Churchill County; Harold Bonham, of the Nevada Bureau of Mines, Washoe and Churchill Counties; J. G. Moore, Lyon, Douglas, and

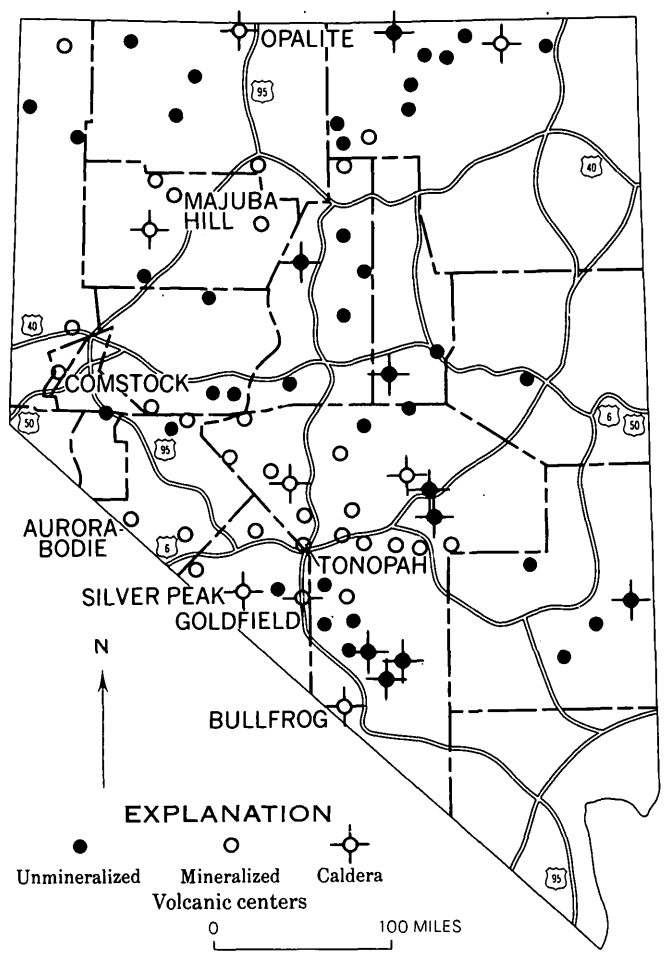

FIGURE 1.—Tertiary volcanic centers, Nevada.

[1] This paper is a somewhat revised version of one presented in February 1968 at the annual meeting of the American Institute of Mining Engineers in New York (Albers and Kleinhampl, 1967). Interest at that time and continuing requests for copies of the paper have led to this publication.

Ormsby Counties; E. H. Pampeyan, Lincoln County; D. B. Tatlock, Pershing County; E. H. McKee, J. H. Stewart, and H. G. Masursky, Lander County; R. J. Roberts and H. G. Masursky, Eureka County; R. O. Fournier and M. C. Blake, White Pine County; and H. R. Cornwall, southern Nye County. In addition, we have obtained information on the Bodie district in several field conferences with C. W. Chesterman and Clifford Gray, of the California Division of Mines, and information on the region encompassed by the U.S. Atomic Energy Commission testing facilities in conference with E. B. Ekren, R. A. Anderson, and other geologists working at the Nevada Test Site, and from their publications. Responsibility for the identification of most of the centers shown in Esmeralda and Mineral Counties rests with Albers; that for those shown in northern Nye County with Kleinhampl.

Although the recognition of most of the 80 centers looks plausible in our present state of reconnaissance, it should be stressed that the nature of a few is speculative and may be disproved in time; no doubt centers not known now will be recognized. The reader should note that most of the centers are in the central and western parts of the State; only a very few are in the eastern and southern parts.

Published maps by Schilling (1964), of the Nevada Bureau of Mines, show 344 established metal mining districts in Nevada. Of these, about 75 are in Tertiary volcanic host rocks; the remaining 269 are in host rocks of pre-Tertiary age. Of the 80 major volcanic centers mentioned above, 35 have spatially related mineral deposits, chiefly mercury, gold, silver, fluorspar, antimony, and possibly manganese. The close spatial relationship suggests a possible genetic relationship and may be a useful guide to exploration.

Some of the more important districts that seem to be spatially related to volcanic centers are the Bullfrog (gold, silver), Daisy (fluorspar), Goldfield (gold, silver), Tonopah (silver), Silver Peak (silver), Bodie and Aurora (gold), Comstock (silver, gold), Opalite (mercury), and Majuba Hill (gold) districts. Most of these are discussed in some detail in subsequent sections of this report, and data concerning them are tabulated in table 1.

Some typical geologic settings of deposits associated with volcanic centers include: (1) rim fracture zones of calderas (Bullfrog, Daisy, Opalite, Goldfield(?)); (2) areas of local uplift that may reflect the intrusion of an igneous body (Tonopah, Goldfield(?), Comstock(?), Bodie and Aurora); and (3) groups of veins, breccia pipes, and breccia zones near the heart of a volcanic center that may dip inward toward the center (Silver Peak, Majuba Hill, Bodie). As seen from this classification, the deposits in some districts, such as Bodie and Goldfield, appear to have composite settings.

TABLE 1.—*Brief description and age of mineralization at major mining districts associated with volcanic centers*

District	Type of center	Type of deposit	Age of mineralization [1] (millions of years)	Source
Aurora	Volcanic center, undifferentiated.	Veins	>12.5	Gilbert and others (1968, p. 283); Yehya Al-Rawi (oral commun., 1968).
Bodie	Intrusion, with uplift(?).	do	7.9 (adularia)	M. L. Silberman (oral commun., 1969).
Bullfrog	Caldera	Deposits along rim fracture zones (veins and bonanza ore).	<11	H. R. Cornwall (oral commun., 1969).
Comstock	Intrusion, with uplift(?).	Veins	13 (adularia)	D. H. Whitebread (oral commun., 1968).
Goldfield	Caldera(?) and (or) intrusion, with local uplift.	do	±21	H. R. Cornwall (oral commun., 1969).
Majuba Hill	Intrusive complex (heart of volcanic center).	Veins, some replacement of rhyolite and breccia.	Tertiary(?)	Trites and Thurston (1958, p. 188, 200–201).
Opalite	Caldera	Deposits along rim fracture zones.	<13	G. W. Walker (oral commun., 1968).
Silver Peak	do	Veins	<5.9	Robinson, McKee, and Moiola (1968, p. 598) taken from J. P. Albers and J. H. Stewart. Unpublished data.
Tonopah	Intrusion, with uplift	do	>17.5, probably >22.	[2].

[1] Primary age control, except for Majuba Hill, is based on K-Ar dating techniques, with the age of mineralization, except where given as an adularia age, deduced from ages of volcanic host rock or rocks adjacent to the host and obtained from sources given. The Majuba Hill age is based on geologic deduction, not on K-Ar work.

[2] Age based on dates obtained by E. B. Ekren (oral commun., 1965) for the Fraction Tuff in the Kawich Range and by R. W. Kistler (see Kleinhampl and Ziony, 1967) for the Toyabe Quartz Latite in the Toiyabe Range.

DEPOSITS RELATED TO CALDERAS

The deposits most clearly related to calderas include those at Bullfrog, possibly Goldfield, Opalite, and Silver Peak.

Bullfrog

The Bullfrog Hills caldera in the Bullfrog district, west of Beatty (fig. 2, table 1), measures 10–13 miles in diameter (Cornwall and Kleinhampl, 1964). The area of the caldera is underlain principally by rhyolitic airfall tuffs and welded tuffs that form a broad faulted dome and dip outward toward the peripheral fault zone of the main caldera rim. Displacement on the peripheral fault where it is exposed along the southeast rim is about 3,500 feet, the northwest or inner side being downdropped. Four well known mineral deposits and most of the smaller deposits in the Bullfrog area are located along marginal faults of the caldera, or near the related subsidence structure that extends outward from the southeast rim of the caldera. Three of the deposits, all gold-silver mines, are on the east rim of the caldera: the Montgomery-Shoshone (*1*, fig. 2), the Mayflower (*2*, fig. 2), and the Pioneer (*3*, fig. 2). The fourth, the Daisy fluorspar mine (*4*, fig. 2), is in Paleozoic rocks adjacent to the southern margin of the subsidence zone that extends tangentially outward from the caldera toward the east. In addition to these deposits, a concentration of small deposits, mostly gold and silver, occurs along the east rim of the caldera, and several other gold deposits occur within the caldera along the north margin of the area of pre-Tertiary basement rocks that have been pushed up into the tuffs and ash flows (see Original Bullfrog mine, *5*, fig. 2).

Goldfield

The Goldfield district, where the U.S. Geological Survey currently has a project, is at the site of a volcanic center that may be a resurgent caldera (table 1, fig. 3). That a volcanic center exists is indicated by the unique pile of volcanic rocks—quartz latites, andesites, and dacites—that thin out away from the area and are not found elsewhere in the region. These rocks are mostly early to middle Miocene in age and are extensively kaolinized, alunitized, and silicified. The silicified and alunitized rocks commonly form tabular ledges that in the aggregate make an eastward-elongate elliptical pattern several miles in diameter (fig. 3) and open on the east. The pattern reflects a concentric fracture system that suggests a collapse structure. However, the presence of the older Tertiary and pre-Tertiary rocks in the central and western parts of the ellipse is not consistent with the idea of collapse and, instead, suggests uplift or doming, possibly by a resurgent igneous body at depth. Modifications of a resurgent caldera by Basin and Range faulting may account for the distribution of

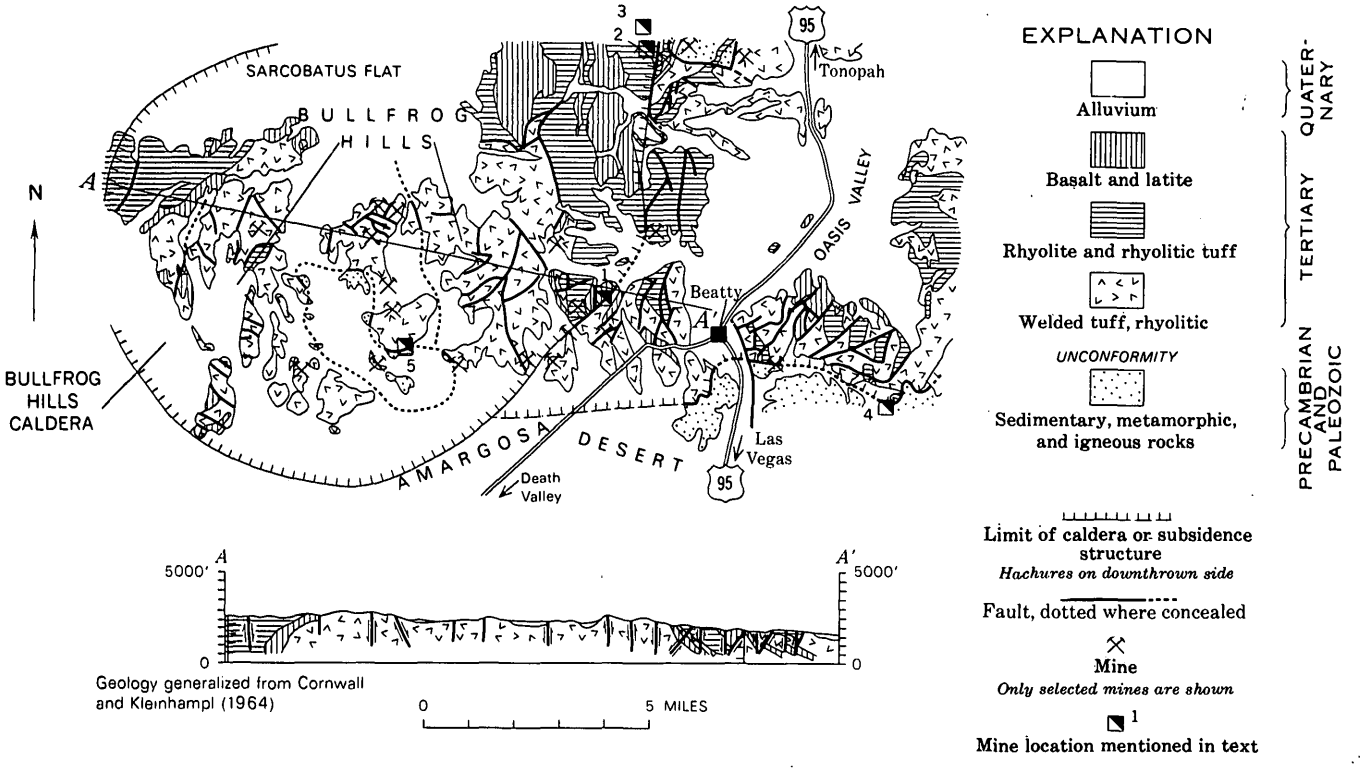

FIGURE 2.—Bullfrog district, Nevada.

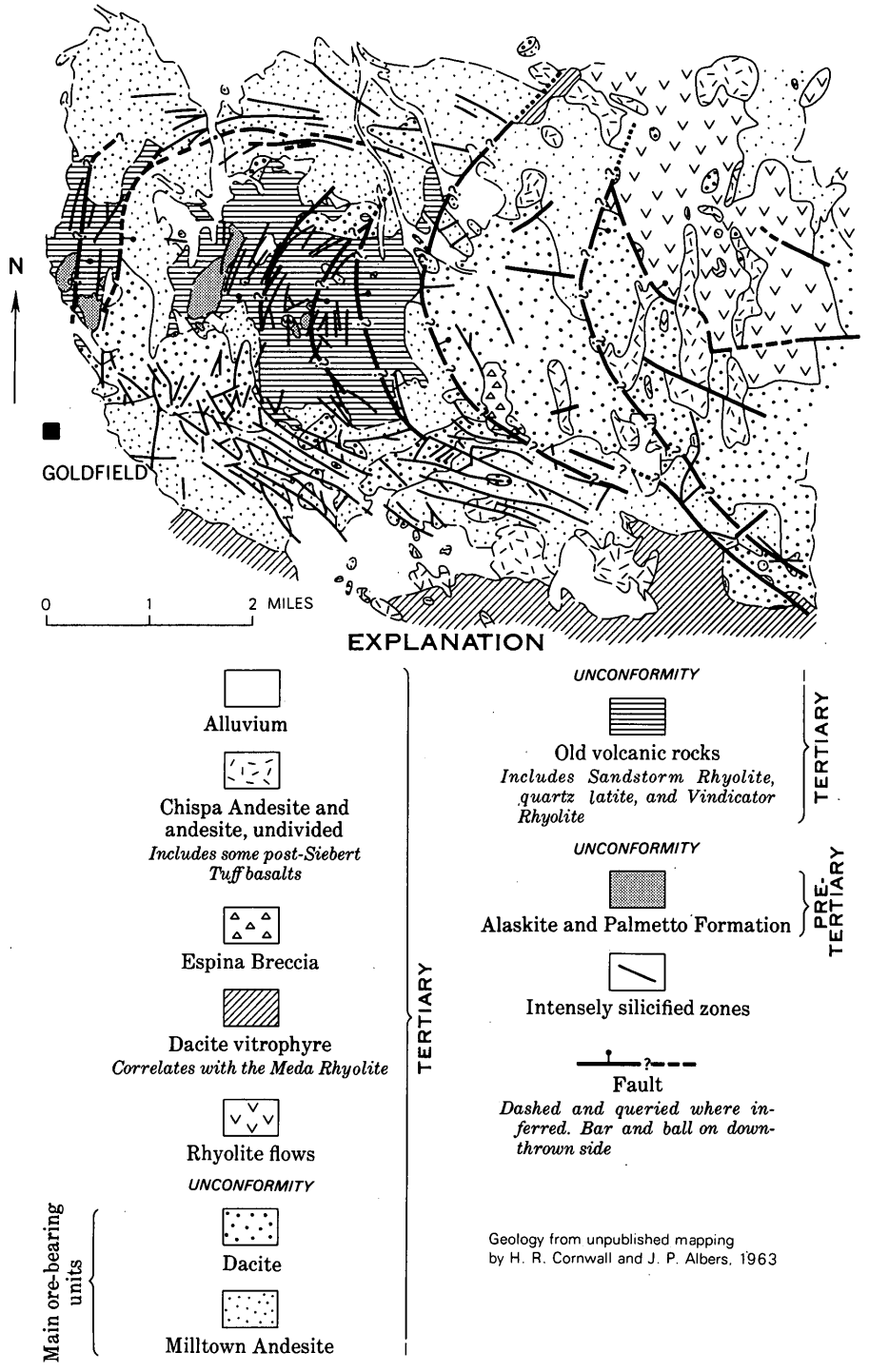

FIGURE 3.—Goldfield district, Nevada.

pre-Tertiary rocks. The known gold and silver deposits are restricted to the western and northern sides of the elliptical structure; 98 percent of the production has come from a segment about three-fourths of a mile long on the western side. The dip of the main mineralized zone at the surface is about 35° eastward, toward the center of the ellipse.

Opalite

The Opalite district (table 1, fig. 4), located along the boundary between Nevada and Oregon, was studied in 1940 by R. G. Yates, who found four quicksilver deposits, including the Cordero, to lie in steep fault zones along a semicircular area about 20 miles in length. The fault zones are in places marked by inward-facing scarps 2,000–3,000 feet high. In this area, Tertiary volcanic rocks, with andesitic to basaltic lavas at the base of the section, followed by extensive welded tuffs, are overlain by late Miocene tuffaceous lakebeds. The andesite and basalt flows may be about 14.5 million years old; the overlying welded tuffs are about 13 million years old (G. W. Walker, oral commun., 1968).

The kinds of rocks, their distribution, and structural relations suggest that the lakebeds fill a calderalike collapse feature. Lake sediments commonly fill such depressions, as shown for example by Smith, Bailey, and Ross (1961, p. D146, D147), at the Valles Caldera, N. Mex. Evidence presented by Yates (1942, p. N326–N328), however, places the major collapse after the deposition of the lakebeds in the Opalite area. More recently, R. G. Yates (oral commun., 1968) states that as caldera structures were not generally recognized in the early 1940's, he only suspected the presence of some kind of a collapsed volcanic structure, and further that the evidence in the Opalite area does not conclusively prove deposition of lacustrine beds prior to faulting. In recent years, workers in the area have recognized it to be underlain by a calderalike structure, with many of the known mercury deposits lying along the northern segment of the rim fracture zone and the large Cordero mine near or on the inferred southeastern rim.

Silver Peak

A volcanic center 5–6 miles in diameter forms the highest part of the Silver Peak Range in Esmeralda

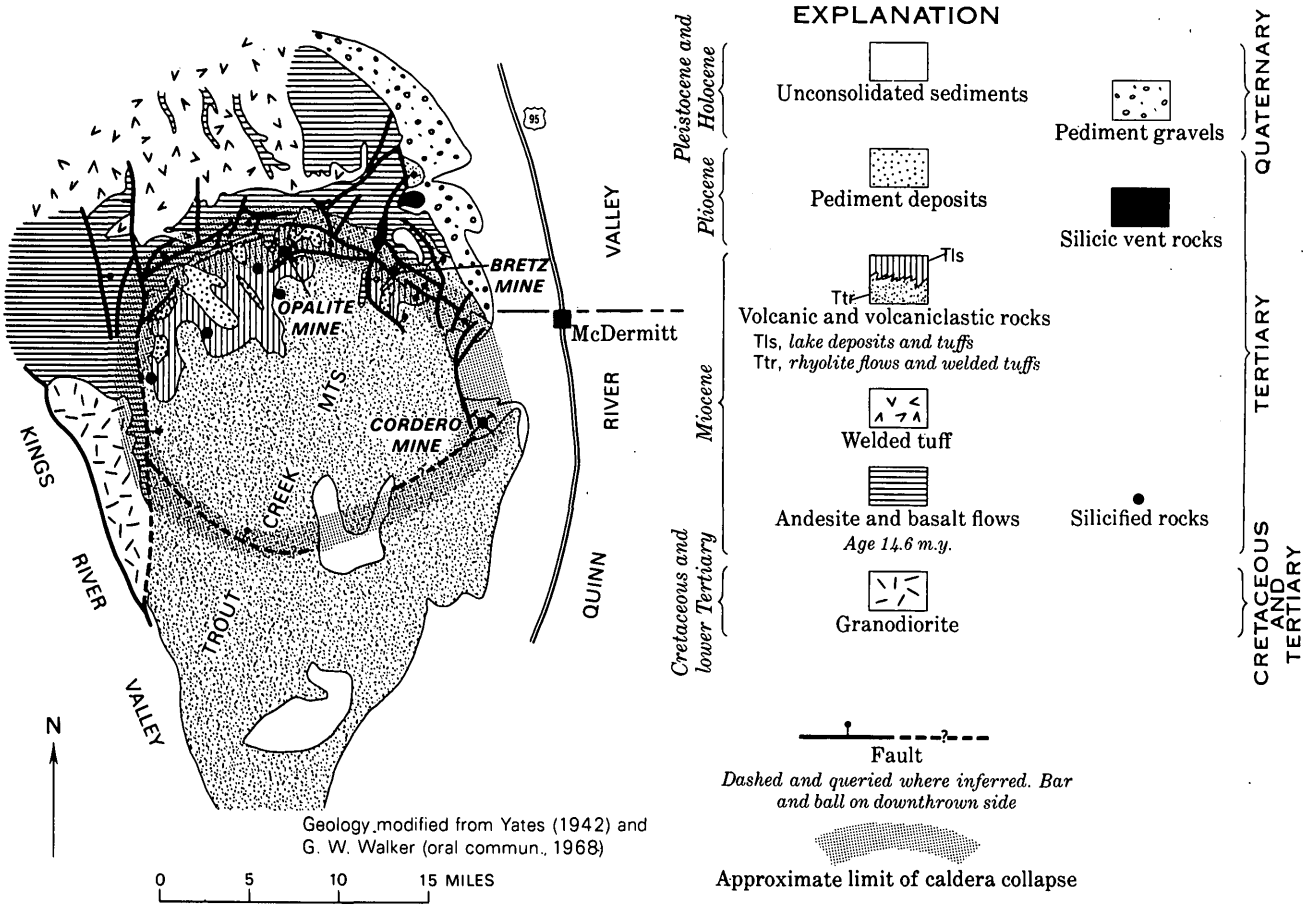

FIGURE 4.—Opalite quicksilver district, Oregon-Nevada.

County (table 1, fig. 5). This center is marked by a thick body of trachyandesite that is the youngest volcanic unit except basalt and appears to fill a calderalike depression. The age of the trachyandesite is only 5.9 m.y., making this center one of the youngest major volcanic centers in Nevada. Cutting the eastern part of the mass of trachyandesite are a group of northeast-striking veins bearing silver chiefly as argentite; barite and calcite are principal gangue minerals. The westernmost veins, including the Mohawk and Sanger, dip northwest toward the presumed center of the caldera (fig. 5). The mineralogically similar veins farther southeast dip steeply either northwest or southeast and cut a complex of volcanic rocks that are older than the trachyandesite and range from andesite to rhyolite in composition. The very youthful age of these rocks and deposits and their close spatial relation are highly suggestive of a genetic relationship.

DEPOSITS RELATED TO INTRUSION AND UPLIFT(?)

Deposits related at least in part to intrusion with possible uplift include those in the districts of Bodie and Aurora, Comstock, and possibly Goldfield and Tonopah.

Aurora-Bodie

Gold- and silver-bearing quartz veins cutting Tertiary propylitized andesitic rocks were the source of ore at Bodie, Calif., and at Aurora, Nev. Aurora lies 8 miles northeast of Bodie and is separated structurally from it, but both districts are related to a volcanic complex that forms an elongate, northeast-trending topographic high, 25 miles long, bordering the north rim of the Mono Lake basin (table 1, fig. 6). Several discrete eruptive centers have been recognized within the volcanic highland complex from which rhyolites, quartz latites, dacites, andesites, and basalts have been erupted.

The Bodie district is more or less centrally located within the highland complex in propylitized and silicified volcanic rocks of intermediate composition. Ore was mined from several systems of north-striking, steeply dipping veins, many of which cut an andesitic plug that underlies the main part of the district known as the Bonanza zone. Chesterman, Silberman, and Gray (1969, p. 10–11) indicate that andesite intrusives were emplaced into andesitic flows and tuff breccias. Ore-bearing solutions, apparently related to a late stage of the intrusion, are considered to have deposited their metals approximately 7.9 m.y. ago, the age obtained by M. L. Silberman on four adularia samples, two from each of two veins in the district.

At Aurora, veins with major production are associated with steeply dipping silicified "reefs" that strike northeast within intensely propylitized and locally pyri-

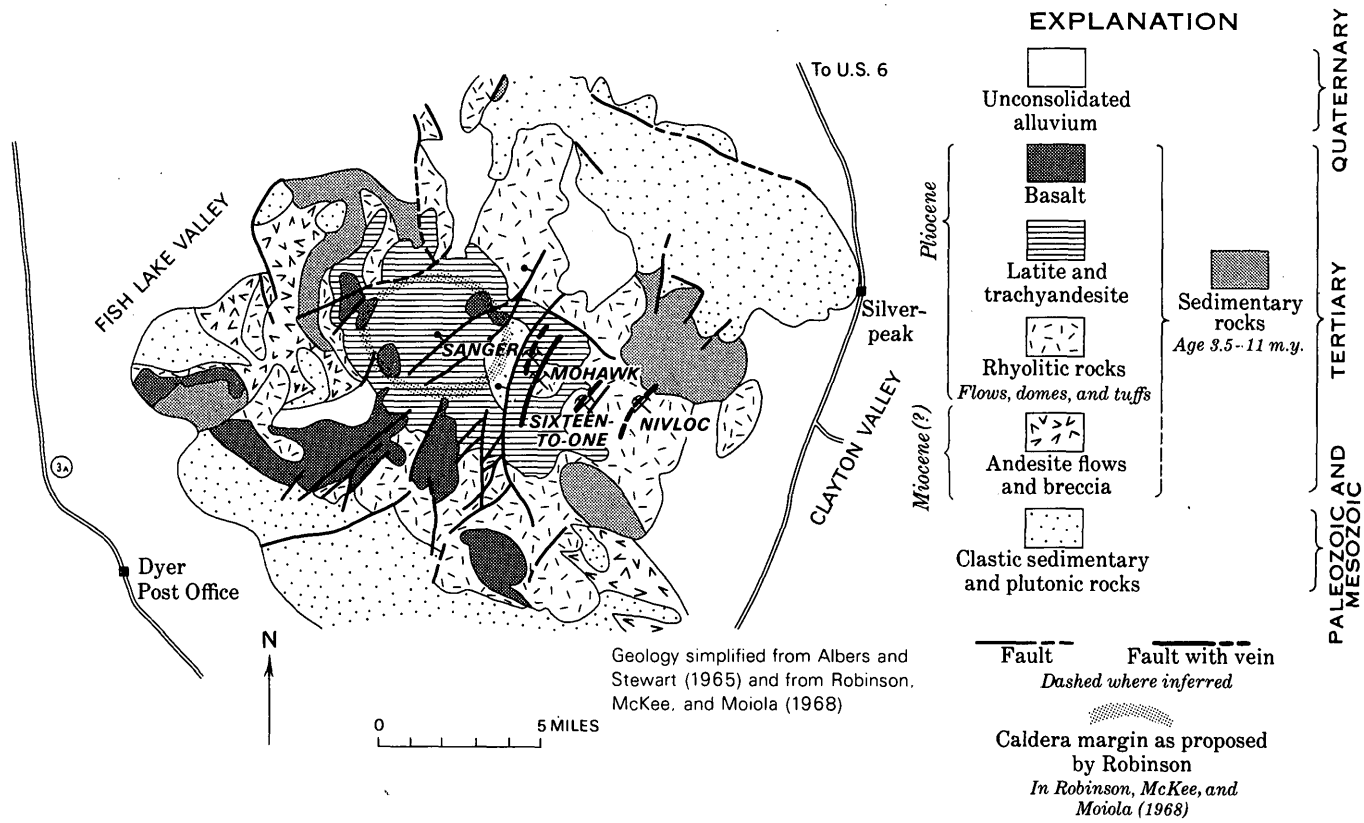

FIGURE 5.—Silver Peak Range, Esmeralda County, Nev.

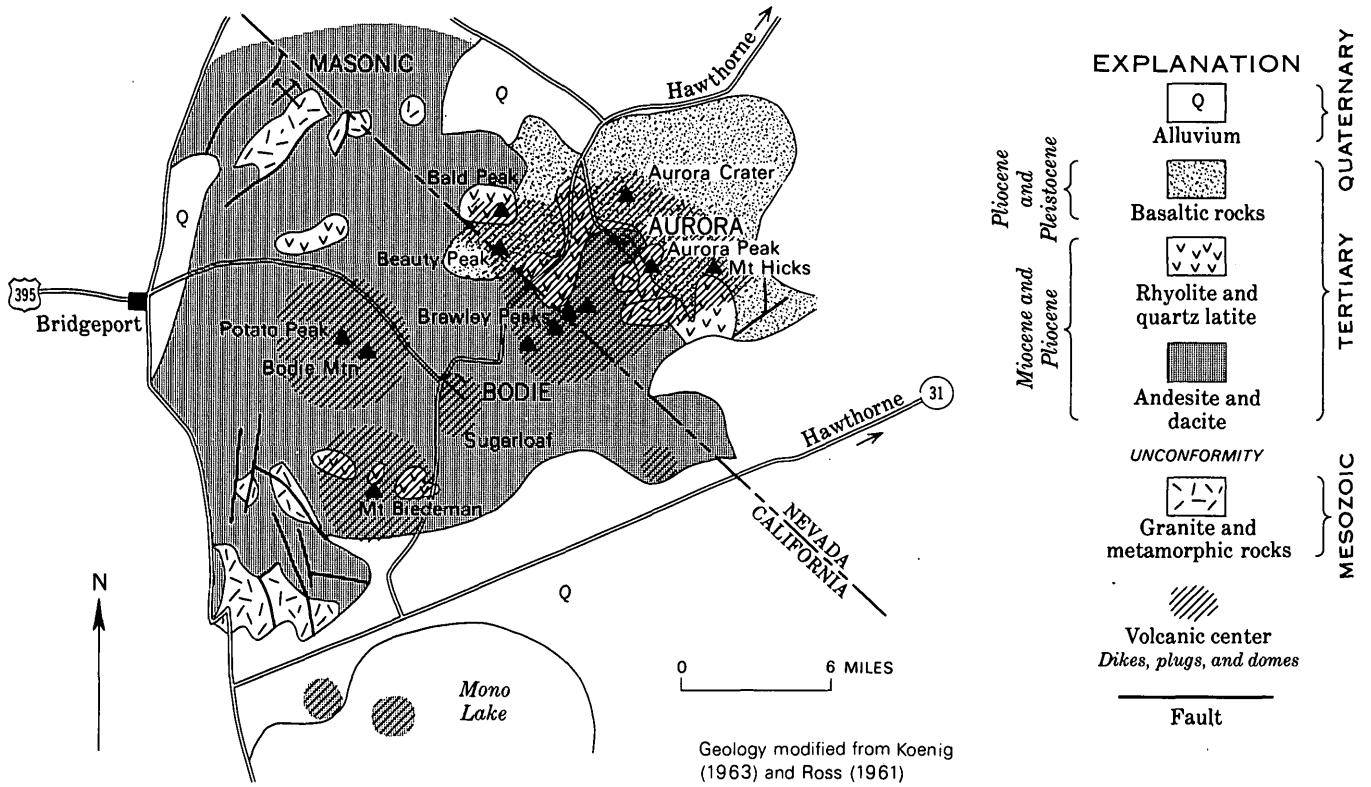

FIGURE 6.—Aurora-Bodie area, California-Nevada.

tized andesitic flows and breccias. Rhyolitic to andesitic intrusives are common in the district. Some are clearly younger than ore mineralization; for others, genetic relationships to the ore deposits is unknown.

Comstock

A strong argument can be made for a large Tertiary volcanic center in the Comstock lode district (table 1, fig. 7). Thompson (1956) points out that the distribution and thickness of the Alta Formation indicates that at least one of the centers from which it was erupted must have been in the Comstock district, and that the younger Kate Peak Formation came from vents in the Virginia Range and nearby areas. Whitebread and Hoover (1968, p. 4–5) also mention intrusive Kate Peak in the Comstock district. Moreover, it is tempting to speculate that the Davidson Granodiorite, which is younger than the Alta and may be in part contemporaneous with the Kate Peak, could mark one of the principal centers from which one or both of the andestic units were derived.

The heart of the Comstock lies directly east of the Davidson Granodiorite, and the principal vein system along the Comstock fault dips eastward away from the stock at about 45°. Ideally, if we subscribe to the classical hypothesis that ore fluids are derived from bodies of cooling magma, we might prefer that the dip of the Comstock fault be westward toward the granodiorite stock. However, the eastward dip is certainly not a flaw in the argument of spatial relationship to a large center in the Comstock area. Nor is it incompatible with the concept of a genetic relationship with the Davidson stock, as little is known of the routes and processes involved in the migration of the ore-forming fluids.

Tonopah

The Tonopah silver district is on the northwestern side of a volcanic center characterized by numerous domes, plugs, and flows of rhyolite quartz latite, and andesite that are of middle Miocene age and mostly younger than the mineral deposits (table 1, fig. 8). The Mizpah Trachyte (andesite) is the host for the ore deposits and is intruded by the other rock types. Part of the same, or a similar, volcanic center is present at the Divide district, several miles south of Tonopah (fig. 8). Here the mineral deposits are younger than those at Tonopah and occur in rocks that overlie or intrude the host andesite there. The abundance of the younger small intrusive bodies in an area otherwise underlain by tuff and andesite lava shows that the general Tonopah area was the site of considerable volcanic activity in Mio-

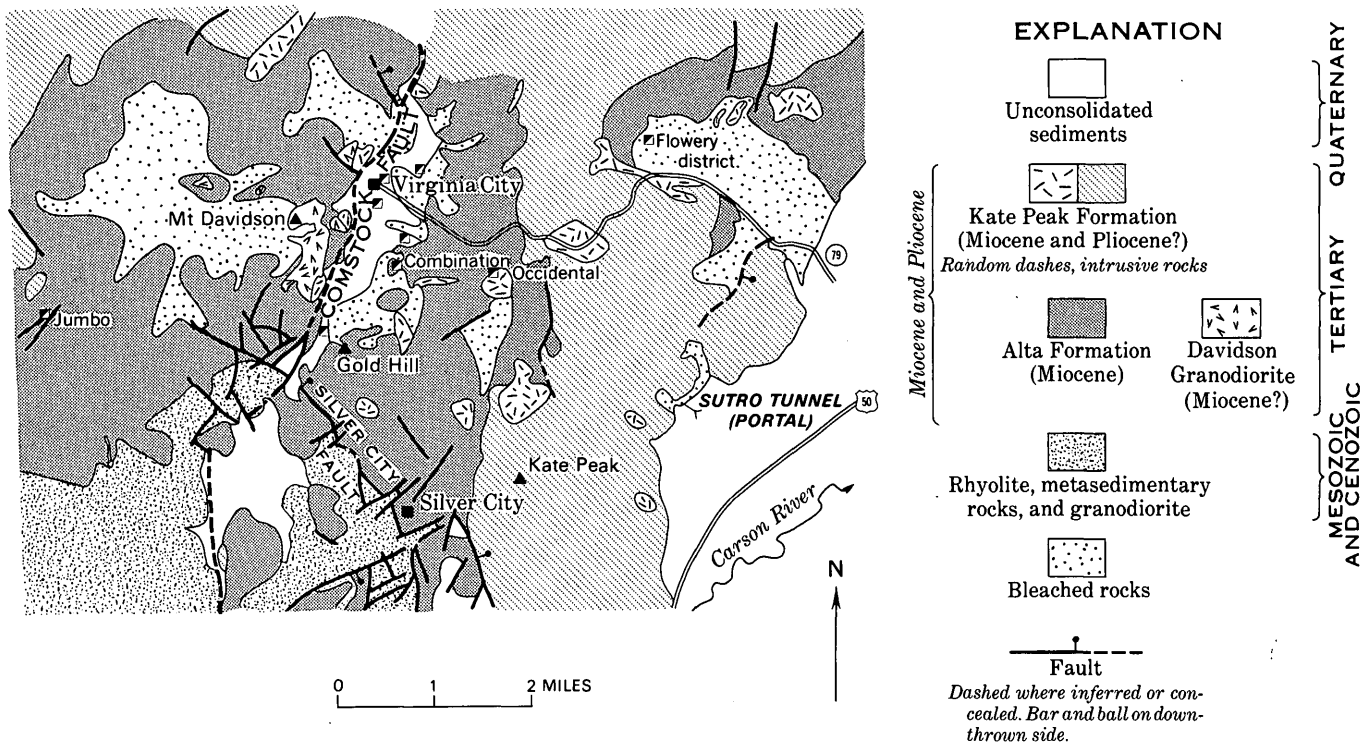

FIGURE 7.—Comstock district, Nevada.

cene time. Upward doming of the Halifax and Tonopah faults, alteration and ore zones, and zones defined by gold-silver ratios led Nolan (1935) to suggest that the Tonopah mine area was domed, possibly above an igneous intrusion prior to deposition of the Esmeralda or Siebert Formations. Inasmuch as several plugs (Oddie Rhyolite, Brougher Dacite) younger than the Siebert are known in the immediate area, this conclusion is certainly reasonable. Quite possibly still another pluglike or stocklike mass representing the intrusive episode is not far beneath the Tonopah workings.

The ore deposits at Tonopah appear to rank about with those at Goldfield as the oldest in the districts herein described (table 1). At Tonopah, the ore is pre-Fraction Breccia where the Fraction overlies the Mizpah Trachyte host. The age of the ore must be greater than 17.5 m.y. if one accepts this as the age of the Fraction Breccia as extrapolated into Tonopah from the dated correlative unit about 45 miles to the east in the Kawich Range (E. B. Ekren, oral commun., 1965).

In addition, the Mizpah Trachyte may be coeval with thin andesite flows that underlie the approximately 22-m.y.-old Toyabe Quartz Latite (Kleinhampl and Ziony, 1967), a welded tuff in the Toiyabe Range about 45 miles north of Tonopah. A lower limit for the age of the Mizpah cannot be set, but the basal Mizpah intertongues (Nolan, 1935, p. 16) with volcanic strata that have affinities with, and may grossly correlate with, a rhyolitic volcanic sequence that underlies the andesite flows in the Toiyabe Range. These rhyolitic volcanic rocks are believed to be early Miocene in age.

OTHER DEPOSITS ASSOCIATED WITH VOLCANIC CENTERS, BRECCIA ZONES, AND PIPES

Deposits belonging to this geologic category, such as Majuba Hill in Pershing County, commonly have features found in deposits related to calderas and to areas of igneous intrusion and uplift, such as Silver Peak and Bodie. But Majuba Hill is clearly not related to a caldera, nor is it obviously related to uplift by intrusion. Majuba Hill is a complex plug of Tertiary(?) rhyolitic rocks, about 5,000 feet in diameter, cutting Triassic(?) sedimentary strata (table 1, fig. 9). As many as five varieties of intrusive breccia form conspicuous dikes and irregular masses cutting the rhyolitic rocks; the latter include an earlier and later rhyolite separated by a rhyolite porphyry. The rhyolitic rocks, as well as the intruded sedimentary strata, are silicified, sericitized, and tourmalinized (Trites and Thurston, 1958). Copper and tin are the principal ore minerals. Apparently the paragenetic sequence is tourmaline (oldest), copper, and tin (youngest), and all are younger than the

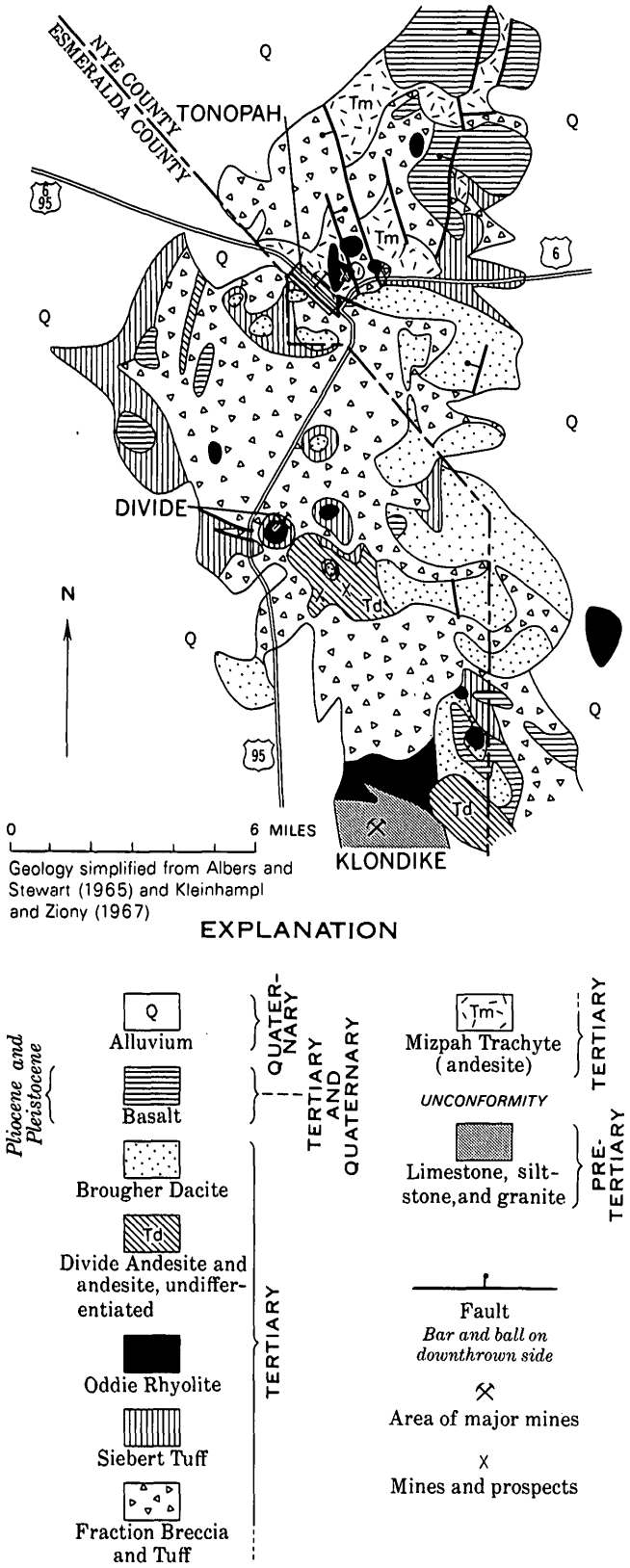

FIGURE 8.—Tonopah area, Nevada.

Majuba fault, which is the principal fracture in the area.

The mineralization of all the deposits discussed here and of others as well occurred after the volcanism and indeed after the volcanic rocks were solidfied. How long afterward is not known. The presently available evidence seems to allow the speculation that many, if not most, of the ore deposits spatially associated with volcanic centers are also genetically related to the centers. Whether or not this is a valid inference, the fact that many deposits are located close to known volcanic centers may be a useful concept in exploration.

REFERENCES

Albers, J. P., and Kleinhampl, F. J., 1967, Spatial relation of mineral deposits to Tertiary volcanic centers in Nevada [abs.]: Mining Eng., v. 19, no. 12, p. 41.

Albers, J. P., and Stewart, J. H., 1965, Preliminary geologic map of Esmeralda County, Nevada: U.S. Geol. Survey Mineral Inv. Field Studies Map MF–298, scale 1:200,000.

Chesterman, C. W., Silberman, M. L., and Gray, C. H., Jr., 1969, Geology and geochronology of the Bodie mining district, Mono County, California [abs.]: Geol. Soc. America, Cordilleran Sec.—Paleont. Soc., Pacific Coast Sec., 65th Ann. Mtg., Eugene, Oreg., 1969, Program, pt. 3, p. 10–11.

Cornwall, H. R., and Kleinhampl, F. J., 1964, Geology of the Bullfrog quadrangle and ore deposits related to the Bullfrog Hills caldera, Nye County, Nevada, and Inyo County, California: U.S. Geol. Survey Prof. Paper 454–J, p. J1–J25.

Gilbert, C. M., Christensen, M. N., Al-Rawi, Yehya, and Lajoie, K. L., 1968, Structural and volcanic history of Mono Basin, California-Nevada, *in* Coats, R. R., Hay, R. L., and Anderson, C. A., eds., Studies in volcanology: Geol. Soc. America Mem. 116 (Howel Williams volume), p. 275–329.

Kleinhampl, F. J., and Ziony, J. I., 1967, Preliminary geologic map of northern Nye County, Nevada: U.S. Geol. Survey open-file map, scale 1:200,000.

Koenig, J. M., compiler, 1963, Geologic map of California, Olaf P. Jenkins edition, Walker Lake sheet: California Div. Mines and Geology, scale 1:250,000.

Nolan, T. B., 1935, The underground geology of the Tonopah mining district, Nevada: Nevada Bur. Mines Bull., v. 29, no. 5, 49 p.

Robinson, P. T., McKee, E. H., and Moiola, R. J., 1968, Cenozoic volcanism and sedimentation, Silver Peak region, western Nevada and adjacent California, *in* Coats, R. R., Hay, R. L., and Anderson, C. A., eds., Studies in volcanology: Geol. Soc. America Mem. 116 (Howel Williams volume), p. 577–611.

Ross, D. C., 1961, Geology and mineral deposits of Mineral County, Nevada: Nevada Bur. Mines Bull. 48, 98 p.

Schilling, J. H., 1964, Metal mining districts of Nevada: Nevada Bur. Mines Map 24, scale 1:1,000,000.

Smith, R. L., Bailey, R. A., and Ross, C. S., 1961, Structural evolution of the Valles Caldera, New Mexico, and its bearing on the emplacement of ring dikes: Art. 340 *in* U.S. Geol. Survey Prof. Paper 424–D, p. D145–D149.

Thompson, G. A., 1956, Geology of the Virginia City quadrangle, Nevada: U.S. Geol. Survey Bull. 1042–C, p. 45–77.

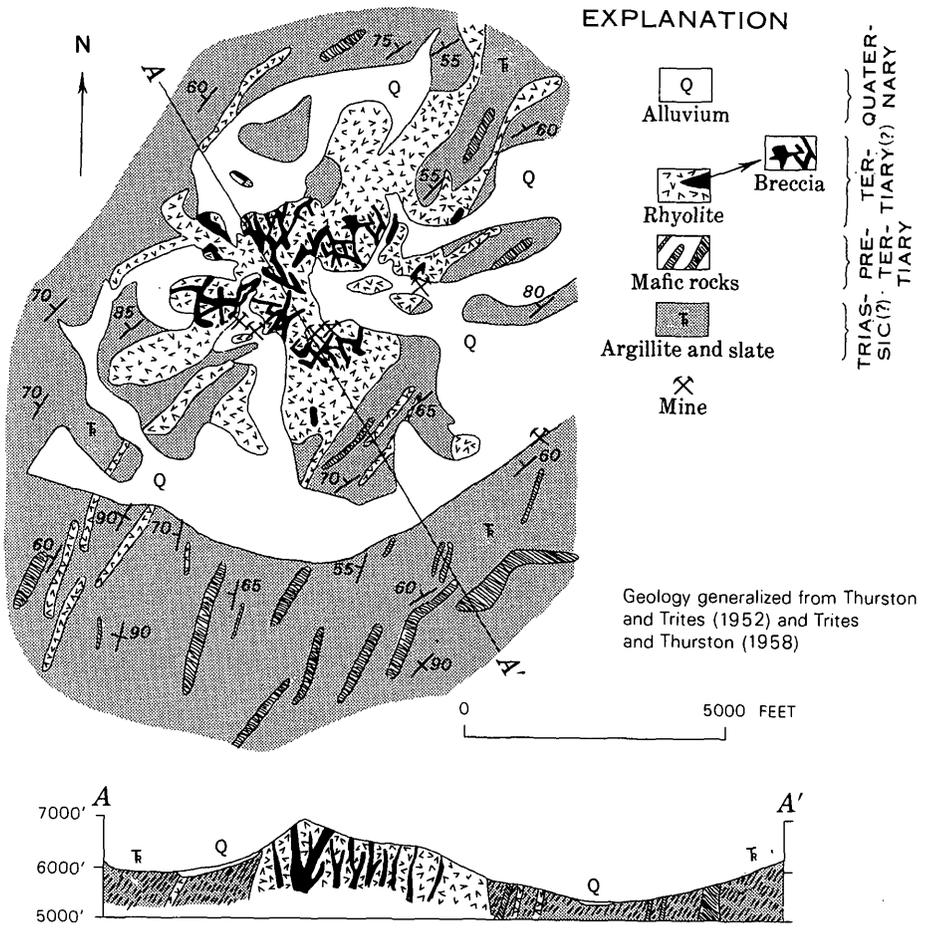

FIGURE 9.—Majuba Hill, Nev.

Thurston, R. H., and Trites, A. F., Jr., 1952, The uranium, tin, and copper deposits at Majuba Hill, Pershing County, Nevada: U.S. Geol. Survey Trace Elements Inv. Rept. 171, 34 p.

Trites, A. F., Jr., and Thurston, R. H., 1958, Geology of Majuba Hill, Pershing County, Nevada: U.S. Geol. Survey Bull. 1046–I, p. 183–203.

Yates, R. G., 1942, Quicksilver deposits of the Opalite district, Malheur County, Oregon, and Humboldt County, Nevada: U.S. Geol. Survey Bull. 931–N, p. 319–348.

Whitebread, D. H., and Hoover, D. B., 1968, Preliminary results of geological, geochemical, and geophysical studies in part of the Virginia City quadrangle, Nevada: U.S. Geol. Survey Circ. 596, 20 p.

QUATERNARY FAULTING AND POTENTIAL EARTHQUAKES IN EAST-CENTRAL COLORADO

By GLENN R. SCOTT, Denver, Colo.

Abstract.—Eight faults in east-central Colorado shifted in Quaternary time. The offsets are only tens of feet, but prove that the rocks beneath some parts of this region were unstable in Quaternary time. Faults along the west flank of the Sangre de Cristo Mountains probably present the greatest likelihood of future earthquakes, owing to their thousands of feet of pre-Quaternary movement and the lateness of their last movement less than 10,000 years ago.

This report about faults with Quaternary displacement in east-central Colorado was prepared after the Denver earthquakes of 1962–67 (Healy and others, 1968) when information was needed about Quaternary fault history in Colorado. Quaternary fault displacements would indicate the probable occurrence of earthquakes, and would be valuable in appraising the likelihood of future earthquakes in the area. Eight faults were found that have stratigraphic evidence for displacement at times ranging from more than 1 million years ago to less than 10,000 years ago (fig. 1). Other faults in the region have probably also been active during the past million years, although evidence for this is lacking.

Quaternary displacement was identified by offset of unconsolidated surficial deposits across the faults. Predominantly vertical movement caused most of the offsets, and evidence for horizontal movement was recognized on only one of the faults. Only one event of Quaternary movement could be confirmed on each of the faults. The displacements in the surficial deposits were caused by movements along observed deep faults; comparable movements today could cause earthquakes.

Most mountain ranges in east-central Colorado are bounded by faults along which there has been hundreds or thousands of feet of cumulative movement. Quaternary movement has been observed along two of these faults but cannot be proved readily along most, because the mountain front is the site of great erosion, and the evidence of displacement is generally destroyed. The Wet Mountain Valley and San Luis Valley are occupied by graben that contain broad basin fills. The Quaternary alluvium is faulted along the borders of these graben. The names and ages of the faulted Quaternary alluvial deposits discussed here are shown in table 1.

TABLE 1.—*Quaternary alluvial deposits in east-central Colorado*

Years before present	Time			Deposit
0	Quaternary	Holocene	Post-Pinedale	Alluvium of several ages (not faulted)
10,000		Pleistocene	Pinedale	Till and outwash
			Bull Lake	Till and outwash
130,000			Sangamon or Illinoian	Slocum Alluvium
			Yarmouth or Kansan	Verdos Alluvium (Douglass Mesa Gravel)
About 1.5 million			Aftonian or Nebraskan	Rocky Flats Alluvium

FAULTS HAVING QUATERNARY DISPLACEMENT

Faults with evidence of Quaternary movement were studied to establish their net Quaternary vertical offset, length of Quaternary displacement, geologic setting, best estimate of time of last movement, and correlative historic seismicity. These are recoverable characteristics that are useful in evaluating likelihood of future fault movement and earthquake generation.

U.S. GEOL. SURVEY PROF. PAPER 700-C, PAGES C11–C18

380-189 O—70——2

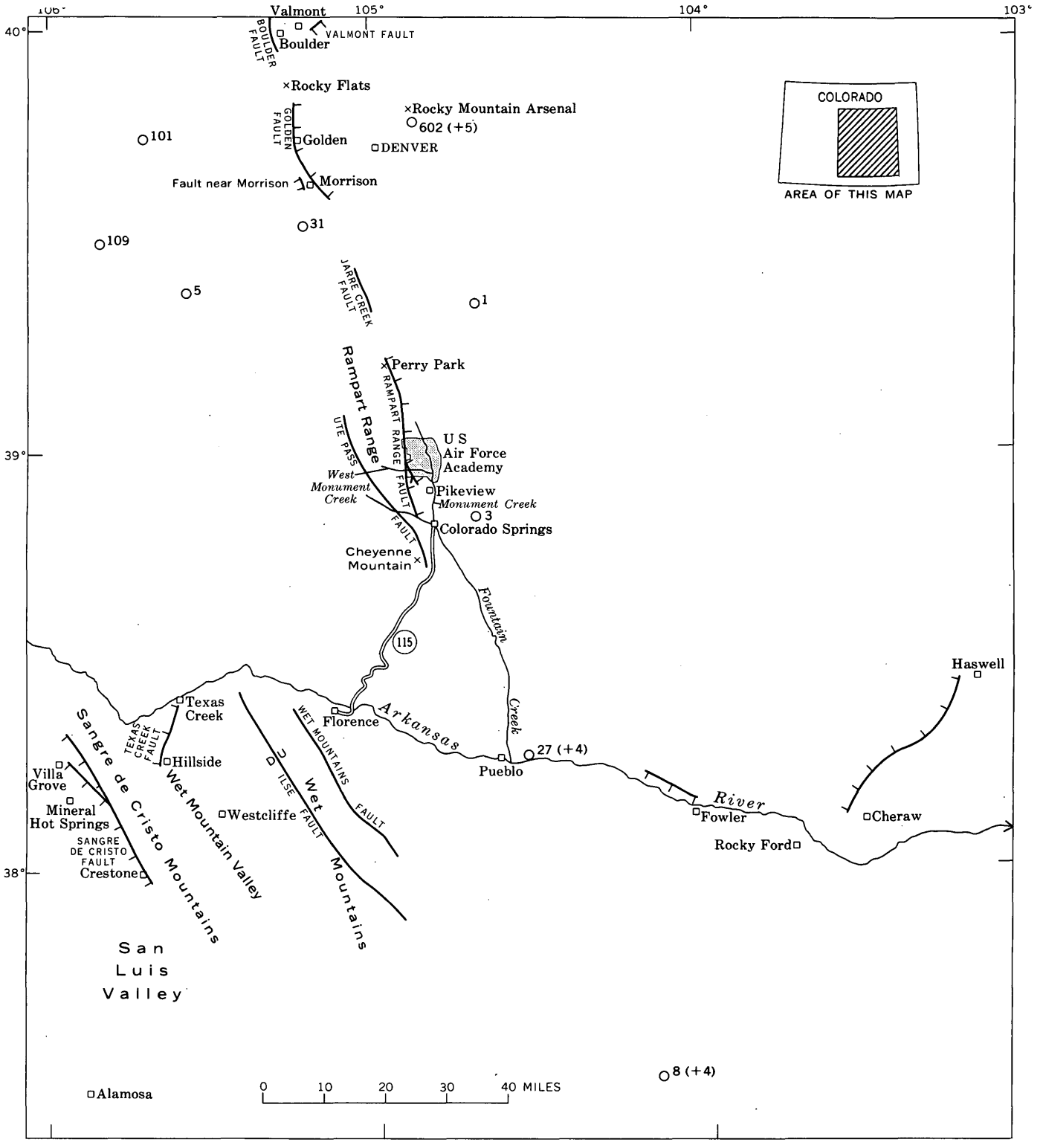

FIGURE 1.—Map of east-central Colorado, showing faults and places mentioned in text. Circles are locations of earthquakes in 1966–68, as shown by Simon (1969), and represent areas approximately 15 km in diameter. Number of events for 3 years is shown beside each circle. Magnitudes of the few shocks of magnitude 4 (Richter scale) or greater are shown in parentheses. Hachures, on downthrown side of faults, indicate Quaternary movement.

The eight faults described in this report are summarized in table 2.

TABLE 2.—*Faults in east-central Colorado having Quaternary displacement*

Name	Net Quaternary displacement (feet)	Youngest material offset	Postulated age
Texas Creek fault.	15+	Miocene and Pliocene basin fill.	Late Pliocene or early Pleistocene.
Fault near Fowler.	60	Rocky Flats Alluvium.	Aftonian(?) or younger.
Fault near Cheraw.	25	-----do---------	Do.
Rampart Range fault.	25	Douglass Mesa Gravel (Verdos Alluvium).	Yarmouth(?) or younger.
Fault near Morrison.	10+	Verdos Alluvium.	Do.
Golden fault-----	5	Verdos Alluvium and overlying colluvium.	Do.
Valmont fault----	5	Slocum Alluvium.	Sangamon(?) or younger.
Sangre de Cristo fault.	25	Pinedale outwash.	Post-Pinedale.

I believe that future displacement on some of the faults described here could result in earthquakes large enough in magnitude to endanger property or people. No one now can predict accurately the time of such an earthquake. I can find no historic record of an earthquake in Colorado having an estimated intensity higher than VII on the modified Mercalli scale. Earthquakes in Colorado in historic time have caused only minor damage to buildings and minor rockslides. The existence of Quaternary ruptures shows that Colorado had high-magnitude earthquakes in Quaternary time, as a magnitude of about 6.5 (Richter scale) (Tocher, 1958) is considered necessary to cause surface rupture, depending on depth of focus, lithology of ruptured material, and other factors.

Texas Creek fault

The Texas Creek fault is a major vertical fault—one having a wide zone of crushed rock—and is believed to have a Precambrian ancestry. It trends slightly west of south about 10 miles from the town of Texas Creek to Hillside and then disappears beneath the fill of the Wet Mountain Valley. A roadcut on the north side of Colorado Highway 69 in the S½ sec. 14, T. 47 N., R. 12 E., shows probable Miocene and Pliocene alluvium on the west downfaulted more than 15 feet against Precambrian gneiss on the east. Outwash deposits of Bull Lake age farther south along the fault are unbroken; therefore the movement along the Texas Creek fault is possibly late Pliocene or early Pleistocene in age, but is no younger than Sangamon. This means that there has been no appreciable movement along the fault for at least 100,000 years.

Inferred fault near Fowler

An inferred minor fault—one having a very narrow zone of crushed shale—lies north of Fowler chiefly in T. 21 S., R. 60 W., and about 2 miles northeast of the Arkansas River. It trends N. 60° W., nearly parallel to the river, and can be traced at least 6 miles (fig. 2). This fault was first suspected by me during a reconnaissance of the surficial deposits of Pueblo County with Harold E. McGovern and Dean O. Gregg in September 1961, when we noted a straight and abrupt scarp between two terraces. The scarp is 60 feet high and separates two flat surfaces, each underlain by Rocky Flats Alluvium. Because the gravel beneath the two surfaces is identical and has a similar soil developed on it, I believe that the gravel is all part of the same deposit, and that the 60-foot scarp represents movement along a fault.

Although faults were not seen in the alluvium, three closely spaced northward-dipping faults were found in the Pierre Shale in an arroyo in the SW¼ sec. 22, T. 21 S., R. 60 W., that crosses the inferred faultline

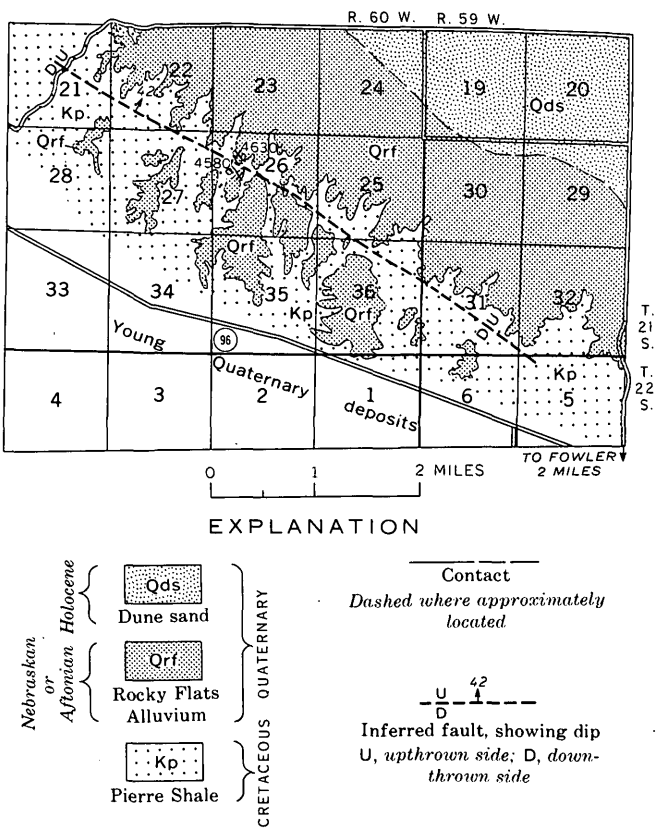

FIGURE 2.—Inferred fault near Fowler, Colo.

(fig. 2). The presence of these faults increases the likelihood that a fault did displace a single terrace. Inasmuch as the terrace was displaced after an Aftonian soil developed in the upper part of the Rocky Flats Alluvium, an age of Aftonian(?) or younger is assigned to the inferred fault.

Fault near Cheraw

A fault north of the Arkansas River extending 25 miles about N. 45° E. from Cheraw to Haswell was discovered in 1968 by J. A. Sharps, U.S. Geological Survey, while he was mapping the geology of the Lamar 1:250,000 quadrangle. Rocks southeast of the fault were displaced upward an estimated 25 feet in relation to those on the northwest. The youngest deposit known to be displaced is the Rocky Flats Alluvium; therefore, the movement is Aftonian(?) or younger.

Rampart Range fault

A branch of the Rampart Range fault at the U.S. Air Force Academy (Varnes and Scott, 1967) is a high-angle reverse fault dipping westward a little steeper than 60°. It trends N. 25° W. obliquely across northward-striking rocks in the N½ sec. 33, T. 12 S., R. 67 W., near the point where West Monument Creek leaves the Rampart Range (fig. 3). Douglass Mesa Gravel (equals Verdos Alluvium) was displaced by the fault, and a swale was eroded along the faultline. The area of bedrock southwest of the fault first moved upward in early Tertiary time; then in Quaternary time the gravels southwest of the fault moved downward about 25 feet. The gravel on the northeast side of the same fault apparently also moved southeastward in Quaternary time. A swale trending south along the remnant of Douglass Mesa Gravel possibly follows an additional

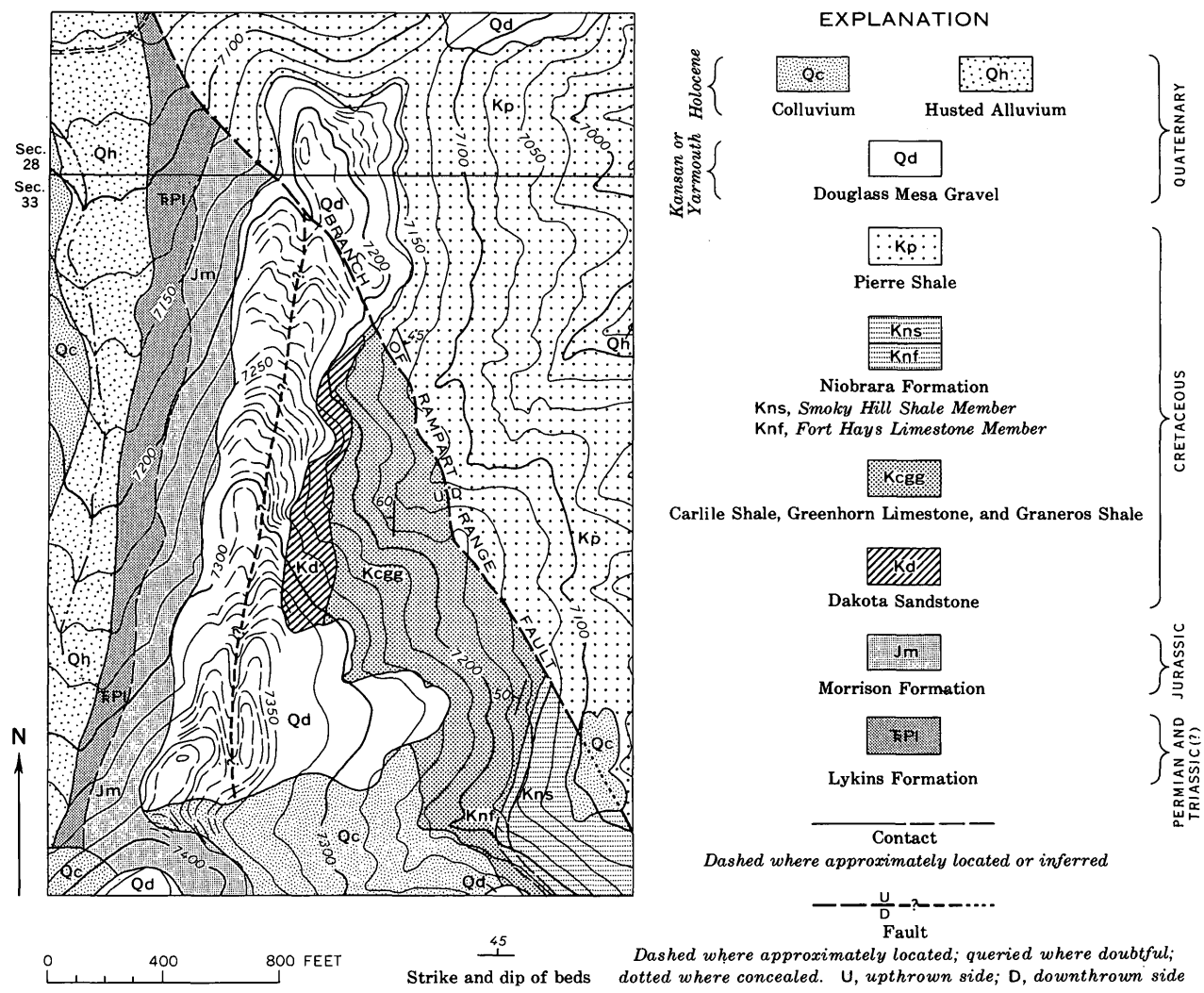

FIGURE 3.—Branch of Rampart Range fault near Pikeview in the southwest part of the U.S. Air Force Academy, in T. 12 S., R. 67 W. Main Rampart Range fault lies west of mapped area. Contour interval 25 feet (with supplemental 5-foot intervals). Geology by Varnes and Scott(1967).

contemporaneous strike-slip branch of the Rampart Range fault (fig. 3). Sandstone dikes associated with the main Rampart Range fault at Perry Park suggest that the fault had a Precambrian ancestry (Scott, 1963). Because faulting took place after a Yarmouth soil was developed on the Douglass Mesa Gravel, the age of the latest faulting is inferred to be Yarmouth(?) or younger.

Fault west of Morrison

Movement occurred along a minor fault at the SE cor. sec. 34, T. 4 S., R. 70 W., three-fourths mile west of Morrison after deposition of the Verdos Alluvium. The fault is vertical and trends N. 20° W. Precambrian gneiss on the east is raised about 10 feet above the base of Verdos Alluvium on the west (fig. 4). In a small patch of Verdos Alluvium preserved along the fault, the stones are skewed so that their long axes parallel the vertical walls of the fault. A Yarmouth soil is developed on the alluvium; therefore, a Yarmouth(?) or younger age is inferred for the most recent fault movement.

Golden fault

The Golden fault is a major mountain-front reverse fault that trends northward through Golden, Colo. The fault has as much as 8,000 feet of stratigraphic throw at Golden, where it dips about 70° W. Two vertical shear zones in a trench in the NE¼SW¼ sec. 28, T. 3 S., R. 70 W., displace Verdos Alluvium and overlying colluvium. The shear zones trend N. 20°–30° W., thus

FIGURE 5.—Golden fault, showing east side of graben. Cobble gravel of Verdos Alluvium is buried on right side of fault. U, upthrown side; D, downthrown side.

forming a graben in which the Quaternary deposits dropped about 5 feet (figs. 5–7). The Verdos Alluvium is a well-sorted cobble gravel deposited by ancestral Clear Creek about 190 feet above the modern stream. The overlying colluvium contains Pearlette-like vol-

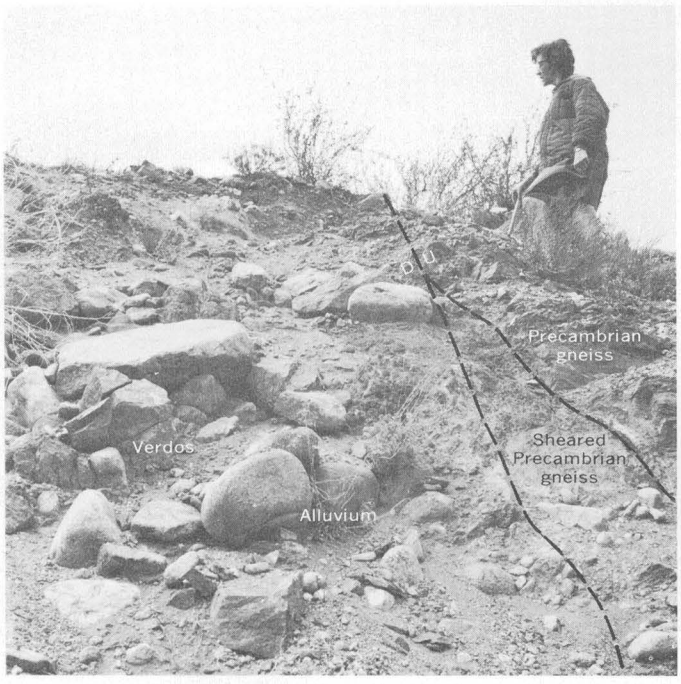

FIGURE 4.—Fault west of Morrison, Colo. U, upthrown side; D, downthrown side. View looking north.

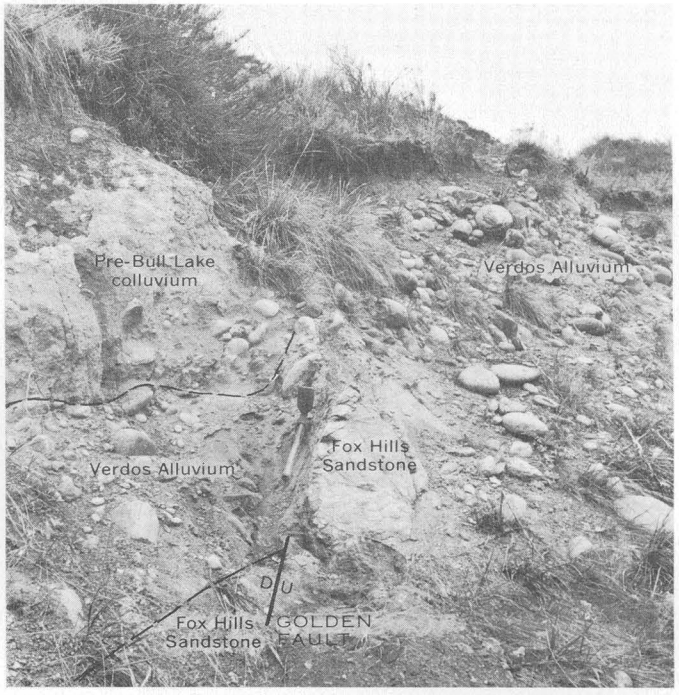

FIGURE 6.—Golden fault, showing west side of graben. U, upthrown side; D, downthrown side.

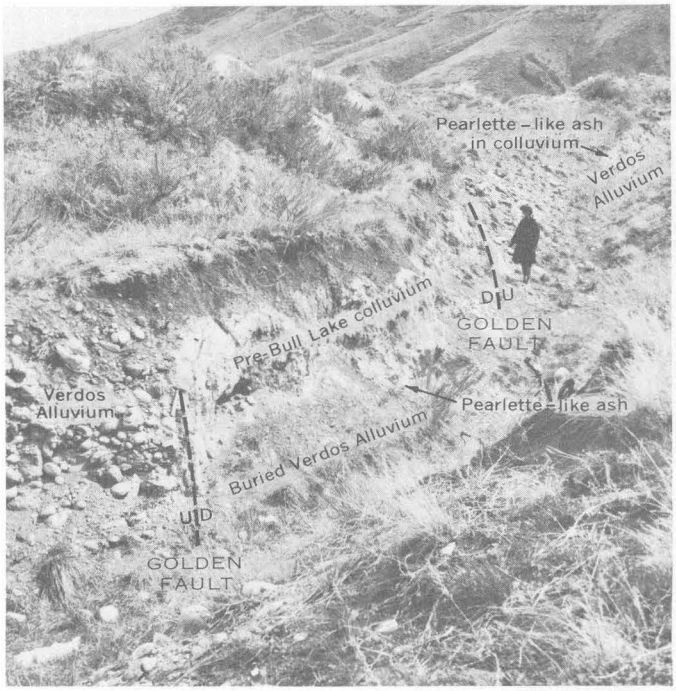

FIGURE 7.—Golden fault, showing full width of graben. Woman is standing just to west of west side of graben. U, upthrown side, D, downthrown side.

canic ash that apparently was carried down over the Verdos from a 5-foot-thick deposit of pre-Verdos water-laid ash about 30 feet upslope. A Yarmouth(?) soil is disrupted by the Golden fault; therefore the age of faulting is judged to be Yarmouth(?) or younger.

Valmont fault

The Valmont fault, a minor vertical fault, trends N. 50° E. across a north-south road in the S½ sec. 24, T. 1 N., R. 70 W. (Scott and Cobban, 1965). It displaced Slocum Alluvium of Illinoian or Sangamon age on the south downward against Fox Hills Sandstone on the north (fig. 8). This Pleistocene movement was first recognized in 1957 by Frank Riley, U.S. Geological Survey. The fault parallels the early Tertiary(?) Valmont igneous dike (Scott and Cobban, 1965) half a mile to the northwest. Movement on the fault created a false shingling of flat stones in the Slocum Alluvium (fig. 8). Displacement of Slocum Alluvium by the fault, which is at least 5 feet in the area exposed, was Sangamon(?) or younger.

Sangre de Cristo fault

The Sangre de Cristo fault, a major fault, forms the boundary between the Sangre de Cristo Mountains and the downfaulted San Luis Valley (figs. 9 and 10), and it extends as a normal fault with nearly vertical dips all along the foot of the mountains. At Valley View Hot Springs (6 miles east of Mineral Hot Springs), a

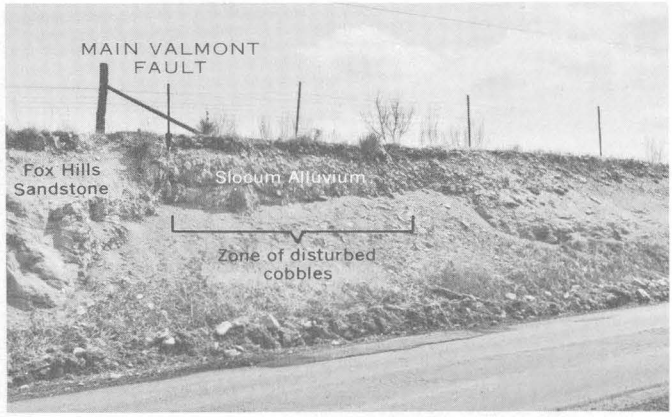

FIGURE 8.—Valmont fault, showing area of near-vertical shingling of cobbles.

branch (fig. 11) of the fault turns northwestward into the center of the valley, where it splits further in the alluvium. This branch apparently bounds the east side of a deep graben, which was discovered by Gaca and Karig (1966) by use of gravity measurements, beneath the San Luis Valley and parallel to the west side of the Sangre de Cristo Mountains. The graben continues northward through Poncha Pass as a major structural trough (Van Alstine, 1968). Both the mountain front fault and the branch fault are expressed at the surface by abrupt scarps in Pleistocene gravel that are as much as 25 feet high (fig. 10). The west side of the graben

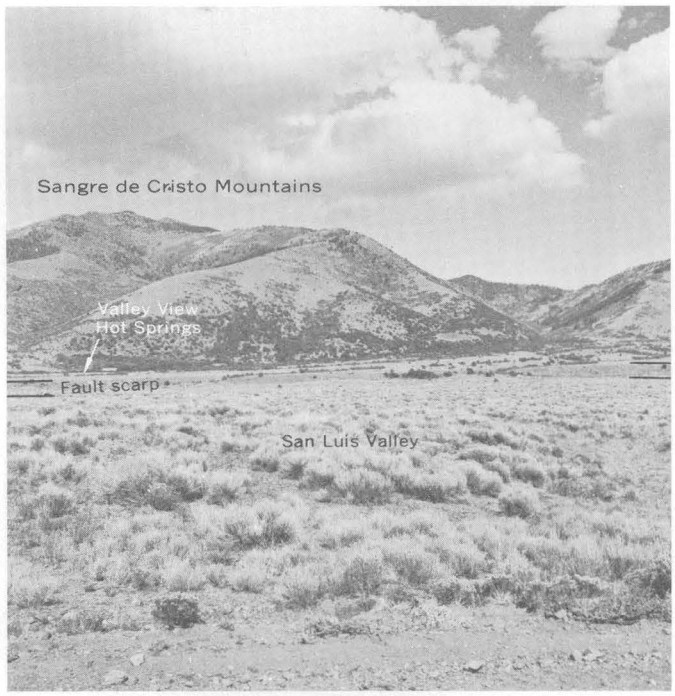

FIGURE 9.—Scarp of branch of Sangre de Cristo fault near mountain front at Valley View Hot Springs. View looking east.

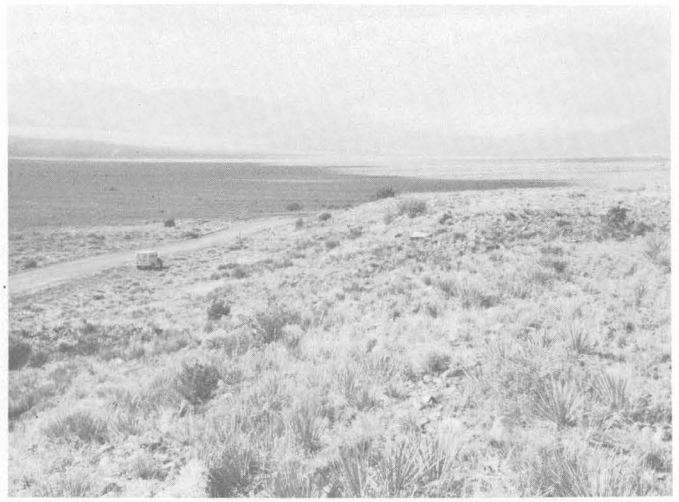

FIGURE 10.—View northwest, from top of scarp near Valley View Hot Springs, of branch of Sangre de Cristo fault, showing a closeup of the scarp shown in figure 9.

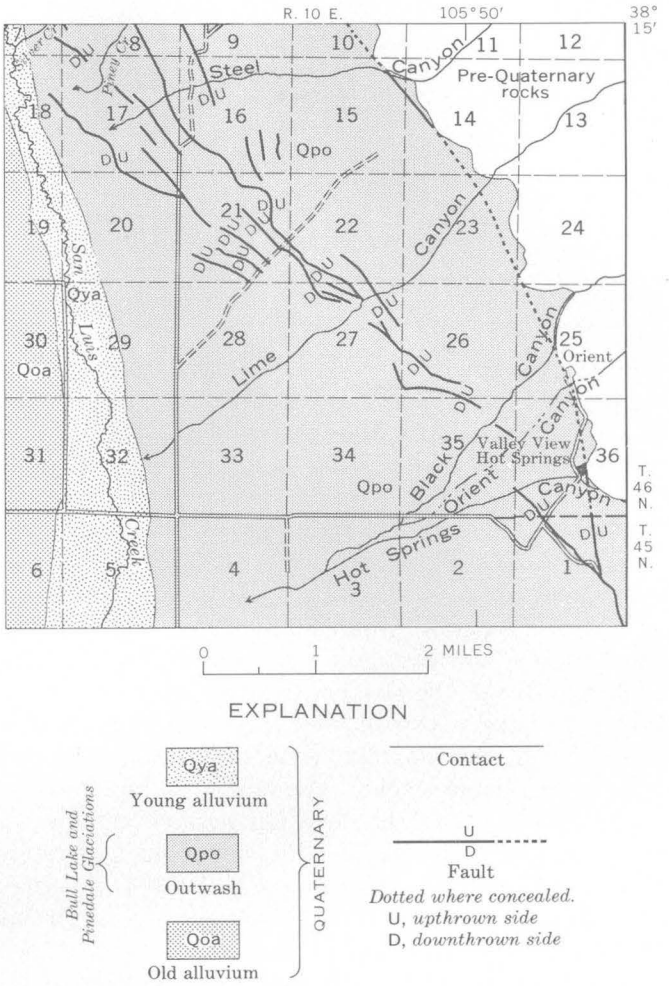

FIGURE 11.—Zone of faults that branches from Sangre de Cristo fault northwestward from Valley View Hot Springs. Fault through Valley View Hot Springs is main Sangre de Cristo fault.

located by Gaca and Karig is not marked by a scarp, but Mineral Hot Springs, 5 miles south of Villa Grove, lies on this trend; the spring water possibly rises along a deep-seated fault.

The mountain front fault has displaced deposits in the mountains as old as Precambrian, and deposits in the basin of the Miocene and Pliocene Santa Fe Formation that fill the San Luis Valley. The faults moved thousands of feet in pre-Quaternary time. They also cut both Bull Lake and Pinedale outwash fans, but not upper Holocene deposits. Thus, the faults have a history of activity from Precambrian to post-Pinedale time less than 10,000 years ago.

POTENTIAL EARTHQUAKES

Many historic fault movements have been accompanied by earthquakes, and the Quaternary faults described in this paper also are inferred to have a potential for future earthquakes. The prediction of future earthquakes in any area is based partly on seismic records. Although few earthquakes are specifically linked to any of the above faults, records of some earthquakes in the same general areas have been assembled by Hadsell (1968, p. 57) as shown in table 3. Earthquakes near the Rocky Mountain Arsenal well at Denver are not listed here.

In addition to the earthquakes listed, F. A. Hadsell (oral commun., May 11, 1967) mentioned an earthquake of intensity IV at Westcliffe, Colo., in 1888, and an earthquake of intensity V at Alamosa in 1952.

Some of the same areas that were seismically active in the historical record gathered by Hadsell (1968) were also active in 1966 through 1968, as shown by a study of seismograms of all Colorado earthquakes in those years (Simon, 1969). Earthquakes near or at three of the faults described here were recorded in those 3 years: at Colorado Springs (Ute Pass or Rampart Range fault?)—three earthquakes in 1968 (magnitude less than 4, Richter scale); Golden fault—31 earthquakes in 1967 (magnitude less than 4); and Pueblo (inferred fault near Fowler?)—five earthquakes in 1966, 12 in 1967, and 10 in 1968 (magnitude less than 4 except in 1967 when some were greater than 4).

An examination of the reports of intensity and of seismograms shows that no earthquake having an estimated modified Mercalli intensity greater than VI is known at or near any of the faults described. These records span only 100 years, whereas the individual faults disturbed the Quaternary deposits from more than 1 million years ago to less than 10,000 years ago. I infer that the reports of intensity and the seismograms

TABLE 3.—*Earthquakes near Quaternary faults in east-central Colorado*

[From Hadsell, 1968, p. 59–62]

Year	Date	Local time	Locality	Lat (N.)	Long (W.)	Circular felt area (thousands of sq mi)	Maximum observed modified Mercalli intensity
1870	Dec. 4	0500	Pueblo	38.5	104	62	VI
1916	Oct. 11	2241	Boulder	40.0	105.0	------	III
1955	Nov. 27	2225	Rocky Ford	38.2	103.7	0.4	IV
1963	Nov. 13	1434	Pueblo	38.3	104.6	------	IV
1965	Jan. 5	1626	Rocky Flats	39.9	105.3	------	III

represent too short a time to be significant in evaluating the potential for future large earthquakes.

Apart from seismic records, the potential for future earthquakes caused by these faults can be evaluated from geologic setting, amount of Quaternary vertical displacement, length of Quaternary fault rupture, and the time of last movement. From the geologic setting, the total displacement and (for some faults) the amount of displacement in different geologic times can be determined. The mountain front faults, such as the Rampart Range, the Golden, and the Sangre de Cristo faults, all have a long history of movement beginning probably in Precambrian time and have produced cumulative displacements measurable in hundreds or even thousands of feet. The Quaternary cumulative movements along the eight faults described here range from 5 to 60 feet. For these faults, Pleistocene displacement probably is only a small part of the total, but permits a comparison of the Quaternary activity of one fault to that of the other faults. An earthquake of intensity V, according to F. A. Hadsell (oral commun., 1967), is likely to be generated by movement on a fault having a length of at least 10 km. By this formula, all except the fault near Morrison and the Valmont fault could produce earthquakes having intensities greater than V. Although the time of latest movement does not allow an estimate of the frequency of movement, the fault that has been active most recently of those described, and shows the greatest cumulative displacement, seems to me to have a greater potential for future displacement than a fault having ancient movement and small cumulative displacement.

The time of latest movement along the eight faults ranges from Pliocene or early Pleistocene to post-Pinedale. The fault in the San Luis Valley near Villa Grove moved most recently, and a possibility of an earthquake seems more likely there than along the other described faults. Further, the possibility of movement along other faults that have a long history of movement cannot be discounted, even though Quaternary movement on some of these faults is not yet demonstrated.

In conclusion, although the available data are inadequate to permit prediction of time of earthquakes in east-central Colorado, the geologic information and seismic record suggest that earthquakes having intensities of IV or less on the modified Mercalli scale will continue as recorded by Simon (1969), and a rare earthquake of intensity VI or VII is probable.

REFERENCES

Gaca, J. R., and Karig, D. E., 1966, Gravity survey in the San Luis Valley area, Colorado: U.S. Geol. Survey open-file report, 21 p., 22-p. app.

Hadsell, F. A., 1968, History of earthquake activity in Colorado, *in* Geophysical and geological studies of the relationships between the Denver earthquake and the Rocky Mountain Arsenal well, pt. A: Colorado School Mines Quart., v. 63, no. 1, p. 57–72.

Healy, J. H., Rubey, W. W., Griggs, D. T., and Raleigh, C. B., 1968, The Denver earthquakes: Science, v. 161, no. 3848, p. 1301–1310.

Scott, G. R., 1963, Bedrock geology of the Kassler quadrangle, Colorado: U.S. Geol. Survey Prof. Paper 421–B, p. 71–125.

Scott, G. R., and Cobban, W. A., 1965, Geologic and biostratigraphic map of the Pierre Shale between Jarre Creek and Loveland, Colorado: U.S. Geol. Survey Misc. Geol. Inv. Map I–439, with 4-p. text.

Simon, R. B., 1969, Seismicity of Colorado; consistency of recent earthquakes with those of historical record: Science, v. 165, no. 3896, p. 897–899.

Tocher, Don, 1958, Earthquake energy and ground breakage [Calif. and Nev.]: Seismol. Soc. America Bull., v. 48, no. 2, p. 147–153.

Van Alstine, R. E., 1968, Tertiary trough between the Arkansas and San Luis Valleys, Colorado, *in* Geological Survey Research 1968: U.S. Geol. Survey Prof. Paper 600–C, p. C158–C160.

Varnes, D. J., and Scott, G. R., 1967, General and engineering geology of the United States Air Force Academy site, Colorado, *with a section on* Ground water, by W. D. E. Cardwell and E. D. Jenkins: U.S. Geol. Survey Prof. Paper 551, 93 p.

RECONNAISSANCE GEOLOGY AND ECONOMIC SIGNIFICANCE OF THE PLATORO CALDERA, SOUTHEASTERN SAN JUAN MOUNTAINS, COLORADO

By PETER W. LIPMAN and THOMAS A. STEVEN, Denver, Colo.

Prepared in cooperation with the Colorado State Mining Industrial Development Board

Abstract.—The Platoro caldera is a composite collapse structure about 20 km in diameter that formed as a result of ash-flow eruption of the upper Oligocene Treasure Mountain Tuff. Three major ash-flow sheets of the Treasure Mountain Tuff—here named the La Jara Canyon, Ojito Creek, and Ra Jadero Members in ascending order—are approximately coextensive and cover about 5,000 km^3 in the southeastern San Juan Mountains. Major collapse of the Platoro caldera occurred during eruption of quartz latitic ash flows that form the La Jara Canyon Member, and late ash flows of this member accumulated within the collapsing caldera to a thickness of more than 800 m. The core of the collapsed block was resurgently domed, and the marginal moat was then filled to overflowing by more than 700 m of andesitic lavas. Renewed ash-flow eruption of the quartz latitic Ojito Creek and Ra Jadero Members resulted in further collapse in the northern part of the main caldera. No resurgence seems to be associated with this late caldera, but it was also filled to overflowing by a thick accumulation of andesitic lavas.

Genetically related quartz latitic dikes and granitic stocks, with associated porphyritic rhyodacitic to quartz latitic lavas, were emplaced repeatedly around margins of the late caldera, and associated hydrothermal alteration and local ore deposition took place in the Summitville and Platoro mining districts, as well as in other nearby mineralized areas at Stunner, Gilmore, Jasper, Crater Creek, and Cat Creek. These mineralized areas, which had previously appeared anomalous, are therefore comparable to other caldera-associated mineralization in the central and western San Juan Mountains.

Recent U.S. Geological Survey investigations of volcanic rocks of the San Juan Mountains have led to recognition of numerous caldera-collapse structures (fig. 1) related to eruption of voluminous ash-flow tuffs in Oligocene time (Luedke and Burbank, 1968; Steven and Ratté, 1965; Steven and Lipman, 1968). It has also become clear that most major ore deposits of the San Juan Mountains, such as those near Creede, Silverton-Telluride-Ouray, and Lake City, are closely associated with calderas (Burbank and Luedke, 1968; Steven, 1968). An apparent exception to this association between mineralization and caldera structure seemed until recently to be the Summitville-Platoro district in the southeastern San Juan Mountains (Steven and Ratté, 1960; Steven, 1968). This paper gives a preliminary description of the newly recognized Platoro caldera and the associated mineral deposits, including those in the Summitville district.

GEOLOGIC SETTING

The San Juan volcanic field, which covers about 25,000 km^2 in southwestern Colorado and adjacent parts of New Mexico (fig. 1), is the largest erosional remnant of a once nearly continuous volcanic field that extended over much of the southern Rocky Mountains in Oligocene and later time (Steven and Epis, 1968). Throughout the San Juan remnant of this field, the general volcanic sequence was relatively simple: initial intermediate lavas and breccias, followed closely in time by more silicic ash-flow tuffs, and ending with a compositionally bimodal association of basalt and rhyolite (Lipman and Steven, 1969).

In the San Juan field voluminous early intermediate-composition lavas and breccias—mainly alkali andesite, rhyodacite, and mafic quartz latite—were erupted from numerous scattered central volcanoes onto an eroded tectonically stable terrane. They formed mostly during the interval 35–30 m.y. (million years) ago (Lipman and others, 1970).

About 30 m.y. ago, major volcanic activity changed to explosive ash-flow eruptions of quartz latite and low-silica rhyolite that persisted until about 26 m.y. ago. Sources areas for the ash flows are marked by large calderas. Two groups of lavas and associated rocks of intermediate composition intertongue with the ash-flow sequence: (1) quartz latitic lavas that were erupted in and adjacent to caldera structures and are genetically related to the ash-flow activity, and (2) other generally more mafic lavas and related rocks that are widely distributed without evident structural relation to the ash-flow eruptive centers. The second group apparently

U.S. GEOL. SURVEY PROF. PAPER 700–C, PAGES C19–C29

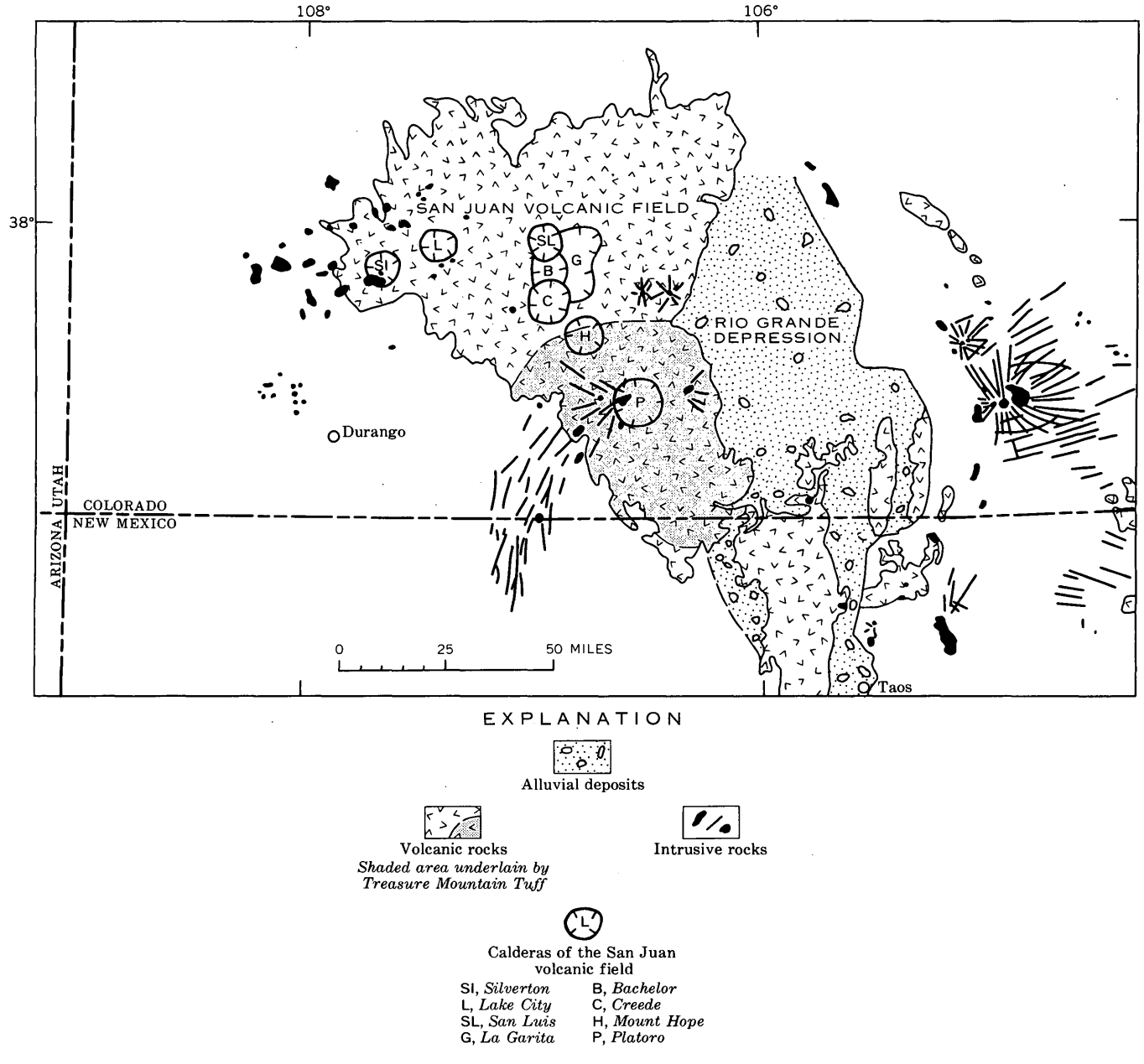

FIGURE 1.—Index map showing location of the San Juan volcanic field, calderas of the San Juan Mountains, and distribution of ash-flow tuffs erupted from the Platoro caldera. In part modified from Cohee (1961).

represents a continuation of the early intermediate activity into the period of major ash-flow eruption.

In the early Miocene the character of volcanism changed notably. Whereas the Oligocene volcanics are predominantly intermediate lavas and related silicic differentiates, the younger rocks are largely a bimodal association of basalt and high-silica alkali rhyolite. Basalt and minor rhyolite were erupted intermittently through the Miocene and Pliocene, and at one time formed a widespread veneer over the older volcanic terrane.

ROCK UNITS

The stratigraphy of the Platoro caldera area is most readily summarized in terms of (1) precaldera intermediate-composition lavas and related rocks of the Conejos Formation, (2) ash-flow sheets of the Treasure Mountain Tuff erupted from the Platoro caldera, (3) lavas and intrusions related to the Platoro caldera, (4) younger ash-flow sheets from calderas farther northwest, and (5) basalt and rhyolite of the Hinsdale Formation.

Conejos Formation

All precaldera rocks in the Summitville-Platoro area are parts of the Conejos Formation (Larsen and Cross, 1956). This unit consists largely of lava flows and breccias that range in composition from calc-alkalic andesite to mafic quartz latite, and also contains varied volcaniclastic rocks, mainly of mudflow origin. Most rocks of the Conejos Formation were erupted in middle Oligocene time from numerous widely scattered central volcanoes, at least three of which contributed to the accumulation within the area of figure 2. Conejos rocks in the east half of the mapped area are predominantly lavas and flow breccias, whereas the bulk of the formation southwest of the Platoro caldera consists of bedded breccias and conglomerates with minor intercalated flows.

Treasure Mountain Tuff

The Treasure Mountain Tuff is here redefined from the Treasure Mountain Rhyolite (Larsen and Cross, 1956) to include only the units present at the type locality at Treasure Mountain, approximately 20 km west of Summitville, Colo., plus additional intertonguing tuffs farther to the south. Excluded from the Treasure Mountain Tuff are thick sections of other welded ash-flow tuffs that were mapped as Treasure Mountain Rhyolite in the western and central San Juan Mountains by Larsen and Cross (1956, pl. 1). The largest body of these in the western San Juan Mountains was designated the Gilpin Peak Tuff by Luedke and Burbank (1963). As redefined, the Treasure Mountain Tuff is a coextensive assemblage of ash-flow tuffs, largely or entirely related to the Platoro caldera. Three large ash-flow sheets in the Treasure Mountain Tuff that have been mapped over nearly 5,000 km^2 are formally designated members in this report: the La Jara Canyon, Ojito Creek, and Ra Jadero Members, in ascending order. Less widespread air-fall and ash-flow tuffs below the La Jara Canyon Member, between the La Jara Canyon and Ojito Creek Members, and above the Ra Jadero Member are informally designated the lower, middle, and upper tuffs, respectively.

The La Jara Canyon Member is a multiple-flow, compound cooling unit of phenocryst-rich quartz latite that makes up the first widespread ash-flow sheet in the eastern and central San Juan Mountains; eruption of these ash flows resulted in the first major collapse of the Platoro caldera. At its type locality in La Jara Canyon (37°10′ N., 106°20′ W.), about 27 km southeast of Platoro, this sheet is about 100 m thick (fig. 3), and its maximum thickness outside the Platoro caldera is about 300 m. Within the caldera it is much thicker; near Jasper (fig. 2), where its top is eroded and its base is not exposed, it is more than 800 m thick. The original total volume of the La Jara Canyon Member was more than 500 km^3 and possibly more than 1,000 km.^{3}

Tuff in the La Jara Canyon Member contains 20–40 percent phenocrysts, mostly plagioclase, accompanied by some biotite, augite, and opaque oxides. Silica content is 65–70 percent. La Jara Canyon tuff within the Platoro caldera is somewhat different from the outflow tuffs that occur outside the caldera: it is lower in silica, contains more phenocrysts, and is propylitically altered. The K-Ar radiometric age of the La Jara Canyon Member at Treasure Mountain is 29.8 m.y. (mean of biotite and plagioclase; Lipman and others, 1970, table 3, No. 1). The tuff is everywhere characterized by reversed magnetic polarity, as indicated by about 25 field determinations.

Outside the Platoro caldera the La Jara Canyon Member is generally separated from the Ojito Creek Member by the middle tuff, consisting of 10–70 m of ash fall and weakly welded ash-flow tuff that is almost everywhere poorly exposed.[1]

The Ojito Creek and Ra Jadero Members are relatively thin widespread ash-flow sheets of similar petrography and megascopic appearance; accordingly, they are described together and combined with the middle tuff in figure 2. Each is typically 10–20 m thick (fig. 3), dark brown where densely welded, and quartz latitic in composition. The initial volume of the two sheets together was probably about 100 km^3. The Ra Jadero Member is virtually coextensive with the La Jara Canyon Member; the Ojito Creek Member does not extend as far north and is missing from the type section of the formation at Treasure Mountain. Both members are well exposed together in their respective type localities: at the head of Ojito Creek (37°20′ N., 106°17′ W.), about 22 km east of Platoro, and in the Ra Jadero Canyon (37°14′ N., 106°16′ W.), about 26 km miles southeast of Platoro.

The Ojito Creek and Ra Jadero Members contain 10–15 percent phenocrysts, and are distinctly less crystal rich than the La Jara Canyon Member. Plagioclase is the major phenocryst constituent in both, accompanied by augite and opaque oxides. The Ra Jadero Member, unlike other tuffs in the Treasure Mountain, contains fairly abundant sanidine. The Ojito Creek Member has normal magnetic polarity; the Ra Jadero Member is reversed. These rocks have not yet been dated radiometrically, but relations to other dated units in the area suggest that they are no more than about 1 m.y. younger than the La Jara Canyon Member (29.8 m.y.).

[1] The lower and upper tuffs, of similar lithology, are not well developed within the area of figure 2. Thick lower tuffs are present a few kilometers to the south, at La Jara Canyon (fig. 3).

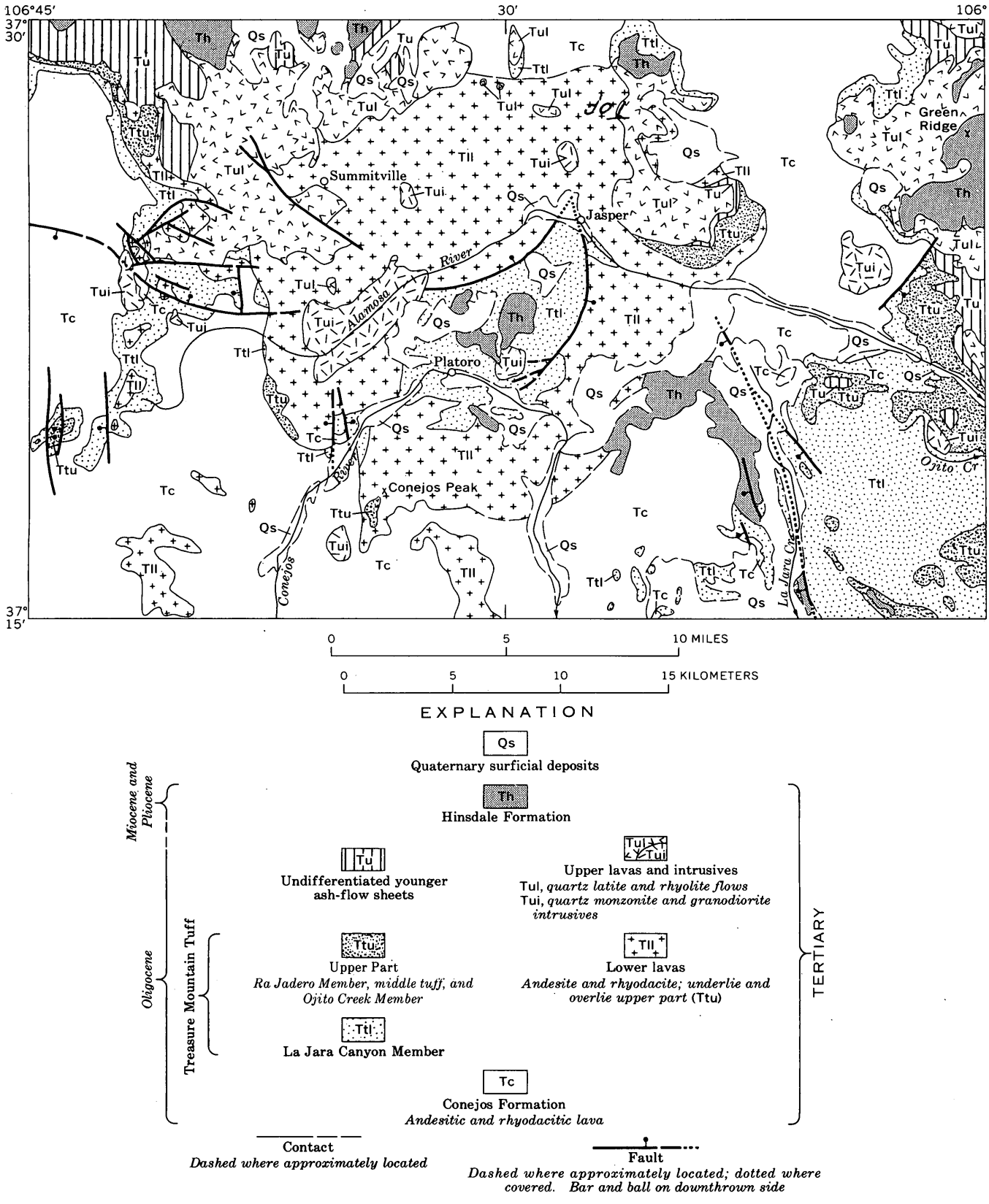

FIGURE 2.—Generalized geologic map of the Platoro caldera area.

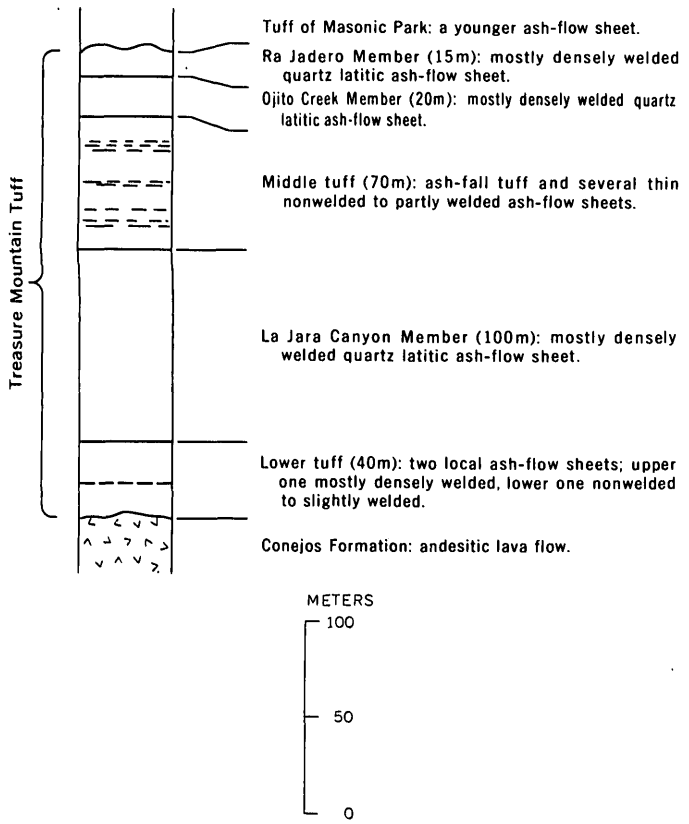

FIGURE 3.—Columnar section of the Treasure Mountain Tuff at La Jara Canyon.

Lavas and intrusions of the caldera

Lavas related to the Platoro caldera are generally divisible into two groups: older nonporphyritic dark-gray to black andesite and rhyodacite (lower lavas, fig. 2), and younger more silicic lavas (upper lavas, fig. 2), mostly light-gray rhyodacite and quartz latite that characteristically contain large feldspar phenocrysts as well as biotite and augite or hornblende.

The dark older lavas flooded the caldera moat to overflowing shortly after the core of the caldera was resurgently domed; they are more than 700 m thick at Conejos Peak in the southern part of the caldera. The obscurity of contacts at caldera walls between these flows and petrographically similar lavas of the Conejos Formation has contributed to the delayed recognition of the Platoro caldera. Although the dark lavas were correctly described as overlying the Treasure Mountain Rhyolite in the Platoro-Summitville area by Patton (1917, p. 36), who designated them the Summitville Andesite, they were mistakenly assigned to the Conejos Formation by Larsen and Cross (1956, p. 36), who also considered the Treasure Mountain Tuff inside the Platoro caldera to represent an older part of the Conejos Formation (p. 101–102). Steven and Ratté (1960) and Calkin (1967) followed Larsen and Cross in assigning the dark lavas, including those at Conejos Peak, to the Conejos Formation.

The younger porphyritic lavas occur in a broad zone along the north side of the Platoro caldera from Summitville to Green Ridge (fig. 2); they are remnants of a partial ring of caldera-margin lava domes. The lavas at Summitville were, until recently, assigned to the Fisher Quartz Latite (Larsen and Cross, 1956, p. 172; Steven and Ratté, 1960), but Steven and Ratté (1965, p. 43–44) later restricted use of this formational name to late lavas and breccias localized around the Creede caldera. The Summitville-Green Ridge assemblage occupies a similar position with respect to the Platoro caldera, and was erupted independently of the type Fisher Quartz Latite. K-Ar ages of porphyritic lavas of the Summitville-Green Ridge zone range from 27.8 to 20.2 m.y., but the distribution of certain younger ash-flow tuffs suggests that most of these lavas were erupted in a relatively brief interval close to the older date (Lipman and others, 1970), and are largely Oligocene in age.

Several fine- to medium-grained granodioritic to quartz monzonitic stocks within and near the Platoro caldera appear to be genetically related to the lava-flow activity at this center. The largest granitic body, the Alamosa River stock, intrudes the dark lavas that filled the moat of the resurgent Platoro caldera, but relations with its alteration halo indicate that at least some of the upper lavas are younger (Steven and Ratté, 1960, p. 38). Dikes that are petrographically similar to the porphyritic lavas define an incomplete radial pattern around this stock (fig. 4), indicating closely associated activity. The Alamosa River stock has yielded a K-Ar age of 29.1 m.y., in good agreement with the other geologic relations (Lipman and others, 1970).

Undivided younger ash-flow sheets

Younger ash-flow sheets that were erupted from calderas farther north in the San Juan volcanic field (fig. 1) are present within the mapped area (fig. 2) around the north side of the Platoro caldera and locally within the caldera. Units present but not shown separately include the tuff of Masonic Park (Lipman and others, 1970) erupted from the Mount Hope caldera (fig. 1), Fish Canyon Tuff (Olson and others, 1968) erupted from the La Garita caldera, Carpenter Ridge Tuff (Olson and others, 1968) erupted from the Bachelor caldera, Wason Park Rhyolite (Ratté and Steven, 1967) erupted from the Creede caldera area, and Snowshoe Mountain Quartz Latite (Ratté and Steven, 1967) erupted from the Creede caldera.

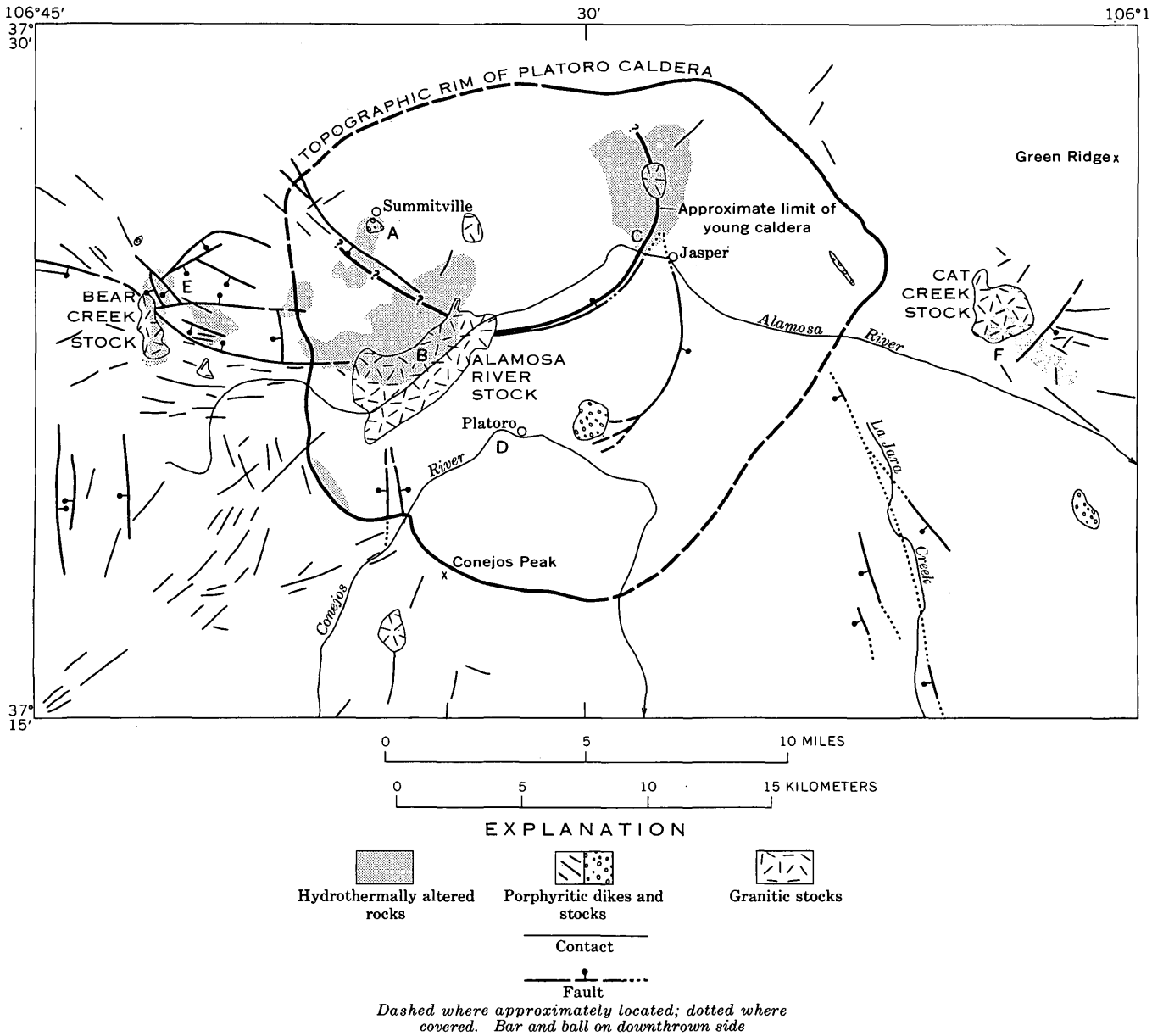

FIGURE 4.—Map showing stocks, dikes, faults, and areas of extensive hydrothermal alteration in the vicinity of the Platoro caldera. A, Summitville district; B, Stunner and Gilmore districts; C, Jasper district; D, Platoro district; E, Crater Creek area; and F, Cat Creek area.

Hinsdale Formation

The last volcanic activity in the Summitville-Platoro area is represented by the Hinsdale Formation, which consists of alkalic olivine basalt, basaltic andesite, and small scattered plug domes of silicic alkali rhyolite. These rocks probably range widely in age and are not closely related in origin to the Platoro caldera. Basalt and rhyolite from Beaver Creek, just north of the area of figure 2, have yielded K-Ar ages of 23.4 and 21.9 m.y., respectively, but other Hinsdale basalts in the southeastern San Juan Mountains are as young as 5 m.y. (Lipman and others, 1970).

STRUCTURAL EVOLUTION OF THE PLATORO CALDERA

Before ash-flow eruptions began in the southeastern San Juan Mountains, the central volcanoes of the Conejos Formation had been extensively eroded and the intervening basins filled with the resultant detritus, producing a widespread surface of low relief. As a result, phenocryst-rich quartz latitic ash flows from sources in the Summitville-Platoro region were able to spread 30–40 km in all directions, depositing the La Jara Canyon Member of the Treasure Mountain Tuff.

Collapse of a subcircular block about 20 km in diameter began before completion of these eruptions, with

the result that the later ash flows of the La Jara Canyon Member were ponded and accumulated to a thickness in excess of 800 m within the caldera. These later tuffs were somewhat more mafic and phenocryst rich than the initially erupted tuff of the widespread thin outflow sheet, reflecting differentiation in the source magma chamber similar to that described for other ash-flow deposits in the San Juan Mountains and elsewhere (Ratté and Steven, 1964; Lipman and others, 1966). The concurrent eruption and collapse at the Platoro caldera clearly differ from those of some other carefully studied areas such as the Valles caldera in New Mexico, where the last erupted units are no thicker inside the caldera than outside, demonstrating that eruption was virtually complete before major subsidence occurred (Smith and Bailey, 1968, p. 638). Other calderas in which thick intracaldera accumulations of ash-flow tuff demonstrate collapse contemporaneous with eruption have been recognized in the San Juan Mountains (Steven and Ratté, 1965, p. 59) and in southern Nevada (Christiansen and others, 1965; Byers and others, 1969). Collapse probably occurs concurrently only with ash-flow eruptions of very large volume; in some such eruptions initial collapse appears to have coincided approximately with abrupt compositional changes in the zoned ash-flow sheets (Lipman and others, 1966, p. F24–F25; Byers and others, 1969, p. 86).

The thick tuffs of the La Jara Canyon Member within the Platoro caldera are topographically and structurally high as a result of resurgent doming (Smith and Bailey, 1968) shortly after collapse. Early resurgence is demonstrated by the presence of monolithologic talus breccias of the La Jara Canyon Member that intertongue with the caldera-filling moat lavas adjacent to the resurgent block. This block dips homoclinally to the southwest and is bounded on its north and east sides by normal faults of large displacement. Prior to disruption by these faults there may have existed a more complete structural dome such as characterizes most resurgent cauldrons (Smith and Bailey, 1968).

The dark andesitic lavas (lower lavas of fig. 2) within the Platoro caldera filled the moat after resurgence was virtually complete, and they lap unconformably onto the uplifted central block. A minimum figure for the amount of collapse of the Platoro caldera is 1,500 m, as shown by the thickness of these lavas in the caldera moat (about 700 m on Conejos Peak) and the thickness of the La Jara Canyon Member within the caldera (about 800 m with the top eroded and the base not exposed). These andesitic lavas, in essence, represent a continuation of the same type of volcanic activity that characterized the Conejos Formation, with which they are readily confused in the field. Continued andesitic volcanic activity during ash-flow eruptions characterizes other portions of the San Juan volcanic field as well, and this relation is significant in reconstructing the petrologic evolution of the volcanic field (Lipman and Steven, 1969).

Upper tuffs of the Treasure Mountain, including the Ojito Creek and Ra Jadero Members, were erupted after the moat of the early, resurgent part of the Platoro caldera was nearly completely filled by andesitic lavas, as these tuffs are found within the caldera only in a few places above thick accumulations of andesitic lavas (fig. 2). The Ojito Creek and Ra Jadero tuffs are nearly coextensive with the La Jara Canyon Member and must have been erupted from the same general area. Although the volumes of these upper two members are much less than the La Jara Canyon, on the order of 50 km^3 each, they are sufficiently large to indicate the likelihood of associated caldera collapse (Smith, 1960, fig. 3). Several features suggest the probability of late collapse related to these tuffs within the northwestern part of the Platoro caldera (fig. 4), although this extensively altered area is not fully understood at the present preliminary stage of study. In this area the arcuate northeast-trending fault that truncates the central resurgent block of La Jara Canyon tuff (fig. 4) has a displacement of more than 800 m in a direction plausible as a younger caldera-margin fault. The andesitic lavas inside the proposed late caldera differ somewhat from those in other parts of the Platoro caldera: as noted by Steven and Ratté (1960, p. 11), they are exceptionally thick, poorly stratified, and highly brecciated. Although not differentiated on the preliminary map (fig. 2), these flows are probably younger than andesitic lavas in other parts of the Platoro caldera and postdate late collapse related to eruption of the upper two members of the Treasure Mountain Tuff.

Extrusion of the porphyritic (upper) lavas and intrusion of dikes and granitic stocks following collapse and filling of the younger caldera constitute the last phase of igneous activity related to the compound Platoro caldera. The existing areas of porphyritic lavas represent remnants of an arc of lava domes around the north side of the Platoro caldera. These lavas may originally have been widely distributed farther to the south as well, having been fed by the numerous dikes and stocks southwest and east of the Platoro caldera (fig. 4), but now completely removed by erosion. Many of the stocks and dikes are petrographically similar to the porphyritic lavas, and they appear to have been emplaced at about the same time. The radiometric age of the Alamosa River stock (29.1 m.y.) is only slightly younger than the La Jara Canyon Member (29.8

m.y.), even though this stock is clearly later than the boundary fault of the late caldera. The Bear Creek stock in the western part of the mapped area (fig. 4) is petrographically similar to the Alamosa River stock, but is later than some of the porphyritic lavas, inasmuch as it intrudes a complex graben of several faults which displace these lavas (fig. 2). This structure is clearly a radial graben related to the Platoro caldera.

MINERALIZATION RELATED TO THE PLATORO CALDERA

Recognition of the Platoro caldera, and of the general sequence of igneous events related to its development, has provided at least partial answers to many puzzling questions of long standing concerning the localization of the mineral deposits in the Summitville mining district and nearby mineralized areas. Earlier studies either were done before the concepts of ash-flow tuffs and associated calderas were developed (Patton, 1917) or were too limited in scope for the regional picture to be discerned (Steven and Ratté, 1960; Calkin, 1967). The preliminary summary by Steven (1968, p. 712–713) clearly reflects the uncertainties concerning localization both of the igneous centers and of related hydrothermal activity in the Summitville area.

We now know that the mineralization at Summitville and in certain nearby areas is closely related to intrusive and extrusive centers localized along margin ring structures formed during compound subsidence of the Platoro caldera, and outlying mineralization was controlled mainly by outward-extending fracture zones. The localization is thus closely comparable to that of other highly mineralized areas in the central and western San Juan Mountains (Steven, 1968; Burbank and Luedke, 1968), and it is instructive to consider other possibly analogous features that may bear on the mineral potential of this generally poorly explored area.

Summitville and Jasper districts

As described by Steven and Ratté (1960), gold-silver-copper ore in the Summitville district was deposited in a very shallow volcanic environment within a then recently erupted volcanic dome of coarsely porphyritic quartz latite. The ore occurs in intensely altered pipes and irregular tabular masses of quartz-alunite rock that replaced the quartz latite along northwest-trending fracture zones. Metallic minerals, chiefly pyrite and enargite, fill irregular vugs that formed by local intense leaching of the quartz-alunite rock. The quartz-alunite masses are surrounded successively by soft argillically altered envelopes (illite-kaolinite zone) and by pervasively propylitized rock (montmorillonite-chlorite zone). The alteration was interpreted to have resulted from shallow solfataric activity similar to that associated with recent volcanic activity.

The alteration and mineralization at Summitville represents a late stage of a sequence of related igneous and hydrothermal episodes along the southwest margin of the younger collapse structure within the compound Platoro caldera (fig. 4). To the south and southeast, along the Alamosa River, a composite granodioritic to quartz monzonitic stock was intruded somewhat earlier, and much rock adjacent to the north margin of this stock was intensely altered. Calkin (1967, p. 123; 1968) noted that a small intrusive body (which he called the Alum Creek Porphyry) within the northern part of the Alamosa River stock is a focus of intense hydrothermal alteration. The subsidiary body contains locally anomalous quantities of several metals (Calkin, 1967, p. 144–146) and in places is cut by numerous closely spaced quartz veinlets containing abundant pyrite and sparse molybdenite (p. 146–147). As described by Patton (1917, p. 98–101), quartz-pyrite veins with ore shoots containing gold and silver tellurides were deposited locally in the Stunner and Gilmore districts within this mass of altered rock. According to W. N. Sharp of the U.S. Geological Survey (oral commun., 1969), these veins strike generally north-northwest and dip steeply. They are largely limited to the south side of the Alamosa River and do not penetrate the most intensely altered rock north of the river.

Some dikes and plugs of coarse porphyry similar to that in the quartz latite dome at Summitville cut both the intrusive mass and the adjacent altered rock, and these in turn were altered in various degrees (Calkin, 1967, p. 74). Sharp and Gualtieri (1968) described zoned anomalous concentrations of lead, copper, molybdenum, and zinc near one of these porphyry dikes.

The Jasper district, about 12 km east of Summitville, is a comparable area of intensely altered rock associated with a granitic stock. The district is localized along the east margin of the same younger collapse structure within the compound Platoro caldera, as are the Summitville, Stunner, and Gilmore districts. Quartz-pyrite veins with ore shoots containing gold and silver (Patton, 1917, p. 105–108) are localized along the south margin of the highly altered rocks.

The whole area from Summitville south across the Alamosa River and east to Jasper thus marks an area of recurrent intrusion, extrusion, and hydrothermal alteration and mineralization along a cauldron ring fault. The environment is similar to that in the intensely altered and mineralized Red Mountain district along the northwest margin of the Silverton cauldron in the western San Juan Mountains (Burbank, 1941; Burbank

and Luedke, 1968). The analogy is even closer when the ores in the Summitville and Red Mountain districts are compared: pyrite and enargite are common in both districts, although numerous other ore minerals, including abundant sulfosalts of copper and silver, are present at Red Mountain. The gangues consist of pipelike masses of strongly leached silicified rock that formed by replacement of preexisting volcanic or shallow intrusive rocks in shallow solfataric environments.

Platoro district

Most veins in the Platoro district are persistent north-northwest-trending quartz-pyrite veins in the thick mass of La Jara Canyon Member within the early, resurgent part of the Platoro caldera. Local ore shoots on these veins containing gold telluride and silver sulfosalt minerals (Patton, 1917, p. 89–96) supplied most of the ore produced in early mining in the district. Most of the La Jara Canyon tuff exposed within the caldera is propylitically altered, apparently unrelated to the later ore deposition. Alteration related to mineralization is restricted to local argillic selvages along the quartz-pyrite veins.

The veins in the Platoro district are about on strike with some of the stronger veins in the Stunner district along the Alamosa River to the north, and the vein mineralogy in the two areas is closely similar. W. N. Sharp (oral commun., 1969) believes that the veins in the two districts are along the same fracture zone. The Platoro veins thus appear to follow radial fractures extending outward from the younger collapse structure in the compound Platoro caldera, and may be only incidentally located within the resurgent dome of the earlier cauldron. Ore deposits are uncommon within resurgent cores of other calderas in the San Juan Mountains, and the closest structural analogy to the Platoro district—the Creede district within the resurgent Bachelor caldera (fig. 1)—is primarily related to radial graben faults of the younger Creede caldera (Steven and Ratté, 1965).

Crater Creek area

Several conspicuous faults comprising a complex radial graben extend westward from the Platoro caldera (figs. 2, 4) and converge toward the north end of the Bear Creek granodioritic stock. Hydrothermally altered rock is apparent at places along these faults, and some rather extensive areas within the faulted zone and around the stock are pervasively altered. Numerous dikes of coarsely porphyritic quartz latite similar to the rock in the plug dome at Summitville fill subparallel fissures within and near the graben.

Shallow prospect pits are scattered through the faulted and discontinuously altered area, and the Crater Creek drainage area near the north end of the Bear Creek granodioritic stock is currently being explored (1967–70). According to Mr. William Ellithorpe of Monte Vista, Colo. (oral commun., 1969) and Mr. Harry V. Ellithorpe, Pueblo, Colo. (written commun., 1970), by the fall of 1969 this exploration had disclosed several veins ranging in width from less than a foot to more than 10 feet that contain significant quantities of lead, zinc, and silver. Through the courtesy of Mr. William Ellithorpe, we examined several selected high-grade samples of the vein consisting almost wholly of galena and sphalerite. As of October 1969, only a limited lateral extent of the vein had been explored.

A close analogy exists between the environment of the lead-zinc-silver vein along Crater Creek and that of the major producing base-metal veins in radial faults around the margins of the Creede caldera (Steven and Ratté, 1965) and the Lake City and Silverton cauldrons (Burbank and Luedke, 1968).

Cat Creek area

An outlying stock of monzonite (Larsen and Cross, 1956, p. 110) is exposed in the Cat Creek drainage basin about 5 km east of the Platoro caldera (fig. 4). An extensive area including the southeastern part of the stock and adjacent volcanic rocks is pervasively altered. Numerous prospect pits and small shafts were noted during reconnaissance mapping, but the altered rock was not examined closely. We know of no recorded production from this area, but its possible mineral potential is not known.

CONCLUSIONS AND ECONOMIC SIGNIFICANCE

The altered and mineralized areas near Summitville and Platoro in the southeastern San Juan Mountains are localized within and adjacent to a compound cauldron subsidence structure that we have called the Platoro caldera. Foci of hydrothermal alteration and mineralization seem to be along the ring-fracture zone of the younger collapse structure in the northern part of the compound caldera, which was the locus of repeated intrusion of equigranular quartz monzonite and coarsely porphyritic quartz latite in stocks, plugs, dikes, and volcanic necks. Radial fracture zones extending outward from the younger subsidence structure localized numerous coarsely porphyritic dikes, as well as hydrothermal alteration and local ore deposition. The older larger cauldron structure apparently exerted little control on either exposed hypabyssal intrusions or related hydrothermal activity.

The areas of most widespread and intense alteration between Summitville and the Alamosa River show evidence of repeated intrusion and hydrothermal activity.

880-189 O—70——3

The composite granodioritic-quartz monzonitic Alamosa River stock apparently was intruded first, and a large block of rock along its northern margin was pervasively altered. Alteration was in part localized around a subsidiary intrusion in the northern part of the Alamosa River stock, and anomalous concentrations of metals were introduced locally (Calkin, 1967, p. 144–147). These altered rocks are overlain by unaltered quartz latitic lavas that were erupted from the vicinity of Summitville to the north (Steven and Ratté, 1960, p. 38) and are locally cut by similar coarsely porphyritic quartz latitic dikes and plugs. Some of the quartz latitic lavas at Summitville were in turn altered and mineralized, and ores from this center have provided most of the metals produced from the Platoro caldera area. Related porphyry dikes and plugs to the south also are altered in various degrees, and at least one area containing anomalous metal concentrations is localized near one of these later dikes (Sharp and Gualtieri, 1968).

The whole environment, with repeated hypabyssal intrusion of differentiated granodioritic to quartz monzonitic (quartz latitic) plutons, widespread and intense hydrothermal alteration, and local anomalous concentrations of gold, silver, copper, and molybdenum, is similar to that in which "porphyry-type" disseminated deposits of copper and molybdenum occur throughout western North America. Presently exposed levels are relatively shallow within the volcanic pile (Steven and Ratté, 1960, p. 51–52), whereas most porphyry-type deposits appear to have formed in lower volcanic levels, or in the upper part of the basement beneath the volcanic pile. Favorable zones for exploration thus still exist at depth.

The granodioritic and quartz monzonitic compositions of the known intrusive bodies in the Summitville–Alamosa River area are more common for predominantly copper-bearing porphyry deposits (Stringham, 1966) than for the predominantly molybdenum-bearing deposits such as those at Climax, Colo. (Wallace and others, 1968), or Questa, N. Mex. (Carpenter, 1968), where mineralization is related to relatively silica-rich rhyolite and granite porphyry. The abundance of copper and the dearth of molybdenum in the known ores at Summitville further suggest this association. Molybdenum and copper, however, both are present in the areas with anomalous metal content south of Summitville described by Calkin (1967, p. 144–147) and by Sharp and Gualtieri (1968).

Mineral deposits in the outward-extending radial fracture zones range from quartz-pyrite veins with shoots of gold and silver tellurides with associated silver and copper sulfosalt minerals in the Stunner, Gilmore, and Platoro districts to a silver-bearing galena-sphalerite vein in the Crater Creek area. The Crater Creek area is appreciably farther from the apparent focus of intrusion and hydrothermal activity between Summitville and the Alamosa River than are the Stunner, Gilmore, and Platoro areas. Although the data are too sparse to be very significant, this general distribution of gold, silver, and copper relatively near the source and of silver, lead, and zinc more distant is reminiscent of the metal zoning around many western mining districts, as previously suggested by Calkin (1967, p. 154). The outward-extending fracture zones have been poorly explored, and would seemingly deserve more attention.

ACKNOWLEDGMENTS

We express our appreciation to W. N. Sharp, U.S. Geological Survey, for making available unpublished data on the veins and the altered and mineralized rocks in the Alamosa River–Platoro area. Russel Burmester assisted P. W. Lipman in reconnaissance geological mapping in and adjacent to the area covered by this report and helped develop the general geologic history of the region.

REFERENCES

Burbank, W. S., 1941, Structural control of ore deposition in the Red Mountains, Sneffels, and Telluride districts of the San Juan Mountains, Colorado: Colorado Sci. Soc. Proc., v. 14, no. 5, p. 141–261.

Burbank, W. S., and Luedke, R. G., 1968, Geology and ore deposits of the western San Juan Mountains, Colorado, *in* Ridge, J. D., ed., Ore deposits of the United States, 1933–1967 (Graton-Sales volume), v. 1: Am. Inst. Mining, Metall., and Petroleum Engineers, Rocky Mtn. Fund Ser., p. 714–733.

Byers, F. M., Jr., Carr, W. J., and Orkild, P. P., 1969, Volcanotectonic history of southwestern Nevada caldera complex, U.S.A. [abs.], p. 84–86 *in* Symposium on volcanoes and their roots: Oxford, England, Internat. Assoc. Volcanology and Chemistry of the Earth's Interior, v. abs., 281 p.

Calkin, W. S., 1967, Geology, alteration, and mineralization of the Alum Creek area, San Juan volcanic field, Colorado: Colorado School Mines unpub. Ph. D. thesis, 177 p.

——— 1968, Geology and petrology of the Alum Creek area, San Juan Mountains, Colorado, *in* Abstracts for 1967: Geol. Soc. America Spec. Paper 115, p. 410.

Carpenter, R. H., 1968, Geology and ore deposits of the Questa molybdenum mine area, Taos County, New Mexico, *in* Ridge, J. D., ed., Ore deposits of the United States, 1933–1967 (Graton-Sales volume), v. 2: Am. Inst. Mining, Metall., and Petroleum Engineers, Rocky Mtn. Fund Ser., p. 1328–1350.

Christiansen, R. L., Lipman, J. W., Orkild, P. P., and Byers, F. M., Jr., 1965, Structure of the Timber Mountain caldera, southern Nevada, and its relation to basin-range structure, *in* Geological Survey Research 1965: U.S. Geol. Survey Prof. Paper 525–B, p. B43–B48.

Cohee, G. V., chm., and others, 1961, Tectonic map of the United States, exclusive of Alaska and Hawaii: U.S. Geol. Survey

and Am. Assoc. Petroleum Geologists, scale 1:2,500,000. [1962]

Larsen, E. S., Jr., and Cross, Whitman, 1956, Geology and petrology of the San Juan region, southwestern Colorado: U.S. Geol. Survey Prof. Paper 258, 303 p.

Lipman, P. W., Christiansen, R. L., and O'Connor, J. T., 1966, A compositionally zoned ash-flow sheet in southern Nevada: U.S. Geol. Survey Prof. Paper 524–F, 47 p.

Lipman, P. W., and Steven, T. A., 1969, Petrologic evolution of the San Juan volcanic field, southwestern Colorado [abs.], p. 254–255 *in* Symposium on volcanoes and their roots: Oxford, England, Internat. Assoc. Volcanology and Chemistry of the Earth's Interior, 281 p.

Lipman, P. W., Steven, T. A., and Mehnert, H. H., 1970, Volcanic history of the San Juan Mountains, Colorado, as indicated by potassium-argon dating: Geol. Soc. America Bull. [In press]

Luedke, R. G., and Burbank, W. S., 1963, Tertiary volcanic stratigraphy in the western San Juan Mountains, Colorado: Art. 70, *in* U.S. Geol. Survey Prof. Paper 475–C, p. C39–C44.

——— 1968, Volcanism and cauldron development in the western San Juan Mountains, Colorado, p. 175–208 *in* Epis, R. C., ed., Cenozoic volcanism in the southern Rocky Mountains: Colorado School Mines Quart., v. 63, no. 3, 287 p.

Olson, J. C., Hedlund, D. C., and Hansen, W. R., 1968, Tertiary volcanic stratigraphy in the Powderhorn-Black Canyon region, Gunnison and Montrose Counties, Colorado: U.S. Geol. Survey Bull. 1251–C, 29 p.

Patton, H. B., 1917, Geology and ore deposits of the Platoro-Summitville mining district, Colorado: Colorado Geol. Survey Bull. 13, 122 p. [1918]

Ratté, J. C., and Steven, T. A., 1964, Magmatic differentiation in a volcanic sequence related to the Creede caldera, Colorado: Art. 131 *in* U.S. Geol. Survey Prof. Paper 475–D, p. D49–D53.

——— 1967, Ash flows and related volcanic rocks associated with the Creede caldera, San Juan Mountains, Colorado: U.S. Geol. Survey Prof. Paper 524–H, 58 p.

Sharp, W. N., and Gualtieri, J. L., 1968, Lead, copper, molybdenum, and zinc geochemical anomalies south of the Summitville district, Rio Grande County, Colorado: U.S. Geol. Survey Circ. 557, 7 p.

Smith, R. L., 1960, Ash flows: Geol. Soc. America Bull., v. 71, No. 6, p. 795–842.

Smith, R. L., and Bailey, R. A., 1968, Resurgent cauldrons, p. 613–662 *in* Coats, R. R., Hay, R. L., and Anderson, C. A., eds., Studies in volcanology—A memoir in honor of Howel Williams: Geol. Soc. America Mem. 116, 678 p.

Steven, T. A., 1968, Ore deposits in the central San Juan Mountains, Colorado, *in* Ridge, J. D., ed., Ore deposits of the United States, 1933–1967 (Graton-Sales volume), v. 1: Am. Inst. Mining, Metall., and Petroleum Engineers, Rocky Mtn. Fund Ser., p. 706–713.

Steven, T. A., and Epis, R. C., 1968, Oligocene volcanism in south-central Colorado, p. 241–258 *in* Epis, R. C., ed., Cenozoic volcanism in the southern Rocky Mountains: Colorado School Mines Quart., v. 63, no. 3, 287 p.

Steven, T. A., and Lipman, P. W., 1968, Central San Juan cauldron complex, Colorado [abs.], p. 209 *in* Epis, R.C., ed., Cenozoic volcanism in the southern Rocky Mountains: Colorado School Mines Quart., v. 63, no. 3, 287 p.

Steven, T. A., and Ratté, J. C., 1960, Geology and ore deposits of the Summitville district, San Juan Mountains, Colorado: U.S. Geol. Survey Prof. Paper 343, 70 p.

——— 1965, Geology and structural control of ore deposition in the Creede district, San Juan Mountains, Colorado: U.S. Geol. Survey Prof. Paper 487, 87 p.

Stringham, Bronson, 1966, Igneous rock types and host rocks associated with porphyry copper deposits, p. 35–40 *in* Titley, S. R., and Hicks, C. L., eds., Geology of the porphyry copper deposits, southwestern North America: Tucson, Ariz., Arizona Univ. Press, 287 p.

Wallace, S. R., Muncaster, N. K., Jonson, D.C., Mackenzie, W. B., Bookstrom, A. A., and Surface, V. E., 1968, Multiple intrusion and mineralization at Climax, Colorado, *in* Ridge, J. D., ed., Ore deposits of the United States, 1933–1967 (Graton-Sales volume), v. 1: Am. Inst. Mining, Metall., and Petroleum Engineers, Rocky Mtn. Fund Ser., p. 605–640.

GOLD DISTRIBUTION ON THE CAROLINA CONTINENTAL MARGIN—A PRELIMINARY REPORT

By ORRIN H. PILKEY[1] and BRIAN D. BORNHOLD,[2] Durham, N.C.

Abstract.—Gold in heavy-mineral fractions of sediments from the Carolina continental margin is restricted to the general vicinity of Cape Lookout and northward. Most of the observed concentrations of gold are very low (0.7 to 7.0 ppb) and at or near the limits of analytical detection.

Rivers emptying onto the Continental Shelf off North Carolina and South Carolina drain gold-bearing areas in the Piedmont province of North Carolina, South Carolina, and Virginia. Hence, concentrations of gold could have formed on the shelf as beach and shelf placers during times of lowered sea level. As part of the research program of the U.S. Geological Survey, gold determinations were made on heavy-mineral fractions of sediment samples from the shelf (fig. 1), as well as from beaches and rivers (fig. 2).

The purposes of this study are to: (1) obtain a "background reading" of the general abundance of gold in local sediments, (2) determine if areas exist where detailed prospecting for gold might conceivably be profitable in the future, and (3) contribute to our knowledge of sedimentary processes, particularly those which distribute heavy metals in geologic environments such as those of the continental margin. The abundance and areal distribution of gold in the study area have been determined through investigation of 57 Continental Shelf samples, 31 beach samples, and 16 river samples.

Acknowledgments.—We wish to thank Captain Milan Willis as well as the crew of Duke University's RV *Eastward* for their splendid cooperation during collecting operations. The three Pamlico Sound samples were collected from RV *Beveridge*. Mr. William Smith processed many of the samples used in this study. We also wish to express our gratitude to Duke University Marine Laboratory for the use of the National Science Foundation-funded RV *Eastward*. The U.S. Geological Survey coordinator of this study was Henry L. Berryhill, Jr., whose helpful cooperation and encouragement were greatly appreciated. John S. Schlee and C. Hans Nelson, of the U.S. Geological Survey, read the manuscript and offered many helpful suggestions.

SEDIMENTARY FRAMEWORK

Much is known about sediment distribution and sedimentary processes on the Continental Shelf off North and South Carolina. Stetson (1939), Gorsline (1963), Uchupi (1963), and Pilkey (1968) discussed regional sedimentation; Pilkey (1963) discussed the heavy minerals of the sediments; Cleary and Pilkey (1968) and Milliman, Pilkey, and Blackwelder (1968) discussed aspects of North Carolina shelf sedimentation; and Meade (1969) reviewed river discharge and suspended-load data.

The rivers in the study area that drain the Piedmont have relatively low discharge and small suspended sediment loads. The most important rivers with respect to both load and discharge are the Roanoke of North Carolina and the Pee Dee of South Carolina (Meade, 1969). The estuaries of these rivers form the northern and southern boundaries of the study area.

Sedimentation rates are low throughout this part of the Continental Shelf. At the present time, rivers are contributing little sand. Much of the nearshore sediment and even estuarine sediment has been derived from landward transport of shelf sediment. The dominant mean grain size of shelf sediment is in the fine- to medium-sand range. The shoals that extend seaward from the capes of the Carolina coast block extensive lateral transportation of sediments on the shelf. The shelf area between Cape Lookout and Cape Fear (Onslow Bay) has received the least amount of sediment because of the complete lack of Piedmont rivers and because lateral transport is blocked by the bounding

[1] Associate Professor, Department of Geology, Duke University, Durham, N.C. 27708.
[2] Graduate student, Department of Geology, Duke University, Durham, N.C. 27708.

shoals. Relict sediments predominate over the entire area, although residual or outcrop-derived sediments are locally abundant. At present, active deposition is restricted to the nearshore area and the Continental slope, while most of the shelf is being subjected to winnowing.

FIELD AND LABORATORY METHODS

Samples from the shelf and slope were collected by using a small Pierce box dredge, which obtains a nonquantitative sample weighing at least 5 kilograms. The heavy-mineral fraction was concentrated by hand panning aboard ship. No visible gold was observed during panning. For the most part, sample locations are based on loran C positions, although some were obtained using radar fixes. River samples were obtained by using the Pierce box dredge on a handline, usually from highway bridges. Beach samples were collected from heavy-mineral-rich sands approximately at the normal high-tide line.

The heavy- and light-mineral fractions of the samples (already pan concentrated) were separated by using standard heavy-liquid techniques. The gold analyses were performed on the heavy-mineral fraction only.

Gold analyses were made at the U.S. Geological Survey laboratory in Denver, Colo., by atomic absorption spectrophotometry following the procedure outlined by Thompson, Nakagawa, and VanSickle (1968). The cold acid procedure was used, as it was found to be faster, and because it permitted use of a larger and, therefore, more representative sample. Analyses were performed using a Model 290 Perkin-Elmer atomic absorption spectrophotometer. The use of heavy-mineral concentrates reduces the particle sparsity effect discussed by Clifton, Hubert, and Phillips (1967).

GOLD IN THE CAROLINAS

Commercial gold deposits in the Carolinas are confined to the Piedmont and Blue Ridge provinces. The gold-bearing formations in these areas have been subdivided into six major belts and represent a wide variety of rock types. These belts cover over half the area of these two States and trend northeast-southwest (Nitze and Hanna, 1896; Bryson, 1936).

Felsic gold-bearing igneous rocks consist mainly of granite, rhyolite, tuff, and breccia; granite is by far the most important. Mafic gold-bearing igneous rocks consist of gabbro, diabase, diorite, andesite, tuff, and breccia. Metamorphic gold-bearing rocks include gneiss, schist, and slate. The principal types of occurrences of gold deposits in the Carolinas have been classified as follows (Bryson, 1936): (1) veins, (2) lodes or mineralized zones, (3) placers, and (4) saprolites.

RESULTS AND DISCUSSION

Gold analyses are summarized in tables 1, 2, and 3 and plotted in figures 1 and 2. Samples containing

TABLE 1.—*Determination of gold content of heavy-mineral fractions of Carolina shelf samples by atomic absorption spectrophotometry*

[N, not detected at detection level cited; D, detected but not measurable at detection level cited]

Sample No.	Coordinates		Depth (meters)	Gold (ppm)
	Lat (N.)	Long (W.)		
1784	34°27. 0′	76°36. 0′	30	0. 15
1785	22. 4′	33. 4′	40	N (0. 013)
1788	09. 0′	23. 9′	40	2. 3
1789	06. 5′	18. 5′	50	N (0. 03)
1815	04. 6′	75°02. 0′	27	N (0. 03)
1816	35°09. 7′	37. 0′	18	. 06
1817	12. 5′	38. 5′	10	. 07
1787	34°12. 5′	76°29. 5′	31	N (0. 03)
2042	03. 2′	46. 6′	15	N (0. 02)
2051	01. 0′	77°11. 5′	26	D (0. 10)
2052	14. 0′	55. 5′	25	N (0. 04)
2084	29. 5′	76°27′	15	D (0. 10)
2085	27′	27′	6	D (0. 10)
2086	28′	30. 5′	7	D (0. 10)
2087	30′	33′	10	D (0. 10)
2099	21. 5′	77°11. 7′	26	N (0. 02)
2104	05. 6′	14. 0′	30	N (0. 10)
2106	33°59. 0′	07. 5′	40	N (0. 10)
2110	38. 6′	19. 0′	40	N (0. 10)
2114	26. 2′	41. 2′	30	N (0. 04)
2115	24. 7′	47. 0′	31	N (0. 06)
2116	22. 7′	54. 0′	32	N (0. 02)
2117	20. 5′	78°00. 0′	32	N (0. 10)
2118	19. 5′	07. 0′	32	N (0. 04)
2120	21. 0′	15. 0′	30	N (0. 02)
2122	30. 5′	19. 0′	27	N (0. 02)
2127	45. 8′	30. 0′	66	N (0. 02)
2128	41. 6′	34. 5′	13	N (0. 03)
2131	30. 0′	30. 6′	16	N (0. 08)
2132	24. 8′	28. 0′	28	N (0. 02)
2133	19. 5′	25. 5′	30	N (0. 02)
2134	14. 5′	23. 3′	32	N (0. 06)
2142	32°57. 6′	55. 7′	30	N (0. 03)
2143	55. 2′	79°01. 1′	30	N (0. 03)
2145	59. 6′	09. 6′	23	N (0. 03)
2146	55. 8′	14. 0′	20	N (0. 04)
2147	52. 4′	18. 6′	18	N (0. 02)
2152	21. 4′	16. 0′	35	N (0. 05)
2153	26. 0′	11. 5′	40	N (0. 04)
2154	22. 0′	09. 0′	43	N (0. 06)
2155	18. 0′	06. 0′	65	N (0. 03)
2156	13. 5′	02. 5′	101	N (0. 03)
2160	25. 5′	28. 5′	18	N (0. 03)
2216	35°07. 5′	75°22. 2′	28	D (0. 02)
2220	47. 5′	23. 8′	58	D (0. 10)
2245	06. 6′	76°28. 6′	4	D (0. 02)
2250	10. 2′	07. 2′	6	D (0. 10)
2252	06. 1′	29. 4′	6	D (0. 10)
2282	34°23. 4′	58. 0′	20	D (0. 10)
2283	21. 0′	58. 0′	20	D (0. 10)
2284	11. 5′	58. 0′	20	D (0. 10)
2318	38. 0′	55. 8′	13	D (0. 02)
2321	33. 5′	44. 8′	16	D (0. 10)
2361	20. 0′	09. 5′	61	D (0. 02)
2364	24. 0′	21. 1′	18	D (0. 10)
2366	30. 7′	31. 8′	13	D (0. 10)
2219	35°47. 5′	75°23. 8′	19	N (0. 02)

TABLE 2.—*Gold content of heavy-mineral fractions of Carolina beach samples*

[N, not detected at detection level cited; D, detected but not measurable at detection level cited]

Sample No.	Location	Gold (ppm)
----------	Sandbridge, Va----------	N (0. 02)
2343--------	Kill Devil Hills, N.C----------	D (0. 02)
2344--------	Whalebone, N.C----------	D (0. 02)
2345--------	Nag's Head, N.C----------	D (0. 02)
2346--------	Nag's Head, N.C----------	D (0. 02)
2347--------	Oregon Inlet, N.C----------	D (0. 02)
2348--------	Milepost 10.5, Cape Hatteras National Seashore (CHNS).	D (0. 02)
2349--------	Milepost 30.0 (CHNS)----------	D (0. 02)
2350--------	39.5 (CHNS)----------	D (0. 02)
2351--------	20.0 (CHNS)----------	D (0. 02)
2351--------	20.0 (CHNS)----------	D (0. 02)
2352--------	Avon, N.C----------	0. 04
2353--------	2 miles north of Buxton, N.C-----	D (0. 02)
2354--------	Cape Hatteras Light House, N.C--	D (0. 02)
2355--------	Hatteras Village, N.C----------	D (0. 02)
2356--------	Milepost 61 (CHNS)----------	D (0. 02)
2357--------	Milepost 65 (CHNS)----------	D (0. 02)
2358--------	Milepost 89 (CHNS)----------	D (0. 02)
----------	Cape Lookout, N.C----------	N (0. 02)
----------	Shackleford Island, N.C----------	N (0. 02)
----------	Atlantic Beach, N.C----------	N (0. 02)
----------	Salter Path, N.C----------	N (0. 02)
----------	Surf City, N.C----------	N (0. 02)
----------	Topsail Beach, N.C----------	N (0. 02)
----------	Wrightsville Beach, N.C---------	N (0. 02)
----------	Carolina Beach, N.C----------	N (0. 02)
----------	Kure Beach, N.C----------	N (0. 02)
----------	Crescent Beach, S.C----------	N (0. 05)
----------	Windy Hill Beach, S.C----------	N (0. 02)
----------	Surfside Beach, S.C----------	N (0. 02)
----------	Sullivan's Island, S.C----------	N (0. 02)

TABLE 3.—*Gold content of heavy-mineral fractions of Carolina river samples*

[N, not detected; D, detected but not measurable at detection level cited]

Sample No.	Location	Gold (ppm)
2325--------	Neuse River, Neuse River Falls, N.C.	D (0.02)
2327--------	Clayton, N.C----------	D (0.02)
2331--------	Near Seven Springs, N.C-----	D (0.02)
2333--------	Near New Bern, N.C----------	D (0.02)
2334--------	Croatan National Forest, N.C..	D (0.02)
2335--------	Haw River, Greensboro, N.C-----	D (0.02)
2337--------	Altamahaw, N.C----------	D (0.02)
2338--------	Saxapahaw, N.C----------	0.60
2339--------	Bynum, N.C----------	D (0.02)
2340--------	Near Pittsboro, N.C----------	D (0.02)
2341--------	Near Sanford, N.C----------	N
2342--------	Lillington, N.C----------	D (0.10)
----------	Gibsonville, N.C----------	D (0.02)
----------	Winyah Bay, S.C----------	D (0.05)
----------	South Santee River, S.C---------	D (0.06)
----------	North Santee River, S.C---------	D (0.06)

detectable and measurable gold in the heavy-mineral fraction are shown by symbols in the figures. The detection limit varies, depending upon the size of the heavy-mineral fraction (from 0.02 to 0.10 ppm gold) available for analysis. Shelf samples with either measurable or detectable gold are restricted to the northern part of the study area (fig. 1).

From the available data, we found no indication of preferred depth range of gold-bearing heavy-mineral fractions, nor any sign of lineation suggesting previous shoreline placers.

Heavy-mineral abundances exhibit a patchy distribution in surface sediments of the study area and are typically less than 2 percent of the calcium carbonate-free sample (Cleary and Pilkey, 1968). According to Milliman, Pilkey, and Blackwelder (1968), the calcium carbonate content of shelf sediments in the study area is highly variable and averages about 15 percent. Table 4 presents the calcium carbonate and heavy-mineral contents, as well as the gold concentration, corrected to total sample, of the four shelf samples containing measurable gold in the heavy-mineral fraction.

All the shelf samples containing measurable gold are from areas of Holocene sedimentation. Evidence for this is indicated by the high mica content of these samples (Doyle and others, 1968) and their fine grain size (Gorsline, 1963). The samples are from plumes of sediment extending seaward from the capes through which fines are presently being transported to the Continental slope. These sediment plumes are clearly illustrated in Apollo 9 photographs (Emery, 1969). Thus, the most gold-rich samples are from areas where sedimentation rates are relatively high.

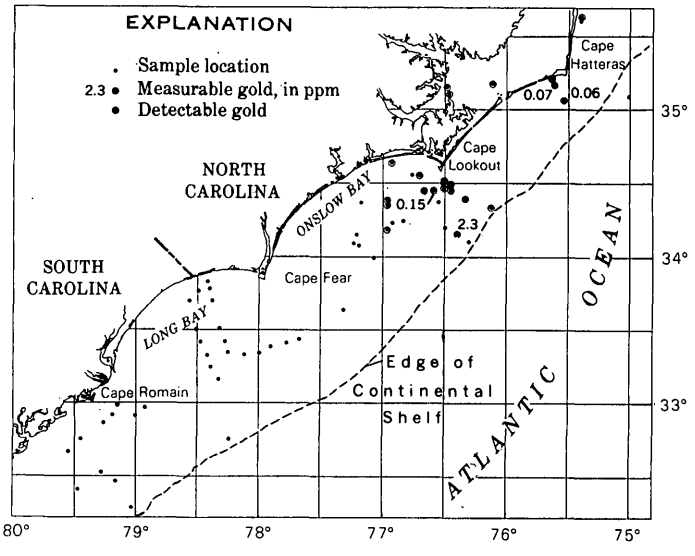

FIGURE 1.—Location and gold content of heavy-mineral fractions of Continental Shelf samples.

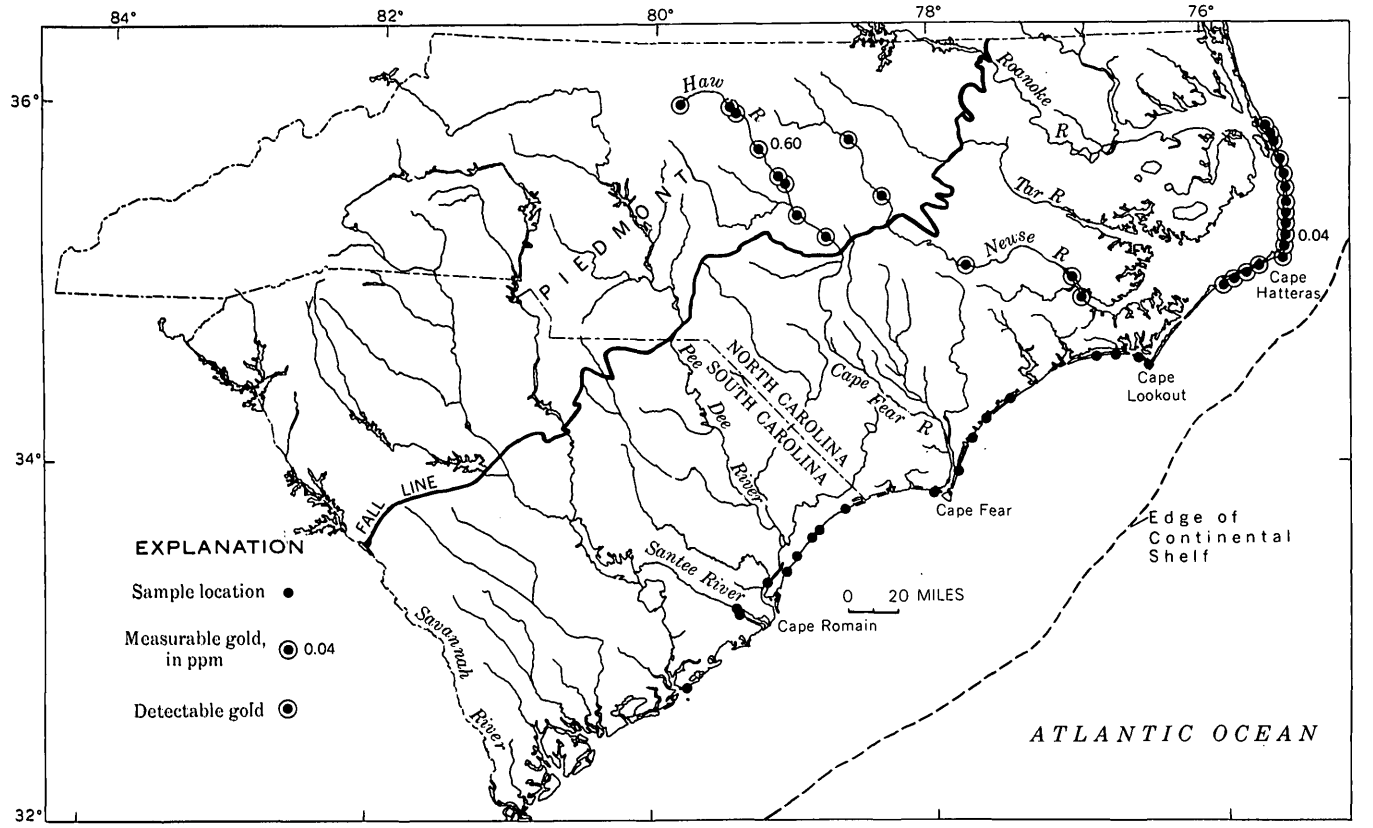

FIGURE 2.—Location and gold content of heavy-mineral fractions of beach and river samples.

TABLE 4.—*Calcium carbonate, heavy minerals, and gold concentration in four shelf samples containing measurable gold in the heavy-mineral fraction*

Sample No.	Calcium carbonate (percent)	Heavy minerals (percent)	Gold in heavy-mineral fraction (ppm)	Gold in total sample (ppb)
1816	8.5	1.9	0.6	1.14
1817	6.4	1.5	.7	1.05
1784	4.4	.46	.15	.69
1788	21.6	.30	2.3	6.9

The beach samples follow the same regional trend as shelf samples (fig. 2, table 2). Samples from most of the beaches north of Cape Lookout have detectable traces of gold, but to the south of this area none have gold. Only one beach sample (sample 2352 from Avon, N.C.) contained gold above the detection level, and this was only 0.04 ppm of the heavy-mineral fraction.

Only a few samples from rivers were studied; hence, generalizations concerning this material are difficult. Most of the samples were collected from the Haw and Neuse Rivers. The heavy-mineral fractions of river sands collected in the Piedmont province contained only detectable levels of gold, even near areas of former small-scale gold mining. It should be noted that the composition of modern river sands is not necessarily the same as during the Pleistocene, when much of the present-day shelf sediment cover was being contributed, because the ancient rivers were responding to different climatic conditions and gradients.

There are three possible explanations for the occurrence of gold in trace amounts in the northern part of the study area and its absence to the south. Perhaps the simplest is that the northern rivers, such as the Tar and Roanoke, are carrying more gold. Not enough river samples have been studied to determine whether this is true, but placer gold deposits occur on all major North Carolina river systems, and not just the Roanoke and Tar. A second possibility is that the gold-bearing sediment is derived from the north, perhaps the Chesapeake Bay system, and carried into the study area by longshore and shelf currents. This is unlikely because the shoals adjacent to both Cape Hatteras and Cape Lookout probably prevent extensive lateral transport. Furthermore, the distance of estuarine transport through the Chesapeake system in all likelihood precludes the contribution of particulate gold to the shelf. Lastly, the general paucity of gold in the southern part of the study area may be ascribed to the great distance from the shelf to the source of gold in the

Piedmont. As discussed by Emery and Noakes (1968), the probability of finding economic concentrations of heavy minerals on beaches or nearshore shelves is low, except where the source area is very near at hand. In the light of this, it seems likely that more gold is found in the northern part of the study area because the effective distance of transport of gold there is least.

CONCLUSIONS

No direct indication of commercial concentration of gold has been detected in surface sediments on the North and South Carolina Continental Shelf or in North or South Carolina beaches. The richest sample contains 6.9 ppb of gold in the total sample and was collected off Cape Lookout. There is a clearcut pattern of gold distribution in both beach and shelf environments. Most samples north of central Onslow Bay contain at least detectable gold in the heavy-mineral fractions. South of this area, none of the samples contain detectable gold. The somewhat remote possibility that significant quantities of gold may occur in buried Pleistocene beach placers has not been investigated.

REFERENCES

Bryson, J. J., 1936, Gold deposits in North Carolina: North Carolina Geol. Survey Bull. 38, 157 p.

Cleary, W. J., and Pilkey, O. H., 1968, Sedimentation on Onslow Bay: Southeastern Geology Spec. Pub. 1, p. 1–17.

Clifton, H. E., Hubert, Arthur, and Phillips, R. L., 1967, Marine sediment sample preparation for analysis for low concentrations of detrital gold: U.S. Geol. Survey Circ. 545, 11 p.

Doyle, L. J., Cleary, W. J., and Pilkey, O. H., 1968, Mica—Its use in determining shelf depositional regimes: Marine Geology, v. 6, p. 381–390.

Emery, K. O., 1969, The continental shelves: Sci. Am., v. 221, p. 106–122.

Emery, K. O., and Noakes, L. C., 1968, Economic placer deposits of the continental shelf: U.N. ECAFE, Tech. Bull., v. 1, p. 95–111.

Gorsline, D. S., 1963, Bottom sediments of the Atlantic shelf and slope off southern United States: Jour. Geology, v. 71, p. 422–440.

Meade, R. H., 1969, Landward transport of bottom sediments in estuaries of the Atlantic coastal plain: Jour. Sed. Petrology, v. 39, p. 222–235.

Milliman, J. D., Pilkey, O. H., and Blackwelder, B. W., 1968, Carbonate sediments on the continental shelf, Cape Hatteras to Cape Romain: Southeastern Geology, v. 9, p. 245–267.

Nitze, H. B. C., and Hanna, G. B., 1896, Gold deposits of North Carolina: North Carolina Geol. Survey Bull. 3, 198 p.

Pilkey, O. H., 1963, Heavy minerals of the U.S. South Atlantic Continental shelf and slope: Geol. Soc. America Bull., v. 74, p. 641–648.

———1968, Sedimentation processes on the Atlantic Southeastern United States Continental shelf: Maritime Sediments, v. 4, p. 49–51.

Stetson, H. C., 1939, Summary of sedimentary conditions on the continental shelf off the east coast of the United States, *in* Trask, P. D., ed., Recent marine sediments, a symposium: Tulsa, Okla., Am. Assoc. Petroleum Geologists, p. 230–244.

Thompson, C. E., Nakagawa, H. B., and VanSickle, G. H., 1968, Rapid analysis for gold in geologic materials, *in* Geological Survey Research 1968: U.S. Geol. Survey Prof. Paper 600–B, p. B130–B132.

Uchupi, Elazar, 1963, Sediments on the continental margin off eastern United States: Article 94 *in* U.S. Geol. Survey Prof. Paper 475–C, p. C132–C137.

DETRITAL GOLD AND SEDIMENTS IN NUKA BAY, ALASKA

By ERK REIMNITZ, ROLAND von HUENE, and F. F. WRIGHT,[1]
Menlo Park, Calif., College, Alaska

Abstract.—A marine geological investigation of Nuka Bay, a fiord system along the northern Gulf of Alaska, was conducted to learn more about the possible occurrence of gold placers on Alaskan shelves and about fiord sedimentation in general. Sediment types, distribution, and thicknesses were outlined by examining 28 bottom samples and a dense pattern of seismic reflection profiles. Nuka Bay is considerably deeper than the adjacent shelf. Holocene marine sediment occurs in thicknesses of nearly 300 m in individual depressions. These sediments are dominantly clayey silt. Sand and gravel are deposited in small, steeply sloping deltas and in recent moraines. Relict sand and gravel, deposited by former glaciers, are exposed on the adjacent open shelf. Numerous streams feeding Nuka Bay carry gold, yet the bottom mud in the bay contains no gold. A small amount of gold was detected in two samples of relict gravel and in relatively unsorted coarse material dumped into the head of the fiord by a glacier. The gold apparently moves with the coarse fraction of the sediment supply and is retained in deltas and moraines where there is little chance of finding an economic concentration.

Numerous fiords indent the coast of the Gulf of Alaska, and many of these, including Nuka Bay, still have tidal glaciers. Sedimentary processes in fiords are not well understood. In 1968 an investigation of Nuka Bay was conducted by the U.S. Geological Survey in cooperation with the University of Alaska. The Nuka Bay area was chosen partly because of the occurrence of gold in the drainage basin and partly because of the recent formation of a new fiord arm by ice retreat, giving the bay special interest for marine geologists. In this report the gold potential of the marine environment in Nuka Bay is evaluated.

METHODS OF INVESTIGATION

The RV *Acona* of the University of Alaska was the operational base for the investigation. This ship was equipped with a Teledyne sparker type continuous reflection-profiling instrument and a Litton Mark 14 Precision Depth Recorder. Sampling devices used include a piston corer, a Shipek sampler, and a bucket dredge. The ship was positioned largely by radar ranges and bearings.

Sediment grain-size distribution was studied by a combined pipet and settling-tube method; sieves were used to size gravel fractions. All surface-sediment samples were analyzed for gold content by atomic absorption. For these analyses, sediment samples weighing between 300 and 5,000 g (dry weight) were available. Each sample was separated into several size classes, and each class was analyzed individually.

GEOGRAPHIC AND GEOLOGIC SETTING

The long precipitous arms of Nuka Bay, whose depths are much greater than those of the open Continental Shelf, empty into a wide bay (fig. 1). The entrance to this bay is partly exposed to the open sea and is rimmed by a broad shoal at about 125 m depth, presumably a terminal moraine. A very conspicuous moraine at an average depth of about 10 m separates McCarty Arm from the rest of the bay. The entire arm was occupied by a glacier in 1912, and probably later. This glacier still extends to tide level and still is retreating. McCarty Arm, being in the initial and probably most rapid phase of fiord filling, allows us to infer the nature of the lower part of the sediment fill in more mature fiords of the bay. This sediment, being beyond reach of available sampling techniques, can only be seen in our seismic records. Glacial streams crossing small deltas are found along the flanks of the older parts of the fiords.

Geologically, Nuka Bay is in a Cretaceous(?) slate-graywacke belt. Interbedded slate and graywacke have been regionally deformed into open, overturned folds and are intruded by granodiorite plutons and associated dikes and sills (Richter, 1968). Numerous quartz veins

[1] University of Alaska, College, Alaska.

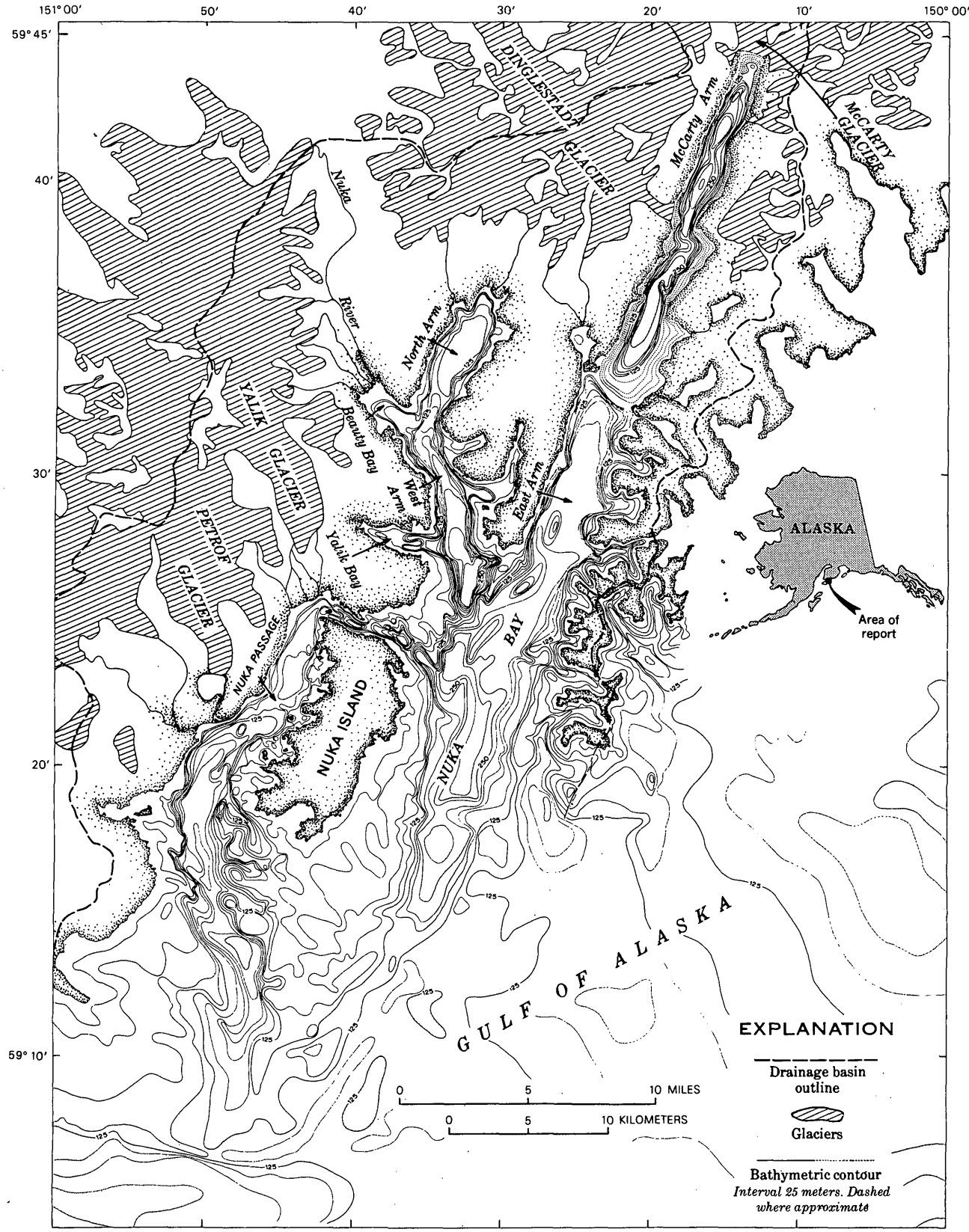

FIGURE 1.—Map of Nuka Bay area, Alaska, showing present extent of glaciers, outline of the drainage basin, major streams, and bathymetry. The bathymetry has been compiled from U.S. Coast and Geodetic Survey chart 8530 and sounding lines shown on figure 2.

containing significant amounts of gold occur in a 6- by 8-mile area around North Arm and West Arm. Total production since 1920 is estimated at $166,000. The streams contributing gold to this part of Nuka Bay and the gold-bearing lodes are shown in figure 4.

OCEANOGRAPHIC SETTING

Very little is known about the hydrology of Nuka Bay. Maximum tide range is 3.6 m, and tidal currents of 8 km/hr are reported in restricted passages (U.S. Coast and Geodetic Survey, 1964). The direct effect of tidal currents on the deep fiord bottoms is not known. Hydrographic studies of Alaskan fiords similar to those of Nuka Bay indicate that, despite the presence of shallow sills, the anoxic condition often found in the water of more temperate fiords does not exist in Alaskan fiords (Picard, 1967). Well-defined plumes of extremely turbid water, observed during the cruise of the RV *Acona* (July), were restricted to within 1 km of river mouths or glaciers. The turbid layer in Beauty Bay was less than 3 m thick, and performance of the sparker indicated saline water immediately below the turbid layer. Nuka Bay is well protected from dominant southeasterly storms except at the southeast shore of Nuka Island, where a terrace apparently is forming at a depth of about 50 m. A long sandspit at the terminus of Petrof Glacier suggests local northerly longshore currents along the partly exposed shore of Nuka Passage.

BOTTOM SEDIMENTS

More than 750 km of continuous seismic profiles (fig. 2), some of which were made in 1965 (von Huene, 1966), show the sediment distribution in Nuka Bay. These records were used to construct an isopach map of the horizontally stratified bottom sediment (fig. 3). Sediment fill of the fiords consists of a number of separate pockets of varying thickness and at different depths below the sea surface. These sediment pockets are interpreted as representing Holocene marine deposits (von Huene, 1966). In comparing the bathymetric contours (fig. 1) with the isopachous contours, we find that the sediment pockets coincide with deep, relatively flat parts of the fiords. Such pockets of Holocene sediment extend only a short distance beyond the mouth of Nuka Bay. Seaward, apparently, glacial drift of Wisconsin age and of great thickness is exposed at the bottom (von Huene, 1966).

In a typical fiord cross section, the steep mountain flanks continue below sea level to a flat, featureless bottom. The juncture of the fiord floor and walls generally is a sharp break, but in some places slump features seem to be indicated by seismic profiles (von Huene, 1966).

Twenty-eight sediment samples were collected for the present investigation. At several stations on the open shelf, where the presence of glacial drift at the surface was indicated by seismic records, a bucket dredge was used, but most samples were collected with a piston corer and (or) a snapper. Cores as long as 2.5 m were obtained. Sample 28 was collected at about sea level at the terminus of McCarty Glacier. Station locations are shown on figure 4. The percentages of gravel, sand, silt, and clay in surface-sediment samples are given in table 1.

The bottom sediment can be divided into two distinct classes: (1) Clayey silt with a small amount of sand occurs within basins outlined on the isopach map. The sand fraction of the clayey silt, which commonly consists largely of foraminiferal tests, ranges from 0 to 15 percent. (2) On the open shelf seaward of the basin, the surface sediment contains 9–95 percent gravel with some sand. The sand fraction in the gravel also consists predominantly of foraminiferal tests and consequently has a high $CaCO_3$ content.

Detailed core analyses, including a study of X-ray photographs, show that the surface sediment generally represents a subsurface condition. However, thin sandy

TABLE 1.—*Percentages of clay, silt, sand, and gravel, and gold content in surface sediment*

[Location of sampling stations on figs. 2 and 4. Gold analyses by atomic absorption. N.d. means gold was not detected]

Sampling station	Clay	Silt	Sand	Gravel	Total gold (parts per billion)
1	14.8	19.8	55.4	10.0	N.d.
2	9.8	6.2	53.6	30.5	N.d.
3	9.8	11.3	38.2	40.7	N.d.
4	11.1	8.3	36.2	44.4	N.d.
5	23.2	16.5	32.3	28.0	4
6	17.8	13.4	39.0	29.8	N.d.
7	34.2	23.1	25.7	17.0	N.d.
8	12.5	9.5	31.2	46.8	N.d.
9	.0	.0	4.6	95.4	N.d.
10	23.4	21.4	3.7	51.5	4
11	48.6	51.2	.0	.2	N.d.
12	38.5	61.5	.0	.0	N.d.
13	43.2	56.8	.0	.0	N.d.
14	50.7	49.3	.0	.0	N.d.
15	22.7	21.9	27.4	28.0	N.d.
16	38.2	61.6	.2	.1	N.d.
17	15.0	12.8	51.8	20.4	N.d.
18	44.0	55.9	.1	.0	N.d.
19	43.2	56.8	.0	.0	N.d.
20	33.2	66.8	.0	.0	N.d.
21	24.2	61.0	14.8	.2	N.d.
22	23.6	53.1	23.3	.0	N.d.
23	19.4	70.4	10.1	.1	N.d.
24	24.9	67.1	7.9	.1	N.d.
25	25.0	63.9	11.1	.0	N.p.
26	45.7	54.3	.0	.0	N.d.
27	42.4	10.5	38.4	8.7	N.d.
28	1.4	17.4	60.7	20.5	4

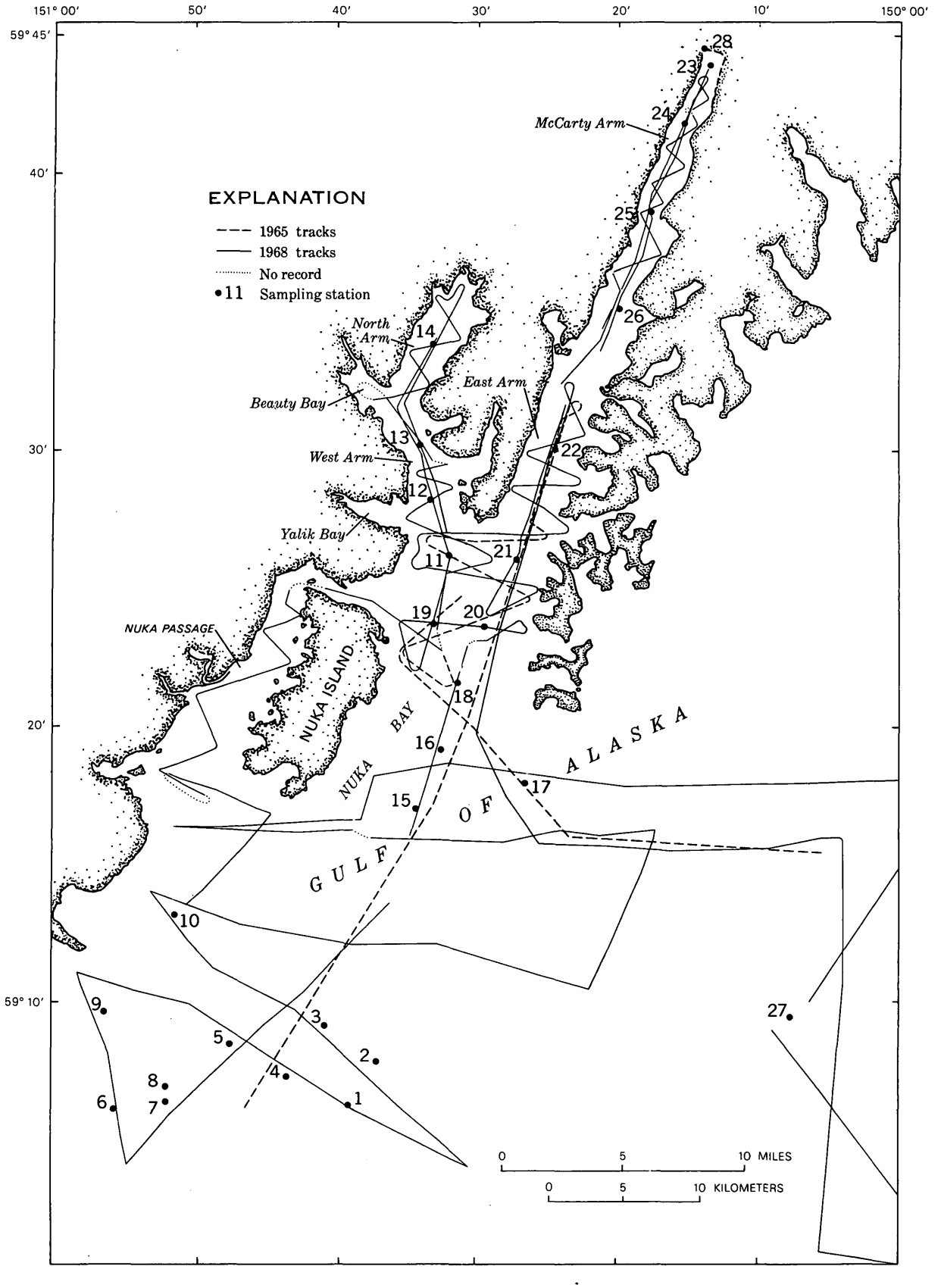

FIGURE 2.—Simultaneous arcer and fathometer transects and sample locations in Nuka Bay. Results of a 1965 survey included (von Huene, 1966).

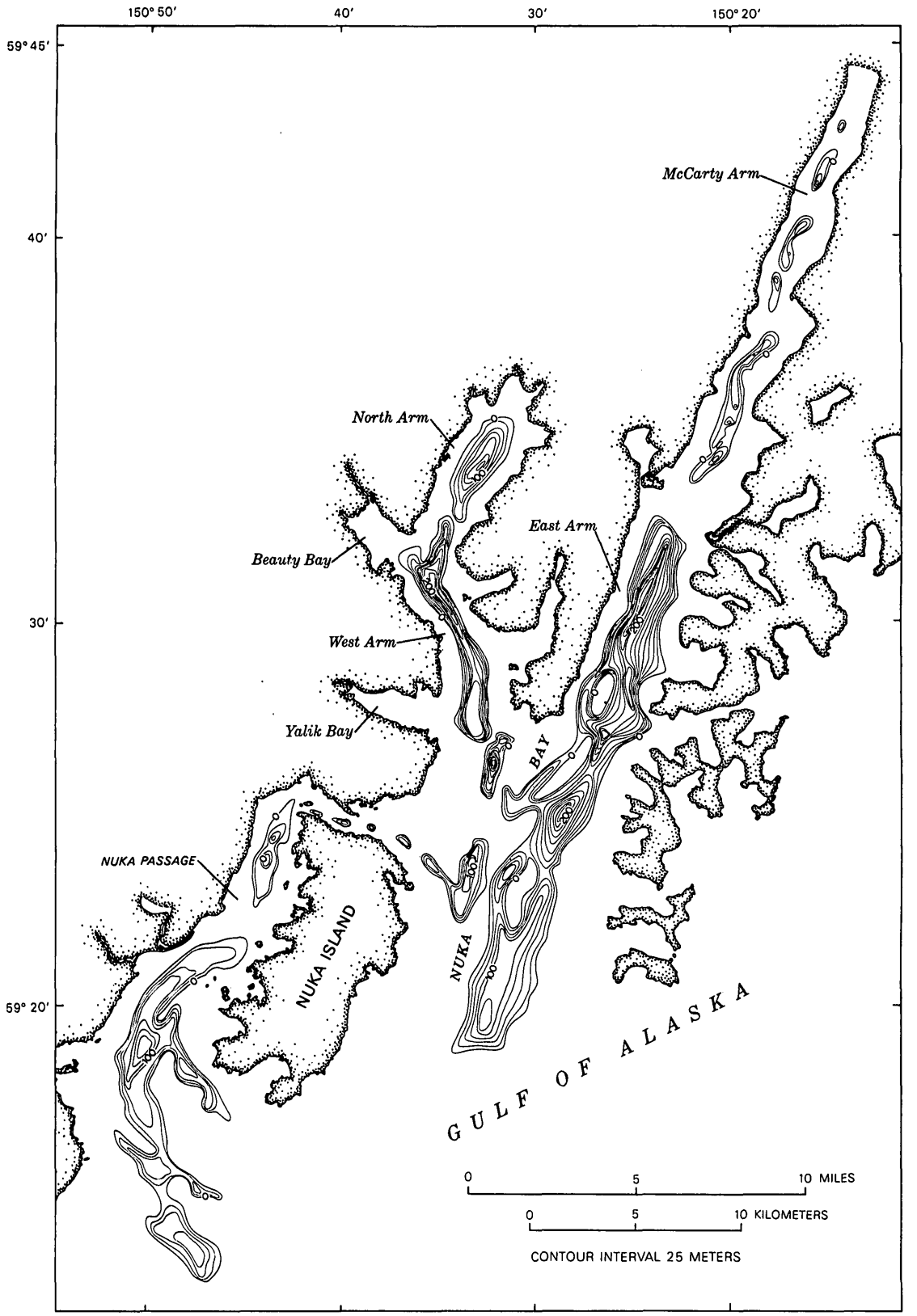

FIGURE 3.—Isopach map of stratified Holocene marine sediment in the bottom of Nuka Bay, Alaska, based on arcer profiles shown on figure 2 and a sediment sound velocity of 1,500 m/sec.

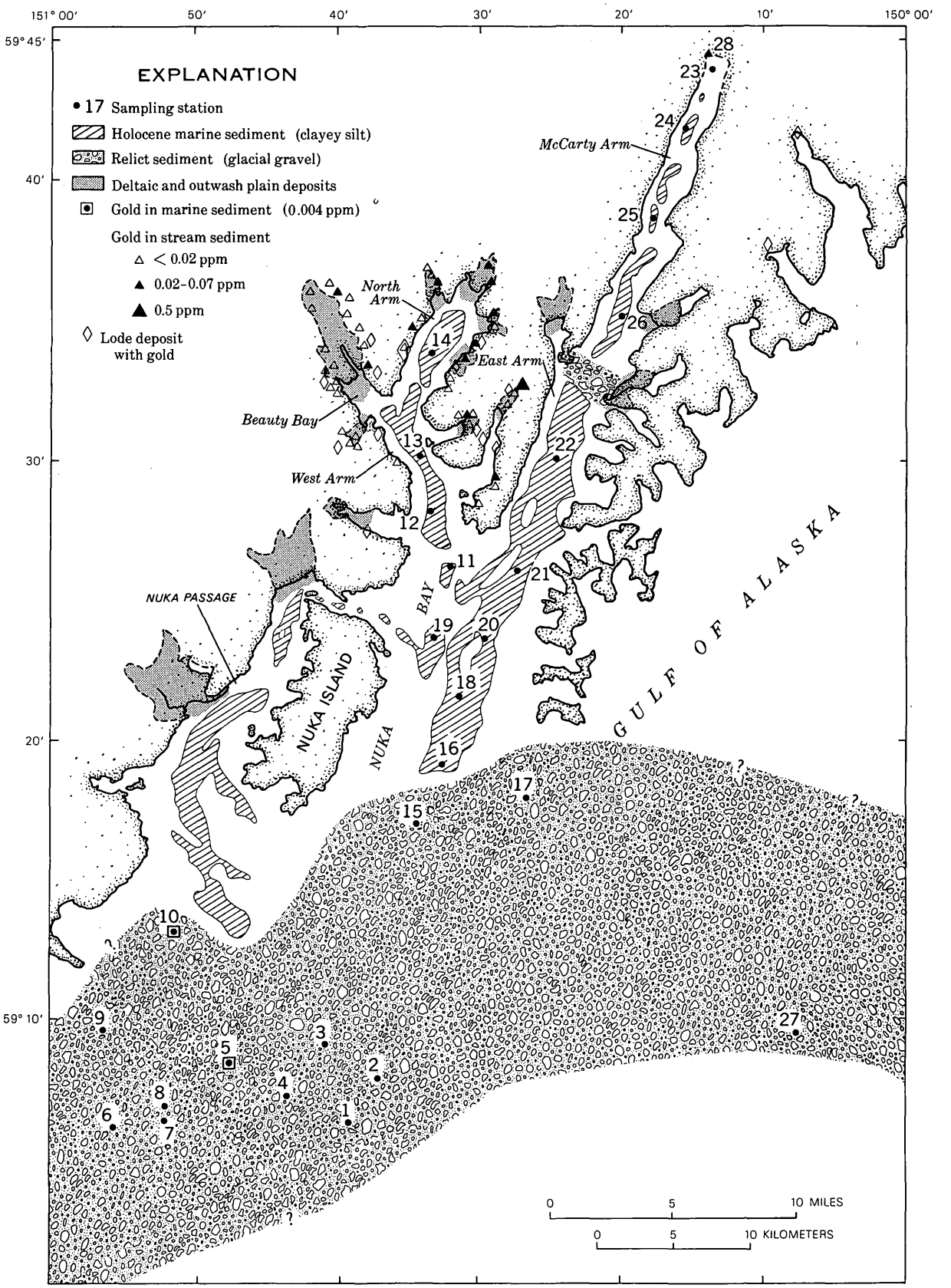

FIGURE 4.—Generalized sediment distribution in Nuka Bay as outlined on the basis of bottom samples and interpretation of arcer profiles. Gold in stream sediment from Richter (1968); gold in lode deposits from Cobb (1969).

layers in several cores occasionally show bedding which grades from coarser to finer upward. Some of these sandy layers are largely fragments of local rocks; others contain large percentages of volcanic glass. Ice rafting is not indicated except for an occasional isolated pebble, nor is there indication of cyclic phenomena suggestive of seasonal variations in sediment supply. The long, thin worm tubes and large-scale burrow structures that are numerous in some cores together with the light-gray to blue-gray sediment suggest that conditions on the fiord floors are not reducing.

GOLD ANALYSIS

The results of the gold analyses are given in table 1. A trace of gold was determined in only three of the 28 samples (fig. 4). Two of these are located in the area of relict glacial drift, the third at the terminus of McCarty Glacier. In the sample from station 5 the gold is in the 0.062–0.125-mm size fraction; in that from station 10, it is in the smaller than 0.062-mm fraction. In the sample from station 28, some gold occurs in the 0.125–0.250-mm size fraction, but it is mainly in the smaller than 0.062-mm fraction.

DISCUSSION

Holocene sediment accumulation in the Nuka Bay area has been restricted to the fiords for the most part. This agrees with observations made during an aerial reconnaissance of the region in July 1968, when the discolored fiord water was seen to extend onto the Continental Shelf for only a short distance.

The Holocene deposits within the bay can be broadly divided into two distinct types: a mud fraction (clayey silt), which lies in deep pockets on the fiord floors, and a sand and gravel fraction, which is retained in small deltas along the inner portions of the fiords and also makes up such distinct morainal features as the sill separating East Arm from McCarty Arm.

A number of seismic profiles show evidence of slumps at the foot of steep fiord walls and deltas. Slump features may result from mass movement of sediment, a common occurrence with steep foreset beds of fiord deltas. Slope failures occur during earthquakes but, in deltas, also during normal conditions of progradation (Coulter and Migliaccio, 1966). Such mass movements occasionally supply relatively coarse-grained material to the deep fiord floors, where it may remain in large masses or transform into turbidity currents that spread sediment in extensive, near-horizontal layers (Holtedahl, 1965). Certain sandy layers found in cores may represent such turbidities. The presence of sills between adjacent sediment pockets and the difference in the level of sediment fill in such pockets suggest that turbidity currents do not travel between individual pockets in Nuka Bay (von Huene, 1966).

Judging by the sparsity of ice-rafted debris in the cores, ice rafting at present is of little importance in the Nuka Bay area. This seems to be true even in McCarty Arm, where a tidal glacier is in retreat.

A slow rain of suspended matter from the overlying water seems to supply the bulk of material to the fiord bottom. The fine grain size of this material and the apparent absence of microrelief on the bottom suggest that tidal currents have no significant effects on the bottom. The presence of burrowing organisms in certain basins of the fiord floor suggests, however, that these basins are not stagnant.

Fine-grained sediment apparently is not being deposited on the open shelf today. The mud matrix in gravelly shelf sediment, therefore, seems to reflect a former environment of deposition by glaciers or by floating ice and suggests that this glacial sediment has not been reworked since the time of deposition.

Fourteen of the 28 sampling stations occupied in the Nuka Bay area lie within the pockets of Holocene marine sediment. None of these contains gold. Two of the three samples with a low gold concentration have been interpreted as representing glacial drift that in turn may be more or less representative of the country rock in general. The third sample with a low gold concentration is from a small delta at the snout of the retreating McCarty Glacier. Forty-four stream-sediment samples from areas surrounding North and West Arm have been analyzed for gold (Richter, 1968). In 12 of these samples, gold was detected with a concentration ranging from 20 to 500 parts per billion.

The distribution pattern and the occurrence of gold in the fine sand–coarse silt size fraction suggest that detrital gold supplied by the drainage basin stays in the coarse part of the total load. It therefore is incorporated into deltas. These fiord deltas are protected from marine reworking, thus making the chance for further concentration of the gold very small.

The bottom of Nuka Bay and other similar fiords does not seem to be a favorable environment for concentrating gold or other heavy metals. Significant concentrations of gold in soupy surface layers, apparently not incorporated into the fiord fill, have been reported from southeastern Alaska. Sampling techniques used in the present investigation were not suitable for proving or disproving the existence of such a soupy layer in Nuka Bay.

CONCLUSIONS

The deep, sheltered fiord environment is an efficient sediment trap for all clastic material supplied since the last major ice retreat, when, apparently, the various basins were for the most part cleaned to bedrock. Subsequent sediment accumulation was rapid, with little sorting. Any detrital gold supplied was incorporated into deltas, together with the coarser part of the load. In Nuka Bay, a lack of sedimentary microenvironments, where the rate of marine reworking would exceed the rate of sediment accumulation, makes the possibility of the occurrence of an economic gold concentration unlikely.

A possible exception to the generalization of low potential gold content is a series of small sediment pockets detected in seismic records of the relatively shallow connection between Nuka Passage and East Arm. In view of strong currents and shallow depths in this area, the sediment accumulated may be coarser grained than that in the deeper basins and therefore may warrant additional sampling.

REFERENCES

Cobb, E. H., 1969, Metallic mineral resources map of the Seldovia quadrangle, Alaska: U.S. Geol. Survey open-file map, scale 1:25,000.

Coulter, H. W., and Migliaccio, R. R., 1966, Effects of the earthquake of March 27, 1964 at Valdez, Alaska: U.S. Geol. Survey Prof. Paper 542–C, p. C1–C36.

Holtedahl, Hans, 1965, Recent turbidites in the Hardangerfjord, Norway, *in* Whitiard, W. F., and Bradshaw, R., eds., Submarine geology and geophysics, Colston Papers: London, Butterworths, n. 17; p. 107–141.

Picard, G. L., 1967, Some oceanographic characteristics of the larger inlets of southeastern Alaska: Canada Fisheries Research Board Jour., v. 24, n. 7, p. 1475–1506.

Richter, D. H., 1968, Geology and lode–gold deposits of the Nuka Bay area, Kenai Peninsula, Alaska: U.S. Geol. Survey open-file report, 52 p.

U.S. Coast and Geodetic Survey, 1964, United States coast pilot 9, Pacific and Arctic coasts, Alaska, Cape Spencer to Beaufort Sea, 7th ed: U.S. Coast and Geodetic Survey, 348 p.

von Huene, Roland, 1966, Glacial-marine geology of Nuka Bay, Alaska, and the adjacent Continental Shelf: Marine Geology, v. 4, p. 291–304.

RUTILE IN THE HARFORD COUNTY, MARYLAND, SERPENTINITE BELT

By NORMAN HERZ and L. B. VALENTINE,[1]
Washington, D.C., Bethesda, Md.

Abstract.—Rutile occurs in an ultramafic chlorite rock of the serpentinite belt of Harford County, Md. At the Dinning prospect, it was found in pockets that contain as much as 16 percent rutile, together with magnetite and apatite. The serpentinite lens that includes the prospect is 300 feet wide and 7,000 feet long; it trends northeast, parallel to the strike of the general regional schistosity. The rutile may have formed during low-grade regional metamorphism when metasomatic exchanges took place between the serpentinite and the enclosing Wissahickon Formation. Analyses of six bedrock and nine stream sediment samples show a maximum value of 5 percent for rutile in hard-rock samples at the prospect and 2 percent in stream concentrates 1.3 miles southwest of the prospect. Magnetite content is 33.5 percent at the prospect and reaches a maximum of 90 percent in a panned stream concentrate 3.5 miles northeast of the prospect. The probable tenor of rutile in most of the serpentinite lens that includes the prospect is 1 percent or less. The lens can be considered a potential economic source for both rutile and magnetite.

The Dinning rutile prospect is in the Fawn Grove, Md.-Pa., 7½-minute quadrangle, 1 mile northwest of Bushs Corner, on Clermont Mill Road in Harford County, Md. It is on the northwestern side of an ultramafic body that consists chiefly of serpentinite and soapstone. The ultramafic body forms an elongated, discontinuous, northeast-striking belt about 10 miles long and as much as 0.3 mile wide (Southwick and Owens, 1968). It is in contact with a fine-grained albite pelitic schist of the upper Wissahickon Formation to the northwest and with metagraywacke and a lower pelitic schist of the Wissahickon Formation to the southeast (fig. 1).

Rutile was found at the prospect itself in pockets that contained as much as 16 percent rutile and averaged 8 percent (Tomlinson, 1946). The present study was made to check the possibility that other parts of the serpentinite were also significantly enriched in rutile. The study is part of a comprehensive research program authorized by the Office of Emergency Planning and undertaken by the Department of the Interior under the Defense Production Act for the purpose of developing a domestic source of rutile.

HISTORY

At the suggestion of Frank L. Hess, U.S. Bureau of Mines, the Old Dominion Soapstone Co., Baltimore, Md., which owned the general area of the Dinning prospect, shipped 80 pounds of concentrates and 10 pounds of tailings on July 25, 1928, to A. Ledoux Co., New York City, for chemical and mineralogical analysis. The results of analysis of the concentrate showed 56.25 percent magnetic minerals (magnetite) and 43.75 nonmagnetic minerals; of the nonmagnetic minerals, 44.4 percent was rutile. The cleaned rutile consisted of 91.20 percent TiO_2, 4.28 percent Fe_2O_3, 2.35 percent SiO_2, and some Al, Ca, and Mg because of a hornblende contamination. The conclusion was that the rutile was a marketable 93.96-percent TiO_2 and that the ore consisted of 6 percent rutile; the magnetite was not considered marketable because of contained TiO_2.

Later in 1928, samples taken from the prospect were examined by D. H. Newland of Albany, N.Y., by Vanadium Corp., New York City, and by Professor J. T. Singewald, Jr., Johns Hopkins University, Baltimore, Md. The Titanium Alloy Manufacturing Co., New York City, expressed an interest in the property, and for the next 4 years detailed sampling and analyses were carried out. The main prospect pit and trenches were dug in 1932 while negotiations with the Titanium Alloys Co. were being carried out. No further developmental work has been done since then.

Robert S. Sanford (in April 1948) and Nils A. Eilertsen (in July 1965) examined the property for the U.S.

[1] Ocean Science and Engineering, Inc., Bethesda, Md. 20014.

U.S. GEOL. SURVEY PROF. PAPER 700-C, PAGES C43–C48

380–189 O—70——4

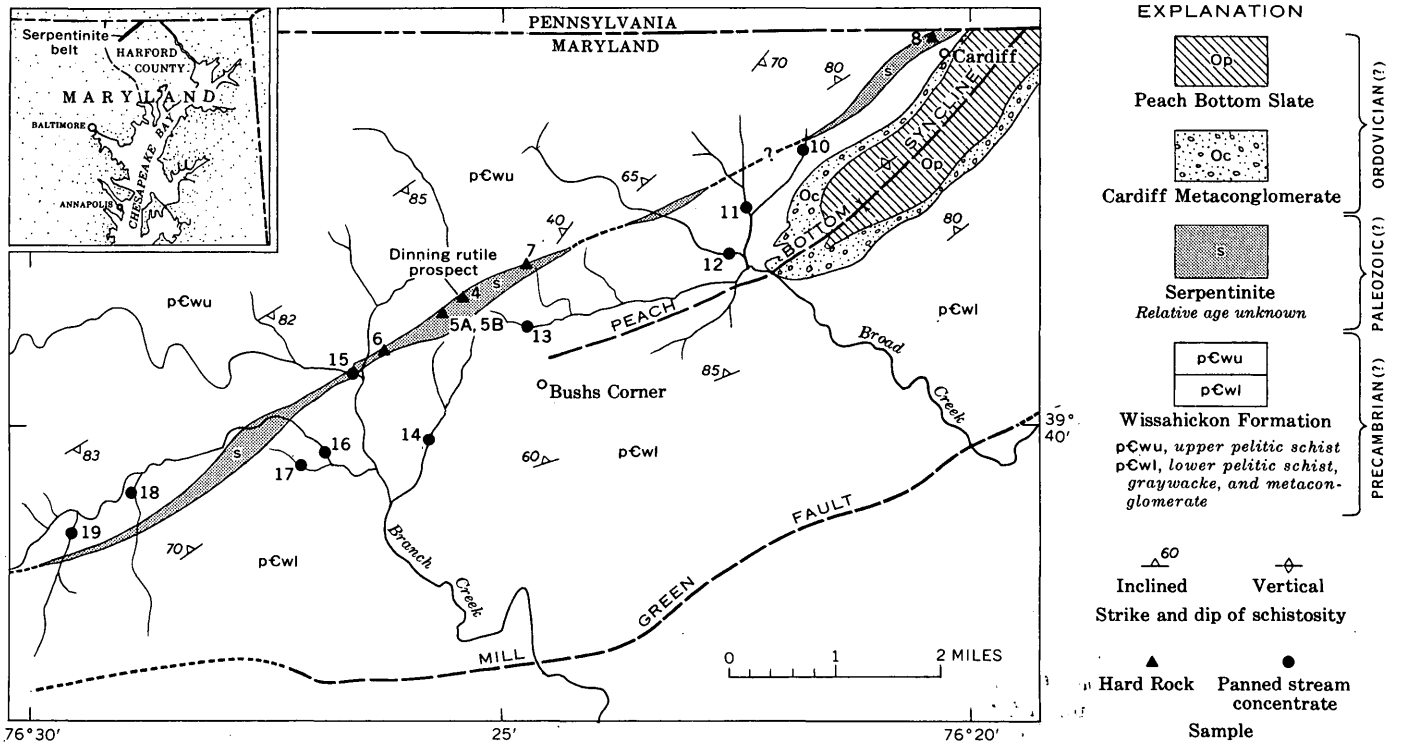

FIGURE 1.—Generalized geologic map of the rutile-bearing serpentinite belt in Harford County, Md., showing sample localities. Modified from Southwick and Owens (1968).

Bureau of Mines, and each concluded that the grade and extent of mineralization of rutile was not sufficient to be commercially attractive. Interest was again renewed in the occurrence because of the U.S. Department of Interior Emergency Rutile Programs and a field conference was arranged on August 14, 1968. Participants were Kenneth N. Weaver, Maryland State Geologist; Jonathan Edwards, Jr., and William P. Crowley, Maryland Geological Survey; L. Y. Marks, U.S. Bureau of Mines; and Norman Herz and F. G. Lesure, U.S. Geological Survey. Further fieldwork was carried out, and hard-rock and panned stream concentrates were collected by Lesure and Herz. The samples were analyzed in laboratories of the U.S. Bureau of Mines and the U.S. Geological Survey. We are indebted to the U.S. Bureau of Mines for making available Mr. Marks' report on the prospect as well as the results of metallurgical testing by their Tuscaloosa, Ala., laboratories.

GEOLOGY

The geology of the rutile occurrence has been described by Tomlinson (1946), Pearre and Heyl (1960, p. 792–793), and Southwick (1968). The following description is taken largely from Southwick.

The rutile at the Dinning prospect occurs in an ultramafic chlorite rock which also contains large amounts of porphyroblastic magnetite, apatite, and ilmenite. Some pockets contain as much as 40 percent magnetite, 15 percent apatite, and 16 percent rutile in rock that commonly contains about 5 percent total iron-titanium oxides and less than 1 percent apatite. This rock is on the northwest edge of a serpentinized and steatized ultramafic rock that ranges in width from less than 10 feet to about 1,000 feet. The body appears to be in a regional fault zone that trends roughly N. 60° E., parallel to the regional strike of the enclosing schists and metagraywackes of the Wissachickon Formation (fig. 1). "This rock was probably formed from a narrow oxide- and apatite-rich gabbro pegmatite dike at the contact between serpentinite and pelitic schist. During low-grade regional metamorphism, it was recrystallized and chloritized by metasomatic exchanges between the much larger serpentinite mass and its pelitic wallrocks" (Southwick, 1968, p. C38).

Rutile replaced much of the ilmenite; iron that was expelled from the ilmenite structure helped form magnetite. A suggested reaction during retrograde metamorphism that would have produced rutile is

$$\underset{\text{ilmenite}}{FeTiO_3} + \underset{\text{hematite}}{Fe_2O_3} \rightarrow \underset{\text{magnetite}}{FeO_4} + \underset{\text{rutile}}{TiO_2}$$

but this did not go to completion everywhere. Much ilmenite is found as skeletal bladed crystals composed of an intimate vermicular intergrowth of ilmenite and rutile with some magnetite and hematite. As rutile con-

tent increases at the expense of ilmenite, it forms large striated prisms as much as 2 cm long that are virtually pure rutile. Magnetite occurs as sharply faceted octahedra, oxidized to hematite along their margins.

X-ray fluorescence analysis, by Robena Brown, U.S. Geological Survey, show two rutile samples to contain 97.5 percent TiO_2 and 1.12 percent FeO (1.25 if Fe_2O_3), and 98.0 percent TiO_2 and 1.44 percent FeO (1.60 if Fe_2O_3), respectively. National stockpile requirements are a minimum of 95 percent TiO_2 and a maximum of 1 percent Fe_2O_3. Two magnetite samples contained 0.1 percent TiO_2. Apatite coexisting with these minerals is a fluorhydroxyl variety, and chlorite is a magnesian sheridanite. A semiquantitative spectrographic analysis of rutile from the Dinning prospect pit (table 1) shows that it meets national stockpile requirements for maximum trace-element content.

TABLE 1.—*Semiquantitative spectrographic analysis, in parts per million, of rutile from Dinning rutile prospect, Harford County, Md.*

[Analyst H. W. Worthing, U.S. Geological Survey, Washington, D.C. Sample probably had some inclusions of chlorite-serpentine as shown by relatively high Si (0.7), Al (0.3), and Mg (0.7). Results are reported in the intervals 1, 0.7, 0.5, 0.3, 0.2, 0.15, 0.1, and so forth. Elements looked for, but below limits of detection (in parentheses in parts per million): As (200), Au (10), Be (1), Bi (10), Cd (20), Co (10), Eu (100), Ga (1), Ge (3), Hf (20), In (100), La (20), Li (30), Mo (2), Nd (70), Pb (10), Pd (1), Pr (100), Pt (3), Re (30), Sb (100), Sm (100), Sr (50), Ta (200), Te (300), Th (200), Tl (50), U (300), W (50), Zn (200)]

Ag	0.03	Ni	15
B	20	Sc	70
Ba	2	Sn	3
Ce	70	V	100
Cr	10	Y	30
Cu	30	Yb	2
Mn	50	Zr	100
Nb	50		

SAMPLING PROCEDURE

Both hard-rock and panned heavy-mineral concentrate samples were collected and analyzed. The hard-rock samples are from the serpentine belt, and were collected from each locality by combining 10 or more ¼- to 1-pound pieces that were taken at the face of the outcrop. Sample 4 (see table 2) is a composite from the Dinning rutile prospect; samples 5A and 5B, are from 0.25 mile southwest, on and north of the road; 6 is from 1 mile southwest of the prospect; and 7 is from 0.7 mile northeast (fig. 1). All these are in a continuation of the serpentinite lens that includes the prospect. Sample 8 is from a serpentinite quarry in Cardiff at the northern end of the serpentinite belt in Maryland.

Panned heavy-mineral concentrates were collected from riffles in streams that drain the serpentinite belt. Because rutile tends to accumulate as a heavy detrital mineral, it should show in samples panned from streams draining the area of weathered rock. Stream samples were dug from the upper 6–12 inches of riffles and bars in the beds of streams. The wet sand was shoveled into a 10-quart bucket (0.34 ft^3) until it was filled. The sample was then sieved through a ⅛-inch opening punch plate; alluvium that passed through the sieve was caught in a 16-inch prospector's pan and shaken to make a heavy-mineral concentrate. The total amount of heavy minerals and the percentage abundance of each heavy mineral can be used to obtain a qualitative idea of the tenor of the streambed material (Theobald, 1957; Overstreet and others, 1968). Samples 10, 11, and 12 are from streams that drain the northeastern part of the serpentine belt; 13, 14, and 15 are from streams that cut the serpentinite lens that includes the prospect, and 16, 17, 18, and 19 are from streams in the southwestern part of the belt (fig. 1).

LABORATORY PROCEDURE

In the laboratory, the hard-rock samples were crushed to pass 10-mesh size; both hard-rock and stream-placer samples were then screened, using 40, 100, and 200 standard sieve sizes. The light minerals were separated in each screen fraction with bromoform (specific gravity 2.86). The heavy minerals were gone over with a hand magnet to remove magnetite and then passed through a Frantz isodynamic separator to concentrate ilmenite. Percentages of magnetite and ilmenite were calculated from the amount of material in each magnetic separate. The nonmagnetic minerals were studied with a binocular microscope to get an idea of the mineral assemblage and were then X-rayed. Percentages of rutile were calculated from X-ray diffractograms from substrates of 800 mg of pulverized sample material mixed with 200 mg of metallic aluminum powder. Standard mixtures had been prepared and working curves drawn relating the peak-height ratios of the 27.5° 2θ:44.8° 2θ (rutile-Al peaks) to the absolute abundance of rutile. The peak-height ratios are a linear function of the weight fraction of each component as the linear absorption coefficient of the mixture, which is an unknown quantity, affects the peak heights of all the components in the same proportion (Cullity, 1956, p. 397). The amount of rutile in any sample can then be obtained by measuring the 27.5° 2θ rutile to 44.8° 2θ Al ratio and comparing it to the working curve.

RESULTS OF MINERALOGICAL ANALYSIS

The results of sample analysis are shown in tables 2 and 3. Magnetite is abundant throughout the length of the serpentine belt and is much more abundant in the stream samples than in the hard-rock samples. This greater abundance of magnetite is probably due to enrichment from rocks other than those occurring within

TABLE 2.—*Results of heavy-mineral analysis of hard-rock samples from the serpentinite belt, Harford County, Md.*

[Na, not analyzed for; Tr., trace]

Sample No.	Screen size	Screened fraction (percent)	Percentage in whole rock (averages given in parentheses)			Other minerals
			Rutile	Magnetite	Ilmenite	
4	40	11	2. 9	51	11	Apatite, chlorite, talc.
	100	35	5. 6	39	9. 6	
	200	25	4. 1	18	10	
	<200	29	6	Na	Na	
			(5. 0)	(33. 5)	(10. 0)	
5A	40	9	0	8. 1	4. 5	Actinolite, chlorite, unidentified amphibole, garnet, serpentine.
	100	45	2. 0	5. 1	1. 3	
	200	7	3. 0	5. 0	0. 3	
	<200	39	Tr.	Na	Na	
			(1. 1)	(5. 5)	(1. 7)	
5B	40	6	3. 6	7. 1	7. 1	Chlorite, apatite, garnet, talc, quartz.
	100	20	4. 9	2. 9	6. 8	
	200	17	0	1. 0	2. 9	
	<200	57	Tr.	Na	Na	
			(1. 2)	(2. 7)	(5. 3)	
6	40	13	0	32	5. 4	Chlorite, serpentine, talc, actinolite(?), apatite.
	100	39	0. 9	25	3. 5	
	200	24	1. 0	19	5. 8	
	<200	24	0	Na	Na	
			(0. 6)	(24. 3)	(4. 6)	
7	40	12	0	3. 9	2. 0	Chlorite, serpentine, apatite, epidote, quartz.
	100	25	0	0. 7	6. 9	
	200	19	0	1. 1	1. 6	
	<200	44	0	Na	Na	
			(0)	(1. 5)	(4. 1)	
8	40	8	0	4. 8	3. 7	Chlorite, serpentine.
	100	54	0	10	2. 0	
	200	16	0	6. 3	1. 0	
	<200	22	0	Na	Na	
			(0)	(8. 7)	(2. 0)	

the belt. Rutile, on the other hand, is most abundant (5 percent) in hard-rock sample 4 taken at the Dinning prospect. It constitutes 2 percent of stream sample 15 taken 1.3 miles southwest of the prospect, but is generally about 1 percent in other samples.

The analyzed samples show that a mineralized zone about 300 feet wide may extend for as much as 7,000 feet along the northwest side of the serpentine belt and may average 1 percent rutile. The Dinning prospect itself probably represents an atypically rich pocket; the probable tenor of most of the zone in rutile is 1 percent or less.

RESULTS OF METALLURGICAL TESTING

The U.S. Bureau of Mines Metallurgy Research Laboratory in Tuscaloosa, Ala., carried out beneficiation tests directed by Mr. W. E. Lamont, project leader, on grab samples taken at the prospect. They concluded that the ore would be easy to beneficiate and would yield both high-grade iron and rutile products (table 4). The ore was ground to pass a 65-mesh sieve and separated magnetically in a Davis Tube separator. The nonmagnetic fraction was sized at 20 microns (sedimentation sizing based on quartz specific gravity) to remove the slimes, and the +20-micron nonmagnetic fraction was separated at a specific gravity of 3.3 to simulate industrial gravity-concentration techniques. Almost 93 percent of the iron was recovered at a grade of 70.4 percent Fe, and more than 90 percent of the total rutile was recovered at a grade of 85.0 percent TiO_2.

CONCLUSIONS

The Harford County serpentinite belt in the vicinity of the Dinning rutile prospect contains enough rutile and magnetite to be considered as a potential, if low-grade resource. However, additional data are needed to establish the economic feasibility of processing this material to recover rutile and coproduct magnetite, or the feasibility of recovering other possibly saleable accessory minerals present, including apatite, ilmenite, garnet, and talc. Further detailed study should include trenching and core drilling to determine (1) the possible existence of other enriched pockets of rutile, (2) whether the rutile content increases or decreases with depth, and (3) whether the entire serpentinite body is indeed mineralized. Chemical analyses should be made of the rutile especially to check for high iron content which would make it unsatisfactory for some purposes.

TABLE 3.—*Results of heavy-mineral analysis of panned stream-concentrate samples from the serpentinite belt, Harford County, Md.*

Sample No.	Total weight heavy mineral (grams)	Screen size	Heavy-mineral content of screened fraction (percent)	Percentage of heavy minerals (average given in parentheses)		Other minerals [1]
				Rutile	Magnetite	
10	95. 0	40	57. 7	1	92	Actinolite, chlorite, epidote, quartz, talc; 1.
		100	36. 3	1	89	
		200	6. 0	2	77	
				(1. 1)	(90. 0)	
11	184. 4	40	50. 4	1	88	Chlorite, actinolite, muscovite, hornblende(?), zoisite(?); 1.
		100	49. 2	<1	92	
		200	0. 4	1	76	
				(<1)	(89. 9)	
12	154. 1	40	42. 4	2	76	Actinolite, chlorite, quartz, ilmenite, zoisite(?); 1.
		100	56. 3	1	82	
		200	1. 4	3	51	
				(1. 5)	(79. 1)	
13	89. 3	40	39. 3	2	84	Ilmenite, garnet, actinolite, quartz; 1.
		100	49. 9	1	79	
		200	10. 8	4	44	
				(1. 7)	(77. 2)	
14	281. 2	40	24. 6	0	76	Actinolite, garnet, quartz, plagioclase; 1.
		100	21. 6	<1	92	
		200	13. 8	1	76	
				(<1)	(85. 9)	
15	58. 9	40	21. 9	2	82	Ilmenite, epidote, actinolite, quartz; 1.
		100	73. 0	2	69	
		200	5. 1	2	65	
				(2)	(71. 6)	
16	125. 1	40	42. 2	0	36	Actinolite, epidote, quartz, ilmenite; 2.
		100	49. 2	1	71	
		200	8. 6	2	47	
				(0. 7)	(54. 2)	
17	193. 2	40	17. 7	0	51	Ilmenite, hornblende(?), actinolite, quartz; 2.
		100	68. 1	1	78	
		200	14. 2	2	66	
				(1. 0)	(71. 5)	
18	249. 0	40	39. 4	0	10	Epidote, ilmenite, garnet, actinolite, quartz; 1.
		100	47. 9	2	67	
		200	12. 7	2	58	
				(1. 2)	(43. 4)	
19	492. 9	40	60. 6	0	54	Epidote, garnet, quartz; 1.
		100	36. 1	<1	73	
		200	3. 3	2	49	
				(<1)	(60. 7)	

[1] The values given are the percentage of sample that passed 200 screen size, and include light and heavy minerals. No further work was done with this fraction.

TABLE 4.—*Response of sample from Dinning rutile prospect, Harford County, Md., to Davis tube magnetic separation and to heavy-media separation of the nonmagnetic fraction*

[W. E. Lamont, project leader, U.S. Bureau of Mines, Tuscaloosa, Ala.]

Product	Weight (percent)	Assay (percent)		Distribution (percent)	
		Fe	TiO_2	Fe	TiO_2
Magnetic:					
30-volt fraction	37. 4	70. 5	1. 3	89. 7	5. 4
90-volt fraction	1. 4	66. 6	2. 1	3. 1	. 3
Total magnetic composite	38. 8	70. 4	1. 3	92. 8	5. 7
Nonmagnetic:					
+20-micron fraction (<3.3 sp gr)	45. 7	2. 5	. 7	3. 9	3. 5
+20-micron fraction (>3.3 sp gr)	9. 6	5. 8	85. 0	1. 9	90. 2
Subtotal	55. 3	3. 1	15. 3	5. 8	93. 7
−20-micron fraction	5. 9	6. 7	. 8	1. 4	. 6
Total nonmagnetic composite	61. 2	3. 4	13. 9	7. 2	94. 3
Total composite ore	100. 0	29. 4	9. 1	100. 0	100. 0

If the entire serpentinite body is assumed to be mineralized, with an average rutile tenor of 1 percent and magnetite of 15 percent, then there would be about 2,700 tons of rutile and 50,000 tons of magnetite per foot of depth. The total volume of easily recoverable material is probably substantial. The major obstacle to opencut mining methods is Deer Creek, which cuts the serpentine belt, but there is a difference of elevation of about 200 feet between the creek bottom and hilltops in the serpentinite. On the basis of a 93-percent recovery of magnetite and 90-percent recovery of an 85-percent grade of rutile, $10 per ton for magnetite and $125 per ton for pure rutile[1], one ton of ore should net about $3.50 in magnetite and rutile. These figures suggest that the value of potential products is sufficient to merit further detailed investigation of the deposit.

[1] If Fe_2O_3 is above 1 percent, the price may be lower.

REFERENCES

Cullity, B. D., 1956, Elements of X-ray diffraction: Reading, Mass., Addison-Wesley Pub Co., 514 p.

Overstreet, W. C., White, A. M., Whitlow, J. W., Theobald, P. K., Jr., Caldwell, D. W., and Cuppels, N. P., 1968, Fluvial monazite deposits in the southeastern United States: U.S. Geol. Survey Prof. Paper 568, 85 p.

Pearre, N. C., and Heyl, A. V., Jr., 1960, Chromite and other mineral deposits in serpentine rocks of the Piedmont Upland, Maryland, Pennsylvania, and Delaware: U.S. Geol. Survey Bull. 1082–K, p. 707–833.

Southwick, D. L., 1968, Mineralogy of a rutile- and apatite-bearing ultramafic chlorite rock, Harford County, Maryland: U.S. Geol. Survey Prof. Paper 600–C, p. C38–C44.

Southwick, D. L., and Owens, J. P., 1968, Geologic map of Harford County: Maryland Geol. Survey, scale 1:62,500.

Theobald, P. K., Jr., 1957, The gold pan as a quantitative geologic tool: U.S. Geol. Survey Bull. 1071–A, 54 p.

Tomlinson, W. H., 1946, Rutile in Harford County, Maryland: Am. Mineralogist, v. 31, nos. 5–6, p. 322–325.

PHOSPHATE OCCURRENCES IN NYE COUNTY AND ADJACENT AREAS, NEVADA

By C. L. ROGERS,[1] F. J. KLEINHAMPL,[2]
J. I. ZIONY,[2] and WALTER DANILCHIK,[1]
[1] Denver, Colo., [2] Menlo Park, Calif.

Abstract.—Recent geologic studies in Nye County and adjacent areas, Nevada, have resulted in the recognition of phosphatic rocks which range in age from Cambrian to Permian(?) and which extend over an area of about 10,000 square miles. The phosphatic rocks are as much as 1.4 feet thick and contain as much as 19.4 percent P_2O_5.

Recent fieldwork in central and southern Nevada, largely in Nye County, has shown that phosphatic sedimentary rocks are widely distributed, both geographically (fig. 1) and stratigraphically (table 1) in that area. This report has been written to focus attention on these discoveries and to encourage geologists working in the southern part of the Great Basin to look for potentially economic concentrations of phosphate.

In 1967 and 1968, the senior author was engaged in geologic mapping for the U.S. Atomic Energy Commission in the Hot Creek Range of northern Nye County and noted the presence of phosphate in formations ranging from early to late Paleozoic age. During reconnaissance mapping of northern Nye County in 1967, Kleinhampl and Ziony (1967) discovered phosphatic rocks in an allochthonous sequence of late Paleozoic age in the Monitor Range, which lies just west of the Hot Creek Range. As a result of these discoveries, Rogers, Kleinhampl, and Danilchik made a brief field trip to Nevada in November 1968 and found several other occurrences in northern Nye County and in the region to the north of Nye County.

The phosphate occurs in marine sedimentary rocks which range in age from Cambrian to Permian(?) and which were deposited in the Cordilleran geosyncline. The richest material discovered to date is largely miogeosynclinal in origin and occurs in rocks of the carbonate and transitional assemblages. However,

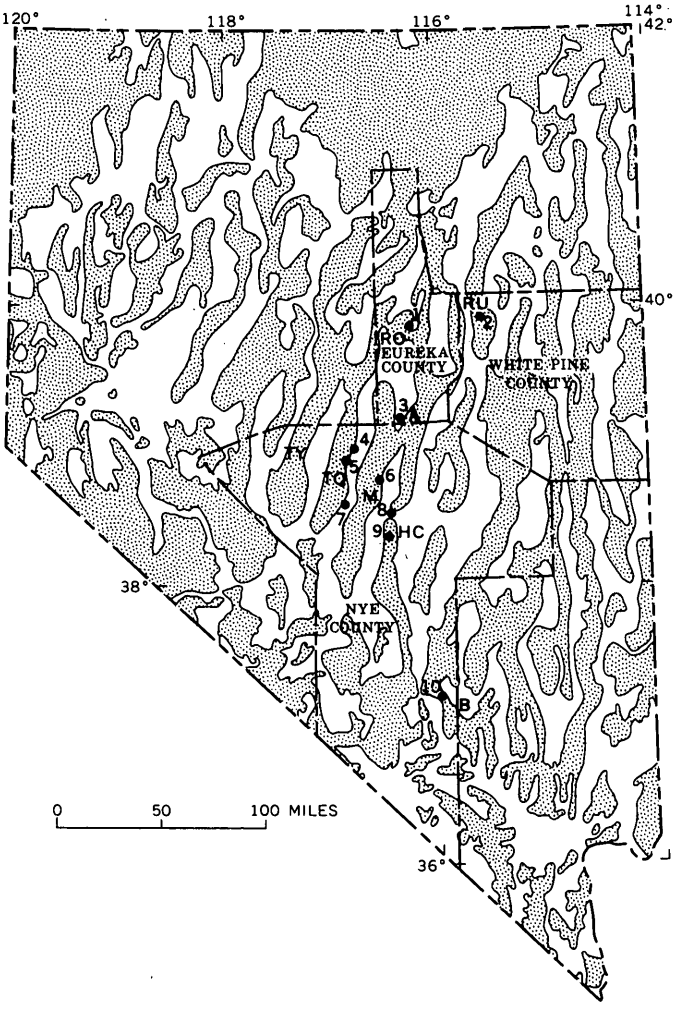

FIGURE 1.—Index map of Nevada, showing phosphate localities mentioned in text. Mountainous areas shown by stipple pattern; alluviated valleys unpatterned. Mountain ranges identified by letters, as follows: A, Antelope Range; B, Banded Mountain; HC, Hot Creek Range; M, Monitor Range; RO, Roberts Mountains; RU, Ruby Mountains; TQ, Toquima Range; TY, Toiyabe Range.

TABLE 1.—*Generalized list of selected Paleozoic stratigraphic units in report area*

[Units mentioned in text are underlined. Units on same line may be only partly equivalent; units on successive lines may overlap in age]

Toiyabe Range (Wall Canyon)	Toquima Range		Roberts Mountains	Monitor Range	Hot Creek Range and Antelope Range	Banded Mountain	Age
	Northern part	Southern part					
Pablo Formation Diablo Formation				Chert, sandstone and shale, [2 3] undifferentiated			Permian and Permian(?)
	Wildcat Peak Formation [1]						Pennsylvanian
					Eleana Formation and lateral equivalents		Mississippian and Devonian
			Nevada Formation	Limestone and dolomite, undifferentiated	Rocks of Cockalorum Wash area [2] — Devils Gate Limestone, Nevada Formation		Devonian
Masket(?) Shale [1] Gatecliff(?) Formation [1]	Masket Shale [1] Gatecliff Formation [1]		Lone Mountain Dolomite Roberts Mountains Formation	Lone Mountain Dolomite Roberts Mountains Formation	Light-gray dolomite (probably correlative with Lone Mountain Dolomite) Dark-gray dolomite (probably correlative with Roberts Mountains Formation)		Silurian

Toquima Formation Zanzibar Limestone [4]	Caesar Canyon Limestone [1] Pogonip Group	Toquima Formation Zanzibar Limestone [4] Mayflower Schist [4]	Hanson Creek Formation Eureka Quartzite Vinini Formation [2] Pogonip Group	Hanson Creek Formation Eureka Quartzite Copenhagen Formation Pogonip Group	Hanson Creek Formation Eureka Quartzite Copenhagen Formation Pogonip Group: Antelope Valley Limestone; Ninemile Formation; Goodwin Limestone		Ordovician
Gold Hill Formation		Gold Hill Formation			Hales Limestone Tybo Shale Swarbrick Formation	Nopah Formation: Smoky Member; Halfpint Member; Dunderberg Shale Member Bonanza King Formation Carrara Formation	Cambrian

[1] Of Kay and Crawford (1964).
[2] Allochthonous or possibly allochthonous.
[3] Age uncertain; contains conodonts in Pennsylvanian(?) to Triassic range, but Permian(?) age suggested by lithology.
[4] Ordovician age uncertain.

phosphate has also been noted in rocks of the detrital-volcanic (eugeosynclinal) assemblage, and these are sufficiently promising to warrant further study. The phosphate localities mentioned in this paper are shown in figure 1, and the occurrences discovered to date are described briefly.

PHOSPHATE IN ROCKS OF THE CARBONATE AND TRANSITIONAL ASSEMBLAGES

Cambrian rocks

The oldest known phosphatic zone occurs in the upper 10 feet of the Bonanza King Formation (of Middle and Late Cambrian age) on the west flank of Banded Mountain, just east of Yucca Flat (fig. 1, loc. *10*; table 1; Barnes and others, 1963). The rock is a dark-brownish-gray limestone, which is characterized by a well-developed bluish-white bloom resembling that associated with the Phosphoria Formation. This zone has not been analyzed, but the rock has been examined in thin section and reveals common phosphatic material occurring in three ways: (1) disseminated throughout the rock matrix; (2) in small irregular pellets that are partly replaced by calcite; and (3) as replacement of abundant fossil debris, which appears to be made up largely of trilobite fragments.

Small dark-gray to black phosphate pellets were also found sparsely distributed through the upper limestone member of the Middle Cambrian Secret Canyon Shale, a partial stratigraphic equivalent of the Bonanza King Formation. The Secret Canyon was examined in the southern Ruby Mountains, White Pine County, in an area about 1.5 miles north-northwest of Big Bald Mountain (fig. 1, loc. *2*).

In the Banded Mountain area (fig. 1, loc. *10*; table 1) the Bonanza King Formation is overlain by the Dunderberg Shale Member of the Nopah Formation, which is 225 feet thick and consists of pale-reddish-brown shale and some nodular to lenticular limestone (Barnes and others, 1963; Barnes and Christiansen, 1967). The limestone in the Dunderberg is generally weakly phosphatic, and a group of lenticular beds that lies about 20 feet above the base of the shale has been sampled and analyzed for P_2O_5 and acid insolubles (table 2). These beds have an aggregate thickness of 3.9 feet and are separated by nonphosphatic shale layers that have an aggregate thickness of 5.4 feet. Phosphate occurs as (1) round to ovoid pellets or nodules which range from silt to fine-pebble size (fig. 2), (2) disseminations in the rock matrix, and (3) replacements of fossil debris. Most of the phosphate is pelletal and is concentrated in thin laminae and thin beds which are separated by weakly phosphatic material.

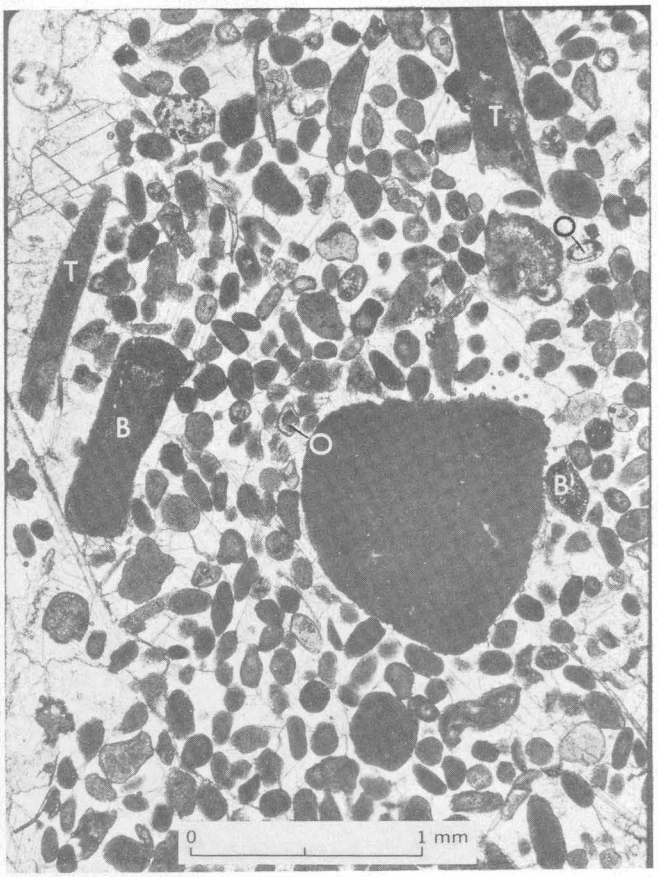

FIGURE 2.—Photomicrograph (plane light) of phosphatic limestone in Dunderberg Shale Member of Nopah Formation of Cambrian age. Phosphate occurs as irregular pellets and fossil fragments in a calcite groundmass; fossil material consists of trilobite debris (T) and cellular fragments that may be bryozoan (B). A few pellets are oolitic (O). The phosphate is medium to dark brown and ranges from anisotropic to wholly opaque.

In the southern Hot Creek Range of northern Nye County (fig. 1, locs. *8* and *9*) the lower 300–400 feet of the Hales Limestone (table 1) contains many weakly phosphatic beds, with the greatest concentration occurring in the basal 20–40 feet. This basal sequence is composed of laminated to thin-bedded limestone, which ranges from nonphosphatic to moderately phosphatic; two layers representative of the richer material have been sampled and analyzed for P_2O_5 and acid insolubles (table 2).

In thin section the phosphate is seen to occur mainly as silt- to sand-sized, round to irregular pellets and as a replacement of trilobite fragments. A few of the pellets exhibit a concentric structure formed by alternate layers of calcite and phosphate, and a few small chert pellets are rimmed by phosphate; however, most of the pellets appear to be wholly structureless. They have a general size range of 0.05–0.3 mm and most are medium to dark brown under the microscope and are wholly opaque.

TABLE 2.—*Analyses of phosphatic rock samples, Nye County, Nev., and adjacent areas*

[N.d., not determined. Colorimetric and volumetric analyses for P_2O_5 and gravimetric analyses for acid insolubles by H. H. Lipp, G. D. Shipley, and C. O. Ingamells, given in percent]

Laboratory No.	Field No.	Locality (fig. 1)	Thickness (feet)	Lithology	P_2O_5 analyses		Acid insolubles
					Colorimetric	Volumetric	
		CAMBRIAN					
		Dunderberg Shale Member of Nopah Formation					
D 131724	R68-4D	Banded Mountain (loc. *10*).	0.6	Phosphatic limestone.	2.3	2.22	10.0
131723	4C	---do---	1.4	---do---	2.0	2.22	11.5
131722	4B	---do---	1.2	---do---	5.7	5.77	10.9
131721	4A	---do---	.7	---do---	1.3	1.40	8.2
		Hales Limestone					
D 132487	R68-8	Hot Creek Canyon, Hot Creek Range (loc. *8*).	1.4	Calcareous phosphorite.	18.8	19.4	13.5
133017	TY67CLR-10	Tybo Canyon, Hot Creek Range (loc. *9*).	.5	Phosphatic limestone.	N.d.	9.92	16.2
		ORDOVICIAN					
		Goodwin Limestone					
D 133019	TY68CLR-26	South of Tybo Canyon, Hot Creek Range (loc. *9*).	0.2	Phosphatic limestone.	N.d.	5.4	1.5
136433	P-2B	Antelope Range (loc. *3*).	<.1	Calcareous siltstone--	N.d.	4.8	62.9
		Ninemile Formation					
D 136434	P-2C	Antelope Range (loc. *3*).	<0.1	Calcareous siltstone--	N.d.	3.4	55.8
		Vinini Formation					
D 136435	P-6A	Roberts Mountains (loc. *1*).	(1)	Phosphorite---	N.d.	28.6	1.6
136436	6B	---do---	0.1	Carbonaceous shale--	N.d.	1.7	91.8
		Toquima Formation					
D 136439	P-10A	Southern part of Toquima Range (loc. *7*).	<0.1	Carbonaceous shale--	N.d.	3.8	67.5
		Caesar Canyon Limestone of Kay and Crawford (1964)					
D 136441	16351-5	August Canyon, Toquima Range (loc. *4*).	0.17	Phosphatic limestone.	N.d.	9.9	9.5
136442	8	---do---	.1	---do---	N.d.	6.4	8.1
		Hanson Creek Formation					
D 133018	TY68CLR-14	Hot Creek Canyon, Hot Creek Range (loc. *8*).	0.2	Phosphatic dolomite-	N.d.	1.28	7.7

See footnote at end of table.

TABLE 2.—*Analyses of phosphatic rock samples, Nye County, Nev., and adjacent areas*—Continued

Laboratory No.	Field No.	Locality (fig. 1)	Thickness (feet)	Lithology	P_2O_5 analyses		Acid insolubles
					Colorimetric	Volumetric	
		SILURIAN					
		Unnamed dark-gray dolomite					
D 131126	TY67CLR-123	Near Old Dominion mine, Hot Creek Range (loc. *8*).	0. 2	Phosphatic dolomite.	2. 26	2. 30	5. 97
131127	124	-----do-----	. 2	-----do-----	1. 64	1. 78	12. 00
132488	TY68CLR-8A	Hot Creek Canyon, Hot Creek Range (loc. *8*).	. 1	-----do-----	5. 40	5. 42	14. 4
		Roberts Mountains Formation					
D 138323	TM68151	Copenhagen Canyon, Monitor Range (loc. *3*).	2. 5	Phosphatic limestone.	N.d.	6. 01	N.d.
		Masket Shale of Kay and Crawford (1964)					
D 136443	19693-9A	Near crest of Toquima Range (loc. *5*).	2. 0	Calcareous siltstone.	N.d.	1. 0	78. 2
		PERMIAN(?)					
		Unnamed unit					
D 136437	P-9A	Danville Canyon, Monitor Range (loc. *6*).	0. 2	Phosphatic sandstone.	N.d.	6. 1	76. 4
M 105472	15368-3	-----do-----	N.d.	-----do-----	N.d.	6. 34	N.d.
D 136438	P-9B	-----do-----	. 1	Calcareous siltstone.	N.d.	. 32	54. 2

[1] Nodule.

Ordovician rocks

Phosphatic material has been found in several dominantly carbonate units of Ordovician age, mainly in northern Nye County and in the Antelope Range of southern Eureka County. At several of the occurrences small grab samples were taken and analyzed for P_2O_5 and acid insolubles (table 2).

In the area south of Tybo Canyon (fig. 1, loc. *9*) the basal 115 feet of the Goodwin Limestone of the Pogonip Group (table 1) consists of platy- to slabby-weathering limestone, which contains a few thin zones of dark-gray to black phosphatic material. One typical zone has been sampled, and pertinent analytical data are reported in table 2 (sample D 133019). The phosphate generally occurs as small pellets and nodules, as a replacement of brachiopod shells, and as finely disseminated material in the rock matrix.

The uppermost part of the Goodwin Limestone and basal beds of the overlying Ninemile Formation are partly phosphatic in the Antelope Range (fig. 1, loc. *3*), although the phosphate is very inconspicuous in outcrop and can be detected easily only with the application of ammonium molybdate solution. The authors used this simple field test extensively. For a description of the test, see Shapiro (1952). For a detailed description of the Goodwin Limestone and the Ninemile Formation in the Antelope Range, see Merriam (1963). In the area visited by the authors, the top of the Goodwin is marked by a zone of light- to medium-gray chert estimated to be about 100 feet thick. Phosphatic rocks below the chert (table 2, sample D 136433) range in lithology from silty limestone to calcareous siltstone and shale, and phosphatic rocks above the chert (table 2, sample D 136434), representing the basal part of the Ninemile Formation, are similar in lithology but contain a larger amount of silty to shaly material. In thin section phosphate is observed to occur in small spherical or irregular sand-sized pellets and stubby rod-shaped grains, and these, along with varying amounts of sand-sized quartz and glau-

conite(?) grains, are embedded in a fine silty carbonate matrix.

In the Hot Creek Range a persistent phosphatic zone occurs near the top of the Hanson Creek Formation (table 1); the Hanson Creek is a thin dolomitic unit underlying the dark-gray dolomite. This zone is 10–15 feet thick and contains scattered dark phosphatic material in small amounts. A small grab sample collected in Hot Creek Canyon contained minor amounts of P_2O_5 (table 2, sample D 133018). The Hanson Creek is accepted as Ordovician in age. According to F. G. Poole (oral commun., 1967), this part of the formation may represent the base of the Silurian, for it lies above a sandy zone that persists over a broad region and may approximate the Ordovician-Silurian boundary.

On the east flank of the Toquima Range (fig. 1, loc. *4*) the Caesar Canyon Limestone of Kay and Crawford (1964) contains phosphate. A good exposure was measured in August Canyon and found to contain about 84 feet of interbedded limestone and dark-gray to black carbonaceous shale. Most of the limestone appears to be phosphatic, and it is silty to sandy in varying degrees, ranging from a relatively pure limestone to calcareous siltstone and sandstone. In thin section (fig. 3) the phosphate is seen in three forms: (1) in silt-sized to small pebble-sized pellets of round to ovoid and irregular form, (2) as a replacement of fossil material, and (3) as fine disseminations through the carbonate matrix. Few of the pellets are wholly phosphate, and many contain calcite patches and silt- to sand-sized quartz grains. The phosphatized fossil material is fragmental and appears to be composed largely of trilobite, brachiopod, graptolite, and bryozoan remains.

Two samples of the limestone contain 9.9 and 6.4 percent P_2O_5 (table 2, samples D 136441 and D 136442).

The Copenhagen Formation, which is at least partly equivalent to the Caesar Canyon Formation (table 1), was examined and tested in the Antelope Range of northern Nye County (fig. 1, loc. *3*), but the results were wholly negative.

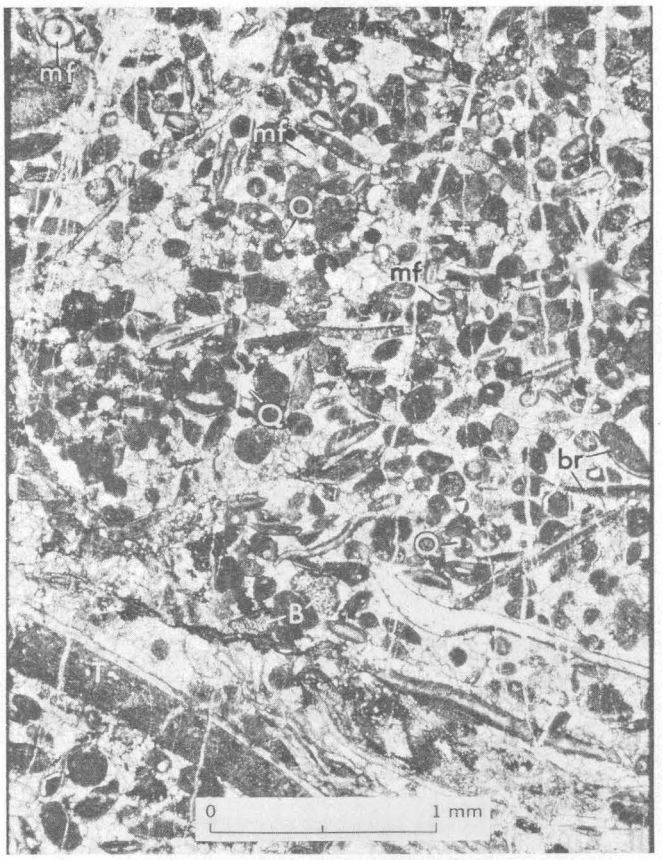

FIGURE 3.—Photomicrograph (plane light) of phosphatic silty limestone in Ordovician Caesar Canyon Limestone of Kay and Crawford (1964). Phosphate occurs as irregular pellets and fossil fragments and is finely disseminated throughout the carbonate matrix. Phosphatized fossil material appears to consist largely of trilobite (T) brachiopod (br), and bryozoan (B) remains. Many pellets are a mixture of phosphate and calcite; the two form alternate layers in round symmetrical pellets that may be microfossils (mf). Subparallel calcite veinlets are common, and calcite irregularly replaces phosphate. Scattered silt-sized quartz grains (Q) occur in the matrix and as inclusions in the phosphate pellets.

Silurian rocks

In the Hot Creek Range of northern Nye County the Silurian is represented by about 1,000 feet of dolomite (Lowell, 1965). The lower half is dark gray and is probably correlative with the Roberts Mountains Formation; the upper half is dominantly light gray, and most of it is probably correlative with the Lone Mountain Dolomite. Phosphate pellets and nodules occur in the lower part of the dark-gray dolomite (fig. 4), which is laminated to thin bedded, is somewhat silty, and is characterized by common nodular to lenticular dark-gray chert. The phosphatic zone appears to extend upward for 20–40 feet above a conspicuous basal cherty sequence. Thin-section study of the phosphatic rock reveals that most of the nodules are pellet aggregates and that many pellets are replaced in part by dolomite.

Two samples from the lower part of the dark-gray dolomite were collected near the Old Dominion mine in the southern Hot Creek Range (fig. 1, loc. *8*), and a third sample was collected from the same zone in Hot Creek Canyon (fig. 1, loc. *8*). All were analyzed for P_2O_5 and acid insolubles (table 2).

T. E. Mullens (oral commun., 1969) has recently discovered an 8-foot zone of phosphatic limestone in an exposure of the Roberts Mountains Formation (table 1) in Copenhagen Canyon in the Monitor Range in southern Eureka County (fig. 1, loc. *3*). The zone lies just above the basal cherty sequence, which in that area is

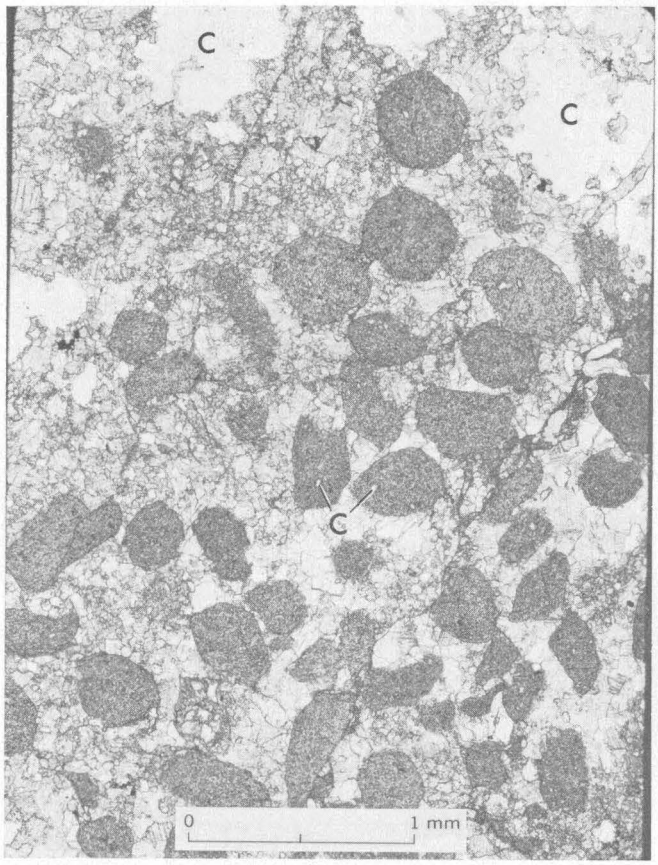

FIGURE 4.—Photomicrograph (plane light) of phosphatic layer in Silurian dolomite. Irregular structureless phosphate pellets occur in fine-grained dolomite matrix. Light areas in upper half of photograph are chert (C), and some pellets appear to contain small chert grains as inclusions. Pellets are dark brown and largely opaque, but contain numerous flecks of, and may be partly rimmed by, lighter anisotropic phosphate.

about 100 feet thick. The upper 2.5 feet of the phosphatic zone contains 6.01 percent P_2O_5 (table 2, sample D 138323); the remainder of the zone has not yet been sampled.

PHOSPHATE OCCURRENCES IN DETRITAL-VOLCANIC ASSEMBLAGE ROCKS

Phosphate in small amounts has been found in several dominantly clastic units of Ordovician, Silurian, and late Paleozoic age that can be assigned to the western detrital-volcanic assemblage.

Ordovician rocks

An allochthonous unit known as the Vinini Formation (table 1) is widely distributed in northern Nye County and the area to the north. It is partly equivalent to the Pogonip Group, having an Early and Middle Ordovician age, and ranges in lithology from sandstone and siltstone to black shale, bedded chert, and limestone. It occurs only as remnants of a major thrust plate. One such remnant was inspected in the vicinity of Vinini Creek at the type locality of the formation, on the east slope of the Roberts Mountains of central Eureka County (fig. 1, loc. *1*; Merriam and Anderson, 1942). In that area the formation consists of black carbonaceous shale and some limestone and bedded black chert. The shale and an enclosed spherical phosphate nodule measuring about 1 inch in diameter (table 2, samples D 136436 and D 136435, respectively) were analyzed for P_2O_5 and acid insolubles, and a semiquantitative spectrographic analysis was made of a sample of the shale (table 3, sample D 136387).

The Toquima Formation, of Ordovician age, and the underlying Zanzibar Limestone of Ordovician(?) age (table 1; Ferguson, 1924) were examined in the Toquima Range, about 1 mile west of Manhattan and near the Flowers mercury mine in Antone Canyon, and in the Toiyabe Range near the mouth of Wall Canyon. These localities contain almost no phosphate. A fourth and more promising locality lies on the east flank of the southern Toquima Range, just east of Belmont (fig. 1, loc. *7*). Bedrock here is largely a graptolitic black, platy to phyllitic, carbonaceous shale, and contains some scattered thin layers of laminated to thin-bedded limestone. A small grab sample of the shale (table 2, sample D 136439) contains 3.8 percent P_2O_5; this sample also received semiquantitative spectrographic analysis and is reported in table 3 (sample D 136388).

Silurian rocks

In the central part of the Toquima Range the lower part of the Silurian is represented largely by the Masket Shale (table 1), which was named by Kay and Crawford (1964). This unit was examined in Mill Canyon on the east flank of the range, and near the crest of the range on the divide between East and West Northumberland Canyons (fig. 1, loc. *5*). In the latter area the rock consists of buff-weathering calcareous siltstone and subordinate amounts of chert and dark-gray shale. A 2-foot channel sample of the siltstone contained minor amounts of P_2O_5 (table 2, sample D 136443).

In Mill Canyon the authors tested the Bastille Limestone Member of the Masket Shale with ammonium molybdate solution and found that many beds, particularly in the lower part, are phosphatic. Unfortunately, no analyses of this material have been obtained. The Masket Shale is underlain by the Gatecliff Formation of Kay and Crawford (1964) (table 1); the cherty unit at the top of the Gatecliff, and a few feet of dolomite underlying the chert, also proved to be phosphatic. It is possible that this sequence is in part Ordovician and equivalent to the upper part of the Hanson Creek Formation, and in part Silurian and

TABLE 3.—*Semiquantitative spectrographic analyses of phosphatic rock*

[G, greater than 10 percent; N.d., not determined; N, not detected at limit of determination or at value shown in parentheses; L, detected, but below limit of determination. Results in percent are to be identified with geometric brackets whose boundaries are 1.2, 0.83, 0.56, 0.38, 0.26, 0.18, 0.12, and so forth, but are reported arbitrarily as midpoints of these brackets: 1.0, 0.7, 0.5, 0.3, 0.2, 0.15, 0.1, and so forth. The precision of a reported value is approximately plus or minus one bracket at 68-percent confidence level, or two brackets at 95-percent confidence level. Elements looked for but not detected: As, Bi, Cd, Dy, Er, Eu, Ge, Gd, Hf, Ho, In, Li, Lu, Pd, Pr, Pt, Re, Sb, Sm, Ta, Tb, Te, Th, Tl, Tm, U, and W. Analyses by J. L. Finley, Leon A. Bradley, D. J. Grimes, and Chris Heropoulos]

Stratigraphic unit	Hales Limestone		Vinini Formation	Toquima Formation	Caesar Canyon Limestone of Kay and Crawford (1964)			Unnamed Permian(?) unit
Lithology	Phosphatic limestone		Phosphatic shale		Phosphatic limestone	Shale	Phosphatic calcareous siltstone	Phosphatic sandstone
Laboratory No.	D131132	D131133	D136387	D136388	D136389	D136390	AEC-235	M105472
Field No.	67HWD8-2	67HWD-22	P-6C	P-10A	16351-5	16351-8A	16351-1B	15368-3
In percent								
Fe	0.2	0.5	0.5	2	5	1.5	7	1.5
Mg	0.1	0.1	0.2	2	0.3	0.5	0.7	0.15
Ca	G	G	5	5	G	0.5	15	5
Ti	0.01	0.07	0.03	0.3	0.1	0.5	0.07	0.07
Si	1.5	2	G	G	5	G	N.d.	G
Al	1.5	1.5	0.5	3	2	G	N.d.	1.5
Na	0.07	0.1	0.1	0.15	0.15	0.2	N.d.	0.07
K	N	N	N	3	1	7	N.d.	N
P	L	5	1	2	10	N	N.d.	3
In parts per million								
Mn	3,000	700	70	50	20	20	20	700
Ag	N	N	L	2	N	N	0.5	4.7
Au	N	N	N	N	N	N	N(10)	N
B	N	N	50	100	500	200	70	100
Ba	70	150	500	3,000	1,000	5,000	700	700
Be	N	N	N	2	1.5	2	1	N
Co	N	5	N	N	N	N	N	2
Cr	7	70	50	200	100	150	100	100
Cu	5	7	70	200	50	15	30	50
La	30	150	N	70	300	50	150	100
Mo	N	50	L	20	20	N	15	N
Nb	N	N	N	L	N	L	N	N
Ni	3	15	50	150	200	20	100	15
Pb	10	15	10	20	10	20	15	15
Sc	N	N	N	10	15	10	7	5
Sn	N	N	N	N	N	N	N(10)	N
Sr	700	2,000	100	300	1,000	200	1,500	200
V	30	150	300	1,500	200	150	70	50
Y	30	300	20	70	500	50	150	150
Zn	N	N	N	1,000	N	N	200	N
Zr	10	50	N	100	100	200	150	70
Ce	N	N	N	N	300	N	N.d.	N
Ga	N	N	N	20	10	50	N.d.	7
Yb	1	10	2	10	15	5	N.d.	5
Nd	N	N	N.d.	N	200	N	N.d.	N

equivalent to the basal cherty unit of the overlying dark-gray dolomite in the Hot Creek Range.

Permian(?) rocks

Reconnaissance mapping in the Monitor Range by Kleinhampl and Ziony (1967) led to the discovery of a significant phosphatic zone in a thick, probably allochthonous sequence that occurs in the Danville Canyon (fig. 1, loc. *6*) area and that was mapped originally as the Vinini(?) Formation. At Danville, the allochthonous rocks, about 1,000 feet thick, consist of gray, green, and reddish-brown chert, commonly laminated, and some brown siliceous siltstone and sandstone and a little partly silicified limestone. In the vicinity of Sawmill Canyon to the north, the rocks may be at least twice as thick; they consist of abundant dark-gray siliceous shale and some intercalated limestone and very sparse greenstone(?). Slightly farther north, these rocks rest on several hundred feet of quartz-sandy limestone conglomerate.

The phosphate at Danville is present in siltstone and sandstone beds in a poorly exposed cherty section; it is at least 2 feet, but no more than 5 feet, thick. Either a fault repeats the phosphatic zone or more than one

phosphatic zone occurs with a stratigraphic separation of perhaps as much as 500 feet. Apatite, which occurs largely as small pellets that weather to light gray and white, and chert and quartz grains are the major constituents of the phosphatic beds. In thin section (fig. 5) the pellets are seen to range from medium to dark brown and to be commonly round to ovoid, although many are irregular in shape. Many have inclusions of chert and silt-sized quartz grains, and some exhibit a concentric structure and can be classed as oolites. Slender rod-shaped sponge spicules and, very rarely, microforaminifera also appear as inclusions in the pellets. Small selected grab samples of phosphatic sandstone and calcareous siltstone were analyzed for P_2O_5 and acid insolubles (table 2).

The strata are considered Permian(?) in age because reworked fragments of the conodont *Gondolella* sp., a late Paleozoic form, are present in the phosphatic siltstone and sandstone (John Huddle, written commun., 1965). Also, the lithology of the unit bears a resemblance to that of the Permian rocks, of Phosphoria age, of northeastern Nevada and adjoining States. Such an age would extend the present-known western and southern limits of Permian phosphate deposition in the Cordilleran geosyncline. The extension suggests that a transitional marine environment of late Paleozoic age, perhaps Phosphoria equivalent, developed virtually parallel to the strike of the Cordilleran miogeosyncline in a southward-protruding lobe from the main basin of phosphate deposition in northeastern Nevada and Utah (Cheney and others, 1956; McKelvey and others, 1959, fig. 2; Roberts and others, 1965, p. 1944, fig. 14). Such a southern bulge might be due to the normal configuration of the depositional basin or to subsequent major structural dislocation. Additional studies should answer some of the questions raised by the Permian(?) strata found at Danville Canyon. K. B. Ketner of the U.S. Geological Survey has recently found significant amounts of phosphate in the Permian rocks of northeastern Nevada (written commun., 1968). The phosphate occurs in a thick section of siltstone, limestone, and chert, which is widely exposed in central Elko County.

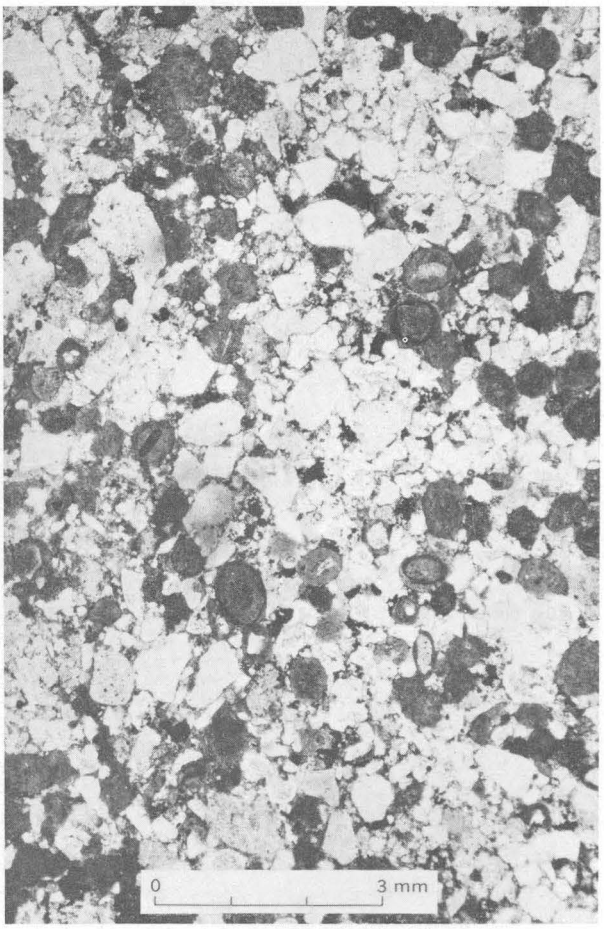

FIGURE 5.—Photomicrograph (plane light) of phosphatic sandstone of Permian(?) age. Dark phosphate grains (some oolitic) are scattered among light subangular to subrounded grains of quartz and chert.

MODE OF OCCURRENCE AND COMPOSITION OF THE PHOSPHATE

Although the phosphatic rocks described in this report vary greatly in age and formed in environments ranging from eugeosynclinal to miogeosynclinal, the mode of occurrence of the phosphate was much the same (fig. 2). The phosphate occurs in three principal ways: (1) in small structureless pellets, oolites, and nodules (which may be pellet aggregates); (2) as fine disseminations through the rock matrix; and (3) as a replacement of fossil material. The pelletal form is the most common, and the pellets are silt to sand size and symmetrical (round or ovoid) to irregular in form. Some pellets contain fine grains of quartz and other minerals and fossil fragments, and these may have served as nuclei for the deposition of apatite. The phosphatic material is generally dark brown to black in outcrop, but may weather to light gray or white. It is light to dark brown and generally isotropic in thin section. The dark color and a characteristic fetid odor are probably due to the presence of organic matter. Only a small part of the material appears to be anisotropic.

An X-ray analysis of a sample of phosphatic limestone from the Cambrian Hales Limestone was made by Jerry D. Tucker of the U.S. Geological Survey. According to James B. Cathcart, who interpreted the results for the authors (oral commun., 1968), the rock consists, in order of abundance, of calcite, apatite, quartz, and some organic material. The phosphate mineral is

carbonate-fluorapatite, which is the phosphate mineral of all marine phosphorites (Altschuler, Cisney, and Barlow, 1953).

Marine phosphorites and the carbonaceous shales with which they are commonly associated contain abnormal concentrations of several minor elements, and for this reason the authors obtained spectrographic analyses for eight samples from central Nevada (table 3). These rocks vary in lithology, and range from phosphatic limestone to phosphatic calcareous siltstone, phosphatic sandstone, phosphatic shale, and shale. The shales are lowest in phosphate and have a P_2O_5 content ranging from almost 0 to about 3 percent. The Nevada samples generally contain abnormal concentrations of the same elements (U, V, Cr, Ni, Zn, Mo, Ag, and Se) that Pettijohn (1958, p. 473) lists as occurring in phosphate deposits. Some metals in the Phosphoria Formation, including Ag?, As, Cd, Cr, Cu, Mo, Ni, Sb, Se, V, and Zn, are associated with organic matter (Gulbrandsen, 1966, p. 774–775); other metals, for example, Sr, U, and Y and the rare earths, La, Nd, Y, and Yb, substitute for Ca in the structure of the apatite.

The Ordovician shale from Belmont (table 3, sample D 136388), in the Toquima Range, carries the greatest amounts of the trace elements listed by Pettijohn and Gulbrandsen, particularly Zn, although the sample was collected very close to the site of one of the major smelters in the district and more sampling would be required to rule out the possible effect of contamination. Several samples appear to contain relatively few elements, and not all of those listed by Pettijohn and Gulbrandsen. Contents of the rare-earth element La and the rare-earth-related Y are consistently high in most of the Nevada samples (table 3), but the other rare earths and Sc are more sporadic. La in the more phosphatic rocks is about the same as the average for the Phosphoria Formation (Gulbrandsen, 1966), but is distinctly lower in the shale samples, which may be natural in view of the probable substitution of La in the apatite lattice. Ba, which is uncommonly low in the Idaho phosphate (Gulbrandsen, 1966, p. 776), is also low in the more phosphatic Nevada samples but is relatively high in the shale samples. This is to be expected, perhaps, if some Nevada barite deposits have a sedimentary origin and are associated with siliceous eugeosynclinal deposits, as postulated by Shawe, Poole, and Brobst (1969).

CONCLUSIONS

The phosphate investigations discussed in this report have been very limited in scope, for they are a by-product of areal geologic mapping initiated for quite different purposes. Nevertheless, they have led to a few general conclusions.

1. Phosphate was deposited in the Cordilleran geosyncline in the central Nevada region throughout much of the history of the geosyncline. Host rocks range in age from Middle Cambrian to Permian(?).

2. Phosphate is geographically widespread in the central Nevada region, for concentrations have been found in rocks of the detrital-volcanic (eugeosynclinal), transitional, and carbonate (miogeosynclinal) sedimentary environments. Some of the observed phosphatic rocks obviously persist for long distances.

3. The discoveries discussed in this report are relevant to stratigraphic studies in the southern Great Basin, because most of the phosphate concentrations are associated with lithologic breaks in the stratigraphic section, which commonly are also formational and (or) systemic boundaries (compare with Pettijohn, 1957, p. 474). Phosphate may have been deposited more or less continuously in the geosyncline, accumulating in significant amounts only during the periods when there was little deposition of carbonates or clastic material. In places the phosphatic materials appear to have been reworked.

Other studies relating to the subject of this report that may be of interest to the reader are those by Ferguson (1924), McKelvey (1967), and McKelvey, Swanson, and Sheldon (1953).

REFERENCES

Altschuler, Z. S., Cisney, E. A., and Barlow, I. H., 1953, X-ray evidence of the nature of carbonate-apatite *in* Origine des gisements de phosphates de chaux: Internat. Geol. Cong., 19th, Algiers 1952, Comptes rendus, sec. 11, pt. 11, p. 9.

Barnes, Harley, Houser, F. N., and Poole, F. G., 1963, Geologic map of the Oak Spring quadrangle, Nye County, Nevada: U.S. Geol. Survey Geol. Quad. Map GQ–214.

Barnes, Harley, and Christiansen, R. L., 1967, Cambrian and Precambrian rocks of the Groom district, Nevada, southern Great Basin: U.S. Geol. Survey Bull. 1244–G, p. G1–G34.

Cheney, T. M., McKelvey, V. E., and Gere, W. C., 1956, Fusulinid-bearing rocks in Sublett Range, southern Idaho: Am. Assoc. Petroleum Geologists Bull., v. 40, no. 7, p. 1716–1719.

Ferguson, H. G., 1924, Geology and ore deposits of the Manhattan district, Nevada: U.S. Geol. Survey Bull. 723, 163 p.

Gulbrandsen, R. A., 1966, Chemical composition of phosphorites of the Phosphoria Formation: Geochim. et Cosmochim. Acta, v. 30, no. 8, p. 769–778.

Kay, Marshall, and Crawford, J. P., 1964, Paleozoic facies from the miogeosynclinal to the eugeosynclinal belt in thrust slices, central Nevada: Geol. Soc. America Bull., v. 75, no. 5, p. 425–454.

Kleinhampl, F. J., and Ziony, J. I., 1967, Preliminary geologic map of northern Nye County, Nevada: U.S. Geol. Survey open-file map, scale 1:200,000.

Lowell, J. D., 1965, Lower and Middle Ordovician stratigraphy in the Hot Creek and Monitor Ranges, central Nevada: Geol. Soc. America Bull., v. 76, no. 2, p. 259–266.

McKelvey, V. E., 1967, Phosphate deposits: U.S. Geol. Survey Bull. 1252–D, p. D1–D21.

380–189 O—70——5

McKelvey, V. E., Swanson, R. W., and Sheldon, R. P., 1953, The Permian phosphorite deposits of western United States, *in* Origine des gisements de phosphates de chaux: Internat. Geol. Cong., 19th, Algiers 1952, Comptes rendus, sec. 11, pt. 11, p. 45–64.

McKelvey, V. E., and others, 1959, The Phosphoria, Park City, and Shedhorn formations in the western phosphate field: U.S. Geol. Survey Prof. Paper 313–A, 47 p.

Merriam, C. W., 1963, Paleozoic rocks of Antelope Valley, Eureka and Nye Counties, Nevada: U.S. Geol. Survey Prof. Paper 423, 67 p.

Merriam, C. W., and Anderson, C. A., 1942, Reconnaissance survey of the Roberts Mountains, Nevada: Geol. Soc. America Bull., v. 53, no. 12, pt. 1, p. 1675–1727.

Pettijohn, F. J., 1957, Sedimentary rocks, 2d ed.: New York, Harper & Bros., 718 p.

Roberts, R. J., Crittenden, M. D., Jr., Tooker, E. W., Morris, H. T., Hose, R. K., and Cheney, T. M., 1965, Pennsylvanian and Permian basins in northwestern Utah, northeastern Nevada, and south-central Idaho: Am. Assoc. Petroleum Geologists Bull., v. 49, no. 11, p. 1926–1956.

Shapiro, Leonard, 1952, Simple field method for the determination of phosphate in phosphate rocks: Am. Mineralogist, v. 37, nos. 3–4, p. 341–342.

Shawe, D. R., Poole, F. G., and Brobst, D. A., 1969, Newly discovered bedded barite deposits in East Northumberland Canyon, Nye County, Nevada: Econ. Geology, v. 64, no. 3, p. 245–254.

PHLOGOPITE AND ACTINOLITE IN LATITIC DIKE ROCKS, BINGHAM MINING DISTRICT, UTAH

By WILLIAM J. MOORE, Menlo Park, Calif.

Abstract.—Latitic dike rocks exposed in underground workings west of the Bingham stock contain primary phlogopite and biotite with actinolite, augite, hornblende, magnetite, and (or) traces of hematite. About 5 percent of the mica occurs in composite crystals: cores of brownish-yellow biotite, some markedly resorbed, are rimmed by euhedral overgrowths of pale-yellowish-green phlogopite. These rocks have a fluidal texture resulting from the subparallel alinement of acicular actinolite in the groundmass. Although not undersaturated, as are most igneous rocks containing phlogopite (ultramafics, carbonatites), the latite dikes contain slightly less SiO_2 and Al_2O_3 and slightly more MgO, total alkalies, and CO_2 than the larger monzonitic stocks in the Bingham Canyon area. The model proposed to explain textural and compositional features of the dikes requires assimilation of magnesian carbonate rocks by a latitic melt with oxygen fugacities controlled externally during later stages of crystallization.

Segments of several northeast-trending latitic dikes are exposed in underground workings west of the Bingham stock. The dikes intrude monzonite of the Last Chance stock and enclosing Pennsylvanian sedimentary rocks. The dikes were not mapped by the author at the surface, but recent work by Bray (1969) indicates that they are extensions of mineralized dikes, exposed in the Utah Copper pit, that have been sampled on several occasions. The present work was undertaken to establish the mineral and chemical composition of the unaltered dike rocks.

GEOLOGIC SETTING

The area studied underground is part of the Utah Metal and Tunnel Co. 450 level, owned by The Anaconda Co. Permission to work in this area and a surveyed base map of the workings were obtained from Anaconda; this assistance and subsequent discussions with Anaconda personnel are gratefully acknowledged. A reconnaissance geologic map was prepared at a scale of 1 inch=200 feet (fig. 1), and spot samples were collected, together with samples along detailed traverses across several dike segments.

Sedimentary rocks of figure 1 consist largely of Upper Pennsylvanian quartzite and cherty limestone. The banded, cherty limestone shown at the west edge of the map, informally termed the Jordan, is one of two major ore horizons in the district; it dips moderately to the northwest in the south limb of the Bingham syncline. Uniformly bleached and locally silicated beds of limestone with bedded chert nodules apparently grade away from the Last Chance stock into a distinctive black-and-white banded zone of incipiently metamorphosed limestone.

The west-trending lobe of the Last Chance stock exposed in the center of the map area is a dark-gray augite-biotite monzonite, identical in texture and composition with the main mass of the stock studied about 1 mile to the southeast in mine workings of the U.S. Smelting, Refining, and Mining Co. (Moore and others, 1968). Alteration consists of spotty occurrences of pyrite, montmorillonite, and (or) chlorite along northeast-trending fractures and shear zones.

Several observations bear on the mechanism of dike emplacement. The dike-wallrock contacts, which are more clearly defined underground than at the surface, are, in most instances, sharp and irregular. Included fragments of quartzite or monzonite and cognate xenoliths in border zones of the dikes suggest that brecciation accompanied forcible emplacement. Perhaps the best example of this is at location *B* (fig. 1), where rounded monzonite fragments as large as 5 by 2 feet occur near the contact in a matrix of silicified latite cut by pyrite-calcite veinlets. Similarly, a 75-foot zone of narrow pebble dikes occurs immediately northwest of the dike contact at sample locality 2. One dike contains sedimentary fragments of mixed lithology with a matrix composed, in part, of latite porphyry; another contains several well-rounded 2-inch porphyry fragments. Apparently the pebble dikes formed during emplacement and crystallization of the latite dike.

U.S. GEOL. SURVEY PROF. PAPER 700-C. PAGES C61-C69

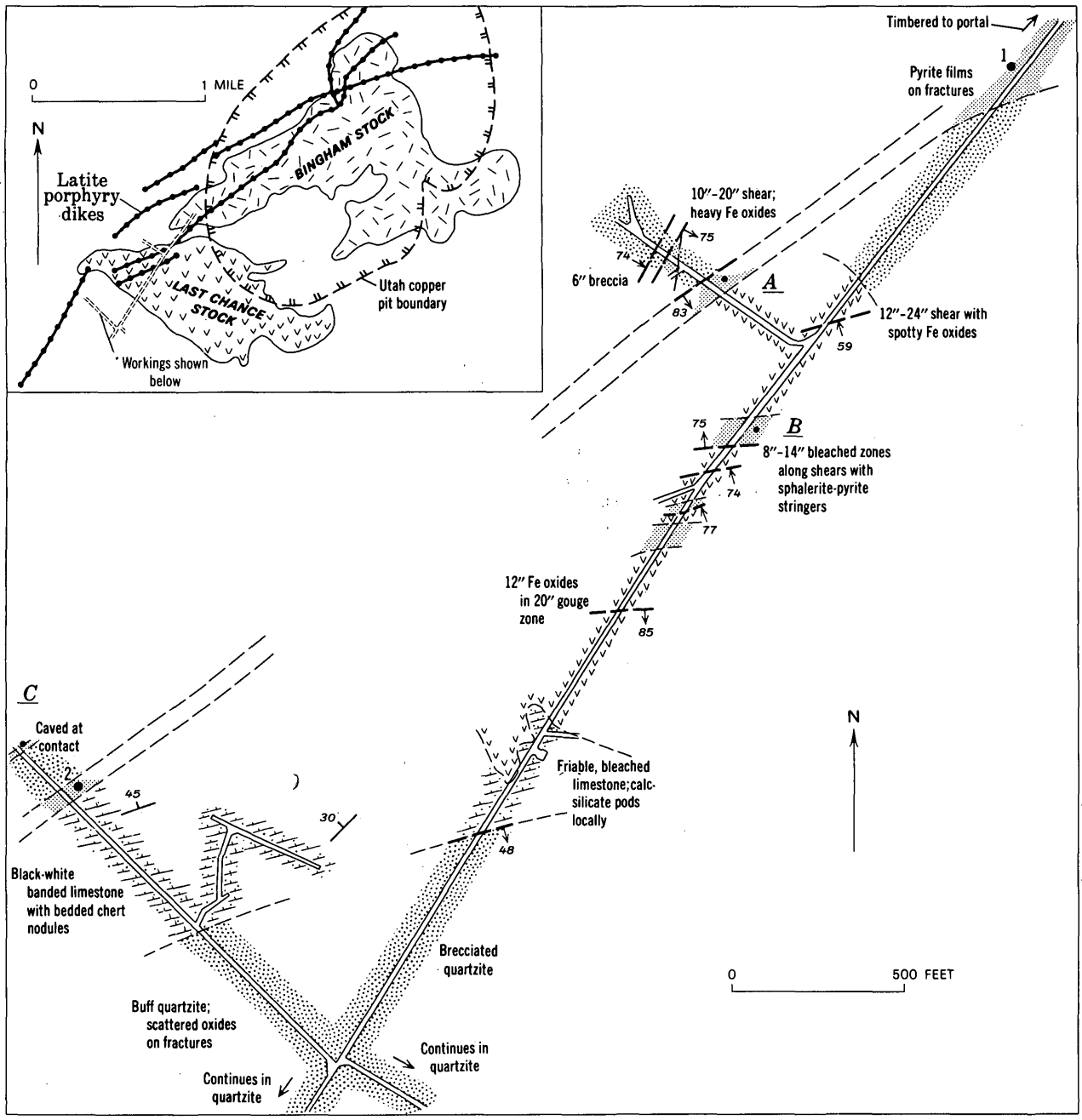

FIGURE 1.

Fragmentation and rounding presumably occurred as a result of explosive release of fluids derived from the crystallizing magma. This implies that the melt was water saturated, at least during terminal stages of crystallization, and that the depth of emplacement was shallow enough for fluid pressure to exceed confining pressure.

In hand specimens the dike rocks are greenish gray and have a porphyritic texture. Megascopic phenocrysts commonly are less than 1 cm long and are randomly oriented. Phenocryst minerals, in order of decreasing abundance, are plagioclase, hornblende, biotite, phlogopite, and alkali feldspar. Phenocrysts make up generally less than half the volume of the rock.

Mineralogical similarities suggest that the dikes represent a single magmatic pulse. K-Ar ages of biotite and phlogopite from sample location 1 (fig. 1) are 37.2±1.2 m.y. and 37.3±1.2 m.y., respectively; ages of igneous rocks in the Bingham area range from 38.9 m.y. to 32.0 m.y. (Moore and others, 1968).

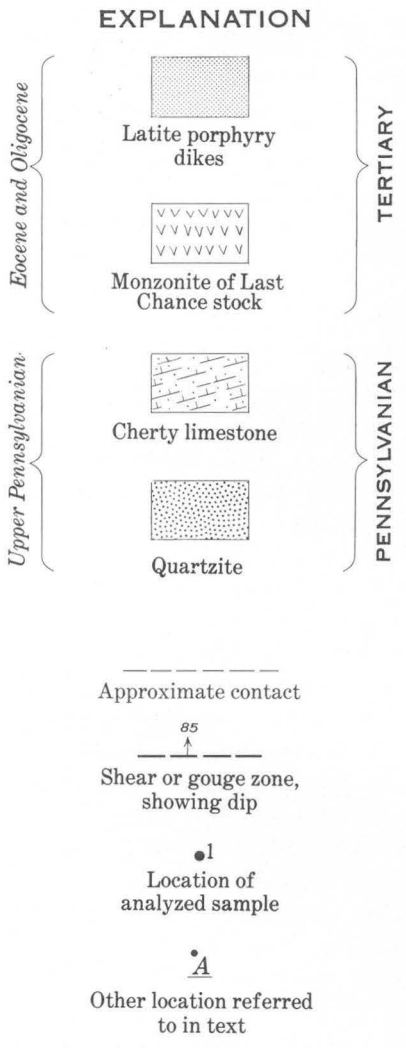

FIGURE 1.—Plan of workings, 450 level (7,000 ft. elev.), Utah Metal and Tunnel Co., Bingham mining district, Utah.

PETROGRAPHY OF THE DIKE ROCKS

The petrography of the dike rocks will be discussed largely in terms of major phenocryst minerals: alkali feldspar and plagioclase, phlogopite, biotite, augite, and (or) hornblende. In thin sections the feldspar phenocrysts have euhedral to subhedral forms and an average length of about 2 mm. Plagioclase commonly displays oscillatory zoning and has an approximate range in composition (by the extinction-angle method for sections cut normal to [010]) of An_{28} to An_{34}. Alkali feldspar phenocrysts are microperthitic orthoclase. The compositions of fragments handpicked from a single sample have been determined by the X-ray methods of Wright and Stewart (1968). The K-rich perthite host, and the bulk phase homogenized by dry heating at 1,000°C for 24 hours contain 90 weight percent orthoclase and 72 weight percent orthoclase, respectively.

The larger mica phenocrysts consist, in about equal amounts, of phlogopite and biotite displaying pseudohexagonal forms. Phlogopite makes up most of the smaller crystals that grade into tiny acicular crystals in the groundmass. Inclusions of zircon, apatite, and traces of rutile are common in the biotite crystals and absent in phlogopite. Rare plates of transparent, blood-red hematite are observed in both micas. Composite mica crystals (fig. 2*A*) make up less than 0.4 percent by volume of the dike rocks. Distribution of phlogopite in the dike rocks is not uniform. At locations 1 and *A* (fig. 1) the mica is found in each section cut across the width of the dikes; at locations 2, *B*, and *C*, it is found only in sections cut from rocks of the border zone. The other dike segments contain no more than trace amounts of phlogopite and will be largely disregarded in the remainder of this report.

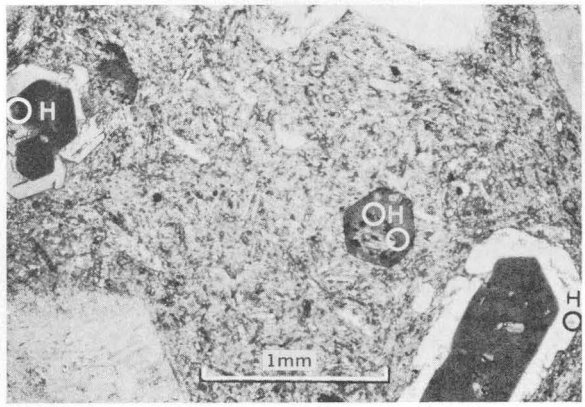

A

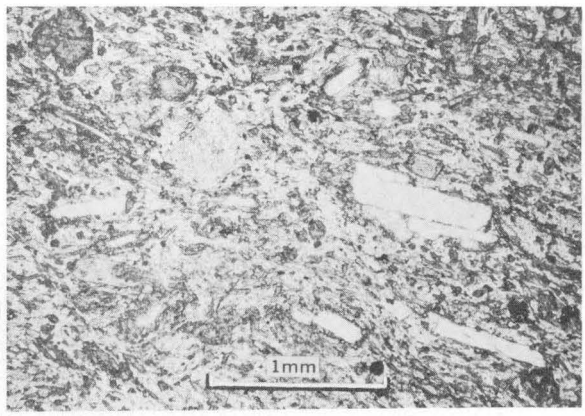

B

FIGURE 2.—Photomicrographs of latitic dike rocks. *A*, Biotite, composite mica, and plagioclase phenocrysts in felted groundmass composed of finely crystalline phlogopite, actinolite, and alkali feldspar. Hematite inclusions, H, in mica crystals are circled. Sample 2 of table 2. *B*, Subparallel alinement of large phlogopite laths and acicular actinolite in groundmass characterizes fluidal texture in dike rocks. Sample 1 of table 2.

The biotite cores of composite crystals are either sharply euhedral (fig. 3*A*) or variably rounded by resorption. In general, the more intricately embayed cores display paler pleochroic colors (fig. 3*B*). In a few crystals a dark-yellow-green transition zone separates core and rim micas.

Optical properties of the micas are summarized in table 1. Both display normal pleochroism with maximum absorption in the γ = Z direction. Color zoning was noted in several phlogopite crystals, a darker central part being separated by a moderately sharp boundary from a lighter outer part of lower refractive index.

The third most abundant phenocryst mineral after plagioclase and mica is either yellow-green hornblende or clinopyroxene; hornblende is less abundant than diopsidic augite in the samples discussed in detail here. Fibrous crystals of pale-yellow to colorless actinolite

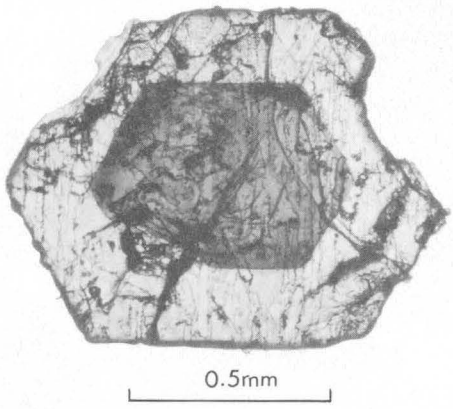

A

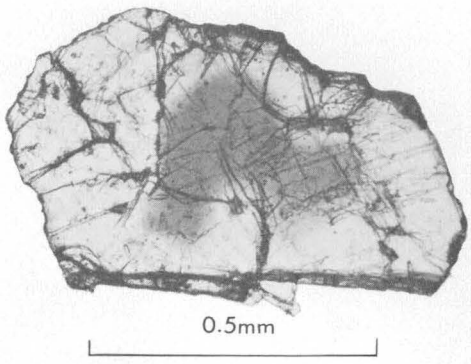

B

FIGURE 3.—Composite mica crystals hand-picked from phlogopite concentrate. *A*, Dark euhedral biotite core with euhedral phlogopite rim. Edges of crystal broken during grinding. *B*, Fragment of pseudo-hexagonal crystal with resorbed biotite core of indeterminate form rimmed by phlogopite. Pale pleochroic colors of core mica suggest preferential loss of Fe and (or) Ti through reaction with magma prior to rimming.

TABLE 1.—*Optical properties of biotite and phlogopite from latitic dike rocks, Bingham mining district, Utah*

	Biotite	Phlogopite
Pleochroic colors	X=pale brownish yellow. Y=Z=dark reddish brown.	X=pale yellow Y=Z=pale greenish yellow.
Refractive index, $(\beta+\gamma)/2$.	1.638 ± 0.002	1.605 ± 0.002
$2V$	$\approx 0°$	$\approx 5°–10°$

($Mg_{0.70}Fe^{+2}_{0.25}Fe^{+3}_{0.05}$) are observed only in the dike extending between sample locations 1 and 2 (fig. 1), giving this particular rock a distinctive fluidal appearance in thin section. The mineral is almost identical in composition with actinolite that occurs locally in monzonite adjacent to large limestone inclusions in the Bingham stock.

Most sections contain rectangular aggregates of calcite with lesser amounts of quartz or fibrous amphibole distinct from actinolite. These aggregates, several of which are surrounded by laths of phlogopite, are presumed to be deuteric reaction products after augite or hornblende. Small patches of calcite in the groundmass likewise appear to be primary rather than post-magmatic additions.

This is not to imply that the dikes are, without exception, unaltered. Rocks in the vicinity of sample location 1 (fig. 1) are in the zone of propylitic alteration surrounding the Bingham porphyry copper deposit. Traces of pyrite occur as scattered grains and fracture coatings, and the calcic cores of some plagioclase phenocrysts are replaced by aggregates of epidote and quartz. Nevertheless, chemical differences between altered and unaltered parts of the same dike are slight.

The dike rocks commonly have a granular groundmass texture consisting of finely crystalline (about 0.04 mm) K-feldspar and plagioclase. Fluidal texture, characterized by subparallel orientation of small actinolite needles and phlogopite laths (fig. 2*B*), is observed only in the throughgoing dike in figure 1. A petrographic examination of eight samples across this dike at location 1 suggests that fluidal and microgranular types merge gradationally.

COMPOSITION OF THE DIKE ROCKS AND MICAS

The samples analyzed (table 2) represent widely separated exposures of a single dike; sample 1 was taken from the center of the exposure and sample 2 from border zone rocks at a quartzite contact. Included for comparison are average values for seven samples from the Last Chance stock, thought to approach the parent magma composition of the igneous rocks in the Bingham Canyon area (Moore and others, 1968).

TABLE 2.—*Composition of latitic dike rocks, Bingham mining district, Utah*

Sample No.	1	2	3
Field No.	63A-109	67U-33A	Last Chance stock (avg. of 7)
Chemical analyses (weight percent) [1]			
SiO_2	57.6	57.4	59.3
Al_2O_3	12.9	14.1	15.1
Fe_2O_3	2.0	1.5	2.3
FeO	3.0	2.3	3.4
MgO	6.3	5.3	4.1
CaO	5.9	5.6	5.5
Na_2O	4.5	4.0	3.7
K_2O	4.3	5.3	4.1
Total H_2O	1.20	1.70	.76
TiO_2	.61	.59	.85
MnO	.19	.10	.09
P_2O_5	.58	.45	.44
CO_2	.82	1.2	<.05
S	.36	<.04	<.04
Total	100.	100.	100.
Minor elements (weight percent) [2]			
B	<0.0007	0.0015	<0.0007
Ba	.2	.15	.2
Be	.0007	.0005	.0002
Ce	.03	.02	.02
Nd	.01	.007	.01
Co	.002	.002	.002
Cr	.05	.02	.01
Cu	.01	.01	.005
Ga	.002	.0015	.002
La	.015	.01	.015
Mo	.0007	.0003	.0005
Nb	.0015	.002	.0015
Ni	.05	.015	.005
Pb	.02	.007	.005
Sc	.002	.0015	.0015
Sr	.1	.15	.15
V	.015	.015	.01
Y	.002	.002	<.001
Yb	.0002	.002	.002
Zr	.02	.03	.02

Sample No.	1	2	3
Field No.	63A-109	67U-33A	Last Chance stock (avg. of 7)
CIPW norms			
Q	------	0.2	7.4
or	25.3	31.5	24.2
ab	38.0	34.0	31.3
an	2.3	4.9	12.9
mt	2.9	2.2	3.4
il	1.2	1.1	1.6
ap	1.4	1.1	1.0
wo	7.5	5.2	4.9
en	14.4	13.3	10.2
fs	2.3	2.2	3.1
ol	1.0	----	----
pr	.7	----	----
cc	1.9	2.7	----
Total	99.0	98.2	100.0
Modal analyses			
Quartz	----	----	7.1
K-feldspar	5.7	1.0	31.3
Plagioclase	2.6	16.2	32.3
Augite	4.3	6.3	10.1
Hornblende	----	----	7.5
Biotite	3.3	5.4	8.3
Phlogopite	5.6	4.6	----
Actinolite	29.2	14.4	----
Opaque	1.7	.8	2.7
Calcite	1.1	.8	----
Apatite	.2	.4	.7
Epidote	.9	----	----
Aphanitic groundmass	45.4	50.1	----
Total	100.0	100.0	100.0

[1] Analyses by rapid methods by U.S. Geological Survey analytical laboratories under the direction of Leonard Shapiro.
[2] Semiquantitative spectrographic analyses by Chris Heropoulos, U.S. Geological Survey. Results are reported in weight percent to the nearest number in the series 1, 0.7, 0.5, 0.3, 0.2, 0.15, 0.1, 0.07, . . .; these numbers represent approximate midpoints of group data on a geometric scale. The precision of a reported value is approximately plus or minus one interval about 68 percent of the time or two intervals 95 percent of the time. Elements looked for but not found: Ag, As, Au, Bi, Cd, Eu, Hf, Hg, In, P, Pd, Pt, Re, Sb, Sn, Ta, Te, Th, Tl, U, W.

In addition to phlogopite and actinolite, the only significant modal difference between the dike samples and stock is the presence of about 7 percent quartz in the stock. Differences in the proportion of feldspar are due largely to the nonuniform distribution of large phenocrysts.

In chemical composition the dike samples contain slightly less SiO_2, and more CO_2 and MgO than the average Last Chance monzonite, and have higher ratios of $(Na_2O+K_2O):Al_2O_3$. Comparable differences are reflected in percentages of Q, en, and an in the norms. The overall similarity in minor-element content of the dike samples and the stock is supporting evidence for consanguinity of these rocks. Noteworthy differences are limited to slight enrichment of Cr, Ni, and Pb in sample 1 (field No. 63A–109); lead may be present as inclusions of galena in pyrite.

Biotite and phlogopite were separated from a bulk sample of the dike rock at location 1 (fig. 1) by conventional heavy-liquid and magnetic methods. Composite mica crystals were concentrated preferentially in the phlogopite separate but made up less than 5 percent of the sample analyzed. In addition to a predictable decrease in the ratios of FeO and TiO_2 to MgO (table 3), the phlogopite is characterized by a twofold increase in F and a puzzling tenfold increase in Cr_2O_3 relative to the biotite. Rough calculations indicate that more than half of the Cr_2O_3 in sample 63A–109 is ac-

counted for in the phlogopite analysis; Cr presumably substitutes for Mg in the crystal lattice, as the mineral contains few inclusions other than rare hematite plates.

The Bingham micas appear to be enriched slightly in Ba and Ni and impoverished in Sc and Cu relative to minor-element data recently summarized by Lovering (1969) for 200 biotites from igneous rocks. Although two samples are hardly an adequate basis for generalizations, it is of interest to note that Cu concentrations of the micas give no positive indication of the nearby porphyry ore deposit.

The computer program described by Jackson, Stevens, and Bowen (1967) was used to calculate mineral formulas for the micas. Mg and Fe^{+2} make up 87–90 percent of the six-coordinated ions; total octahedral occupancy is slightly less than 6.0 ions. Likewise, the sum of 12-coordinated cations, of which K makes up at least 87 percent, is slightly less than 2.0. The sum of (OH+F) closely approaches, or slightly exceeds, the expected value of 4.0 ions. The largest single deviation from ideal compositions of the phlogopite-annite series is the presence of 0.8 F ions in the Mg-rich mica.

PROPOSED HISTORY OF DIKE EMPLACEMENT AND CRYSTALLIZATION

Petrographic features indicate a shift in mafic mineralogy at some intermediate stage of dike-rock crystallization from "normal" assemblages consisting of biotite with hornblende and (or) augite to magnesian assemblages characterized by phlogopite and Mg-rich actinolite. No single process can entirely account for the resulting chemistry and mineralogy of the dikes. Contamination of a latitic melt would appear necessary to explain the high concentrations of Mg andCO_2 in later stages of crystallization. Assimilation of dolomitic carbonate rocks is an obvious possibility; such rocks make up about 25 percent of the Cambrian section exposed in Ophir Canyon, 10 miles southwest of the Bingham Canyon area. Unexplained, however, is the lack of enrichment in calcium, either in anorthite content in the norm or anorthite content of the plagioclase phenocrysts.

Textural evidence of two types suggests that crystallization of biotite was terminated abruptly. The biotite cores of composite crystals are euhedral in most instances; furthermore, the proportion of biotite in late-stage, flow-oriented laths is small relative to biotite-to-total mica proportions in pseudohexagonal phenocrysts. If early-formed biotite phenocrysts reacted slowly with an Mg-rich contaminated melt, the expected frequency of resorbed and rimmed crystals would be greater than that actually observed. As most of the larger crystals are composed entirely of biotite or phlogopite, the possibility remains that a contaminated melt containing phlogopite crystals was mixed with a latitic melt containing biotite prior to final emplacement. Such mixing could account for the occurrence of both fluidal and microgranular textures in the exposure at location 1.

Recent experimental results may be used to place limits on pressure-temperature conditions at the time of dike emplacement. Wones and Eugster (1965, fig. 15) have calculated stability curves for biotites of given mole fraction annite, $KFe_3AlSi_3O_{10}(OH)_2$, coexisting with K-feldspar and with f_{O_2} buffered by mixtures of hematite+magnetite and quartz+magnetite+fayalite. By comparison with the solidus curve for the "granite minimum melting" composition, they estimate approximate stability limits for the micas in this melt.

Similar calculations have been made for the Mg-rich mica in the Bingham dike rocks by using equation 6'' derived by Wones and Eugster (1965, p. 1249):

$$\log f_{H_2O}=\frac{3428-4212(1-x)^2}{T}+\log x+\tfrac{1}{2}\log f_{O_2}+8.23 -\log a_1-\log a_2,$$

where

f_{H_2O}=fugacity of water,
f_{O_2}=fugacity of oxygen,
T=temperature (°K),
x=concentration of annite in biotite,
a_1=activity of $KAlSi_3O_8$ in alkali feldspar, and
a_2=activity of Fe_3O_4 in magnetite.

Oxygen fugacities used were those determined by the assemblage magnetite-hematite, and $a_{Fe_3O_4}$ in magnetite was taken to be 1.0. As an approximation, $a_{KAlSi_3O_8}$ in alkali feldspar was set equal to 0.71, the mole fraction of orthoclase in the analyzed phenocrysts. From table 3, concentration of annite in the Mg-mica (the fraction of Fe^{+2} in the octahedral layer) is about 0.10.

In figure 4 the resulting biotite stability curve is shown together with the water-saturated solidus curve, *TO*, for a tonalite from the central Sierra Nevada batholith (Piwinskii, 1968). Biotite with 0.10 mole fraction annite can exist stably in crystal-liquid mixtures of tonalitic bulk composition in the f_{H_2O}–temperature field between the curves.

Of the rocks studied by Piwinskii (1968), the tonalite is closest in chemical composition to the latites, although the dike rocks contain about twice as much MgO and two-thirds as much Al_2O_3. Thus the position of the latite solidus should be similar to (or shifted to the right of) the tonalite solidus, and the minimum water fugacity at the time of dike emplacement is estimated from figure 4 to be about 750 bars. With even less certainty, emplacement temperatures of the order of 750°–800°C are suggestd.

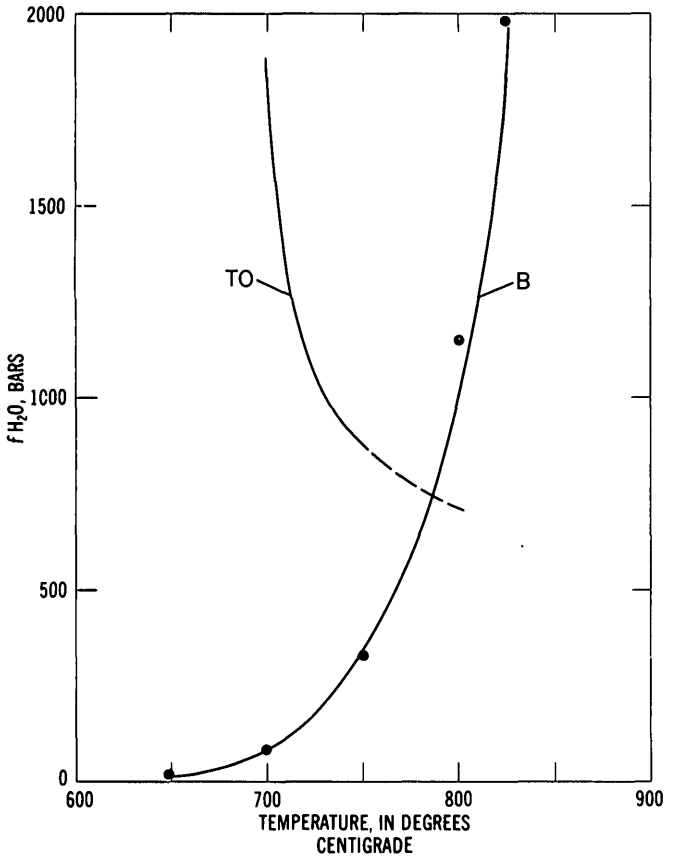

FIGURE 4.—Stability curve for a biotite with 0.10 mole fraction annite (B) relative to solidus curve for a Sierra Nevada tonalite (TO). Biotite is stable in field between curve B and solidus curve. Curve TO from experimental data of Piwinskii (1968) converted from P_{H_2O} to f_{H_2O} using fugacity ratios calculated by Anderson (1964).

Limiting water pressures can also be estimated for the occurrence of actinolite in the latitic melt from stability curves for tremolite and ferrotremolite summarized by Ernst (1968). It was noted that the composition of the actinolite is about $Mg_{0.70}Fe^{+2}{}_{0.25}F^{+3}{}_{0.05}$. By neglecting Fe^{+3}, a very approximate minimum water pressure for the actinolite can be obtained by linear extrapolation between dehydration curves for the Mg and Fe^{+2} end members (fig. 5). For an intrusion temperature of 750°C, a minimum P_{H_2O} of about 1,500 bars (f_{H_2O}=1,140 bars) is indicated. This value exceeds the f_{H_2O} of 750 bars for phlogopite stability estimated from figure 4, and thus is a minimum for stable coexistence of the actinolite-phlogopite pair.

A final point concerns variations in oxygen fugacity during crystallization of the latites. The experimental work of Wones and Eugster (1965) clearly demonstrates the importance of oxygen buffers in determining the composition and stability limits of micas in the phlogopite-annite series. Their work is summarized in figure 6, together with two contrasting trends of magmatic crystallization expressed in terms of f_{O_2} and temperature. According to Wones and Eugster, trend II "represents a magma which, because of low H_2O content, is buffered by anhydrous mineral assemblages." Compositions of biotites from granitic rocks of the central Sierra Nevada batholith parallel this trend (Dodge and others, 1969).

TABLE 3.—*Composition and structural formula of coexisting biotite and phlogopite from latitic dike, Bingham mining district, Utah*

	Biotite	Phlogopite
Major elements (weight percent) [1]		
SiO_2	37.9	40.4
Al_2O_3	13.3	14.5
Fe_2O_3	1.7	1.5
FeO	12.4	4.6
MgO	15.5	22.0
CaO	.72	.24
Na_2O	.43	.50
K_2O	8.5	9.2
Total H_2O	3.3	3.4
TiO_2	4.3	.90
MnO	.13	.05
F	.94	1.82
BaO	.42	.47
Cr_2O_3	.06	.60
Less O=F	.39	.76
Total	99.2	99.5
Minor elements (weight percent) [2]		
Co	0.007	0.005
Cu	.001	.0005
Ga	----	.0015
Nb	.003	----
Ni	.03	.07
Sc	.001	.001
Sr	.003	.005
V	.05	.015
Zr	.005	.0015
Structural formulas [3]		
Si (Z)	5.70	5.81
Al^{iv} (Z)	2.30	2.19
Z total	8.00	8.00
Al^{vi} (Y)	.06	.26
Fe^{+3} (Y)	.19	.16
Ti (Y)	.49	.10
Mg (Y)	3.47	4.71
Fe^{+2} (Y)	1.56	.55
Mn (Y)	.02	.01
Y total	5.79	5.89
Ca (X)	.11	.04
Na (X)	.13	.14
K (X)	1.63	1.69
X total	1.87	1.87
OH	3.31	3.26
F	.45	.83

[1] Analyses by U.S. Geological Survey analytical laboratories using methods of Ingamells (1962, 1966), Suhr and Ingamells (1966), and Medlin, Suhr, and Bodkin (1969). Marcelyn Cremer, analyst.

[2] Semiquantitative spectrographic analyses by Chris Heropoulos, U.S. Geological Survey. Results are reported in percent to the nearest number in the series 1, 0.7, 0.5, 0.3, 0.2, 0.15, 0.1, 0.07, . . . ; these numbers represent approximate midpoints of group data on a geometric scale. The precision of a reported value is approximately plus or minus one interval about 68 percent of the time or two intervals 95 percent of the time. Elements looked for but not found: Ag, As, Au, B, Be, Bi, Cd, Ce, Ge, Hf, Hg, In, La, Li, Mo, Pb, Pd, Pt, Re, Sb, Sn, Ta, Te, Th, Tl, U, W, Y, Yb, Zn.

[3] Calculated on the basis of 24 (O, OH, F) per formula unit. $X_2Y_{4-6}Z_8O_{20}(OH,F)_4$ is assumed to be the general structural formula.

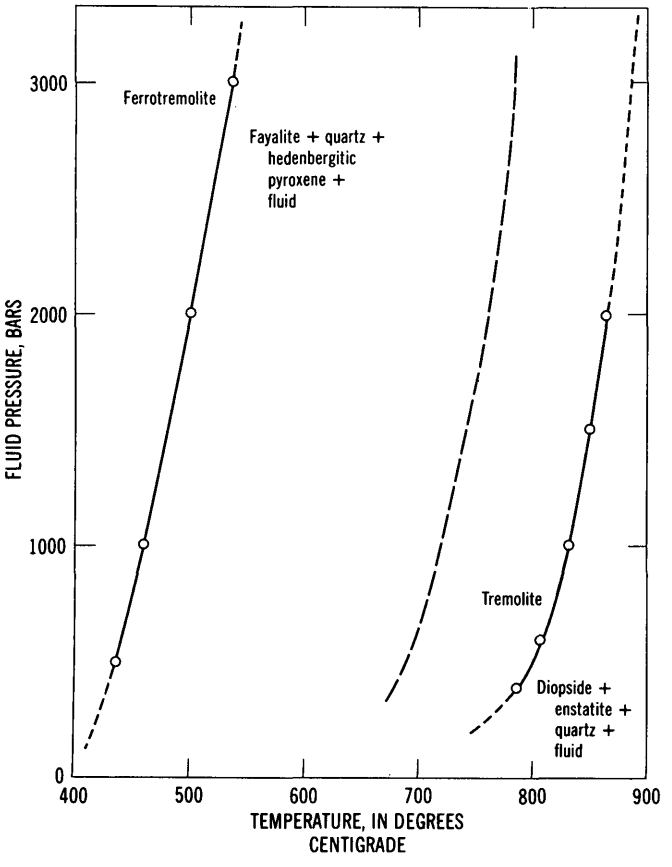

FIGURE 5.—Thermal stability limits of tremolite and ferrotremolite from Ernst (1968, fig. 31). Dashed curve for composition $Mg_{0.7}Fe_{0.3}$ obtained by linear extrapolation between end members.

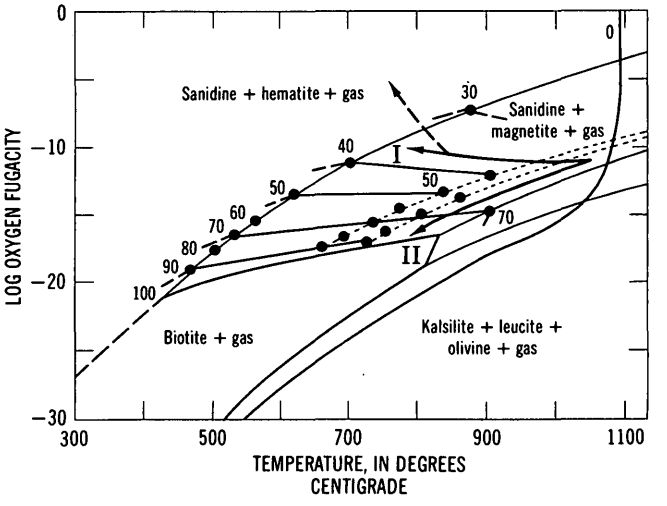

FIGURE 6.—Stability of biotites as function of f_{O_2} and temperature at 2,070 bars total pressure. Heavy solid lines and dashed lines indicate compositions of given biotite as 100 Fe/(Fe+Mg). Lightweight lines and dotted lines represent various experimental oxygen-buffer curves. The postulated trend in f_{O_2} during crystallization of the latitic dikes is represented by trend I, modified by a dashed extension at the lower temperature end. Diagram from Wones and Eugster (1965, figs. 4 and 13).

Trend I represents a magma that becomes water saturated during crystallization and one in which the Fe:(Fe+Mg) ratio of biotites in equilibrium with the melt may decrease in later stages of crystallization. Micas with Fe:(Fe+Mg) ratios of about 0.35, similar to the early-formed phenocrysts in the dike rocks, can coexist with magnetite and sanidine within the temperature range 800°–1,000°C with $f_{O_2} \approx 10^{-11}$ bars. Biotite in equilibrium with magnetite and sanidine at the estimated temperature of emplacement for the Bingham dike rocks (≈750°C) contains appreciably more iron than the analyzed phlogopite in table 3. Only at temperatures above 1,000°C can biotites with Fe:(Fe+Mg) ≈0.15 coexist stably with magnetite, but dashed extensions of the biotite composition contours suggest that Mg-rich biotites can coexist with hematite and sanidine at temperatures of the order of 750°C. As the dike rocks contain small amounts of hematite and give indications of having become water saturated during crystallization, it is thought that relatively high f_{O_2} was a contributing factor in stabilizing late-stage Mg-rich micas in the Bingham dike rocks. Trend I of Wones and Eugster (1965), as modified in figure 6, is the general crystallization path suggested by this interpretation. The increase postulated for f_{O_2} (from about 10^{-11} to 10^{-5} bars) implies that oxygen fugacities during the later stages of crystallization were controlled by an external but otherwise undefined oxygen supply. A similar model has been proposed by Haslam (1968) to account for the high magnesium content of ferromagnesian minerals in salic igneous rocks at Ben Nevis, Scotland, although he suggests that the partial pressure of oxygen was high throughout the crystallization history.

REFERENCES

Anderson, G. M., 1964, The calculated fugacity of water to 1,000° C and 10,000 bars: Geochim. et Cosmochim. Acta, v. 28, no. 5, p. 713–715.

Bray, R. E., 1969, Igneous rocks and hydrothermal alteration at Bingham, Utah: Econ. Geology, v. 64, p. 34–49.

Dodge, F. C. W., Smith, V. C., and Mays, R. E., 1969, Biotites from granitic rocks of the central Sierra Nevada batholith, California: Jour. Petrology, v. 10, p. 250–271.

Ernst, W. G., 1968, Amphiboles; crystal chemistry, phase relations, and occurrence: New York, Springer-Verlag, New York, Inc., 125 p.

Haslam, H. W., 1968, The crystallization of intermediate and acid magmas at Ben Nevis, Scotland: Jour. Petrology, v. 9, pt. 1, p. 84–104.

Ingamells, C. O., 1962, The application of an improved steam distillation apparatus to the determination of fluoride in rocks and minerals: Talanta, v. 9, p. 507–516.

———1966, Absorptometric methods in rapid silicate analysis; Anal. Chemistry, v. 38, p. 1228–1234.

Jackson, E. D., Stevens, R. E., and Bowen, R. W., 1967, A computer-based procedure for deriving mineral formulas from

mineral analyses, *in* Geological Survey Research 1967: U.S. Geol. Survey Prof. Paper 575–C, p. C23–C31.

Lovering, T. G., 1969, Distribution of minor elements in samples of biotite from igneous rocks, *in* Geological Survey Research 1969: U.S. Geol. Survey Prof. Paper 650–B, p. B101–B106.

Medlin, J. H., Suhr, N. H., and Bodkin, J. B., 1969, Atomic absorption analysis of silicates employing Li BO_2 fusion: Atomic Absorption Newsletter 8, p. 25–29.

Moore, W. J., Lanphere, M. A., and Obradovich, J. D., 1968, Chronology of intrusion, volcanism, and ore deposition at Bingham, Utah: Econ. Geology, v. 63, p. 612–621.

Piwinskii, A. J., 1968, Experimental studies of igneous rock series, central Sierra Nevada batholith, California: Jour. Geology, v. 76, p. 548–570.

Suhr, N. H., and Ingamells, C. O., 1966, Solution technique for analysis of silicates: Anal. Chemistry, v. 38, p. 730–734.

Wones, D. R., and Eugster, H. P., 1965, Stability of biotite—Experiment, theory, and application: Am Mineralogist, v. 50, no. 2, p. 1228–1272.

Wright, T. L., and Stewart, D. B., 1968, X-ray and optical study of alkali feldspar—I, Determination of composition and structural state from refined unit-cell parameters $2V$: Am. Mineralogist, v. 53, p. 38–87.

ON-LAND MESOZOIC OCEANIC CRUST IN CALIFORNIA COAST RANGES

By EDGAR H. BAILEY, M. C. BLAKE, JR.,
and DAVID L. JONES, Menlo Park, Calif.

Abstract.—The basal mudstones of the Upper Jurassic to Upper Cretaceous Great Valley sequence rest despositionally on a typical ophiolite ultramafic-mafic succession of igneous rocks. The ophiolite succession from top downward typically consists of chert; keratophyric to basaltic lavas; diabase, gabbro, or norite; and serpentinized peridotite, although not all parts are present everywhere. The volcanic rocks have an average thickness of 3,000 feet (900 m), and the serpentine may be as much as 5,000 feet (1,500 m) thick above a basal thrust fault. Comparison of occurrence, lithology, and thickness with the present in situ sea floor indicates that the ophiolite is the exposed Mesozoic oceanic crust on which sedimentary rocks of the Great Valley sequence were deposited. Coeval eugeosynclinal rocks of the Franciscan assemblage have been dragged below the rocks of the Great Valley sequence by sea-floor spreading. A great thrust fault, herein named the Coast Range thrust, separates the Franciscan and Great Valley sequence. Serpentine immeditaely above the thrust, previously thought to have been intruded into the fault zone, is the basal part of the Mesozoic oceanic crust lying beneath the Great Valley sedimentary rocks and thus was present before thrusting commenced.

The California Coast Ranges and adjacent Great Valley contain two coeval Upper Jurassic to Upper Cretaceous sequences, both possibly as much as 50,000 feet (15,000 meters) thick (see fig. 1). The western unit is the eugeosynclinal Franciscan assemblage of Bailey and others (1964), consisting of graywacke, shale, mafic volcanic rock, chert, limestone, and metamorphic rocks of zeolite and blueschist facies. The eastern unit is the Great Valley sequence, which consists predominantly of graywacke and shale with some conglomerate. This sequence was deposited in an area lying continentward from the site of accumulation of the eugeosynclinal Franciscan rocks, and it was referred to as miogeosynclinal by Bailey and others (1964) and as shelf and slope facies by Irwin (1964). Although its base is not exposed, the eugeosynclinal Franciscan assemblage has been regarded as having been deposited in a deep ocean environment on oceanic crust. In contrast, geologists have tended to regard the Great Valley sequence as having been deposited on continental crust because Cretaceous clastic strata of this sequence in the northern and eastern parts of the valley rest depositionally on the metamorphic and granitic rocks of the Klamath Mountains and Sierra Nevada. As is described herein, however, the Jurassic part of the Great Valley sequence, exposed west of the valley, rests depositionally upon an accumulation of generally mafic volcanic rocks that in turn rest on serpentinized ultramafic rocks (Bailey and Blake, 1969). This basal ultramafic-mafic sequence is similar in lithology to other composite igneous piles elsewhere referred to as ophiolite, a term we use throughout the paper in a descriptive sense without genetic implication. Because of its resemblance to present in situ oceanic crust, we believe that the ophiolite is the Mesozoic oceanic crust on which the Great Valley sediments were deposited.

The significance of the ultramafic-mafic sequence as oceanic crust has not been generally recognized; and even though these rocks are widespread and fairly well exposed in many places in the California Coast Ranges, they remain little studied. We, as well as others, are only beginning to study in detail their occurrence, structure, petrography, and chemistry. This preliminary paper, therefore, leans heavily on the available descriptions of other geologists, most of whom had no idea that they were studying or writing about ancient oceanic crustal material. However, focusing attention on these rocks seems worthwhile, especially as recognition of the character of the serpentine has an important bearing on the geologic history of a major part of the Pacific margin, now being widely discussed under the impetus of concepts of sea-floor spreading and new global tectonics.

U.S. GEOL. SURVEY PROF. PAPER 700–C, PAGES C70–C81

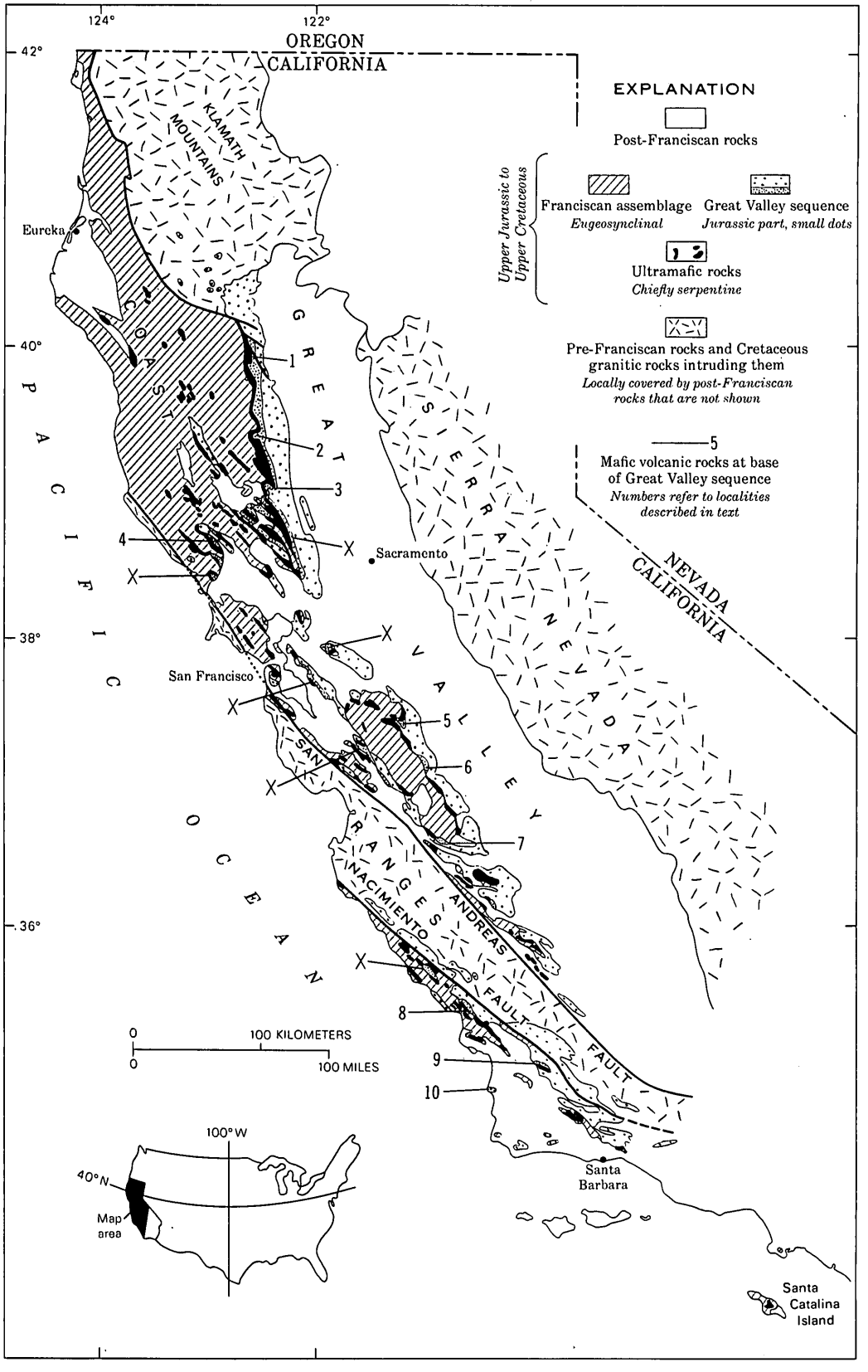

FIGURE 1.—Map of western California, showing the distribution of the coeval Great Valley sequence and Franciscan assemblage and the serpentine that in most places lies between these major units. Numbers indicate localities, described in text, where mafic volcanic rocks underlie Upper Jurassic sedimentary rocks of the Great Valley sequence; other similar localities not described are indicated by X's.

DISTRIBUTION OF THE OPHIOLITE

More than a dozen localities where Jurassic sedimentary rocks of the Great Valley sequence rest directly upon volcanic rock, which in turn lies on serpentine, are shown by numbers and X's in figure 1. Also shown is the distribution of the younger rocks of the Great Valley sequence, the coeval Franciscan assemblage, and the sheet of serpentine separating the two units. The localities where the ophiolitic succession is known to underlie Jurassic sedimentary rocks of the Great Valley sequence are widely distributed and coextensive with the outcrop area of the Jurassic strata. Furthermore, near the north end of the Great Valley, the volcanic rocks and serpentine both terminate abruptly at the fault that limits the northern extent of the Jurassic sedimentary strata, as they would if they formed the basal beds of the sedimentary sequence.

DESCRIPTION OF LOCALITIES

Columnar sections showing the succession of rocks from the lowest exposure of serpentine upward through the mafic igneous rocks and overlying sedimentary strata at 10 localities are shown on figure 2. We have examined some of these localities and modified published geologic descriptions; for localities not visited, we have liberally reinterpreted the published reports and maps in light of the ophiolite or oceanic crust concept. Such preliminary reinterpretations are necessary at this time because the relations of one kind of igneous rock to another commonly are not stated, and from available reports we could not be certain, for example, whether a gabbro occurs above or below a diabase. In such instances, we have stacked the mafic igneous rocks in the most probable order. Similarly, on some maps the original sequence in the ophiolite has been obscured by cover or by real or postulated faults. Additional work can be expected to modify the columns as drawn, but probably only to a limited degree. Most thicknesses shown are averages based on sections through mapped areas, and again, because of lack of data on dips, are in part "best guesses." Despite these limitations, the section proved to be surprisingly uniform with respect to thickness, kind, and succession of rocks, especially in the ophiolite sequences. The areas represented by the columns are discussed below in geographic order from north to south as shown on figure 1, and from left to right as shown on figure 2.

Paskenta

West of Paskenta, a succession of at least 10,000 feet (3,000 m) of Jurassic mudstone with some sandstone and conglomerate (*1*, figs. 1 and 2) lies depositionally on mafic igneous breccias that lie on gabbro, banded gabbro, pyroxenite, and serpentinized peridotite and dunite. The kinds of ophiolitic rocks are not discriminated on any published geologic map, although they extend from the foothills west of Paskenta westward for a distance of 3 miles (5 km) and to an altitude almost 4,000 feet (1,200 m) above the valley. Most of this section is basalt occurring as breccia or pillow lava, but about one-quarter is ultramafic rock, chiefly serpentinized peridotite. As the rocks stand nearly vertical, the apparent thickness is nearly 15,000 feet (4,600 m), but because of repetition of ultramafic-mafic successions, we believe the main section is repeated at least once by faulting.

Of special interest in this area is an uncontestable depositional succession, extending up from ultramafic rock through mafic volcanic rock to mudstone, exposed in the channel of the South Fork of Elder Creek. The contact of the Jurassic mudstone on volcanic basaltic breccia is shown on figure 3, and the contact of the breccia on pyroxenite on figure 4. The breccia immediately above the massive pyroxenite contains 6-inch cobbles of pyroxenite along with pieces of other coarse-grained mafic and ultramafic rocks, such as gabbro, quartz gabbro, and diorite. The total thickness of the ophiolite sequence here is only a few hundreds of feet, but because mudstone is again exposed in the canyon west of the ultramafic rock, the lower part of the ophiolite is believed to be faulted off. Farther west, beneath the mudstone, is more ophiolite containing considerable gabbro, part of which is segregated into anorthosite and pyroxenite layers; mafic breccias with coarse-grained pieces cemented by fine-grained igneous material of similar composition; and pyroxenite, peridotite, and dunite that are almost completely serpentinized.

Stonyford

Within the Stonyford quadrangle (*2*, figs. 1 and 2), which has been studied by Brown (1964), the Upper Jurassic portion of the Great Valley sequence consists of about 10,000 feet (3,000 m) of siltstone, sandstone, and conglomerate. The lower half is largely tuffaceous siltstone containing interbeds of basaltic sandstone and tuff. These sedimentary rocks in turn rest on a volcanic section, as much as 3,000 feet (1,000 m) thick, that is made up chiefly of mafic pillow lavas and breccias but includes numerous thin diabase sills as well as altered tuffs and radiolarian chert lenses. Below this unit is a wedge of peridotite and serpentine having a thickness of about 5,000 feet (1,500 m). In Brown's interpretation, a major thrust fault, the Stony Creek fault zone, occurs between serpentine and Jurassic siltstone in the eastern part of the map area, and between serpentine and mafic volcanic rocks farther west. Although minor faults undoubtedly occur at the positions shown on

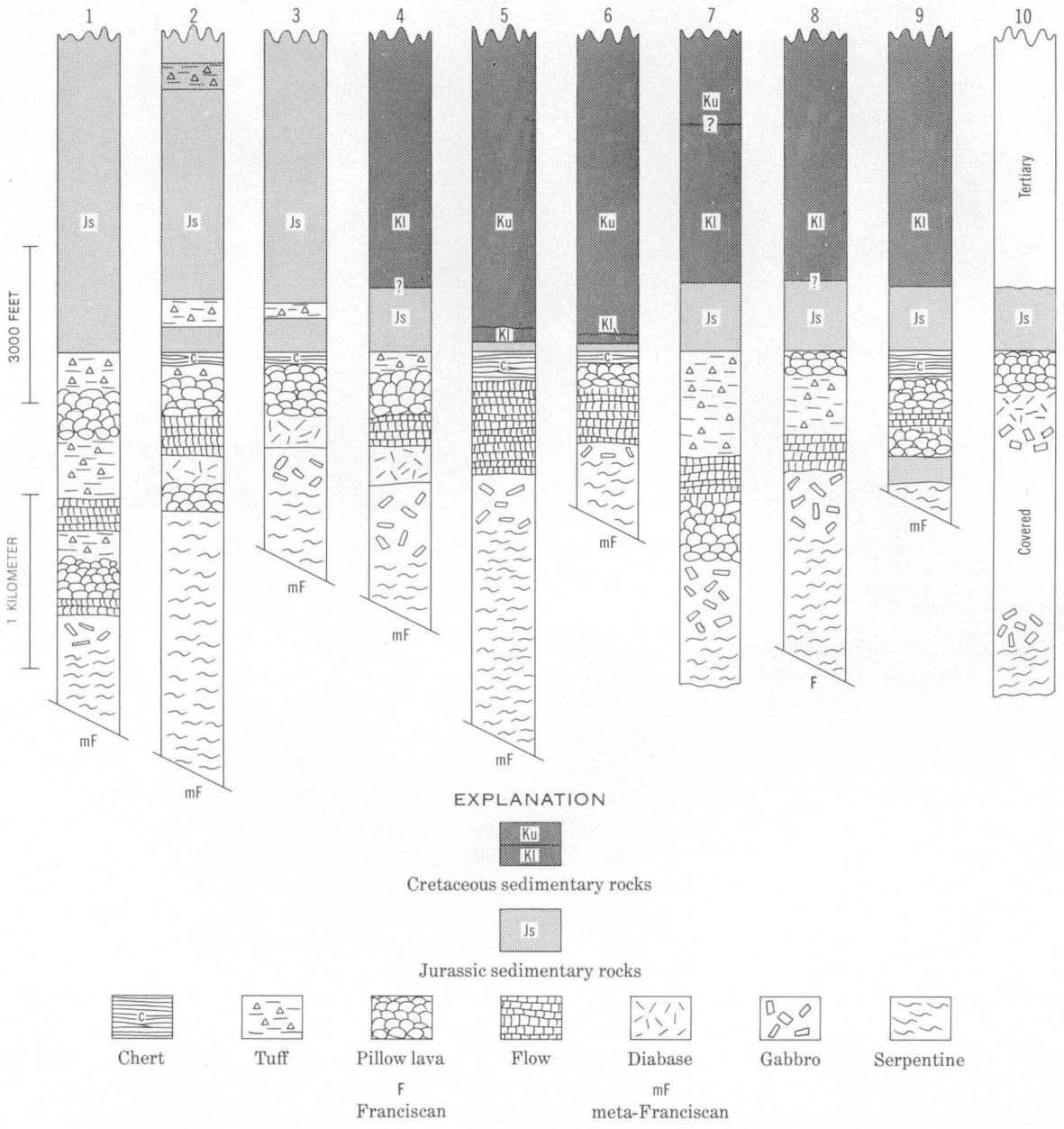

FIGURE 2.—Columnar sections showing details of the ophiolite succession at the numbered localities on figure 1.

Brown's map, the regional relations described in this paper suggest that the main zone of thrusting separating the Great Valley sequence from the underlying deformed and metamorphosed Franciscan rocks lies at the base of the serpentine, not at the top.

Wilbur Springs

The Wilbur Springs area (*3*, figs. 1 and 2) has been studied by several geologists, including Taliaferro (1943), Lawton (1956), Rich (1968), and Moisseeff (1966, 1968). Taliaferro (1943, p. 196–197, 210) described basalt, agglomerate, and chert as being present in the lower part of the Jurassic strata of the Great Valley sequence and, noting their similarity to rocks in the Franciscan, believed that there was a gradational contact between the Franciscan and Great Valley units. He described a section going upward from slaty Franciscan rocks as consisting of 1,200 feet (380 m) of serpentine overlain by 2,000 feet (600 m) of pillow basalts with interbeds of red chert and black shale, intruded by autobrecciated diabase. Moisseeff, who mapped the area in detail, indicates that the rocks above the serpentine range from tachylite to coarse gabbro and diabase and include soda-rich and hornblende-bearing varieties.

FIGURE. 3.—Upper Jurassic shale and minor graywacke of the Knoxville Formation lying depositionally on mafic volcanic breccia exposed in the canyon of the South Fork of Elder Creek, Tehama County, Calif.

FIGURE. 4.—Igneous breccia containing blocks of pyroxenite lying depositionally on massive pyroxenite exposed in canyon of South Fork of Elder Creek. Finger points to contact.

Basalts are most abundant and generally have pillow structure; coarse-grained igneous rocks are mainly restricted to the lower part. Prehnite and pumpellyite are found in the diabase near the basal serpentine. Sedimentary rocks are "scarce," except for beds of radiolarian chert. Higher in the section the effusive rocks are overlain by tuff, graywacke, and shale. Moisseeff (1966) initially considered the section to be ophiolite, and clearly states (p. 15) "the serpentine unit belongs to the Lower Knoxville Formation and is therefore a part of the Great Valley sequence." He later (Moiseyev (Moisseeff), 1968, p. 170) seems to have had some reservations regarding this conclusion, for he states, "The serpentinized ultramafic mass that has been intruded between Franciscan and Great Valley assemblages * * *.", though he still regards the basalt flows, tuffs, and radiolarian cherts as the base of the Great Valley sequence.

Healdsburg

The Healdsburg quadrangle, which is 30 miles (50 km) west of the western edge of the Great Valley, has been mapped and reported on by Gealey (1951). It contains near its northwestern corner (*4*, figs. 1 and 2) an unusually complete, though poorly exposed, ophiolite succession beneath unfossiliferous black shales of the Great Valley sequence that he regarded as Jurassic in age. Above a tabular mass of sheared serpentine, possibly 1,000 feet (300 m) thick, is a mafic "sill" about 2,000 feet (600 m) thick with gabbro at the base and diabase at the top. Locally the sill is layered with olivine- or pyroxene-rich bands. Overlying the sill, and barely distinguishable in some places, is basalt that locally has pillow structure, and above the basalt is volcanic breccia and agglomerate. At least part of the rocks referred to as basalt we have found to be keratophyre and very siliceous quartz keratophyre. Gealey suggests that the gabbro, olivine gabbro, enstatite rock, and serpentinized periodite were all differentiates from a single sill. Here we are still concerned with the problems of relations between various ultramafic and mafic rocks, and whether or not they are intrusive or extrusive—problems that are typical of ophiolites in other areas.

At another locality, 15 miles (24 km) to the east near Mount Saint Helena, Bezore (1969) has studied ophiolite at the base of the Great Valley sequence. Here, above a tectonic contact with Franciscan rock, is a succession of 2,000 feet (600 m) of serpentinized harzburgite cut by dikes of pyroxenite and olivine gabbro, overlain by 1,200 feet (370 m) of mixed serpentinized dunite and gabbro that is overlain by 500 feet (160 m) of massive olivine-free gabbro, in turn capped by 1,000 feet (300 m) of diabase breccia. The overlying black shales and conglomerates have not yielded fossils but are believed to be of Late Jurassic age. Bezore suggests that this ophiolite on which the sedimentary rocks of the Great Valley sequence were deposited might be oceanic crust.

Mount Boardman

The ultramafic rocks of the Mount Boardman area (*5*, figs. 1 and 2) were described by Hawkes and others (1942), and a larger area was mapped in detail by Mad-

dock (1964). Here beneath Jurassic shale of the Great Valley sequence is a typical ophiolite succession, but Maddock mapped major faults between some of the units. Beneath the Jurassic shale is his Lotta Creek Tuff Member, a unit 900 feet (275 m) thick consisting of mafic or keratophyric material with increasingly abundant siliceous shales or impure chert near the top. The tuff lies on a pile of keratophyre and quartz keratophyre flows 1,500 feet (450 m) thick with no sedimentary interbeds. Beneath the keratophyre, though everywhere mapped as separated by a fault, is hornblende gabbro cut by aplite, or perhaps trondjemite, dikes containing secondary prehnite. The gabbro in one area is in the center of a synclinal tabular mass of ultramafic rock, which we believe it overlies but which Maddock has separated by a fault. The sill-like ultramafic sheet is about 4,000 feet (1,200 m) thick and is largely serpentinized peridotite, although some dunite is present locally both near its base and top. The sheet is banded in places and contains segregations of chromite. It was mapped as intrusive into the Franciscan rocks by Maddock (1964), but its lower contact is shown as a fault by Hawkes and others (1942). We regard the surface below the serpentine as the major thrust fault that separates the Franciscan and Great Valley units.

Quinto Creek

There is no published large-scale map of the exposures at the base of the Great Valley sequence along Quinto Creek (*6*, figs. 1 and 2), but the San Jose sheet of the 1:250,000 geologic map of California depicts the distribution of rock types reasonably well, although it is incorrect on age assignments. Fossil-bearing black shale only a few hundred feet thick in this locality is definitely of Jurassic age. It dips steeply eastward and is underlain by a few tens of feet of tuff, which is considerably silicified and has been correlated with the Lotta Creek Tuff Member of the Mount Boardman area. The tuff lies depositionally on light-colored pillow lavas that are probably keratophyre, and these lavas are underlain by a volcanic succession, more than 1,000 feet (300 m) thick, containing basalt, diabase, and, locally, breccias cut by deep-green volcanic glass. Underlying the volcanic rock is a few hundred feet of mixed coarse-grained mafic rocks including quartz gabbro, leucogabbro, hornblende gabbro, and hornblendite. The coarse-grained rocks overlie about 1,000 feet (300 m) of serpentinized peridotite with some dunite. The exact thickness of the ultramafic and mafic units is unknown, as are their contact relations, but there is nothing to suggest that this is not a typical ophiolite succession.

380-189 O—70——6

Vallecitos

The Vallecitos area (*7*, figs. 1 and 2) has been mapped by Enos (1963, 1965), who described a succession of Jurassic and Lower Cretaceous sedimentary rocks of the Great Valley sequence lying depositionally on a pile of volcanic rocks 3,500 feet (1,100 m) thick. However, he assigned the volcanic rocks to the Franciscan Formation, and emphasized that the relations demonstrated the pre-Portlandian age of these Franciscan rocks. We believe that the volcanic pile, which contains no sedimentary rocks, is not Franciscan but a part of the ophiolitic succession on which the Great Valley sequence was deposited.

As described by Enos, the thick volcanic pile consists of andesite tuff and tuff breccia, underlying flow layered andesite porphyry, keratophyre, and quartz keratophyre, and in the lower part subolivine basalt with well-developed pillow structure. Locally the volcanic rocks lie upon hornblende gabbro, which in turn seems to be above norite. The norite is in contact with serpentinized periodotite that in at least part of the area overlies Franciscan jadeitic metagraywacke and glaucophane schist. Enos showed no fault below the serpentine and considered it as intrusive into the Franciscan. To interpret this area as ophiolite beneath the Great Valley sequence requires drastic reinterpretation of Enos' data. However, all parts of the ultramafic-mafic sequence are shown in the typical ophiolite order on his geologic map, though partly covered by younger rocks so that the stacking is not immediately obvious.

Black Mountain

The Black Mountain area (*8*, figs. 1 and 2), about half way between Morro Bay and Atascadero, has been mapped in detail by Fairbanks (1904). The oldest sedimentary rocks of the Great Valley sequence are black shales, which he named the Toro Formation and listed as Cretaceous in age, but the shales are now known to include rocks of Late Jurassic age. These sedimentary rocks are underlain by 2,800 feet (850 m) of volcanic rock, termed Cuesta Diabase, which is in turn underlain by 3,500 feet (1,100 m) of serpentinized peridotite and some dunite. The sedimentary strata, which are more than 3,000 feet (900 m) thick, occupy the central part of a long syncline; the mafic and ultramafic rocks are found on both limbs, as is well shown on Fairbanks' cross sections. He regarded the Cuesta Diabase as an intrusive sill, although he mentions that it is generally amygdaloidal and has friction breccia or tuffaceous facies at its top. Other workers (Taliaferro, 1944, p. 545) have reported pillows and pillow breccias, indicating that at least part of the Cuesta is extrusive. Fair-

banks' "diabase" shows great variation, and apparently includes keratophyre and quartz keratophyre as well as gabbro. Gabbro and norite are also mentioned as occurring along the edges of the serpentinized peridotite.

Stanley Mountain area

The Stanley Mountain area (*9*, figs. 1 and 2), 15 miles (25 km) northeast of Santa Maria, has been known for many years a place where well-bedded Jurassic shale is interlayered with mafic volcanic rocks and chert. Taliaferro (1943) presented a map showing these relations and cited the area as one where the Franciscan Formation graded into the Jurassic (Knoxville) part of the Great Valley sequence, which included abundant volcanic rocks in its lower part. A different interpretation was supplied by Easton and Imlay (1955), who used the data afforded by fossils found in the shale, which they assigned to the Franciscan Formation, to prove the Jurassic age of this part of the Franciscan. Recently Brown (1968) mapped the area in detail, and he concluded that the fossiliferous Jurassic shale and volcanic rocks were a part of the Great Valley sequence that had been tectonically superposed over much more deformed and metamorphosed Franciscan rocks.

The ophiolite sequence has at its top interbedded red chert and black shale 400 feet (120 m) thick lying conformably beneath graywacke. The chert and shale unit lies depositionally on a pile of mafic volcanic rocks 1,500 feet (460 m) thick consisting chiefly of flows, pillow lavas, and tuffs. Most of the lava is described as spilitic andesite; the remainder is referred to as basalt. In the upper and lower parts of the pile, the lavas commonly show pillow structure, and throughout the pile most of them are vesicular. Amygdules contain epidote and quartz, and in some varieties both minerals also occur as metamorphic replacements that make up a major part of the rock. Pumpellyite is present also as a metamorphic mineral, and in one tuff layer near the base, prehnite is abundant. The chert and underlying volcanic pile have features typical of an ophiolite sequence, but beneath the volcanic rocks is black shale with fossiliferous limestone nodules in place of the usual ultramafic rocks. This occurrence of shale below the volcanic part of a presumed ophiolite sequence is the only such occurrence that we know of in the California Coast Ranges. As shown on Brown's map, both volcanic rocks and the shale believed to underlie it have attitudes strongly divergent from the intervening contact, suggesting that the contact might be a thrust fault that has brought the volcanic rocks over the shale. Beneath the lower shale is the major thrust that carries the Great Valley sequence over metamorphosed Franciscan rocks, but only locally is a little serpentine found along it.

Point Sal

The geology of Point Sal (*10*, figs. 1 and 2), about 30 miles south of San Luis Obispo, was mapped by Fairbanks (1896). In this area, upper Jurassic shale of the Great Valley sequence lies upon volcanic rocks, which are shown on the 1:250,000 San Luis Obispo sheet of the geologic map of California as belonging to the Franciscan Formation, although no sedimentary rocks are included. Just below the shales is nearly 1,000 feet (300 m) of pillow basalt containing amygdules of epidote and quartz. Cutting the basalt locally are dikes of andesite and diabase. Beneath the basalt is a mass of diabase grading downward to gabbro that is at least 1,000 feet (300 m) thick, but the base is concealed by overlapping Tertiary strata. About a mile to the south, gabbro again crops out in a belt that trends southeastward along the coast. At this northwestern end, this gabbro is uniform in texture and composition, but farther to the southeast it becomes regularly banded with layers of diorite and hornblende gabbro. Still farther southeast, and presumably lower in the sequence, is olivine pyroxenite, anorthosite, hypersthene gabbro, serpentinized peridotite, and serpentinized dunite. Mafic dikes of various kinds transect the layered mass, and the sequence of rock types may be even more complex than indicated herein. Nevertheless, within this area an ultramafic-mafic succession generally similar to the ophiolite found elsewhere in the Coast Ranges appears to underlie the oldest rocks of the Great Valley sequence. Because of the good exposure provided by the sea cliffs, it is an area where future work might be rewarding.

SUMMARY OF OCCURRENCES OF OPHIOLITE

The ophiolite lying beneath the Jurassic strata of the Great Valley sequence seems remarkably similar from place to place. The lowest part everywhere, except perhaps in the Stanley Mountain area, is a completely hydrated serpentine, and most of the parent rock was a pyroxene-bearing peridotite. As its base is everywhere a fault, its original thickness is unknown, but the thickness of the portion present generally does not exceed 5,000 feet (1,500 m) except where repeated by imbrication. Dunite, where present, is not consistently confined to the base, and pyroxenite is widespread but occurs only in small amounts, usually as thin layers or dikes. The upper part of this zone commonly gives way to a feldspathic banded or layered complex consisting of norite, gabbro, hornblende gabbro, anorthosite, hornblendite, and, rarely, trondjemite. Overlying these coarse-grained rocks everywhere is a layer of mafic, or locally even silicic, volcanic rock that ranges in thickness from 2,000 to 5,000 feet (600–1,500 m) and

averages about 3,000 feet (900 m). Its lower part is diabasic or basaltic, and may show pillow structure. Locally, prehnite, epidote, and quartz occur in amygdules and as alteration products in the lavas. Higher in the succession, keratophyre or quartz keratophyre is locally dominant. The upper rocks tend to be breccias or tuffs. At the top of the volcanic pile chert is common in some areas as a result of silification of the tuffs, or more locally as rhythmically layered radiolarian cherts possibly precipitated directly as silica. Intrusions, especially dikes, are commonly noted in the mafic volcanic succession but are rarely described as occurring in the underlying ultramafic rocks. Exceptions are found in the Mount Boardman area, where gabbro dikes intrude the upper part of the serpentinized peridotite (Maddock, 1964; Himmelberg and Coleman, 1968), and perhaps locally in the lower ultramafic mass of Point Sal (Fairbanks, 1896).

COMPARISON OF MESOZOIC OPHIOLITE WITH MODERN OCEANIC CRUST

Because of its mode of occurrence, there is little doubt that the ophiolite described here is the Mesozoic oceanic crust on which the Great Valley sequence was deposited. Several authors have suggested that ophiolite sequences elsewhere in the world represent ancient oceanic crust (Hess, 1962; Dietz, 1963; Davies, 1968; Gass, 1968; Thayer, 1969; Varne and others, 1969). Their view is based on comparison of ophiolites with present oceanic crust, but unfortunately, knowledge of the characteristics of this crust is obtained mainly through interpretation of geophysical data supported by scattered dredging and drilling. According to widely spaced seismic data, the average oceanic structure consists of ultramafic rock (mantle) overlain by: (1) an "oceanic" layer about 4.8 km thick of gabbro or serpentine; (2) an intermediate layer about 1.7 to 2.0 km thick probably of basalt and consolidated sediment; and (3) an upper layer, 0.2–0.3 km thick, of unconsolidated sediments (Dietz, 1961; Raitt, 1963). The existence of the upper layer of consolidated sediments and underlying basalt has been well documented by the JOIDES deep drilling program (California Univ., Scripps Inst. Oceanography, 1969). Dredge hauls have provided data on the deeper structure. For example, peridotite was dredged from the lower slopes, gabbros and greenschists from intermediate levels, and basalt from the upper slopes of the deep fracture zones that intersect the Mid-Atlantic Ridge (Bonatti, 1968). Distribution appears to be similar along the rifted crest of the Mid-Indian Ocean Ridge (Engel and Fisher, 1969), where tholeiitic basalt overlies coarse-grained gabbro, anorthosite, and lherzolite. The lithology and thickness of the layers in the present oceanic crust appear to be grossly similar to those of the ophiolite at the base of the Great Valley sequence. This similarity supports our conclusion that these rocks do indeed represent the ancient oceanic crust upon which the Late Jurassic sediments were deposited.

TECTONICS RESPONSIBLE FOR EXPOSURE OF OCEANIC CRUST

The depositional and tectonic activities responsible for the onland exposure of Mesozoic oceanic crust in the California Coast Ranges have recently been discussed by Bailey and Blake (1969) and by Hamilton (1969). The present distribution of the major Mesozoic units is shown on figure 5, and our concept of the sedimentation and tectonism leading to this distribution is illustrated, on figure 6, by a series of sequential cross sections drawn northeastward through the northern Coast Ranges from a point on the coast about 70 miles north of San Francisco. These cross sections show that in the late Mesozoic in this area the Franciscan and Great Valley sequence rocks were being deposited in parallel basins, and from mid-Cretaceous onward were being simultaneously deformed by underthrusting due to seafloor spreading. Superposition of the two units was brought about by movement along the great thrust fault, whose position is nearly everywhere marked by serpentine. Beneath the thrust, the Franciscan rocks were sheared and converted to blueschists in an inverted sequence, in which higher grade jadeite- or lawsonite-bearing metagraywacke near the fault grades downward to mildly altered pumpellyite-bearing graywacke. The distribution of this great thrust through the Coast Ranges and the metamorphic zones in the Franciscan are shown on figure 5. Prior to its recognition throughout the Coast Ranges, different parts of the thrust had received several different names; for simplicity, we recommend that it be referred to everywhere as the Coast Range thrust. The cross sections making up figure 6 make it clear that the ultramafic-mafic succession is a part of the Mesozoic oceanic crust that has been brought into view mainly because it has overridden the Franciscan rocks along the Coast Range thrust.

SIGNIFICANCE OF THE ON-LAND MESOZOIC OCEANIC CRUST

Recognition that the ultramafic-mafic rock at the base of the Great Valley sedimentary sequence is oceanic crust is significant for several reasons. For one, it provides an unusual opportunity for geologists to study on-land exposures of oceanic crust. At the present time much effort is being put forth to learn more about the oceanic crust through dredging, deep-sea drilling, and

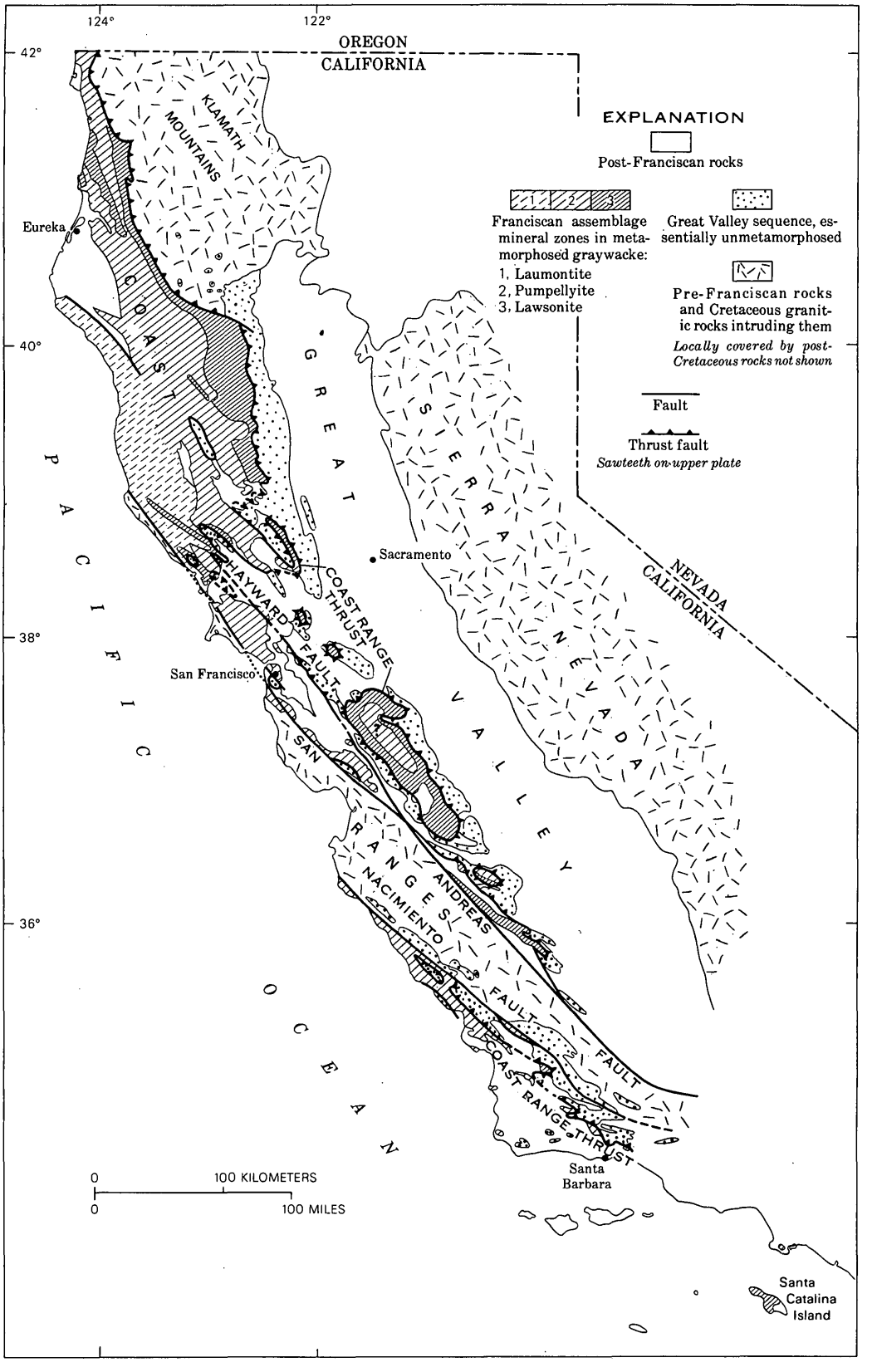

FIGURE 5.—Map of western California, showing the position of the Coast Range thrust beneath the rocks of the Great Valley sequence and the inverted metamorphic zones in the Franciscan rocks below the thrust.

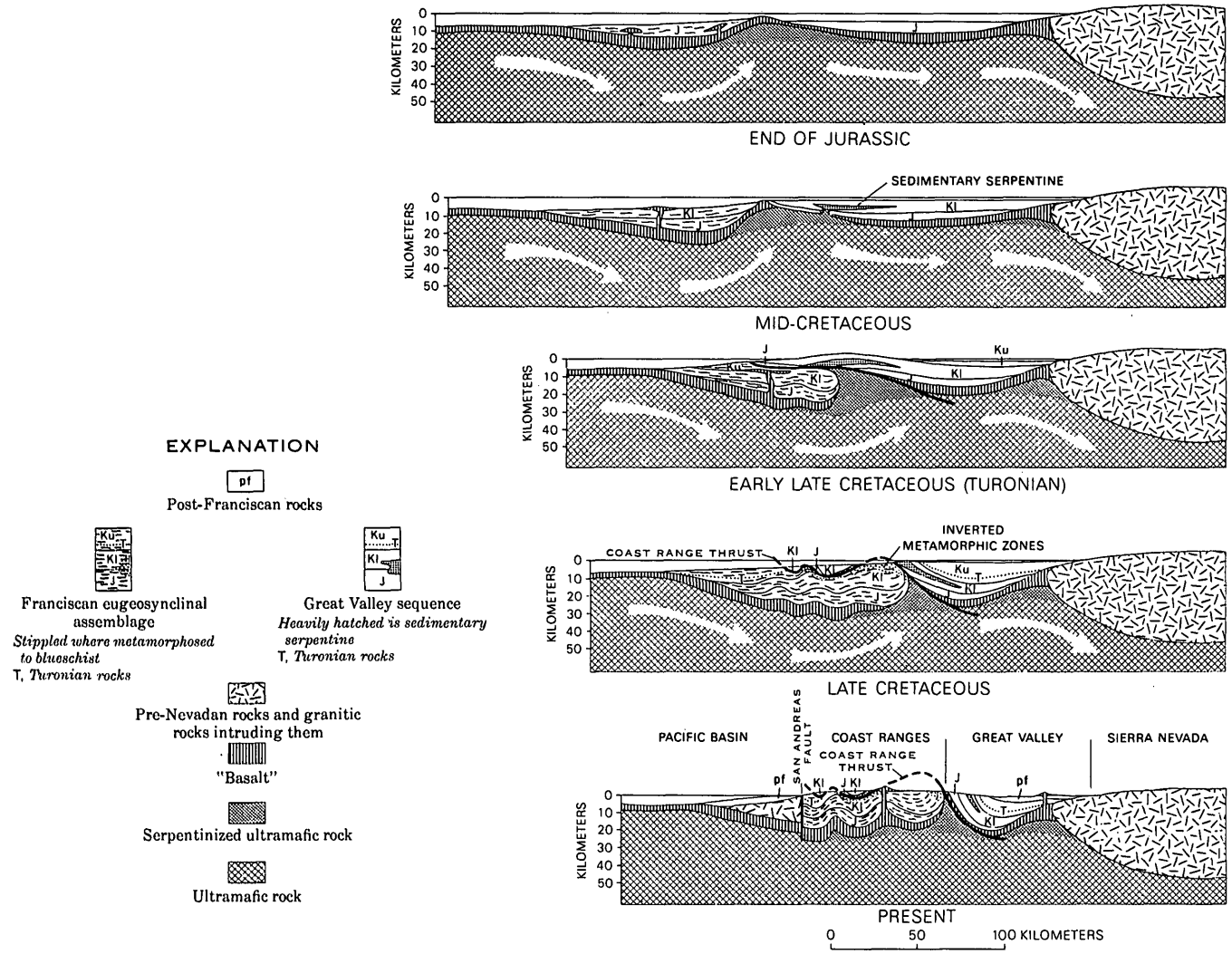

FIGURE 6.—Sequential sections through the Coast Ranges northeastward from a point on the coast 70 miles north of San Francisco. No attempt has been made to show the contemporaneous tectonism and intrusion in the Sierra Nevada block at right edge of sections or to show the complex structure within the Franciscan assemblage. Symbols: J, Jurassic; Kl, Lower Cretaceous; Ku, Upper Cretaceous.

remote sensing in the ocean basins. A few hours spent in examing the on-land exposures can yield more about the lithologic character and sequence than can weeks of dredging, although of course one cannot assume that the crust of the vast ocean basins will prove to be everywhere like the sample provided by examination of a limited on-land area.

Recognition of the character of the ultramafic-mafic rocks is also significant in interpreting the history of the Coast Ranges, especially as it leads to a new concept regarding the age, origin, and emplacement of the serpentine at the base of the Great Valley sequence. As was noted by Taliaferro (1943) and emphasized by Irwin (1964), the serpentine makes up a great sheet that intervenes nearly everywhere between the rocks of the Great Valley sequence and the underlying Franciscan rocks (see fig. 1). Prior to its dissection by faulting and erosion, this sheet of sheared serpentine extended many thousands of square miles, for at least the length of the Great Valley and from its western edge to the Pacific coast. It marks the position of the extensive Coast Range thrust, and the serpentine has been regarded by most geologists as having been injected into the thrust as a cold intrusion squeezed up from the upper mantle. As the serpentine was thought to have intruded along the plane of the fault, between its two walls, geologists were faced with the problem of where to show the fault on a geologic map. Virtually all geologists somehow decided that the serpentine was more like the Franciscan assemblage than the Great Valley sequence, and consequently drew the fault at the base of the Great Valley sequence so that the serpentine would be in the Franciscan side. The recognition of the serpentine as a part of the ophiolite beneath the Great Valley clastic

strata requires that the thrust fault be placed below it, and that the serpentine be in existence prior to faulting and to deposition of the Great Valley rocks. The depositional contacts on the serpentine, together with the occurrence of ultramafic fragments in overlying volcanic breccia and in the Jurassic strata lying on the ophiolite, proves that the serpentine antedates the sedimentation and faulting.

The total extent of the ultramafic sheet and overlying volcanic and sedimentary rocks that formed the upper plate of the thrust is not known because of dissection by later faulting and erosion. It is at least 15,000 square miles, and this is a minimum for the area that was initially oceanic crust and has now been welded to the continent. This figure, however, includes only rocks in the upper plate, and because the Franciscan rocks in the lower plate were also deposited on oceanic crust still farther from the continental margin, the total width of material added to the continent is at least 150 miles (250 km). Underthrusting has telescoped this new material with the result that the effective continental growth along this part of the Pacific margin during late Mesozoic time has been reduced to about 100 miles (160 km).

REFERENCES

Bailey, E. H., and Blake, M. C., 1969, Tectonic development of western California during the late mesozoic: Geotektonika, pt. 3, p. 17–30; pt. 4, p. 24–34.

Bailey, E. H., Irwin, W. P., and Jones, D. L., 1964, Franciscan and related rocks, and their significance in the geology of western California: California Div. Mines and Geology Bull. 183, 177 p.

Bezore, S. P., 1969, The Mount Saint Helena ultramafic-mafic complex of the northern California Coast Ranges [abs.]: Geol. Soc. America Abstracts with Programs 1969, pt. 3, Cordilleran Sec., Eugene, Oreg., 1969, p. 5–6.

Bonatti, Enrico, 1968, Ultramafic rocks from the Mid-Atlantic Ridge: Nature, v. 219, p. 363–364.

Brown, J. A., Jr., 1968, Thrust contact between Franciscan group and Great Valley sequence northeast of Santa Maria, California: Univ. Southern California, Los Angeles, Calif., Ph. D. thesis (geology), 236 p.

Brown, R. D., Jr., 1964, Geologic map of the Stonyford quadrangle, Glenn, Colusa, and Lake Counties, California: U.S. Geol. Survey Mineral Inv. Field Studies Map MF–279, scale 1: 48,000.

California University, Scripps Institution of Oceanography, 1969, Initial reports of the Deep Sea Drilling project, prepared for the National Science Foundation, National Ocean Sediment Coring Program, v. 1: 672 p.

Davies, H. L., 1968, Papuan ultramafic belt, *in* Upper mantle (Geological processes): Internat. Geol. Cong., 23d, Prague, 1968, Repts., v. 1, Proc. Sec. 1, p. 209–220.

Dietz, R. S., 1961, Continent and ocean basin evolution by spreading of the sea floor: Nature, v. 190, no. 4779, p. 854–857.

——— 1963, Alpine serpentinites as oceanic rind fragments: Geol. Soc. America Bull., v. 74, no. 7, p. 947–952.

Easton, W. H., and Imlay, R. W., 1955, Upper Jurassic fossil localities in Franciscan and Knoxville Formations in southern California: Am. Assoc. Petroleum Geologists Bull., v. 39, no. 11, p. 2336–2340.

Engel, C. G., and Fisher, R. L., 1969, Lherzolite, anorthosite, gabbro, and basalt dredged from the Mid-Indian Ocean Ridge: Science, v. 166, p. 1136–1141.

Enos, Paul, 1963, Jurassic age of Franciscan Formation south of Panoche Pass, California: Am. Assoc. Petroleum Geologists Bull., v. 47, no. 1, p. 158–163.

——— 1965, Geology of the Western Vallecitos syncline, San Benito County, California: California Div. Mines and Geology, Map sheet 5, scale 1:31,680.

Fairbanks, H. W., 1896, The geology of Point Sal: California Univ. Dept. Geology Bull., v. 2, no. 1, p. 1–92.

Fairbanks, H. W., 1904, Description of the San Luis quadrangle [California]: U.S. Geol. Survey Geol. Atlas, Folio 101, 14 p.

Gass, I. G., 1968, Is the Troodos Massif of Cyprus a fragment of Mesozoic ocean floor?: Nature, v. 220, no. 5162, p. 39–42.

Gealey, W. K., 1951, Geology of the Healdsburg quadrangle, California: California Div. Mines Bull. 161, 50 p.

Hamilton, Warren, 1969, Mesozoic California and the underflow of Pacific mantle: Geol. Soc. America Bull., v. 80, p. 2409–2429.

Hawkes, H. E., Jr., Wells, F. G., and Wheeler, D. P., Jr., 1942, Chromite and quicksilver deposits of the Del Puerto area, Stanislaus County, California: U.S. Geol. Survey Bull. 936–D, p. 79–110.

Hess, H. H., 1962, History of ocean basins, *in* Petrologic studies: Geol. Soc. America, Buddington volume, p. 599–620.

Himmelberg, G. R., and Coleman, R. G., 1968, Chemistry of primary minerals and rocks from the Red Mountain–Del Puerto ultramafic mass, California, *in* Geological Survey Research 1968: U.S. Geol. Survey Prof. Paper 600–C, p. C18–C26.

Irwin, W. P., 1964, Late Mesozoic orogenies in the ultramafic belts of northwestern California and southwestern Oregon, *in* Geological Survey Research 1964: U. S. Geol. Survey Prof. Paper 501–C, p. C1–C9.

Lawton, J. E., 1956, Geology of the north half of the Morgan Valley quadrangle and the south half of the Wilbur Springs quadrangle [California]: Stanford Univ., Ph. D. thesis, 259 p.

Maddock, M. E., 1964, Geology of the Mount Boardman quadrangle, Santa Clara and Stanislaus Counties, California: California Div. Mines and Geology Map Sheet 3, scale 1: 62,500.

Moisseeff, A. N., 1966, The geology and the geochemistry of the Wilbur Springs quicksilver district, Colusa and Lake Counties, California: Stanford Univ., Ph. D. thesis, 214 p.

Moiseyev (Moisseeff), A. N., 1968, The Wilbur Springs quicksilver district (California) example of a study of hydrothermal processes by combining field geology and theoretical geochemistry: Econ. Geology, v. 63, no. 2, p. 169–181.

Raitt, R. W., 1963, The crustal rocks, *in* The sea, v. 3: London, Interscience Publishers, p. 85–102.

Rich, E. I., 1968, Geology of the Wilbur Springs quadrangle, Colusa and Lake Counties, California: Stanford Univ., Ph. D. thesis, 101 p.

Taliaferro, N. L., 1943, Franciscan-Knoxville problem: Am. Assoc. Petroleum Geologists Bull., v. 27, no. 2, p. 109–219.

——— 1944, Cretaceous and Paleocene of Santa Lucia Range, California: Am. Assoc. Petroleum Geologists, v. 28, no. 4, p. 449–521.

Thayer, T. P., 1969, Peridotite-gabbro complexes as keys to petrology of mid-oceanic ridges: Geol. Soc. America Bull., v. 80, no. 8, p. 1515–1522.

Varne, Richard, Gee, R. D., and Quilty, P. G. J., 1969, Macquarie Island and the cause of oceanic linear magnetic anomalies: Science, v. 1966, p. 230–233.

COMPOSITE DIKES IN THE LITTLE BELT MOUNTAINS, CENTRAL MONTANA

By IRVING J. WITKIND, Denver, Colo.

Abstract.—Three, and possibly four, composite dikes have been recognized in the Little Belt Mountains, central Montana. These dikes, marked by basic margins that contain quartz xenocrysts, and by acidic interiors that contain quartz phenocrysts, imply that two magmas of contrasting composition coexisted and were emplaced almost synchronously. The basic margins consist of kersantite, interpreted as a lighter fraction that formed during the differentiation of an alkalic magma of shonkinitic composition. The acidic interiors consist of quartz porphyries that may stem from acidic magmas which possibly formed by selective fusion of certain metasedimentary rocks of the Belt Supergroup.

At least three composite dikes are in the Little Belt Mountains, central Montana (fig. 1). These dikes, characterized by basic margins and acidic interiors, assume an importance far beyond that of their size and number, for they imply that two primary magmas of diverse composition coexisted and were emplaced almost simultaneously. The basic margins are composed of a dark-gray, fine-grained lamprophyre in which the dominant mafic mineral is biotite, and the dominant felsic mineral is plagioclase. Comparable rocks exposed elsewhere in the area have been called kersantites by Weed (1900, p. 353) and Pirsson (1900, p. 539). The acidic interiors are quartz porphyries—granophyres—in which conspicuous phenocrysts of quartz and feldspar are enclosed in a microgranular intergrowth of the same minerals. Similar rocks exposed elsewhere in the area have been called the porphyry of Galena Creek (Witkind, 1970) and the Carpenter Creek Porphyry (Weed, 1900, p. 376).

Other dikes and minor intrusions in this area are composed of either kersantite or granophyre; they testify to the former presence of basic and acidic magmas, but they indicate nothing about the time and sequence of emplacement of these magmas. The composite dikes, however, in which the kersantite and the granophyre are in close association, strongly imply that these two contrasting magmas were emplaced almost synchronously in the same fracture while both were still fluid and mobile.

The physical behavior and ultimate origin of intimately associated acidic and basic magmas have been discussed repeatedly. Most recently the subject has been reviewed thoroughly in a series of six papers by King (1962–1965).

DESCRIPTION OF DIKES

Of the composite dikes recognized in the Little Belt Mountains, two are exposed near Barker, Mont., and one is exposed about 7 miles to the southwest, along Carpenter Creek near Neihart (fig. 1). The fourth dike, possibly composite, was intersected in a diamond drill hole along the south valley wall of Carpenter Creek. It is highly likely that similar dikes are exposed elsewhere in the mountains, but these either have not been recognized or are concealed beneath the vegetative cover so characteristic of the mountains.

Composite dikes near Barker

One of the two composite dikes near Barker, the Maytee dike (fig. 1), is particularly well exposed along an old road near the portal of the Maytee tunnel of the Block P mine—a once-famous producer of lead, silver, and zinc. The other dike, the Annie E (fig. 1), can be examined only underground where it has been cut through by the Annie E tunnel of the Liberty mine. Both dikes intrude the Hughesville syenite stock (fig. 2).

Maytee dike.—The Maytee dike is a near-vertical body that trends about N. 30° W. for about 1 mile from Galena Creek to its distal end near the northwest edge of the Hughesville stock (fig. 2). It extends through the SW¼ sec. 6 and the NW¼ sec. 7, T. 15 N., R. 9 E. (unsurveyed). For most of this distance the dike is about 24 feet wide. Of this width each basic margin occupies about 2 feet, each transitional zone another

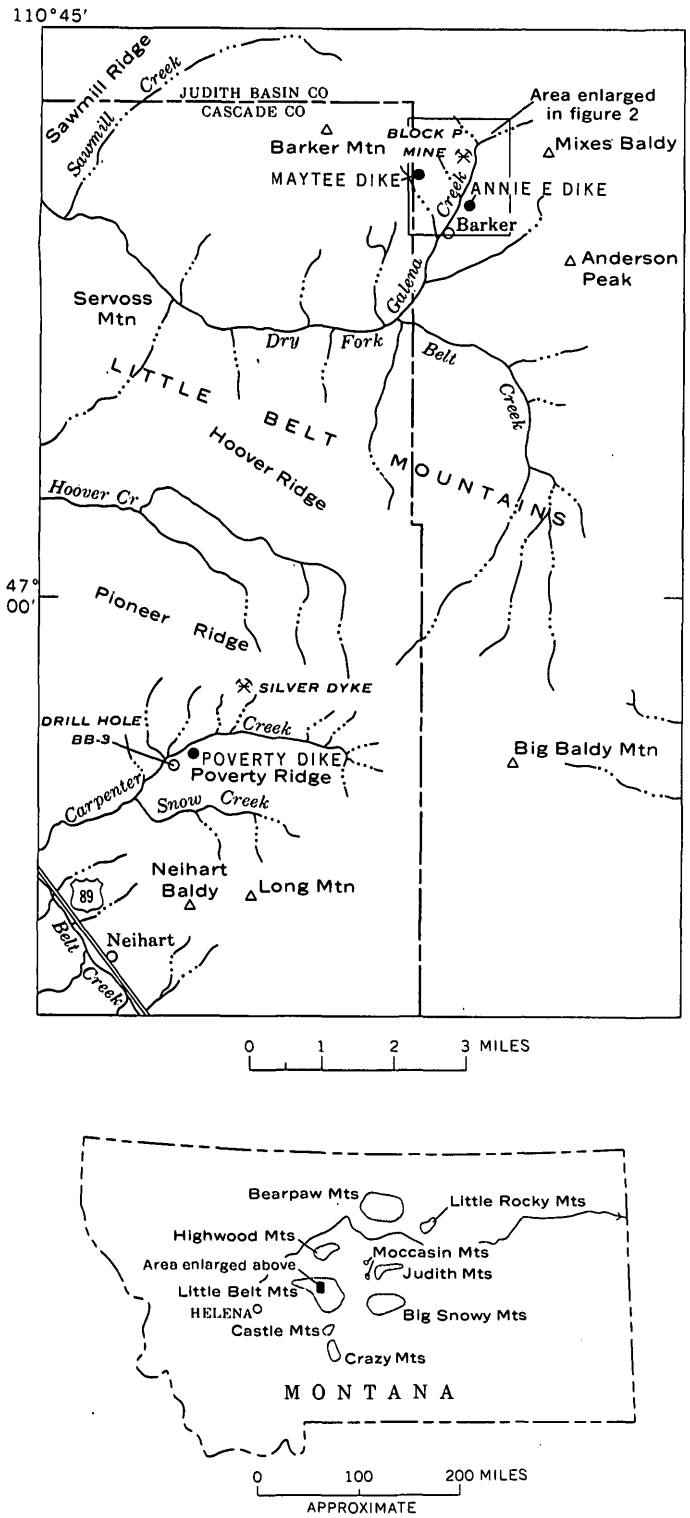

FIGURE 1.—Index map of Montana and a part of the Little Belt Mountains, Cascade and Judith Basin Counties, Mont.

2 feet, and the remainder of the dike—some 17 feet—consists of the acidic interior. The widths of all zones remain remarkably constant. Exposures are poor, and nowhere is the full width of the dike available for examination. Here and there, parts of it crop out on ridges and in old roadcuts (fig. 3*A* and *B*).

The basic margin of the dike is in sharp contact with the country rock, and the contact is marked by a change in both color and rock type. As the basic margin is traced toward the center of the dike—toward the acidic interior—it maintains a uniform dark-gray color for about 2 feet, and then grades into a transitional zone, also about 2 feet wide, in which the rock becomes light gray and seemingly passes smoothly and imperceptibly into the light-tan granophyre of the acidic interior. Contacts between the various phases of the dike cannot be detected in outcrop. Xenoliths of country rock are found in both the basic margin and the acidic interior. Small angular blebs of galena also are in the granophyre.

In hand specimen the kersantite of the basic margin is a dark-gray dense porphyritic rock in which conspicuous grains of angular feldspar, round, glassy, fractured quartz, and irregular-shaped books of biotite are scattered through a fine-grained, almost aphanitic, groundmass (fig. 3*C*).

Thin sections suggest that both phenocrysts and xenocrysts are present. The phenocrysts include plagioclase feldspar (chiefly oligoclase, An_{13}) and biotite. Most of the plagioclase grains are subhedral and partly rounded; a few are encircled by reaction rinds. The biotite, by contrast, is euhedral and fresh. Xenocrysts include both fractured quartz grains and a few grains of angular to rounded sanidine. All the quartz grains are rounded, many are embayed, and a few are encircled by reaction rims composed of minute grains of an unknown mineral, possibly orthopyroxene. Most of the sparse sanidine grains are embayed and encircled by reaction rinds. The groundmass is a felted mixture of slender plagioclase microlites, irregular blebs of alkalic feldspar, and biotite flakes. Some mosaic quartz fills voids in the groundmass.

Also included are a few grains of clinopyroxene and a unique amphibole. *Z* is the acute bisectrix in the latter rather than *X* as in most amphiboles, and its optic angle ranges from 82° to 88°. Refractive indices are: $n_x = 1.649$ to 1.651, $n_y = 1.655$, and $n_z = 1.665$ to 1.667. This mineral is probably pargasite (Tröger, 1959, p. 65).

The granophyre contrasts sharply with the kersantite (fig. 3*D*). In hand specimen the granophyre is a light-tan rock in which conspicuous grains of round smoky quartz and angular claylike feldspar laths are scattered through a fine-grained to aphanitic light-tan groundmass. Many of the feldspar phenocrysts are rimmed by a thin brown (limonite?) stain which imparts a brown speckled appearance to the rock. Biotite flakes are sparse and inconspicuous.

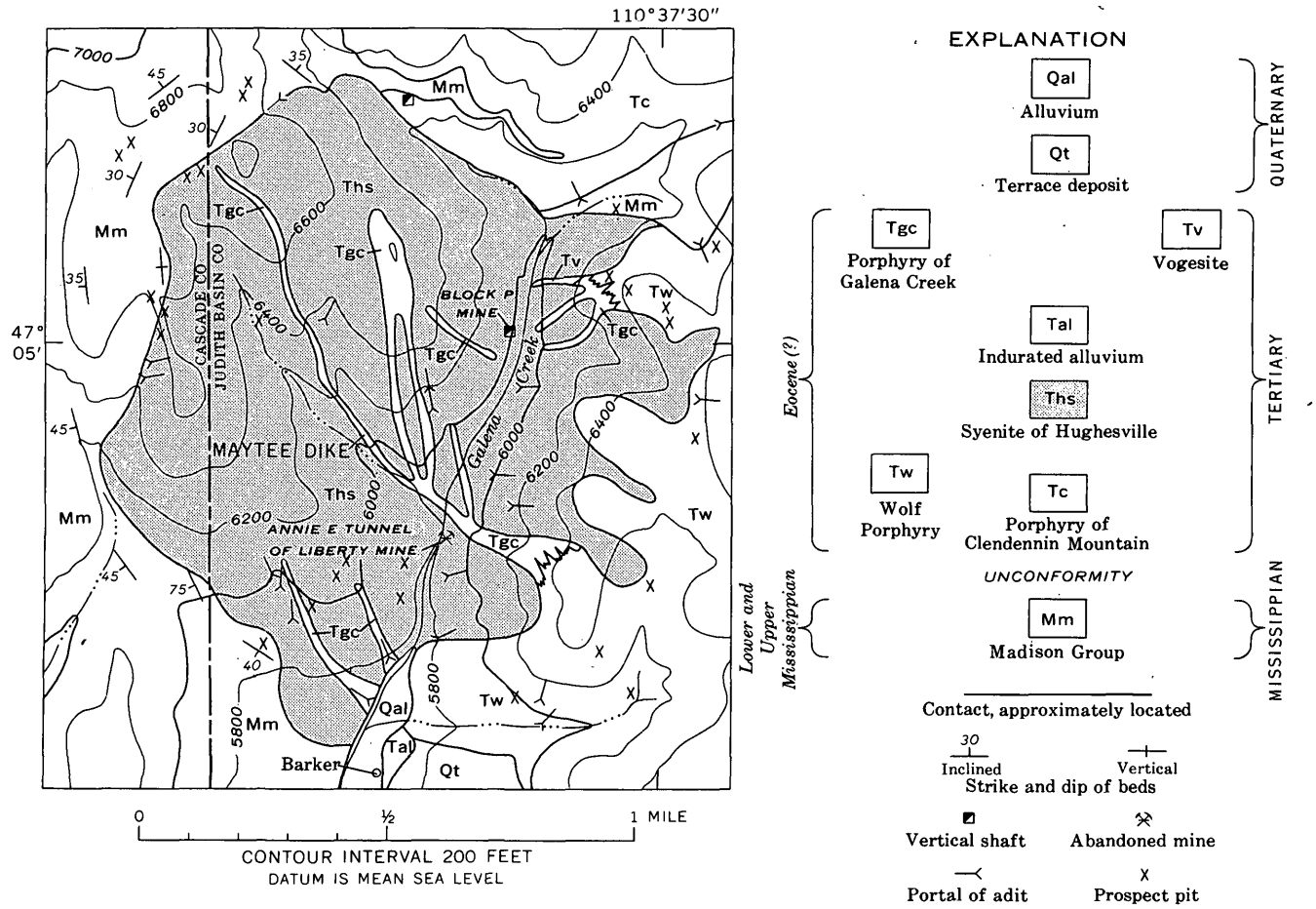

FIGURE 2.—Geologic map of the Hughesville stock. Geology by I. J. Witkind, assisted by T. E. Redlinger, 1966. Base from U.S. Geological Survey Barker quadrangle, 1961.

In thin section much of the quartz is euhedral, and a few grains are bipyramidal. Some of the larger quartz grains are partly rounded, and all the smaller ones are completely rounded. Many of the grains are embayed. A few large angular to subrounded grains of sanidine are scattered through the groundmass, and all are corroded. No plagioclase was noted. A little biotite is present, and much of it has been bleached and altered. Here and there rectangular voids in the thin section suggest the former presence of biotite flakes. The groundmass is a microgranular intergrowth of quartz and alkalic feldspar. A few large grains of clinopyroxene have been found, and these are interpreted as xenocrysts possibly derived from the kersantite magma. A special search was made for xenocrysts of pargasite(?), but none were found.

The sharp contrast in color and mineralogy between the basic margin and the acidic interior is reemphasized when the chemical compositions of the two phases are contrasted (table 1). Compared to the granophyre, the basic margin (kersantite) is low in silica but high in almost every other component with the exception of potash. Whereas the granophyre is practically devoid of magnesia and lime, the kersantite is high in these components (≈3–4 percent), reflecting the abundant biotite and various other mafic minerals. The kersantite is also rich in soda (≈3 percent) presumably owing to the abundant sodic plagioclase, whereas the granophyre, virtually free of plagioclase, contains only about half a percent of soda. Only when potash content is compared does the granophyre (≈6 percent), with its abundant alkalic feldspar as both sanidine phenocrysts and intergrowths in the groundmass, exceed the kersantite (4 percent).

Annie E dike.—The Annie E composite dike is exposed in the Annie E tunnel of the Liberty mine. The portal of the tunnel is in the center of sec. 7, T. 15 N., R. 9 E., along the east bank of Galena Creek (fig. 1).

The exact relations between the Annie E and the Maytee dikes are not clear; possibly they are one and the same, but inadequate surface exposures preclude correlation. They are here considered to be closely related but separate bodies.

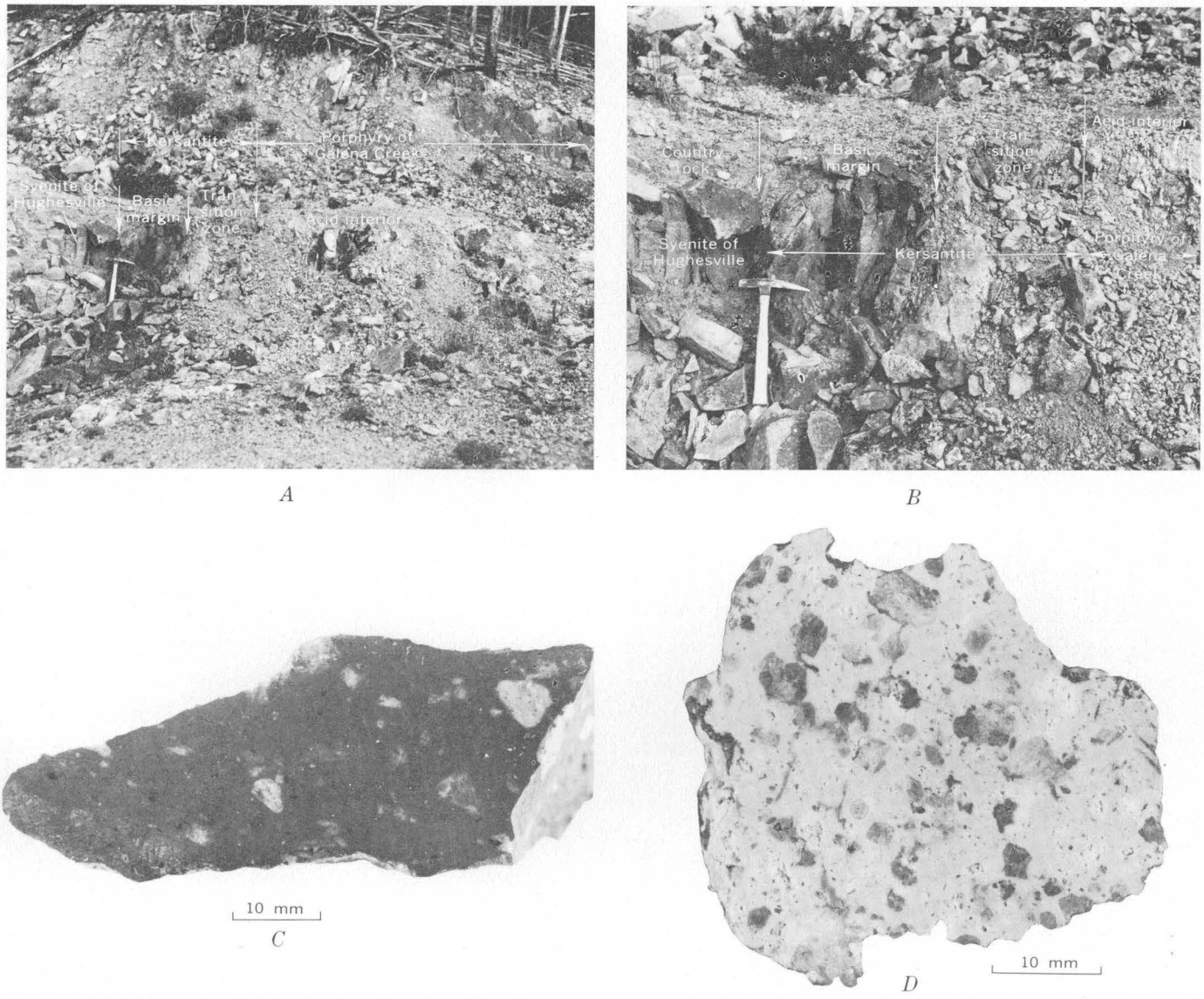

FIGURE 3.—Views of and specimens from the southwest flank of the Maytee dike in contact with the syenite of Hughesville. *A* and *B*, Basic margin and transitional zone are each about 2 feet wide; acidic interior is about 17 feet wide. *C*, Hand specimen from the basic margin (kersantite). *D*, Hand specimen from the acidic interior (porphyry of Galena Creek). *C* and *D* photographed by R. B. Taylor, U.S. Geological Survey.

The Annie E dike trends about N. 10° W., is vertical, and is about 25 feet thick. The Annie E vein—lead-silver-zinc—narrows abruptly where it cuts across the dike; the vein postdates the dike.

The rock types that make up the Annie E composite dike are similar in color, lithology, and mineralogy to those in the Maytee dike. Kersantite (biotite-plagioclase) forms the basic margins, and granophyre (quartz-sanidine) forms the acidic interior.

The basic margins are about 2 feet thick, and they grade somewhat abruptly into the acidic interior. They contain a host of angular xenoliths both of the syenite of Hughesville (the country rock) and of the Wolf Porphyry, a granite porphyry that forms an adjacent asymmetric laccolith. These xenoliths, 1–3 inches on a side, are all so deeply decomposed that they crumble and disintegrate when touched. No xenoliths were noted in the granophyre, but by analogy with other dikes composed of the granophyre they are believed to be present.

Composite dike (Poverty dike) near Carpenter Creek

A composite dike (called the Poverty dike) in the Neihart area is exposed along the south valley wall of Carpenter Creek; a second may have been intersected at a depth of about 625 feet by a diamond drill hole

TABLE 1.—*Analyses, in weight percent, of basic margins, transitional zones, and acidic interiors of two composite dikes in the Little Belt Mountains, Mont.*

[All rapid rock analyses. Analysts: P. L. D. Elmore, G. W. Chloe, James Kelsey, S. D. Botts, H. Smith, Lowell Artis, and J. L. Glenn]

	Barker area			Carpenter Creek area			
	Maytee dike [1]			Poverty dike [2]			
	Basic margin	Transitional zone	Acid interior	Basic margin	Transitional zone	Acid interior	Hypothetical acidic magma [3] (fused Belt rocks)
Rock name	Kersantite	Kersantite(?)	Porphyry of Galena Creek	Kersantite	Kersantite(?)	Carpenter Creek Porphyry	
Lab. No.	W-170181	W-171084	W-171083	W-171086	W-171087	W-171085	
Field No.	WL-270-c	WL-552-a	WL-551-a	WL-566-a	WL-567-a	WL-565-a	
Chemical analyses							
SiO_2	57.5	68.6	75.9	59.4	56.7	69.3	76.5
Al_2O_3	16.0	15.7	13.0	16.4	16.2	15.5	8.0
Fe_2O_3	2.4	1.4	.74	4.2	3.9	1.1	2.0
FeO	2.8	.92	.60	2.8	3.6	.60	2.2
MgO	3.1	.88	.29	3.0	3.5	1.3	2.6
CaO	3.9	1.0	.11	3.5	3.3	1.1	1.9
Na_2O	3.3	2.9	.53	3.9	3.9	3.7	.1
K_2O	4.0	4.6	6.3	3.8	4.3	5.0	1.6
H_2O^-	.22	.69	.51	.25	.25	.81	2.6
H_2O^+	.78	2.1	1.7	1.2	2.0	.89	.3
TiO_2	.89	.77	.15	.87	.97	.46	.3
P_2O_5	.42	.33	.02	.63	.74	.20	.1
MnO	.16	.03		.07	.07	.03	0.0
CO_2	3.9	<.05	<.05	<.05	.28	<.05	2.6
Sum	99.37	99.97	99.90	100.07	99.70	100.04	100.80
CIPW norms							
Q	19.33	31.74	48.12	11.95	7.22	25.05	61.41
ar	23.79	27.18	37.23	22.46	25.41	29.55	9.46
ab	28.10	24.54	4.49	33.00	33.00	31.31	.85
an	0	2.49	.10	12.93	9.83	3.83	8.46
C	6.28	5.04	5.27	1.13	1.53	2.60	3.01
hy{en	4.85	2.19	.72	7.47	8.72	3.24	6.48
hy{fs	2.00	0	.24	.37	1.92	0	1.89
mt	3.50	.83	1.07	6.09	5.66	.70	2.90
ap	1.00	.78	.05	1.49	1.73	.47	.24
il	1.70	1.46	.29	1.65	1.84	.87	.57
hm	0	.83	0	0	0	.62	0

[1] Composite dike, secs. 6 and 7, T. 15 N., R. 9 E. (unsurveyed), Judith Basin County, Mont.
[2] Composite dike, NE¼ sec. 21, T. 14 N., R. 8 E. (unsurveyed), Cascade County, Mont.
[3] Hypothetical magma that might result if 600 feet of Neihart Quartzite, 2,000 feet of Chamberlain Shale, and 600 feet of Newland Limestone—all of Belt Supergroup—were fused. Based on weighted average of one sample of each rock type. Analytical data from Ross (1963, tables 16 and 20).

testing the Big Ben molybdenum properties along Carpenter Creek (fig. 1). It is highly likely that others are in the same area.

The Poverty dike crops out along the crest of a narrow, heavily forested ridge that forms part of the north flank of Poverty Ridge (NE¼ sec. 21, T. 14 N., R. 8 E., unsurveyed). The dike trends about N. 35° E., is vertical, and is about 35 feet wide. It is moderately well exposed along an old, abandoned, timber road.

Locally the full width of the dike is exposed, and its makeup is strikingly similar to that of the Maytee dike about 7 miles to the north. Three rock types are recognizable: dark-gray basic margins (each about 2 feet wide), gray to light-gray transitional zones (each also about 2 feet wide), and the central acidic interior (about 25 feet wide). All types maintain a uniform width wherever exposed.

The contact with the light-tan country rock, which is an Eocene(?) quartz rhyolite porphyry known as the Snow Creek Porphyry, is sharp and distinct, with the darkest part of the basic margins adjacent to the country rock.

The basic margins of the dike are kersantite formed chiefly of two generations of biotite and plagioclase

feldspar. The acidic interior consists of a granite porphyry identical in all respects with the Carpenter Creek Porphyry, the youngest and one of the more distinctive igneous rocks in the Neihart area. In hand specimen the acidic interior is a pinkish-gray, fine-grained rock speckled with large (10×5 mm) angular phenocrysts of tabular pink feldspar, rounded (about 5 mm in diameter) smoky quartz, and black biotite flakes. The pink feldspars are conspicuous and distinguish the Carpenter Creek Porphyry from all other porphyries exposed in the area.

In thin section most of the feldspar phenocrysts are orthoclase (a few perthitic), but a few are plagioclase (oligoclase, An_{13}). Most of these are partly resorbed, and they are embayed by a micrographic groundmass of intergrown quartz and feldspar. The quartz grains are rounded and embayed, and a few have faintly corroded rims.

In the Poverty dike, as in the Maytee dike, chemical analyses accentuate the sharp differences between the basic margins and the acidic interior (table 1).

DISCUSSION

The xenocrysts of quartz and sanidine in the kersantites are optically identical with the phenocrysts in the granophyres. In like fashion the clinopyroxene xenocrysts(?) in the granophyre of the Maytee dike are optically similar to the clinopyroxene phenocrysts in the kersantite. This suggests that the xenocrysts are transferred phenocrysts. Such an interchange of crystals could only have occurred as a result of a physical exchange between two magmas of different composition in which blebs of each were engulfed and partly assimilated by the other.

This mingling probably occurred as a highly mobile basic magma moved up through a viscous acidic one when a fissure tapped two magma chambers—a basic one beneath an acidic one. This relative position of basic beneath silicic has been inferred repeatedly, and seemingly is essential in the development of composite dikes (Simons, 1963; King, 1964; Blake and others, 1965; Holmes, 1931; Tomkeieff and Marshall, 1935; Wilcox, 1944).

Once through the acidic magma the basic magma filled the fissure, and parts of it chilled against the country rock to form narrow selvages. Between these crystallized edges the remainder of the basic magma remained fluid and mobile. Shortly thereafter mobile acidic magma invaded the fissure and flushed out the still-fluid core of basic material. The end result is a composite dike marked by a core of acidic rock flanked by margins of basic rock.

The corrosion rims that envelop the sanidine and some of the quartz grains in the granophyres support this sequence. It is likely that immediately prior to the upward surge of the basic magma well-formed quartz and sanidine phenocrysts were suspended in an acidic magmatic liquid. When the temperature of this liquid was raised (owing to upward passage of the hotter basic magma) the established equilibrium was disturbed, and the liquid attacked and corroded both the sanidine and some of the quartz phenocrysts.

A few of the quartz xenocrysts in the basic margins have corrosion rims, but most do not, in marked contrast to other quartz xenocrysts in dikes and sills of kersantite and vogesite exposed elsewhere in the area. These latter quartz xenocrysts, I believe, were suspended in basic magmatic liquids long enough for them to react and develop reaction rinds. The quartz and sanidine xenocrysts enclosed in the basic margins of the composite dikes, by contrast, probably lacked time to react with the basic magma, which probably chilled and crystallized before reaction could occur.

The kersantite margins of the dikes probably represent the lighter fraction of a differentiating alkalic magma having the composition of shonkinite. It seems unlikely, however, that the acidic cores stem from the same magma, for the silica deficiency of shonkinitic magmas is evidenced by the presence of feldspathoids in rocks evolved therefrom. Larsen (1940, p. 939–940) recognized that the rocks in the Little Belt Mountains could not have evolved from such a magma without the assimilation of large amounts of silicic material. Thus, it seems much more likely that the acidic material came from a separate chamber, one possibly derived from the palingenesis of the highly silicic Belt metasedimentary rocks (table 1).

REFERENCES

Blake, D. H., Elwell, R. W. D., Gibson, I. L., Skelhorn, R. R., and Walker, G. P. L, 1965, Some relationships resulting from the intimate association of acid and basic magmas: Geol. Soc. London, Quart. Jour., v. 121, pt. 1, p. 31–49.

Holmes, Arthur, 1931, The problem of the association of acid and basic rocks in central complexes: Geol. Mag., v. 68, p. 241–255.

King, B. C., 1962–1965, Geology—the nature of basic igneous rocks and their relations with associated acid rocks: Sci. Progress, Pt. I, 1962, v. 50, no. 200, p. 616–629; Pt. II, 1963, v. 51, no. 202, p. 259–275; Pt. III, 1963, v. 51, no. 204, p. 610–628; Pt. IV, 1964, v. 52, no. 206, p. 282–292; Pt. V, 1965, v. 53, no. 209, p. 117–125; Pt. VI, 1965, v. 53, no. 211, p. 437–446.

Larsen, E. S., Jr., 1940, Petrographic province of central Montana: Geol. Soc. America Bull., v. 51, no. 6, p. 887–948.

Pirsson, L. V., 1900, Petrography of the igneous rocks of the Little Belt Mountains, Montana: U.S. Geol. Survey 20th Ann. Rept., pt. 3, p. 463–581.

Ross, C. P., 1963, The Belt Series in Montana: U.S. Geol. Survey Prof. Paper 346, 122 p.

Simons, F. S. 1963, Composite dike of andesite and rhyolite at Klondyke, Arizona: Geol. Soc. America Bull., v. 74, p. 1049–1056.

Tomkeieff, S. I., and Marshall, C. E., 1935, The Mourne dyke swarm: Geol. Soc. London Quart. Jour., v. 91, p. 251–288.

Tröger, W. E., 1959, Optische Bestimmung der gesteinbildenden Minerale, Teil 1, Bestimmungstabellen [3d ed.]: Stuttgart, E. Schweizerbart Verlagsbuchhandlung, 147 p.

Weed, W. H., 1900, Geology of the Little Belt Mountains, Montana, with notes on the mineral deposits of the Neihart, Barker, Yogo, and other districts: U.S. Geol. Survey 20th Ann. Rept., pt. 3, p. 257–461.

Wilcox, R. E., 1944, Rhyolite-basalt complex on Gardiner River, Yellowstone Park, Wyoming: Geol. Soc. America Bull., v. 55, p. 1047–1080.

Witkind, I. J,, 1970, Geologic map of the Barker quadrangle, Cascade and Judith Basin Counties, Montana: U.S. Geol. Survey Geol. Quad. Map GQ–898. [In press.]

MINERALOGY OF UNDERCLAYS IN THE PENNSYLVANIA ANTHRACITE REGION

By JOHN W. HOSTERMAN, GORDON H. WOOD, JR., and M. J. BERGIN, Beltsville, Md., Washington, D.C.

Abstract.—The underclays of anthracite beds in eastern Pennsylvania contain kaolinite, illite (2M), chlorite, pyrophyllite, and phlogopite, all identified by X-ray diffraction; quartz is the only nonclay mineral. The association of these clay minerals indicates that the anthracite formed in the greenschist range of temperature and pressure; that is, between 250° and 450° C and 2,000 to 9,000 bars, respectively.

The Anthracite region of northeastern Pennsylvania is erosionally separated from the Bituminous region of central and western Pennsylvania. Northwest-directed tangential pressures of the Appalachian orogeny uplifted, folded, and faulted the coal-bearing rocks of both regions but were more intense in the Anthracite region. As a result of these pressures and of temperature differences, anthracite formed nearer the orogenic centers in the Valley and Ridge province, and bituminous coal formed at a distance from the centers in the Appalachian Plateaus province.

Mineralogical and chemical studies have been made on the underclays of the anthracite beds. In general, the chemical composition of these underclays is similar to that of the plastic underclays of the bituminous coal field. However, the clay mineralogy of the two types of underclays is very different. The mineralogical difference indicates that the underclays of anthracite beds have been subjected to low-grade metamorphism. The section on mineralogy in this report gives detailed information on the clay-mineral composition.

The anthracite beds and associated underclays occur in rocks of Pennsylvanian age that underlie four fields named according to their relative geographic location: Northern, Eastern Middle, Western Middle, and Southern. These fields cover parts of 10 counties: Carbon, Columbia, Dauphin, Lackawanna, Lebanon, Luzerne, Northumberland, Schuylkill, Susquehanna, and Wayne (fig. 1). The anthracite fields trend northeastward and have an en echelon arrangement. They range from 24 to 70 miles in length and from less than 1 mile to 8 miles in width. The coal-bearing rocks are as much as 4,900 feet thick, and the thickest part contains 50 or more coal beds (Arndt and others, 1968, p. 122).

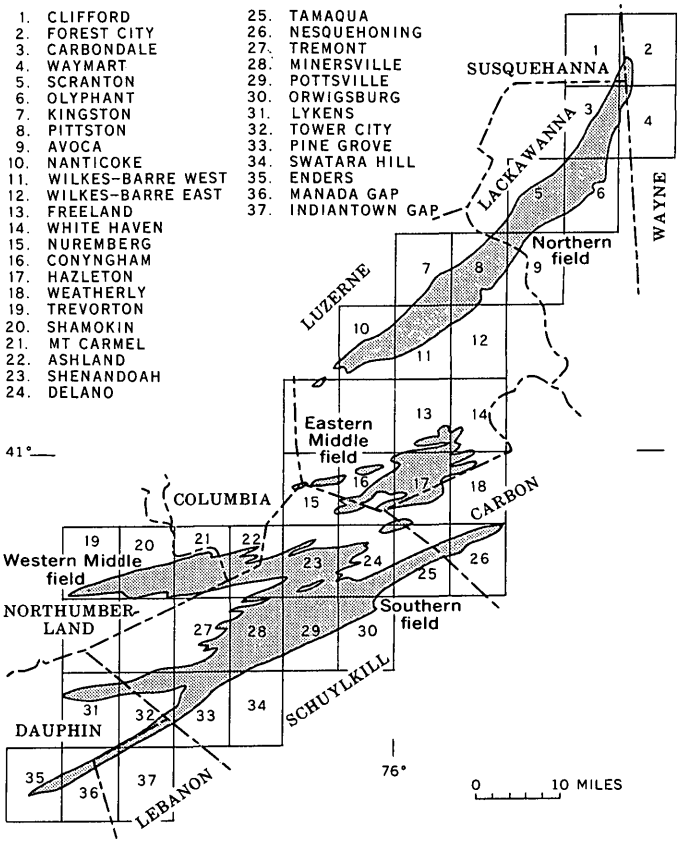

FIGURE 1.—Index map of the anthracite fields of eastern Pennsylvania, showing outline of the Pottsville Formation (patterned) and location of U.S. Geological Survey 7½-minute topographic quadrangles. Modified from Wood and others (1962, p. 183) and Arndt and others (1968, p. 123).

The coal-bearing sequence has been subdivided into the Pottsville Formation of Early and Middle Pennsylvanian age and the Llewellyn Formation of latest Middle and Late Pennsylvanian age.

U.S. GEOL. SURVEY PROF. PAPER 700-C, PAGES C89–C97

In most of the Anthracite region, the Pottsville Formation overlies the Mauch Chunk Formation of Late Mississippian and Early Pennsylvanian age and underlies the Llewellyn Formation. However, in the northern part of the Northern field, the Pottsville may overlie the Pocono Formation of Mississippian age or the Catskill Formation of Devonian age. The Pottsville ranges in thickness from less than 100 feet in the Northern field to more than 1,500 feet in the Southern field (Wood and others, 1969, p. 77). The formation is composed of light- to dark-gray quartz pebble and cobble conglomerate and quartzose sandstone interbedded with lesser amounts of siltstone, shale, anthracite, semianthracite, and underclay (bottom rock). Wood and others (1956) subdivided the Pottsville Formation of the Southern field into the Tumbling Run Member, Schuylkill Member, and Sharp Mountain Member. These members are also present in the Western Middle and Eastern Middle fields, but only the upper member is recognized in the Northern field. The Pottsville contains many anthracite beds. Nine of the more widespread of these in the Southern field, five in the Western Middle field, and one in the Eastern Middle field are shown on figure 2. As much as 3 feet of carbonaceous black shale and interbedded anthracite, known as the Campbell Ledge Shale Member, locally underlies the Sharp Mountain Member in the Northern field.

The Llewellyn Formation rests conformably on the Pottsville Formation and is overlain by Quaternary sediments or truncated by the present erosion surface. It contains most of the anthracite beds mined in eastern Pennsylvania. The formation is composed chiefly of gray and brown conglomeratic sandstone, quartzose sandstone, and siltstone with lesser amounts of conglomerate, carbonaceous shale, anthracite, semianthracite, and underclay. The maximum preserved thickness is about 3,500 feet in the Southern field, about 2,200 feet in the Northern field, about 1,900 feet in the Western Middle field, and about 1,500 feet in the Eastern Middle field. Generally, the lower 400–500 feet consists mainly of medium-gray to dark-gray coarse-grained sandstone and conglomeratic sandstone interbedded with dark-gray to grayish-black sandstone, siltstone, and shale. This lower sequence in some places includes as many as eight persistent coal beds which are extensively mined. Commonly, the middle part of the formation consists of light-gray to light-olive-gray and moderately yellowish-brown fine- to medium-grained sandstone, siltstone, and shale and includes as many as 15 persistent coal beds, many of which are extensively mined. The upper several hundred feet of Llewellyn is similar to the lower 400–500 feet. It includes five or more persistent coal beds in the Southern field. Elsewhere, the upper sequence has been removed by erosion.

Seventy-two samples of underclay from 68 localities representing 34 different coal beds were collected throughout the 4 anthracite fields (table 1). Ten samples were from 10 coal beds of the Pottsville Formation in the Southern field, and 62 samples were from 24 coal beds of the Llewellyn Formation in all 4 anthracite fields. In addition, one sample of an unnamed black shale and two samples of black shale from the Campbell Ledge Shale Member were from the Pottsville Formation. One sample of black shale was taken from the Llewellyn Formation.

MINERALOGY

The underclays of the Pottsville and Llewellyn are dark-gray to black nonbedded silty clayey argillites and clayey argillites. The clay minerals identified by X-ray diffraction are kaolinite, illite, chlorite, pyrophyllite, and phlogopite. Quartz is in all samples as angular grains of very fine sand and silt. In thin sections, most of the quartz grains have irregular boundaries, indicating that silica has been leached. Overgrowths on some of the quartz grains indicate that silica deposition followed leaching. In one sample the quantity of pyrite is large enough to be detected by X-ray diffraction.

The X-ray diffraction method for mineralogical identification and X-ray fluorescence method for chemical composition are routine. Details of the sample preparation have been described by Hosterman (1969, p. 6–7). For X-ray diffraction, all samples were treated with ethylene glycol to check for expandable clay (montmorillonite) and were heated to 300°C to check for collapsible clay (vermiculite). Neither montmorillonite nor vermiculite was found to be present. Several samples were treated with 3*N* hydrochloric acid to check the presence of chlorite and kaolinite. The clay mineral-quartz ratios (table 1) are based on the peak-area ratios obtained from the X-ray diffraction traces. This gives the amount of each mineral present to an accuracy of about ± 10 percent.

The clay mineral-quartz ratios (table 1) are derived from the peak-area ratios of the following X-ray diffraction peaks: kaolinite at 7 A, illite at 9.8 A, chlorite at 7 A, pyrophyllite at 9.2 A, phlogopite at 10.1 A, and quartz at 4.26 A. When both koalinite and chlorite are present in a sample, a ratio between the two minerals is obtained from the kaolinite peak at 3.57 A (24.9° for Cu$K\alpha_1$ radiation) and the chlorite peak at 3.52 A (25.2°). This ratio is then applied to the 7 A peak area to obtain a ratio of kaolinite and chlorite with the other minerals. This method is used only when a 14 A peak is present because an assumption had to be made that

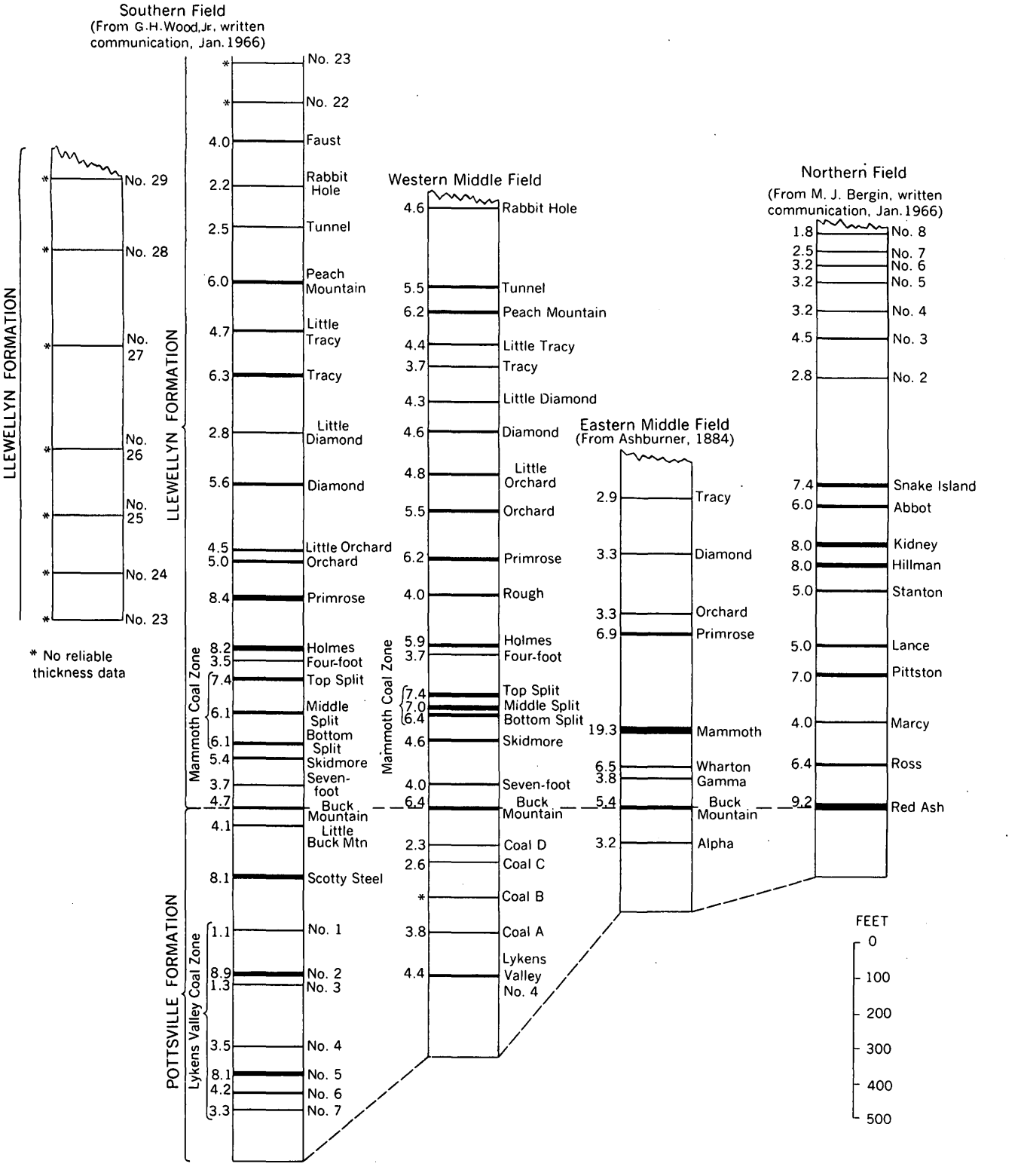

FIGURE 2.—Generalized columnar sections showing names, average thickness of coal (in feet), and intervals between coal beds in the eastern Pennsylvania anthracite fields (from Arndt and others, 1968, p. 130).

380-180 O - 70 - 7

TABLE 1.—*Chemical composition and mineralogy of some underclays in the eastern Pennsylvania anthracite fields*

[Analyses by X-ray fluorescence methods; chemical results in weight percent. Tr., trace]

Sample No.	Coal bed name and No.	7½-minute quadrangle	Coordinates		SiO_2	Al_2O_3	Fe_2O_3[1]	MgO	K_2O	TiO_2	Loss on ignition (1,000°C)	Sum	Peak-area ratio					
			Long. (W.)	Lat. (N.)									Kaolinite	Chlorite	Pyrophyllite	Illite	Phlogopite	Quartz
Southern field																		
1	No. 22	Pottsville	40°42′00″	76°11′26″	61	21	1.2	1.0	4.5	1.3	7.1	97.1	Tr.	------	--------	6	------	4
2	Rider (No. 21).	---do-----	42′00″	11′26″	59	22	3.0	1.4	4.2	1.3	7.5	98.4	------	2	--------	5	------	3
3	Faust (No. 21).	---do-----	42′00″	11′26″	54	17	3.7	1.4	4.1	1.1	18.5	99.8	------	2	--------	4	------	4
4	Rabbit Hole (No. 20).	---do-----	42′00″	11′26″	58	20	5.4	2.1	4.4	1.2	8.8	99.9	------	3	--------	4	------	3
5	Tunnel (No. 19).	---do-----	42′08″	11′26″	68	21	.8	.7	3.7	1.2	3.6	99.0	1	------	--------	4	------	5
6	Peach Mt. (No. 18).	---do-----	42′00″	11′26″	58	21	4.4	2.5	3.7	1.2	8.6	99.4	------	4	--------	3	------	3
7	-----do------	---do-----	42′00″	11′26″	55	22	5.4	2.5	4.2	1.2	9.3	99.6	------	3	--------	4	------	3
8	-----do------	---do-----	41′44″	11′23″	72	18	.7	1.0	3.6	1.4	4.0	100.7	------	Tr.	--------	5	------	5
9	Mammoth (No. 8).	---do-----	40′42″	11′15″	60	21	3.4	1.4	3.4	1.1	8.8	99.1	1	1	Tr.	5	------	3
10	Skidmore (No. 7).	---do-----	40′42″	11′15″	59	23	3.8	1.0	4.1	1.2	6.0	98.1	2	Tr.	1	5	------	2
11	Seven Foot (No. 6).	---do-----	40′42″	11′15″	68	19	1.0	1.4	2.3	1.0	6.7	99.4	4	Tr.	Tr.	2	------	4
12	Rider (No. 5).	---do-----	40′42″	11′15″	56	23	4.1	2.1	4.3	1.2	8.5	99.2	Tr.	2	Tr.	5	------	3
13	Buck Mt. (No. 5).	---do-----	40′42″	11′15″	55.2	26.8	1.6	.9	4.8	1.2	9.8	[2] 100.3	2	Tr.	Tr.	4	2	2
14	-----do------	---do-----	39′53″	14′07″	65	20	2.1	1.8	3.6	1.1	6.7	100.3	2	1	--------	3	------	4
15	-----do------	---do-----	44′28″	09′11″	60	25	1.1	1.8	4.3	1.1	6.8	100.1	Tr.	------	--------	5	2	3
16	Little Buck (No. 4).	---do-----	40′42″	11′15″	66	23	.9	1.8	3.5	1.2	3.9	100.3	1	------	4	3	Tr.	2
17	Scotty Steel (No. 3).	---do-----	40′42″	11′15″	61	26	1.2	1.0	3.5	1.3	4.4	98.4	------	1	4	3	------	2
18	Black shale	---do-----	40′42″	11′15″	53.8	26.5	4.7	1.8	4.3	1.2	7.2	[2] 99.5	1	3	Tr.	4	------	2
19	Lykens valley No. 1.	---do-----	40′42″	11′15″	54	22	6.5	2.5	4.6	1.3	9.3	100.2	------	3	1	4	------	2
20	Lykens valley No. 2.	---do-----	40′42″	11′15″	69	19	1.1	1.0	2.9	1.3	6.0	100.3	1	Tr.	2	3	------	4
21	Lykens valley No. 3.	---do-----	40′42″	11′15″	55	24	3.5	1.8	5.3	1.0	8.7	99.3	2	2	--------	4	------	2
22	Lykens valley No. 3½.	---do-----	40′42″	11′15″	57	15	3.2	1.4	4.0	1.0	19.0	100.6	1	1	--------	4	------	4
23	Lykens valley No. 4.	---do-----	40′42″	11′15″	56	17	3.5	2.1	5.0	1.1	14.9	99.6	------	2	--------	4	------	4
24	Lykens valley No. 5.	---do-----	40′42″	11′15″	55	18	7.9	2.5	5.4	1.0	9.4	99.2	------	3	--------	4	------	3
25	Lykens valley No. 6.	---do-----	40′42″	11′15″	62	20	3.3	1.8	5.5	1.1	6.5	100.2	------	1	--------	5	------	4
26	Lykens valley No. 7.	---do-----	40′42″	11′15″	60	17	7.3	1.4	4.5	1.1	7.7	99.0	------	1	--------	5	------	4
Western Middle field																		
27	Holmes (No. 10).	Shamokin.	40°47′18″	76°30′56″	59	24	2.4	1.0	4.1	1.2	5.8	96.5	1	2	--------	4	Tr.	3
28	Mammoth (No. 8).	Shenandoah.	48′40″	14′56″	54	25	7.3	1.8	4.5	1.1	7.2	100.9	------	------	--------	5	3	[3] 2
29	----do--------	Ashland..	48′18″	16′00″	61	25	1.4	1.0	4.3	1.1	6.4	100.2	1	------	--------	5	1	3
30	----do--------	----do----	48′15″	19′31″	58	26	1.1	2.5	4.9	1.3	6.1	99.9	Tr.	------	--------	6	2	2
31	----do--------	Shamokin	45′49″	35′48″	63	23	1.0	1.4	4.2	1.1	6.1	99.8	Tr.	------	--------	6	1	3
32	Black shale	Trevorton	45′30″	43′29″	59	19	6.9	1.8	3.3	1.2	9.0	100.2	1	2	--------	4	------	3
33	Buck Mt. (No. 5).	Shenandoah.	49′48″	13′40″	60	27	1.0	1.4	4.5	1.3	4.5	99.7	1	------	2	5	------	2
34	----do--------	Ashland..	48′30″	20′38″	61	25	1.5	1.4	4.0	1.2	5.7	99.8	Tr.	------	3	5	------	2
Eastern Middle field																		
35	Mammoth (No. 8).	Hazleton.	40°59′57″	75°56′45″	59	26	1.2	1.0	5.3	1.2	6.5	100.2	1	------	--------	6	------	3
36	----do--------	----do----	59′57″	56′45″	62	22	2.5	1.4	3.9	1.2	6.8	98.4	1	1	1	3	Tr.	3
37	Buck Mt. (No. 5).	Nuremberg.	54′04″	76°09′40″	68.9	21.6	.9	.4	2.7	1.3	4.5	[2] 100.3	Tr.	------	3	3	1	3
38	----do--------	----do----	54′09″	09′40″	58	27	1.2	1.4	4.7	1.2	5.6	99.1	Tr.	------	2	5	1	2
39	----do--------	----do----	54′08″	08′39″	61.6	24.5	1.4	.7	4.6	1.2	5.6	[2] 99.6	Tr.	------	--------	6	1	3
40	----do--------	Hazleton.	52′46″	75°59′05″	64	25	.8	1.4	3.6	1.2	3.6	99.6	Tr.	------	3	4	------	3
41	----do--------	----do----	54′29″	58′46″	63	25	.8	1.8	4.6	1.2	3.7	100.1	Tr.	------	2	5	------	3
42	----do--------	Nuremberg.	54′04″	76°09′40″	58	28	1.2	2.1	5.0	1.2	3.8	99.3	------	------	2	5	2	1
43	----do--------	----do----	54′04″	09′40″	64	26	.7	.7	2.9	1.3	4.1	99.7	Tr.	------	4	3	1	1
44	----do--------	----do----	54′04″	09′40″	66	23	.9	1.0	2.9	1.3	5.2	99.3	------	------	3	4	1	1

See footnotes at end of table.

TABLE 1.—*Chemical composition and mineralogy of some underclays in the eastern Pennsylvania anthracite fields*—Continued

[Analyses by X-ray fluorescence methods; chemical results in weight percent. Tr., trace]

Sample No.	Coal bed name and No.	7½-minute quadrangle	Coordinates		SiO_2	Al_2O_3	Fe_2O_3[1]	MgO	K_2O	TiO_2	Loss on ignition (1,000°C)	Sum	Peak-area ratio					
			Long. (W.)	Lat. (N.)									Kaolinite	Chlorite	Pyrophyllite	Illite	Phlogopite	Quartz
Northern field																		
45	No. 6	Wilkes-Barre West.	41°12′10″	75°56′19″	62	22	4.5	2.1	5.1	1.2	3.1	100.0	.....	3	.....	3	.....	4
46	Abbott	....do....	11′43″	57′08″	62	21	1.6	1.8	3.5	1.2	8.8	99.9	.....	2	.....	4	.....	4
47	Kidney	....do....	10′53″	59′03″	63	22	1.0	1.4	4.7	1.2	6.2	99.5	1	.....	.....	5	.....	4
48	Hillman	....do....	11′05″	58′16″	65	18	1.3	1.6	3.5	1.2	8.7	99.3	1	1	.....	4	.....	4
49	Lower Stanton	....do....	11′59″	55′06″	60	24	1.0	1.4	3.2	1.3	8.8	99.7	3	.....	.....	4	.....	3
50	.....do.....	....do....	11′59″	55′06″	57	21	3.5	1.5	5.8	1.3	9.1	99.2	2	1	.....	4	.....	3
51	.....do.....	....do....	10′55″	58′43″	55	25	1.9	1.9	5.8	1.2	9.9	100.7	.....	2	.....	5	.....	3
52	Lower Pittston	Wilkes-Barre East.	14′56″	51′08″	59	25	1.3	1.8	4.0	1.2	7.4	99.7	.....	.....	.....	5	3	2
53	.....do.....	Nanticoke.	09′58″	76°03′16″	59	24	2.5	1.4	4.5	1.1	6.8	99.3	2	.....	.....	5	.....	3
54	.....do.....	Pittston	17′09″	75°49′35″	53	23	1.3	.9	4.8	1.2	15.3	99.5	1	.....	.....	5	.....	4
55	Upper Marcy	....do....	17′02″	49′35″	65	23	1.4	1.3	2.9	1.1	3.9	98.6	.....	2	.....	4	.....	4
56	Lower Marcy	....do....	21′16″	47′07″	59	24	1.5	1.8	4.1	1.6	7.4	99.4	2	.....	.....	5	.....	3
57	.....do.....	Scranton	23′14″	41′06″	59	22	4.5	1.4	4.3	.9	7.3	99.4	1	.....	.....	5	1	3
58	.....do.....	Carbondale.	33′43″	31′19″	61	23	2.4	2.0	4.5	1.1	5.9	99.9	2	1	.....	4	.....	3
59	Upper Ross	Wilkes-Barree West.	11′44″	55′12″	62	24	2.1	2.3	4.1	1.2	4.4	100.1	1	1	1	4	.....	3
60	.....do.....	Pittston	16′50″	48′58″	65	22	1.0	1.0	2.4	1.1	6.2	98.7	3	.....	1	2	.....	4
61	Lower Ross	Wilkes-Barre West.	12′00″	54′25″	58	23	1.4	1.4	7.5	1.3	5.5	98.1	.....	.....	.....	7	.....	3
62	.....do.....	....do....	11′36″	55′12″	60	25	1.2	1.4	4.1	1.1	6.8	99.6	2	.....	.....	4	.....	4
63	.....do.....	Pittston	15′50″	48′58″	56	23	5.6	2.5	3.7	1.2	7.9	99.9	1	2	2	3	.....	2
64	.....do.....	Olyphant	23′52″	35′57″	61	23	1.5	1.7	3.2	1.4	8.2	100.0	3	.....	.....	3	.....	4
65	.....do.....	Carbondale.	31′21″	30′51″	50	14	.4	1.8	2.3	.8	30.1	99.4	2	.....	.....	3	.....	5
66	Upper Red Ash	Wilkes-Barre West.	11′35″	55′16″	59	24	1.7	1.4	2.1	1.1	10.3	99.6	3	.....	.....	4	.....	3
67	.....do.....	Kingston	16′12″	56′04″	57	25	2.0	1.9	3.3	1.1	7.4	97.7	3	.....	.....	4	1	2
68	.....do.....	Carbondale.	31′21″	30′51″	50	15	1.1	.9	3.5	.7	27.9	99.1	2	.....	.....	4	.....	4
69	Lower Red Ash	Wilkes-Barre West.	12′38″	53′18″	60	25	1.3	1.4	5.0	1.3	5.6	99.6	1	.....	.....	5	2	2
70	.....do.....	Wilkes-Barre East.	13′04″	51′45″	56	26	1.5	1.4	4.7	1.3	8.1	99.0	2	.....	.....	5	1	2
71	.....do.....	Wilkes-Barre West.	11′57″	54′30″	60	24	2.2	1.8	4.0	1.1	7.4	100.5	1	1	.....	4	1	3
72	.....do.....	....do....	11′31″	55′17″	61	25	1.2	1.8	3.7	1.5	5.0	99.2	2	.....	.....	4	1	3
73	.....do.....	Nanticoke.	11′01″	76°03′47″	59	24	1.5	1.0	2.8	1.6	9.9	99.8	3	.....	.....	4	.....	3
74	.....do.....	Wilkes-Barre West.	13′52″	75°59′04″	46	20	1.6	1.5	3.3	1.3	26.1	99.8	3	.....	.....	4	.....	3
75	Campbell Ledge Member.	Pittston	20′54″	48′08″	35	15	.9	....	1.6	.7	47.4	100.6	6	.....	.....	1	.....	3
76	.....do.....	Wilkes-Barre West.	12′11″	53′48″	62	27	.9	2.0	3.6	1.3	3.2	100.0	1	.....	3	4	.....	2

[1] Includes FeO and Fe_2O_3.
[2] Analysis by rapid rock method.
[3] Contains pyrite.

chlorite is not present if there is no 14 A peak. Also, it is assumed that kaolinite is not present if there is no 3.57 A peak. Phlogopite is very difficult to identify by X-ray diffraction methods when present with 2M illite; therefore, it may be overlooked, especially if it occurs in small amounts. On an X-ray machine using maximum resolution, the following three peaks can be separated from the 2M illite peaks: the basal (001) peak at 10.1 A, the basal (002) peak at 5.08 A, and the (022) reflection at 3.40 A (fig. 3). By removing quartz and chlorite from the sample, the 060 reflection can be observed at 1.54 A.

Kaolinite occurs randomly throughout the underclays of the Pottsville and Llewellyn Formations. It occurs in amounts ranging from a trace to about 80 percent in 55 of 76 samples, but only 33 samples have significant amounts of 10 percent or more, and only one sample contains more than 40 percent kaolinite. The kaolinite is the well-crystallized variety with a basal spacing (001) of 7.13 A. The poorly crystalline variety which is typical

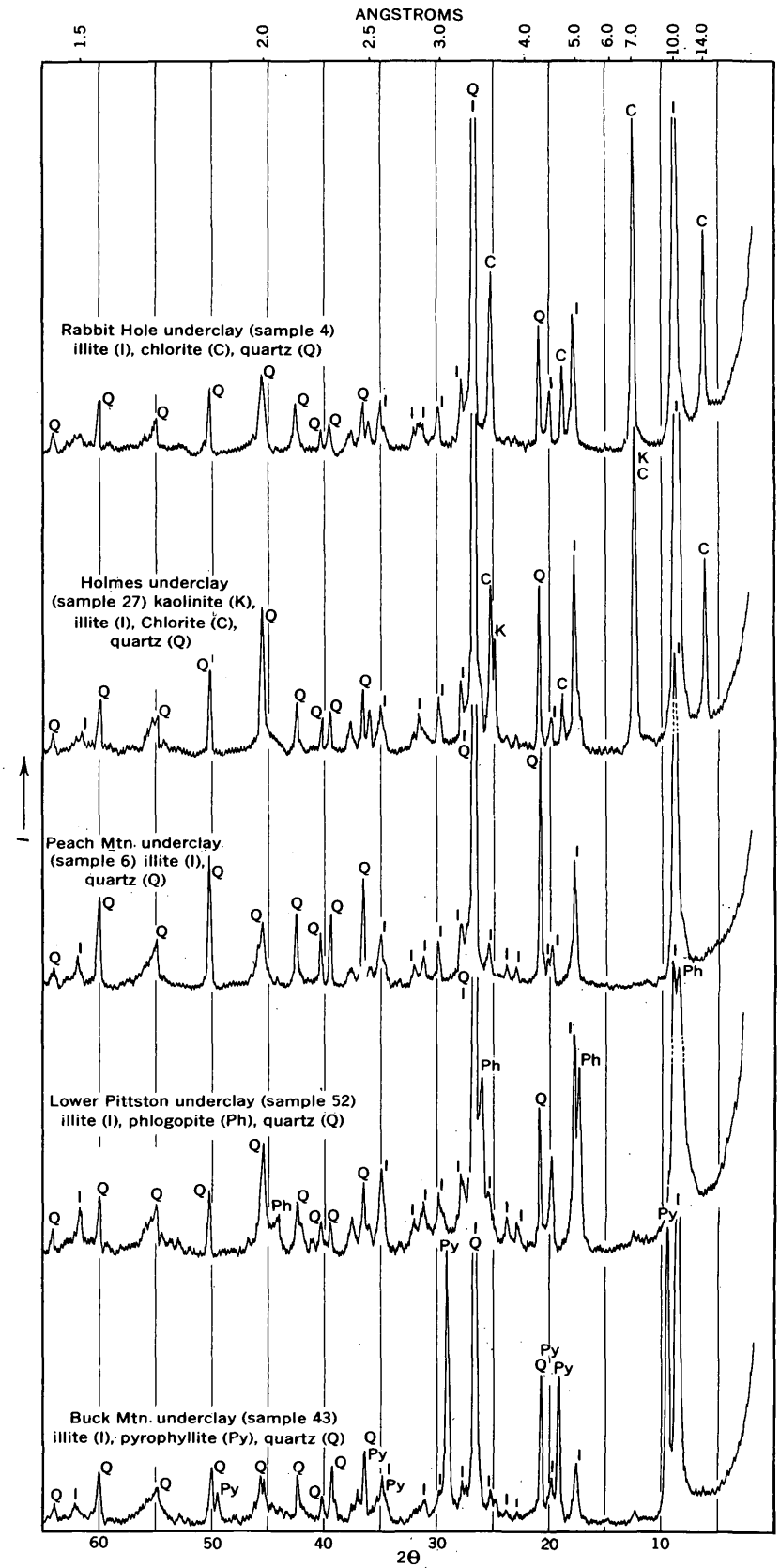

FIGURE 3.—X-ray diffraction traces of underclay samples from eastern Pennsylvania anthracite fields.

of the semiflint and plastic underclays of the Bituminous coal region (Patterson and Hosterman, 1962, p. 60) is absent. Two vague trends in the kaolinite can be observed in table 1. In general, the kaolinite content is low or absent when chlorite is present in large quantities (this is easily checked by removing the chlorite with hydrochloric acid), and kaolinite seems to be more abundant in the Northern field than it is in the Southern or Middle fields.

The occurrence of pyrophyllite in the underclays and black shales may be a clue to the temperature and pressure prevailing when the anthracite formed. Pyrophyllite occurs in 24 of the 76 samples. It is easily distinguishable from the other clay minerals by its basal 002 spacing of 9.21 A on the X-ray diffraction traces (fig. 3).

In thin sections, pyrophyllite was found disseminated throughout and as filling in small cracks. Amounts range from 5 to 45 percent throughout all the coal fields, but pyrophyllite seems to be more prevalent in the Southern and two Middle fields than in the Northern field. The distribution of samples indicates that pyrophyllite is concentrated in the upper part of the Pottsville and lower part of the Llewellyn and is absent below the underclay of the Lykens Valley No. 2 coal bed of the Pottsville and in the underclays or shales lying stratigraphically above the younger Mammoth or Upper Ross coal beds (table 1 and fig. 2).

Illite occurs in every sample of underclay and black shale (table 1) in amounts ranging from 10 to 70 percent, with an average of about 40 percent. Illite as used here is defined as a clay-size dioctahedral mica (muscovite). All the illite was found to be the 2M polymorph. However, instead of a basal spacing (002) of 10.01 A found in synthetic muscovites (Yoder and Eugster, 1955, p. 247), this illite has a basal spacing (002) of 9.8 A (fig. 3). The only trends observed from the illite are that it occurs in every sample of underclay and black shale and that the 1M or *Md*[1] polymorphs are not present.

Chlorite is randomly distributed throughout the underclays and black shales of the anthracite fields. It occurs in amounts ranging from a trace to 40 percent in 35 of 76 samples; 18 samples contain more than 10 percent. Chlorite was not identified by X-ray diffraction traces in the samples from which thin sections were made. However, a very few grains can be observed under the optical microscope in all the sections.

Chlorite is identified on X-ray diffraction traces by its 001 basal peak at 14 A which does not expand to 17 A with ethylene glycol treatment and is not collapsed to 10 A by heating to 550°C. If both kaolinite and chlorite are suspected in a sample, the kaolinite can be positively identified by treating the sample with hydrochloric acid. The acid decomposes chlorite but not kaolinite; therefore, on X-ray diffraction traces, the 002 basal spacing of chlorite at 7 A will be removed, leaving the 001 basal peak of kaolinite. Two trends in the occurrence of chlorite can be observed in table 1. As has been pointed out, chlorite is low or absent where kaolinite is present in large quantities. Also, chlorite seems to be much more prevalent in the Southern field than it is in the Middle or Northern fields.

Phlogopite, a trioctahedral mica containing magnesium and iron, is found to occur in at least 22 of 76 samples (table 1) and may be present in others. The spacing of the basal (001) peak at 10.1 A, the second-order basal peak at 5.08 A, and (022) reflections at 3.40 A and 2.03 A indicate that the phlogopite is a 1M or 3T polymorph type (Yoder and Eugster, 1954, p. 170). Under the optical microscope, a very pale brown mica with weak pleochroism, strong birefringence, and small $2V$ can be seen in some of the thin sections. This observation supports the X-ray diffraction data that phlogopite is present in some of the underclays of eastern Pennsylvania. The phlogopite seems to be concentrated in the lower part of the Llewellyn Formation; it does not occur in the underclays of the Lykens Valley coal beds of the Pottsville Formation, and it is not found in the underclays in the upper part of the Llewellyn Formation. In addition, it is more abundant in the two Middle coal fields.

ORIGIN

Throughout the bituminous coal field of the Appalachian Plateau, the presence of root fossils, the absence of a soil profile, the lack of bedding, the intimate association with overlying coal beds, and the marine or brackish-water fossils in the enclosing black shales suggest the deposition of clay in coastal swamps. The mineralogical and chemical evidence indicates that the underclays were formed in low-gradient swamps whose acidic and reducing environment altered the ordinary fine-grained sediments of Pennsylvanian age. This is supported by the observations of Schultz (1958, p. 363, 377–378) and Patterson and Hosterman (1962, p. 79). Theoretically, alteration of clay by a leaching process takes place shortly after deposition but before burial by overlying sediments. Three types of underclay—plastic, semiflint, and flint—appear to represent progressive stages in the leaching process. "Juvenile" or unaltered underclay is plastic and composed of poorly crystalline kaolinite, *Md* illite, and mixed-layer clay minerals. The amount of kaolinite increases successively from

[1] The term "1M*d*" is commonly used in the literature. The authors, however, prefer to use M*d* because it represents disordered stacking of the unit cells in which the random stacking must be one or more.

plastic to semiflint to flint clay, and this increase is accompanied by an increase in the crystallinity of the kaolinite and a decrease in the amount of illite and mixed-layer clay minerals. Quartz is present in all types of clay in amounts ranging from 0 to almost 50 percent. According to the leaching theory, kaolinite recrystallizes and forms concurrently with the removal of alkalies, iron, and silica from the illite and mixed-layer clay (Patterson and Hosterman, 1962, p. 80–81). Also, if the leaching process is sufficiently intensive or long lasting enough, almost all the silica from quartz is leached, and diaspore and boehmite are formed as a result of silica being removed from the kaolinite.

The origin of underclays in the Pennsylvania Anthracite region is probably similar to that described above, except that the clays were deposited in freshwater swamps rather than coastal swamps, and these underclays have also undergone low-grade metamorphism. The mineral composition indicates that the anthracite underclays were recrystallized under conditions of elevated temperature and pressure. As mentioned previously in the section on mineralogy, these underclays are composed of kaolinite, pyrophyllite, illite, phlogopite, and chlorite, and quartz is the only nonclay mineral. There are no experimental data on this mineral assemblage that can give the temperature and pressure of metamorphism. However, the stability fields of the minerals may be a clue. The upper stability limit of kaolinite with quartz has been the subject of experimental work (Roy and Osborn, 1954; Carr and Fyfe, 1960). These experiments are based on gel crystallizations and short-term unreversed thermal decomposition; therefore, the true stability limit is probably lower than the 405° to 420°C indicated by these experiments (Reed and Hemley, 1966, p. C164). Hemley and Jones (1964, p. 552) observed that the reaction of kaolinite plus quartz alters to pyrophyllite at about 380°C at 1,000 bars partial water pressure. Reed and Hemley (1966, p. C164) state that this reaction takes place at temperatures as low as 300°C and 1,000 bars when allowed to run for a long period of time. The stability of pyrophyllite has been studied by Yoder and Eugster (1954), Roy and Osborn (1954), Winkler (1957), Carr and Fyfe (1960), Carr (1963), Aramaki and Roy (1963), Althouse (1966), Hemley (1967), and Kerrick (1968). From the results of these experiments, the upper stability limit of pyrophyllite ranges from 400°C at 1,000 bars to 580°C at 2,000 bars. Pyrophyllite was observed to form from mica at about 350°C and 1,000 bars in some experiments by Hemley and Jones (1964, p. 548). The 2M polymorph of illite (muscovite), derived from the *Md* illite in the original sediment, is found to be stable at temperatures above 200°–350°C at 1,000 bars water pressure by Yoder and Eugster (1955, p. 246) and at temperatures above 125°C by Velde (1965, p. 442). According to Winkler (1957, p. 65), when illite (*Md*) is changed to muscovite (2M), iron and magnesium are released in addition to silica, and these form chlorite. He also states that chlorite and muscovite change to biotite, aluminum-rich chlorite, and quartz. If magnesium is more abundant than iron, it seems that phlogopite would form instead of biotite. Yoder and Eugster (1954, p. 164) made phlogopite synthetically at temperatures between 400° and 1,000°C at 1,000 bars water pressure. Muscovite, chlorite, and phlogopite represent the greenschist facies which has a metamorphic temperature range of 250° to 450°C and a pressure range of 2,000 to 9,000 bars (5–30 km in depth) (Turner, 1968, p. 366).

The possible diagenesis and low-grade metamorphism of the underclays is summarized as follows: The first stage of alteration is the recrystallization of illite from *Md* to 2M polymorphic type which occurs at about the time of burial and lithification. As illite is recrystallized, Si, Fe, and Mg are released to form chlorite (Winkler, 1957, p. 65). If the temperature of this recrystallization is as low as 125°C (Velde, 1965, p. 442), this is equivalent to a depth of about 14,000 feet and a lithostatic pressure of about 1,300 bars. The second stage of alteration is the formation of pyrophyllite from kaolinite and quartz and from illite (2M) and quartz (Hemley and Jones, 1964, p. 548). This reaction probably takes place between 300° and 350°C. The author suggests that the postassium from illite may combine with chlorite to form phlogopite. However, the experimental studies on chlorite, phlogopite, and biotite are too imperfect to throw any light on the critical reactions mentioned above.

REFERENCES

Althouse, E., 1966, Die Bildung von Pyrophyllit und Andalusit zwischen 2,000 und 7,000 Bar H_2O Druck: Naturwissenschaften, v. 53, p. 105–106.

Aramaki, Shigeo, and Roy, Rustum, 1963, A new polymorph of Al_2SiO_5 and further studies in the system Al_2O_3-SiO_2-H_2O: Am. Mineralogist, v. 48, nos. 11–12, p. 1322–1347.

Arndt, H. H., Averitt, Paul, Dowd, James, Frendzel, D. J., and Gallo, P. A., 1968, Coal, *in* U.S. Geol. Survey and U.S. Bur. Mines, Mineral resources of the Appalachian region: U.S. Geol. Survey Prof. Paper 580, p. 102–133.

Ashburner, C. A., 1883–85, Atlas of anthracite fields; Eastern Middle anthracite fields, pts. 1–3: Pennsylvania Geol. Survey, 2d.

Carr, R. M., 1963, Synthesis fields of some aluminum silicates—further studies: Geochim. et Cosmochim. Acta, v. 27, p. 133–135.

Carr, R. M., and Fyfe, W. S., 1960, Synthesis fields of some aluminum silicates: Geochim. et Cosmochim. Acta, v. 21, p. 99–109.

Hemley, J. J., 1967, Stability relations of pyrophyllite, andalusite, and quartz at elevated pressures and temperatures [abs.]: Am. Geophys. Union Trans., v. 48, p. 224.

Hemley, J. J., and Jones, W. R, 1964, Chemical aspects of hydrothermal alteration with emphasis on hydrogen metasomatism: Econ. Geology, v. 59, no. 4, p. 538–569.

Hosterman, J. W., 1969, Clay deposits of Spokane County, Washington: U.S. Geol. Survey Bull. 1270, 96 p.

Kerrick, D. M., 1968, Experiments on the upper stability limit of pyrophyllite at 1.8 kilobars and 3.9 kilobars water pressure: Am. Jour. Sci., v. 266, no. 3, p. 204–214.

Patterson, S. H., and Hosterman, J. W., 1962, Geology and refractory clay deposits of the Haldeman and Wrigley quadrangles, Kentucky: U.S. Geol. Survey Bull. 1122–F, 113 p.

Reed, B. L., and Hemley, J. J., 1966, Occurrence of pyrophyllite in the Kekiktuk Conglomerate, Brooks Range, northeastern Alaska *in* Geological Survey Research 1966: U.S. Geol. Survey Prof. Paper 550–C, p. C162–C166.

Roy, Rustum, and Osborn, E. F., 1954, The system Al_2O_3-SiO_2-H_2O: Am. Mineralogist, v. 39, nos. 11–12, p. 853–885.

Schultz, L. G., 1958, Petrology of underclays: Geol. Soc. America Bull., v. 69, no. 4, p. 363–402.

Turner, F. J., 1968, Metamorphic petrology—Mineralogical and field aspects: New York, McGraw-Hill Book Co., 403 p.

Velde, B., 1965, Experimental determination of muscovite polymorph stabilities: Am. Mineralogist, v. 50, nos. 3–4, p. 436–449.

Winkler, H. G. F., 1957, Experimentelle Gesteinsmetamorphose—I, Hydrothermale Metamorphose karbonatfreier Tone: Geochim. et Cosmochim. Acta, v. 13, p. 42–69.

Wood, G. H., Jr., Trexler, J. P., Arndt, H. H., Yelenosky, Andy, and Soren, Julian, 1956, Subdivision of Pottsville Formation in Southern Anthracite field, Pennsylvania: Am. Assoc. Petroleum Geologists Bull., v. 40, no. 11, p. 2669–2688.

Wood, G. H., Jr., Trexler, J. P., and Kehn, T. M., 1969, Geology of the west-central part of the Southern Anthracite field and adjoining areas, Pennsylvania: U.S. Geol. Survey Prof. Paper 602, 150 p.

Wood, G. H., Jr., Trexler, J. P., Yelenosky, Andy, and Soren, Julian, 1962, Geology of rocks of Pennsylvanian age in the southern half of the Tremont quadrangle, Schuylkill County, Pennsylvania: U.S. Geol. Survey Bull. 1112–F, p. 181–208.

Yoder, H. S., and Eugster, H. P., 1954, Phlogopite synthesis and stability range: Geochim. et Cosmochim. Acta, v. 6, no. 4, p. 157–185.

———1955, Synthetic and natural muscovites: Geochim. et Cosmochim. Acta, v. 8, nos. 5–6, p. 225–280.

A CORUNDUM OCCURRENCE IN THE EASTERN ALASKA RANGE, ALASKA

By DONALD H. RICHTER, Anchorage, Alaska

Abstract.—Crystals of gray corundum, as much as 8 cm long, occur in alkali pegmatite dikes in the Mentasta Mountains of the eastern Alaska Range. The pegmatite dikes cut a syenite-monzonite gneiss that is part of a large metaigneous complex consisting principally of diorite and diorite gneiss. Field relations and K-Ar dates suggest that the rocks of the complex were syntectonically emplaced during late Permian or Triassic time. The pegmatite dikes are composed almost entirely of orthoclase, orthoclase microperthite, and soda feldspar; biotite and hornblende are minor constituents. Corundum has only been recognized in three dikes and where present is generally associated with muscovite. Asteriated stones have been cut from the larger corundum crystals, but the poor quality and scarcity of the crystals preclude an economic gem industry.

In 1964, Mr. Ray Gatz, an Alaskan prospector, brought news of an occurrence of blue sapphire in the Mentasta Mountains of the eastern Alaska Range. The area was visited briefly by the author in 1967 and 1968, but it was not until the summer of 1969 that the author's U.S. Geological Survey field party examined the area in more detail.

Scattered fragments of claim posts(?) and an old weathered sieve in the vicinity of the corundum deposits indicate that Gatz had rediscovered a locality that had been prospected probably prior to and during the early part of World War II when a nearby molybdenum deposit was being explored (Moffit, 1954, p. 209). The occurrence may also have been known much earlier and perhaps was the source of an ambiguous report by Kunz (1899, p. 520), who mentioned seeing "good grey and pink specimens of asteriated corundum from a locality on the Copper River in the Juneau Indian Reservation [sic], Alaska." Kunz' report was referred to in a description of corundum deposits in the United States (Pratt, 1901, p. 88), but since then no mention of corundum in Alaska has appeared in the literature.

The corundum occurs in thin pegmatite dikes that cut a syenite-monzonite gneiss, and although probably of value only as a mineralogical curiosity, its uniqueness and geologic setting warrant description.

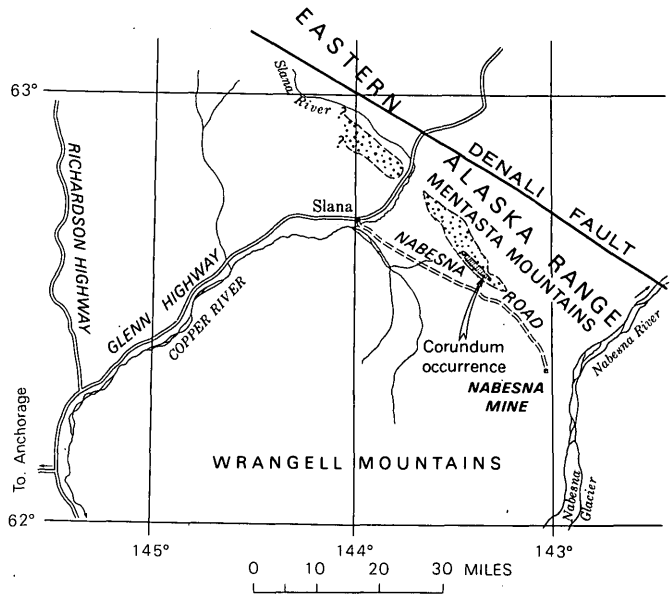

FIGURE 1.—Sketch map of a part of south-central Alaska, cipal geologic features. Ruled area shows zone of syenite-monzonite gneiss within metaigneous complex (stippled).

LOCATION AND ACCESSIBILITY

The known corundum-bearing pegmatites are restricted to a ¼-mile-square area at an elevation of between 5,300 and 5,500 feet on the southern flank of the Mentasta Mountains in the eastern Alaska Range (figs. 1 and 2). The area is within the Nabesna C–5 quadrangle (scale 1:63,360), and the map coordinates are lat 62°36′ N. and long 143°21′ W.

The area is easily accessible from the Nebesna Road, an intermittently maintained gravel road that leaves the Glenn Highway at the small community of Slana about 263 miles northeast of Anchorage (fig. 1). Approximately 20 miles east of Slana on the Nabesna Road, an old trail a little over 3 miles long leads to an adit at an abandoned molybdenite prospect, which is a few hundred feet west of the westernmost corundum occurrence (fig. 2).

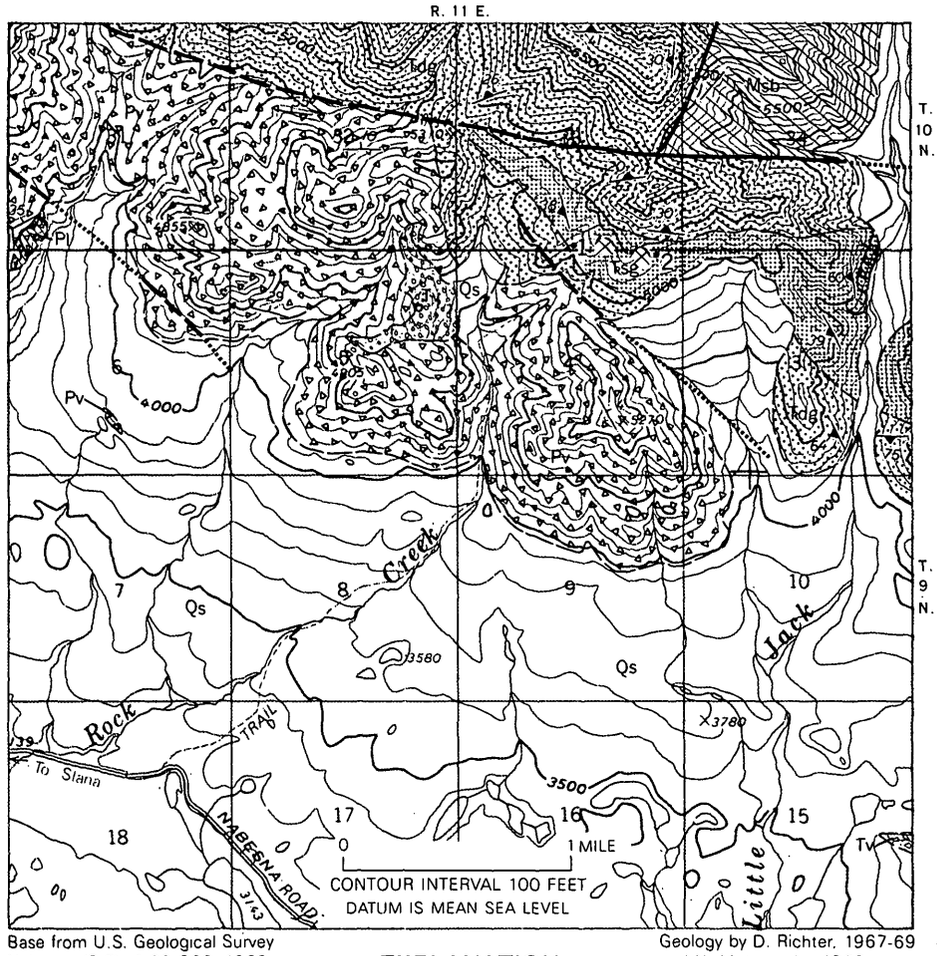

FIGURE 2.—Geologic map of the corundum-bearing area, Mentasta Mountains, eastern Alaska Range, Alaska.

GEOLOGIC SETTING

The host rock for the corundum-bearing pegmatites is a unique peraluminous syenite-monzonite gneiss that is part of a large metaigneous complex consisting principally of diorite gneiss and a variety of nonfoliated diorites with subordinate amphibolite, metagabbro, and schistose cataclasite. Most of the alkali gneisses, including those that are host to the alkali pegmatites, are confined to a well-defined zone approximately 6 miles long and as much as 1 mile wide in the extreme southeastern end of the metaigneous complex (fig. 1). The contact between the alkali gneiss zone and the enclosing diorite gneiss is broadly gradational. A few layers of diorite gneiss occur within the alkali gneiss zone, and thin layers of alkali gneiss are scattered throughout much of the complex but appear to be especially common near the alkali gneiss zone.

Gneissic banding, foliation, and lineation directions within the metaigneous complex trend generally northwest, parallel to the major structural features of the eastern Alaska Range. Foliation dips are steep and generally to the northeast, but anomalous reversals indicate strong local folding.

Although the gneissosity displayed by much of the rock in the complex indicates high-grade regional metamorphism, the common mineral assemblage of horn-blende-biotite-plagioclase (-quartz-alkali feldspar-epidote) in the diorite gneisses suggests a metamorphic environment no higher than the greenschist facies. Local schistose cataclasites containing the assemblage quartz - muscovite - plagioclase-almandine-potassium feldspar provide evidence of strong dislocation metamorphism. All rocks show the effects of retrograde metamorphism by the development of chlorite after biotite and hornblende.

The metaigneous complex, although predominantly fault bounded, locally appears to exhibit gradational intrusive relations with a thick unit of andesite volcanics and volcaniclastics of Permian age. These apparent intrusive contacts consist of a complex metamorphic and dioritized aureole as much as a mile wide. The rocks within the aureole are principally albite-epidote to hornblende hornfels with irregular segregations of both normal and foliated diorite.

K–Ar dating of coexisting hornblende and biotite from an alkali pegmatite in the alkali gneiss at the molybdenite prospect (fig. 2) indicates concordant ages of 199 and 198 m.y., respectively, for the minerals. The alkali pegmatites probably represent an extremely late stage of igneous activity within the complex; thus, the K–Ar dates indicate that emplacement of the complex probably culminated in late Triassic time. The intimate association of normal igneous rocks, metamorphic rocks, and cataclasites further suggests that emplacement occurred during a prolonged and complex tectonic event in an ancestral Alaska Range.

The syenite-monzonite gneisses are light pink and contrast boldly with the dark-gray diorite gneisses. Gneissosity in the syenites and monzonites is characterized by biotite- and (or) hornblende-rich layers alternating with feldspathic bands poor in mafic minerals. Thicknesses of the layers range from less than a tenth of an inch to more than a foot; the mafic layers are conspicuously thinner and less continuous than the feldspathic layers. The syenite gneisses and monzonite gneisses are indistinguishable in hand specimen, and even in thin section more than cursory examination is necessary to differentiate the two types. Apparently, changes in the potassium feldspar to plagioclase ratio are subtle and may occur even within single bands over relatively short distances. The alkali gneisses exhibit a typical xenoblastic texture; very few individual crystals are more than 2 mm in diameter. Locally, the rocks are porphyroblastic, with porphyroblasts of microperthite as much as 30 mm long. Some of the larger feldspar porphyroblasts and most of the late accessory minerals including the corundum are poikiloblastic.

In most places, the alkali gneisses have a low color index and consist principally of potassium feldspar and albite-oligoclase and minor biotite and hornblende. Accessory minerals are muscovite, corundum, sphene, zircon, opaque minerals, zoisite, and carbonate. Modal analyses of the syenite and monzonite gneiss and a diorite gneiss occurring within the alkali gneiss are listed in table 1. Most of the potassium feldspar in the gneisses is orthoclase or orthoclase microperthite. The large porphyroblasts in the porphyroblastic variants, however, are apparently microcline microperthites that have undergone some rotation. Not all the soda feldspars exhibit multiple twinning, and where twinning is absent, they are difficult to distinguish from orthoclase unless stained. In general, both feldspars are fresh, although locally the plagioclase is saussuritized. Both brown and green biotite are present in the gneisses, but the green variety predominates. Both also show alteration to chlorite. Corundum is present in all sections examined and occurs as small (<0.5 mm) euhedral crystals. Euhedral crystals of sphene, typically diamond shaped in cross section and as much as 1 mm long, are locally abundant in some of the gneisses, especially in the mafic-rich bands. The opaque minerals are probably magnetite or magnetite-ilmenite mixtures and are generally associated with white opaque leucoxene. Carbonate minerals and zoisite occur as small irregular aggregates scattered through the gneiss.

TABLE 1.—*Modal analyses of alkali gneisses and related rocks, Mentasta Mountains, eastern Alaska Range, Alaska*

[Tr., trace]

Field No.	67–ARh–172	68–ARh–325	69–ARh–1	69–ARh–2	69–ARh–3b
Rock name	Monzonite gneiss	Syenite gneiss	Syenite gneiss	Porphyroblastic monzonite gneiss	Diorite gneiss
Potassium feldspar.	45	65	61	[1] 43	----
Plagioclase	45 (An_{10})	26 (An_{8-10})	31	48 (An_{10-14})	30 (An_{46-55})
Biotite [2]	5	1	4	3	----
Hornblende	----	3	----	----	59
Clinopyroxene	----	----	----	----	5
Muscovite	1	----	----	----	2
Zoisite	----	----	3	5	----
Corundum	1	Tr.	Tr.	Tr.	----
Sphene	1	2	----	1	----
Zircon	Tr.	----	Tr.	Tr.	----
Carbonate	Tr.	----	----	----	----
Opaque minerals	2	3	1	Tr.	4

Location of samples:
67–ARh–172: Elevation 4,600 feet, 1.6 miles S. 65° E. of loc. 2, figure 2.
68–ARh–325: Elevation 5,500 feet, 2.8 miles N. 55° W. of loc. 2, figure 2.
69–ARh–1, 69–ARh–2: Elevation 5,020 feet, loc. 1, figure 2.
69–ARh–3b: Elevation 5,400 feet, loc. 2, figure 2.

[1] Includes microcline microperthite porphyroblasts (26 percent) and matrix orthoclase (17 percent).
[2] Predominantly green biotite locally altered to chlorite.

GEOLOGY AND MINERALOGY OF THE CORUNDUM-BEARING PEGMATITES

Pink, coarse-grained to pegmatitic syenite dikes are relatively common throughout the alkali gneiss zone in the complex, but only in one small area are they known to contain corundum crystals of any size. The dikes are small and discontinuous; most are less than 3 feet wide. They are massive and exhibit clear, distinct crosscutting relations with the host gneiss; however, the actual contact may be either sharp or gradational. The easternmost corundum-bearing dike cuts a fine-grained schistose rock less than 1 foot thick consisting of epidote, white mica, plagioclase, and carbonate with veinlets of fibrous calcite and fresh andesine. Crystals are as large as 10 to 15 cm in the dike rocks, but the average grain size is 3 cm or less. Commonly a matrix of medium-grained crystals is present. The mineralogy of the dikes is simple, with orthoclase, orthoclase microperthite, and soda feldspar the principal constituents. Antiperthite, consisting of soda feldspar with streaky blebs of potassium feldspar, was observed in one thin section. Small crystals of dark-green biotite are common minor constituents. Locally, dark massive hornblende is present, but the mafic minerals do not constitute more than 2 percent by volume of the dikes at any locality. Sporadic aggregates or groups of gray corundum crystals occur in at least three of the dikes at the localities shown in figure 2. Small books of light-gray to very pale grayish-lavender muscovite as large as 3 cm in diameter are generally associated with the corundum. The muscovite is a dioctahedral mica; it does not have an unusually high lithium content, contrary to what its color suggests. The trace-element chemistry of the pegmatites is also comparatively simple, as indicated by a spectrographic analysis of bulk material from one of the corundum-bearing localities (table 2). Neither the rare earth elements nor the other elements commonly found in alkali rocks, such as Mo, Be, W, Zr, and Nb, are present in amounts exceeding the average crustal abundance.

The corundum crystals occur as elongate, doubly terminated hexagonal pyramids as much as 2 to 8 cm long and 2 to 3 cm in diameter (fig. 3). Many of the

TABLE 2.—*Semiquantitative spectrographic analysis of corundum-bearing alkali pegmatite, Mentasta Mountains, eastern Alaska Range, Alaska*

[Looked for, but not detected: P, Ag, As, Au, Cd, Co, Cr, Ge, Hf, Hg, In, Li, Mo, Ni, Pd, Pt, Re, Sb, Sc, Sn, Ta, Te, Th, Tl, U, V, W, Yb, Zn, Pr, Nd, Sm, and Eu. Analyst: Chris Heropoulos]

Element	Content (weight percent) [1]	Element	Content (weight percent) [1]
Si	10	Be	.00015
Al	10	Ce	.01
Fe	.5	Cu	.0005
Mg	.15	Ga	.002
Ca	.5	La	.005
Na	3.0	Nb	.005
K	3.0	Pb	.002
Ti	.07	Sr	.007
Mn	.01	Y	.001
B	.002	Zr	.005
Ba	0.02		

[1] Results are reported in percent to the nearest number in the series 1, 0.7, 0.5, 0.3, 0.2, 0.15 and 0.1, and so forth, which represent approximate midpoints of interval data on a geometric scale. The assigned interval for semiquantitative results will include the quantitative value about 30 percent of the time.

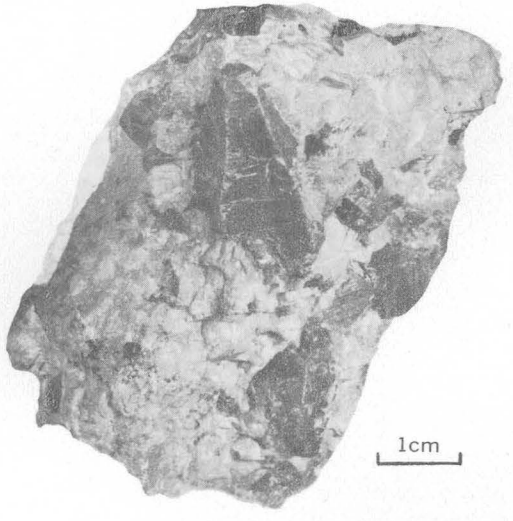

FIGURE 3.—Corundum crystals in alkali pegmatite (sample 69–ARh–3).

crystals are bent or badly misshapen. Inclusions of feldspar are common, and a thin microselvage of fine-grained white mica generally coats the outside of a crystal. Most of the crystals are badly fractured, breaking along the perfect basal parting (0001), and are difficult to remove whole from the pegmatite matrix. Although gray when fresh, the corundum becomes bluish gray after exposure to sunlight.

Since the original discovery of the corundum, prospectors and miners have optimistically viewed the deposits as a source of gem sapphire. Within the last 2 years, Mr. Robert McGrane, an Anchorage jeweler, has cut cabochons from some of the weathered corundum, producing attractive blue-gray stones that generally show asterism. However, the badly fractured habit of the crystals, the abundance of feldspar inclusions, the poor color in fresh material, and the overall paucity of crystals preclude the development of an economic gem enterprise.

REFERENCES

Kunz, G. F., 1899, Precious stones, pt. VI of Mineral resources of the United States: U.S. Geol. Survey 20th Ann. Rept., p. 557–602.

Moffit, F. H., 1954, Geology of the eastern part of the Alaska Range and adjacent area: U.S. Geol. Survey Bull. 989–D, p. 63–218.

Pratt, J. H., 1901, The occurrence and distribution of corundum in the United States: U.S. Geol. Survey Bull. 180, 98 p.

MALACHITE- AND SPECULARITE-BEARING TRIASSIC SANDSTONE LOCALITIES NEAR CHANTILLY, VIRGINIA

By JOHN P. D'AGOSTINO and PENELOPE M. HANSHAW,
Beltsville, Md., Washington, D.C.

Abstract.—A zone of gray sandstone in predominantly red Triassic beds, in a pipeline trench exposure near Chantilly, Fairfax County, Va., contains noticeable malachite and azurite. A specularite-bearing conglomeratic sandstone containing minor malachite was noted about 1 mile southeast of the copper locality in a housing-development excavation near a diabase intrusion. At the first locality, all mineralization is secondary and is not in contact with diabase. Semiquantitative spectrographic analyses showed as much as 20,000 ppm copper and 50 ppm silver. Similar mineralized rock has been economically important in the past elsewhere in Triassic rocks of the Eastern United States and conceivably could become so again in the future.

Malachite-bearing gray Triassic sandstone was noted during October 1968 in a trench excavation of the Transcontinental Gas Pipeline Co. The pipeline trends N. 40° E. and crosses U.S. Route 50, 1.2 miles east of Chantilly, in Fairfax County, Va. Copper mineralization was noted about 0.3 mile south along the pipeline trench from U.S. Route 50, northeast of the point where Tabscott Road ends at the pipeline (see fig. 1). The land surface is nearly flat to gently rolling; mineralized rock is not present at the surface. Natural outcrops are few and poor in this area. The trench was 8 feet deep and 6 feet wide and was open for only a few days. It was studied by several geologists of the U.S. Geological Survey as part of a project by Penelope M. Hanshaw to compile and revise the geology of Fairfax 15 minute quadrangle on 7½ minute quadrangles at 1 : 24,000 scale.

James P. Owens and Penelope M. Hanshaw noted the occurrence first, John P. D'Agostino then sampled the site, had the rocks analyzed, and interpreted the results. Because the trench had already been backfilled, bulldozed, and seeded south of this locality in October 1968, a search for similar occurrences there was not fruitful.

PREVIOUS WORK

The geology of the Fairfax 15 minute quadrangle was mapped by Allan P. Bennison and Charles Milton at 1:62,500 in 1950; Richard E. Eggleton used their map and his own field observations to produce a 1 : 24,000-scale geologic map of the Herndon quadrangle in 1958–59 in connection with an engineering geology report on the proposed Dulles Airport (unpub. data, U.S. Geol. Survey).

Copper minerals were noted by Charles Milton and Edward C. T. Chao 0.3 mile northwest of this occurrence (oral commun., 1958). Milton and Chao traced the minerals more than 1 mile southwest and postulated an origin by solutions moving up along a fault.

HISTORICAL BACKGROUND

Copper-silver-barium mineralization in red Triassic sandstones and shales associated with basalt flows and dikes is quite common along the Atlantic coast from Virginia to Massachusetts (Roberts, 1928, p. 132–136; Tyson, 1860, p. 17; Brown, 1968, p. 2–18). These near-surface deposits were extensively prospected and mined during colonial times for copper, barium, and silver until ore reserves at shallow depth were depleted. The largest commercial deposits were along the western part of the Triassic basin of Connecticut (Bateman, 1923; Richardson, 1854; Silliman and Whitney, 1855) and northeastern New Jersey (Lewis, 1907, p. 251; Woodward, 1944).

The copper ore minerals of such deposits were supergene and primary chalcocite and chalcopyrite with minor amounts of bornite, chrysocolla, malachite, azurite, and native copper. Nearly all silver was obtained as a minor byproduct from the copper and galena ores (Schairer, 1931, p. 48); some native silver was obtained from the copper mines in northeastern New Jersey (Lewis, 1907, p. 251). The mined barite deposits were usually massive veins (Rice and Gregory, 1906, p. 196). Meager nonvisible gold values are also associated with these deposits (Wherry, 1908, p. 732).

U.S. GEOL. SURVEY PROF. PAPER 700-C, PAGES C103–C106

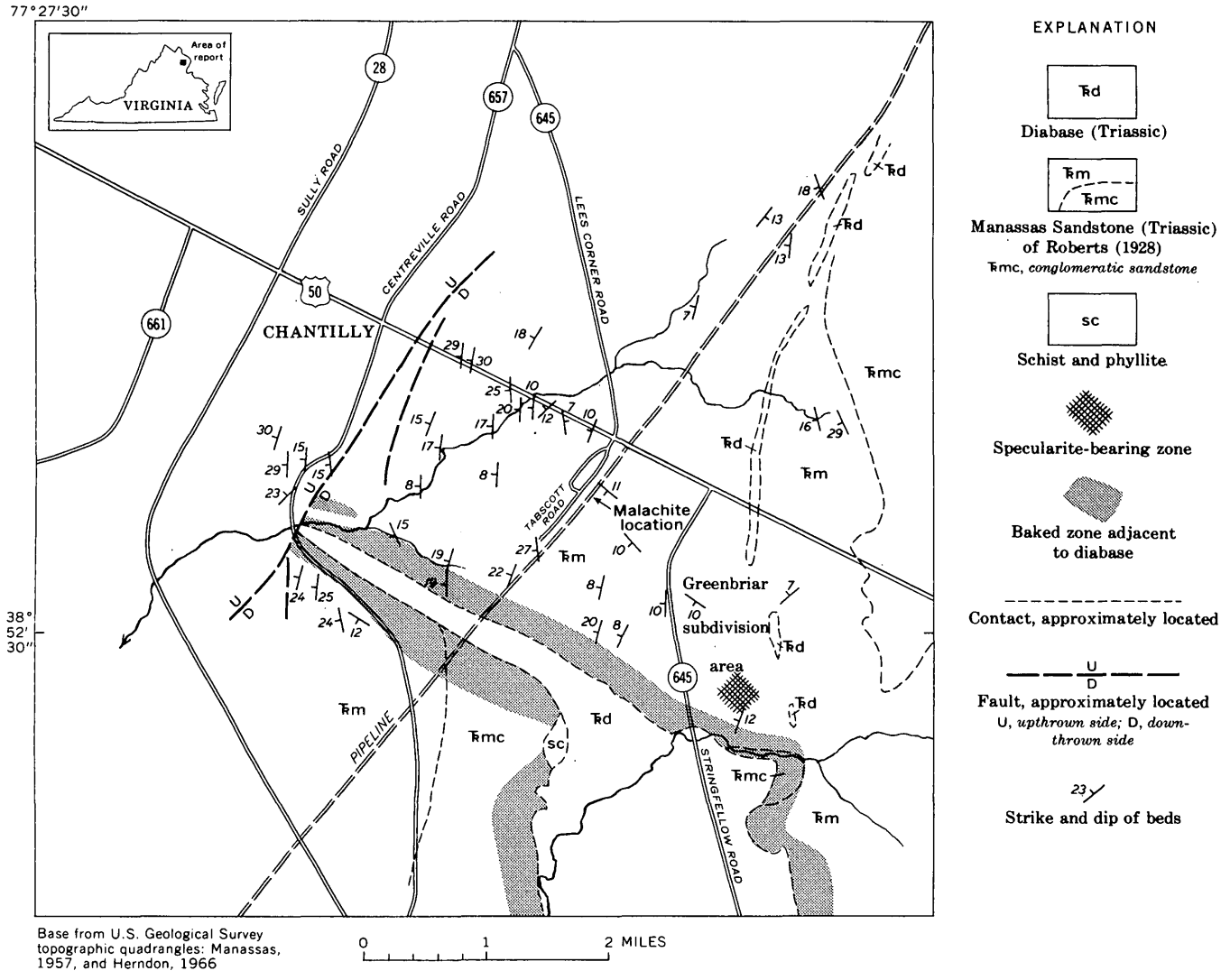

FIGURE 1.—Generalized geologic map of the Chantilly, Va., area, showing malachite and specularite localities. Geology by A. P. Bennison, Charles Milton, Manual Bass, and E. C. T. Chao, modified by R. E. Eggleton and P. M. Hanshaw.

GENERAL GEOLOGY

Rocks underlying the Triassic sediments are schist and phyllite of unknown age mapped at Wissahickon Schist by Bennison and Milton. The contact between Triassic and basement rocks were exposed about 3.7 miles northeastward along the trench from the copper locality. Basement rock at the contact is a fine lustrous sericite-quartz phyllite with interlayered sandstone lenses.

The copper minerals occur in the Manassas Sandstone as mapped by Roberts (1928). In this area it is composed of red mudstone, siltstone, and fine sandstone; medium to coarse arkosic sandstone and conglomerate lenses increase in abundance near the base of the unit. The Manassas is probably several hundred feet thick at the copper locality. The sandstone in the trench at the copper locality is composed of well-sorted rounded quartz grains ranging from very fine sand to silt size in a massive bed several feet thick containing many small irregular laminations. Mica and chlorite are the chief accessory minerals. Carbonized plant remains, mainly stems and leaves, are common in the gray to olive-gray layers and sparse in the reddish-brown layers.

About 1 mile southeast of the malachite locality, conglomeratic lenses are common and, in places, contain fragments of sericite schist as much as 3 feet in maximum diameter and fragments of quartz as much as 4 inches across. Such rocks are lacking in the pipeline trench near Tabscott Road. The coarseness suggests a basal stratigraphic position for the conglomerate and associated beds.

Numerous dikes and sill-like masses of diabase intrude the Triassic sedimentary rocks in a north-northeast-trending belt throughout much of the area and may signify structural weakness in the basement. Faults occur within the Triassic basin and especially along its outer margins. The sedimentary rock shows the effects of thermal metamorphism by the diabase; the finer grained beds are bleached white, light tan, or pink within 400 to 600 feet of the diabase, the coarse grained beds as much as 1,200 feet from it.

The diabase zone south of the malachite locality shown on figure 1 consists of closely spaced dikes which form an "arm" about 500 feet wide which trends N. 60° W. and merges with the main body of diabase. This main body, farther south and only partly shown on figure 1, measures about 2½ miles north-south and 1¼ miles east-west. Each dike consists of several feet of fine-grained chilled diabase that grades inward to coarser textured diabase.

COPPER LOCALITY

The malachite-bearing zone is 5 feet thick in the trench and contains anomalous quantities of copper and silver (table 1). Owing to lack of good exposures and because of local deviations in strike of the sandstone, the surficial malachite-bearing zone could not be traced

TABLE 1.—*Semiquantitative spectrographic analyses and fire assay of samples from a malachite-bearing zone, Chantilly, Va.*

[Analyst: William B. Crandell, U.S. Geol. Survey; N, looked for but not detected]

Description	5-foot mineralized zone		2-foot malachite-rich zone	1-foot malachite-rich zone	Grab of mixed bedrock
	Upper 3 feet	Lower 2 feet			
Field No.	V-JO-3	V-JO-4	V-JO-6A	V-JO-6B	V-JO-8
Tag No.	AHK-044	AHK-045	AHK-046	AHK-047	AHK-048
SPECTROGRAPHIC ANALYSES (percent)					
Fe	3	5	3	3	3
Mg	2	5	3	3	2
Ca	.5	.5	.5	.5	.3
Ti	.5	.5	.5	.5	.5
Parts per million					
Mn	1,000	1,000	1,000	1,000	1,000
Ag	10	5	50	7	3
As	N	N	N	N	N
Au	N	N	N	N	N
B	30	30	30	30	30
Ba	500	700	1,000	700	700
Be	2	2	2	2	2
Bi	N	N	N	N	N
Cd	N	N	N	N	N
Co	15	20	15	20	20
Cr	50	50	70	70	70
Cu	5,000	5,000	20,000	10,000	5,000
La	50	50	50	70	100
Mo	N	3	N	3	3
Nb	20	20	20	20	20
Ni	30	30	30	30	30
Pb	15	7	7	7	15
Pd	N	N	N	N	N
Pt	N	N	N	N	N
Sb	N	N	N	N	N
Sc	15	15	15	15	15
Sn	N	N	N	N	N
Sr	100	100	100	100	70
Te	N	N	N	N	N
U	N	N	N	N	N
V	70	200	70	100	150
W	N	N	N	N	N
Y	70	50	30	50	50
Zn	N	N	N	N	N
Zr	500	300	500	300	500
FIRE ASSAY (ppm)					
Au	<0.05	0.08; 0.09	<0.05	<0.05	<0.05

southward into the altered baked zone of the Manassas Sandstone.

The rock was sampled for semiquantitative spectrographic analysis, to determine the kind and amount of trace metals present, and for X-ray analysis, to determine some of the minerals present. The 5-foot exposure was vertically channeled and divided into an upper 3-foot sample (V–JO–3) and a lower 2-foot sample (V–JO–4). In addition, two samples were taken in malachite-rich layers 50 feet downdip to the southwest from samples V–JO–3 and V–JO–4. These also were vertical channel samples, one of a 2-foot section (V–JO–6A) and one of a 1-foot section (V–JO–6B).

Malachite, azurite, and barite were identified by X-ray analysis. The malachite and less abundant azurite are on laminae and joints as thin coating ($\frac{1}{32}$ inch thick) throughout the 5-foot zone. Malachite is concentrated in layers containing carbonized plant remains, especially stems, and in places the original plant structure is preserved in the malachite replacement. Conspicuous colloform malachite and some azurite, $\frac{1}{16}$–$\frac{1}{8}$ inch thick, are also associated with the carbonaceous material. Barite was identified only in the carbonaceous material. Barite in the very fine grained sandstone is not noticeable in hand specimen, and the barium may be contained within the feldspar. No silver mineral was identified by X-ray, but elsewhere in the Eastern United States, silver in Triassic rocks is contained in galena (Schairer, 1931, p. 48) and chalcopyrite (Wherry, 1908, p. 732); native silver was commonly found in some New Jersey deposits (Lewis, 1907, p. 251).

The minor gold value in sample V–JO–6A (see table 1) may be a result of gold either from a fossil placer deposit or, more likely, associated with redepositonal limonite by ground-water transport. A heavy-mineral separation from a crushed whole-rock sample revealed one crystal of chacopyrite and three of pyrite.

IRON LOCALITY

The specularite-bearing rock was noted in 12-foot-deep trenches excavated at the Greenbriar subdivision; the trenches are about 1 mile southeast of the copper locality. They are on the east side of Stringfellow Road and north of Big Rocky Run in the Manassas quadrangle. The trenched area is just north of the main body of diabase (see fig. 1).

In the altered zone nearest the diabase, hematite occurs as massive, coarsely crystalline specularite within siliceous zones as much as 2 feet thick; it also occurs as rosettes in scattered segregations. Vitreous quartz and mica are associated with specular hematite. Disseminated fine-grained metallic hematite and some red hematite also occur as compact layers. Small amounts of malachite occur with hematite in a few samples. Farther from the diabase but still in the baked zone, fine hematite crystals occur with quartz in solid rounded clots.

CONCLUSIONS

The location of the primary copper minerals that produced the supergene minerals at the pipeline occurrence is unknown. However, mineralized solutions from the "arm" of the diabase body 0.7 mile southwest of the pipeline exposure could have moved updip along bedding planes or along joints and fractures until they reached the organic-rich rock in the area of the pipeline trench. The en echelon diabase dikes 0.7 mile east of the copper locality are a less likely source because of their small size and because of the many deviations in strike and dip of bedding planes in the sedimentary rock between the dikes and the copper locality.

Most other occurrences of copper mineralization in Triassic rocks of the Eastern United States suggest at least partial control of primary ore minerals by faults. In contrast, at Chantilly only supergene minerals occur, and these are deposited mainly along bedding planes. Perhaps such secondary minerals exist elsewhere in Triassic rocks and may be of economic importance.

REFERENCES

Bateman, A. M., 1923, Primary chalcocite; Bristol copper mine, Connecticut: Econ. Geology, v. 18, no. 2, p. 122–166.

Brown, J. S., 1968, Ore deposits of the northeastern United States, *in* Ore deposits of the United States, 1933–1967 (Graton-Sales Volume), v. 1: New York, Am. Inst. Mining, Metall., and Petroleum Engineers, p. 1–19.

Lewis, J. V., 1907, Copper deposits of the New Jersey Triassic: Econ. Geology, v. 2, p. 242–257.

Rice, W. N., and Gregory, H. E., 1906, Manual of the geology of Connecticut: Connecticut Geol. Survey Bull. 6, 273 p.

Richardson, C. S., 1854, The old Bristol copper mine, Connecticut: Mining Mag., v. 3, p. 251–255.

Roberts, J. K., 1928, The geology of the Virginia Triassic: Virginia Geol. Survey Bull. 29, 205 p.

Schairer, J. F., 1931, The minerals of Connecticut: Connecticut Geol. and Nat. History Survey Bull. 51, 121 p.

Silliman, Benjamin, Jr., and Whitney, J. D., 1855, Notice of the geological position and character of the copper mine at Bristol, Connecticut: Am. Jour. Sci., 2d ser., v. 20, p. 361–368.

Tyson, P. T., 1860, Mineral resources of Maryland: Maryland State Agr. Chemist, First Rept., App., 20 p.

Wherry, E. T., 1908, The Newark copper deposits of southeastern Pennsylvania: Econ. Geology, v. 3, p. 726–738.

Woodward, H. P., 1944, Copper mines and mining in New Jersey: New Jersey Geol. Survey Bull. 57, 156 p.

APPLICATION OF MAGNETIC AND ELECTRICAL RESISTIVITY METHODS TO PLACER INVESTIGATIONS IN THE FAIRBANKS DISTRICT, ALASKA

By L. A. ANDERSON and G. R. JOHNSON, Denver, Colo.

Abstract.—Magnetic and electrical resistivity sounding surveys were made in an area of known placer gold deposits near Fairbanks, Alaska, to evaluate the effectiveness of these methods in locating placer deposits containing magnetic minerals. Near Happy, where bedrock is several hundred feet beneath the surface, it was necessary to apply a low-pass filtering process to the observed magnetic data in order that magnetic anomalies associated with placer deposits be recognized. In the narrow valley of Goldstream Creek, where bedrock is at a depth of about 170 feet, the placer minerals can easily be detected by the magnetic method. Bedrock depth determinations from resistivity soundings in areas free of permafrost agreed favorably with existing drill hole data. However, in areas underlain by permafrost no meaningful bedrock depths could be determined from the resistivity data.

Direct-current resistivity soundings and magnetic geophysical prospecting methods were tested in an area of known placer deposits in parts of the Fairbanks district, Alaska (fig. 1). The Fairbanks district was selected for these investigations because of the known placer gold deposits and the availability of geologic control to aid in interpreting the geophysical data. The control came largely from a report by Joesting (1941), the geologic quadrangle map of Fairbanks (D–2) (Péwé, 1958), and a report by the Fairbanks Exploration Co. detailing the results of an extensive drilling program designed to evaluate the gold content of virtually every active drainage channel within the Fairbanks district. The company report has not been made public but was recently made available to the U.S. Geological Survey for restricted use. The report was extremely helpful in selecting traverses for magnetic surveying and was essential in constructing the geologic cross sections shown in conjunction with the magnetic profile data. Magnetic surveys were also made north of the University of Alaska campus to examine an untested area for possible placer deposits.

Although geophysical methods cannot determine the gold content of a placer deposit, the magnetic method is useful for detecting and delineating concentrations of magnetite, which are commonly associated with gold in the gravels, and the resistivity sounding method has a proven capability of resolving depths to bedrock and thus indicating channels that may be favorable for placer accumulation. If the gold content of a placer is determined by drilling, these methods provide a relatively inexpensive means of outlining the extent of a deposit with a minimum of additional drilling.

GEOLOGIC SETTING

The generalized geology of the Fairbanks area is shown in figure 1. The entire area is underlain by the Birch Creek Schist of Precambrian or Paleozoic age. The upper slopes of the exposed schist are covered with Fairbanks Loess, which grades into undifferentiated Quaternary silt covering the lower slopes and valley bottoms. The Tanana River drainage basin, which makes up the southern part of the Fairbanks district, consists of thick flood-plain alluvium.

MAGNETIC SURVEYS

Magnetic measurements were made along traverse *A–A′*, across the valley near Happy, herein called the Cripple-Ester-Goldstream valley, and along traverse *B–B′*, crossing Goldstream Creek (figs. 2, 3). Magnetic measurements were made using a vertical intensity fluxgate magnetometer. The magnetic data were corrected for instrument drift, regional gradient, and diurnal variations; the last correction was made from the magnetic observations by the U.S. Coast and Geodetic Survey office at College, Alaska.

The location of the Cripple-Ester-Goldstream valley traverse, *A–A′* (fig. 2), was chosen to coincide with a series of drill holes, spaced 1,000 feet apart, all of which penetrated bedrock. Bedrock is as much as 370 feet below ground surface, and though this depth is well

U.S. GEOL. SURVEY PROF. PAPER 700–C, PAGES C107-C113

380-189 O - 70 - 8

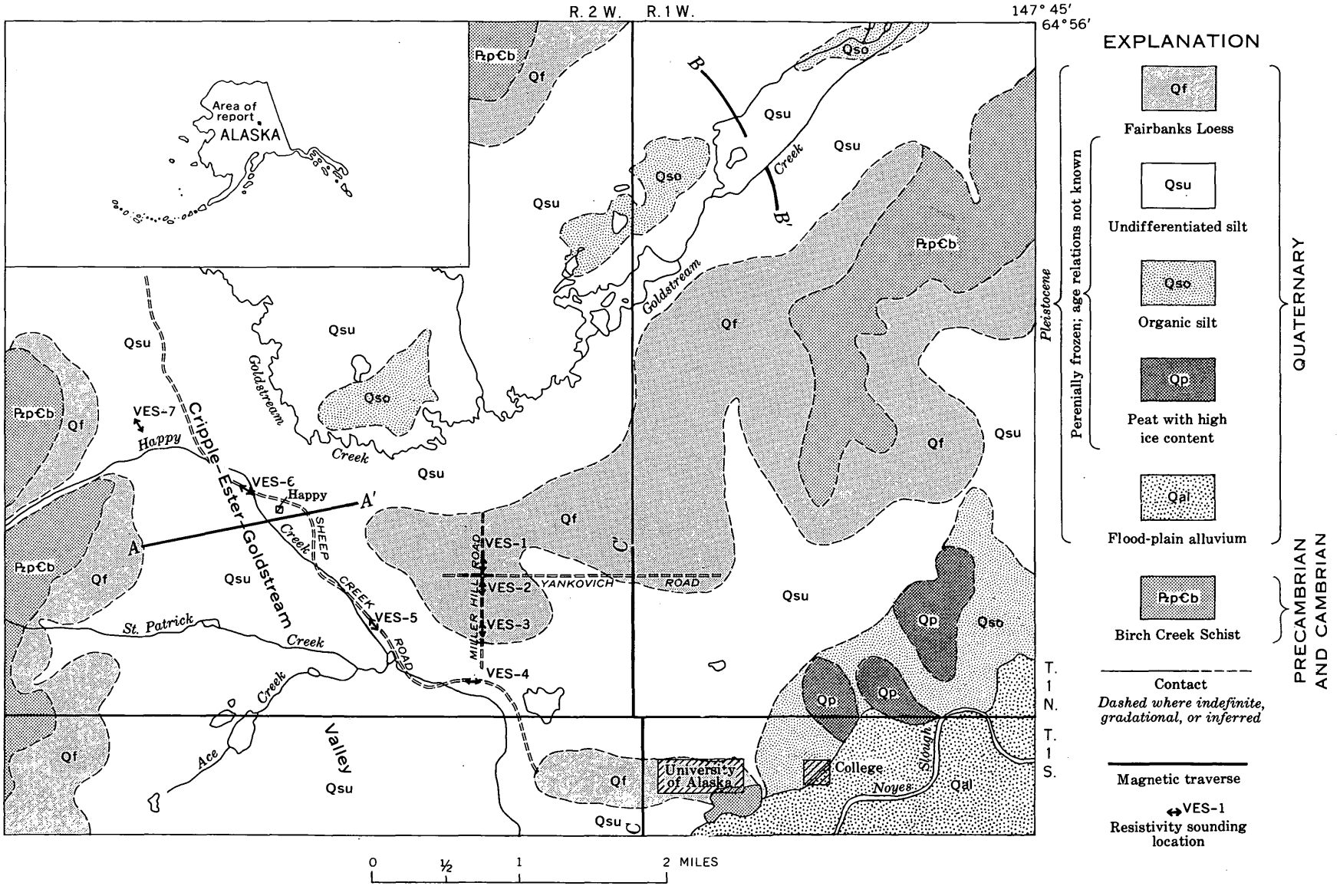

FIGURE 1.—Generalized geologic map of the area northwest of Fairbanks, Alaska, showing location of magnetic traverses and resistivity soundings. Geology modified from Péwé (1958).

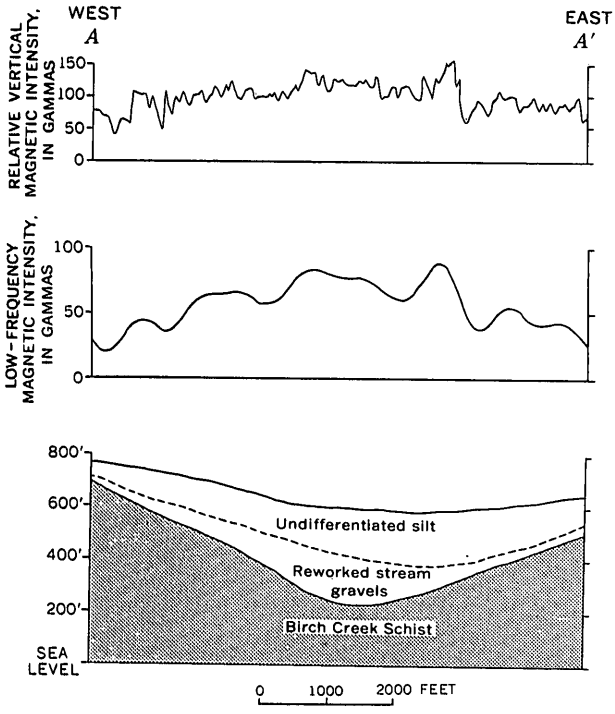

FIGURE 2.—Observed and filtered profiles of magnetic data obtained across the valley near Happy (*A–A'*).

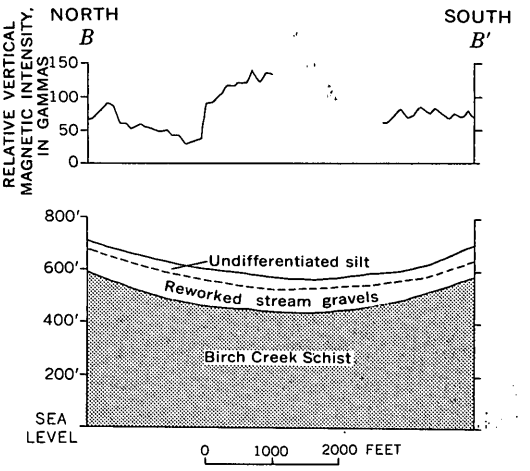

FIGURE 3.—Magnetic profile obtained across Goldstream Creek (*B–B'*).

beyond the excavating depth capabilities of any known dredge, the deeply buried placer deposits provided a good test area for the magnetic method.

The magnetic profile along traverse *A–A'* (fig. 2) shows high-frequency changes superimposed upon a broad magnetic high. The high-frequency variations are particularly pronounced because of the 50-foot station interval used in making the measurements but are primarily the result of "geologic noise"—the effects of near-surface magnetic minerals—and possibly meter reading error by the operator. The manufacturer of the magnetometer specifies a ±5-gamma accuracy for the instrument.

To eliminate these high-frequency effects, the magnetic data were filtered by using a low-pass digital filtering computer program. All frequencies above $\frac{1}{20}$ of highest possible frequency contained in the observed magnetic profile were removed. The processed data are shown beneath the field data on figure 2. This profile gives a clear indication of the general increase in the magnetic intensity over the center of the valley and the effects of concentrations of placer minerals near the bedrock surface. The larger deposits are evidently concentrated within and along the east flank of the deepest channel in the bedrock.

Although gold has been dredged from the gravels near the headwaters of Goldstream Creek, no dredging was ever attempted in the area where the magnetic traverse was made. The bedrock depth is approximately 170 feet, too deep for the dredges then in use in the Fairbanks district.

Traversing across Goldstream valley is especially difficult because of the swamp areas adjacent to Goldstream Creek. Traverse *B–B'* (fig. 3) did not coincide with an alinement of drill holes but was located where the valley crossing was easiest. Even then a continuous profile was not obtainable because of swamp.

The 100-foot station interval along traverse *B–B'* (fig. 3) produced a smoother magnetic profile than that observed along *A–A'*. A broad incompletely measured anomaly can be observed in the approximate center of the traverse, presumably the result of a concentration of magnetic minerals near bedrock. The anomaly is quite conspicuous, and for this reason no further processing of the magnetic data was thought necessary. A small anomaly near the north end of the traverse may be caused either by a placer deposit or by magnetic variations within bedrock. Joesting (1941) determined that local magnetic variation in the bedrock is on the order of ±20 gammas in the vicinity of Goldstream Creek. That the anomaly has a magnetic intensity of about 30 gammas and the bedrock is more than 100 feet below the ground surface together suggest a placer deposit as the probable magnetic source.

The Goldstream valley magnetic profile demonstrates that magnetic mineral concentrations can rather easily be detected by conventional magnetic ground methods. The greater the depth, the more difficult the recognition of this type of deposit; nevertheless, that deep deposits might be identified is shown by the Cripple-Ester-Goldstream magnetic profile. It would seem advantageous to utilize an airborne magnetometer in future placer investigations, especially in those areas where

the depth to bedrock is less than 150 feet and the terrain will permit the survey to be flown at an elevation of 100–200 feet above the ground. Airborne surveying would eliminate the problem of diurnal variations and instrument drift by significantly reducing the time required to obtain these data. In addition, "geologic noise" would be subdued, thereby facilitating the recognition of anomalies caused by deeply buried magnetic sources.

A ground magnetic profile, along traverse *C–C′* (fig. 4), was also made over the area west and northwest of the University of Alaska. In this area, the unconsolidated deposits covering the southernmost flanks of the upland ridges have never been evaluated for possible gold content.

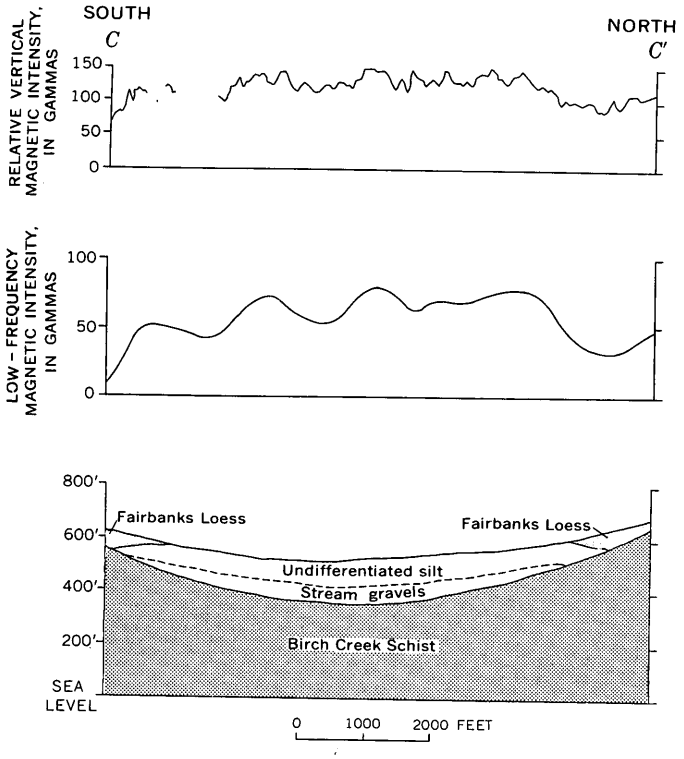

FIGURE 4.—Observed and filtered profiles of magnetic data obtained north of the University of Alaska.

Profile *C–C′*, constructed from magnetic measurements made at 50-foot intervals, traverses the entire silt section except for a few gaps near the south end where manmade objects interfered with the magnetometer readings. The north and south ends of the traverse are over loess, which rests directly on bedrock.

The magnetic profile obtained along traverse *C–C′* shows high-frequency background effects superimposed on a broad magnetic high which coincides with the silt. A much clearer portrayal of the placer mineral distribution can be seen in the digitally filtered magnetic profile plotted below the observed data in figure 4.

Individual placer deposits can easily be recognized when the high-frequency noise has been eliminated. The relatively low-amplitude magnetic anomalies do not indicate strong concentrations of magnetic minerals within the gravels, in view of the fact that bedrock is only about 100 feet below the surface.

RESISTIVITY SURVEYS

The Schlumberger array (Keller and Frischknecht, 1966) was used in measuring the earth resistivity. The resulting resistivity curves obtained were interpreted using an album of three-layer Schlumberger theoretical curves (Orellana and Mooney, 1966) in conjunction with the auxiliary point diagrams (Kalenov, 1957; Orellana and Mooney, 1966; Keller and Frischknecht, 1966; Zohdy, 1965). The geologic section at each sounding station, obtained on the basis of the geophysical interpretation of each sounding curve, was then modeled by means of a digital computer to approximate the curve described by the field data.

Three vertical electrical resistivity soundings were made along Miller Hill Road and one at the foot of this road along the Sheep Creek Road (fig. 1). Of the four sounding curves, two (VES–1 and VES–3) contained offsets in the continuity of data points owing to lateral effects possibly caused by lenses of permanently frozen ground; they have been omitted from the following discussion.

Sounding VES–2 had its midpoint 600 feet south of the intersection of Miller Hill and Yankovich Roads, and sounding VES–4 was centered on Sheep Creek Road 950 feet west of the south end of Miller Hill Road. The sounding curves with their corresponding interpreted geologic sections are shown in figure 5.

At the VES–2 sounding location, according to drillhole information, loess overlies Birch Creek Schist. Interpretation of the resistivity data indicates that the schist is 72 feet below the ground surface. A conductive layer within the Birch Creek Schist is presumed to be graphitic schist.

Sounding VES–4 was located on silt covering the valley bottom. The silt, known to contain large masses of permanently frozen ground, overlies stream gravel which rests on schist bedrock. The VES–4 interpretive section on figure 5 shows the top of a 10-foot-thick permafrost layer 18 feet beneath the surface underlain by a single layer having a resistivity of 185 ohm-m. This resistivity value represents an average value for a section composed of silt, gravel, and possibly graphitic schist. The vertical electrical sounding method requires a significant contrast in the resistivity of the layered

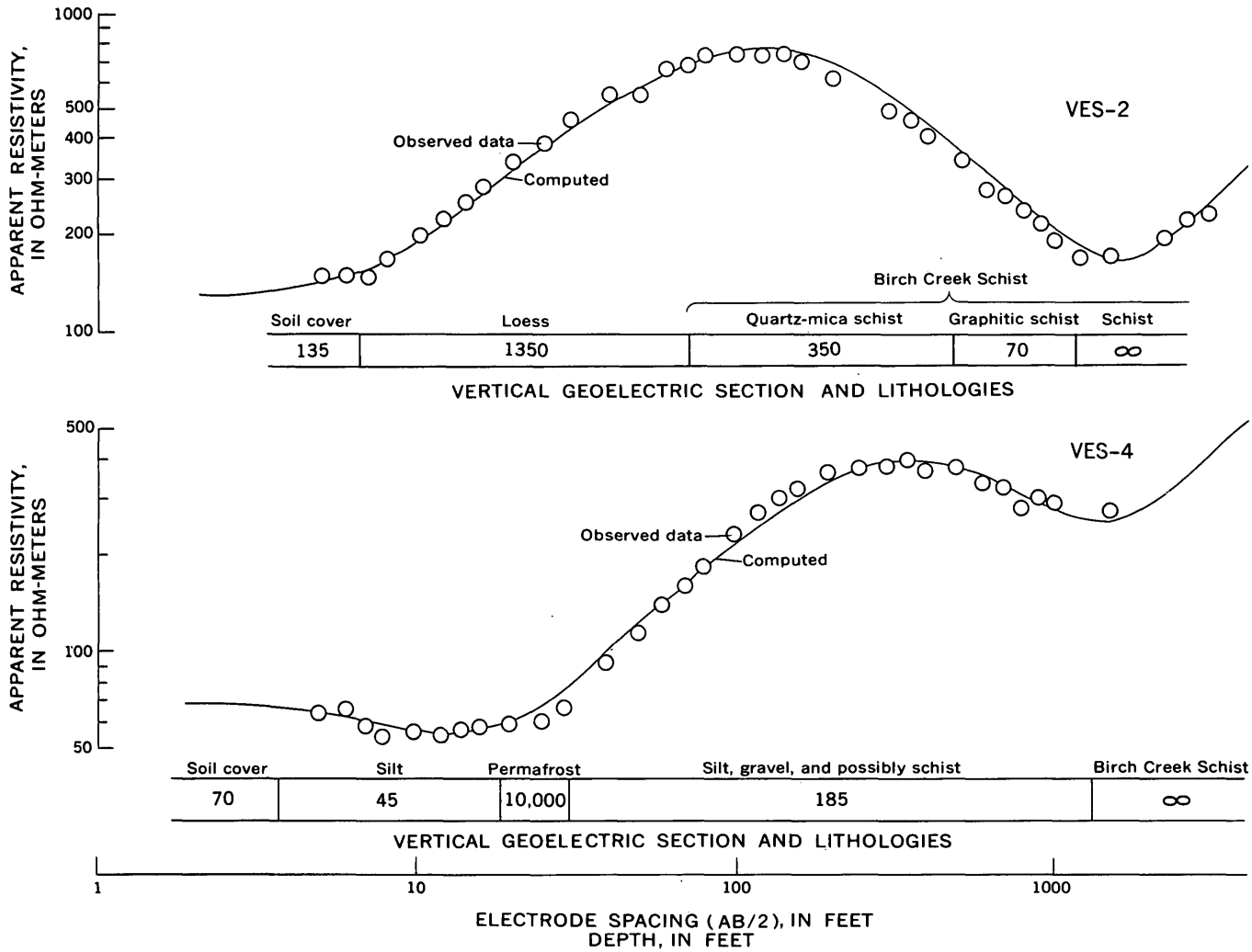

FIGURE 5.—Vertical electrical soundings made on Miller Hill Road (VES–2) and Sheep Creek Road (VES–4), showing interpreted geoelectric section and corresponding lithology. True resistivity values are indicated in the geoelectric column.

materials in order that they be recognized as individual layers. Here the resistivity difference between the silt, gravel, and schist is slight when compared to the 10,000-ohm-m resistivity of the permafrost; therefore the layering beneath the permafrost cannot be resolved from the resistivity field measurements.

The effect of the permafrost or any high-resistivity layer on the interpretive qualities of a vertical electrical sounding is to combine the layers beneath the permafrost into a single composite layer showing only the total thickness and average resistivity of the section. If the bedrock has a very high resistivity it is possible to determine the depth to the bedrock contact, the principal objective of the resistivity surveys. This is not the situation in the Fairbanks area, however, and at least the upper parts of the schist bedrock seem to be included in the 185-ohm-m section at the VES–4 sounding location.

Three additional soundings—VES–5, VES–6, and VES–7—were made in the Cripple-Ester-Goldstream valley to see if gaps in the permafrost layer would permit a usable resistivity sounding to be made (fig. 1). VES–5, made on Sheep Creek Road, approximately 1 mile northwest of sounding VES–4, also detected a permafrost layer within the silt. Sounding VES–6 was made on an airstrip adjacent to the Sheep Creek Road, 1,100 feet west of the railroad track (fig. 6). This site had been cleared, and some thawing of the permafrost layers was anticipated. Our interpretation indicates a 10-foot soil cover underlain by a 290-foot layer of silt and gravel. The bedrock resistivity is at least 900 ohm-m, which suggests that the schist there does not contain graphite. A calculated depth of approximately 300 feet to the bedrock is confirmed by drill hole data which show a depth of 285 feet.

VES–7 was made along a new road leading to the

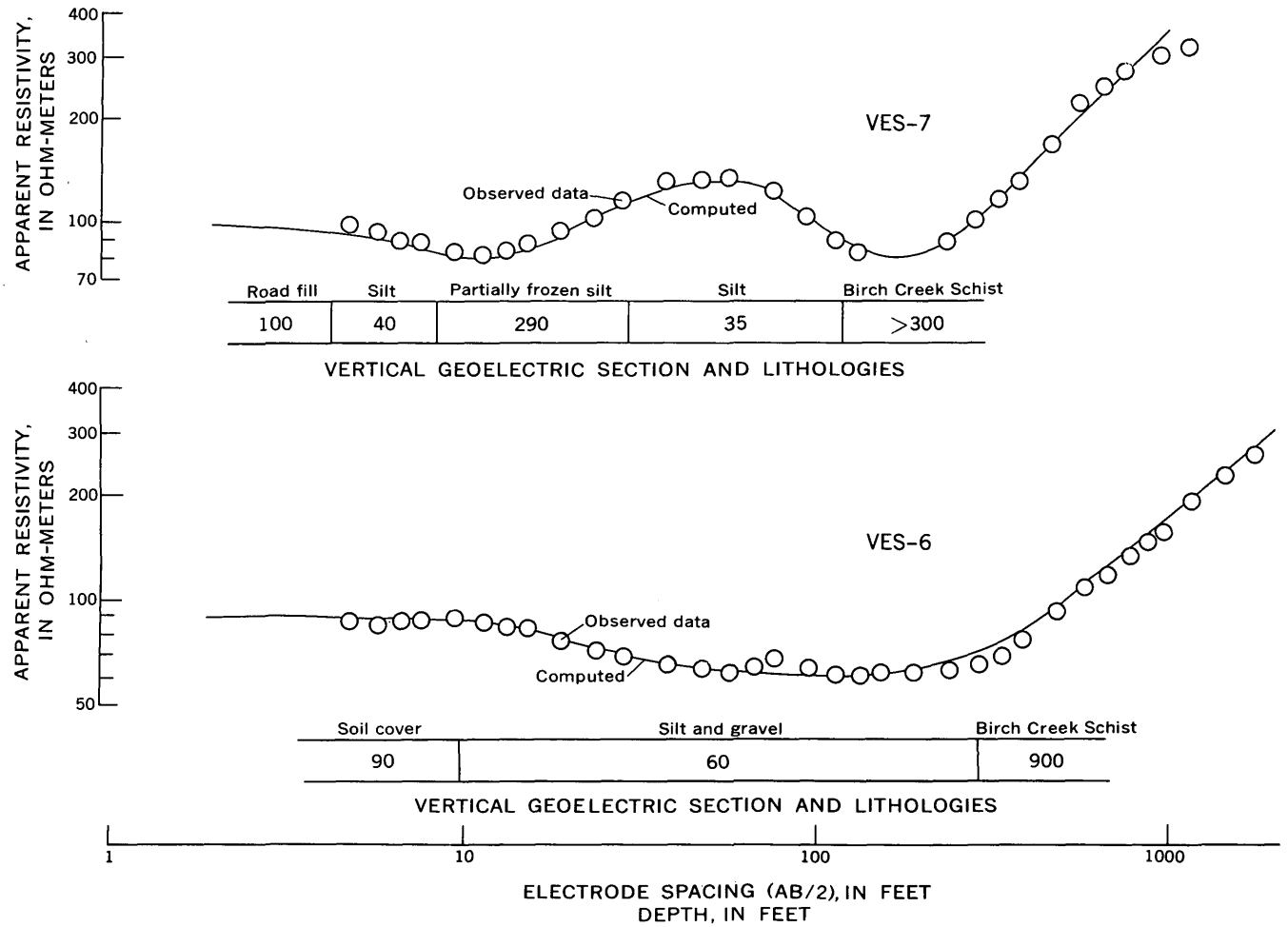

FIGURE 6.—Vertical electric soundings made on airstrip adjacent to Sheep Creek Road (VES–6) and on the new road leading to Ester Dome (VES–7), showing interpreted geoelectric section and corresponding lithology. True resistivity values are indicated in the geoelectric column.

summit of Ester Dome (fig. 6). Interpretation of this sounding shows 4.5 feet of road fill and 120 feet of silt resting on a schist bedrock. There is a 32-foot layer of 290-ohm-m material within the silt. This higher resistivity layer may be a partially frozen section within the silt. A drill hole immediately south of the survey location shows a depth of 126 feet to bedrock, which is in excellent agreement with the 125-foot depth determined by the resistivity method. The interval within the silt which is assumed to be partially frozen had no effect on the interpretation of the resistivity sounding data.

SUMMARY AND CONCLUSIONS

The magnetic profile across the Cripple-Ester-Goldstream valley indicates a general increase in the magnetic intensity caused by magnetic minerals within the stream gravel, but concentrations of these minerals are difficult to recognize from the observed magnetic data. After these data are filtered through a digital filtering computer process, however, the magnetic anomalies associated with placer deposits at depths in excess of 300 feet become quite apparent. In Goldstream valley, depth to bedrock is approximately 170 feet and the valley is much narrower than the Cripple-Ester-Goldstream valley; the placer minerals are well concentrated and can be delineated by magnetic surveys.

A magnetic profile across an area west and northwest of the University of Alaska indicates that magnetic minerals are contained within stream gravels resting on schist bedrock. The filtered magnetic data indicate that individual placer deposits exist, but the amplitudes of the magnetic anomalies suggest a relatively sparse concentration of magnetic minerals within these deposits.

The resistivity sounding method was tested for bedrock depth determinations in the Cripple-Ester-Goldstream valley and in an area adjacent to the valley

where stream deposits are notably absent. In areas free of permafrost, bedrock depths determined from the resistivity data compared favorably with drill-hole data. However, resistivity soundings made over permafrost were useful only for determining the depth to the top of the permafrost. The electrical current can be made to penetrate the permafrost by the use of very large electrode separations, but the underlying layers are then detected as a single layer having a resistivity which represents an average of the individual layers in the geoelectric layer. If the resistivity of the bedrock were extremely high, then possibly depth to bedrock might be determined. Owing to the low resistivity of the schist in the Fairbanks district, the resistivity sounding method can be applied only to areas where permafrost does not interfere with soundings.

REFERENCES

Joesting, H. R., 1941, Magnetometer and direct-current resistivity studies in Alaska: Am. Inst. Mining and Metall. Engineers Tech. Pub. 1284 (class L, geophysics, no. 72), 20 p.

Kalenov, E. N., 1957, Interpretation of vertical electrical sounding curves: Vses. Nauchno-Issled. Inst. Geofiz. Metodov Razved. Trudy, no. 1, 471 p. [In Russian]

Keller, G. V., and Frischknecht, F. C., 1966, Electrical methods in geophysical prospecting: New York, Pergamon Press, 517 p.

Orellana, Ernesto, and Mooney, H. M., 1966, Master tables and curves for vertical electrical sounding over layered structures: Madrid, Spain, Interciencia, 125 p.

Péwé, T. L., 1958, Geology of the Fairbanks (D–2) quadrangle, Alaska: U.S. Geol. Survey Geol. Quad. Map GQ–110.

Zohdy, A. A. R., 1965, The auxiliary point method of electrical sounding interpretation, and its relationship to the Dar Zarrouk parameters: Geophysics, v. 30, no. 4, p. 644–660.

GRAVITY ANOMALIES IN CACHE VALLEY, CACHE AND BOX ELDER COUNTIES, UTAH, AND BANNOCK AND FRANKLIN COUNTIES, IDAHO

By DONALD L. PETERSON and STEVEN S. ORIEL, Denver, Colo.

Work done in cooperation with the Utah Department of Natural Resources, Division of Water Rights

Abstract.—A large, complex gravity anomaly coincides with Cache Valley and reveals a complex basin structure. Interpretations of two-dimensional models prepared along four gravity profiles indicate the approximate thickness of water-bearing Cenozoic strata in the valley and the gross structure of underlying Paleozoic and older bedrock. The thickest Cenozoic strata, 7,000 and 8,000 feet, occur in two fault-bounded troughs near the Idaho-Utah State line. The troughs are separated by a basement high indicated by high gravity values that extend from the Bannock Range southward through Bergeson Hill to Little Mountain. The eastern trough is bounded on the east by a buried block of Paleozoic rock extending southwestward from Mount Smart. Farther north, a block of Precambrian rock exposed at Clifton Hill extends southward beneath thin Cenozoic fill for at least 4 miles; this block is bounded on the east by a fault. Belts of high and low gravity values in Idaho along the west edge of the Bear River Range coincide with belts of pre-Cenozoic and Salt Lake strata.

A gravity survey was made of Cache Valley in 1968 as part of an investigation of the water resources of the valley. The purpose of the survey was to determine the approximate thickness of low-density Cenozoic strata in the valley and the gross structure of the underlying pre-Cenozoic bedrock. Geophysical investigations of adjacent valleys had been reported by Mabey and Armstrong (1962) and Stewart (1958).

Cache Valley is one of several large valleys which lie along the eastern part of the Basin and Range physiographic province (fig. 1). The valley is north trending, approximately 55 miles long, and 7–12 miles wide. Strata exposed within the valley consist of poorly indurated tuffaceous siltstone, marlstone, and conglomerate which are assigned to the mainly Pliocene Salt Lake Formation, unconsolidated sediments of the Pleistocene Lake Bonneville Group, and younger alluvium, eolian sand, and tufa (Williams, 1962). The valley is bounded on the east by the Bear River and Wasatch Ranges, and on the west by the Wellsville Mountains, Junction Hills, and the Malad and Bannock Ranges. The ranges consist mainly of sedimentary rocks of Precambrian through Paleozoic age, but parts of the ranges are covered by Tertiary sedimentary rock (Williams, 1958; Stokes, 1963; Oriel and Platt, 1968). Altitudes range from about 4,400 to 4,800 feet in the valley to almost 10,000 feet in the ranges. Cache Valley is drained by the Bear River, which enters the valley in the northeast corner through a narrow gorge (Oneida Narrows) and leaves through Bear River canyon along the western edge. The Bear River flows southward into Great Salt Lake.

GRAVITY SURVEY

Gravity observations were made at 345 stations in Cache Valley and the adjoining ranges. The gravity data are referenced to the Liberty Park gravity base station in Salt Lake City, Utah (Behrendt and Woollard, 1961). Terrain corrections were computed outward to a distance of 19 km for 156 selected stations by means of Hayford-Bowie templates (Swick, 1942). Terrain corrections for the remaining stations were interpolated. The largest terrain correction was 17.4 mgal for a station in Logan Canyon. Corrections in the center of the valley approach zero. A density of 2.67 g per cm^3 was assumed for the rock between sea level and station elevations in reducing the data to the complete Bouguer anomaly.

A large, complex negative gravity anomaly coincides with Cache Valley (fig. 2); an appended low extends northwestward through Clarkston. Two-dimensional interpretations of the gravity anomaly (figs. 3 and 4) were made along four profiles across the valley.

The models assume that the gravity anomaly is produced by a single density contrast of 0.5 g per cm^3 between Cenozoic strata and older denser rocks, which

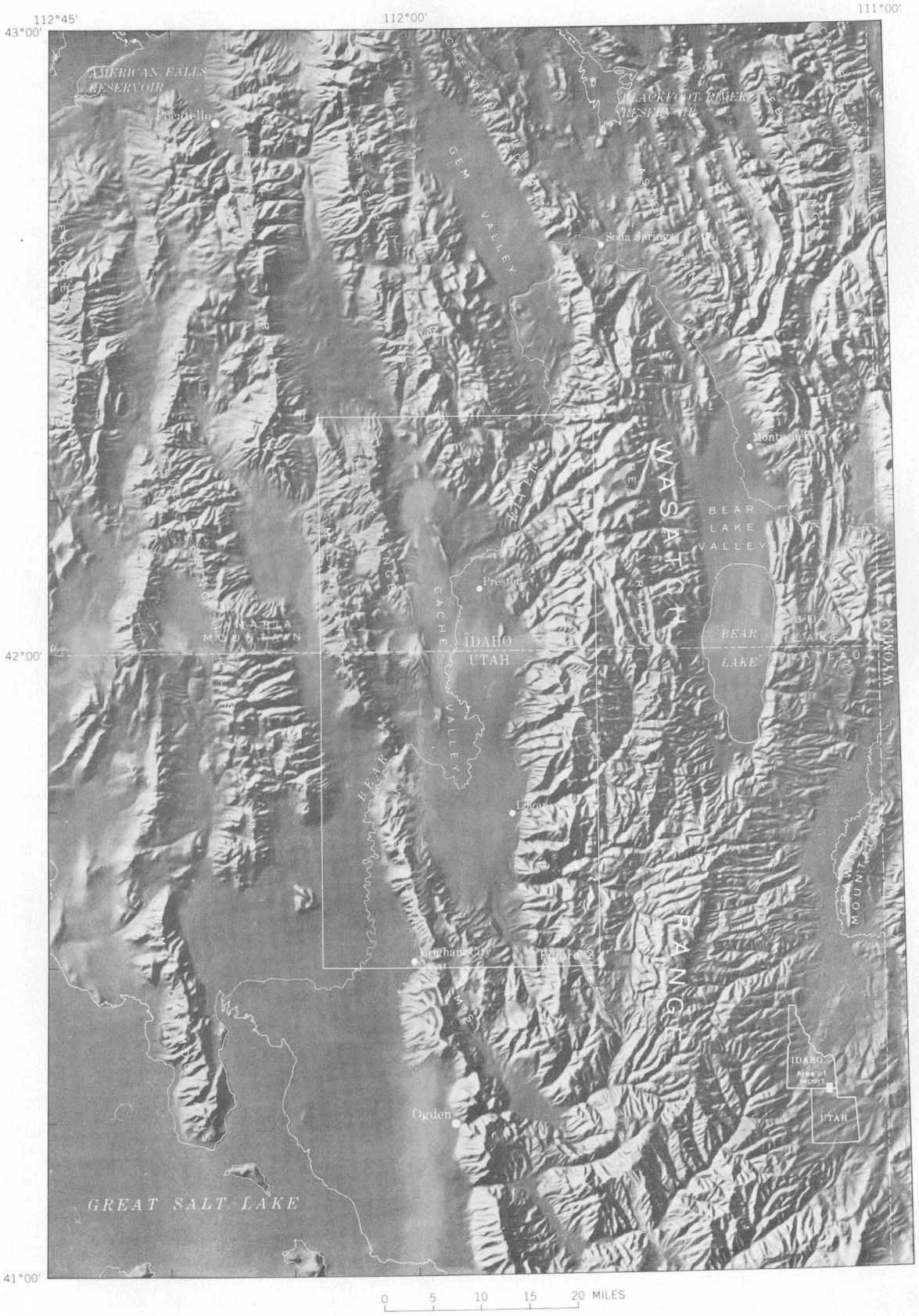

FIGURE 1.—Relief map of Cache Valley and surrounding area, Utah and Idaho.

consist mainly of Precambrian quartzite and Paleozoic limestone. Although the actual mass distribution is undoubtedly much more complex, a density contrast of 0.4–0.6 g per cm³ has proved applicable to other areas of the Basin and Range province in determining the gross structure of a basin. Steeply dipping slopes shown on the models indicate faults; but lateral variations in the density of the basin fill, particularly along the margins of the basin, limit the usefulness of gravity data in determining the precise position and attitude of bounding faults. Gravity interpretations are inherently ambiguous, and the thickness of valley fill shown on the models may differ substantially from the actual thickness if the assumed density contrast is not correct. The accuracy of thickness estimates can be much improved by means of other subsurface control, such as deep drill holes and other geophysical techniques.

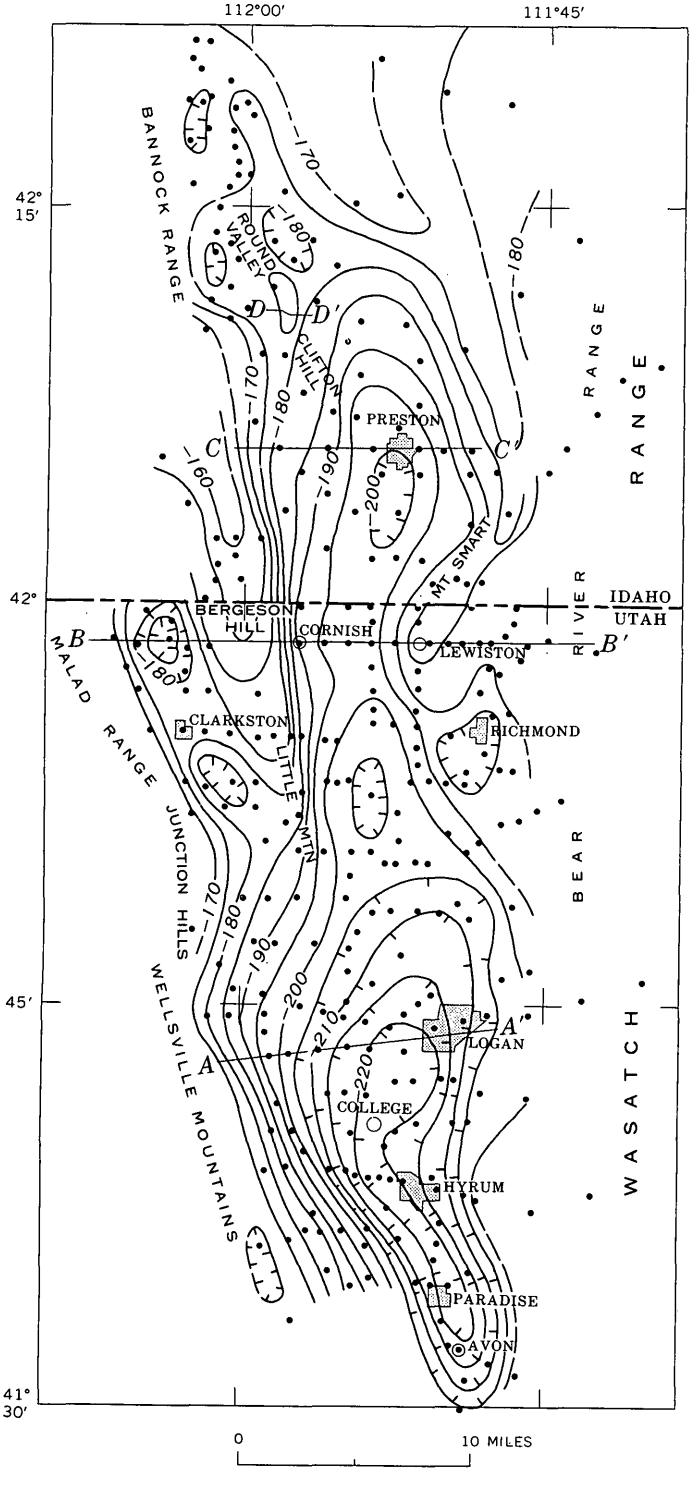

FIGURE 2.—Bouguer gravity map of Cache Valley, Utah and Idaho. Gravity contours are dashed where approximately located; contour interval 5 mgal; hachured contours enclose areas of low gravity. Dots indicate gravity stations.

Regional gravity decreases eastward across the valley 1–2 mgal per mile. The regional gravity field is probably related mainly to undetermined features of greater depth and extent than Cache Valley, but may be relatively complex in the area of the valley.

INTERPRETATION

A gravity low in the southern part of Cache Valley is bounded on the east and west by steep gradients, which reflect major faults or fault zones, many of which are shown by Williams (1958) and by Stokes (1963). The gravity low narrows in the area of Hyrum and Paradise, Utah, and pinches out south of Avon, thus indicating a narrow trough of Cenozoic rock. Between College and Hyrum the anomaly decreases in magnitude, probably reflecting a buried westward-protruding bedrock nose. The model computed along profile *A–A′* (fig. 3) suggests that about 6,000 feet of Cenozoic strata is present near the east side of Cache Valley. Moreover, gravity data reveal two faults rather than one fault, or a step-fault feature [1]—on the east side of the profile. A single fault is inferred at the west side of the profile, but gravity data are too few to properly define the gradients.

Near the Idaho-Utah State line a gravity saddle separates the southern gravity low from a low near Preston, Idaho. The gravity saddle is flanked on the east by a gravity high which extends southwestward into the valley near Lewiston, Utah. The high no doubt reflects the concealed southwestward extension of a block of bedrock that is exposed at Mount Smart, where it consists mainly of limestone but also contains some quartzite of Cambrian and Ordovician age (Oriel and Platt, 1968).

Another gravity high on the west side of the valley extends from the Bannock Range southward through

[1] Two faults were mapped by Williams (1958) along the west flank of the Wasatch Range east of Richmond and east of Paradise, but only one was mapped near Logan. The gravity data indicate that the westernmost fault near Paradise may continue northward through Logan; whether this fault is the same as the western fault near Richmond is not clear.

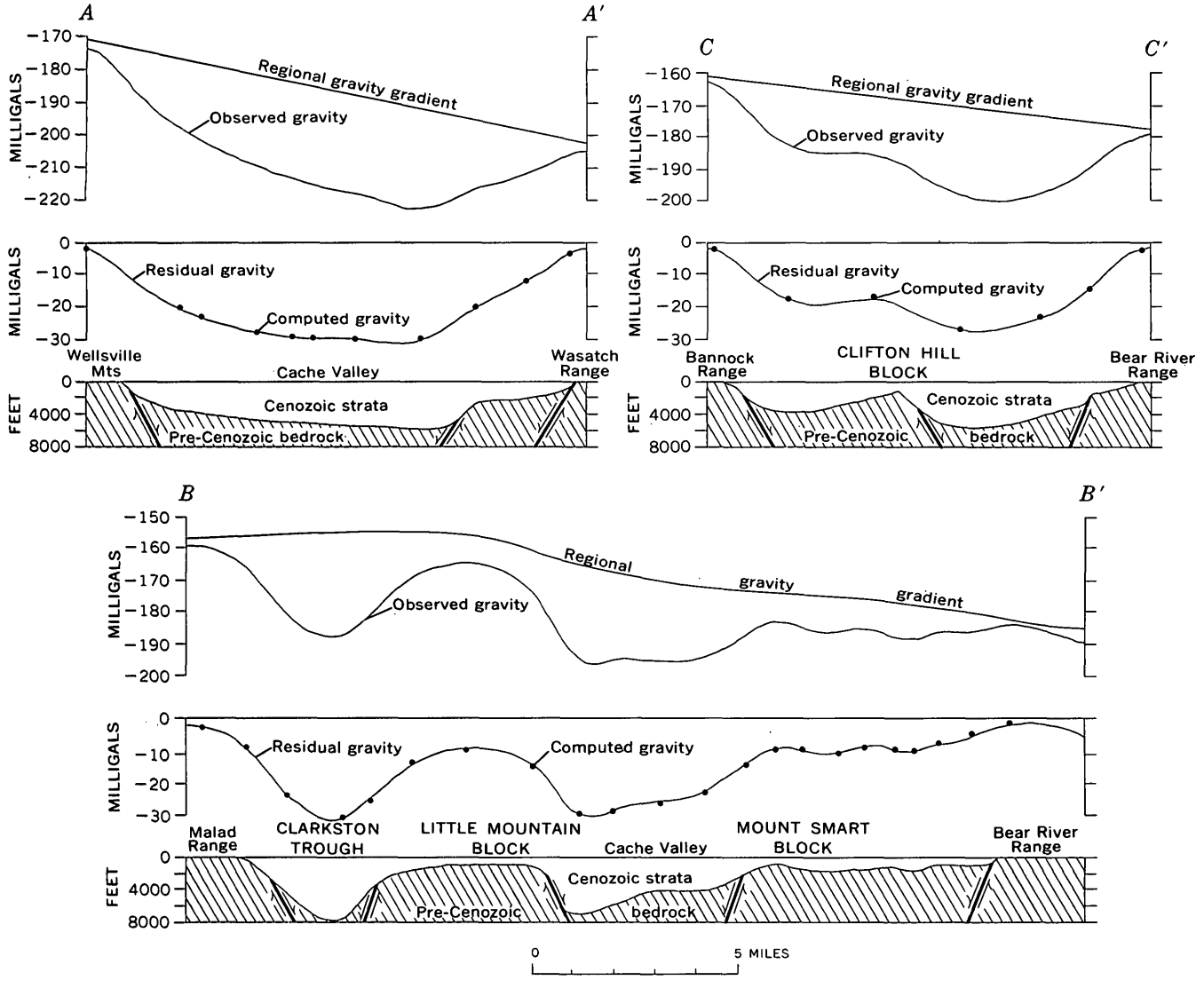

FIGURE 3.—Two-dimensional models computed along gravity profiles *A–A'*, *B–B'*, and *C–C'*. Location of profiles shown on figure 2.

Bergeson Hill to Little Mountain. (Little Mountain is referred to as Newton Hill on the geologic map of northeastern Utah; Stokes, 1963.) Although strata exposed along this belt consist dominantly of the Tertiary Salt Lake Formation and overlapping Quaternary units (Stokes, 1963), gravity data indicate that these sediments are thin. Cambrian rocks are exposed beneath Cenozoic strata on Little Mountain, at the south, and Precambrian rocks are exposed to the north in the Bannock Range. The Precambrian rocks comprise metagraywacke and metadiabase which probably belong to such units below the Brigham Quartzite as the Pocatello Formation and the Bannock Volcanic Formation of the Pocatello area (Ludlum, 1943).

The bedrock profile computed along section *B–B'* (fig. 3), about 2 miles south of the Idaho-Utah State line, assumes a nonlinear regional gravity gradient and indicates that a basement high separates two deep troughs. The eastern trough, the Cache Valley trough, is bounded on the east by the Mount Smart block and is there buried by 1,000–2,000 feet of Cenozoic strata. More than 7,000 feet of Cenozoic strata fills the Cache Valley fault-bounded trough between Lewiston and Cornish, Utah. This trough is separated from the Clarkston trough to the west by a basement high, here designated the Little Mountain block. The western, the Clarkston trough, is deep and narrow and contains at least 8,000 feet of Cenozoic fill; this northwesterly trending trough shows two areas of low gravity closure.

Farther north, a gravity low is located just south of Preston, Idaho. An interpretation across this low along profile *C–C'* (fig. 3) indicates a thickness of Cenozoic fill of about 5,500 feet. A bedrock high is located just west of the center of the model and is probably bounded

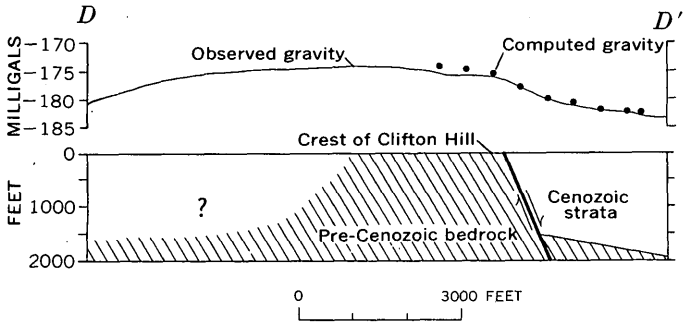

FIGURE 4.—Two-dimensional model computed along gravity profile *D–D'*. Location of profile shown on figure 2.

on the east by a fault. This bedrock high probably is the subsurface extension of Clifton Hill, about 4 miles to the north, where Precambrian rock is exposed (Oriel and Platt, 1968). The gravity data indicate faulting along the east and west margins of the valley.

A detailed gravity survey was made of Clifton Hill in an attempt to determine whether the hill represents a rooted fault block (Oriel and Platt, 1968) or a block of Precambrian rock that slid eastward from the Bannock Range over Salt Lake strata. Gravity stations were spaced approximately 300 feet apart, and horizontal and vertical positions were obtained by transit surveying. An interpretation of these data (profile *D–D'*, fig. 4) indicates that Clifton Hill is bounded by a fault along its east side and that the bedrock is near the surface west of the hill. Whether the hill is bounded on the west by another fault cannot be determined from the available gravity data. Clifton Hill is interpreted to be the exposed part of a rooted and tilted northwesterly trending block of Precambrian bedrock that lies east of and lower than the Precambrian rock that forms the Bannock Range. Therefore, the slide interpretation is denied by the gravity data. Two small gravity lows occur north and northwest of Clifton Hill and indicate local thickening of the Cenozoic rock in the Round Valley area.

The gravity high along the west edge of the Bear River Range, north of the Idaho-Utah State line, is bordered on the east and northeast by an area of lower gravity values. The gravity high coincides with exposures of Brigham Quartzite and Cambrian limestone (Oriel and Platt, 1968) and connects with the Mount Smart block. The lower gravity values to the east and northeast coincide with a belt of exposed Salt Lake strata. A small closed gravity low (fig. 2) near Richmond, Utah, represents the wedge of Cenozoic sediments southeast of the Mount Smart block.

CONCLUSIONS

Gravity data in Cache Valley reveal a relatively complex basin. The estimates of thickest Cenozoic fill are 7,000–8,000 feet for two fault-bounded troughs near the Idaho-Utah State line. The gravity survey amplifies information that has been gathered from surface mapping, answers questions raised in the course of mapping, and indicates the gross structure of the basin. The work provides a basis for developing programs of drilling and for conducting more intensive geophysical studies to evaluate the ground-water resources in the basin.

REFERENCES

Behrendt, J. C., and Woollard, G. P., 1961, An evaluation of the gravity control network in North America: Geophysics, v. 26, no. 1, p. 57–76.

Ludlum, J. C., 1943, Structure and stratigraphy of part of the Bannock Range, Idaho: Geol. Soc. America Bull., v. 54, no. 7, p. 973–986.

Mabey, D. R., and Armstrong, F. C., 1962, Gravity and magnetic anomalies in Gem Valley, Caribou County, Idaho: Art. 140 *in* U.S. Geol. Survey Prof. Paper 450–D, p. D73–D75.

Oriel, S. S., and Platt, L. B., 1968, Reconnaissance geologic map of the Preston quadrangle, southeastern Idaho: U.S. Geol. Survey open-file map, 2 sheets.

Stewart, S. W., 1958, Gravity survey of Ogden Valley in the Wasatch Mountains, north central Utah: Am. Geophys. Union Trans., v. 39, no. 6, p. 1151–1157.

Stokes, W. L., 1963, Geologic map of northwestern Utah: Utah Geol. and Mineralog. Survey, scale 1:250,000.

Swick, C. H., 1942, Pendulum gravity measurements and isostatic reductions: U.S. Coast and Geod. Survey Spec. Pub. 232, 82 p.

Williams, J. S., 1958, Geologic atlas of Utah—Cache County: Utah Geol. and Mineralog. Survey Bull. 64, 104 p.

——— 1962, Lake Bonneville—Geology of southern Cache Valley, Utah: U.S. Geol. Survey Prof. Paper 257–C, p. 131–152.

THICKNESS OF UNCONSOLIDATED TO SEMICONSOLIDATED SEDIMENTS IN JORDAN VALLEY, UTAH

By ROBERT E. MATTICK, Denver, Colo.

Work done in cooperation with the Utah Department of Natural Resources, Division of Water Rights

Abstract.—A maximum thickness of about 5,000 feet of unconsolidated to semiconsolidated sediments in Jordan Valley is indicated on an isopach map constructed on the basis of previously published geophysical data. The map is based on a gravity survey of Jordan Valley, a seismic-refraction profile in the northern part of the valley, an aeromagnetic survey in the southern part of the valley, and on the data from 10 wells which penetrated underlying consolidated rocks and which are located throughout the valley.

Jordan Valley is an intermontane basin extending south from the southeast corner of Great Salt Lake, Utah. The valley lies between two great upthrown fault blocks—the Wasatch fault block to the east and the Oquirrh-Boulter-Tintic fault block to the west. At the south end of Jordan Valley the east-trending Traverse Mountains extend between the Wasatch Range and the Oquirrh Mountains and separate Jordan Valley from Utah Valley to the south. The Traverse Mountains (approximately at the Utah-Salt Lake County boundary) are bisected at the Jordan Narrows by the Jordan River, which conveys fresh water from Utah Lake northward into Great Salt Lake. Wells within Jordan Valley have revealed thickness of valley fill in excess of 3,000 feet.

As part of an investigation of the water resources of Jordan Valley, the U.S. Geological Survey must determine the amount of ground water that is in storage in the valley fill. To construct an isopach map that might help in this determination, previously published geophysical and well data from Jordan Valley were reviewed. The available geophysical data are (1) a gravity survey by Cook and Berg (1961), (2) a seismic-refraction survey by Arnow and Mattick (1968), and (3) an aeromagnetic survey in southern Jordan Valley by Books (1954).

GRAVITY SURVEY AND WELL DATA

A Bouguer gravity map of Jordan Valley and vicinity together with the locations of 10 wells that penetrated consolidated rock are shown on figure 1. Gravity highs correspond to the surrounding Wasatch Range, and the Traverse and Oquirrh Mountains. The highest gravity values occur near the northwest corner of the mapped area. This high correlates with an area of relatively high density rock consisting of Precambrian gneisses and schists which are exposed on Antelope Island about 2 miles northwest of the mapped area (Eardley, 1939).

According to Cook and Berg (1961), Jordan Valley is a graben as indicated by the steep gravity gradients that outline the valley along parts of its east, west, and south boundaries. Along the Wasatch Range, the graben is bounded by the Warm Springs and Limekiln faults to the north and the Wasatch fault zone to the south. The curving character of these faults is indicated by the trends of the steep gravity gradients. To the south, near the Traverse Mountains, steep gravity gradients and the occurrence of warm springs suggest that the thick fill in Jordan Valley possibly terminates against an east-trending fault or fault zone.

The conspicuous southeast-trending gravity nose in the vicinity of Kearns is coextensive with a bedrock pediment of Paleozoic rocks and upper Tertiary rocks, including tuffs, that extends at shallow depth beneath a thin veneer of unconsolidated sediments out into Jordan Valley (Marsell and Jones, 1955). Paleozoic rocks crop out at the east edge of Magna and probably occur at shallow depths beneath this nose.

The relatively low gravity values over the Jordan Valley graben probably are caused, at least in part, by a density contrast between unconsolidated to semicon-

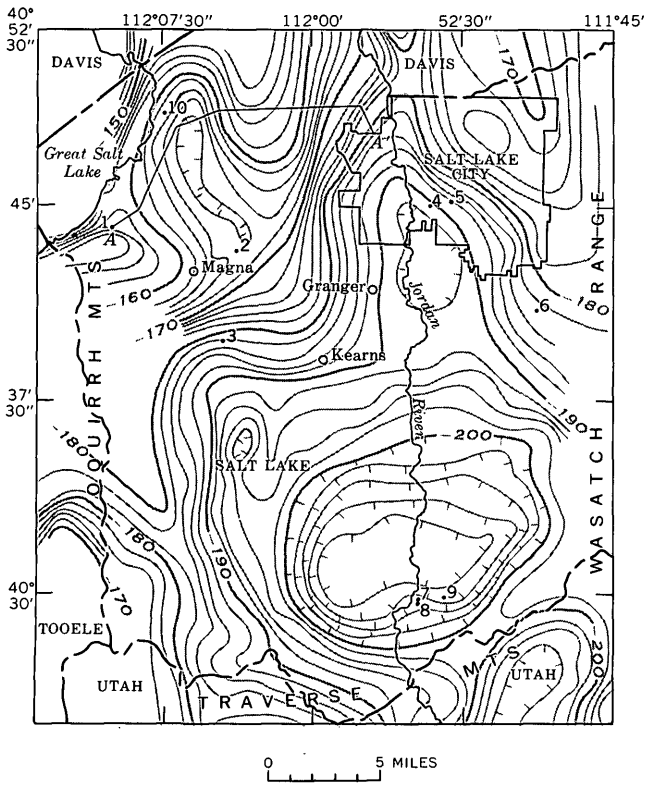

Description of wells

Well No.	Name and field number	Depth to consolidated rock (feet)
1	(C–1–3)15bca–2 (Kennecott Copper Corp., Garfield No. 5 replacement).	882
2	(C–1–2)21adb–1 (Kennecott Copper Corp.).	520
3	(C–2–2)9bdb–1 (Hercules Inc.)	480
4	(C–1–1)12bdb–1 (American Foundry and Machine Co.).	1, 168
5	(D–1–1)7bba–1 (Clover Leaf-Harris Dairy).	741
6	(D–2–1)2bbb–1 (County Water System)	398
7	(C–4–1)2ddb–1 (Utah State Prison Farm No. 1).	722
8	(C–4–1)2ddc–1 (American Smelting and Refining Co. No. 2).	370
9	(C–4–1)1dad–1 (Utah State Prison Farm No. 2).	300
10	(B–1–3)24bdd–1 (L. E. Whitlock, Morton Salt No. 1).	3, 650

FIGURE 1.—Map of Jordan Valley, Utah, showing the location of seismic-refraction profile *A–A′*, wells (1–10) that penetrated consolidated rock, and Bouguer gravity contours (interval 2 milligals). (Bouguer gravity contours from Cook and Berg, 1961, pl. 13.)

solidated valley fill and the more dense underlying consolidated rocks. However, superimposed on this anomaly are anomalies resulting from (1) changes in underlying consolidated rocks and (2) a regional gradient.

The heterogeneity of the underlying consolidated rocks is shown by well data. Wells 1 and 2, near the west side of the valley, bottomed in limestone. Well 3 (Hely and others, 1967, p. 15), near the west side of the valley, and wells 4 and 5, near the east side of the valley, bottomed in shale. A description of the bedrock from well 6 is not available. At the south end of Jordan Valley, wells 7 and 8 bottomed in andesite and well 9 penetrated quartzite. Near the northwest corner of the valley, well 10 penetrated consolidated rock, possibly conglomerate, at a depth of 3,650 feet. Although the different rock types probably give rise to gravity anomalies of at least relatively small amplitude, most of these smaller anomalies cannot be distinguished from the larger anomalies that are attributable to a density contrast between the unconsolidated to semiconsolidated sediments and the more dense underlying consolidated rocks.

The change in gravity values from above —150 mgals (milligals) in the northwest corner of the mapped area to below —200 mgals in the southeast corner suggests a regional gradient of 1–2 mgal per mile in a north-northwest direction. (See fig. 4.) This gradient, at least in part, is associated with regional topographic features and is believed to indicate isostatic compensation for regional topography (Mabey and others, 1963).

SEISMIC-REFRACTION SURVEY

Arnow and Mattick (1968) interpreted a seismic-refraction survey along profile *A–A′* near the north end of Jordan Valley (fig. 2). They recorded three major velocity layers with average P-wave velocities of about 5,800, 9,200, and 15,400 feet per second. The following description of these layers is mostly from their report.

The uppermost layer, which is believed to be of Quaternary age, is traced continuously along the seismic profile, and the average velocity of 5,800 fps is characteristic of an unconsolidated water-saturated material. Logs of wells drilled near the profile indicate that this material is predominantly interbedded clay, silt, fine

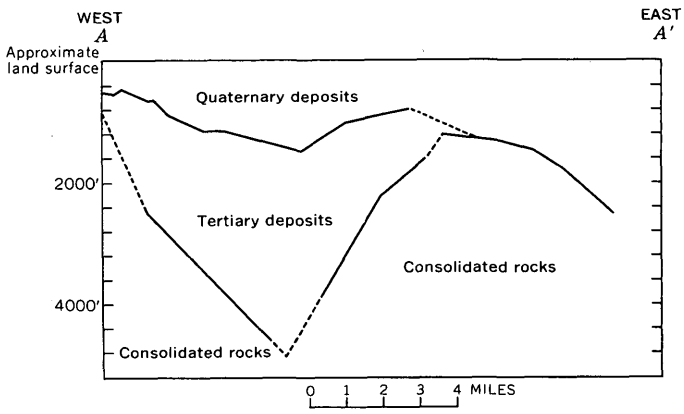

FIGURE 2.—Computed depth of three velocity layers along seismic-refraction profile *A–A′* in Jordan Valley. Boundaries are dashed where inferred. From Arnow and Mattick (1968, fig. 2).

sand, and medium sand. The computed thickness of the Quaternary deposits ranges from about 600 to 2,500 feet.

The intermediate velocity layer, which is believed to be of Tertiary age, appears only in the central and west-central parts of the seismic profile. Although the average velocity in this layer is characteristic of semiconsolidated sediments, the log of well 10 indicates that the layer contains unconsolidated sediments with a total of about 300 feet of volcanic rock, possibly andesite, between depths of 2,300 and 2,800 feet. Part or all of the second layer may be in the Salt Lake Formation, but without diagnostic fossils or an age determination a definite identification cannot be made.

The lowest layer, which can be traced across almost the entire profile, is limestone near the west end of the profile, according to the driller's log for well 1 (Iorns and others, 1966, p. 88), and possibly a conglomerate near the center of the profile, according to a core from well 10.

AEROMAGNETIC SURVEY

A total-intensity aeromagnetic map of southern Jordan Valley is shown in figure 3. Data from wells 7 and 8, which penetrated andesite at depths of 722 and 370 feet, respectively, indicate that the elongate, closed, east-trending magnetic high near the south end of Jordan Valley is caused by an andesite body buried at shallow depth. Although the more extensive magnetic high, which covers the southeast and southwest corners of Jordan Valley and includes the previous high could be coextensive with andesite rock, it probably is related, at least in part, to granitic rock similar to that which crops out at the southeast corner of Jordan Valley.

Four magnetic depth estimations, calculated by using the technique described by Vacquier, Steenland, Henderson, and Zietz (1951), are located on figure 3.

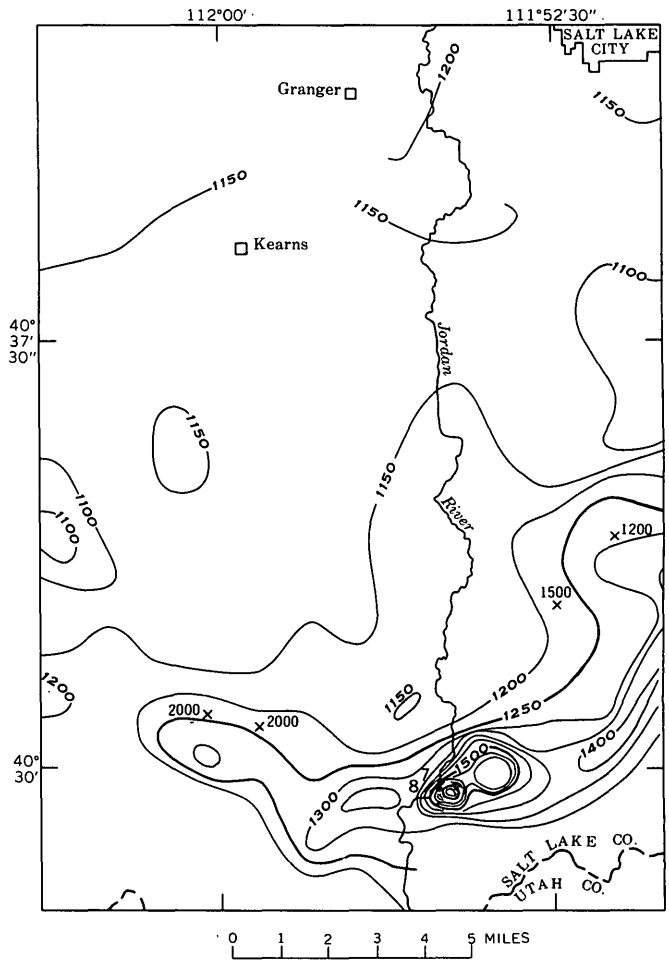

FIGURE 3.—Total intensity aeromagnetic map of southern Jordan Valley, showing the localities (X) where depths (in feet) from ground surface to bedrock were calculated from magnetic data and the locations of wells 7 and 8 and the depths (722 and 370 feet, respectively) below ground surface at which andesite was penetrated. Modified from Books (1954). Interval is 50 gammas.

DENSITY ESTIMATIONS

The well data indicate that the consolidated rock that underlies unconsolidated to semiconsolidated sediments in Jordan Valley is limestone and shale in the western part of the valley, shale along the Wasatch Range in the northern part of the valley, andesite and quartzite in the extreme southern part of the valley, and limestone and possibly conglomerate along seismic-refraction profile A–A'. Density measurements for these rock types in Jordan Valley are not available; however, the literature provides enough information to make reasonable density estimates. According to Birch (in Birch and others, 1942, table 2), the density of pre-Tertiary limestone average about 2.65 g/cm^3, and the average density of water-saturated pre-Tertiary shale is about 2.43 g/cm^3; however, there is an overlap in the spread of densities for these two rock types. According to the composite velocity-density relations for clastic sediments reported by Woollard (1962), clastic sediments with a recorded velocity of about 15,800 fps (as recorded along seismic-refraction profile A–A') have a density of about 2.5–2.7 g/cm^3. Comparison of these densities with an average density for the unconsolidated Quaternary and unconsolidated to semiconsolidated Tertiary deposits (a reasonable average density for these two units is probably about 2.0–2.2 g/cm^3) suggests that the consolidated rock types occurring in the northern and central parts of the valley (limestone, shale, and the 15,800-fps layer) can be lumped together in considering the major gravity anomalies. Therefore the gravity map, at least in the northern and central

parts of the valley, should be useful in constructing an isopach map of the unconsolidated to semiconsolidated sediments. The density relations in the southern part of the valley are discussed in a later section of this paper.

REGIONAL GRAVITY GRADIENT

To construct an isopach map of the unconsolidated to semiconsolidated sediments from the gravity data a regional gradient must be removed. As shown on figure 1, gravity values, which are on or near consolidated rock, are above −150 mgals in the northwest corner of the mapped area and below −200 mgals in the southeast corner. This change in gravity values suggests that the average regional gravity gradient trends northwesterly with a magnitude of about 1–2 mgal per mile. To more precisely define this gradient, a second-degree polynomial surface was fitted by computer to the gravity data of figure 1. The resultant planar surface, part of which is shown in the bottom half of figure 4, indicates that the average regional gravity gradient trends N. 20° W. and has a magnitude of 1.4 mgal per mile. In the north half of figure 4, the average regional gradient has been adjusted by hand to more closely fit the depths to consolidated rock obtained along seismic-refraction profile A–A' and from wells 1–6 and 10.

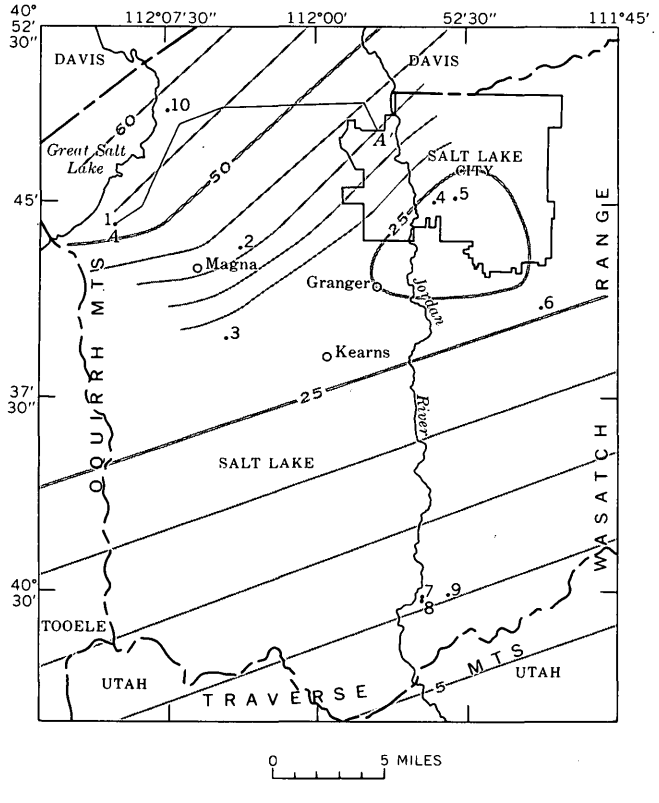

FIGURE 4.—Map showing assumed regional gravity in the Jordan Valley area. Contour interval is 5 mgal. A–A', seismic refraction profile. 1–10, locations of wells.

It should be noted that this method for calculating a so-called regional gradient actually isolates more than just a regional gradient. The term "regional gradient" normally refers to those anomalies that are much larger in areal extent than the anomalies ordinarily of interest and are usually attributed to deep-seated structural features (for example, isostatic compensation for regional topography). However, the adjusted regional gravity shown in the north half of figure 4 probably represents the combined effect of both a true regional gradient and anomalies due to changes in the underlying consolidated rocks. The areal extent of the latter anomalies could be about equal to the areal extent of any residual anomalies.

An area in which the magnitude of the regional gradient is relatively low appears in the central part of figure 4. This area, which extends from the left-central boundary of figure 4 and includes the area enclosed by the closed 25-mgal contour, cannot be correlated with known geologic structure. All the wells in this area from which bedrock information is available (wells 3, 4, and 5) penetrated shale. Therefore, it might be speculated that this area is underlain by shale whose density is lower than that of other consolidated rocks in the Jordan Valley area.

A residual gravity map (fig. 5) was obtained by subtracting the contoured values of figure 4 from the contoured values of figure 1. The conspicuous anomalies shown on the residual gravity map are (1) a closed gravity low of about 15 mgal near the northwest corner of the mapped area, (2) a lobed, elongate gravity low of 15–20 mgal extending northward through the east-central part of the mapped area, and (3) an east-trending gravity nose between Granger and Magna. These three anomalies correlate with known geologic structures. The gravity low shown near the northwest corner of the map correlates with the thick section of Quaternary unconsolidated and Tertiary unconsolidated to semiconsolidated deposits recorded on seismic-refraction profile A–A'. The second anomaly is coextensive with the Jordan Valley graben. The salient gravity nose between Granger and Magna, which has shifted significantly from a northwest-trending position in figure 1 to an east-trending position in figure 4, probably is related to a bedrock pediment discussed earlier.

ISOPACH MAP

Figure 6 is an isopach map of unconsolidated to semiconsolidated sediments in Jordan Valley. The northern and central sections of this map were constructed on

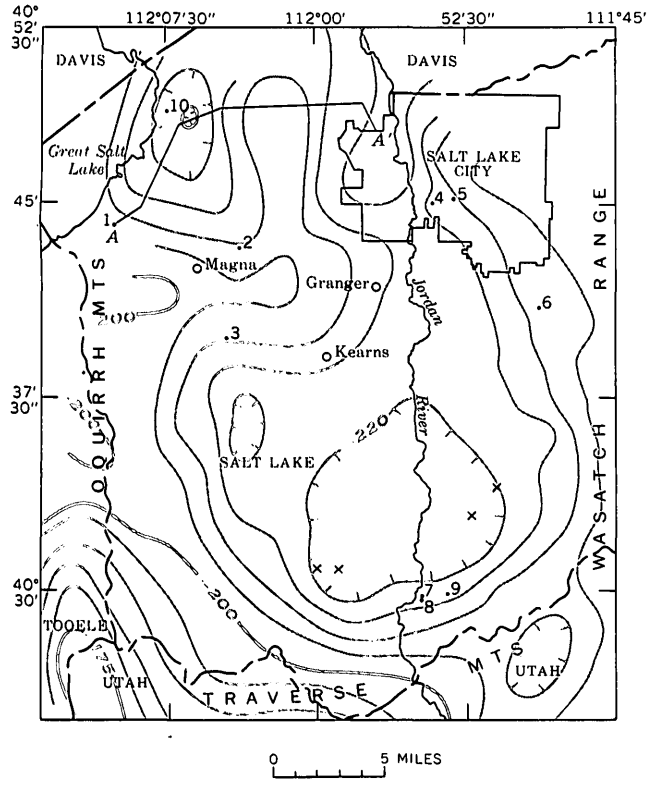

FIGURE 5.—Map showing residual gravity in the Jordan Valley area. Contour interval 5 mgal. The residual values were obtained by subtracting the contoured values of figure 4 from the contoured values of figure 1. *A–A'*, seismic refraction profile. 1–10, locations of wells. X indicates location where depth to bedrock was calculated from magnetic data.

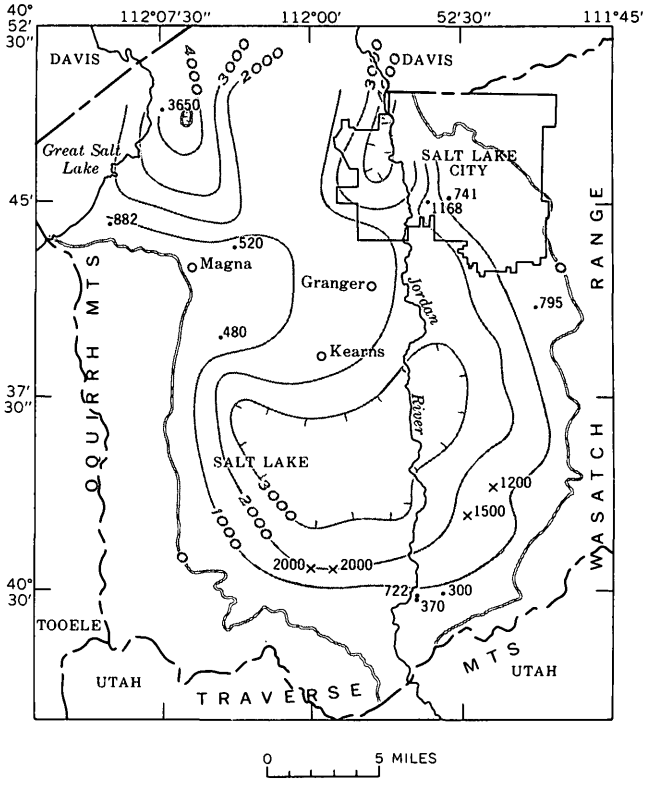

FIGURE 6.—Isopach map of unconsolidated to semiconsolidated sediments in the Jordan Valley area. Interval 1,000 feet. Number beside dot is thickness, in feet, of unconsolidated to semiconsolidated sediments in control well (fig. 1); number beside X is depth to bedrock calculated from magnetic data (fig. 3). The zero contour line is from boundary of valley fill as interpreted by Marine and Price (1964).

the basis of well depths and using the residual gravity map for extrapolation between wells.

In southern Jordan Valley, in the vicinity of wells 7 and 8, the isopach map is based on well depths and the four depths calculated from the aeromagnetic data rather than the gravity data. Wells 7 and 8 penetrated andesite at depths of 722 and 370 feet, respectively. However, the magnitude of the residual gravity anomaly in the vicinity of these wells is greater than could be produced by this thickness of valley fill. A part of the gravity anomaly is assumed to be produced by the andesite, which is less dense than the normal bedrock.

Although this isopach map is somewhat general, it will be useful in preparing a more detailed isopach map of that part of the valley fill material that is readily water bearing.

REFERENCES

Arnow, Ted, and Mattick, R. E., 1968, Thickness of valley fill in the Jordan Valley east of the Great Salt Lake, Utah, *in* Geological Survey Research 1968: U.S. Geol. Survey Prof. Paper 600–B, p. B79–B82.

Birch, A. F., Schairer, J. F., and Spicer, H. C., eds., 1942, Handbook of physical constants: Geol. Soc. America Spec. Paper 36, 325 p.

Books, K. G., 1954, Geophysical surveys in Salt Lake Valley, Utah: Science, v. 119, no. 3094, p. 513–514.

Cook, K. L., and Berg, J. W., Jr., 1961, Regional gravity survey along the central and southern Wasatch Front, Utah: U.S. Geol. Survey Prof. Paper 316–E, p. 75–89.

Eardley, A. J., 1939, Structure of the Wasatch-Great Basin region: Geol. Soc. America Bull., v. 50, no. 8, p. 1277–1310.

Hely, A. G., Mower, R. W., and Horr, C. A., 1967, Hydrologic and climatologic data, 1966, Salt Lake County, Utah: U.S. Geol. Survey open-file report (duplicated as Utah Basic-Data Release 13, 85 p.).

Iorns, W. V., Mower, R. W., and Horr, C. A., 1966, Hydrologic and climatologic data collected through 1964, Salt Lake County, Utah: U.S. Geol. Survey open-file report (duplicated as Utah Basic-Data Release 11, 91 p.).

Mabey, D. R., Tooker, E. W., and Roberts, R. J., 1963, Gravity and magnetic anomalies in the northern Oquirrh Mountains, Utah: Art. 187 *in* U.S. Geol. Survey Prof. Paper 450–E, p. E28–E31.

Marine, I. W., and Price, Don, 1964, Geology and ground-water

380-189 O - 70 - 9

resources of the Jordan Valley, Utah: Utah Geol. and Mineralog. Survey Water-Resources Bull. 7, 67 p.

Marsell, R. E., and Jones, D. J., 1955, Geomorphology of Jordan Valley, Utah [abs.]: Geol. Soc. America Bull., v. 66, no. 12, pt. 2, p. 1656–1657.

Vacquier, Victor, Steenland, N. C., Henderson, R. G., and Zietz, Isidore, 1951, Interpretation of aeromagnetic maps: Geol. Soc. America Mem. 47, 151 p.

Woollard, G. P., 1962, The relation of gravity anomalies to surface elevation, crustal structure and geology: Wisconsin Univ. Geophys. and Polar Research Center Rept. Ser., Rept. 62–9, pt. 2, 30 p.

COPRECIPITATION OF CARBONATE AND PHOSPHATE FROM SEA WATER

By R. A. GULBRANDSEN and MARCELYN CREMER,
Menlo Park, Calif.

Abstract.—A precipitate composed dominantly of aragonite was obtained from sea water by increasing the pH of the solution. Analysis of the precipitate showed it to contain 0.064 percent P_2O_5, an amount that comes close to the average for analyzed limestones. The results of the experiment thus indicate that coprecipitation of carbonate and phosphate may be an important natural process.

Chemical analyses show that most limestones contain a very small amount of phosphate. Clarke's (1924, p. 30) often-cited average limestone contains 0.04 percent P_2O_5; Ronov and Korzina (1960, p. 821) give an average for 289 composites of 0.068 percent; and we have calculated that in 385 published analyses of limestones containing less than 10 percent MgO and less than 0.5 percent P_2O_5, the average P_2O_5 content is 0.067 percent. A histogram of this latter group (fig. 1) shows a high frequency of P_2O_5 content around 0.05 percent, which may have resulted from the dominant action of a particular process. Ronov and Korzina (1960, p. 813) suggest that the phosphate in limestone is biologically derived from associated organic matter, but although this possibility cannot be ruled out in the present state of knowledge, it offers no clear explanation for the frequency of P_2O_5 percentages close to 0.05 percent.

Another possibility is that the phosphate (presumably in carbonate fluorapatite, the marine variety of apatite) was precipitated with the calcium carbonate. The theoretical basis for this is treated by Gulbrandsen (1969) as a part of a summary and synthesis of physical and chemical data bearing on the formation of apatite in sea water. The relationship in general terms is based on the two compounds having an ion of calcium in common, on their similar reactions to sea water within its prevailing pH range, and on the fact that sea water is apparently nearly saturated with both of them. This inference was tested by an experiment, in which both compounds were found to be precipitated when the pH of the sea water was raised. It was known beforehand that this procedure would bring about the precipitation of calcium carbonate, but although it was indicated by theory that the very small amount of phosphate in sea water would also be precipitated, the fact had not been demonstrated experimentally. Sodium hydroxide was used to raise the pH of the sea water because, since the amount of sodium added would be negligible as compared with the amount already in sea water, the pH would be the only variable that was materially changed.

The sea water used in the experiment was taken from Half Moon Bay, south of San Francisco, Calif. It was pumped through a 0.45-micron ultrafilter from a level several feet below the water surface. Its original tem-

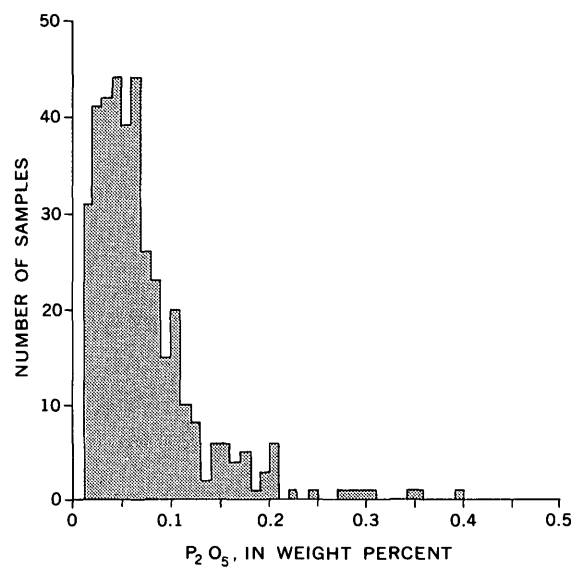

FIGURE 1.—Histogram of P_2O_5 content in weight percent of 385 limestone samples that contain less than 10 percent MgO and less than 0.5 percent P_2O_5. Data from Graf (1960), Hill, Werner, and Horton (1967), and Muir, Hardie, and Mitchell 1956).

U.S. GEOL. SURVEY PROF. PAPER 700-C, PAGES C125-C126

perature was 16°C, and its original pH was 7.8. In the laboratory the temperature rose to about 24°C and the pH to 8.2. The pH of 20 liters of the sea water, contained in a glass bottle, was then raised by adding 1-ml increments of 5*M* NaOH at approximately 1- to 2-hour intervals during the day. The solution was mechanically stirred while this was being done, and the stirring was continued during most of the experiment. Globules of precipitate immediately formed around the drops of NaOH solution, but were rapidly dissolved. In about 3 days, when 12 ml of NaOH solution had been added, the water became turbid. The pH of the solution at this time was 9.9. Adding 6 ml more of NaOH solution markedly increased the amount of precipitate but did not change the pH. Within 2 hours of the last addition of NaOH nearly all the precipitate had settled to the bottom of the bottle. It was left in contact with the solution for 4 days, during which the mixture was occasionally stirred. The pH dropped during this period to 9.6. The precipitate from these 20 liters of sea water weighed about 3.9 g.

X-ray analysis showed that the precipitate consisted mainly of aragonite but contained a significant amount of brucite. In an oil mount under the microscope the aragonite was seen to form spherical aggregates of microcrystalline particles, laths, and dumbbell-shaped aggregates of laths. The brucite formed irregularly shaped aggregates of microcrystalline particles. No phosphate mineral was observed, and because of the very small amount possible, none was expected to be seen.

The precipitation of brucite was unexpected, but it should have been expected in view of the high pH of the solution. In a second experiment we found that the calcium carbonate was nearly all precipitated before brucite began to come out, a finding in agreement with the fact that brucite is not known as a naturally occurring sedimentary mineral. The precipitate from this experiment was lost in a laboratory accident before it could be analyzed for phosphate.

A chemical analysis of the precipitate from the first experiment (table 1) shows it to contain 0.064 percent P_2O_5. The amount of phosphate would be somewhat higher if brucite were absent, but the limestones used for comparison here also contained diluting minerals, such as quartz and clay minerals. The phosphate content of the precipitate is close to two of the above-cited averages for limestone and within the range of all three. The significance of this kind of comparison is clearly difficult to assess. The results of the experiment do show, however, that phosphate can be precipitated from sea water along with calcium carbonate and that the amount of phosphate precipitated is of a magnitude that is consistent with the observed amounts in many limestones.

Acknowledgments.—We are especially grateful to Ivan Barnes for his help and the use of his equipment in collecting the sea water. We thank R. J. McLaughlin for his compilation of limestone analyses and C. E. Roberson for lending some laboratory equipment.

TABLE 1.—*Partial chemical analysis of precipitate from sea water*

[Semiquantitative spectrographic analysis of SrO by Chris Heropoulos]

Constituent	*Amount (weight percent)*
MgO	12.1
CaO	43.0
SrO	0.8
P_2O_5	0.064
CO_2	35.99

REFERENCES

Clarke, F. W., 1924, The data of geochemistry: U.S. Geol. Survey Bull. 770, 841 p.

Graf, D. L., 1960, Geochemistry of carbonate sediments and sedimentary carbonate rocks—Pt. 4–A, Isotopic composition, chemical analyses: Illinois Geol. Survey Circ. 308, p. 5–42.

Gulbrandsen, R. A., 1969, Physical and chemical factors in the formation of marine apatite: Econ. Geology, v. 64, no. 4, p. 365–382.

Hill, T. P., Werner, M. A., and Horton, M. J., 1967, Chemical composition of sedimentary rocks in Colorado, Kansas, Montana, Nebraska, North Dakota, South Dakota, and Wyoming: U.S. Geol. Survey Prof. Paper 561, 241 p.

Muir, A., Hardie, H. G. M., and Mitchell, R. L., 1956, Tables of chemical analyses of Scottish limestones, chap. IV, *in* The limestones of Scotland: Geol. Survey of Great Britain, Dept. Sci. and Industrial Research, Spec. Repts. on the Mineral Resources Great Britain, v. 37, 150 p.

Ronov, A. B., and Korzina, G. A., 1960, Phosphorus in sedimentary rocks: Geochemistry, no. 8, p. 805–829.

THE MOBILITY OF GOLD IN MULL (FOREST HUMUS LAYER)

By GARY C. CURTIN, HUBERT W. LAKIN,
and ARTHUR E. HUBERT, Denver, Colo.

Abstract.—Three gold-bearing samples of mull were leached with demineralized water. The leachate from the first sample was passed through a 0.45-micron average pore diameter membrane filter. The remaining two leachates were passed through 0.05-micron average pore diameter membrane filters. The filtered leachates contained 110, 27, and 120 parts per trillion (1×10^{-12}) gold, respectively. The relatively high gold content of two of the leachates suggests that in the mull layer of the soil, gold is slightly mobile principally as extremely small colloidal particles (<0.05 micron diameter) and in minor amounts as gold cyanide and gold thiocyanate ions.

The movement of gold as an organic complex in the zone of weathering has been studied by several investigators. Lungwitz (1900, p. 501), after detecting as much as about 0.07 oz gold per ton (valued at $1.17 per ton) in ash of branches of ironwood trees, postulated that gold chloride may be formed during the leaching of gold deposits by surface waters containing chloride ion and nitric and sulfuric acids derived from the decomposition of organic matter. The gold chloride then may form double salts with water-soluble organic compounds, such as those present as brown coloring matter in tropical streams, that can be absorbed by the trees. Freise (1931, tables 2 and 3) reported that gold was dissolved in solutions of organic compounds derived from brown coal and from black river water in Brazil that was rich in dissolved organic compounds. V. V. Sherbina (cited in Manskaya and Drozdova, 1968, p. 271) suggested in 1956 that gold may react with humic acids to form soluble compounds in soil and that the products probably would have low stability constants and low positive oxidation-reduction potentials. Steelink (1963, p. 380–381) suggested that, in the presence of oxygen, gold may react with humic acids to form soluble compounds. Garces (1942, p. 1137–1138) and Fetzer (1946, p. 50–52) attempted to duplicate Freise's results using humic acids extracted from peat and lignite, but their experiments yielded no gold in solution. Ong and Swanson (1969, p. 420–422) showed that gold is neither dissolved, complexed, nor oxidized by organic acids, but that gold in solution in the form of gold chloride is reduced to a negative colloid of metallic gold in the presence of organic acids. Further, they observed that the resulting gold sol is stabilized, probably by the simultaneous formation of a protective layer of organic molecules around the gold, permitting mobility of the colloidal gold in soil and sediment waters.

This report presents information on a part of the studies done on gold-bearing samples of mull, the organic surface layer of the soil, which is defined by the U.S. Department of Agriculture (1951, p. 245) as "a humus-rich layer consisting of mixed organic and mineral matter, generally with a gradational boundary to the underlying mineral horizon."

The gold content of the mull probably reflects a biogeochemical cycle in which gold is leached from the bedrock, is absorbed by vegetation, and is concentrated in the mull as the vegetation decays.

The results of the laboratory experiments described in this paper suggest that gold is slightly mobile in the mull layer of the soil, either in solution as an organic complex or in a sol as a very fine colloid (<0.05 micron).

LABORATORY EXPERIMENTS

The experiments consisted of the determination of gold in the solution obtained by leaching three composite gold-bearing mull samples with demineralized water. Gold content was determined by an atomic absorption method (Thompson and others, 1968). Physical and chemical data on the composite mull samples and leachates are shown in table 1.

Composite 1 (table 1) was fractionated according to particle size and density using demineralized water as a dispersing agent. The leachate formed by leaching action of the water used in the fractionation of composite 1 was filtered (table 1) to remove suspended particles. The leachate was then evaporated to dryness in

a new laboratory free from any gold contamination. The residue was ashed and analyzed. Because gold was found in the residue of the leachate from composite 1 (table 1), composite 2 was treated in the same way as composite 1 except that, in addition, the leachate was filtered through a 0.05-micron average pore diameter membrane filter to insure that the gold content determined represented only gold in solution or very fine colloidal suspension. To further test the mobility of gold in the mull layer of the soil, composite 3 was immersed in demineralized water. The mixture was allowed to stand, covered except for vigorous stirrings twice each day, for a 240-hour period (table 1). The leachate from composite 3 was treated in the same way as the leachate from composite 2.

DISCUSSION OF RESULTS

Though less than 1 percent of the total gold in the mull samples is in the leachates (table 2), in composites 1 and 3 the gold content of the leachates—110 and 120 ppt (parts per trillion, 1×10^{-12}), respectively, (table 1)—is more than twice the general maximum gold content (50 ppt) of waters draining gold-bearing areas in Colorado (Jenne and others, 1968, p. 421). The lowest gold content occurs in a leachate that is straw yellow (fig. 1), whereas the two high gold contents occur in leachates that are light to dark brown, suggesting a positive correlation of gold content with density of color of the leachates. Because dissolved organic compounds probably are the primary coloring agents in the solution, the gold may be present either as a gold-organic complex ion or as an organic-protected colloid.

Whether gold is dissolved, complexed, or reduced by organic acids is controversial. The apparent positive correlation between gold and organic compounds in the leachates implies that the gold in the leachates is in the form of soluble organic-gold complexes.

Cyanide and thiocyanate ions, which are products of hydrolysis of plant glycocides by enzymatic action (Kingsbury, 1964, p. 23–27; Armstrong and Armstrong, 1931, p. 67; Timonin, 1941, p. 404), have the ability to complex gold in moderately oxidizing environment (Jacobson, 1949, p. 554; Manskaya and Drozdova, 1968, p. 271). Where the dry surface layer of the mull is loosely packed and periodically saturated by rain and snowmelt water, a biogeochemical process may take place in which cyanide and thiocynate ions are produced during the decay of vegetation, and these ions, in turn, form stable, water-soluble gold complexes in the aerated water solution.

The gold in the reducing environment of the well-packed, water-soaked mull beneath the loose surface layer, however, probably is in the colloidal state and may reflect the release of gold from decaying vegetation either as extremely small colloidal particles or as ionic gold which is subsequently reduced to the colloidal state.

TABLE 1.—*Physical and chemical data on the composite mull samples, filtered leachates, and residues*

No.	Composite samples			Evaporated residue (weight in grams)	Ash of evaporated residue		
	Dry weight (grams)	Average gold content (ppm)	Soaking time (hours)		Weight (grams)	Percent	Gold content (ppm)
1	392	0.8	24	2.0	0.7	35	1.1
2	509	1.4	24	2.3	.7	30	.34
3	928	.6	240	5.5	1.8	33	.45

No.	Filtered leachates			Filter		
	Volume (liters)	Color	Gold content (ppt)	Size (microns)	Type	Gold content of residue on filter (micrograms)
1	7	Light brown	110	4	Glass	0.18
				.45	Membrane	<.04
2	9	Straw yellow	27	4	Glass	.36
				.45	Membrane	.16
				.05	do	<.04
3	7	Dark brown	120	4	Glass	.48
				.45	Membrane	<.04
				.05	do	<.04

1. Composite of two samples of mull collected under single-leaf pinyon pine (*Pinus monophylla*) growing in residual soil on the Wenban Limestone of Devonian age in the Mill Canyon area in the northeastern part of the Cortez quadrangle, T. 27 N., R. 48 E., Eureka County, Nev. Trees were adjacent to a steeply dipping auriferous pyrite vein.
2. Composite of eight samples collected under lodgepole pine (*Pinus contorta*) growing in colluvial soil, derived principally from granite and gneiss, in the Empire district, 37 miles west of Denver, in Clear Creek County, Colo. Trees were growing over or in the immediate vicinity of auriferous pyrite veins.
3. Composite of nine mull samples collected under lodgepole pine growing over or in the immediate vicinity of auriferous pyrite veins in the Empire district.

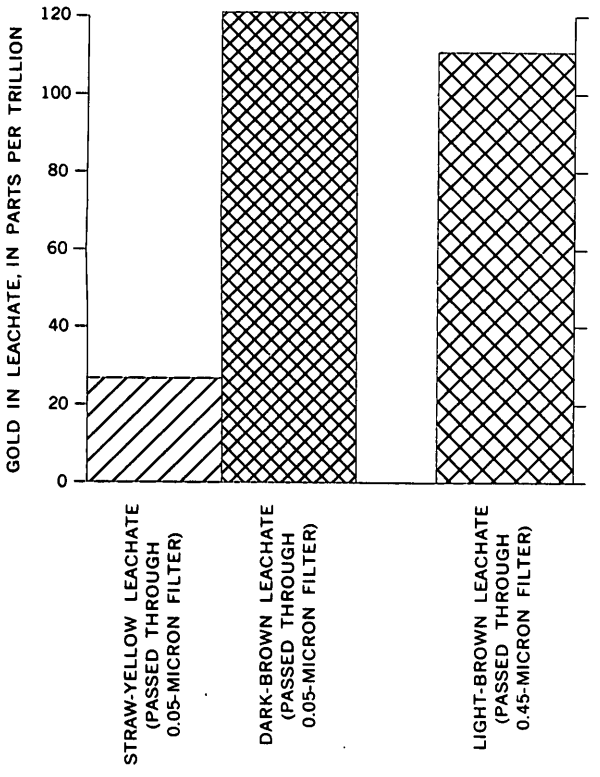

FIGURE 1.—Comparison of gold content and color of leachates.

In summary, gold in the form of extremely small colloidal particles (<0.05 micron diameter) is probably the principal source of gold in the leachates, and gold cyanide and gold thiocyanate ions may be present in minor amounts.

REFERENCES

Armstrong, E. F., and Armstrong, K. F., 1931, The glycosides: London, Longmans, Green & Co., 123 p.

Fetzer, W. G., 1946, Humic acids and true organic acids as solvents of minerals: Econ. Geology, v. 41, no. 1, p. 47–57.

Freise, F. W., 1931, The transportation of gold by organic underground solutions: Econ. Geology, v. 26, no. 4, p. 421–431.

TABLE 2.—*Gold content of composite mull samples and of leachates from the samples and percentage of total gold in the leachates*

No.	Gold in composite mull sample (micrograms)	Gold in leachate from composite mull sample [1] (micrograms)	Total gold in leachate (percent)
1	278. 5	0. 78	0. 28
2	222. 12	. 24	. 11
3	301. 6	. 84	. 28

[1] Leachate from composite 1 filtered through 0.45-micron filter; leachates from composites 2 and 3 filtered through 0.05-micron filter.

Garces, Hernán, 1942, Solubilidad del oro en acides humicos: Anales Primer Cong. Panamericano Ingenieria Minas y Geologia, v. 3, p. 1135–1138.

Jacobson, C. A., ed., 1949, Encyclopedia of chemical reactions: New York, Reinhold Pub. Co., v. 3, 842 p.

Jenne, E. A., Chao, T. T., and Heppting, L. M., 1968, Use of mercurous chloride to recover trace amounts of gold from waters: Econ. Geology, v. 63, no. 4, p. 420–421.

Kingsbury, J. M., 1964, Poisonous plants of the United States and Canada: Englewood Cliffs, N.J., Prentice Hall, Inc., 626 p.

Lungwitz, E. E., 1900, The lixiviation of gold deposits by vegetation: Eng. and Mining Jour., v. 69, no. 17, p. 500–502.

Manskaya, S. M., Drozdova, T. V., 1968, Geochemistry of organic substances: New York, Pergamon Press, Internat. Ser. Mons. Earth Sci., v. 28, 345 p.

Ong, H. L., and Swanson, V. E., 1969, Natural organic acids in the transportation, deposition, and concentration of gold: Colorado School Mines Quart., v. 64, no. 1, p. 395–425.

Steelink, Cornelius, 1963, What is humic acid?: Jour. Chem. Education, v. 40, no. 7, p. 379–384.

Thompson, C. E., Nakagawa, H. M., and VanSickle, G. H., 1968, Rapid analyses for gold in geologic materials, *in* Geological Survey Research 1968: U.S. Geol. Survey Prof. Paper 600–B, p. B130–B132.

Timonin, M. I., 1941, The interaction of higher plants and soil micro-organisms—III. Effect of by-products of plant growth on activity of fungi and actinomycetes: Soil Sci., v. 52, p. 395–413.

U.S. Department of Agriculture, 1951, Soil survey manual: U.S. Dept. Agriculture, Agriculture Handb. 18, 503 p.

NATURAL ORGANIC ACIDS AS AGENTS OF CHEMICAL WEATHERING

By H. LING ONG,[1] VERNON E. SWANSON, and RAMON E. BISQUE,[2]
Bandung, Indonesia, Denver, Colo., Golden, Colo.

Abstract.—Naturally occurring organic acids, commonly called "humic acids," are effective agents in the colloidal transport of copper, lead, zinc, iron, and aluminum. Concentrations of organic acids in the range of 4–40 ppm carbon in water can effect increases of several orders of magnitude in the amount of these metals "stabilized" in solution. Stability of these metal-organic colloids increases with increasing organic acid concentration and increasing pH. The optimum condition for the stability, in general, lies between pH 6 and pH 9. Chemical weathering due to differential leaching of cations by organic acids may be largely responsible for the formation of sedimentary aluminum and lateritic deposits, which are restricted to tropical and subtropical regions where organic acids are abundant.

In chemical weathering processes, the role of organic or "humic" acids in the decomposition of rocks by differential leaching of the cations is commonly cited (for example, Krauskopf, 1967; Gorshkov and Yakushova, 1962). These naturally occurring soluble organic substances give a brown color to the water of many streams, lakes, and soils, and are largely derived by aqueous leaching of decaying plant material, or humus, at or near the surface.

The term "humic acids" as commonly used in the geologic literature is a misnomer according to generally accepted soil nomenclature, and its further usage should be discouraged. Similarly, use of the term "fulvic acids," which has been used in the literature on natural water, should be discouraged. Naturally occurring organic acids are actually composed of both humic and fulvic acids which are separated in the laboratory according to several soil-science procedures.

At the present time there are no grounds for doubting that organic acids are high-molecular-weight substances (Kononova, 1966); the most commonly cited molecular weight is in the range $2.0–5.0\times10^4$ (Steelink, 1963). The acidity of these organic acids in water is due to functional groups such as –COOH and phenolic –OH which become more or less dissociated or ionized and form polyelectrolytes (Mukherjee and Lahiri, 1956; Piret and others, 1960). Organic acids dispersed in water therefore can be considered either as true solutions of macro-ions or as dilute suspensions of negative hydrophilic colloids.

In their summary of geochemical processes, Rankama and Sahama (1950) described the associations of organic-rich water with iron, silica, phosphorus, and manganese. There is evidence that appreciable amounts of copper in tropical sea water are present as soluble organic complexes (Lee and Hoadley, 1967), and that other transition metals are perhaps similarly bound and transported. Nesterova (1960) found that the amount of copper, nickel, and cobalt in the Ob River increases as the amount of dissolved organic matter increases. Strakhov (1967) determined that more than half the total quantity of iron, manganese, nickel, and copper in the water of the Dnieper River is transported in the form of organic acids. Shapiro (1963) noted that organic acids in natural water are capable of maintaining iron, copper, and other metals in a filterable state at high pH and high Eh. Freise (1931) and Steelink (1963) postulated that river water containing organic acids transports gold; Ong and Swanson (1969), as a result of subsequent experimental work, indicated that organic acids can serve as a mechanism for transporting colloidal metallic gold under natural conditions. And Fetzer (1946) showed that platinum can be solubilized by organic acids.

Laboratory experiments on the role of organic acids in the decomposition of rocks and minerals have been conducted by several investigators. Gruner (1922) found that peat solutions dissolved iron, silica, calcium oxide, and magnesium oxide from various minerals. Moore and Maynard (1929) solubilized iron and aluminum using natural water containing soluble organic matter, and Kee and Bloomfield (1961) experimented with the solubilization of a series of metals from their oxide forms by fermenting plant material. Graham (1941) re-

[1] Bagian Geologi, Institut Teknologi Bandung.
[2] Department of Chemistry, Colorado School of Mines.

ported the effectiveness of humic acid extracted from peat in the weathering of anorthite. The influence of organic acids in the weathering of the more widespread and common rock-forming minerals has been studied by Schatz, Cheronis, Schatz, and Trelawny (1954), Schatz, Schatz, and Martin (1957), Schalscha, Appelt, and Schatz (1967), and Ginzburg, Yashina, Matveeva, Belyatskii, and Nuzhdelovskaya (1966).

Although the geologic role of organic acids, which are abundant in tropical areas, is often emphasized, precise data on the variable geochemical parameters involved in weathering processes remain unclear. The objectives of this investigation were to determine (1) the amounts and stability of copper, iron, aluminum, lead, and zinc in natural organic acid solutions; and (2) the mechanism of mobilization of these metals in organic acid solutions.

This paper was initially presented by the senior author at a symposium, "Different Aspects of Tropical Weathering," at Bandung, Indonesia, November 17–22, 1969, sponsored by UNESCO in cooperation with the International Society of Soil Science. The investigation was in part supported by a U.S. Geological Survey grant (No. 14–08–001–G–12) to the Colorado School of Mines.

EXPERIMENTS AND RESULTS

Conventional chemical extraction techniques were used in the laboratory to obtain soluble organic matter representative of organic acids found in nature. In this study, an alkali-soluble fraction of peat was employed to represent the soluble organic substances. Peat from Michigan was extracted with a mixture of 0.2*N* $NaHCO_3$ and 0.2*N* Na_2CO_3, ratio 2 : 1, with a pH of 9.4. The organic-acid liquor was then purified by treatment with anion (Amberlite IRA–400) and cation (Amberlite IR–120) resins as suggested by Hori and Okuda (1961).

The concentration of the organic acids was determined by carbon analysis, following the Walkley-Black method as described by Allison (1965). Standard solutions were prepared by diluting the extracts to make solutions containing 400 ppm carbon. The organic acids in solutions will be subsequently referred to as OA.

Elemental and infrared analyses of the OA were made after freeze-drying the OA solution. Ultimate analyses, on an ash-free basis, are listed in table 1. These values are very similar to the average composition of organic acids extracted from humate sand and soil, as well as organic acids in surface water (table 1). Infrared spectra of the freeze-dried OA contain the few sharp bands indicating hydroxyl and carboxyl functional groups, similar to the spectra of many soil organic extracts. Therefore, the OA obtained are believed to be representative of dissolved organic matter as found in nature.

Experiments with copper

In order to study some of the reactions between cupric ions and the organic acids, a series of solutions was prepared. A stock copper solution was made up of 200 ppm copper sulfate in hydrochloric acid at a pH of 2.2, and 50-ml aliquots of this stock solution were pipetted into each of five 500-ml volumetric flasks and diluted to volume. They were then poured into five beakers, and the pH of each was adjusted with solid Na_2CO_3 to individual pH levels of 5.0, 6.0, 7.0, 8.0, and 9.0, respectively. These solutions, each containing 20 ppm copper and having different pH values, were placed in tightly stoppered polyethylene bottles.

At the end of 30 days the bottles were opened and about 30 ml of each solution was passed through Whatman No. 42 filter paper, which has a pore size of 0.4–1.2 microns. The filtering removed suspended and, at least, the larger colloidal-size particles of $Cu(OH)_2$ and $CuCO_3$ precipitates. The concentrations of the cupric

TABLE 1.—*Comparison of ash-free organic element analyses of organic acids, in weight percent*

[Leaders (....) indicate data not given in cited report]

Type of organic matter	C	H	N	S	O	Reference
OA–1, peat extract	54. 02	4. 86	0. 94	0. 32	39. 84	This paper.
Humate-sand extract (mean of 5 analyses).	55. 00	4. 4	1. 4	. 7	38. 5	Swanson and Palacas (1965, table 4).
Soil extracts:						
Humic acid (mean of 5 analyses).	57. 20	4. 80	3. 9	------	34. 10	Kononova (1966).
Fulvic acid (mean of 5 analyses).	48. 80	4. 00	2. 9	------	44. 60	Do.
Organic acids from surface water:						
Water humus	45–54	3. 9–5. 1	1. 5–4. 2	Small	38. 8–47. 9	Waksman (1938).
Fulvic acid	41. 50	5. 72	1. 98	------	50. 80	Black and Christman (1963, table 4).

ions in the filtrates were then determined by the 2,2′-biquinoline procedure (Sandell, 1959).

The entire series of determinations was repeated with stock solutions containing the same amount of copper, having the same pH values, plus 4, 8, or 40 ppm carbon of the OA.

Figure 1 summarizes the behavior of the two series of solutions at the end of 30 days of storage. The behavior of copper in the test solutions containing no organic acids can be roughly explained from data given by Latimer (1952), which indicate that the Eh at which copper is oxidized from Cu^{+} to Cu^{++} in acid solution is about +0.15 v. This Eh is much less than the expected Eh in most solutions in contact with air. Consequently, cupric ions were to be expected in the test solutions.

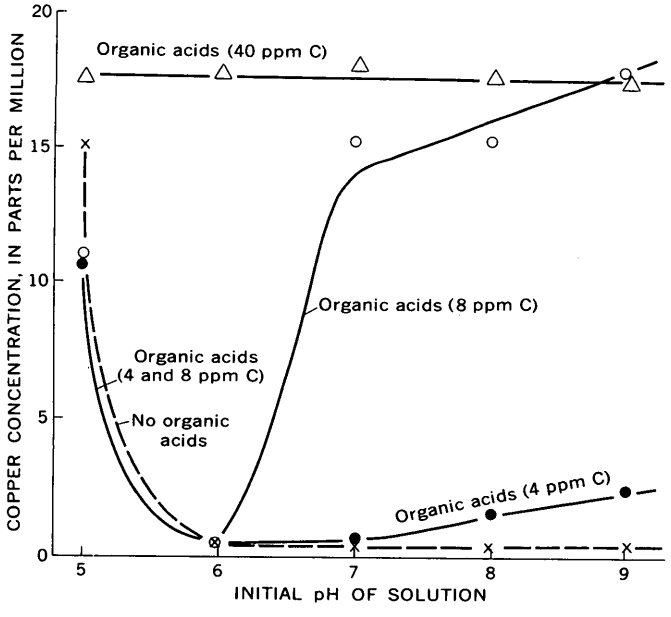

FIGURE 1.—Effect of organic acids on the stability of dissolved copper as a function of pH at the end of 30 days of storage. Initial copper content, 20 ppm.

The compounds of lowest solubility that cupric ions might form in these test solutions are the hydroxide ($K_{sp}=3.0\times10^{-20}$) and carbonate ($K_{sp}=2.5\times10^{-10}$). In a 20-ppm copper solution with activity of $3.14\times10^{-4}M$, $Cu(OH)_2$ will start to precipitate at pH 6, and $CuCO_3$ at pH 7. In the latter computation the carbonate concentration is taken as that in the initial Na_2CO_3 added, before any loss of CO_2 to the air.

These solubility calculations as a whole are in agreement with the experimental results. Figure 1 shows that for solution of pH 5 the amount of copper in solution is greater than 15 ppm, whereas at pH 6 and greater the amount of copper is only 0.5 ppm. This latter value is somewhat greater than that expected from the theoretical calculations, even after the ionic strength of the solution is taken into account; probably some of the copper in colloidal form passed through the 0.4- to 1.2-micron filter paper.

In the presence of organic acids, however, the behavior does not follow the theoretical solubility calculations. OA in the amounts of 4 and 8 ppm C have no retaining power for copper when the pH is 6 or less. At pH greater than 6 the amount of copper in solution/suspension increases as the pH increases. OA in the amount of 40 ppm C cause almost all the copper to remain in solution/suspension. In other words, the amount of copper mobilized increases with increasing organic acid concentration and increasing pH of the medium.

In another set of experiments the copper was added as a copper hydroxide to a known organic acid solution. (The amount of copper brought into solution or suspension is termed the copper-uptake capacity.) The pH levels of this set of solutions were adjusted to the desired values, 6 and 9, by addition of small amounts of Na_2CO_3 or HCl. The volume used in these experiments was 100 ml containing 24 ppm C of the OA and 5.00 g copper hydroxide. Static (no shaking) and dynamic (agitation) uptake experiments were conducted. The agitated solutions were stirred with a magnetic stirrer. Aliquots of 5 ml were decanted and filtered through Whatman No. 42 filter paper, and the copper in the filtrates was analyzed by the biquinoline procedure. The first aliquots were analyzed after 15 minutes, and thereafter at periods of 1 to 7 days aliquots were similarly analyzed for copper.

Blank solutions at pH 6 and 9 were prepared and analyzed by a procedure identical with that above, except that distilled water was used instead of organic acid solutions.

Results of the uptake experiment (fig. 2) show that the amount of copper brought into solution/suspension is greatly dependent on the presence of organic acids.

In the blank solution the copper that was brought into solution/suspension remained constant for the whole period of the experiment, the average concentration being 0.3 ppm. Agitation had no effect. This low value is reasonable considering the solubility of copper hydroxide ($K_{sp}=3.0\times10^{-20}$).

In the presence of organic acids, the amount of copper brought into solution or suspension depends on the condition of the experiment as well as the pH of solution. Under the static condition, the copper uptake increases with time, and at the end of the seventh day the amounts of copper in solution/suspension were 3.2 and 3.7 ppm at pH 6 and 9, respectively. Agitation increases the uptake capacity considerably; at the end of the seventh day, the amount of copper in solution of pH 6 was 38.5

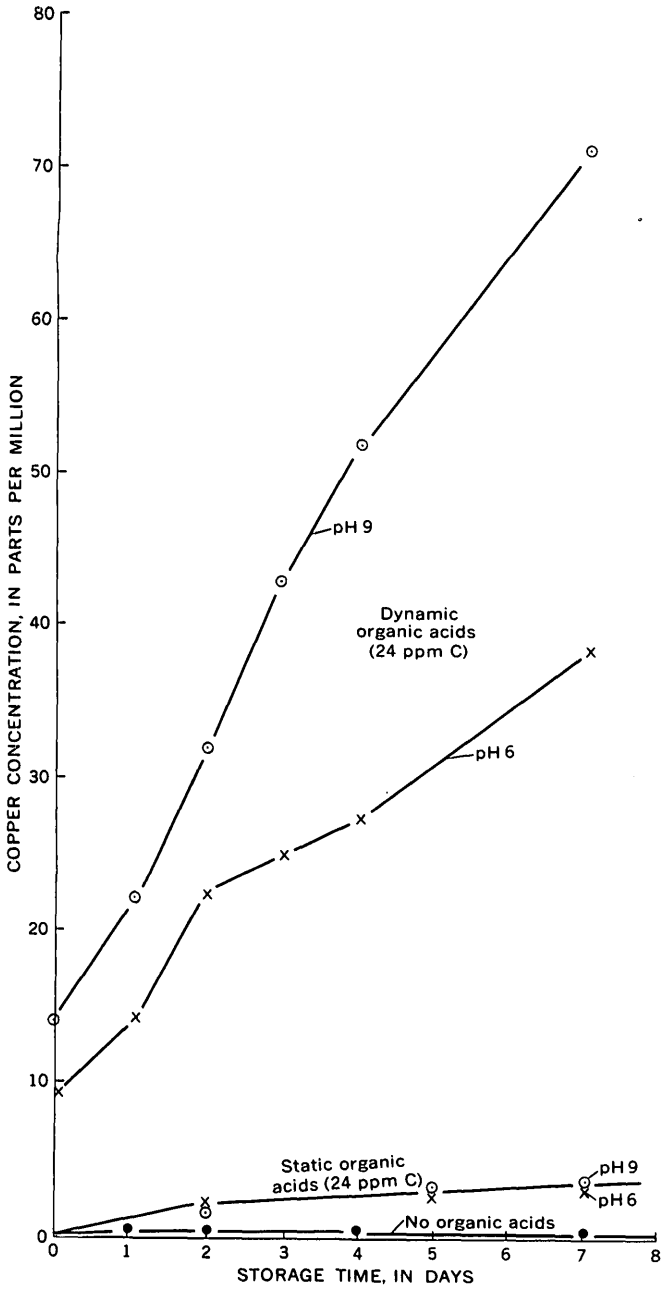

FIGURE 2.—Copper uptake in the presence and absence of organic acids under static and dynamic conditions at pH 6 and pH 9.

ppm and in solution of pH 9 was 71 ppm. These values are more than two orders of magnitude greater than if no organic acids were present. Some of the copper, however, was in the colloidal state and passed through the 0.4- to 1.2-micron-size filter paper, as indicated by the cloudiness of the filtrate. Centrifugation at 20,000 rpm for 15 minutes caused some of the colloids to accumulate at the bottom of the tubes. The organic acids, nevertheless, have the capacity and power to break down large particles of copper hydroxide into smaller colloidal ones. This probable peptization is more effective in a basic solution.

Experiments with other metals

In order to study the mobility of aluminum, ferric iron, zinc, and lead in organic acid solution, the coagulation method was employed; this is a different method from that used for copper. The coagulation experiments were carried out in a series of beakers containing equal amounts of the OA. The saturation capacity was determined by adding increments of a metal salt solution, in the form of $AlCl_3$, $FeCl_3$, $ZnSO_4$, or $Pb(NO_3)_2$, and subsequently adjusting the pH with solid Na_2CO_3 to pH levels of 5, 6, 7, 8, and 9. After the solutions were mixed with a magnetic stirrer they were immediately transferred to a series of test tubes and allowed to stand for 24 hours. Coagulation or the appearance of a precipitate was ascertained by viewing the solution before an illuminator. With due care even a slight colloidal precipitate can be detected in this fashion.

The method for determining the critical concentration or "solubility" of an electrolyte was to interpolate the value between the concentration in the test tube that produced precipitation and the concentration in the subsequent tube in which no precipitation or coagulation could be detected. This coagulation method is commonly used in colloid chemistry, and is also used by soil scientists (for example, Wright and Schnitzer, 1963) to determine the "metal holding capacity" of a soil organic extract.

The results for aluminum, ferric iron, zinc, and lead are presented in figures 3, 4, 5, and 6 respectively. Except at low pH values the amount of the metals held in solution/suspension is always greater when organic acids are present.

The amount of the metals retained in solution/suspension is much greater in the presence of organic acids. As the pH of OA solutions increases, the amount of the metals retained in solution/suspension greatly increases, though the relative amount of zinc and lead decreases slightly in the pH 7–9 range. The metal retention of the blank solution always decreases with the increase of pH, except for aluminum, which is soluble in a basic solution owing to the formation of the anion AlO_2^{-1}.

The solubility pattern of aluminum, which is commonly the major component of laterite, indicates very low solubility in solutions at or near neutral pH (fig. 3). Consequently, water with organic acids would readily solubilize the other metals, but aluminum would be left, and thus would be residually concentrated to form the laterite typical in tropical areas.

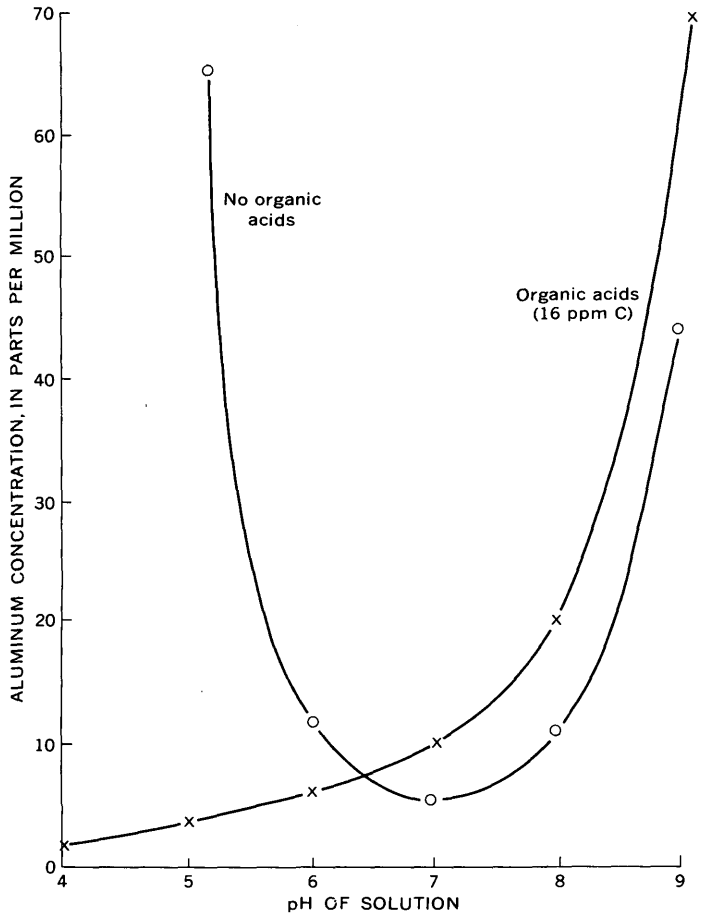

FIGURE 3.—Solubility of aluminum as a function of pH in the presence and absence of organic acids.

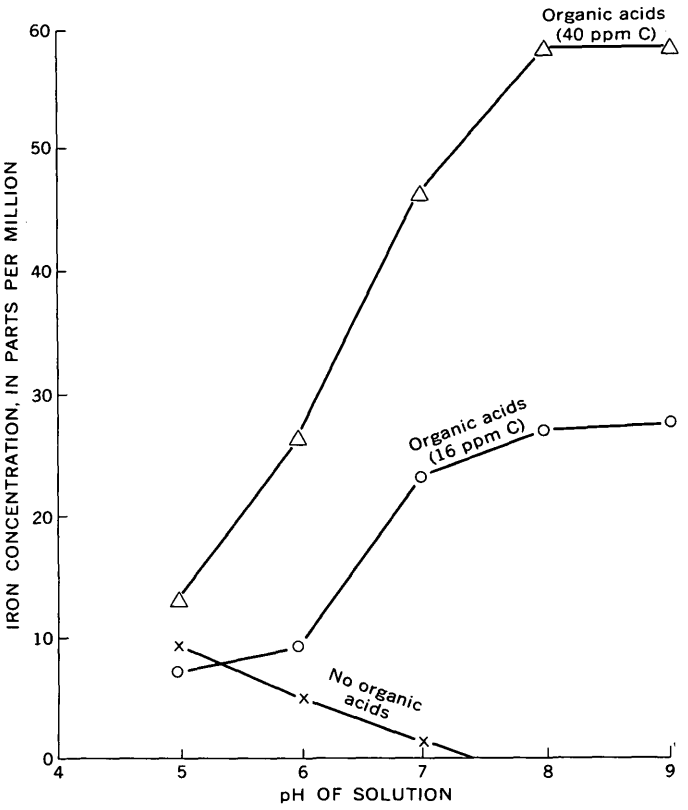

FIGURE 4.—Solubility of ferric iron as a function of pH in the presence and absence of organic acids.

METAL-ORGANIC ASSOCIATIONS

Several possibilities exist for a mechanism of fixation or bonding between the metals and the organic acids: (1) the metal ions may have been brought into solution by reduction to the more soluble lower valence state, for example ferric to ferrous iron, in the presence of organic acids; (2) the metal ions may have formed a soluble chemical complex with the organic acids; and (3) the metal ions may have formed a colloidal suspension with the organic acids.

Reduction

Reduction from the higher to lower valence state of a metal is the solubility mechanism suggested by some investigators working with natural organic substances. Examples are the reduction of iron and manganese by tannic acid (Hem, 1960; Rawson, 1963), reduction of uranium and vanadium by peat, wood, and lignite (Garrels and Pommer, 1959; Andreyev and Chumachenko, 1964), and reduction of vanadium by humic acid (Szalay and Szilágyi, 1967). Reduction of metals due to organic matter in soil has been postulated by many investigators, although it is not yet certain whether the reducing action is inherent in the humus molecule, is due to a contaminant, or is the result of bacterial activity (Kononova, 1966).

Reduction may play a role in solubilizing metal ions, but it is probably only a minor factor and, alone, cannot apply to all the metals studied here. Aluminum, for example, is very stable in the trivalent state and is impossible to reduce under the experimental conditions described. In the experiments with iron, hydrogen peroxide was added to the test solutions to secure a definite ferric species; no changes were observed in the coagulation values.

Chemical complex formation

Most present-day investigators are of the opinion that the nature of the association between organic acids and various metal ions is of the so-called complex formation, or sometimes referred to as chelation or coordination compounds (for example, see review by Saxby, 1969). Methods used by these investigators for the confirmation of complex formation are potentiometric titration, changes in infrared spectra, electrical conductance, solubility, oxidation potentials, and chromatography.

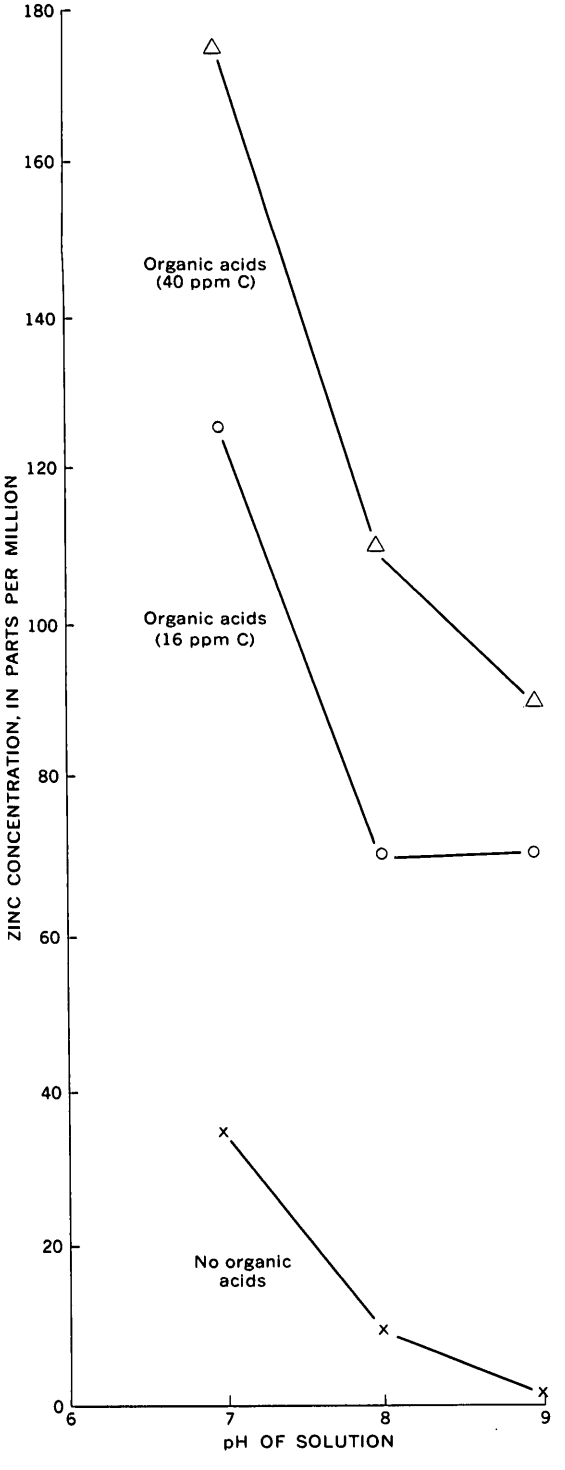

FIGURE 5.—Solubility of zinc as a function of pH in the presence and absence of organic acids.

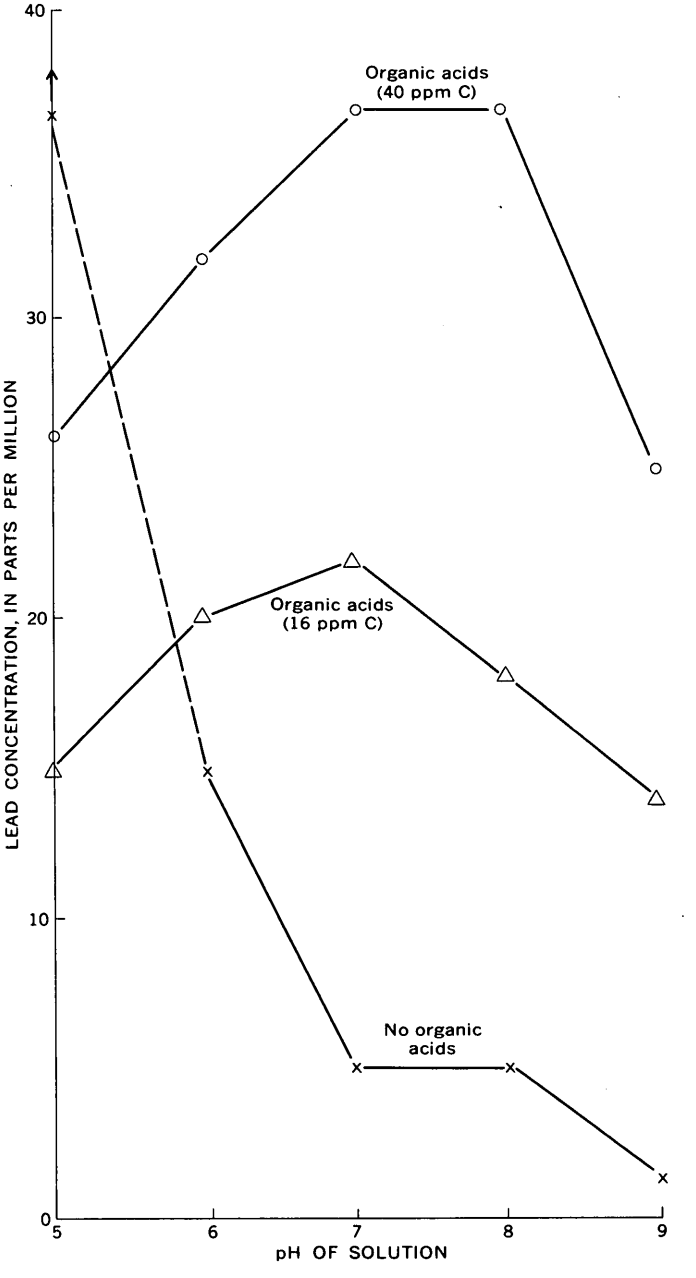

FIGURE 6.—Solubility of lead as a function of pH in the presence and absence of organic acids.

Colloidal formation

The colloidal properties of organic acids as transporting agents of metal ions were known in the early history of soil science (Waksman, 1938) and were studied during the development of colloidal chemistry in the first three decades of the 20th century. General acceptance of organic acids as colloidal transporting agents faded, however, with the more recent advances in coordination chemistry. For example, Schnitzer and DeLong in 1955 reported that the primary function of organic matter in solutions is to act as a peptizing agent and as a protective colloid, a conclusion that was apparently changed in 1963 in favor of multidentate chelate formation (Wright and Schnitzer, 1963).

However, a recent study on the coagulation of organic acids by metal ions (Ong and Bisque, 1968) has shown that iron-organic association can be considered as a

hydrophobic colloid, and has properties generally attributed to this type of colloid. In other words, metal-organic associations can be considered as purely physical phenomena and metal ions added to the metal-organic colloids will be absorbed into the Stern layer with a resulting decrease in the zeta potential.

Theory of metal-organic associations

Here a theory of the metal-organic associations will be postulated. Such a theory should be capable of accommodating at least two actions: (1) it should be able to explain the formation of a complex between the functional groups of the organic acids and the several metals, as predicted by most investigators, and (2) it should be capable of explaining the colloidal phenomena, as shown in our recent studies.

These two requirements are met in a theory developed by Fuoss and Strauss (1948) and Fuoss and Cathers (1949). The so-called Fuoss effect is well accepted in polymer chemistry and was based mainly on viscosity observations (electroviscous effect). Addition of salt to a polyelectrolyte causes the stretched configuration to become coiled, which is statistically the most probable configuration. Because of the coiling of the polyelectrolyte, the contribution of the large molecules to reduced viscosity decreases. This viscosity phenomenon has been observed for organic acids (Mukherjee and Lahiri, 1956; Piret and others, 1960.)

According to the Fuoss effect theory, the effect of adding salt to a humus polyelectrolyte, or to organic acids, may be explained in the following way: When the polyelectrolytes are dissolved in water the macromolecules assume a stretched configuration due to mutual repulsion of the negative charges on dissociated or ionized functional groups. Upon the addition of salts, this behavior is radically modified in that the cations are attracted to the carboxylate and phenoxide anions (complex formation). Once the cations are combined there is a marked decrease in the intramolecular coulombic repulsion in the polymer chain, which in turn results in coiling of the chain. Thus, the humus or organic acid macromolecule changes in shape.

This coiled geometry causes part of the water of hydration surrounding the colloid to be expelled from the structure. The process can be visualized as squeezing the water of hydration out of the molecule and leaving it less solvated. Thus, the humus macromolecule changes from a hydrophilic (much water) to a hydrophobic (little water) type of colloid. That is, in the presence of cations the charge of the polyelectrolyte is reduced, and, because water is a polar molecule, this reduction decreases the amount of water of hydration that can be held by the colloids. Consequently the macromolecule takes the properties of a hydrophobic colloid, which obeys the double-layer theory (physical).

The above-described theory of metal-organic associations is summarized in the following diagram (in which M^+=metal ion):

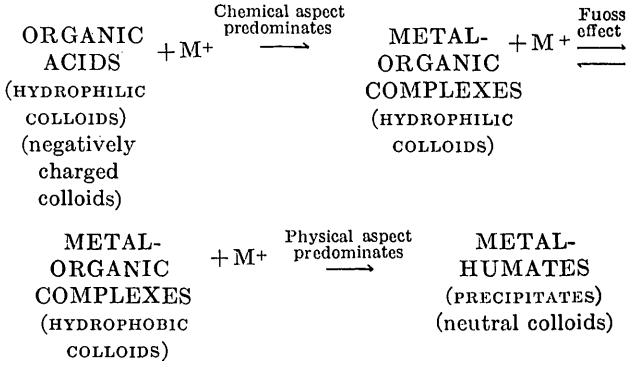

SUMMARY AND CONCLUSIONS

Organic acids have long been widely recognized as effective agents in chemical weathering processes; however, their quantitative significance under different climatic conditions on different rock types, and a clear understanding of the chemical mechanism or mechanisms in the dissolution, transportation, and deposition of metal ions are still largely subjective.

The experimental studies reported here show quantitatively that (1) organic acids, in concentrations (4–40 ppm) common in natural water, readily solubilize copper, aluminum, iron, zinc, and lead; (2) the organic acids exert a stabilizing effect to retain these metals in solution for transportation; and (3) the controlling factors that determine the increase in amount of these metals that are dissolved and transported are the increase in concentration of organic acids and the increase in pH (4–9) of the solutions, with the exception that the relative amount of zinc and lead decreases slightly in the pH 7–9 range. The low solubility of aluminum at or near pH 7, with or without organic acids, may largely explain the concentration of aluminum in lateritic deposits typical in tropical areas.

Natural organic acids are considered as negatively charged hydrophilic colloids or polyelectrolytes, and the stability of metal-organic acid associations is explained by the Fuoss effect and the double-layer theory of colloid coagulation.

REFERENCES

Allison, L. E., 1965, Organic carbon, p. 1367–1378 *in* Black, C. A., ed., Methods of soil analysis, pt. 2: Madison, Wis., Am. Soc. Agronomy, Inc., 1,572 p.

Andreyev, P. F., and Chumachenko, A. P., 1964, Reduction of uranium by natural organic substances: Geochemistry Internat., v. 1, p. 3–7.

Black, A. P., and Christman, R. F., 1963, Chemical characteristics of fulvic acids: Am. Water Works Assoc. Jour., v. 55, no. 7, p. 897–912.

Fetzer, W. G., 1946, Humic acids and true organic acids as solvents of minerals: Econ. Geology, v. 41, no. 1, p. 47–56.

Freise, F. W., 1931, The transportation of gold by organic underground solutions: Econ. Geology, v. 26, no. 4, p. 421–431.

Fuoss, R. M., and Cathers, G. I., 1949, Polyelectrolytes; 3, Viscosities of butyl bromide addition compounds of 4-vinylpyridine-styrene copolymers in nitromethane-dioxane mixtures: Jour. Polymer Sci., v. 4, p. 97–120.

Fuoss, R. M., and Strauss, U. P., 1948, Electrostatic interaction of polyelectrolytes and simple electrolytes: Jour. Polymer Sci., v. 3, p. 602–603.

Garrels, R. M., and Pommer, A. M., 1959, Some quantitative aspects of the oxidation and reduction of ores, pt. 14 *of* Garrels, R. M., and Larsen, E. S., 3d, compilers, Geochemistry and mineralogy of the Colorado Plateau uranium ores: U.S. Geol. Survey Prof. Paper 320, p. 157–164.

Ginzburg, I. I., Yashina, R. S., Matveeva, L. A., Belyatskii, V. V., and Nuzhdelovskaya, T. S., 1966, Decomposition of certain minerals by organic acids, p. 304–320 *in* Vinogradov, A. P., ed., Chemistry of the Earth's crust, v. 1: Israel Program Sci. Translations Ltd., 458 p.

Gorshkov, G. P., and Yakushova, A. F., 1962, General geology [2d ed.]: Moscow, Moskva Univ., 565 p. [In Russian]

Graham, E. R., 1941, Colloidal organic acids as factors in the weathering of anorthite: Soil Sci., v. 52, p. 291–295.

Gruner, J. W., 1922, Organic matter and the origin of the Biwabik iron-bearing formation of the Mesabi Range: Econ. Geology, v. 17, no. 6, p. 407–460.

Hem, J. D., 1960, Complexes of ferrous iron with tannic acid: U.S. Geol. Survey Water-Supply Paper 1459–D, p. 75–94.

Hori, Shiro, and Okuda, Azuma, 1961, Purification of humic acid by means of ion-exchange resins: Soil Sci. and Plant Nutrition, v. 7, no. 4, p. 4.

Kee, N. S., and Bloomfield, C., 1961, The solution of some minor element oxides by decomposing plant materials: Geochim. et Cosmochim. Acta, v. 24, nos. 3/4, p. 206–225.

Kononova, M. M., 1966, Soil organic matter; its nature, its role in soil formation and in soil fertility [2d English ed.]: New York, Pergamon Press, 544 p.

Krauskopf, K. B., 1967, Introduction to geochemistry: New York, McGraw-Hill Book Co., Inc., 721 p.

Latimer, W. M., 1952, Oxidation states of the elements and their potentials in aqueous solutions [2d ed.]: Englewood Cliffs, New Jersey, Prentice-Hall, Inc., 392 p.

Lee, G. F., and Hoadley, A. W., 1967, Biological activity in relation to the chemical equilibrium composition of natural waters, [chap. 16] *in* Equilibrium concepts in natural water systems—Am. Chem. Soc. 151st Ann. Mtg., Pittsburgh, 1966, Water, air and waste chemistry symposium: Am. Chem. Soc. (Adv. chemistry ser. 67), p. 319–338.

Moore, E. S., and Maynard, J. E., 1929, Solution, transportation, and precipitation of iron and silica: Econ. Geology, v. 24, no. 3, p. 272–303; no. 4, p. 365–402; no. 5, p. 506–527.

Mukherjee, P. N., and Lahiri, A., 1956, Studies on the rheological properties of humic acid from coal: Jour. Colloid Sci., v. 11, p. 240–243.

Nesterova, I. L., 1960, Chemical composition of the suspended and dissolved loads of the Ob River: Geochemistry, no. 4, p. 424–431.

Ong, H. L., and Bisque, R. E., 1968, Coagulation of humic colloids by metal ions: Soil Sci., v. 106, no. 3, p. 220–224.

Ong, H. L., and Swanson, V. E., 1969, Natural organic acids in the transportation, deposition, and concentration of gold, *in* International geochemical exploration symposium: Colorado School Mines Quart., v. 64, no. 1, p. 395–425.

Piret, E. L., White, R. G., Walther, H. C., Jr., and Madden, A. J., Jr., 1960, Some physicochemical properties of peat humic acids: Royal Dublin Soc. Sci. Proc., ser. A, v. 1, p. 69–79.

Rankama, K. K., and Sahama, T. G., 1950, Geochemistry: Chicago, Ill., The University of Chicago Press, 912 p.

Rawson, Jack, 1963, Solution of manganese dioxide by tannic acid: Art. 117 *in* U.S. Geol. Survey Prof. Paper 475–C, p. C218–C219.

Sandell, E. B., 1959, Colorimetric determination of traces of metals [3d ed.]: New York, Intersci. Publishers, 1,032 p.

Saxby, J. D., 1969, Organometallic chemistry of the geochemical cycle: Rev. Pure and Appl. Chemistry, v. 19, p. 131–150.

Schalscha, E. B., Appelt, H., and Schatz, Albert, 1967, Chelation as a weathering mechanism—1, Effect of complexing agents on the solubilization of iron from minerals and granodiorite: Geochim. et Cosmochim. Acta, v. 31, no. 4, p. 587–596.

Schatz, Albert, Cheronis, N. D., Schatz, Vivian, and Trelawny, G. S., 1954, Chelation (sequestration) as a biological weathering factor in pedogenesis: Pennsylvania Acad. Sci. Proc., v. 28, p. 44–51.

Schatz, Albert, Schatz, Vivian, and Martin, J. J., 1957 Chelation as a biochemical weathering factor [abs.]: Geol. Soc. America Bull., v. 68, no. 12, pt. 2, p. 1792–1793.

Schnitzer, M., and DeLong, W. A., 1955, Investigations on the mobilization and transport of iron in forested soils; 2, The nature of the reaction of leaf extracts and leachates with iron: Soil Sci. Soc. America Proc., v. 19, p. 363–368.

Shapiro, Joseph, 1963, Natural coloring substances of water and their relation to inorganic components [abs]: Geol. Soc. America Ann. Mtgs., New York, 1963, Program, p. 148A.

Steelink, Cornelius, 1963, What is humic acid?: Jour. Chem. Education, v. 40, no. 7, p. 379–384.

Strakhov, N. M., 1967, Principles of lithogenesis, v. 1 [1st English ed.]: Edinburgh, Oliver & Boyd, Ltd., 245 p.

Swanson, V. E., and Palacas, J. G., 1965, Humate in coastal sands of northwest Florida: U.S. Geol. Survey Bull. 1214–B, 29 p.

Szalay, A., and Szilágyi, 1967, The association of vanadium with humic acids: Geochim. et Cosmochim. Acta, v. 31, no. 1, p. 1–6.

Waksman, S. A., 1938, Humus; origin, chemical composition, and importance in nature [2d ed.]: Baltimore, The Williams & Wilkins Co., 526 p.

Wright, J. R., and Schnitzer, M., 1963, Metallo-organic interactions associated with podzolization: Soil Sci. Soc. America Proc., v. 27, p. 171–176.

THORIUM- AND TITANIUM-BEARING ORGANIC MATERIAL IN THE DAKOTA SANDSTONE NEAR DURANGO, COLORADO

By ROBERT S. HOUSTON and JOHN F. MURPHY,
Laramie, Wyo., Washington, D.C.

Abstract.—Organic material similar to thucholite is present in the Dakota Sandstone at a locality north of Durango, Colo. The organic material resembles asphaltite in the field, but chemical analyses suggest that it was derived from coal or humic substances. It is especially enriched in Th and Ti, but also contains anomalous amounts of Au, U, Nd, Zr, Yb, Y, V, Sr, La, Cr, Cu, Ba, and Ce. Heavy minerals in the Dakota Sandstone at this locality probably are inadequate to supply the elements present in the organic material. Because of the variable chemical properties of the elements enriched in the organic material and the tendency of certain of the elements, such as Th, Ti, and Zr, to precipitate with the hydrolyzates, it seems unlikely that these elements would be transported in a single ionic solution to the organic material where they could be adsorbed to form thucholite. It is suggested that ground water carried humic substances in solution or as colloidal suspensions through the Dakota Sandstone and that these substances adsorbed the various elements from local interstitial solutions or surface films on minerals of the sandstone.

Sandstone impregnated with a radioactive black substance resembling asphaltite is localized in a medium-grained sandstone of the Dakota Sandstone, near Chapman Lake, 4 miles north-northwest of Durango, Colo. The sandstone crops out on the south face of a cliff in the SW¼NW¼NE¼ sec. 6, T. 35 N., R. 9 W., La Plata County, Colo. (fig. 1).

The organic material is enriched in thorium, titanium, gold, uranium, neodymium, zirconium, ytterbium, yttrium, vanadium, strontium, lanthanum, chromium, copper, barium, and cerium. It resembles "asphaltite" described in epigenetic uranium deposits in sandstone of the Western United States by Finch (1967) Breger and Deul (1959), and Bell (1960). It differs from this material in that the major enriched element is thorium rather than uranium. The "asphaltite," therefore, is similar to the organic substance thucholite (Ellsworth, 1928; Davidson and Bowie, 1951) that has been reported in pegmatites, as well as in uranium- and gold-bearing conglomerates.

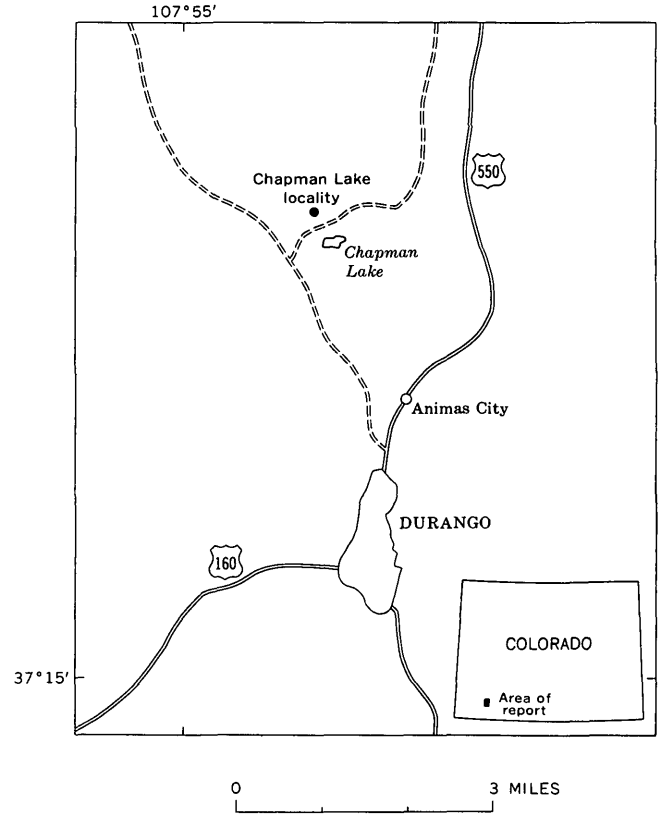

FIGURE 1.—Index map showing Chapman Lake locality.

Acknowledgments.—We would like to express our appreciation to Vernon E. Swanson, Frederick N. Ward, and Tom G. Ging, of the U.S. Geological Survey, for advice and assistance in preparing this report. We do not wish to imply that they are necessarily in agreement with the conclusions of the report.

FIELD OCCURRENCE AND PETROGRAPHY

The sandstone that contains the organic material is in the lower part of the Dakota Sandstone of Cretaceous age. The base of the Dakota Sandstone is not ex-

posed, but the "asphaltite" is estimated to be about 30 feet above the contact of the Dakota with the underlying Morrison Formation of Jurassic age. According to Zapp (1949) the Dakota Sandstone of this area is 213 feet thick and the lower 67 feet consists of cliff-forming light-gray conglomeratic sandstone and a thin unit of gray-green soft argillaceous sandstone that is locally carbonaceous. Zapp suggested that the lower conglomeratic sandstone may correlate with the Burro Canyon Formation as used by Stokes and Phoenix (1948).

The lower 8 feet of the sandstone that contains the organic material is covered by a slump block (fig. 2), but is exposed in the slump block itself. The upper 6 feet of the sandstone contains lenses of sandstone, impregnated with organic material, that are more highly radioactive than the surrounding sandstone. Stringers of impregnated sandstone are exposed on the walls of an exploration adit, terminated by a stope, that has been driven a short distance into the cliff face.

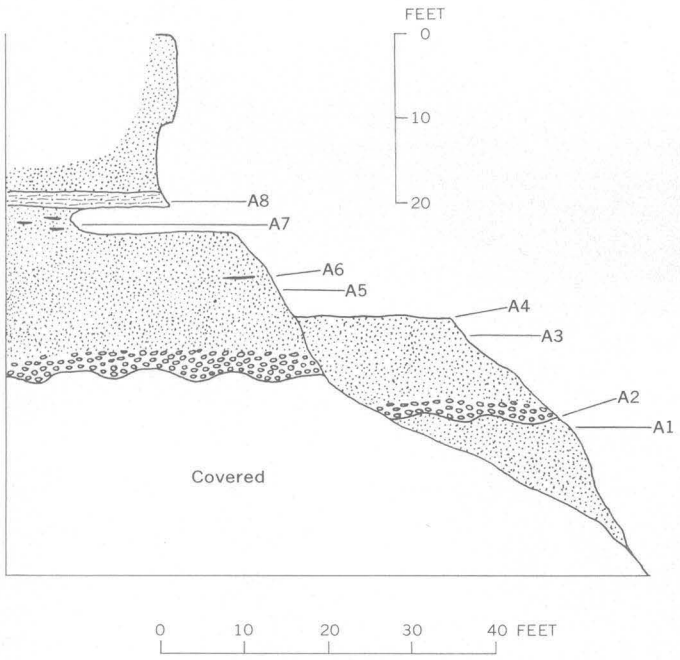

FIGURE 2.—Cross section of the Dakota Sandstone at the Chapman Lake locality near Durango, Colo., showing positions of samples (*A*1 to *A*8). Heavy dashes indicate "asphaltite" lenses; stipple, sandstone; dot-dash pattern, siltstone; circles, conglomerate.

The host rock is a gray to light-green friable medium-grained sandstone unit that is 20 feet thick and includes a well-developed pebble conglomerate at its base. The host rock is composed largely of quartz, but contains grains of white chert and green claystone as well as grains of limonite that may be ghosts of opaque minerals. The upper 10 feet of the host sandstone is richer in organic material than the lower part. Some beds there are dark gray and contain stringers of purple to black organic material. Quartz grains may be coated with a purple to black organic substance. These darker sandstones are about 10 times as radioactive as the light-colored sandstone.

The conglomerate has a coarse-grained sandstone matrix that encloses 30–50 percent pebble-sized clasts that average 10 mm in diameter and that are as long as 20 mm. The host sandstone is overlain by 1.8 feet of green to bluish-green siltstone.

The stringers of sandstone impregnated with the organic material pinch and swell locally along the same stratigraphic horizon, but they may occur at more than one stratigraphic level in the host rock. The stringers are as much as 20 feet long and as much as 6 inches thick (fig. 3). Where concentrated, the organic material is a dense black substance that resembles black obsidian in outcrop; but, in general, it has an earthy dull luster and is purplish black. It acts as poor cement for the sandstone; and where it is concentrated, the sandstone has an open framework with quartz grains suspended in the matrix of organic material. Radioactivity, as determined in the field by means of scintillometer is 33–60 times greater in the richer lenses than in the sandstone that contains no organic material.

The radioactivity of the host sandstone is directly related to the concentration of organic material. Samples from sandstone and pebble conglomerate (*A*1, *A*2, *A*3, *A*5, and *A*8, fig. 2) that contain little visible organic material did not show radioactivity above background.

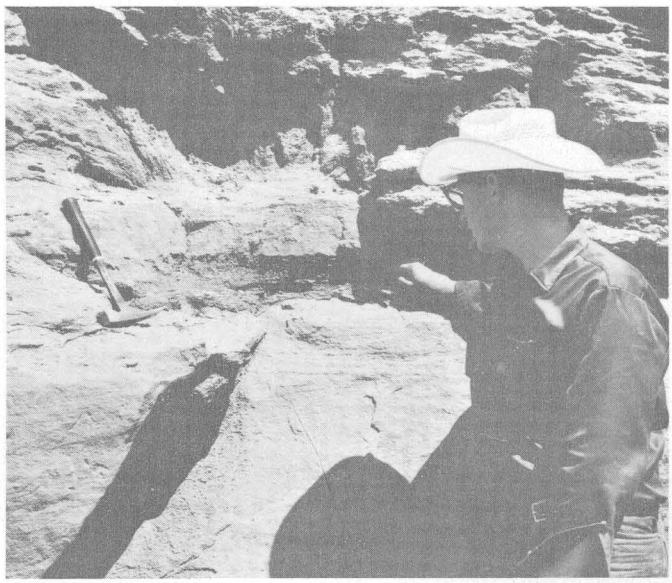

FIGURE 3.—Lens of sandstone impregnated with organic material in Dakota Sandstone from Chapman Lake locality near Durango, Colo.

380-189 O - 70 - 10

Heavy minerals

Heavy minerals constitute <0.03 percent of the samples of sandstone studied (table 1), and with the exception of marcasite, their occurrence bears no relation to the content of organic material. About 85 percent of the heavy minerals are opaque, and in polished section these appear to be highly altered iron-titanium oxides, probably ilmenite. Many of the opaque mineral grains have alterations rims of anatase, and some of the grains are anatase pseudomorphic after a titanium-bearing oxide mineral. Zircon is next in abundance followed by tourmaline and garnet. Marcasite is present only in the samples containing organic material.

Organic material

The organic material will not ignite when subjected to heat but does partly liquefy after prolonged heating. The specific gravity of the organic material is less than 2.

In polished section the organic material is seen to be light gray, streaked, and moderately but variably anisotropic. Quartz grains in contact with the organic material are irregular in shape, which suggests etching by the organic material. The organic material contains inclusions of marcasite, quartz, minute crystals of anatase, very small dark-gray crystals that are non-opaque, and some larger irregular masses, most of which are altered to anatase. Neither the irregular masses nor the total amount of included material is abundant in the more massive organic material.

Detrital grains, largely quartz, were separated by grinding these samples to a particle size smaller than quartz and floating off the organic material in a liquid with a specific gravity of about 2. Most of the detrital quartz was removed by this method, but a few small grains could still be seen in the "purified" samples. X-ray patterns of the organic material purified in this manner show that the dominant or best crystallized residual constituents of the organic material are quartz and anatase. In addition, thorite, brookite, and muscovite were tentatively identified and one X-ray pattern gave a broad line at about 3.95 A. An earlier X-ray examination of a sample of organic material from this deposit by S. R. Austin (written commun., 1956) also indicated anatase and thorite in the most radioactive fraction. Thorite, however, is not detectable in the heavy-mineral suite nor could it be identified in polished or thin sections of the organic material.

ANALYTICAL RESULTS

Samples from sandstone and pebble conglomerate (*A*1, *A*2, *A*3, *A*5, and *A*8, fig. 2) that contain little visible organic material are not significantly enriched in thorium, cerium, zirconium, and other elements (table 2). Sandstone sample A4 is not rich in organic material, but its quartz grains are coated with purplish organic material. It is about 8 times as radioactive as sandstone that contains no organic material, and it is slightly enriched in titanium, cerium, copper, lead, scandium, thorium, vanadium, yttrium, ytterbium, and neodymium (table 2). Samples A6 and A7 are from sandstone rich in organic material and are 33–60 times more radioactive than typical Dakota Sandstone. Sample A6 is significantly enriched in thorium, titanium, barium, cerium, copper, lanthanum, lead, scandium, strontium, vanadium, yttrium, ytterbium, zirconium,

TABLE 1.—*Heavy-mineral content, in percent, of Dakota Sandstone, Chapman Lake locality near Durango, Colo.*

[Tr., trace]

Sample No. (C-) (fig. 2)	CL-A1	CL-A2	CL-A3	CL-A4	CL-A5	CL-A6	CL-A7	[1]SR-1
Percentage of heavy minerals in sample	0.016	0.016	0.024	0.006	0.005	0.024	0.026	0.004
Altered opaque mineral	75	86	68	78	81	95	96	74
Unaltered opaque mineral	6	2	5	4				6
Anatase pseudomorphs	6	8	8	16	2		2	3
Zircon (euhedral, colorless)	2		1		2			5
Zircon (well-rounded, violet)	5	2	12		6	2	Tr.	3
Zircon (metamict)	Tr.							Tr.
Zircon (well-rounded, colorless)	2		1	Tr.	2			Tr.
Marcasite				1		2	1	4
Tourmaline (blue-green)	Tr.		Tr.					Tr.
Tourmaline (blue)			Tr.					
Tourmaline (brown)	2		3	Tr.	6	Tr.		
Garnet	Tr.	2						2
Rutile	Tr.		Tr.			Tr.		Tr.
Sphene								Tr.
Biotite								Tr.
Epidote								Tr.
Allanite								Tr.
Kyanite			Tr.					

[1] Sample SR-1 grab sample from "asphaltite"-rich zone.

gold, and uranium. Sample A7 is enriched in thorium, titanium, barium, lead, scandium, strontium, vanadium, yttrium, ytterbium, zirconium, and uranium.

Two samples that contained organic material were analyzed by F. N. Ward, T. G. Ging, Jr., and A. H. Love, of the U.S. Geological Survey, to determine the nature of the material. One sample of hand-sorted organic material, studied by an infrared scan method, showed the presence of saturated hydrocarbons and inorganic and organic functional groups such as silanes, perchlorates, nitrates, and mercaptans. A 500-gram sample that contained disseminated organic material was crushed to 100- to 150-mesh size and subjected to benzene extraction. The benzene extract was passed through a copper amalgam to remove sulfur and was then evaporated to dryness. This was taken up in cyclohexane and passed through a silica gel column. Aromatics were removed by benzene, and a benzene-methanol mixture was used to collect the asphaltic fraction. The analysis gave the following results:

	Part of extract (in milligrams)	*Percentage of total extract*
Saturated hydrocarbons	1. 31	8. 09
Aromatic hydrocarbons	8. 22	50. 74
Asphaltic fraction	6. 05	37. 34
Remaining on column (by difference)	0. 62	3. 83

The 500-gram sample therefore yielded a total of 16.20 mg of extract or 32 ppm (0.0032 percent) of the sample. This means that if the sample contained even as much as 10 percent organic material, only about 320 ppm (0.032 percent), or less than 99.9 percent of this organic material is hydrocarbon and asphaltic compounds. Even if the sample contained only 1 percent organic material, still, more than 99.5 percent of the organic material is insoluble in an organic solvent.

ORIGIN

Thorium and uranium in the organic material, thucholite, have been considered by some (Davidson and Bowie, 1951; Ramdohr, 1958) to be locally derived and concentrated from uranium- and thorium-bearing minerals in the host rock. The hydrocarbon in the thucholite is thought to have been introduced as a fluid with polymerization (if a liquid) or condensation (if a gas) around the uranium- or thorium-bearing minerals. The uranium and thorium were partly dissolved by the organic complex which finally consolidated in place. Probably the only minerals in the Dakota Sandstone that could contain adequate uranium and thorium (mainly thorium) are heavy minerals. However, no significant amount of heavy minerals is noted in the Dakota, and those heavy minerals that are present are not thorium rich. The possibility should be acknowledged that thorium- and uranium-bearing heavy minerals may have been destroyed by solutions. Thorite may be present in the "asphaltite," but is probably authigenic because it has not been identified in any of the heavy-mineral suites from the Dakota Sandstone. The thorium and uranium probably were not derived locally from the heavy minerals in the host rock.

The origin of the thorium and uranium in the organic rich sandstone may be the same as for the thorium and uranium in the epigenetic uranium deposits in sandstone. These organic-rich deposits, however, show an unusual enrichment in thorium, titanium, cerium, lanthanum, yttrium, ytterbium, neodymium, and gold and contain less uranium than is normal for epigenetic deposits (Bell, 1960).

If the organic material (thought of here as having been at its present site since shortly after deposition of the sediments) simply acted as an extractor or adsorbent of metals from solution, then consideration must be given to the nature of a solution or solutions that could have transported the metals in question. Hostetler and Garrels (1962) have constructed Eh–pH diagrams for hydrous systems that contain uranium and vanadium at 1 atmosphere and 25°C. They show that addition of CO_2 to this system causes the development of uranyl carbonate complexes and increases the solubility of uraninite and schoepite. One set of conditions necessary for solubility of uranium and vanadium is a mildly reducing, neutral to alkaline environment that contains fairly abundant CO_2. Some natural ground waters meet these criteria (Hostetler and Garrels, 1962, p. 161).

Such a concept might satisfactorily explain how uranium and vanadium were transported to the organic material, but elements of the titanium family (titanium, zirconium, and thorium) in which these deposits are especially enriched may not be as available for transportation even if they could be carried in some type of ground water that contains alkaline bicarbonate. Minerals that contain elements of the titanium family (that is, zircon, ilmenite) are generally more resistant to chemical weathering than are common rock-making minerals, but even if these elements were released in trace amounts during the breakdown of pyroxenes, amphiboles, and micas, they have a strong tendency to hydrolyze and remain in the rocks with the hydrolyzates.

This tendency is noted by Shoemaker, Miesch, Newman, and Riley (1959, p. 40), who showed that titanium and zirconium are not essential or major constituents of any of the ore minerals in sandstone-type uranium deposits and are only rarely reported even as trace constituents in uranium ores. These elements are thus probably not carried in the ore-bearing solution and are

TABLE 2.—*Chemical, radiometric, and spectrographic analyses, in percent, of*

[Samples C-CL-A1 to C-CL-A8 shown on fig. 2 as A1-A8. All analyses are in percent except for gold, which is in parts per million. A, not detected; N.d., not determined · determined by fluorometric method by E. J. Fennelly; eU determined by J. Gardner and E. J.

	Sample No.	Laboratory No.	Type of sample	Field radio-activity (mr/hr)	eU	U	eTh	Th	Au (ppm)	Ti	Fe	Mg	Mn	Ba
1	C-CL-A1	ABT-392	Barren Dakota Sandstone.	0.3	0.001	A	A	A	<0.02	0.07	0.5	0.1	0.01	0.015
2	A2	393	-----do-----------	.3	<.001	A	A	A	<.02	.07	.7	.1	.01	.015
3	A3	394	-----do-----------	.3	.001	A	A	A	<.02	.05	.3	.15	.01	.015
4	A4	395	Sandstone grains coated with organic material.	2.4	.032	0.0005	0.18	0.15	<.02	.7	.7	.15	.003	.007
5	A5	395	Barren Dakota Sandstone.	.3	<.001	A	A	A	<.02	.07	.3	.15	.007	.007
6	A6	396	Sandstone impregnated with organic material.	18.0	.35	.011	2.0	1.5	.16	8.0	.7	.3	.007	.03
7	A7	398	-----do-----------	10.0	.26	.005	1.5	1.5	<.02	3.0	.3	.3	.007	.03
8	A8	399	Barren green siltstone.	.3	.002	A	A	A	<.02	.3	.15	.15	.005	.01
9	1H	499	Sandstone impregnated with organic material.[1]	N.d.	N.d.	N.d.	N.d.	N.d.	.19	N.d.	N.d.	N.d.	N.d.	N.d.
10	2H	500	-----do.[1]---------	N.d.	N.d.	N.d.	N.d.	N.d.	.04	N.d.	N.d.	N.d.	N.d.	N.d.
11	C-DU-1	388	Sandstone with disseminated organic material.[2]	N.d.	.058	.002	N.d.	A	N.d.	1.0	1.0	.2	.007	.01
12	2	389	-----do.[2]---------	N.d.	.076	.003	N.d.	A	N.d.	1.0	1.5	.2	.02	.015
13	3	390	-----do.[2]---------	N.d.	<.001	A	N.d.	A	N.d.	.07	.5	.1	.007	.005
14	4	391	-----do.[2]---------	N.d.	.003	A	N.d	A	N.d.	.1	.3	.1	.005	.007

[1] Grab sample.

thus not precipitated with the ore minerals. Shoemaker, Miesch, Newman, and Riley (1959, p. 40) further pointed out a strong statistical correlation in the occurrence of titanium and zirconium in both ores and mineralized sandstone; this correlation suggests that factors controlling the distribution of these elements are similar. Titanium and zirconium are probably simply intrinsic (either (1) contained originally in clastic components or simultaneously deposited with clastic components, or (2) introduced during diagenesis by processes unrelated to uranium mineralization) elements in mineralized sandstone. This concept may also apply to gold which, from geochemical and geological considerations (Krauskopf, 1967, p. 525), is also unlikely to be transported in solution for appreciable distances.

The foregoing seems to indicate that gold, titanium, zirconium, and thorium are not as likely to be transported in solution (we must emphasize that this solution would be inorganic, rather than organic, without soluble humic material) to a site of deposition as are uranium and vanadium, and that processes governing their enrichment in the "asphaltite" are not the same as those governing enrichment of uranium and vanadium. Furthermore, these elements are not deposited from solution as discrete minerals as a result of a local reducing environment generated by the presence of organic material but they are clearly localized in the organic material proper.

The origin of the organic material is unknown, but crude oil and coal or a humic-type material may be the two best possible sources. Benzene or other organic solvents generally extract 0.1–5 percent of coal (except anthracite) and 0.005–0.1 percent of humates. These same solvents generally extract 85–100 percent of asphalt, tar, or oil (Vine, Swanson, and Bell, 1958, p. 187). As noted above, organic solvents extracted only 0.032–0.32 percent of the organic material in the 500-gm sample of sandstone that was impregnated with organic material. This small amount suggests that the source material was coal or a humic-type material rather than crude oil.

The conclusion that the organic material in the Dakota Sandstone is a type derived from coal or a humic-type material is compatible with conclusions reached by Breger and Deul (1959, p. 149) concerning similar organic materials from the Colorado Plateau. These authors (Breger and Deul, 1959, p. 149) suggested that, "It is possible that uranium- and vanadium-bearing solutions extracted organic matter from degraded plant debris in the sediments and that the mixture of carbonaceous material, uranium, and vanadium was sub-

host sandstone and "asphaltite" from Chapman Lake locality near Durango, Colo.

Gold determined by atomic absorption method by Claude Huffman, except for samples A1–A7, which were determined by cyanide method by G. T. Burrow; uranium Rowe; all other elements determined by six-step spectrographic analysis by J. L. Finley]

Ce	Co	Cr	Cu	La	Nb	Pb	Sc	Sr	V	Y	Yb	Zr	Nd	
A	0. 0005	0. 0003	0. 001	A	A	0. 0015	0. 0003	0. 003	0. 002	0. 0002	0. 0001	0. 015	A	1
0. 02	. 0007	. 0015	. 0015	0. 007	A	. 002	. 0005	. 015	. 002	. 002	. 0003	. 01	A	2
. 015	. 0003	. 0003	. 0002	. 003	A	. 001	. 0015	. 003	. 0015	. 0015	. 0005	. 01	A	3
. 03	. 0003	. 001	. 003	. 005	A	. 005	. 003	. 007	. 007	. 007	. 0015	. 015	0. 007	4
A	A	. 0002	. 0001	A	A	. 001	. 0015	. 003	. 001	. 0015	. 0003	. 015	A	5
. 3	. 0007	. 003	. 03	. 03	0. 001	. 015	. 015	. 03	. 015	. 15	. 05	. 07	. 07	6
. 03	. 0015	. 0007	. 0007	. 005	. 0003	. 007	. 015	. 015	. 01	. 07	. 03	. 30	. 015	7
. 015	. 0003	. 0015	. 0002	. 005	A	. 002	. 002	. 007	. 002	. 003	. 0007	. 05	A	8
N.d.	N.d.	N.d.	N.d.	N.d.	N.d.	N.d.	N.d.	N.d.	N.d.	N.d.	N.d.	N.d.	N.d.	9
N.d.	N.d.	N.d.	N.d.	N.d.	N.d.	N.d.	N.d.	N.d.	N.d.	N.d.	N.d.	N.d.	N.d.	10
. 03	. 0003	. 0005	. 005	. 005	A	. 002	. 007	. 007	. 005	. 015	. 007	. 03	A	11
A	. 0005	. 0005	. 002	A	A	. 003	. 015	. 003	. 005	. 02	. 015	. 05	N.d.	12
A	. 0003	. 0002	. 0002	A	A	A	. 003	. 002	. 002	. 001	. 0007	. 01	N.d.	13
A	. 0003	. 0003	. 0015	A	A	A	. 0015	. 0015	. 001	. 001	. 0007	. 01	N.d.	14

[3] Grab sample from adit.

sequently deposited in porous sandstones." This conclusion also agrees with that of Vine, Swanson, and Bell (1958, p. 190), who stated that "uraniferous asphaltite" of Colorado Plateau uranium deposits is derived from humic matter.

If the organic material of this report is indeed from coal or humic-type material, the enrichment in gold, titanium, zirconium, and thorium remains a problem. Perhaps as stated by Breger and Deul (1959, p. 149), it is possible that solutions carrying elements such as uranium and vanadium that are readily soluble in ground water can extract organic matter from plant debris in sediments and thus the mixture eventually be deposited as uranium- and vanadium-rich organic material. However, it seems very unlikely that relatively insoluble elements, such as gold, titanium, zirconium, and thorium, would be present in ground water or, if present, would move significant distances in aquifers.

Furthermore, if we consider the total list of elements (thorium, barium, cerium, copper, chromium, lanthanum, strontium, vanadium, yttrium, ytterbium, zirconium, neodymium, gold, and uranium) that enrich this organic material, it is clear that we deal with elements of such diverse chemical properties that they are not likely to be transported in the same type of solution. A much simpler approach is to hypothetically move the organic material through the aquifer and have it collect (perhaps by adsorption) traces of these various elements from local interstitial fluids or from films on grain boundaries. Swanson and Palacas (1965) have pointed out that soluble or colloidally dispersed humic substances can be derived from decomposed plants and animals. This humic material is soluble in neutral to slightly alkaline ground water and may be transported many miles prior to deposition. Swanson, Frost, Rader, and Huffman (1966) have also shown that this water-soluble organic material can sorb (sorb as used by these authors is an indefinite process that may be adsorption, ion-exchange, or chelation) between 1 and 17 percent by dry weight of such metals as cobalt, copper, iron, lead, manganese, molybdenum, nickel, silver, vanadium, and zinc.

Perhaps the organic material of this report was humic material transported in ground water that came into contact with local metal-bearing solutions in the sandstone and that it extracted (sorbed) a part of the metals and continued to move until it was flocculated or precipitated by a change in chemical environment. This type of solution that contains soluble humic substances would, of course, be quite different from the "inorganic" solution considered incapable of transporting certain of these elements.

POSSIBLE ECONOMIC SIGNIFICANCE

This occurrence of thorium-rich organic material is too small to be of economic significance in itself. The presence of gold in the organic material may be of indirect economic interest. If the gold was extracted from the Dakota Sandstone it may indicate that this unit is gold bearing in places. It also suggests that other "asphaltites" should be tested for gold and that the analyses be used as a reconnaissance tool in exploration.

Another interesting economic aspect of this study is the bearing it may have on the genesis of some uranium deposits. Granger (1968) has suggested that the southern San Juan mineral belt in northwestern New Mexico is localized where the uptilted edges of Morrison sandstones of Late Jurassic age (the host rocks) were exposed to erosion during Early Cretaceous time. The Dakota Sandstone of Early(?) and Late Cretaceous age was deposited by transgression on this erosion surface. The Dakota Sandstone consists partly of nonmarine sediments rich in organic debris that were deposited in swamps marginal to the transgressive sea. These nonmarine rocks are especially abundant at the base of the Dakota and are thought by Granger to have been the source of soluble humic substances that were transported downward and were eventually precipitated in the more permeable beds of the Morrison Formation at the water table. Uranium is considered to have been introduced in the organic debris later, and the site of the mineral belt was therefore controlled by the position of the organic debris in the Morrison Formation.

One of the problems considered by Granger is the timing of uranium deposition. Was the uranium deposited contemporaneously with the organic material or was it introduced later? Granger (1968, p. B66–B67) preferred a concept of introduction of uranium after precipitation of the organic material, and he noted that uranium in coalified limbs and trunks of fossil trees that are associated with the ore bodies is not uniformly distributed in this material but is localized in fusain or vitrain zones along microfractures. He believed, therefore, that this original plant material was not highly uraniferous and that the uranium was introduced after coalification. This concept may not apply, however, to the much more extensive uraniferous carbonaceous residue that may have been derived from soluble humic substances. If uranium was present in sufficient quantity during deposition of the nonmarine Dakota, it may have been sorbed by the soluble humic material prior to deposition in the Morrison. A test of this hypothesis might come from a study of the metal content of organic material in the Dakota Sandstone. If most of the organic material in the Dakota is relatively uranium poor, as is true of the organic material of this study, uranium may not have been available in quantity during Dakota deposition and this lack would support Granger's contention of late introduction of uranium in the deposits of the southern San Juan mineral belt.

REFERENCES

Bell, K. G., 1960, Uranium and other trace elements in petroleums and rock asphalts: U.S. Geol. Survey Prof. Paper 356–B, p. 45–65. [1961]

Breger, I. A., and Deul, Maurice, 1959, Association of uranium with carbonaceous materials, with special reference to the Temple Mountain region [Utah], pt. 12 *of* Garrels and Larsen, compilers; Geochemistry and mineralogy of the Colorado Plateau uranium ores: U.S. Geol. Survey Prof. Paper 320, p. 139–149.

Davidson, C. F., and Bowie, S. H. U., 1951, On thucholite and related hydrocarbon-uraninite complexes: Geol. Survey Great Britain Bull. 3, p. 1–19.

Ellsworth, H. V., 1928. Thucholite, a remarkable primary carbon mineral from the vicinity of Parry Sound, Ontario, pt. 1: Am. Mineralogist, v. 13, no. 8, p. 419–439.

Finch, W. I., 1967, Geology of epigenetic uranium deposits in sandstone in the United States: U.S. Geol. Survey Prof. Paper 538, 121 p.

Granger, H. C., 1968, Localization and control of uranium deposits in the southern San Juan Basin mineral belt, New Mexico, *in* Geological Survey Research 1968: U.S. Geol. Survey Prof. Paper 600–B, p. B60–B70.

Hostetler, P. B., and Garrels, R. M., 1962, Transportation and precipitation of uranium and vanadium at low temperatures, with special reference to sandstone-type uranium deposits: Econ. Geology, v. 57, no. 2, p. 137–167.

Krauskopf, K. B., 1967, Introduction to geochemistry: New York, McGraw-Hill Co., 721 p.

Ramdohr, Paul, 1958, New observations on the ores of the Witwatersrand in South Africa and their genetic significance: Geol. Soc. South Africa Trans., v. 61, annexure, 50 p.

Shoemaker, E. M., Miesch, A. T., Newman, W. L., and Riley, L. B., 1959, Elemental composition of the sandstone-type deposits, pt. 3 *of* Garrels and Larsen, compilers, Geochemistry and mineralogy of the Colorado Plateau uranium ores: U.S. Geol. Survey Prof. Paper 320, p. 25–54.

Stokes, W. L., and Phoenix, D. A., 1948, Geology of the Egnar-Gypsum Valley area, San Miguel and Montrose Counties, Colorado: U.S. Geol. Survey Oil and Gas Inv. Prelim. Map 93.

Swanson, V. E., Frost, I. C., Rader, L. F., Jr., and Huffman, Claude, Jr., 1966, Metal sorption by northwest Florida humate, *in* Geological Survey Research 1966: U.S. Geol. Survey Prof. Paper 550–C, p. C174–C177.

Swanson, V. E., and Palacas, J. G., 1965, Humate in coastal sands of northwest Florida: U.S. Geol. Survey Bull. 1214–B, 29 p.

Vine, J. D., Swanson, V. E., and Bell, K. G., 1958, The role of humic acids in the geochemistry of uranium, *in* United Nations, Survey of raw material resources: Internat. Conf. Peaceful Uses Atomic Energy 2d, Geneva, Sept. 1958, Proc., v. 2, p. 187–191.

Zapp, A. D., 1949, Geology and coal resources of the Durango area, La Plata and Montezuma Counties, Colorado: U.S. Geol. Survey Oil and Gas Inv. Prelim. Map 109.

K-AR AGES OF LAMPROPHYRE DIKES NEAR GREAT FALLS, MARYLAND–VIRGINIA

By JOHN C. REED, JR., RICHARD F. MARVIN,
and JOHN H. MANGUM, Denver, Colo.; Washington, D.C.

Abstract.—Biotite from small undeformed dikes of biotite lamprophyre cutting the complexly folded metasedimentary rocks of the Wissahickon Formation at Great Falls, Maryland-Virginia, has K-Ar ages of about 360 million years. This suggests that the age of dike emplacement is no later than Middle Devonian and is consistent with the interpretation that major deformation and regional metamorphism in this part of the Piedmont had ended by Late Ordovician or Early Silurian. The lamprophyre dikes are cut by a fault, one of a family of faults that controlled gold mineralization in the Great Falls area, indicating that the mineralization is of post-Middle Devonian age.

Complexly folded metasedimentary rocks of the Wissahickon Formation are spectacularly exposed along the Potomac River near Great Falls about 8 miles west of Washington, D.C. (index map, fig. 1). The stratigraphy, structure, and metamorphic history of the rocks exposed there have been discussed by Cloos and Anderson (1950), Reed and Jolly (1963), and Fisher (1963, 1970); the regional metamorphic and stratigraphic problems of this part of the Piedmont have been summarized by Hopson (1964).

The rocks in the immediate vicinity of Great Falls are interbedded metagraywackes and pelitic schists containing garnet and aggregates of sericite replacing staurolite and kyanite(?). The metamorphic grade rises rather abruptly to the southeast, reaching sillimanite grade in a small area on Bear Island, about 0.3 mile southeast of the area of figure 1. The sedimentary rocks display at least four generations of folds and three generations of cleavage (Fisher, 1963, 1970); the major folds (B of Reed and Jolly, 1963, F_3 folds of Fisher, 1963, 1970) formed during the climax of regional metamorphism. After formation of these folds, the sillimanite-grade rocks on Bear Island were invaded by numerous small plugs, dikes, and veinlets of light-colored granitic rocks and pegmatite. Subsequently, all rocks in the area, including the granites, were subjected to local shearing and retrogressive metamorphism which resulted in local chloritization, sericitization, and saussuritization of many of the earlier minerals.

Fisher (1963) discovered and described a set of 2-inch to 2-foot-thick dikes of unmetamorphosed biotite-rich lamprophyre exposed in cliffs along the river about 0.5 mile southeast of Great Falls (fig. 1). The dikes Fisher found have been followed for about 1,000 feet to the east using a ground magnetometer to trace a distinct magnetic low and flanking highs associated with them. They have also been traced for about 300 feet to the west in float and scattered outcrops. Similar lamprophyre dikes have been found nearby. One crops out at the south end of Falls Island and along strike immediately west of the main channel of the Potomac River (fig. 2). Another is exposed north of Rocky Islands between the Chesapeake and Ohio Canal and Olmsted Island.

The dikes are composed of a fine-grained dark-greenish-gray rock containing conspicuous phenocrysts of biotite as much as 5 mm in diameter. The phenocrysts are larger and more abundant near the centers of the dikes and are absent in a zone a few inches wide at the walls. Thin sections show that the phenocrysts are chestnut brown, undeformed, and strongly zoned. The matrix consists of finely crystalline quartz, albite, calcite, olive-green partly chloritized biotite, epidote, sphene, and apatite. The dikes south of Rocky Islands also contain spongy prisms of colorless to light-green or bluish-green actinolite (n_α=1.620; n_β=1.636; n_γ=1.644). Fisher (1963) reports $2V$ is −75°. Several of the dikes contain amygdules 1–2 mm in diameter filled with quartz and calcite. Fisher (1963) reported zeolitized microcline in the groundmass in some of the dike rocks, but no zeolites or potassium feldspars were identified in our specimens in thin section or by X-ray diffraction.

U.S. GEOL. SURVEY PROF. PAPER 700-C, PAGES C145–C149

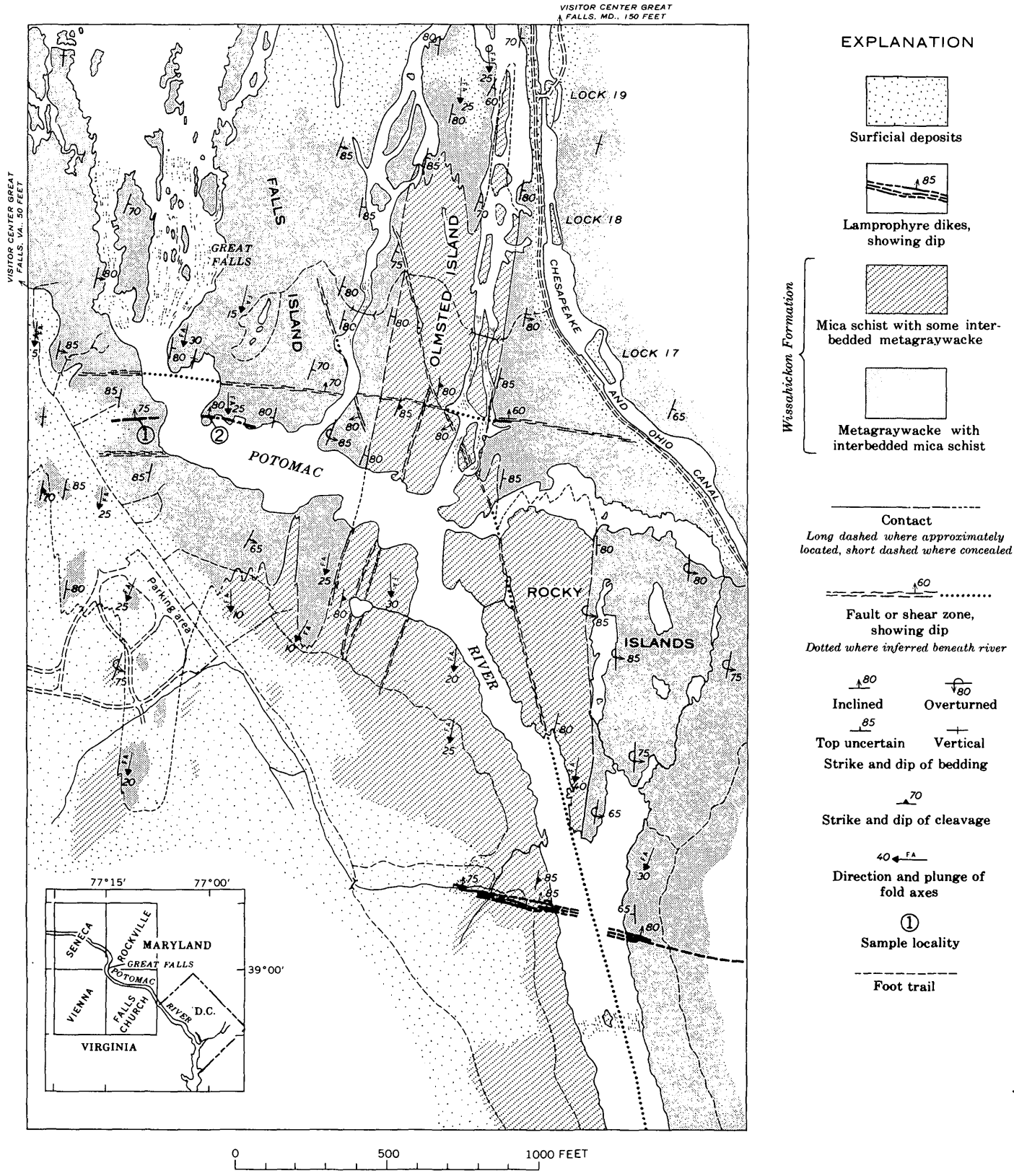

FIGURE 1.—Geologic map of the Great Falls area, Maryland-Virginia, showing dikes, faults, and sample localities.

A

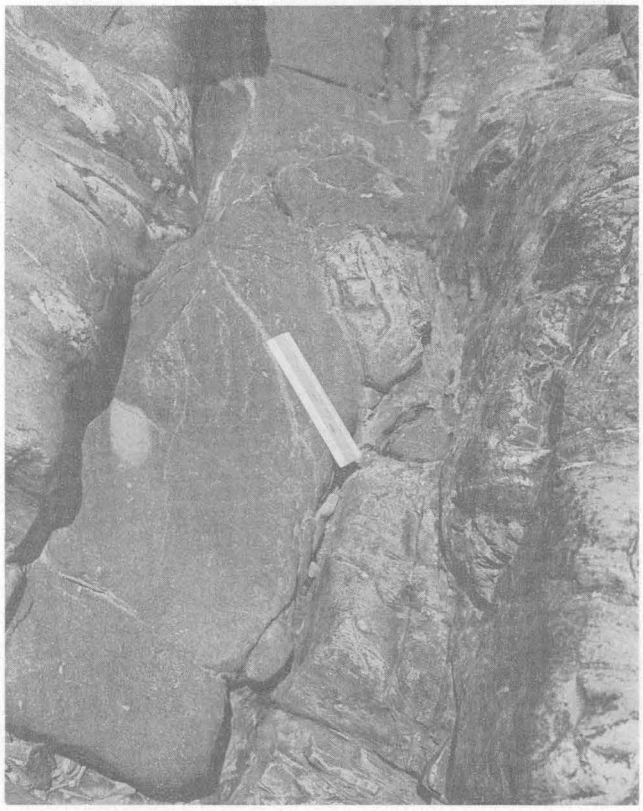

B

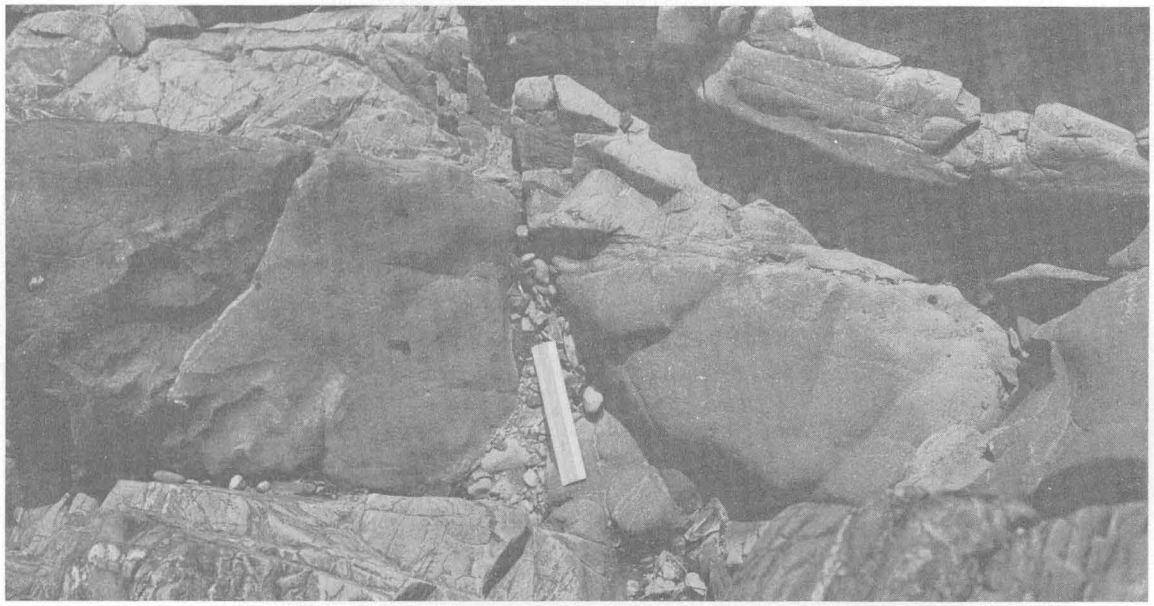

C

FIGURE 2.—Photographs of dike outcrops showing—

A. View toward the west at the southwest tip of Falls Island, showing dike outcrops and sample localities 1 and 2 (arrows). Main channel of the Potomac River is between the sample localities, but is hidden by outcrop in foreground. Width of dike in foreground is about 1 foot.

B. Closeup view of part of dike at sample locality 2, showing sharp contacts and partly detached blocks of wallrock. Note folded quartz-albite pods and veinlets in wallrocks. Scale is approximately 6 inches long.

C. Closeup view of part of dike at sample locality 2, showing minor right lateral offset along small north-northwest-trending fault. Scale is approximately 6 inches long.

The dikes all occupy cross joints normal to the axes of the principal folds (B folds or F_3 folds). Most of them strike about N. 80° W. and dip from 75°–85° N. They range in thickness from a few inches to as much as 2 feet. The swarm of dikes south of Rocky Islands is offset 80–100 feet in an apparent right-lateral sense by a fault that controls the straight course of the river in this part of the gorge. Fisher (1963, p. 80) estimates that the displacement along this fault has been at least 1,000 feet down on the southwest side on the basis of truncation of fold axes in metagraywacke beds. The fault is exposed along the western side of Rocky Islands and cuts diagonally across Olmsted Island. In one exposure on the southeast corner of Olmsted Island it is marked by a 3- to 4-inch-thick zone of gouge that dips 80° SW., flanked by a few inches of sheared and retrograded schist in which the foliation shows right-lateral drag. The fault is almost certainly part of the group of similarly oriented shear zones and fault-controlled quartz veins from which considerable quantities of gold have been mined about a mile to the east (Reed and Reed, 1967, 1969).

Because the emplacement of the dikes clearly postdates the climax of regional metamorphism and predates the faulting that controlled the gold mineralization, their age is of considerable interest in the interpretation of the metamorphic and tectonic history of this part of the Piedmont.

Table 1 gives K-Ar ages of biotite separated from two samples of lamprophyre from the dike just south of Great Falls. Table 2 gives chemical analyses, modes, and petrographic descriptions of the dike rocks. The dike at Great Falls was chosen for sampling because its outcrops are farthest from the fault zone and the biotite showed the least evidence of alteration.

The agreement (table 1) between the ages determined for the two samples is very good and indicates that the time of dike emplacement could be no later than Middle Devonian. This is consistent with ages of postkinematic pegmatites near Baltimore (Wetherill and others, 1966) which show that the major deformation in this part of the Piedmont had ended by Late Ordovician or Early Silurian (Hopson, 1964; Harper, 1968; Fisher,

TABLE 1.—K-Ar *ages and analytical data for biotites from lamprophyre dikes*

[Analysts: R. F. Marvin, R. E. Zartman, C. E. Hedge, and Violet Merritt]

Sample No.	K_2O [1] (weight percent)	*Ar^{40} (moles per gram)	*Ar^{40} (percent)	Age (m.y.)$\pm 2\sigma$
1	9. 31	55.04×10^{-10}	99	363 ± 13
2	9. 24	54.09×10^{-10}	99	360 ± 13

*Ar^{40}, radiogenic argon.
Decay constants, K^{40}; $\lambda_\epsilon=0.584\times10^{-10}$/yr, $\lambda_\beta=4.72\times10^{-10}$/yr.
Atomic abundance: $K^{40}/K=1.19\times10^{-4}$.

[1] Determined by Perkin-Elmer flame photometer with Li internal standard.

TABLE 2.—*Chemical analyses of dike rocks from Great Falls, Maryland-Virginia*

	Samples 1	2
Major oxides [1] (weight percent):		
SiO_2	49. 4	50. 4
Al_2O_3	11. 5	11. 8
Fe_2O_3	1. 8	1. 4
FeO	5. 4	5. 6
MgO	8. 8	8. 3
CaO	7. 8	7. 3
Na_2O	1. 4	1. 6
K_2O	4. 2	4. 1
H_2O+	2. 6	2. 1
H_2O-	. 07	. 12
TiO_2	1. 4	1. 4
P_2O_5	1. 0	. 87
MnO	. 12	. 11
CO_2	4. 1	4. 11
Other		
Total	100	99
Minerals [2] (volume percent):		
Quartz	22. 3	22. 8
Plagioclase	12. 0	13. 6
Biotite	45. 2	43. 0
Calcite	11. 3	7. 6
Sphene	. 9	. 4
Epidote	3. 1	7. 6
Chlorite	3. 5	2. 6
Talc	. 7	. 7
Apatite	1. 1	1. 7

Description of specimens:

1. Biotite lamprophyre from near center of dike exposed in cliff about 600 feet S. 55° E. of south entrance of Visitor Center at Great Falls Park, Va. (38°59′40″ N., 77°15′15″ W.). Sample is from about 30 feet below top of cliff (fig. 2*A*). Dike is 2 feet thick where sampled, but pinches out entirely 20 feet from top of cliff. Rock consists of ragged to subhedral, randomly oriented phenocrysts of biotite 0.5–2 mm in diameter in a groundmass of fine-grained quartz, plagioclase, and stubby, olive-green partly chloritized biotite. Plagioclase is irregular, untwinned, and has blotchy extrusions. Most seems to be An_0 to An_5. Matrix is partly replaced by blotchy grains of calcite. A few 0.5–1-mm quartz grains may be xenocrysts, and scattered 0.1–2-mm aggregates of talc and chlorite rimmed by biotite may represent pyroxene or olivine phenocrysts. Biotite phenocrysts are conspicuously zoned from colorless cores to dark-reddish-brown rims. Outer fringe is olive green and choked with sagenitic webs. Indices of refraction are: α, 1.564 (core) to 1.568 (rim); β and γ, 1.612 (core) to 1.620 (rim). $2V=0$ to 5° (estimated).
2. Biotite lamprophyre from dike exposed at southwestern tip of Falls Island. Sample locality is 300 feet east of locality 1 and about 240 feet due south of southwesternmost overlook on Olmsted Island trail, Great Falls Park, Md. (fig. 2*A*) (38°59′40″ N., 77°15′14″ W.). Dike is about 1 foot wide where sampled (fig. 2*B* and 2*C*), but pinches out entirely 80 feet to the west and 60 feet to the east. Rock is practically the same as sample 1, but biotite phenocrysts are larger and more nearly euhedral. Indices of refraction are: α, 1.564 (core); β and γ, 1.612 (core) to 1.616 (rim). Plagioclase is largely albite, but index suggests some is An_{20-25}.

[1] Rapid rock analyses using methods described by Shapiro and Brannock (1962), supplemented by atomic absorption. Paul Elmore, Lowell Artis, J. Kelsey, Gillison Chloe, H. Smith and John Glenn, analysts.
[2] Based on counts of 333 points in each of three perpendicular thin sections of each specimen. Ratio of plagioclase and quartz adjusted to fit chemical analysis.

1970). It is not entirely clear whether the alteration that produced chlorite, actinolite, epidote, and calcite in the groundmass of the dike rocks was deuteric or the result of the late retrogressive metamorphism and hydrothermal alteration that affected all the enclosing rocks (Reed and Jolly, 1963; Fisher, 1963, 1970). However, the lack of any indication of shearing of the contacts of the dikes or of deformation of the nearly euhedral biotite phenocrysts suggests that it was deuteric. If so, the measured ages are probably close to the true age of emplacement. The offset of the dikes by the fault related to the nearby gold deposits shows that the gold mineralization is post-Middle Devonian and may be as young as Triassic as suggested by Reed and Reed (1967, 1969).

The dike rocks were classed as minettes by Fisher (1963). The lack of potassium feldspar would suggest that they might better be termed kersantites, but the chemical analyses (table 2) are not particularly like either the average minette or average kersantite quoted by Johannsen (1937, p. 36, 190).

REFERENCES

Cloos, Ernst, and Anderson, J. L., 1950, The geology of Bear Island, Potomac River, Maryland, Guidebook 2: Johns Hopkins Univ. Studies Geology, no. 16, pt. 2, p. II–1–II–13.

Fisher, G. W., 1963, The petrology and structure of the crystalline rocks along the Potomac River near Washington, D.C.: Johns Hopkins Univ., Ph. D. dissertation, 241 p.

——— 1970, The metamorphosed sedimentary rocks along the Potomac River near Washington, D.C., *in* Fisher, G. W., Pettijohn, F. J., Reed, J. C., Jr., and Weaver, K. N., eds., Studies of Appalachian geology—central and southern: New York, Interscience Publishers, p. 299–315.

Harper, C. T., 1968, Isotopic ages from the Appalachians and their tectonic significance: Canadian Jour. Earth Sci., v. 5, no. 1, p. 49–59.

Hopson, C. A., 1964, The crystalline rocks of Howard and Montgomery Counties, *in* The geology of Howard and Montgomery Counties: Baltimore, Maryland Geol. Survey, p. 27–215.

Johannsen, Albert, 1937, A descriptive petrography of the igneous rocks; v. III, The intermediate rocks: Chicago, Univ. Chicago Press, 360 p.

Reed, J. C., Jr., and Jolly, Janice, 1963, Crystalline rocks of the Potomac River gorge near Washington, D.C.: U.S. Geol. Survey Prof. Paper 414–H, p. H1–H16.

Reed, J. C., Jr., and Reed, J. C., 1967, Gold deposits near Great Falls, Maryland: Washington Acad. Sci. Jour., v. 57, p. 213–223.

——— 1969, Gold veins near Great Falls, Maryland: U.S. Geol. Survey Bull. 1286, 22 p. [1970]

Shapiro, Leonard, and Brannock, W. W., 1962, Rapid analysis of silicate, carbonate, and phosphate rocks: U.S. Geol. Survey Bull. 1144–A, 56 p.

Wetherill, G. W., Tilton, G. R., Davis, G. L., Hart, S. R., and Hopson, C. A., 1966, Age measurements in the Maryland Piedmont: Jour. Geophys. Research, v. 71, no. 8, 2139–2155.

K–Ar AGE OF THE LOWER PART OF THE BROWNS PARK FORMATION, NORTHWESTERN COLORADO

By G. A. IZETT, N. M. DENSON, and J. D. OBRADOVICH,
Denver, Colo.

Abstract.—Biotite separated from a chalky-white rhyolitic ash in the lowermost part of the Browns Park Formation in northwestern Colorado has a K-Ar age of 24.8±0.8 million years. On the basis of combined radiometric (early Miocene) and paleontologic (late Miocene) evidence, the age of the Browns Park ranges from earliest Miocene through most of Miocene and possibly into early Pliocene time.

The age span of the Browns Park Formation in the type locality, northwestern Colorado, has not been well bracketed owing to the paucity of diagnostic fossil mammal remains in the formation. An understanding of the age of the formation has been important to geologists including Powell (1876), Rich (1910), Sears (1924), Bradley (1936), Hansen (1965), and Hunt (1969), who have attempted reconstructions of the geomorphic history in the Uinta Mountains area. In recent years, the U.S. Geological Survey has considered the age of the Browns Park Formation to be Miocene(?). In the past, on the basis of stratigraphy and geomorphology the formation was considered Pliocene by Hayden (1872, p. 64), "Green River group" age by Emmons (1877, p. 222), Miocene(?) by Sears (1924), late Miocene or early Pliocene by Bradley (1936), and Miocene(?) by Hansen (1965). The only fossil mammals reported from the Browns Park Formation in its type locality were described by Peterson (1924, 1928). In 1924 he judged the age of the formation to range "* * * from the uppermost Oligocene to the middle Miocene." In 1928 (p. 88, 111) Peterson revised his opinion on the basis of newly discovered fossil mastodon remains and restudy of fossils previously described in 1924 and concluded that the Browns Park Formation was middle and late Miocene and Pliocene in age.

To determine more closely the age of the lower part of the Browns Park Formation in its type locality, we collected a sample of a chalky-white rhyolitic air-fall ash bed, about 7 feet thick, that occurs in the lowermost part of the formation. The ash bed crops out 20–30 feet above the road on the west bank of the Little Snake River in the NW¼SE¼ sec. 30, T. 8 N., R. 97 W., Moffat County, Colo. (fig. 1).

The white ash bed used for the isotope age determination is rhyolitic, as shown by the partial chemical analysis of the ultrasonically cleaned glass phase of the ash (table 1).

The ash is composed chiefly of glass shards, but it includes phenocrysts of quartz, sanidine, oligoclase, biotite, allanite, zircon, apatite, magnetite, and ilmenite. Biotitic white rhyolitic ash beds are common in lower Miocene rocks in the Western United States, and they differ chemically and petrographically from nonbiotitic gray-toned rhyolitic ashes in upper Miocene and Pliocene rocks. Two gray-toned ash beds (fig. 2) crop out west of the Little Snake River in the SE¼SE¼ sec. 27, T. 9 N., R. 101 W., and occur in the upper part of the formation. A chemical analysis of the glass phase of the lower of the two ash beds is given in table 2.

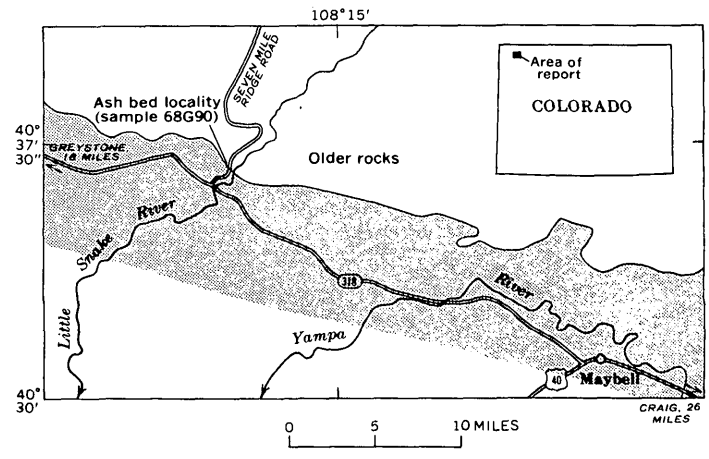

FIGURE 1.—Sketch map showing location of ash bed used for isotopic age determination (sample 68G90) in the lowermost part of the Browns Park Formation. Stippled area is Browns Park Formation modified after Sears (1924).

U.S. GEOL. SURVEY PROF. PAPER 700–C, PAGES C150–C152

TABLE 1.—*Chemical analysis, in weight percent, of glass phase of air-fall ash (sample 68G90) from lower part of the Browns Park Formation in the NW¼SE¼sec. 30, T. 8 N., R. 97 W., Moffat County, Colo.*

[Analysis by G. T. Burrow, Violet Merritt, and Elsie Rowe]

SiO_2	74. 1	K_2O	3. 50
Al_2O_3	12. 9	TiO_2	. 10
Fe as Fe_2O_3	. 75	MnO	. 071
MgO	. 06	SrO	. 007
CaO	. 47	Rb_2O	. 022
Na_2O	3. 88	Zn	. 004

TABLE 2.—*Chemical analysis, in weight percent, of glass phase of gray rhyolitic air-fall ash in the upper part of the Browns Park Formation in the SE¼SE¼ sec. 27, T. 9 N., R. 101 W., Moffat County, Colo.*

[Analysis by G. T. Burrow, Violet Merritt, and Elsie Rowe]

SiO_2	74. 7	K_2O	5. 55
Al_2O_3	12. 2	TiO_2	. 16
Fe as Fe_2O_3	1. 64	MnO	. 003
MgO	. 07	SrO	. 004
CaO	. 55	Rb_2O	. 021
Na_2O	2. 42	Zn	. 005

Gray-toned rhyolitic ashes characteristically contain from 1 to 3.5 percent iron (calculated as Fe_2O_3), whereas chalky-white rhyolitic ash beds contain less than 1.0 percent iron (calculated as Fe_2D_3).

The generalized position of the ash bed dated by isotope methods is shown in figure 2. At the sample locality (fig. 1) the ash bed is about 100 feet stratigraphically above the top of a red conglomeratic sandstone unit, about 80 feet thick, that was mapped by Sears (1924) and Bradley (1964) as the basal conglomerate of the Browns Park Formation. To the west and the east of the sample locality the thickness of the conglomeratic sandstone ranges from 0 to as much as 300 feet (Sears, 1924, p. 295).

This red conglomerate unit differs markedly from the overlying sandstone of the Browns Park Formation, and it is possible that the red conglomeratic sandstone is not genetically related to the Browns Park Formation but may be an Oligocene rock unit equivalent to the Bishop Conglomerate (compare Bradley, 1964, p. A55). Current stratigraphic studies by the U.S. Geological Survey field parties in northwestern Colorado, northeastern Utah, and southwestern Wyoming may solve this problem. Heavy minerals from the Browns Park Formation and equivalent rocks in northwestern Colorado, southern Wyoming, and the Northern High Plains are currently being studied by N. M. Denson.

Results of a potassium-organ age determination made on biotite separated from the ash indicate that the lowermost part of the Browns Park Formation, where there is no paleontologic evidence, is about 25 million years old, or earliest Miocene. The Oligocene-Miocene boundary is currently believed to be 26 million years (Harland and others, 1964). The pertinent isotope age data are given in table 3.

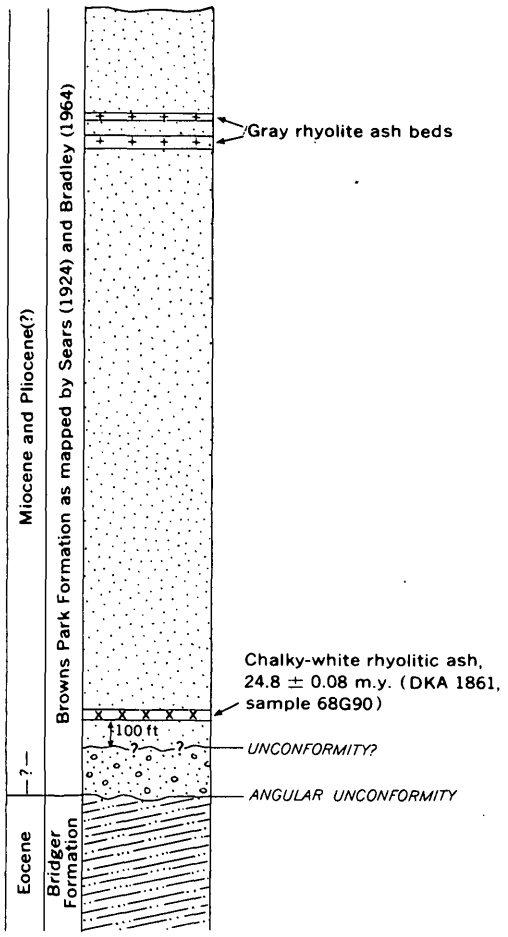

FIGURE 2.—Generalized stratigraphic column in the type locality of the Browns Park Formation, Colorado, showing the stratigraphic position of the rhyolitic ash bed dated by isotope methods. Total thickness of the Browns Park Formation is 1,200+ feet (Sears, 1924, p. 295).

In conclusion, the age of the Browns Park Formation is established by radiometric and paleontologic evidence. The potassium-argon age establishes that the lower part of the formation is earliest Miocene. The fossil mastodon "*Serridentinus*" *fricki* Peterson, 1928, was found at the "Weller Horizon" in the Browns Park

TABLE 3.—*Laboratory data for* K-Ar *age determination of biotite in rhyolitic ash in the Browns Park Formation*

Laboratory No.	Sample No.	Mineral	K (percent)	$*Ar^{40}$ (10^{-10} moles/g)	$*Ar^{40}$ (percent)	Age (m.y.)
DKA 1861	68G90	Biotite	7. 28	3. 24	90. 0	24.8±0. 8

Decay constants, K^{40}: $\lambda_\epsilon = 0.584 \times 10^{-10}$ yr^{-1}
$\lambda_\beta = 4.72 \times 10^{-10}$ yr^{-1}
Atomic abundance: $K^{40}/K = 1.19 \times 10^{-4}$
* Ar^{40}=radiogenic argon.

Formation (Peterson, 1928, p. 111), and because the earliest known mastodon remains in North America occur in upper Miocene rocks (G. E. Lewis, written commun., Sept. 26, 1969), the upper part of the formation is late Miocene to Pliocene(?) in age.

REFERENCES

Bradley, W. H., 1936, Geomorphology of the north flank of the Uinta Mountains [Utah]: U.S. Geol. Survey Prof. Paper 185–I, p. 163–199.

——— 1964, Geology of Green River Formation and associated Eocene rocks in southwestern Wyoming and adjacent parts of Colorado and Utah; U.S. Geol. Survey Prof. Paper 496–A, 86 p.

Emmons, S. F., 1877, Descriptive geology: U.S. Geol. Explor. 40th Parallel (King), v. 2, 890 p.

Hansen, W. R., 1965, Geology of the Flaming Gorge area, Utah-Colorado-Wyoming: U.S. Geol. Survey Prof. Paper 490, 196 p.

Harland, W. B., Smith, A. G., and Wilcock, Bruce, eds., 1964, The Phanerozoic time scale—a symposium: Geol. Soc. London Quart. Jour., supp., v. 120s, 458 p.

Hayden, F. V., 1872, Preliminary report of the United States Geological Survey of Wyoming and portions of contiguous territories (being a second annual report of progress): U.S. Geol. Geog. Survey Terr., 4th Ann. Rept., 511 p.

Hunt, C. B., 1969, Geologic history of the Colorado River, *in* The Colorado River region and John Wesley Powell: U.S. Geol. Survey Prof. Paper 669–C, p. 59–130.

Peterson, O. A., 1924, Discovery of fossil mammals in the Brown's Park formation of Moffat County, Colorado: Carnegie Mus., Annals, v. 15, nos. 2 and 3, p. 299–304.

——— 1928, The Brown's Park formation: Carnegie Mus., Mem., v. 11, no. 2, p. 87–121.

Powell, J. W., 1876, Report on the geology of the eastern portion of the Uinta Mountains and a region of country adjacent thereto: U.S. Geol. Geog. Survey Terr., 218 p.

Rich, J. L., 1910, The physiography of the Bishop conglomerate, southwestern Wyoming: Jour. Geology, v. 18, p. 601–632.

Sears, J. D., 1924, Geology and oil and gas prospects of part of Moffat County, Colorado, and southern Sweetwater County, Wyoming: U.S. Geol. Survey Bull. 751–G, p. 269–319.

LUNAR CRATER MORPHOLOGY AND RELATIVE-AGE DETERMINATION OF LUNAR GEOLOGIC UNITS—PART 1. CLASSIFICATION

By H. A. POHN and T. W. OFFIELD, Flagstaff, Ariz.

Abstract.—Lunar craters appear to occur in a morphologic continuum from very sharp to very subdued. Superposition relations show that younger craters are fresher in appearance than older craters. The assumption is made that morphology correlates generally with crater age. Change in crater form with time probably occurs as a result of mass wasting, mantling, and structural modifications effected by micrometeorite and meteorite bombardment, volcanic processes, and crustal vibrations. Craters in three size classes have been assigned relative ages expressed as decimals in an arbitrary scale—0.0 (oldest) to 7.0 (youngest)—on the basis of a detailed succession of morphologic differences attributed to aging processes. The criteria used are preservation of rays, radial ejecta facies, and satellitic craters; rim-crest sharpness and rim texture; and development of terraces and interior radial channels. Type examples of crater stages of defined age are established as a basis of comparison in determining relative ages of craters anywhere on the moon.

If certain assumptions, discussed below, are granted, relative ages of lunar craters can be determined by the degree of apparent freshness of their major topographic components such as the rim crest, walls, and surrounding rim deposits. Such apparent freshness was used in the past by Baldwin (1949) and by Arthur (1963) to construct very generalized correlations of age with four or five morphologic classes of craters. Crater morphologic classes somewhat more closely defined from telescopic observations and believed to represent age classes have been recognized from the outset of the U.S. Geological Survey's lunar mapping program (Hackman, 1961; Wilhelms, 1970). N. J. Trask (unpub. rept.) proposed that numbers be used to express the dependence of morphology on age in young craters smaller than 3 km within Apollo landing sites.

The system described here is a detailed refinement of these earlier basic approaches, made possible mostly by the moonwide coverage of Orbiter IV photographs, which permits relative-age determination and stratigraphic correlation of lunar geologic units for most of the lunar surface. Most craters larger than about 1 km, anywhere on the moon, can be assigned relative ages by means of the system described here, if adequate photographs are available.

A morphologic continuum from the most subdued to the sharpest lunar craters is defined, and this sequence is interpreted to reflect the relative ages of the craters. Evidence for correlation of age with progressive morphologic change has already been presented for small craters (Trask and Rowan, 1967), and a recent statistical evaluation appears to show the same correlation for craters of all sizes (Ronca and Green, 1968). Basic to the correlation of age with morphologic stage is our assumption that most lunar craters formed by impact and, therefore, in any given size category had a common initial form. The assumption that departures from this initial form reflect real age differences is borne out by observable superposition relations. For example, where one crater is superposed on another, the younger crater appears fresher: it has a sharper rim, more widely distributed and less subdued ejecta (relative to crater size), less subdued terraces, and fewer superposed craters. We also assume that a relatively regular progression of morphologic changes occur as a crater "ages". This "aging" may result from mass wasting, mantling, and structural modifications effected by micrometeorite and meteorite bombardment, volcanic processes, and crustal vibrations.

CRATER-AGE CLASSIFICATION

In examining pictures of more than 1,000 young lunar craters, we have found that with few exceptions they can be ordered into three classes on the basis of the planimetric shape of their rim crests. The actual size classes exhibit some overlap, as follows: <20 km crater diameter (round), 16–48 km (polygonal), >45 km (round, with distinct rim crenulations). For simplicity, in this paper the overlap is ignored, and class size limits are taken at 20 and 45 km; thus, class I, >45 km; class II, 20–45 km; and class III, 8–20 km.[1] Because of differ-

[1] Class III can be extended to include craters as small as 1 km, but assignment of age to craters smaller than 8 km poses some problems, discussed by Offield and Pohn (1970) (p. C163–C169, this chapter).

ences in the initial shape of craters, a slightly different morphologic continuum can be defined for each of the three size classes.

Within each class, the morphologic stage of any crater is determined by evaluation of a number of morphologic components (fig. 1). All components must be considered in this evaluation, but the most important single criterion is rim-crest sharpness. Other diagnostic features are the freshness of textural detail of ejected materials, morphology of terraces, and size-frequency distribution of superposed craters. On the assumption that craters become progressively degraded in appearance with increasing age, a morphologic continuum of crater forms ranging from very sharp to barely discernible represents an age hierachy. We have identified and closely defined such hierarchies for craters of the three size classes by choosing crater forms such that morphologic features in each stage, at scales proportionate to the sizes of the craters, have identical appearances in craters of all three classes.

As a convenience of notation, and to permit fine distinctions among generally similar craters, we have chosen to assign numbers to morphologic stages within these hierarchies. Our number scale is a completely arbitrary convention based on examination of thousands of pictures of craters, which indicated that approximately seven general types of crater forms could be discriminated easily and consistently. We chose seven stages and assigned them numbers ranging from 0.0 (most degraded, barely discenible) to 7.0 (least degraded, fresh, sharp). Because stage is here assumed generally to be a function of age, the numbers will hereafter be called "age numbers". It should be noted that this is relative age and that no relation of absolute time to these age numbers is implied.

Figure 2 shows craters that we have selected as type examples representing points in the general inferred aging sequence in each of the three size classes, and the caption describes their diagnostic features. Location of craters shown in figure 2 is given in table 1. Craters not exactly like those shown can be assigned intermediate decimal numbers by comparing their features with those of the defined type-example craters they most resemble, and subjectively interpolating between the age numbers of these craters. Some of the age criteria in any crater may be slightly equivocal, but a crater's place on the decimal scale can generally be expressed within specified limits. Trial of the numbering system by several lunar mappers indicates that the error increases with increasing age, owing to degradation and loss in definition of morphologic features. The error is represented typically by ± 0.1 in craters of age 6.0, ± 0.2 at age 4.0, and by about ± 0.4 in craters of age 1.0

Progressive change of several crater features from stage to stage in each size-class hierarchy, as a function of inferred age, is shown in figure 3. The figure demonstrates the observed points in the inferred apparent-age sequences of the three crater classes at which various features first develop, attain maximum development, and become obliterated. For rays, the points are defined from Earth-based full-Moon observations and for other features from Orbiter IV photographs with 70- to 100-meter resolution. Specific features are:

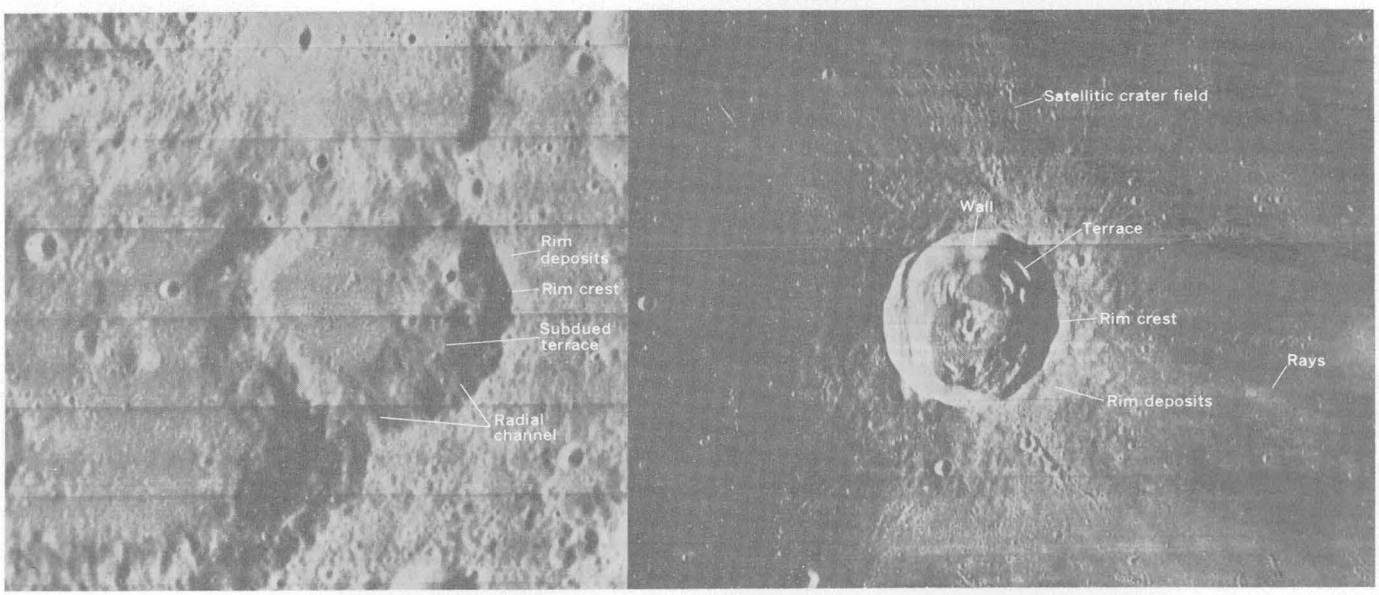

FIGURE 1.—Morphologic components of young (right) and old (left) craters used in relative-age determinations.

Rays.—The preservation of bright rays, best for all craters at age 7.0, is dependent on crater size as crater age increases.

Radial ejecta.—The continuous blanket of material surrounding a crater beyond ¼–⅓ crater diameter from the rim crest, characterized by ridges and grooves radial to the crater, is termed "radial ejecta." Radial ejecta is best developed and most easily distinguished on planar surfaces but can generally be discerned on rougher terrain by careful examination.

Satellitic craters.—Satellitic craters are generally arranged in subradial strings, in loops and arcs, or in clusters around fresh craters. Their size is dependent on the size of the primary crater, and small craters may not exhibit satellitic fields at Orbiter IV resolution. The ages shown in figure 3 for obliteration of satellitic craters are for mare or plains surfaces and may be displaced upward 0.1–0.3 in uplands because of poorer preservation of small craters in rough terrain.

Rim-crest sharpness.—Crater rim crests are considered sharp if they do not exhibit minute crenulations or rounding indicative of modification by small cratering events or mass wasting. Thus example III–6.5 (fig. 2*r*) would be considered sharp, whereas III–4.0 (fig. 2*w*) would be considered subdued.

Terracing and interior radial channels.—These two features are closely associated and are not generally size dependent, except that class III craters lack terraces. Terraces in the freshest large craters form as many as seven large sharp-edged tiers on the crater walls. From that initial configuration, the large terraces appear to break up by slumping, so that more and smaller terraces with somewhat rounded edges are characteristic of the fairly fresh to intermediate geomorphic stages. This phenomenon is at a maximum at age 4.5–5.0. In craters older than this, the terraces are progressively more subdued and appear to coalesce, so that fewer discrete terraces are present. By age 4.3, the first interior radial channels are observed on the crater walls in all three classes. These channels dissect the terraces and become more abundant and deeper toward a maximum at age 2.5. In craters older than this, the channels progressively are obliterated, concomitant with destruction of the terraces to form massive hummocky deposits along the lower walls of the craters.

Polygonality.—Class I craters are generally circular when formed and become slightly to markedly polygonal after age 4.0, depending on influences such as local fracture pattern and superposed cratering events. Class II craters form with polygonal outlines and remain obviously polygonal throughout all stages of modification. Class III craters form with circular outline; polygonality develops by age 4.5 and reaches a maximum at age 2.5.

Rim texture.—Rim materials of fresh craters are irregularly hummocky and are broken by short, curved terraces which are convex outward. As craters approach age 2.5, the hummocks and terraces are progressively smoothed. In craters older than age 2.5, the frequency of superposed craters approaches saturation, resulting in an increase of rim roughness.

For craters in Class III, an additional age criterion not seen in the larger classes is variation in the geometry of the interior shadow and of the associated photometric darkening pattern (subresolution shadow effects in microtextured slope material). This criterion is most useful at sun angles of 15° to 30°, the illumination of most Orbiter photographs. Figure 4 shows idealized drawings of six small craters in order of inferred age on our defined scale. (The shadow geometry and photometric darkening depend partly on sun angle, exposure, print contrast, and other variables of the Orbiter photographs.) In craters of age 6.0 and 6.5 the shadow impinges on a slightly raised floor and is therefore convex toward the sun; photometric darkening is present only as a small flare on each side of the shadow in the upper part of the sunward wall. By age 5.5 and 5.0, craters may or may not have small areas of flat floor which slightly affect the shadow geometry; by age 4.5 no floor remains. With progressive aging, the shadows curve more broadly and become irregular as they reflect increasing jaggedness in the rim crests; the photometric darkening extends as cusps which enlarge to cover the whole nonshadowed wall by age 4.0. In craters of age 4.0, development of flat floors is common and therefore shadows are again convex sunward; photometric darkening is irregularly distributed.

TIME SIGNIFICANCE OF THE RELATIVE-AGE SCALE

The intervals between morphologic stages chosen as integers on our scale probably do not represent equal spans of time because erosional modification of lunar landforms is almost certainly a nonlinear process. This nonlinearity stems from sequential erosion in which material eroded from the uppermost meter in height of a crater rim or terrace is redeposited downslope and must be removed over and over as the overall crater form is degraded. The erosion rate therefore probably is approximately exponential, but the exact function cannot be determined from present data.

If craters are eroded mainly by micrometeorite bombardment, then the rate of erosion is dependent on the flux rate of infalling particles. Any variations in size and frequency of these particles which may have

380-189 O - 70 - 11

Class I (>45 km) Class II (20–45 km) Class III (8–20 km)

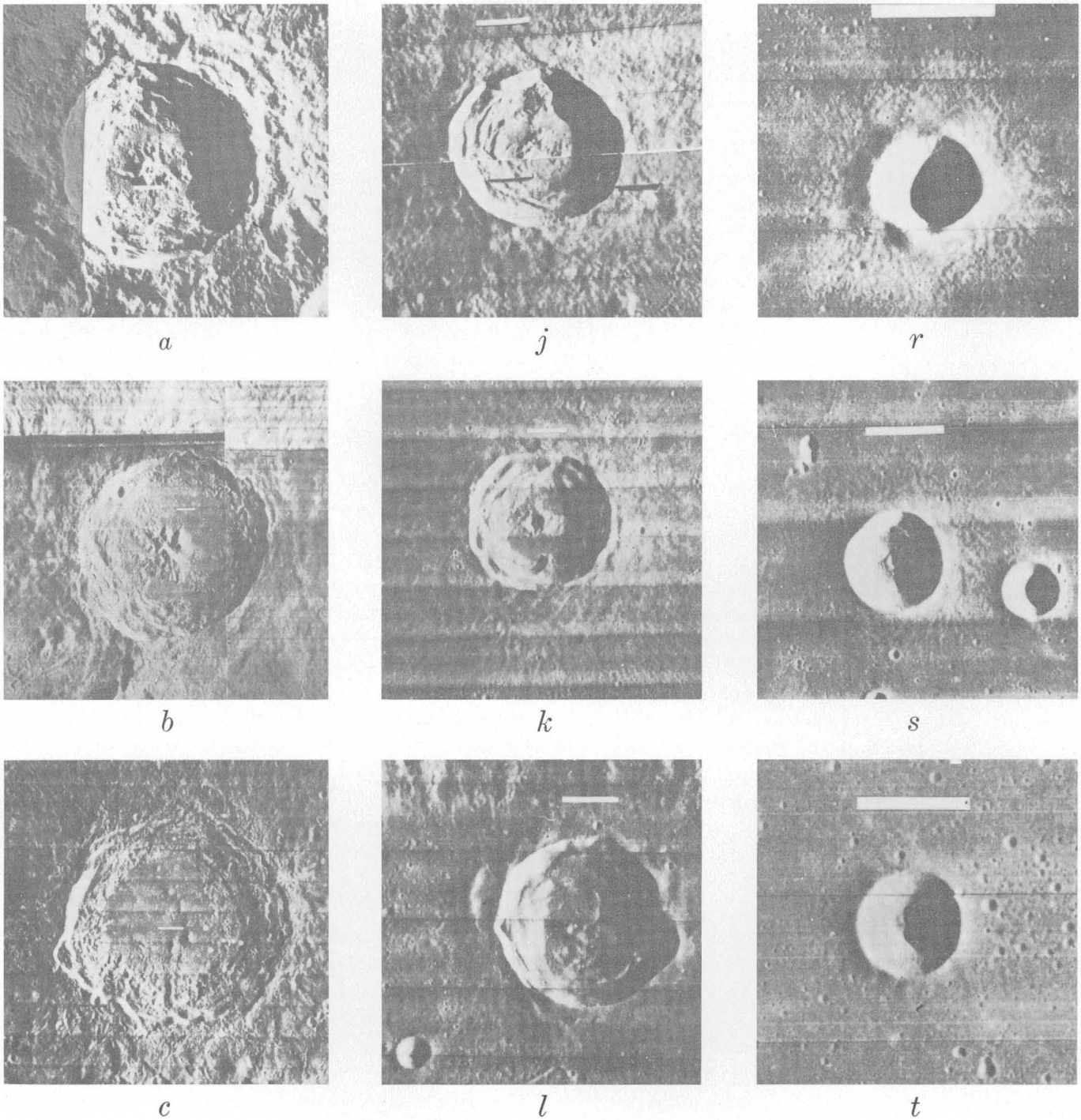

FIGURE 24.

FIGURE 2A.—Craters typical of the three classes of craters described in text. Criteria listed are with reference to Orbiter IV resolution (70–100 m; white bar in each picture 10 km, for scale). Upper size limit in classes II and III may be larger for old craters, owing to enlargement by slumping. Subdual rate increases markedly for craters smaller than 8 km; ages may be assigned by establishing offset from scale for larger craters. Names, relative ages (in parentheses), and descriptions of craters of class I (a–i), class II (j–q), and class III (r–x) are as follows:

CLASS I (>45 km)

Zuchius (6.5) (fig. 2*a*)

Rim crest.—Circular in plan view, with numerous crenulations. Sharp.
Walls.—Terraced; uppermost terrace never as deep as ⅓ crater depth and generally ⅓–⅙ crater depth. Terraces typically discontinuous; no single terrace occupies more than 1/10 of the crater circumference. Slump features commonly angular and blocky.
Rim.—Gently concave upward but irregularly terraced. Hummocky from rim crest outward, grading rapidly into radial "braided" texture which, in turn, grades into satellitic crater field. Satellitic craters fresh enough to be readily seen on rough upland surfaces. Conspicuous ray pattern.

Theophilus (6.0) (fig. 2*b*)

Rim crest.—Circular in plan view. Very slightly subdued (rounded).
Walls.—Terraces very slightly subdued.
Rim.—Hummocky and terraced; very low frequency of superposed craters. Satellitic craters conspicuous on mare but barely visible on rough upland terrain. Rays conspicuous but less bright than around late Copernican craters.

Aristoteles (5.5) (fig. 2*c*)

Rim crest.—Circular. Slightly subdued.
Walls.—Terraces slightly subdued.
Rim.—Exterior terraces more subdued than wall terraces; low frequency of superposed craters. Well-preserved radial facies. Rays virtually absent.

CLASS II (20–45 km)

Kepler (6.5) (fig. 2*j*)

Rim crest.—Polygonal in plan view, commonly hexagonal. Sharp.
Walls.—Terraced; uppermost terrace most commonly occurs at ¼–⅓ crater depth but may occur just below rim crest. Terraces angular but may have appearance of slight subdual of surface roughness. Individual terraces commonly longer than ¼ crater circumference.
Rim.—Gently concave upward, but irregularly terraced. Moderately hummocky from rim crest outward, grading rapidly into "braided" pattern which, in turn, grades into grooved field of satellitic craters. Conspicuous ray pattern.

Timocharis (6.0) (fig. 2*k*)

Rim crest.—Polygonal in plan view. Very slightly subdued.
Walls.—Terraces very slightly subdued.
Rim.—Terraces conspicuous but considerably subdued; overall surface texture fairly smooth. Satellitic craters subdued but conspicuous on smooth terrain; barely visible on rough terrain. Rays conspicuous but not extensive.

Horrocks (5.5) (fig. 2*l*)

Rim crest.—Polygonal. Slightly subdued.
Walls.—Terraces slightly to moderately subdued.
Rim.—Terraces generally inconspicuous. Near radial facies very subdued; extreme radial facies and satellitic craters barely visible on smooth terrain.

CLASS III (8–20 km)

Lansberg A (6.4–6.5) (fig. 2*r*)

Rim crest.—Circular in plan view. Sharp.
Walls.—Smooth, no terraces.
Rim.—Continuously concave upward. Smooth to slightly undulating from rim crest outward, with break in slope (rampart) just outside rim crest. At ⅓–⅔ crater diameter smooth raised-rim facies grades rapidly into discontinuous "dune" facies which, in turn, grades into radially grooved facies at about one crater diameter. Satellitic craters subdued but visible on smooth terrain. Conspicuous rays.

Marius C (6.0) (fig. 2*s*)

Rim crest.—Circular in plan view. Very slightly subdued.
Walls.—Smooth. Albedo slightly lower than that of late Copernican craters.
Rim.—Smooth; rampart subdued. "Dune" facies has braided appearance, with distal part markedly subdued. Satellitic craters barely discernible on smooth terrain. Rays virtually absent.

Le Verrier D (5.5) (fig. 2*t*)

Rim crest.—Circular. Slightly subdued.
Walls.—Smooth.
Rim.—Faint exterior radial channels in rampart. No radial facies at one crater diameter. "Dunes" inconspicuous.

occurred throughout lunar geologic time will have increased the nonuniformity of the proposed numbering scale with respect to time.

Absolute ages and particle flux rates can be determined only by radiometric dating of lunar materials. When this is done, it should be possible, by means of the relative-age criteria proposed here, to extrapolate the absolute-age data over much of the lunar surface.

VARIABLES AFFECTING THE CRATER-NUMBERING SYSTEM

Factors that may contribute to an erroneous assessment of crater ages are:

Rock strength.—Lunar materials probably vary considerably in their response to the stresses produced by impact and generated during subsequent crater modification. A crater on a contact between different geologic units might therefore be expected to show differences in internal morphology. Although such differences may be present in very small craters, they have not been observed in craters larger than 1 km, even where the craters (for example, Menelaus and Eratosthenes) cross contacts between presumably very different geologic materials such as those which form mare and terra.

Volcanic materials.—Although most craters described in the age sequence are presumed to be of impact origin and, in a given size class, have similar initial forms, it is quite likely that endogenetic (volcanic or tectonic) craters with variable initial forms also occur on the moon (McCauley, 1967). Such craters may not only be of

Class I (>45 km) Class II (20–45 km) Class III (8–20 km)

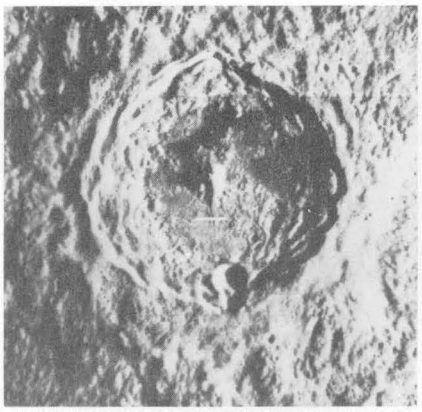

d

m

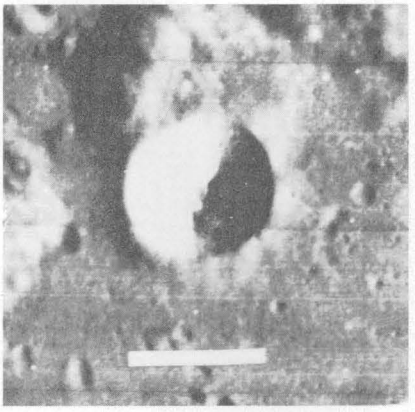

u

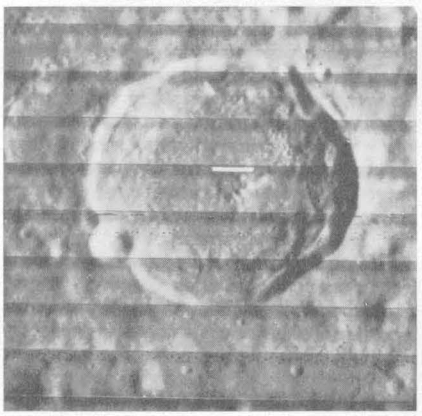

e

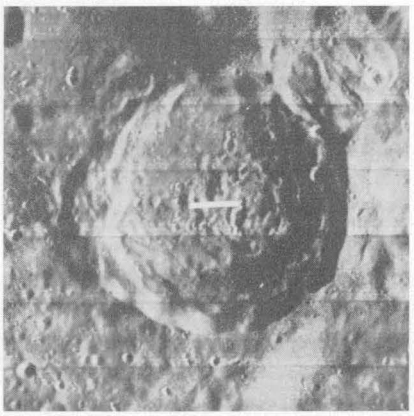

n

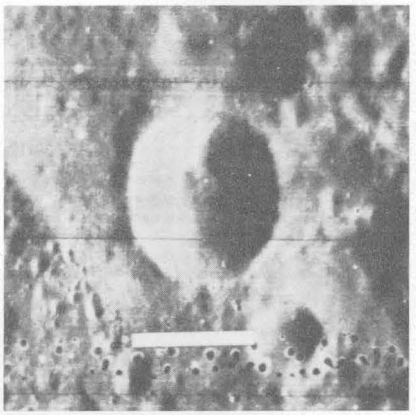

v

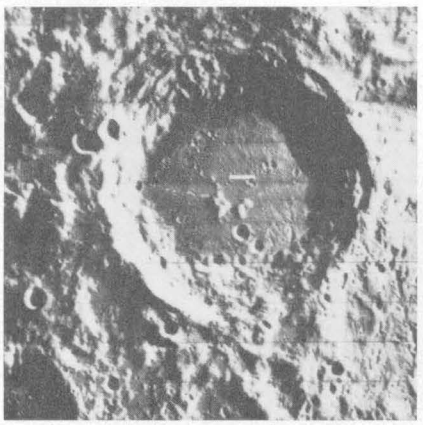

f

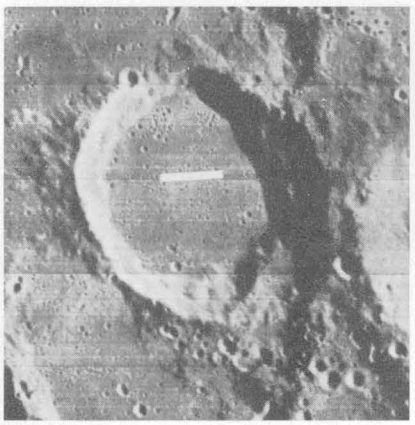

o

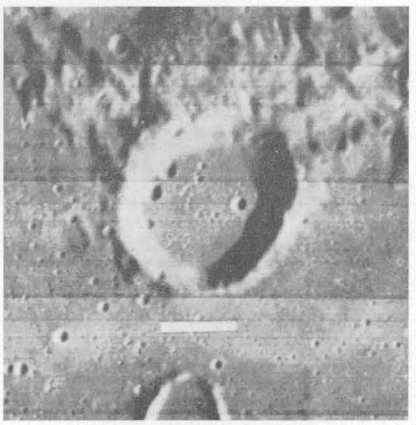

w

FIGURE 2*B*.

FIGURE 2*B*.—Craters typical of the three classes of craters described in text (continued).

Schlüter (5.0) (fig. 2*d*)

Rim crest.—Ranges from sharp to slightly subdued.
Walls.—Terraces subdued but not coalesced.
Rim.—Exterior terraces very subdued and conspicuously cratered. Superposed craters are small (<3 km). Radial facies barely discernible.

Macrobius (4.5) (fig. 2*e*)

Rim crest.—Entire rim crest very slightly subdued.
Walls.—Terraces subdued with some coalescence.
Rim.—Generally at least one crater (>3 km) superposed on rim deposits. No radial facies, hummocky facies very subdued.

Blancanus (4.0) (fig. 2*f*)

Rim crest.—Entire rim crest somewhat subdued.
Walls.—Terraces exhibit considerable subduing and are very coalesced, but still distinct.
Rim.—Generally at least one large crater superposed on the rim. Hummocky facies all but obliterated.

Eichstädt (5.0) (fig. 2*m*)

Rim crest.—Partly subdued.
Walls.—Terraces slightly subdued, but well developed.
Rim.—Cratering apparent on rim, radial facies absent, hummocky facies quite subdued.

Nasireddin (4.5) (fig. 2*n*)

Rim crest.—Partly subdued.
Walls.—Maximum development of terraces. Individual terraces subdued.
Rim.—Cratering conspicous on rim. Hummocky facies absent.

Rost A (4.0) (fig. 2*o*)

Rim crest.—Entire rim crest slightly subdued. Sone resolvable craters intersect crestline.
Walls.—Subdued and partly coalesced. No radial channelling.
Rim.—Numerous small craters superposed on rim. Outer limit of morphologic unit commonly ill defined.

Römer L (5.0) (fig. 2*u*)

Rim crest.—Circular. Subdued, with no rampart.
Walls.—Smooth.
Rim.—Few very small craters on rim. No "dunes." Very slight evidence of radial facies.

Riccius M (4.5) (fig. 2*v*)

Rim crest.—Circular to slightly elliptical. Entire crestline slightly subdued.
Walls.—Smooth.
Rim.—Several small craters in rim. No evidence of radial facies.

Nöggerath G (4.0) (fig. 2*w*)

Rim crest.—Slightly polygonal. Subdued; intersected by numerous craters on crestline.
Walls.—Faint radial channels.
Rim.—Coarsely hummocky owing to cratering.

forms different from impact craters initially, but because of different compositions and physical makeup may also be modified at a different rate, resulting in an incorrect appraisal of age under the proposed crater-numbering system. The effect of these factors on the numbering system cannot be assessed at this time because the range in form and the abundance of endogenetic craters are not known.

Fill and mantling units of probable volcanic origin, with hummocky, undulating, and planar topographic expression are common in the uplands and appear to mantle many craters. A result of this mantling is that crater features are subdued even more than they would be by erosion alone. Thus, such craters appear to be older than they actually are.

Proximity aging.—A crater within range of ejecta from an impact event will be mantled, as well as subdued, by secondary impacts. A crater thus modified will appear older than it really is. Modification of this sort results in what we have termed "proximity aging" and presents one of the most difficult problems in assigning relative ages to craters. In youthful craters, proximity aging appears to result more from secondary impacts than from ballistic deposition of blanketing materials. However, the distribution of impacting secondary particles typically is nonuniform; thus, only part of the rim crest of a crater may be subdued. The least affected part reveals the true geomorphic stage of the crater. Proximity aging by a single event will have contributed

TABLE 1.—*Location of crater examples shown in figure 2*

[−, S. lat or W. long; +, N. lat or E. long]

Crater name	Diameter (km)	Long	Lat	Orbiter IV photo
Class I (>45 km)				
Zuchius	64.2	−50.9	−61.5	H 154
Theophilus	100.0	+26.3	−11.4	H 74, 84
Aristoteles	87.2	+17.3	+50.1	H 103
Schlüter	90.7	−83.5	−6.0	H 181
Macrobius	64.0	+46.0	+21.2	H 66
Blancanus	105.3	−21.5	−63.6	H 130
Manzinus	98.1	+26.7	−67.7	H 94
Sacrobosco	95.9	+16.9	−24.0	H 89
Regiomontanus	109.9			
	126.3	−1.0	−28.5	H 107
Class II (20–45 km)				
Kepler	31.5	−38.0	+8.1	H 138
Timocharis	35.2	−13.1	+26.7	H 121
Horrocks	30.5	+5.9	−4.0	H 101
Eichstädt	49.2	−78.4	−22.6	H 181
Nasireddin	51.4	+0.2	−41.1	H 112
Rost A	39.0	−36.7	−56.5	H 154
Baco E	27.5	+16.2	−52.9	H 107
Rosenberger A	48.9	+47.0	−53.5	H 83
Class III (8–20 km)				
Lansberg A	8.6	−31.1	+0.2	H 133
Marius C	12.1	−47.5	+13.9	H 150
Le Verrier D	9.1	−12.3	+39.7	H 127
Römer L	10.6	+34.7	+23.2	H 78
Riccius M	13.6	+26.5	−37.9	H 88
Nöggerath G	21.1	−45.7	−50.2	H 160
Baco J	18.8	+19.3	−54.7	H 107

Class I (>45 km) Class II (20–45 km) Class III (8–20 km)

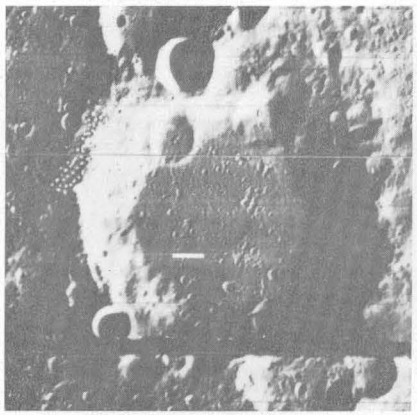

g

p

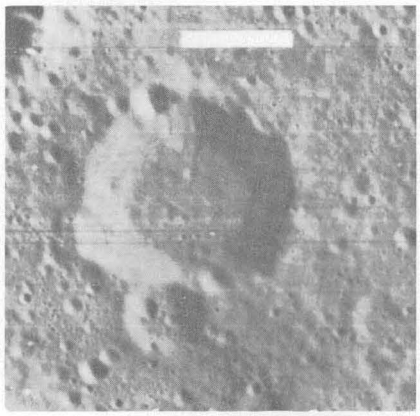

x

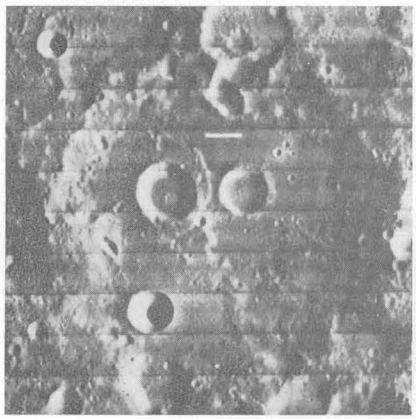

h

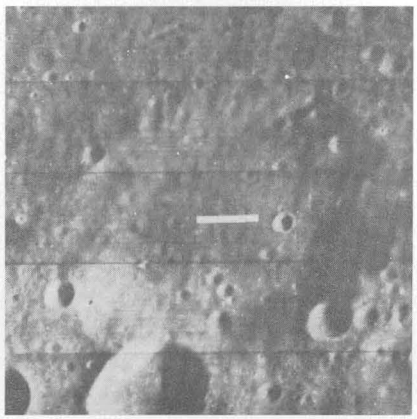

q

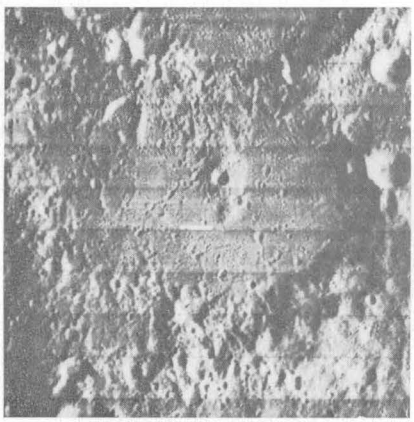

i

FIGURE 2C.

FIGURE 2C.—Craters typical of the three classes of craters described in text (continued).

Manzinus (3.0) (fig. 2*g*)

Rim crest.—Somewhat polygonal in plan view. Moderately to highly subdued; typically interrupted by numerous superposed craters.
Walls.—Terraces coalesced, highly subdued, and moderately cratered. Radial channels poorly developed.
Rim.—Heavily cratered but readily distinguishable as morphologic unit.

Sacrobosco (2.0) (fig. 2*h*)

Rim crest.—Somewhat polygonal. Highly subdued; commonly disrupted by one or more craters whose sizes are a large fraction (>¼) of the crater diameter; crestline apparent in some segments.
Walls.—Terraces very subdued; occupy only a small part of the crater circumference. Hummocky slump masses more typical than terraces. Radial channels well developed.
Rim.—Heavily cratered; faintly discernible.

Regiomontanus (1.0) (fig. 2*i*)

Rim crest.—Somewhat polygonal. Broadly rounded, discontinuous; no distinct crestline.
Walls.—Hummocky slump masses dominant; no significant terraces. Only remnants of radial channels visible.
Rim.—Heavily cratered, dissected, coarsely hummocky; barely mappable as unit.
Craters older than Regiomontanus within the lower pre-Imbrian series are barely discernible and do not have mappable subunits.

Baco E (3.0) (fig. 2*p*)

Rim crest.—Polygonal. Highly subdued; broken by numerous superposed craters.
Walls.—Terraces mostly coalesced; absent in many craters. Radial channels well developed.
Rim.—Heavily cratered; disrupted by some large craters; poorly and irregularly mappable as unit.

Rosenberger A (2.0) (fig. 2*q*)

Rim crest.—Polygonal. Present as highly subdued remnant segments.
Walls.—Terraces virtually absent. Hummocky slump masses characteristic. Radial channels moderately well developed.
Rim.—Heavily cratered; segments destroyed by large superposed craters, remainder difficult to map as unit.

No Example.

Baco J (3.0) (fig. 2*x*)

Rim crest.—More polygonal than circular in plan view. Highly subdued; breached.
Walls.—Commonly breached. Radial channels conspicuous.
Rim.—Largely destroyed; extent of unit vaguely discernible in remnant segments. Numerous large superposed craters. Barely discernible craters in which no subunits are mappable. Probably no preserved examples.

No Example.

No Example.

little to the present form of older craters (0.0–4.0). The apparent age of most older craters thus reflects proximity aging by many events as well as the more continuous processes of meteorite bombardment and seismic vibrations, so that proximity aging, not specifically identifiable, is intrinsic in the geomorphic development of old craters and therefore need not receive special attention in assigning age numbers to these craters.

SUMMARY

Lunar craters range in form from very sharp to barely discernible and appear to make up a morphologic continuum in which degradation of crater form is progressive with age. On the assumption that craters have a common initial form, and change in appearance as a function of age (owing to meteoritic bombardment, seismic shaking, and mantling processes), hierarchies of crater forms have been identified and morphologic stage inferentially equated with age. Numbers representing relative age have been assigned to crater stages in three size classes of craters. Type examples of crater stages of defined age are established as a basis of comparison in determining relative ages of craters anywhere on the moon.

Part 2 of this study (Offield and Pohn, 1970) (p. C163–C169, this chapter) details tests of the proposed crater numbering system in areas where geologic units have known relative ages, and discusses applications to lunar geologic problems.

REFERENCES

Arthur, D. W. G., Agnieray, A. P., Horvath, R. A., Wood, C. A., and Chapman, C. R., 1963, The system of lunar craters, quadrant I: Arizona Univ. Lunar and Planetary Lab. Commun. 2, p. 1–60.

Baldwin, R. B., 1949, The face of the moon: Univ. Chicago Press, 239 p.

——— 1963. The measure of the moon: Univ. Chicago Press, 488 p.

Hackman, R. J., 1961, Photointerpretation of the lunar surface: Photogramm. Eng., v. 27, no. 3, p. 377–386.

McCauley, J. F., 1967, Geologic results from the lunar precursor probes: Am. Inst. Aeronautics and Astronautics Paper 67–862, 8 p.

Offield, T. W., and Pohn, H. A., 1970, Lunar crater morphology and relative-age determination of lunar geologic units—Part 2. Applications, *in* Geological Survey Research 1970: U.S. Geol. Survey Prof. Paper 700–C, p. C163–C169.

Ronca, L. B., and Green, R. R., 1968, Large-scale evolution of the lunar surface: Boeing Sci. Research Lab. Doc. D1–82–0773, 28 p.

Trask, N. J., and Rowan, L. C., 1967, Lunar Orbiter photographs—Some fundamental observations: Science, v. 158, no. 3808, p. 1529–1535.

Wilhelms, D. E., 1970, Summary of lunar telescopic stratigraphy: U.S. Geol. Survey Prof. Paper 599–F. [In press]

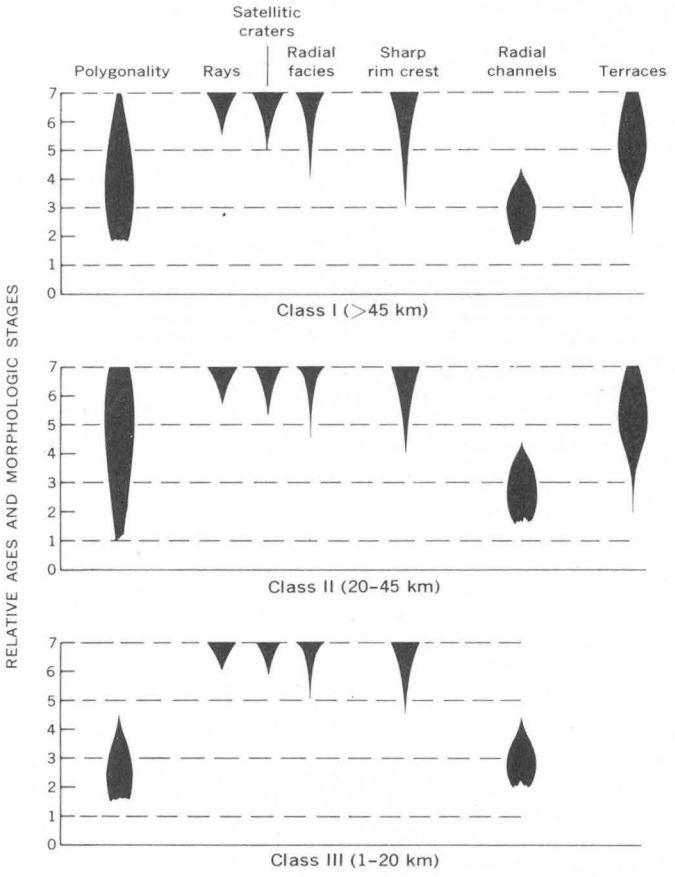

FIGURE 3.—Changes in diagnostic crater features with age. The numerical values denote seven morphologic stages and relative ages ranging from 0.0 (most degraded—greatest relative age) to 7.0 (least degraded—least relative age).

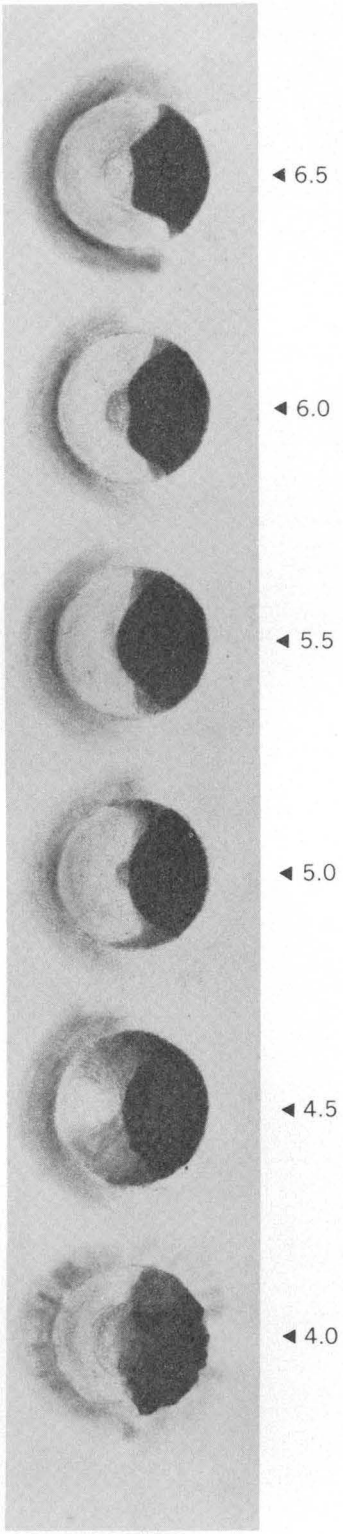

FIGURE 4.—Idealized relative-age sequence of small craters, showing diagnostic shadow shapes.

LUNAR CRATER MORPHOLOGY AND RELATIVE-AGE DETERMINATION OF LUNAR GEOLOGIC UNITS—PART 2. APPLICATIONS

By T. W. OFFIELD and H. A. POHN, Flagstaff, Ariz.

Abstract.—Lunar craters larger than 8 km have been assigned inferred ages expressed as decimals—0.0 (oldest) to 7.0 (youngest)—on the basis of a detailed succession of morphologic differences attributed to aging processes. Relative ages of lunar basins and regional geologic units can be determined by dating the oldest craters superposed on them, and moonwide age sequences and correlations are thus made possible. Such age determinations indicate that mare basins formed in the following order: Nectaris, Serenitatis, Humorum, Crisium, Imbrium, and Orientale. Mare surface units were emplaced in the following generalized order: Fecunditatis, Tranquillitatis, Imbrium, Crisium, Humorum, eastern Procellarum, western Procellarum. Regional light plains units are dated as the same age as some dark mare units; albedos and crater abundances are not valid age criteria for these units. A further application is the identification of basin ejecta blankets and possible basin secondary craters.

An inferred continuum of morphologic stages observed in lunar craters was described in part 1 of this study (Pohn and Offield, 1970) (p. C153–C162, this chapter), and a numbering system to express these differences in form was proposed. Because superposition relations nearly everywhere on the moon show that craters with subdued morphologic features are older than craters with sharper, apparently fresher, features, numbers assigned to craters according to the aforementioned system are believed to correlate generally with crater age. If such a correlation does, in fact, exist, regional geologic units and lunar events can be assigned relative ages independently of inferred superposition or interselection relations or other less direct methods such as crater size-frequency counts (Shoemaker and Hackman, 1962; Shoemaker and others, 1962; McCauley, 1967b). Any unit extensive enough to contain a large population of craters can be dated as slightly older than the oldest crater superposed on it. The circular multiringed mare basins can be dated by determining the age of the oldest craters which cut structures related to the formation of the basin or are superposed on the circumbasin deposits construed to be basin ejecta blankets.

RELATIVE-AGE DETERMINATION OF SURFACES AND EVENTS

The numbering system was tested by determining the relative ages of the oldest craters on three regional lunar geologic units. Each of these units is believed to be isochronous. In addition, the sequence of relative ages of these units is indicated by superposition relations, superposed-crater abundance, and freshness of detail. These units were the hummocky materials surrounding the Imbrium basin and inferred to be its ejecta blanket (oldest), the Orientale basin ejecta blanket, and the western Oceanus Procellarum mare material (youngest). The test results agreed with the established relative-age sequence of the three isochronous units. Other similar tests (for example, Sinus Iridum crater ejecta blanket relative to the inferred Imbrium ejecta blanket, Serenitatis basin relative to the inferred Imbrium ejecta blanket, and the relative ages of many crater pairs such as Copernicus-Eratosthenes, Aristoteles-Audoxus, and Aristoteles-Plato) also showed agreement between ages assigned by the numbering system and ages determined from clear-cut superposition relations.

Figures 1 and 2 give the results of crater-age determinations for several mare basins and regional geologic units on the earthward face of the moon, and for a few features on the far side. Table 1 shows the basis for the ages in figures 1 and 2; data for features on the far side are not given because of difficulty in citing precise locations.

The oldest reasonably well preserved basin dated thus far (fig. 1) is the double-ring Schiller basin. Other basins apparently formed in the following order: Nectaris, Serenitatis, Muscoviense, Humorum, Crisium, Imbrium, and Orientale. Tsiolkovsky, perhaps a large crater and not a multiring basin, is slightly younger than Orientale. The above age sequence differs somewhat from that of Hartmann (1964), who estimated that the

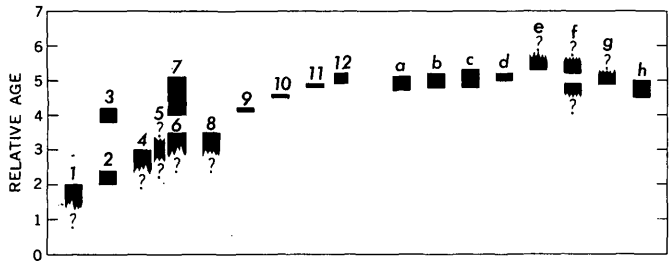

FIGURE 1.—Crater-age determinations of lunar basins and associated units and of plains units. Broken-ended boxes indicate uncertainty in maximum or minimum age. Basins: *1*, Schiller; B, Nectaris; C, Nectaris "blanket"; D, Serenitatis; *5*, Muscoviense; *6*, Humorum; *7*, Humorum "blanket"; *8*, Crisium; T, Imbrium "blanket"; VJ, Iridum; VV, Orientale; *12*, Tsiolkovsky. Plains: *a*, southern-region crater-fill plains; *b*, northern-region plains; *c*, central-region plains; *d*, Orientale inner-ring fill; *e*, southwest of Mare Smythii; *f*, Tsiolkovsky region; *g*, far-side plains (east); *h*, far-side plains (central).

Nectaris basin is relatively young (between Crisium and Imbrium in age).

Each basin may have been partly filled shortly after it formed, but the present major surface units in the maria are much younger than the basins they occupy. The ages given in figure 2 are upper and lower limits generalized for very large mare areas. On a more local scale, especially in the western maria, superposition relations of individual fresh craters and mare materials typically reveal the presence of several local geologic units of different ages within the limits shown. The oldest mare surface units dated so far (fig. 2) are little older than the Orientale basin, and most are decidedly younger.

In high-resolution Orbiter II and III photographs, the eastern maria in the equatorial region appear to have more highly battered small craters than the western maria; thus, the former may be older (U.S. Geological Survey, 1968). This suggested age relation is confirmed by our crater-age numbers which show that, although relatively young units are present in places, generally the Fecunditatis and Tranquillitatis mare units are older than those of the western maria. Crisium mare material is, however, as young as some of the western mare material. Its relative youthfulness was suggested earlier as one explanation of its low crater frequency at telescopic resolution (Shoemaker and others, 1962). Also, lunar night thermal infrared observations (R. L. Wildey, written commun., 1969) show that Crisium is relatively warm among maria, presumably an indication that the insulating regolith material is thinner than in other maria and, thus, that Crisium mare material has been subjected to erosion for a shorter time.

The mare material in Tsiolkovsky is about the same age as the surface units in eastern Oceanus Procellarum, and the mare filling of the Muscoviense basin is slightly younger, perhaps correlative with the units of western Procellarum.

Surface units of the light terra plains all appear to have formed in the relative-age interval 4.5–5.6 (fig. 1); most units which can be dated satisfactorily are younger than the Orientale basin. Light plains units near Tsiolkovsky are in part younger and in part older than that crater. None of the extensive light plains units is as young as the youngest mare units.

SIZE DEPENDENCE OF CRATER-AGE CHARACTERISTICS

The effect of size on the apparent age of craters must be considered if crater age is to be used in dating geologic units upon which the craters are superposed, particularly if craters as small as 1 km in diameter are to be used for dating purposes. At the outset, we supposed intuitively that where two craters differed in size, the smaller would be degraded more rapidly than the larger crater and that this would be true throughout the complete spectrum of sizes.

To determine the relation between crater size and morphologic modification (apparent aging), we used identical morphologic criteria to assign age numbers to the most subdued craters of several sizes superposed on four regional geologic units, each of which has been interpreted as isochronous (Eggleton, 1964; Shoemaker and Hackman, 1962; McCauley, 1967a). The curve connecting ages of these oldest superposed craters of different sizes on each surface is nearly flat for craters larger than 8 km (fig. 3). This shows that craters larger than 8 km do not change markedly in apparent age assignable on the basis of geomorphic characteristics.

Craters smaller than 8 km, however, are affected by modifying processes in such a way that they are subdued more rapidly than larger craters, resulting in an offset in the changes of morphologic detail. For example, if a surface is dated as age 4.5 on the basis of craters larger than 8 km, then by using the same morphologic characteristics, a crater 3 km in diameter will show an apparent age as much as 1.5 integers younger (fig. 3). Still smaller craters will show greater apparent ages on the same surface. However, the numbering system proposed in part 1 for class III craters can be used for craters smaller than 8 km if a crater-number offset curve (like those in fig. 3) is made for each unit being dated. Interpolation from figure 3 may make construction of a new offset curve unnecessary for many craters. On most extensive geologic units older than age 5.5, the population of craters 8–15 km in diameter generally is large enough to assure the presence of the oldest possible superposed crater for determining the age of the unit. Craters in this size range should be used for dating such units because smaller craters will appear to be older

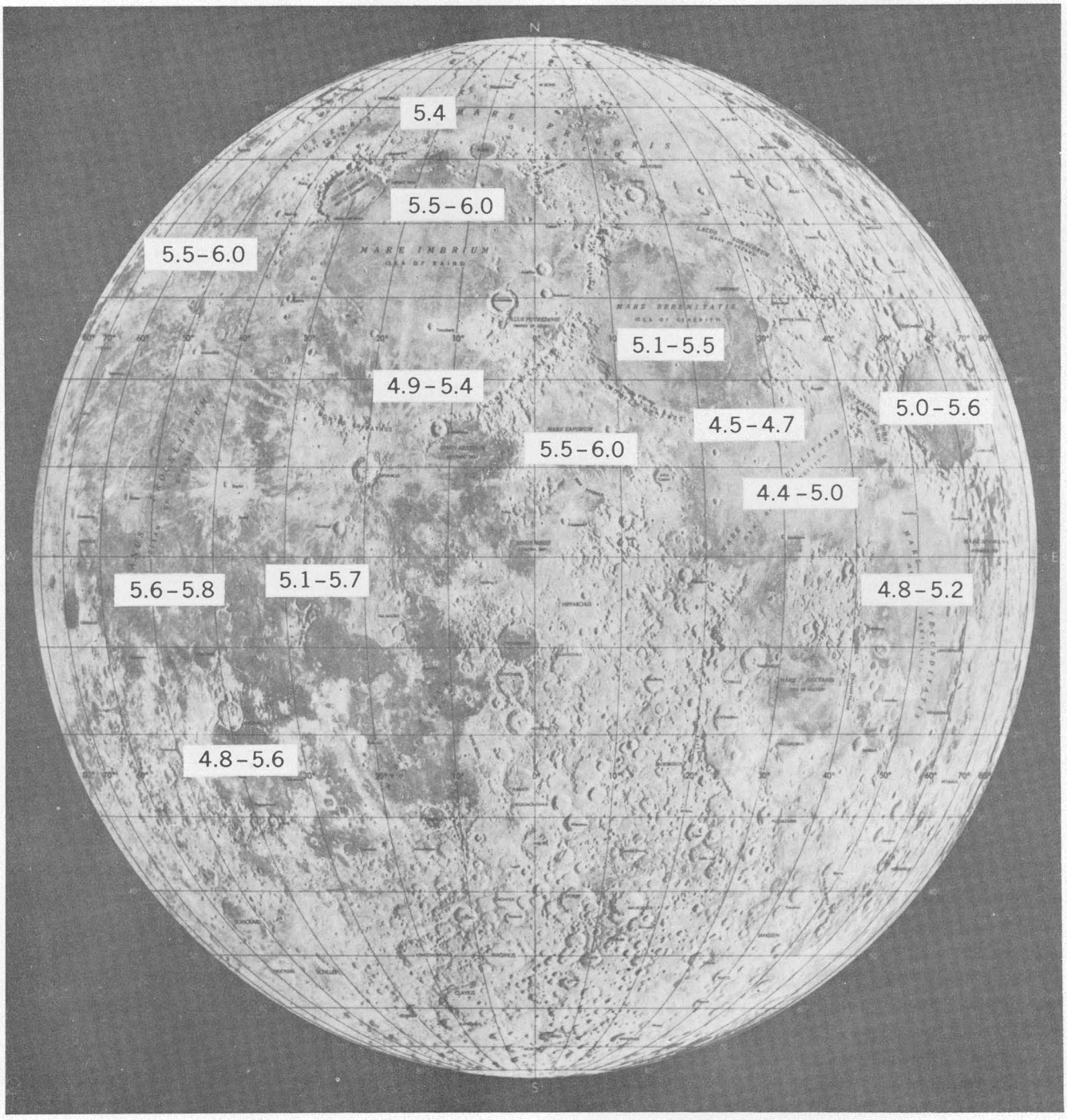

FIGURE 2.—Relative ages of regional mare surfaces. (Base map is USAF Lunar Reference Mosaic.)

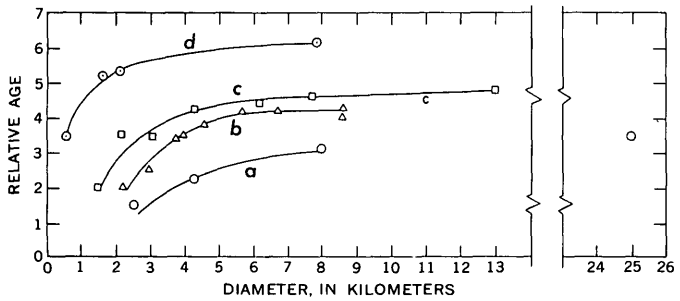

FIGURE 3.—Change in apparent age as a function of size for craters on isochronous surfaces: *a*, Crisium rim; *b*, Imbrium blanket; *c*, Orientale blanket; *d*, Copernicus ejecta.

than they actually are, and larger craters may not be numerous enough to provide the oldest possible example on any given unit. For dating younger units, it generally will be necessary to use smaller craters and to deduce the age by means of individual offset curves or interpolation from figure 3.

The similarity and smoothness of the curves for surfaces of considerably different relative ages are interpreted as showing that (1) the proposed crater-numbering system is internally consistent (although equal intervals probably do not represent equal periods of time), and (2) changes in crater morphologic characteristics are a fairly regular progression with time.

RAMIFICATIONS OF THE CRATER-NUMBERING SYSTEM

A number of observations and conclusions about local and moonwide geologic correlations have already resulted from use of the crater-numbering system, and others will be made possible by it. Some of the relative-age determinations bear out earlier geologic inferences from telescopic data; in general, there is good correspondence between the relative ages determined by this system and those arrived at by systematic geologic mapping. Other relative-age determinations refute or cast doubt on older interpretations, and open the way to new and more precise interpretations. Some important points are discussed briefly below.

1. A marked discrepancy is found in dating the Humorum basin and the hummocky, partly blanketing materials around it. On the basis of telescopic observations, these hummocky materials had been thought to be basin ejecta (Titley, 1967; Titley and Eggleton, 1964), but crater-age determinations show them to be approximately a whole integer younger than the basin on our proposed number scale (fig. 1; table 1). This age difference seems to be confirmed qualitatively by a paucity of 1–10-km craters superposed on the hummocky materials as compared with the abundance of such craters on large areas which appear to be original basin rim and not covered by the hummocky materials. Because of the age difference, and other considerations, such as the fresh appearance and patchy distribution of the hummocky materials, we suspect that they are relatively young volcanic blanketing units not directly related to the formation of the Humorum basin. Figure 1 shows a similar discrepancy between the relative ages of the Nectaris basin and the widespread hummocky blanketing materials around it, which supports the conclusion by Milton (1968) that the hummocky materials are volcanic rather than basin ejecta.

TABLE 1.—*Superposition relationships supporting relative-age determinations shown on figures 2 and 3*

Superposition relationships: A, named crater superposed on unit or structure; B, materials of unit found in crater interior; C, materials of unit embay crater rim; D, materials of unit superposed on crater; E, crater appearance (see Pohn and Offield, 1970) (p. C153-C162, this chapter)]

Unit	Crater or feature used for dating	Relative age	Superposition relationships
Schiller basin	Segni	2. 0	A
Nectaris basin	Catharina	2. 4	A
	Rothmann G	2. 0	D
Nectaris "blanket"	Tacitus	4. 2	A
	Pons	3. 8–3. 9	C
Serenitatis basin	Littrow	3. 0	A
Humorum "blanket"	Fontana G	4. 2	D
	Fontana C	3. 8	D
	Lepaute	3. 6–3. 8	D
	Hainzel L	4. 1–4. 2	D
	Ramsden H	4. 0–4. 2	D
	Vitello	4. 8–4. 9	A
	Hansteen	4. 9–5. 1	A
	Western plains	4. 8–5. 1	A
Crisium basin	Proclus P	3. 2–3. 5	A
	Proclus S	3. 4–3. 6	A
	Tisserand A	3. 4–3. 6	A
	Picard G	3. 5	A
	Cleomedes	3. 5	A
Imbrium "blanket"	Arata A	4. 2	A
Iridum	Iridum	4. 6	E
Orientale basin and "blanket".	Schlüter	5. 0–5. 1	A
	Eichstadt	5. 0	A
	Shaler	4. 8	(1)
	Rocca	4. 2	C
	Crüger	4. 8	A
Southern and western plains.	Orientale blanket.	4. 8	D
	Zagut	4. 9–5. 1	A
	Lilius B	4. 7–4. 9	B, C
	Deluc C	4. 8–4. 9	B
Northern plains	Timaeus	5. 2–5. 3	A
	3 craters 126 km north of Pascal.	4. 8–5. 0	B, C
Central plains	Cayley	5. 5	A
	Whewell	4. 9	C
	Arzachel	4. 8	C
	Thebit	5. 1–5. 2	A
Frigoris mare	Protagoras	5. 1–5. 3	C
	Timaeus	5. 2–5. 3	C
	Aristoteles	5. 5	A
	Archytus	5. 5–5. 6	A
	Phythagoras	5. 4	A
	J. Herschel F	5. 0	B, C
Tranquillitatis mare	Ross D	4. 7	A, C[2]
	Sinas E	5. 0	A
	Maraldi B	5. 0	A
	Cauchy A	4. 4	B, C
	Römer J	5. 1	A

See footnotes at end of table.

TABLE 1.—*Superposition relationships supporting relative-age determinations shown on figures 2 and 3*—Continued

[Superposition relationships: A, named crater superposed on unit or structure; B, materials of unit found in crater interior; C, materials of unit embay crater rim; D, materials of unit superposed on crater; E, crater appearance (see Pohn and Offield, 1970) (p. C153–C162, this chapter)]

Unit	Crater or feature used for dating	Relative age	Superposition relationships
Northwestern Tranquillitatis mare.	DeSeilligny A	4.5	B, C
	Ross P	4.7	A
Serenitatis mare	Posidonius P	5.5	A
	Bessel E	5.1	C
	Eudoxus	5.6	A
	Posidonius N	5.3	A, C[2]
Vaporum mare	Manilius	5.5	C
	Manilius D	6.0–6.1	A
Eastern Imbrium mare	Archimedes	4.9–5.3	B, C
	Feuillée	5.1	C
	Eratosthenes	5.7	A
	Eratosthenes B	5.4	A
Mare south of Copernicus.	Lansberg	5.1–5.3	C
	Lansberg D	6.0	A
	Bonpland E	5.7	A
Southern Procellarum mare.	Flamsteed A	5.5–5.6	C
	Flamsteed	5.8	A, C[2]
	Herigonius	5.5–5.6	A, C[2]
	Euclides B	6.0	A
Northwestern Imbrium mare.	Bullialdus	5.7	A, C[2]
	Helicon	5.1–5.4	C
	Carlini	5.6–5.8	C
	Heis	5.9–6.1	A
	Leverrier	5.9–6.0	A
	Leverrier D	5.5	A
	Kirch	5.6	A
Northern Procellarum mare.	Dechen	5.5	C
	Lavoisier	5.1–5.4	C
	Harding	6.0–6.1	A
	Markov	5.3	C
	Naumann	5.8–5.9	A
Western Procellarum mare.	Cavalerius	5.9–6.0	A, C[2]
	Lohrmann BA	6.0	A
	Lohrmann A	6.0	A
	Reiner	5.9	A, C[2]
	Kraftt E	5.7–5.8	A
	Galilaei	5.8–5.9	A
	Schiaparelli	5.3–5.5	C
	Marius D	5.3–5.4	C
Humorum mare	Vitello	4.8–4.9	C
	Liebig F	5.6	A
Crisium mare	Cleomedes G	4.5	B, C
	Cleomedes FA	5.6	A
	Messala	5.7–5.8	A
	Eimmart C[3]	5.0	C
Fecunditatis mare	Petavius	4.5	C
	Messier G	5.2	A
	Goclenius A	4.8	C

[1] Synchronous with basin?
[2] Part embayment of rim materials.
[3] Determination from Orbiter IV front-side apolune photograph with poorer resolution and lower lighting than usual photographs.

2. The identification of basin ejecta blankets has rested hitherto on distinctive morphology of the deposits and their distribution around a basin. It now should be possible to determine the presence and extent of basin ejecta blankets too old to have a distinctive morphology. Small craters (1–8 km) existing before the blankets (here called preblanket) will be absent or indistinct (mantled), and larger preblanket craters, particularly those close to the basin, will be subdued to the extent that they appear older than they actually are. Postbasin craters (those younger than the basins) should have normal age characteristic. Thus a noticeable break in the crater-age versus crater-frequency data will occur at the age just before the oldest postbasin crater and will mark the presence and age of a suspected ejecta blanket. The extent of the blanket will be indicated by a line or zone around the basin where the crater-age distribution becomes continuous. Such determinations, however, may be ambiguous where extensive blankets of volcanic materials are present.

3. Superposition relations of craters so consistently confirm the relative age numbers assigned that any anomaly seems to require a special explanation. One such anomaly, noted by D. E. Wilhelms, is provided by the craters Isidorus and Capella, northeast of Mare Nectaris (fig. 4). The apparent age of Capella is greater than that of Isidorus by 1.5 on the proposed number scale, yet Capella is clearly superposed on Isidorus. Capella and Isidorus apparently had different initial morphologies, and we believe that Capella is a volcanic crater. It is one of a few craters which have "overfit" central peaks and unusually irregular rim morphology. These unusual craters generally occur in groups and most are located in areas of complex structure.

4. Use of the crater-numbering system also offers a possibility of identifying secondary craters associated with some of the younger lunar basins, that is, those craters produced by impact of fragments ejected from the basins or from volcanic vents along basin-radial fractures. Strings or clusters of craters radial to the Orientale basin are dated on our scale as the same rela-

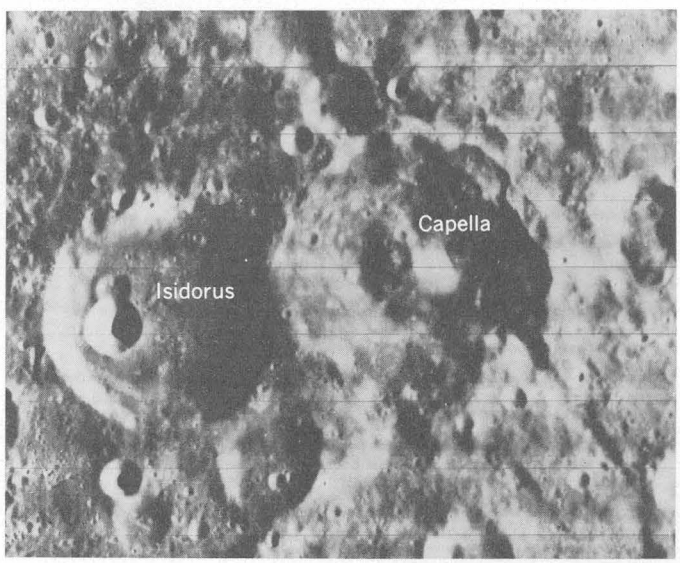

FIGURE 4.—Anomalous crater-age and superposition relationship of Isidorus and Capella. Framelet strip spans about 10 km.

tive age (4.8) as the basin. In addition to these, individual 5- to 15-km craters of this age are uncommonly abundant in a belt around Orientale and almost certainly are secondary craters formed by impact of material ejected from the basin. By applying the numbering system to craters in the central and southern highlands, clusters of 10- to 20-km craters of the same age as the Imbrium basin have been identified; these may well be Imbrium secondary craters.

5. If craters everywhere on the moon are degraded at about the same rate, then assignment of age numbers on the basis of geomorphic stage permits moonwide stratigraphic correlations. This will facilitate refinement of the present moonwide time-stratigraphic sequence.

6. Light (relatively high albedo) terra plains are difficult to date precisely because they typically occur in small areas such as in crater floors: the dates given in figure 1 are generalized to show probable age limits for numerous separate plains areas within broad regions of the moon. Nevertheless, the data (table 1) suggest that terra plains, believed to be generally of volcanic origin, formed all over the moon in a relatively brief period of time; they formed in age interval 4.5 to 5.6 on the proposed number scale, and most are in the age range 4.7–5.2. This period coincides with the emplacement of mare surface units in many areas, although the mare units are mostly younger. It is interesting to compare small-crater frequencies on various light plains and mare surfaces of similar ages. Craters on light plains (age 4.8–5.1) north of Mare Frigoris are an order of magnitude more abundant than on light plains (age 4.9–5.1) in the southern terra or on mare materials of Tranquillitatis (age 4.4–5.0) and Fecunditatis (age 4.8–5.2). That these age differences are too small to explain such crater-abundance variations in terms of impact frequency is indicated by the fact that ejecta blankets around craters of relative ages 4.2 and 4.8 or 4.8 and 5.2 do not show nearly the disparity in crater abundances seen in the compared mare and plains surfaces. From these observations, we believe that most of the craters on the highly cratered plains are probably of endogenetic origin. In addition, comparison of albedos for mare and light plains units of similar ages suggests that the relatively greater brightness of plains is an intrinsic property and that the plains are formed of different materials than the mare units. Although the time involved is not known, the emplacement of so many light plains and mare units in a small interval on the crater evolution scale suggests that this was a relatively short period of widespread volcanic activity on the moon.

SUMMARY

Tests of the proposed crater-numbering system by dating geologic units from the oldest craters superposed on them show that relative ages thus determined consistently agree with known superposition relations of the units. The success of this empirical approach appears to demonstrate that in general the correlation of geomorphic stage with crater age is a valid assumption. Major geologic events and units are assigned relative ages on the basis of the numbering system. Circular mare basins are determined to have formed in the order: Schiller, Nectaris, Serenitatis, Muscoviense, Humorum, Crisium, Imbrium, Orientale. Western mare units are generally younger than eastern mare units, except for relatively young material in Mare Crisium. Plains units are found to be little older than many mare units, and we infer that their greater crater frequency is due to endogenetic processes, and that their higher albedo is a compositional property. Numerous craters not obviously related to the Orientale and Imbrium basins are determined to be of the same age as the basins and are tentatively identified as basin secondary craters. These examples indicate the utility of the proposed system as a relatively precise means of deciphering local geologic relationships and correlating the geology of widespread areas on the moon.

REFERENCES

Eggleton, R. E., 1964, Preliminary geology of the Riphaeus quadrangle of the Moon and definition of the Fra Mauro Formation, *in* Astrogeol. Studies Ann. Progress Rept., Aug. 25, 1962 to July 1, 1963, pt. A: U.S. Geol. Survey open-file report, p. 46–63.

Hartmann, W. K., 1964, Radial structures surrounding lunar basins. II—Orientale and other systems; conclusions: Arizona Univ. Lunar and Planetary Lab. Commun., v. 2, no. 36, p. 175–188.

McCauley, J. F., 1967a, The nature of the lunar surface as determined by systematic geologic mapping, *in* Runcorn, S. K., ed., Mantles of the earth and terrestrial planets: London, John Wiley and Sons, p. 431–460.

——— 1967b, Geologic results from the lunar precursor probes: Am. Inst. Aeronautics and Astronautics Paper 67–862, 8 p.

Milton, D. J., 1968, Geologic map of the Theophilus quadrangle of the Moon: U.S. Geol. Survey Misc. Geol. Inv. Map I–546.

Pohn, H. A., and Offield, T. W., 1970, Lunar crater morphology and relative-age determination of lunar geologic units—Part 1. Classification, *in* Geological Survey Research 1970: U.S. Geol. Survey Prof. Paper 700–C, p. C153–C162.

Shoemaker, E. M., and Hackman, R. J., 1962, Stratigraphic basis for a lunar time scale, *in* Kopal, Zdenek, and Mikhailov, Z. K., eds., The Moon—Internat. Astron. Union Symposium 14, Leningrad 1966, Proc.: London, Academic Press, p. 289–300.

Shoemaker, E. M., Hackman, R. J., and Eggleton, R. E., 1962, Interplanetary correlation of geologic time, *in* Advances in the astronautical sciences, v. 8: New York, Plenum Press, p. 70–89.

Titley, S. R., 1967, Geologic map of the Mare Humorum region of the Moon: U.S. Geol. Survey Misc. Geol. Inv. Map I–495.

Titley, S. R., and Eggleton, R. E., 1964, Description of an extensive hummocky deposit around the Humorum basin, *in* Astrogeol. Studies Ann. Prog. Rept., July 1, 1963 to July 1, 1964, pt. A: U.S. Geol. Survey open-file report, p. 85–89.

U.S. Geological Survey, 1968, Apollo site maps: U.S. Geol. Survey open-file repts.

AGE AND STRATIGRAPHY OF THE HECETA LIMESTONE IN NORTHERN SEA OTTER SOUND, SOUTHEASTERN ALASKA

By A. T. OVENSHINE and G. D. WEBSTER, [1]
Menlo Park, Calif., Pullman, Wash.

Abstract.—The Heceta Limestone in the northern Sea Otter Sound area, Alaska, is more than 10,000 feet thick and contains two major zones of terrigenous clastic rocks. On the basis of sparse conodonts, graptolites, and bachiopods, it is late Early through Late Silurian in age. This new age assessment of the formation requires extension of the range in southeastern Alaska of the stromatoporoid *Amphipora* and the pelecypod *Pycinodesma*, both previously considered no older than Middle Devonian.

The Heceta Limestone (Eberlein and Churkin, 1970) is 10,000 to 16,000 feet thick, consists mainly of limestone and conglomerate, and is widely distributed in the southern parts of southeastern Alaska. The clastic wedge of the Karheen Formation (Eberlein and Churkin, 1970; Ovenshine and others, 1969) above it, and the unconformity below it, record significant early Paleozoic tectonic events; thus it is useful to know the time span represented by the Heceta Limestone. The purpose of this paper is to present paleontological evidence that the limestone is late Early through Late Silurian in age.

Acknowledgments.—The writers identified the conodont elements but wish to acknowledge helpful comments by Gilbert Klapper, of the University of Iowa. Dr. Klapper also advised us on the stratigraphic position of the *amorphognathoides*-Zone fauna. Dr. J. G. Johnson, of Oregon State University, kindly identified brachiopods from Marble Island and suggested their stratigraphic range. Claire Carter and Michael Churkin, Jr., of the U.S. Geological Survey, identified the graptolites found in the Heceta Limestone. The use made of this information is the responsibility of the writers.

HECETA LIMESTONE

Limestone, conglomerate, sandstone, and shale of the Heceta Limestone are well exposed around Sea Otter Sound in the northwest coastal area of Prince of Wales Island, Alaska (fig. 1). The area where we have mapped and studied the formation is indicated by the fossil localities in figure 1; in the southern part of Sea Otter Sound the formation has been investigated by G. D. Eberlein. The contact between the Heceta Limestone and the underlying Descon Formation of Early Ordovician through Early Silurian age (Eberlein and Churkin, 1970) is an angular unconformity at both Cap Island (locality 67AOv1381 in fig. 1) and east of Tokeen Bay (locality 67AWd423 in fig. 1). Basal conglomerates less than 300 feet thick are present at both localities and consist of rounded megaclasts of gray chert, red chert, and limestone from an unknown source, as well as angular fragments of basalt, argillite, and graywacke derived from the underlying Descon Formation. The upper contact of the Heceta Limestone with the Karheen Formation (Eberlein and Churkin, 1970) is conformable where exposed on Kosciusko Island (locality 67AOv1741).

Figure 2 portrays gross lithic aspects of the Heceta Limestone and also shows some of the subdivisions that have been recognized in the geologic mapping of the northern Sea Otter Sound area. About half of the formation is limestone, the most common variety of which is very light gray and finely crystalline. The limestone generally lacks bedding and primary texture. Acetic acid insoluble residues amount to less than 1 percent of sample weight and consist principally of 0.25-mm dolomite rhombs. Fossils other than dasycladacean algae are very rare. That the original nature of much of this limestone may have been a coarse breccia is suggested by the presence of this texture in places such as beneath the water of some tidepools, areas where fires have baked outcrops, and weathered surfaces beneath the roots of recently fallen trees. Strongly contrasting with the light-colored massive limestone is the dark-gray bedded limestone locally present in the for-

[1] Washington State University, Pullman, Wash.

U.S. GEOL. SURVEY PROF. PAPER 700-C, PAGES C170-C174

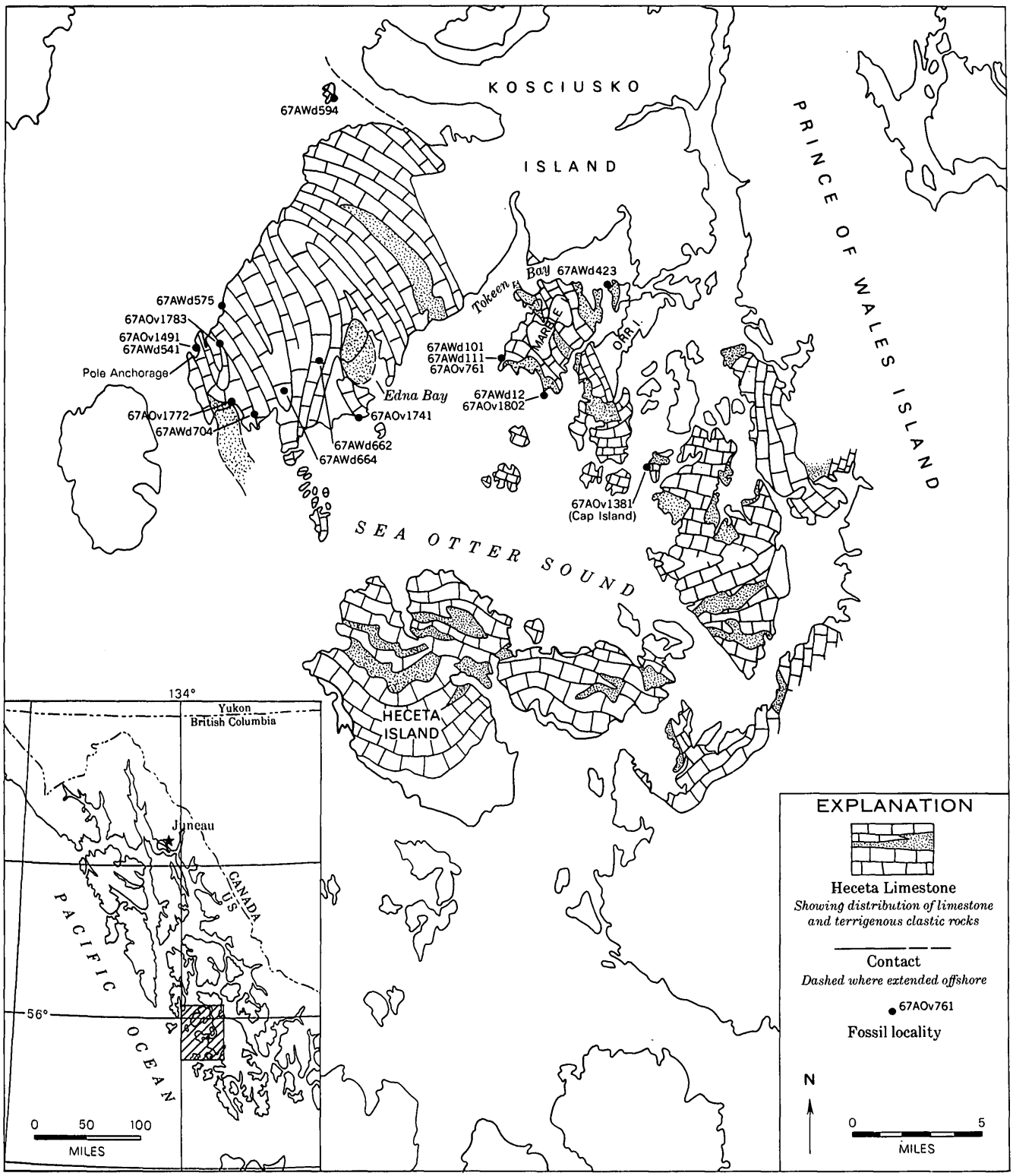

Geology modified from unpublished mapping by G.D. Eberlein, 1947–49; Eberlein and M. Churkin, 1965–66; and A.T. Ovenshine and G. D. Webster, 1967

FIGURE 1.—Distribution of the Heceta Limestone in the Sea Otter Sound area, and locations of fossil collections discussed in this report.

380-189 O - 70 - 12

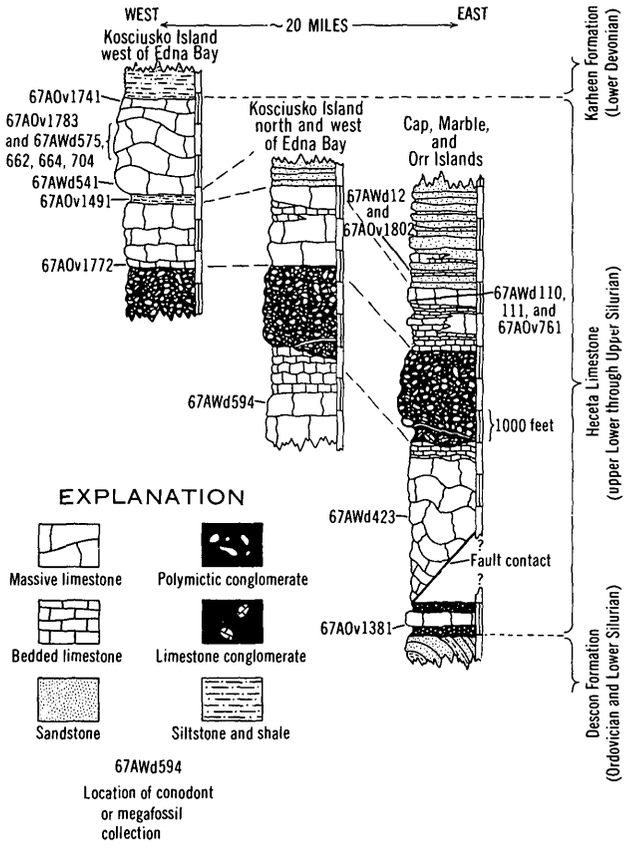

FIGURE 2.—Stratigraphy of the Heceta Limestone in northern Sea Otter Sound, southeastern Alaska.

mation, particularly above or below terrigenous clastic strata. The bedded limestone, which is commonly argillaceous biomicrite and less commonly argillaceous biopelmicrite, in places contains abundant stromatoporoids, corals, and gastropods and less commonly brachiopods, pelecypods, crinoids, and conodonts. The bedded limestone yields insoluble residues that may amount to several percent of sample weight and consist chiefly of carbonaceous matter, pyrite, and dolomite. Rare limestone varieties in bedded zones are crinoidal, pelletoidal, and oolitic limestones and roundstone and edgewise conglomerate.

In the northern Sea Otter Sound area there are two thick zones of terrigenous clastic rocks within the Heceta Limestone. The lower zone, which is about 2,500 feet thick, is dominantly coarse conglomerate in which the subrounded pebble- to boulder-sized megaclasts of andesite, red and gray chert, limestone, and graywacke greatly predominate over pebbles of gabbroic to granitic plutonic rock and milky quartz. The megaclast fraction is moderately closely packed and moderately sorted so that bedding is well expressed; the matrix is calcareous lithic graywacke. The base of the lower clastic zone on Marble and Orr Islands and the eastern part of Kosciusko Island is a disconformity overlain by 50 to 300 feet of monomictic conglomerate consisting of rounded limestone megaclasts closely packed in a tan limestone matrix.

The upper clastic zone is well exposed at the south end of Marble Island where it consists of more than 3,000 feet of lithic graywacke (shown by sandstone pattern in fig. 2) and minor argillaceous limestone. This graywacke unit thins westward rapidly; on western Kosciusko Island (near locality 67AOv1491) it is represented by only a few hundred feet of black shale and arenaceous limestone. The lower contact of the graywacke is gradational with the underlying limestone on Marble Island.

PALEONTOLOGIC DATA

Conodonts

Limestone samples averaging 0.8 kilogram in weight were digested in 10-percent acetic acid; the heavy portions of the residues were isolated by 2.85-bromoform separation and searched for conodonts. Approximately two-thirds of the 100 samples yielded from one to five specimens, but most contained only distacodontid conodont elements. Fifteen samples yielded compound conodonts, and for these, locality numbers and forms identified are listed in table 1. Localities of conodonts and other fossils are also shown on the map in figure 1 and on the stratigraphic sections of figure 2. Of the 15 compound conodont faunas, 3 contains from 25 to 200 specimens. These three are discussed in the following paragraphs.

Sample 67AOv1381 is from the base of the Heceta Limestone on Cap Island and contains the zone fossil and other elements of the *Pterosphathodus amorphognathoides* Zone recognized in the Silurian of Europe by Walliser (1964). Walliser regarded the *P. amorphognathoides* Zone as of late Llandoverian and early Wenlockin age. Gilbert Klapper (oral commun., 1968) believes that the *P. amorphognathoides* Zone is entirely within the late Llandoverian. Accepting Klapper's age assessment, we consider the base of the Heceta Limestone on Cap Island to be of late Early Silurian age. Eberlein and Churkin (1970) report graptolites of late Early or early Middle Silurian age 1,500 feet below the base of the Heceta in its type area. They correlated the base of the Heceta approximately with the Lower-Middle Silurian boundary.

Samples 67AWd111 and 67AWd101 are from limestone within the middle part of the Heceta and yield conodont species, most of which have known ranges from Silurian to early Devonian (Walliser, 1964, table 1). The presence of *Polygnathoides emarginatus*, which

TABLE 1.—*Conodonts from the Heceta Limestone*

Conodont	Locality number															Age
	67AWd12	67AWd101	67AWd111	67AWd423	67AWd541	67AWd575	67AWd594	67AWd662	67AWd664	67AWd704	67AOv1381	67AOv1491	67AOv1741	67AOv1772	67AOv1783	
Belodella resima						X		X	X				X			Ludlow (Upper Silurian)
triangularis								X								
Hindeodella equidentata	X		X				X		X	X				X		
? *Lonchodina* sp					X								X			
Neoprioniodus excavata					X		X		X					X		
Ozarkodina sp. aff. *edilhae*									X					X		
media	X		X	X			X		X							
Plectospathodus extensus	X		X		X				X							
Polygnathoides emargina		X														
Spathognathodus inclinatus	X		X	X					X			X		X		
Trichonodella excavata			X	X					X							
T. sp. aff. *inconstans*					X										X	
Neoprioniodus planus											X					*Amorphognathoides* Zone (Uppermost Lower Silurian)
Ozarkodina sp. aff. *gaertneri*											X					
Pterospathodus amorphognathoides											X					
Roundya trichonodelloides											X					
Scolopodus sp											X					
Trichonodella brassfieldensis											X					

in Europe is found only in the upper *crassa* to *siluricus* Zones (Walliser, 1964, p. 66), implies a lower to middle Ludlow age. The samples are from the same beds that yielded the brachiopod fauna discussed later under locality 67AOv761.

Sample 67AWd664 is from massive limestone approximately 1,500 feet below the red and green shales which are stratigraphically above the Heceta Limestone in the Kosciusko Island area. Conodont species from this sample all have known ranges from Late Silurian to Early Devonian (Walliser, 1964, table 1). The composition and general aspect of the conodont fauna, however, suggest a correlation with conodonts from the Ludlovian Aymestry Limestone of England (Rhodes, 1953). In particular, *Spathognathodus inclinatus* (sensu Rhodes non Walliser) shows close correspondence. Moreover, lacking are typical Lower Devonian conodont elements like those recovered from the overlying Karheen Formation. For these reasons, the horizon of 67AWd664 is considered as late Silurian in age, equivalent to that of the Aymestry Limestone.

Graptolites

Graptolites have been found in dark-gray silty limestone at two places at approximately the same stratigraphic position within the Heceta Limestone. Approximately 30 specimens were found at locality 67AOv1491 at Pole Anchorage on western Kosciusko Island, and 2 specimens were found at locality 67AOv1802 on a small island near the south end of Marble Island. These graptolites have been examined by Michael Churkin, Jr., and Claire Carter, of the U.S. Geological Survey, who state (oral commun., 1968) that the graptolites are *Monograptus* sp. indet. Churkin and Carter note that all the poorly preserved specimens probably represent a single species of a small monograptid with straight, simple thecae. But because of the poor preservation of the graptolites and because of the difficulty in assigning a precise age on the basis of a single monograptid species, refinement in age beyond Late Silurian is unwarranted.

Brachiopods

An abundant, well-preserved brachiopod fauna (67AOv761) found in dark-gray limestone a few hundred feet stratigraphically below the *Monograptus* sp. horizon on Marble Island has been examined by J. G. Johnson, of Oregon State University. Johnson (written commun., June 25, 1968) identifies:

Atrypella sp. (lenticular)
Atrypella carinata
Gracianella sp. aff. *umbra*
Hedeina sp. aff. *balchaschensis*
Rhynchotrema? sp.

Johnson states:

> All of these brachiopods except the questionable *Rhynchotrema* occur in the Ludlow interval of the Roberts Mountains Formation in the Roberts Mountains in beds that are well dated by the brachiopods, conodonts, and graptolites. However, I can't say for sure what part of the Ludlow is indicated.

The brachiopods of locality 67AOv761 are from the same beds that yielded the Ludlow-age conodont fauna of samples 67AWd111 and 67AWd101.

AGE OF THE HECETA LIMESTONE

The *amorphognathoides*-Zone conodont fauna from near the base of the Heceta Limestone (67AOv1381) on

Cap Island indicates the onset of limestone deposition no later than late Early Silurian time. Ludlow-age brachiopods and conodonts beneath the upper clastic zone and the graptolites from the basal part of the clastic zone indicate that the lower approximately 9,000 feet of the formation is no younger than Late Silurian. The uppermost important conodant fauna (67AWd-664), which comes from a horizon no more than 1,500 feet below the top of the formation, also suggests a Silurian age at least as high as this stratigraphic level. Thus, only the upper 1,500 feet of the formation could contain deposits of Devonian age. In the Heceta-Tuxekan Islands area, the lowest known Devonian fossils are approximately 1,400 feet above the base of the overlying Karheen Formation (Eberlein and Churkin, 1970), or approximately 3,000 feet above the horizon of 67AWd664.

RANGES OF AMPHIPORA AND PYCINODESMA

The consistent results provided by the study of conodonts, graptolites, and brachiopods are not mirrored in the results obtained from other fossil groups. In particular, corals, stromatoporoids, and mollusks, the more common fossils in the Heceta Limestone, have yielded inconclusive or conflicting results. Two that have been most vexing are discussed in the following paragraphs.

The small, tubelike stromatoporoid *Amphipora* and the large, thick-shelled pelecypod *Pycinodesma* are locally abundant in bedded limestone throughout the Heceta. Both have been used as guide fossils to the Middle or early Late Devonian in southeastern Alaska and elsewhere (Loney and others, 1963, p. C17).

Amphipora has been recognized in Devonian rocks in Europe and North America, and in southeastern Alaska it has been found in the Kennel Creek Limestone of Freshwater Bay, Chicagof Island, by Loney, Condon, and Dutro (1963, p. C17). These writers note:

> *Amphipora* is extremely common in rocks of Middle and early Late Devonian age throughout the Western United States, Canada, and in other parts of Alaska. This stromatoporoid genus has been recorded from the Silurian of Russia, but the faunal evidence supporting this age assignment is either absent or inconclusive.

Amphipora occurs in the Heceta Limestone at many places below the upper clastic zone; thus its range into the Silurian should be accepted for southeastern Alaska.

Kirk's (1927) assignment of a Late Silurian age to *Pycinodesma* was questioned by Loney, Condon, and Dutro (1963, p. C17). Eberlein and Churkin (1970) noted that *Pycinodesma* is present in the upper part of the Heceta Limestone and also in the Devonian Wadleigh Limestone. We have found *Pycinodesma* in association with *Amphipora* and the brachiopod *Conchidium* in parts of the Heceta Limestone well below the upper clastic zone. Thus, the range of *Pycinodesma* into the Silurian, as Kirk originally suggested, should also be accepted.

SUMMARY

On the basis of sparse conodonts, graptolites, and brachiopods, the Heceta Limestone is largely of late Early through Late Silurian age. Although the uppermost 1,500 feet of the formation could be of Devonian age, there is no reliable fossil evidence that it is. The southeast Alaska ranges of *Amphipora* and *Pycinodesma* should be extended into the Silurian.

REFERENCES

Eberlein, G. D., and Churkin, Michael, Jr., 1970, Paleozoic stratigraphy in the northwest coastal area of Prince of Wales Island, southeastern Alaska: U.S. Geol. Survey Bull. 1284 [In press].

Kirk, Edwin, 1927, *Pycnodesma*, a new molluscan genus from the Silurian of Alaska: U.S. Natl. Mus. Proc., v. 7, art. 20, p. 1–9.

Loney, R. A., Condon, W. H., and Dutro, J. T., Jr., 1963, Geology of the Freshwater Bay area, Chichagof Island, Alaska: U.S. Geol. Survey Bull. 1108–C, p. C1–C54.

Ovenshine, A. T., Eberlein, G. D., and Churkin, Michael, Jr., 1969, Paleotectonic significance of a Silurian-Devonian clastic wedge, southeastern Alaska [abs.]: Geol. Soc. America, Cordilleran Sec. Ann. Mtg. Program. Eugene, Oreg., 1969, pt. 3, p. 51.

Rhodes, F. H. T., 1953, Some British lower Paleozoic conodont faunas: Royal Soc. London Philos. Trans. ser. B, no. 647, v. 237, p. 261–334.

Walliser, O. H., 1964, Conodonten des Silurs: Hesse Landesamt Bondenforschung, Abh., no. 41, 106.

THE HONDO SANDSTONE MEMBER OF THE SAN ANDRES LIMESTONE OF SOUTH-CENTRAL NEW MEXICO

By ROBERT L. HARBOUR,[1] Denver, Colo.

Abstract.—The Glorieta Sandstone and the Hondo Sandstone Member of the San Andres Limestone are separate stratigraphic units in the Permian sequence in south-central New Mexico. The Glorieta Sandstone wedges out toward the south and southeast; whereas the Hondo, stratigraphically above the Glorieta, thickens toward the southeast. It is possible that the Glorieta and Hondo merge into one body of sandstone toward the north, but proof of this is lacking from the area of study. Although additional studies of grain size, mineralogy, and structural features are needed to determine the environment of deposition and means of transportation of these clastic sediments, the present study does resolve some basic correlation problems.

Along the Rio Hondo, south-central New Mexico, two similar Permian sandstone units are present: (1) the Glorieta Sandstone which separates the Yeso Formation from the overlying San Andres Limestone, and (2) the thicker Hondo Sandstone Member of the San Andres Limestone. These are separate stratigraphic units. In many areas outside the present study area only one or the other of these units is present.

Inasmuch as the Hondo Sandstone Member is a distinctive lithologic unit along the Rio Hondo, its relationship to the Glorieta Sandstone of northern New Mexico has been discussed. Nye (in Fieldler and Nye, 1933, p. 55–60) measured and described the Permian sandstone units 3.9 miles east of Picacho on the Rio Hondo and stated that geologists were in disagreement as to which of the two units was the Glorieta Sandstone and that it was not at all improbable that these two sandstones were lenticular and possibly represented a sandstone zone rather than continuous stratigraphic units. The upper and more conspicuous sandstone unit was named the Hondo Sandstone Member of the Chupadera Formation by Lang (1937, p. 850), who designated its type locality as "the Hondo and its tributaries" and expressed doubt as to its correlation with the Glorieta. In 1940, King abandoned the name Chupadera and raised the San Andres to formation rank. The Hondo was changed then to a member of the San Andres. In a review of type sections of some Permian formations in southern New Mexico, Needham and Bates (1943, p. 1664) considered the Glorieta to be "identical to the Hondo sandstone of Lang." Sandstone near the base of the San Andres in the southern Sacramento Mountains was correlated with the Glorieta by Skinner (1946, p. 1863), and sandstone layers along the crest of the Sacramento Mountains were tentatively correlated with the Hondo by Pray (1954, p. 101–102; 1961, p. 115).

In an effort to establish the relationship between the Hondo and Glorieta, the author examined their stratigraphic interval within the area shown by the stippled pattern in figure 1. In the southeast part of the report

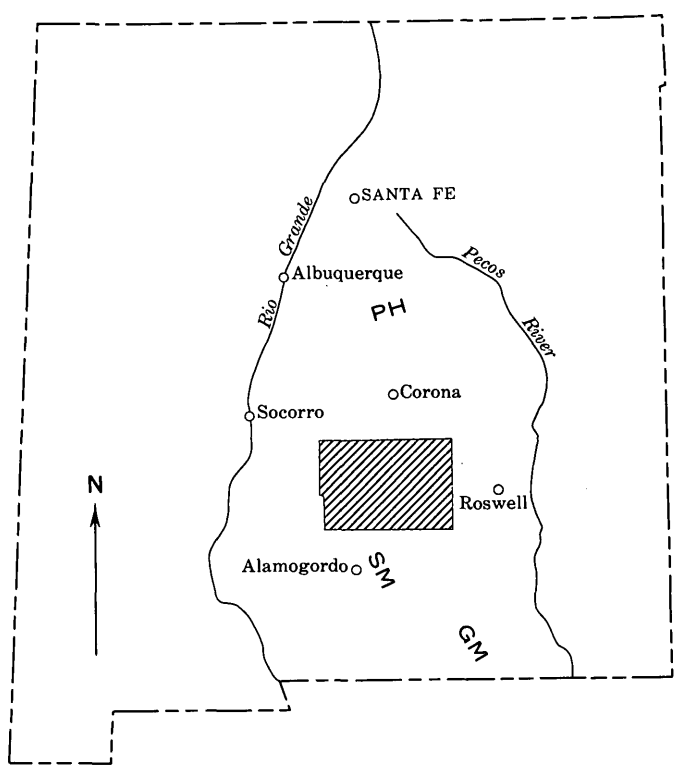

FIGURE 1.—Index map of New Mexico, showing location of map on figure 2 (stippled), PH, Pedernal Hills; SM, Sacramento Mountains; GM, Guadalupe Mountains.

[1] Deceased November 10, 1966.

area is Rio Hondo, the type locality of the Hondo Sandstone Member; in the northwest is the southern part of Chupadera Mesa, where the Glorieta was mapped and described in detail by Wilpolt and Wanek (1951). Between Rio Hondo and Chupadera Mesa, the interval is intermittently exposed by structural deformation on the flanks of Sierra Blanca, the Capitan Mountains, and the Jicarilla Mountains. The author measured stratigraphic sections through the upper part of the Yeso Formation and the lower part of the San Andres Limestone at the localities described in table 1 and shown on the map in figure 2 to determine the distribution of the Hondo and Glorieta.

A comparison of the stratigraphic sections indicates that the Hondo and Glorieta are not equivalents. The Hondo occupies a slightly higher stratigraphic position than the Glorieta of Chupadera Mesa, and the lower sandstone unit in Rio Hondo is apparently the Glorieta equivalent.

DESCRIPTION OF THE ROCKS

The measured sections *A–A′*, *B–B′*, and *C–C′* (fig. 2) show the gross lithology of the stratigraphic interval in the report area. Both the Yeso and the San Andres Formations are largely composed of limestone, dolomite, and gypsum of such uniform appearance that the clastic rocks, the siltstone and sandstone, serve as the best stratigraphic markers and permit identification of lithologic units.

Although all gradations of limestone and dolomite apparently occur in the Yeso and San Andres, pure varieties of either are sparse; the carbonates are fine grained and so similar in appearance that acid must be used to differentiate the varieties. Color is confined to a narrow range of grays; texture is almost invariably very fine grained but not aphanitic. Bedding ranges from thin to medium in both formations, and a few of the limestone or dolomite beds are laminated. All the carbonate rocks yield black clay upon solution despite

TABLE 1.—*Location of stratigraphic sections*

[Sections shown on figure 2]

No. (fig. 2) and name	Sec.	T. (S.)	R. (E.)	Description of locality
1. Chupadera Mesa	8	6	7	Hillside scar.
2. West of The Malpais	15	7	9	Upper 123 feet; hillside near center of section.
	14, 15	7	9	Lower 173 feet; hillside near quarter corner of sections.
3. Lone Mountain	SE¼SE¼ 22	6	11	Upper 140 feet, canyon wall.
	NE¼SW¼ 22	6	11	Lower 75 feet, canyon bottom.
4. North of Patos Mountain	SW¼ 2	6	13	Roadcut.
5. Block Ranch	1	7	15	Upper 100 feet, east wall of Arroyo del Macho.
	NW¼ 7	7	16	Lower 228 feet, Twin peaks.
6. Pine Lodge	NW¼ 11	8	17	Roadcut.
7. Bluewater Creek	NE¼ 8	9	18	East wall of canyon.
8. Blackwater Creek	SW¼ 29	9	19	South wall of canyon.
9. Riverside	SW¼ 21	11	19	Do.
10. Crockett Ranch	6	8	9	Hillside.
11. Phillips Hills	8	10	8	Northwestern part.
12. Rinconada Canyon	NE¼SE¼ 8	13	10	North side of canyon.
13. ----do	NW¼SW¼ 9	13	10	Do.
14. ----do	SE¼SW¼ 3	13	10	South wall of canyon.
15. ----do	NW¼NW¼ 7	13	11	Do.
16. Dry Canyon		12	11	Hillside north of canyon, a fourth of a mile southeast of triangulation station VABM 6611 in unsurveyed township.
17. Mescalero	SW¼NE¼ 27	13	12	Hillside.
18. Ruidoso	26	11	13	North side of Rio Ruidoso near center of section.
19. Fox Cave	NW¼ 7	11	15	Upper 125 feet, Fox Cave.
	NW¼ 7	11	15	Lower 45 feet, U.S. Highway 70 roadcut a fourth of a mile southwest of Fox Cave.
20. Little Creek	SW¼ 16	10	15	North wall of canyon.
21. Rio Bonito	SW¼ 15	9	15	Canyon.
22. Salazar Canyon	12	9	15	North wall, near center of section.
23. Pfingston Orchards	SE¼ 2	10	16	North wall of Rio Bonito Canyon.
24. Tinnie	NW¼ 12	11	17	North side of U.S. Highway 70.

absence of shale or claystone beds, but they yield very little sand even where they are in contact with sandstone. Gray aphanitic chert occurs as partially replaced lenses and fossils in carbonate beds of the Yeso Formation and is rather common at the base of the San Andres in the limestone that normally separates the Glorieta and Hondo.

Beds of white granular gypsum form much of the Yeso and San Andres Formations, especially in the western part of the area. Lateral gradation of gypsum to carbonate (usually dolomite or dolomitic limestone) occurs in both formations.

Siltstone is confined to the Yeso and contributes the diagnostic salmon-pink color of that formation. The siltstone is in thick, unlaminated beds which, though homogeneous, are poorly sorted. The grains, some of which are rounded and frosted, are mostly clear quartz, but a few are feldspar, tourmaline, zircon, and muscovite. Although grains as large as fine sand are abundant, most of the particles are smaller than 0.062 mm, the upper limit of the silt range. Very little clay is present, and the salmon-pink color is due to iron-oxide staining of the grains. The siltstone is very poorly cemented by gypsum and calcite, and it erodes more easily than the gypsum which is interbedded with it.

Sandstone is confined to the Glorieta Sandstone and to the Hondo Member of the San Andres. Both units are evenly bedded and have some small-scale cross-lamination; their color is gray with yellow iron staining. The Hondo Sandstone Member is slightly coarser grained than the Glorieta at most localities, and measurements from several specimens gave the following estimates of grain size:

	Average medium grain size (mm)	*Average maximum grain size (mm)*
Hondo Sandstone Member.	0. 25 (finely medium)	0. 60 (finely coarse)
Glorieta Sandstone----	0. 15 (fine)	0. 40 (medium)

No lateral gradation of grain size in the area is apparent in either unit. The Hondo consists of clear quartz grains and very sparse fragments of rose quartz, smoky quartz, and an undetermined pink mineral aggregate. The Glorieta contains some material of silt size and, as in the underlying Yeso siltstone, some detrital feldspar in the silt size range. Rounding and frosting of grains in both units are typical, and secondary crystal enlargements are common. The quartz grains of both units are mostly clear—free from strain shadows—and contain similar mineral inclusions. In summary, the Hondo is slightly coarser grained than the Glorieta, but the two units are composed of very similar material.

Conspicuous yellow layers of edgewise breccia, which is composed of limestone fragments set in a matrix of earthy lime, clay, and limonite, are common in the San Andres, especially in the Rio Hondo area. Despite persistence of these breccias at confined stratigraphic horizons over large areas, the author believes that the breccias are cave deposits due to solution and refill after deposition, and, as a result, shows them on the stratigraphic sections as sandy solution breccia or solution breccia horizon. One such deposit in Rinconada Canyon is largely composed of the Hondo Sandstone Member, along which solution took place, but it contains some limestone fragments which were derived from the overlying thin-bedded limestone. The limestone has a distinctive aphanitic texture and a dark-gray color. The brecciation in the limestone is confined along a small fault, and the limestone fragments in the Hondo persist for many feet in the canyon walls.

OBSERVATIONS IN LOCAL AREAS

Poor exposures prevent bed-by-bed correlation in the upper part of the Yeso Formation; the measured sections (fig. 2), however, permit two generalizations. The clastic (siltstone) content of the Yeso increases northward in the report area, and the ratio of evaporites to carbonates increases westward. At Rinconada Canyon in the southwestern part of the area (loc. 12), gypsum constitutes more than half of the upper 200 feet of the formation, and very thin beds of limestone or dolomite are present. At Chupadera Mesa in the northwestern part (loc. 1), siltstone dominates the same interval, and two thin beds of limestone are present. To the east in the northern foothills of the Capitan Mountains and in Rio Hondo valley, the Yeso contains several thick limestone beds and in its upper part gypsum as a minor constituent.

The Glorieta Sandstone forms a southward-thinning wedge in the area. In the western part of the area, the Glorieta is 48 feet thick at Chupadera Mesa (loc. 1), but southward in the Tularosa Valley it pinches out between the Phillips Hills (loc. 11) and Rinconada Canyon (loc. 12). Eastward from Chupadera Mesa, the Glorieta is about 50 feet thick in the Jicarilla Mountains area (locs. 3 and 4) and thins to 4 feet at the Block Ranch headquarters north of the Capitan Mountains (loc. 5). In the Rio Hondo valley area, the Glorieta equivalent is but a featheredge, and it is no longer recognizable near Fox Cave on the Rio Ruidoso (loc. 19).

A cliff-forming unit of massive dark-gray limestone, which commonly contains chert and poorly preserved megafossils, separates the Glorieta and Hondo at most localities in the area. This unit thickens southward and ranges from 23 feet at Lone Mountain (loc. 3) to 80 feet in the Ruidoso area. The limestone is spectacularly displayed at Fox Cave (loc. 19) on U.S. Highway 70. 10

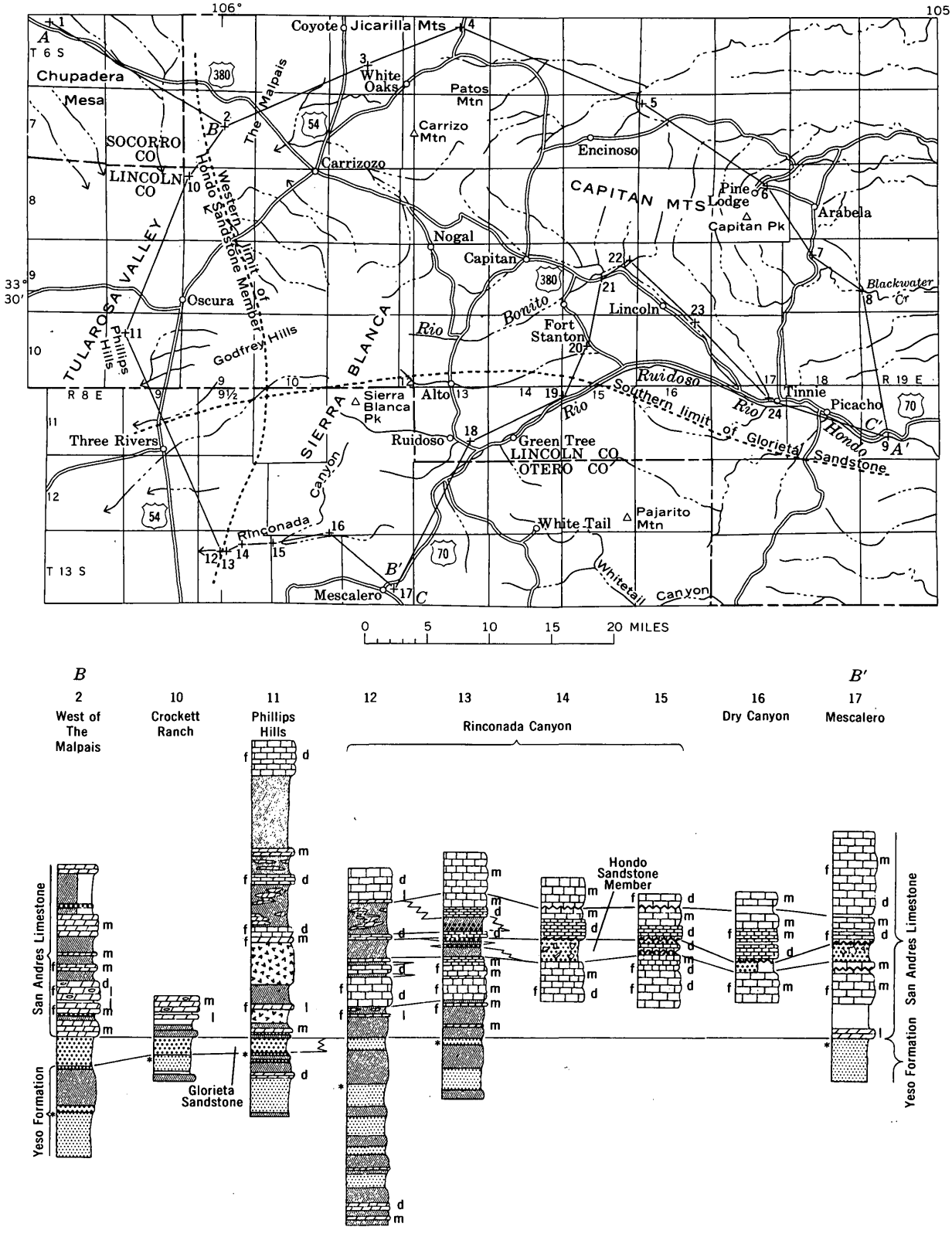

FIGURE 2.—Measured stratigraphic sections of the Hondo Sandstone Member and map showing their locations, which are described in table 1.

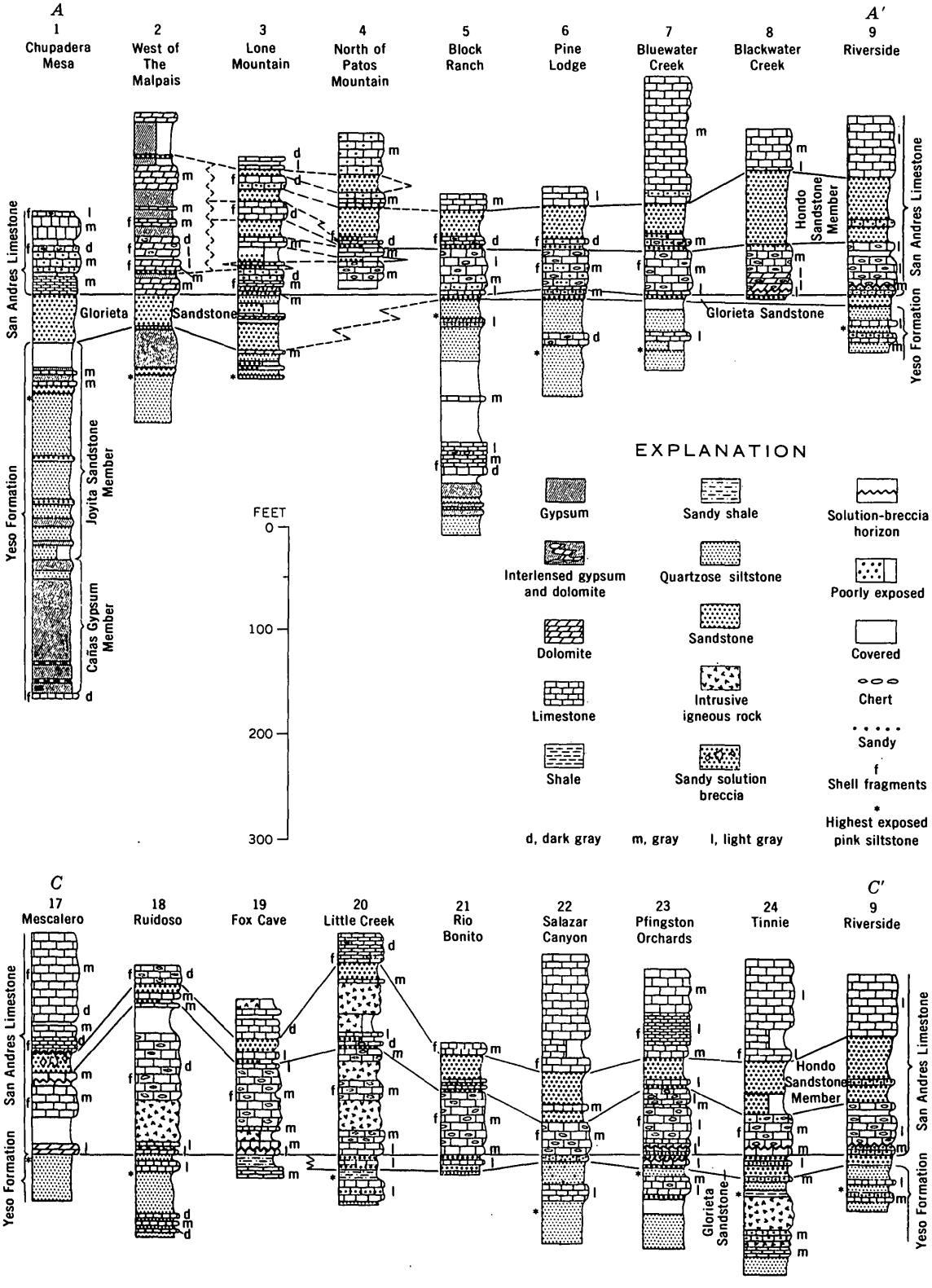
A
A'
1 Chupadera Mesa
2 West of The Malpais
3 Lone Mountain
4 North of Patos Mountain
5 Block Ranch
6 Pine Lodge
7 Bluewater Creek
8 Blackwater Creek
9 Riverside
San Andres Limestone
Yeso Formation
Glorieta
Sandstone
Glorieta Sandstone
Hondo Sandstone Member
Joyita Sandstone Member
Cañas Gypsum Member
FEET
0
100
200
300
EXPLANATION
Gypsum
Interlensed gypsum and dolomite
Dolomite
Limestone
Shale
Sandy shale
Quartzose siltstone
Sandstone
Intrusive igneous rock
Sandy solution breccia
Solution-breccia horizon
Poorly exposed
Covered
Chert
Sandy
Shell fragments
Highest exposed pink siltstone
d, dark gray
m, gray
l, light gray
C
C'
17 Mescalero
18 Ruidoso
19 Fox Cave
20 Little Creek
21 Rio Bonito
22 Salazar Canyon
23 Pfingston Orchards
24 Tinnie
9 Riverside

FIGURE 2.—(CON.)

miles east of Ruidoso. South of the Glorieta pinchout, the limestone unit rests directly on siltstone of the Yeso Formation; and in Rinconada Canyon, part of it grades laterally into gypsum (locs. 12–15). Partially silicified remnants of tightly coiled gastropods and of productid brachiopods are characteristic of the unit.

The Hondo Sandstone Member, though separated from the Glorieta by only a few feet of limestone, shows a very different distribution: the Hondo is thickest in the eastern part of the area and pinches out to the west in the vicinity of the Tularosa Valley. The maximum thickness of the Hondo (69 feet) was measured in Blackwater creek (loc. 8). Throughout the Rio Hondo valley, the Hondo Sandstone Member thins progressively westward toward Sierra Blanca, and the pinchout is well displayed in the lower part of Rinconada Canyon (locs. 12–15). The Hondo thins irregularly northwestward from Rio Hondo, but, in the Jicarilla Mountains area (locs. 3 and 4), several sandstone beds lie above the Glorieta, and distinguishing between the Glorieta and the Hondo is difficult. Westward from the Jicarilla Mountains, the Hondo pinches out in the vicinity of The Malpais as shown in sections measured at localities 1, 2, and 3.

The western limit of the Hondo, shown on the map in figure 2, corresponds very closely to a lateral change in the basal part of the San Andres from a limestone facies on the east to an evaporitic facies on the west. The eastern limestone facies, with which the Hondo is interbedded, consists of even, widespread beds of limestone. The western evaporitic facies consists of complexly intergrading gypsum and carbonate, which indicate that environment in the San Andres Sea must have hovered between conditions favorable to gypsum deposition and those favorable to carbonate deposition. The transition from the eastern limestone facies at Lone Mountain (loc. 3) to the western evaporitic facies at locality 2 is so complete that no beds, with exception of those of the Glorieta, can be correlated with assurance between the two localities. Although this relationship suggests existence of a barrier such as a land mass or reef between the two localities, the lateral gradation of the limestone facies into the evaporitic facies, as well as the westward pinchout of the Hondo into the western evaporatic facies, can be observed in Rinconada Canyon where the Hondo passes westward into sandy gypsum and disappears and the enclosing limestone is replaced westward by gypsum (locs. 12–15, fig. 2).

SEDIMENTARY ENVIRONMENT

The Yeso, Glorieta, and San Andres Formations, and overlying red beds of the Artesia Group apparently were deposited in a single marine cycle by a sea which advanced northward, then retreated southward across the area. In such a cycle, the Yeso might represent the transgressive clastic deposits, the San Andres the offshore lime muds, and the overlying red beds the near-shore regressive deposits. However, the Glorieta Sandstone, coarser than the underlying clastic rocks of the Yeso, does not easily fit such a concept. If the Glorieta resulted from an uplift in source areas to the north, then it only coincidentally marked the end of siltstone deposition (Yeso), and beginning of lime deposition (San Andres).

Source of the sand deposits must have been to the north in the vicinity of the New Mexico–Colorado boundary where the Yeso and San Andres shoal against an older land surface. Island monadnocks of granitic and associated rocks existed at the Pedernal arch in Torrance County (Pedernal Hills, fig. 1), but absence of arkosic detritus in the onlapping Yeso and San Andres Formations there indicates that little, if any, sediment was furnished by these hills. However, the westward pinchout of the Hondo Sandstone Member and the westward transition from carbonate to gypsum in the basal part of the San Andres in this area may be due to vagaries in currents flowing from the northern source area past these Permian islands.

The interval between the Glorieta and Hondo thins northward in the report area, and the two units probably merge to the north. It seems rather unlikely that disconnected lenses of sand, sandwiched conformably between carbonates, could have been deposited far from their source. After further study, the Hondo may be best classified as an upper tongue of the Glorieta Sandstone, but until this relationship is demonstrated, the Hondo is retained as a member of the San Andres Limestone.

CONCLUSION

In absence of diagnostic fossils, direct tracing of the sandstone beds appears to be the best means of correlation in the Permian of the northwest shelf. Distribution of the sandstone beds in this area, shown in figure 3, may aid in selecting the contact between the Yeso and San Andres Formations in the Sacramento Mountains and Guadalupe Mountains to the south, as well as the region around Corona, N. Mex., to the north. The Glorieta pinches out southward in the report area, and sandstone units near the base of the San Andres to the south probably correlate with the Hondo. In the Sacramento Mountains, limestone just beneath the Hondo is more naturally classified as San Andres than Yeso, or Glorieta, because equivalents of this limestone overlie the Glorieta at Chupadera Mesa. Farther south in the Guadalupe Mountains, no sandstone is present, but because of relations in the report area the Yeso–

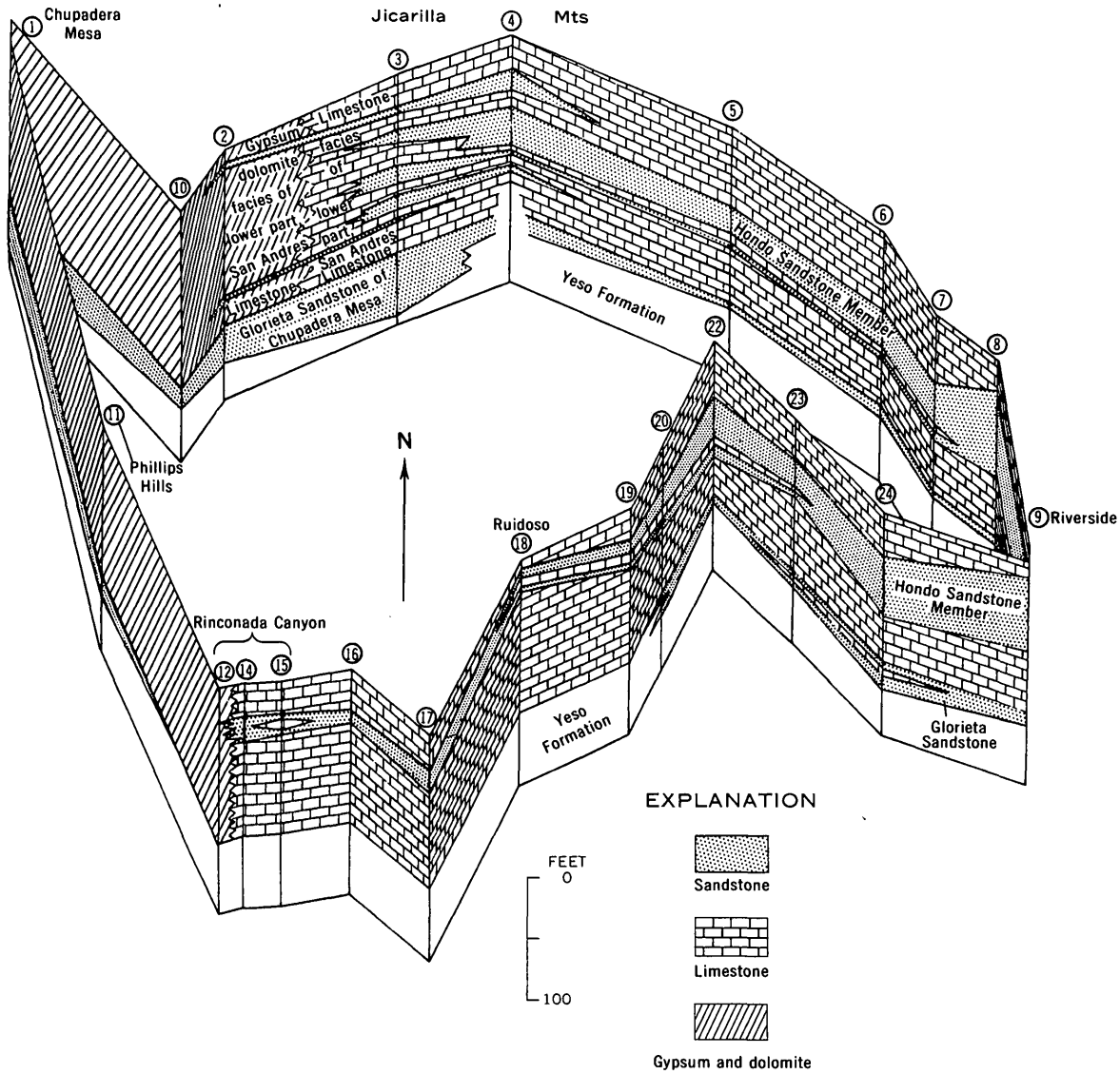

FIGURE 3.—Inferred distribution of Hondo Sandstone Member of San Andres Limestone and Glorieta Sandstone. Location of numbered localities is shown on figure 2.

San Andres contact has been placed at the top of the highest siltstone or gypsum beneath the scarp-forming limestone of the San Andres (Hayes, 1964, p. 23, 24). North of the report area in the vicinity of Corona, separation of Glorieta and San Andres is complicated by complex interfingering of limestone and sandstone, which may have been caused by proximity to the island masses of the Pedernal arch. Eventual classification of the rock units there will probably require careful mapping and measurement of individual limestone and sandstone beds on the theory that the sandstone beds, presumably derived from a source far to the north, eventually merge into the main body of the Glorieta in that direction.

The aspects of the Yeso, Glorieta, and San Andres rocks suggest peculiar conditions of sedimentation. Fairly strong currents would be required to carry sand grains far from their source, yet the Glorieta and Hondo are interbedded with limestone and show no evidence of scour and very little intermixing of sand and lime. The siltstone beds, which are invariably associated with evaporites, are almost clay free and are of a distinctive salmon-pink color. Future investigation of these problems should include careful analysis of grain size in the clastic sediments, and study of prevailing attitudes of crossbedding to determine direction of currents and the source of the clastic sediments.

REFERENCES

Fiedler, A. G., and Nye, S. S., 1933, Geology and ground-water resources of the Roswell artesian basin, New Mexico: U.S. Geol. Survey Water-Supply Paper 639, 372 p.

Hayes, P. T., 1964, Geology of the Guadalupe Mountains, New Mexico: U.S. Geol. Survey Prof. Paper 446, 69 p.

King, P. B., 1940, Permian of west Texas and New Mexico, pt. 2 *of* DeFord and Lloyd, eds., West Texas–New Mexico symposium: Am. Assoc. Petroleum Geologists Bull., v. 26, no. 4, p. 535–763.

Lang, W. T. B., 1937, The Permian formations of the Pecos valley of New Mexico and Texas: Am. Assoc. Petroleum Geologists Bull., v. 21, no. 7, p. 833–898.

Needham, C. E., and Bates, R. L., 1943, Permian type sections in central New Mexico: Geol. Soc. America Bull., v. 54, no. 11, p. 1653–1667.

Pray, L. C., 1954, Outline of the stratigraphy and structure of the Sacramento Mountains escarpment, *in* New Mexico Geol. Soc. Guidebook, 5th Field Conf., Southeastern New Mexico: p. 92–107.

———1961, Geology of the Sacramento Mountains escarpment, Otero County, New Mexico: New Mexico Bur. Mines and Mineral Resources Bull. 35, 144 p.

Skinner, J. W., 1946, Correlation of Permian of west Texas and southeast New Mexico: Am. Assoc. Petroleum Geologists Bull., v. 30, no. 11, p. 1857–1874.

Wilpolt, R. H., and Wanek, A. A., 1951, Geology of the region from Socorro and San Antonio east to Chupadera Mesa, Socorro County, New Mexico: U.S. Geol. Survey Oil and Gas Inv. Map OM–121.

A MICROPROCEDURE FOR THE DETERMINATION OF CARBON DIOXIDE IN MINERALS

By ROBERT MEYROWITZ, Washington, D.C.

Abstract.—Carbon dioxide in minerals is determined after hydrochloric acid decomposition by a gravimetric microprocedure using a modified Schroedter alkalimeter as reaction flask. The carbon dioxide after purification is absorbed in a tube containing Ascarite (sodium hydroxide on asbestos).

Many of the mineral samples received by the analytical laboratories of the U.S. Geological Survey are too small (100–1,000 mg) for complete analysis by macroprocedures. This paper describes a microprocedure for the gravimetric determination of carbon dioxide by acid decomposition which has proved to be useful in the analysis of minerals containing carbonate (Meyrowitz and others, 1963, 1964). The apparatus and method are based on the microprocedures described by Kemmerer and Hallet (1927), Reich-Rohrwig (1933), Wyatt (1942), and Colson (1945).

REAGENTS AND APPARATUS

Reagents

Hydrochloric acid, (1+1) : Freshly boiled and cooled.
Sodium hydroxide pellets.
Pumice, impregnated with anhydrous copper sulfate: Transfer 60 g of 10–12-mesh pumice to a casserole. Cover with a concentrated solution of 30–35 g $CuSO_4 \cdot 5H_2O$. Evaporate to dryness. When the volume of liquid is small, stir constantly. Heat for 3–4 hours at 150°–160°C in an air bath. Cool in a desiccator and preserve in a glass-stoppered bottle in a desiccator.
Anhydrone or Dehydrite (anhydrous magnesium perchlorate), 10–20 mesh.
Nitrogen, oxygen-free.
Sulfuric acid-potassium chromate solution: Dissolve K_2CrO_4 in concentrated H_2SO_4. Discard when solution turns green.
Ascarite (sodium hydroxide on asbestos), 8–20 mesh.
Kroenig glass cement.
Wool, glass, Pyrex brand.
Absorbent cotton.

Apparatus

Figure 1 illustrates the train used. Figure 2 (*D* of fig. 1) is a diagram of the reaction flask, which differs from that of Wyatt (1942) in that the gas-scrubbing tube of the Schroedter alkalimeter, adapted from the Liebig alkalimeter (Kunberger and others, 1929), is replaced by a microcondenser as an integral part of the reaction flask. Letter preceding each piece of apparatus listed below refers to apparatus as shown in figure 1.

(*A*) Rubber tubing.
(*B*) Drying tower, without glass joint, 250 mm high, filled with NaOH pellets.
(*C*) Pregl gas-pressure regulator, micro, American Chemical Society specifications (hereafter referred to as A.C.S.), filled with water.
(*D*) Reaction flask. Constructed from a standard Schroedter alkalimeter and a West-type microcondenser with 100-mm water jacket; overall height, 180 mm; outlet tube, 5–6 mm OD. The outlet stopper becomes the gas-inlet tube and is inserted into the separatory funnel. The gas scrubber is replaced by the microcondenser.
(*E*) Heating mantle, electric, hemispherical, 2⁹⁄₁₆ inch diameter.
(*F*) Niederl bubble counter, micro. This is the bubble counter, micro, A.C.S., without the U-tube part.
(*G*) Drying tube, U-form, glass-stoppered, Schwartz; height without stoppers, 150 mm. The ground-glass stoppers are sealed in the open position with Kroenig glass cement (Steyermark, 1961, p. 239). The space 10 mm below each stopper is filled with glass wool. The tube is filled with Anhydrone (*H*) except for a 45-mm part of the right arm which contains copper sulfate impregnated pumice (*I*). The pumice is separated from the Anhydrone above and below by 10-mm layers of glass wool. The bottom of the pumice layer is approximately 90 mm below the glass stopper.
(*J*) Pregl rubber tubing, microchemical, impregnated, 34–40 mm long.
(*K*) Pregl absorption tube, micro, combustion, A.C.S.; length, 190 mm. Tube is filled with Ascarite (*L*) and Anhydrone (*H*) as described by Steyermark (1961, p. 240).
(*M*) Pregl drying tube, micro, A.C.S. (also called "guard" tube); filled with Anhydrone (*H*) as described by Steyermark (1961, p. 240).
(*N*) Mariotte bottle, micro, A.C.S.
(*O*) Cylinder, graduated, 500 ml.
Combustion boats, platinum; Pregl, micro, 4×5×16 mm (A.C.S.), and 4×5×35 mm, or porcelain equivalents.

U.S. GEOL. SURVEY PROF. PAPER 700–C, PAGES C183–C185

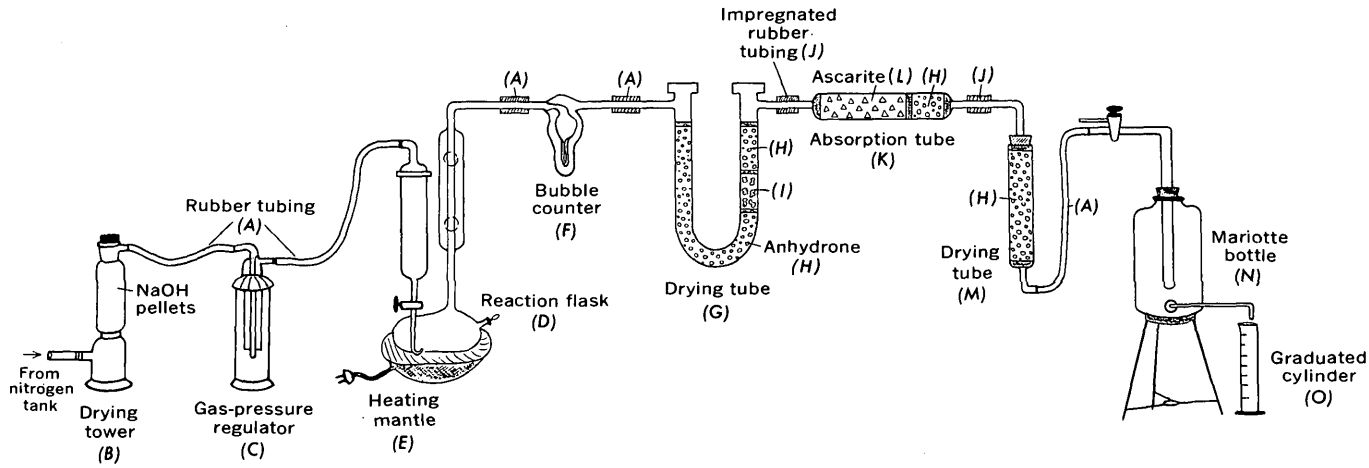

FIGURE 1.—Apparatus for the determination of carbon dioxide. Description is given in text. Components are not drawn to scale.

PROCEDURE

1. Insert reaction flask into train. The CO_2 absorption tube is not in position in the train. Turn on condenser water.
2. Weigh a sample estimated to contain no more than 8 mg of CO_2 in a platinum or porcelain microboat. Transfer the boat and sample to the reaction flask.
3. Add sufficient freshly boiled and cooled redistilled water to the reaction flask to cover the tip of the acid inlet tube.
4. Remove the glass-rod plug at the end of the U-tube. Open stopcock to the reaction flask and pass nitrogen through the train for 15 minutes at the rate of 10–15 ml per minute. Insert the glass plug and close the stopcock.
5. The CO_2 absorption tube is wiped, as described by Steyermark (1961, p. 252–253), and weighed.
6. Insert absorption tube into train between the U-tube and the guard tube of the Mariotte bottle, using a trace of glycerine to lubricate the ends of the absorption tube. Open the Mariotte bottle to the train.
7. Disconnect the gas-inlet tube of the reaction flask and add to the bulb approximately 6 ml of 1+1 HCl. Close the end of the inlet tube with a finger and hold until maximum pressure in the pressure regulator is obtained. Pinch rubber tubing as close to the glass inlet tube as is possible. Remove the finger from the inlet tube and connect the tube to the reaction flask as quickly as possible.
8. Turn on the heating mantle so that it will be hot when needed.
9. Open the stopcock slightly so that the acid will flow very slowly into the reaction flask. Close the stopcock while there is still a small amount of acid remaining in the bulb. Watch the bubbler, and when the decomposition reaction begins to slow, raise heating mantle into position and heat the contents of the flask to boiling and boil for 1 minute.
10. Open stopcock slowly and pass nitrogen through the train at the rate of 10–15 ml per minute. If the solution in the bubbler begins to back up before the boiling has been completed, begin to pass nitrogen through the flask by slowly opening the stopcock. Remove the heating mantle. Collect 500 ml of water. Close the stopcock to Mariotte bottle.
11. Disconnect the CO_2 absorption tube from the guard tube. Plug guard tube with a glass rod. Disconnect the CO_2 absorption tube from the U-tube and plug the U-tube. Close stopcock of the reaction flask. Disconnect the flask from bubbler and plug bubbler.

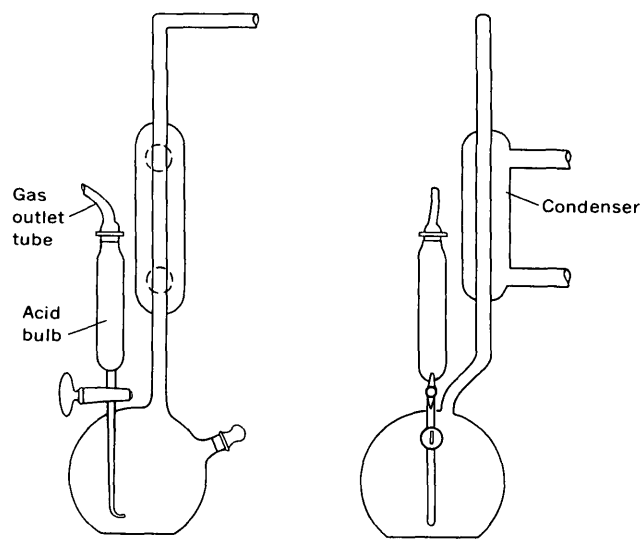

FIGURE 2.—Two views of reaction flask.

12. Wipe and weigh the absorption tube as in step 5.
13. Run procedural blank before and after the sample, using an empty boat.

DISCUSSION

The analyst should read the chapter on the determination of carbon and hydrogen in organic compounds by Steyermark (1961) to obtain the details of the technique used in carrying out the procedure described above. The boats are cleaned by boiling in 1+1 HCl, rinsing with water, and igniting. The outside diameters of the glass tubes held together by rubber tubing should match to prevent leakage between the condenser and bubbler, and between the U-tube and absorption tube. If necessary, draw out the glass tubing of the pieces affected or use adapters made from glass tubing. The rubber tubing on either side of the NaOH tower is clamped off when the train is not in use.

The purpose of the condenser in the train is to remove as much water and HCl vapor as possible from the gas passing through the bubbler and the U-tube. The H_2SO_4–K_2CrO_4 solution in the bubbler removes traces of H_2S as well as hydrocarbons. The Anhydrone in the U-tube removes the last traces of water vapor in the gas, and the $CuSO_4$ in the pumice absorbs the chlorine, residual HCl, and H_2S not absorbed in the bubbler. The volume of solution in the bubbler should be the minimum required to cover the tip of the inner tube but enough to show bubbles as an indicator that gas is flowing through the train. Avoid violent surges of gas through the train which would force the concentrated H_2SO_4 solution into the U-tube so that it would come in contact with the magnesium perchlorate, possibly causing an explosion.

Before the analysis of samples, the train is conditioned by carrying out the procedure on an unweighed sample of carbonate containing approximately 4 mg of CO_2. A new absorption tube is conditioned by the use of two such unweighed samples in successive runs.

REFERENCES

Colson, A. F., 1945, The rapid gravimetric micro and semi-micro determination of carbon dioxide in carbonates: Soc. Chem. Industry Jour., v. 64, p. 225–227.

Kemmerer, George, and Hallett, L. T., 1927, Micro determination of carbonate carbon: Indus. Eng. Chemistry, v. 19, p. 1352–1354.

Kunberger, A. F., and others, eds., 1929, Gas chemists' handbook, 3d ed.: New York, Am. Gas. Assoc., 795 p.

Meyrowitz, Robert, Ross, D. R., and Ross, Malcolm, 1964, A new uranyl tricarbonate, $K_2Ca_3(UO_2)_2(CO_3)_6 \cdot 9\text{–}10H_2O$ *in* Geological Survey Research 1964: U.S. Geol. Survey Prof. Paper 501–B, p. B82–B83.

Meyrowitz, Robert, Ross, D. R., and Weeks, A. D., 1963, Synthesis of liebigite: Art 43 *in* U.S. Geol. Survey Prof. Paper 475–B, p. B162–B163.

Reich-Rohrwig, Wilhelm, 1933, Über die mikrochemische Bestimmung der Kohlensaure in Carbonaten: Zeitschr. Anal. Chemie, v. 95, p. 315–323.

Steyermark, Al, 1961, Quantitative organic microanalysis: 2d ed.: New York, Academic Press, 665 p.

Wyatt, G. H., 1942, An improved apparatus for the microdetermination of carbonates: Analyst, v. 67, p. 260–261.

A RAPID METHOD FOR THE DETERMINATION OF FLUORIDE IN ROCKS AND SOILS, USING AN ION-SELECTIVE ELECTRODE

By WALTER H. FICKLIN, Denver, Colo.

Abstract.—A rapid method for the direct determination of fluoride in rocks and soils is presented. No prior separation of fluoride by distillation is required. Results are listed for 19 rock samples from the Cripple Creek mining district of Colorado, 8 U.S. Geological Survey standard rock samples, and 5 soil samples from New Mexico. The results determined by the proposed method agree to within about 20 percent of the values obtained by other methods and are reproducible to within about 15 percent. The minimum fluoride content detected is 40 ppm.

Conventional chemical methods of determining fluorine require that the fluorine be separated by distillation from interfering elements. These methods are reliable but time consuming and are not really satisfactory for use in geochemical exploration where a large number of samples must be analyzed with minimum effort and cost. Direct measurement of the fluoride ion in the presence of other ions found in solutions of soil or rock samples would obviously be helpful in the development of an exploration method, and the selectivity of a fluoride ion electrode suggests an application for such use (Frant and Ross, 1966).

Other applications of the fluoride ion electrode provide additional evidence of its usefulness. For example, Lingane (1967) used the electrode in the titration of fluorine solutions with thorium, lanthanum, and calcium salts. Van Loon (1968) employed a sodium hydroxide fusion and a fluoride electrode in the analysis of fluoride minerals. Recently, Edmond (1969) developed a method for determining the fluoride content of phosphate rock.

The method described here is comparatively simple and is free from notable interferences. The sample is sintered with a mixture of sodium carbonate and potassium nitrate. The sinter is dissolved with water and the flux neutralized with citric acid. The fluorine ion activity of the solution is compared to standards on a specific ion meter.

APPARATUS AND REAGENTS

Apparatus

Orion Model 94–09 fluoride specific ion electrode.
Orion Model 407 Ionalyzer specific ion meter.
Orion Model 90–01 single-junction reference electrode with a filling solution of saturated KCl and Ag ion.
16×150-mm culture tubes.
Fusion rack.

Reagents

Sodium fluoride: Reagent grade, oven dried at 110°C overnight. A solution containing 1 percent F is prepared with distilled water and diluted to 100 μg/ml F. These solutions are stored in polyethylene bottles.
Flux: Two parts by weight of reagent-grade sodium carbonate and 1 part by weight of potassium nitrate.
Citric acid: 100 g of reagent-grade citric acid dissolved in 1 liter of distilled water.
Ammonium carbonate: Reagent grade.

PROCEDURE

Weigh 0.25 g of sample of rock or soil, which has been ground to at least 80 mesh, into a culture tube. Add 1 g of flux to this and mix thoroughly. The sample and flux are then sintered for 10 minutes using a fusion rack (Marranzino and Wood, 1956). After cooling, 20 ml of water is added to dissolve the melt. After 1 hour the sample solution is poured into a 100-ml polypropylene beaker. The remaining residue in the culture tube is loosened with a glass stirring rod and added to the rest of the sample in the polypropylene beaker. The culture tube is rinsed with water, and the sample solution is then allowed to stand for 1 hour. The tube is discarded after use.

After at least 1 hour, 10 ml of citric acid solution is added and the final volume brought up to 100 ml with water. A Teflon-coated magnet is placed in the beaker, and the solution is gently stirred with a magnetic stirrer. The fluoride-ion activity of the sample solutions is read on the previously calibrated specific ion meter. The pH of the solution should be from 5.5 to 6.5.

U.S. GEOL. SURVEY PROF. PAPER 700–C, PAGES C186–C188

The instrument is calibrated with standard solutions prepared as follows:

Add 1 g of flux to a polypropylene beaker that contains 15–20 ml of distilled water. The appropriate volume of 100-μg/ml fluoride solution is added, followed by 10 ml of the citric acid solution. The final volume is made up to 100 ml with distilled water. The standard solutions contain 100, 50, 10, 5, 1, 0.5, and 0.1 μg/ml of fluorine. Blank solutions are also prepared in this manner with no addition of fluorine. The specific ion meter is set so that when the 10 μg/ml of fluorine solution is adjusted to 100 on the scale, a 1-μg/ml solution will read 10. Thus the fluoride-ion activity of the sample solution is obtained directly from the reading on the instrument.

DISCUSSION AND RESULTS

The analytical results for fluorine on U.S. Geological Survey standard rock samples are compared in table 1 with published average values (Flanagan, 1969; Fleischer, 1969). Analytical data for fluorine content on 19 rock samples from the Cripple Creek mining district, Colorado and 5 soils samples from New Mexico are shown in table 2. Replicate analyses made by this method are compared with those obtained by a distillation method (W. D. Goss, oral commun., 1969). (In the Goss method the sample is sintered with a carbonate flux, leached with water, acidified with sulfuric acid, and steam distilled. The estimation of fluorine is then made volumetrically or colorimetrically.) The values obtained by the ion-selective method, described here, agree with those of the older method by approximately 20 percent. The reproducibility of the method as shown by the replicate analyses is approximately 15 percent, with one exception: More accurate determinations of fluorine contents in phosphate rocks are made by the method of Edmond (1969).

TABLE 1.—*Comparison of analytical data for fluorine content, in parts per million, in U.S. Geological Survey standard rock samples*

Sample No.	Rock type	Average content (Fleisher, 1969, p. 73; Flanagan, 1969, p. 109)	Content (method of this report)
DTS-1	Dunite	12	<40
G-2	Granite	1, 200	1, 120
AGV-1	Andesite	435	500
PCC-1	Peridotite	13	<40
GSP-1	Granodiorite	1, 940	2, 400
BCR-1	Basalt	485	510
G-1	Granite	700	600
W-1	Diabase	250	180

TABLE 2.—*Comparison of analytical data for fluorine content, in parts per million, in rocks and soils*

[N.d., not determined]

Sample No.	Sample description	Distillation method (W. D. Goss, oral commun., 1969)	Method of this report, replicate analyses		
			1	2	3
CC-103	Breccia	1, 000	840	1, 160	820
104	do	1, 300	1, 120	960	1, 100
129	Granite	4, 000	3, 600	3, 520	3, 600
129A	do	8, 500	5, 200	4, 800	4, 800
132	do	4, 700	3, 720	4, 600	4, 400
164	Breccia	900	1, 180	1, 100	940
168	do	700	1, 000	860	720
169	do	1, 000	900	940	880
183	do	1, 100	1, 080	1, 040	960
188	do	1, 200	1, 040	1, 000	840
189	do	1, 000	1, 040	920	920
193	do	1, 200	920	880	1, 080
196	do	1, 500	1, 320	1, 280	N.d.
197	do	1, 300	1, 080	1, 240	1, 300
268	do	2, 700	1, 600	1, 960	1, 600
272	do	2, 400	1, 440	1, 520	1, 760
354	Granite	1, 000	960	720	760
355	do	400	420	420	400
356	do	200	170	160	175
HC-2-67	Soil	1, 000	700	790	735
4-67	do	250	200	245	245
12-67	do	560	530	720	665
14-67	do	230	195	210	205
22-67	do	200	260	330	270

380-189 O - 70 - 13

The possibility that fluoride will be complexed by aluminum ion in the solution is obviated by the addition of citric acid to the carbonate solution. In order to determine if other common ions would reduce the free fluoride in the test solutions, we adapted a simple chemical separation from that described by Hall and Walsh (1969). Samples of 0.2 g were sintered with 1 g of flux. Enough water was added to effect a solution and permit removal of the samples from the culture tube to polypropylene beakers. One gram of ammonium carbonate was added to each of the samples. The samples were heated gently for 30 minutes, then allowed to stand overnight. After filtering, the solutions were made just neutral with 1+1 HCl. The final volume was made up to 100 ml. The samples were compared by means of the specific ion meter with standards made in the same manner. The results as shown in table 3 indicate that aluminum and iron do not interfere when this method is used.

TABLE 3.—*Comparison of analytical data for fluorine content in random samples*

[Data in parts per million, except as noted otherwise]

Sample No.	Method	
	$(NH_4)_2CO_3$ (Hall and Walsh, 1969)	Citrate solution (this report)
D132685	3, 800	3, 800
132695	750	700
132724 (percent)	1. 7	1. 7
CL129A	4, 800	4, 700
193	1, 150	1, 200
CC356	220	200

Frant and Ross (1966) have shown that at pH 5, or less, fluorine is likely to be present as associated species of fluoride. Srinivasan and Rechnitz (1968) have shown these species to be HF and HF_2^{-1}, which are not detected by the electrode. In basic solutions the hydroxyl ion is an interfering ion. Therefore, in this procedure the pH is maintained at or near 6.

REFERENCES

Edmond, C. R., 1969, Direct determination of fluoride in phosphate rock samples using the specific ion electrode: Anal. Chemistry, v. 41, no. 10, p. 1327–1328.

Flanagan, F. J., 1969, U.S. Geological Survey standards—II. First compilation of data for the new U.S.G.S. rocks: Geochim, et Cosmochim. Acta, v. 33, no. 1, p. 81–120.

Fleischer, Michael, 1969, U.S. Geological Survey standards—I. Additional data on rocks G–1 and W–1, 1965–1967: Geochim. et Cosmochim. Acta, v. 33, no. 1, p. 65–79.

Frant, M. S., and Ross, J. W., Jr., 1966, Electrode for sensing fluoride ion activity in solution: Science, v. 154, p. 1553–1554.

Hall, J., and Walsh, J. N., 1969, A rapid method for the determination of fluorine in silicate rocks and minerals: Anal. Chim. Acta, v. 45, no. 4, p. 341–342.

Lingane, J. S., 1967, A study of the lanthanum fluoride membrane electrode for end point detection in titrations of fluoride with thorium, lanthanum, and calcium: Anal. Chemistry, v. 39, no. 8, p. 881–887.

Marranzino, A. P., and Wood, W. H., 1956, Multiple-unit fusion rack: Anal. Chemistry, v. 28, no. 2, p. 273–274.

Srinivasan, K., and Rechnitz, G. A., 1968, Activity measurements with a fluoride-selective membrane electrode: Anal. Chemistry, v. 40, no. 3, p. 509–512.

Van Loon, J. C., 1968, The rapid determination of fluoride in mineral fluorides using a specific ion electrode: Anal. Letters, v. 1, no. 6, p. 393–398.

EFFECTS OF URBANIZATION ON THE QUALITY OF SELECTED STREAMS IN SOUTHERN NASSAU COUNTY, LONG ISLAND, NEW YORK

By ELLIS KOCH, Mineola, N.Y.

Prepared in cooperation with the Nassau County Department of Public Works; the Suffolk County Water Authority; the Suffolk County Board of Supervisors; and the New York State Department of Conservation, Division of Water Resources

Abstract.—The water quality of the streams in southern Nassau County has diverged noticeably from natural conditions because of extensive urbanization. The quality of two streams in sparsely populated areas in Suffolk County was compared with the quality of three streams in moderately to densely populated parts of Nassau County. The estimated load of dissolved solids of all the southern Nassau County streams presently is about 10.5 tons per day greater than the estimated load under natural conditions. Furthermore, analysis of the data for certain constituents directly affected by man shows that the detergent content of the three streams in Nassau County ranges from about 9 to 18 times the detergent content of the two Suffolk County streams; the nitrate content is 14 times that of the Suffolk County streams; and the dissolved-solids content is about 3 to 4 times that of the Suffolk County streams.

The disposal of domestic and industrial waste water by means of hundreds of thousands of cesspools, septic tanks, and disposal basins has caused widespread pollution of the upper glacial aquifer, a major shallow water-bearing unit on Long Island, N.Y. (Perlmutter and others, 1963, 1964). Since 1966, the U.S. Geological Survey, in cooperation with the Nassau County Department of Public Works, has been studying the nature and extent of the pollution in Nassau County and the possible abatement of the pollution as a result of construction of a sanitary-sewer system in part of the county. The purpose of this report is to describe the preliminary results of one aspect of that study—namely, a comparison of the chemical quality of selected streams in Nassau and Suffolk Counties (fig. 1).

Except for short periods after intense storms, virtually all of the water in Long Island's streams is derived from the shallow aquifers of the ground-water reservoir. Accordingly, the quality of the streamflow commonly is closely representative of the quality of the shallow ground water. Thus, a comparison of the quality of selected streams in Nassau County, where the shallow aquifer is known to contain pollutants, with the quality of selected streams in Suffolk County, where the shallow ground water locally is comparatively free of pollutants, affords an excellent opportunity to describe the gross aspects of ground-water pollution in Nassau County.

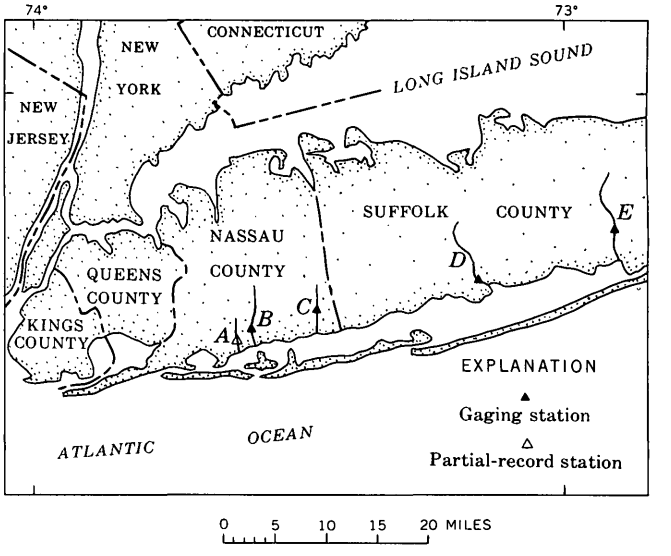

FIGURE 1.—Location of selected streams in southern Nassau and Suffolk Counties, Long Island, N.Y., *A*, Millburn Creek; *B*, East Meadow Brook; *C*, Massapequa Creek; *D*, Connetquot River; and *E*, Carmans River.

METHODS OF INVESTIGATION

Among the many streams in Suffolk County, several have drainage basins which are still largely undeveloped and generally free from contamination resulting from the influence of man's activities. Two of these streams, Connetquot and Carmans Rivers (*D* and *E*, fig. 1), were chosen for this study because the quality of these streams probably is very similar to what the quality of Long Island streams was under natural conditions. Conversely, southern Nassau County is highly urbanized, and the quality of the water in the streams draining this county is directly affected by man's activities. Three major streams in southern Nassau County—Millburn Creek, East Meadow Brook, and Massapequa Creek (*A*, *B*, and *C*, fig. 1)—were chosen for comparison with the two Suffolk County streams.

Periodic sampling of all the major streams in Nassau and Suffolk Counties for chemical analyses was begun in 1966 and has continued to the present (1969). Standard chemical analyses were made of selected samples by the U.S. Geological Survey, and analyses of additional selected constituents were made by the Nassau County Department of Health. Stream samples were collected at base flow to obtain a representative sample of groundwater outflow uncontaminated by overland runoff from intermittent storms.

Continuous records of discharge were available at the sampling points which were at the regular stream-gaging stations of the U.S. Geological Survey (1968). At the other sampling sites spot discharge measurements were made by current meter, or the discharge was estimated by correlation with the records of continuously gaged streams. All the streams used in this report are tidal in their lower reaches. Therefore, gaging and sampling operations were restricted to reaches upstream from tidal influence, or were conducted during periods of low tide.

The changes in dissolved-solids content and the changes in three of the determined constituents—nitrate, phosphate, and detergent (referred to as MBAS in this report)—were considered to be principally related to urbanization. The average concentration of these principal chemical indicators was calculated for each stream.

CHARACTERISTICS AND PHYSICAL ENVIRONMENT OF THE STREAMS

The land surface of southern Nassau and Suffolk Counties is a broad plain with an average slope of 20 feet per mile toward the southeast. The streams are small and occupy narrow shallow channels. The material underlying the plain and the stream channels is highly permeable glacial outwash deposits of sand and gravel. Under natural conditions about 95 percent of the streamflow is derived from the ground-water reservoir, and only about 5 percent is direct runoff (Pluhowski and Kantrowitz, 1964, p. 35).

Some general hydraulic characteristics of the streams selected for this study are summarized in table 1. The two streams selected from Suffolk County flow through virtually unpopulated areas. Connetquot River flows through an undeveloped game preserve, and Carmans River to the east flows through sparsely populated and undeveloped land. However, both drainage basins contain very scattered developments of low population density, which undoubtedly contribute small quantities of contaminants to the ground water.

TABLE 1.—*Characteristics of selected streams in southern Nassau and Suffolk Counties, N.Y.*

Name of stream	Period of record	Average discharge for period of record (cubic feet per second)	Surface drainage area (square miles)	Approximate length [1] in April 1968 (miles)
Suffolk County:				
Carmans River	1942–67	23. 3	71	4. 1
Connetquot River	1943–67	38. 3	24	4. 3
Nassau County:				
Massapequa Creek	1936–67	11. 7	38	2. 0
East Meadow Brook	1937–67	16. 2	31	4. 2
Millburn Creek	1940–65	8. 5	4. 5	1. 6

[1] Stream lengths are measured from the start of perennial flow to the gaging station.

The three streams in Nassau County have heavily urbanized drainage basins whose average population densities range from about 5,000 to 10,000 people per square mile (adapted from Nassau-Suffolk Regional Planning Board, 1969). Thousands of cesspools and septic tanks discharge waste into the shallow ground-water reservoir in the vicinities of East Meadow Brook and Massapequa Creek (Perlmutter and others, 1964). Some industrial plants also discharge waste into sumps which drain into the shallow aquifer (Perlmutter and others, 1963). The drainage basin of Millburn Creek has been sewered since the mid 1950's, and probably few cesspools or septic tanks are in operation in that area at the present time. However, prior to the construction of sewers, thousands of cesspools and septic tanks contributed waste to the shallow aquifer in this area.

QUALITY OF STREAMS UNDER NATURAL CONDITIONS

Representative chemical analyses of the two Suffolk County streams are listed in table 2. Table 2 shows that the concentration of most of the constituents is very low; only the dissolved-solids content, bicarbonate and sul-

TABLE 2.—*Representative chemical analyses of selected streams in southern Nassau and Suffolk Counties, N.Y.*

[Analyses by U.S. Geological Survey; concentrations in milligrams per liter]

Stream	Date of collection	Silica (SiO_2)	Iron (Fe)	Calcium (Ca)	Magnesium (Mg)	Sodium (Na)	Potassium (K)	Bicarbonate (HCO_3)	Sulfate (SO_4)	Chloride (Cl)	Fluoride (F)	Nitrate (NO_3)	Phosphate (PO_4)	Detergent (MBAS)	Hardness as $CaCO_3$	Dissolved solids	Specific conductance (micromhos at 25°C)	pH
Carmans River at Yaphank.	May 11, 1966.	10	0.51	6.2	3.0	5.2	1.0	17	12	8.2	0.1	1.7	----	0.0	28	62	86	6.9
	June 6, 1968.	10	----	6.2	2.4	5.6	.6	20	9.0	7.0	.2	1.2	0.09	.04	26	56	86	6.7
Connetquot River near North Great River.	May 6, 1966.	8.5	.35	4.2	2.8	5.5	.6	1.8	5.1	7.9	.0	1.5	----	.0	22	54	71	6.8
	June 6, 1968.	9.5	----	4.0	2.1	4.7	.4	18	4.9	6.5	.1	1.7	.15	.18	18	50	65	6.8
Massapequa Creek at Massapequa.	May 11, 1966.	6.8	.36	13	4.3	16	2.6	12	32	20	.1	12	----	.4	50	146	211	6.2
	June 6, 1968.	8.0	----	20	4.2	24	5.0	36	37	27	.1	28	.1	.44	67	171	301	6.5
East Meadow Brook at East Meadow.	April 22, 1966.	6.8	----	18	3.9	32	4.1	10	38	47	.0	22	----	.4	61	198	326	5.9
	June 7, 1968.	7.6	----	23	4.5	44	4.7	32	41	64	.1	20	.08	.29	76	229	411	6.8
Millburn Creek at Baldwin.	May 11, 1966.	------	.71	----	----	----	----	32	43	17	----	10	----	.2	75	----	239	6.4
	May 6, 1968.[1]	------	.08	----	----	----	----	48	------	25	----	26	.04	.31	102	242	350	6.7

[1] Analysis by Nassau County Department of Health.

fate content, and the hardness (as $CaCO_3$) exceeded 10 mg/l. The concentrations of all the listed constituents are below the limits established by the U.S. Public Health Service for drinking water (U.S. Public Health Service, 1962).

Average values of the concentration of selected constituents that are directly affected by man's activities are shown in figure 2. The average dissolved-solids content of the two Suffolk streams is about 50 mg/l. The average dissolved-solids content, weighted with respect to discharge at the time of sampling, is 52 mg/l, and that of nitrate is 1.6 mg/l for the two streams. These values are probably nearly equal to the average dissolved-solids and nitrate content of all the streams emptying into Long Island's south-shore bays under natural conditions.

COMPARISON OF NATURAL WATER WITH THAT AFFECTED BY MAN'S ACTIVITIES

From the data in table 2 and figure 2 it is evident that the dissolved-solids content of the streams in southern Nassau County is markedly higher than that of the two streams in Suffolk County. The average nitrate content is about 14 times greater, MBAS content ranges from 9 to 18 times greater, and the average dissolved-solids content is about 3 to 4 times greater in the Nassau streams than in the Suffolk streams. MBAS is almost nonexistent in the two Suffolk streams, but at times the

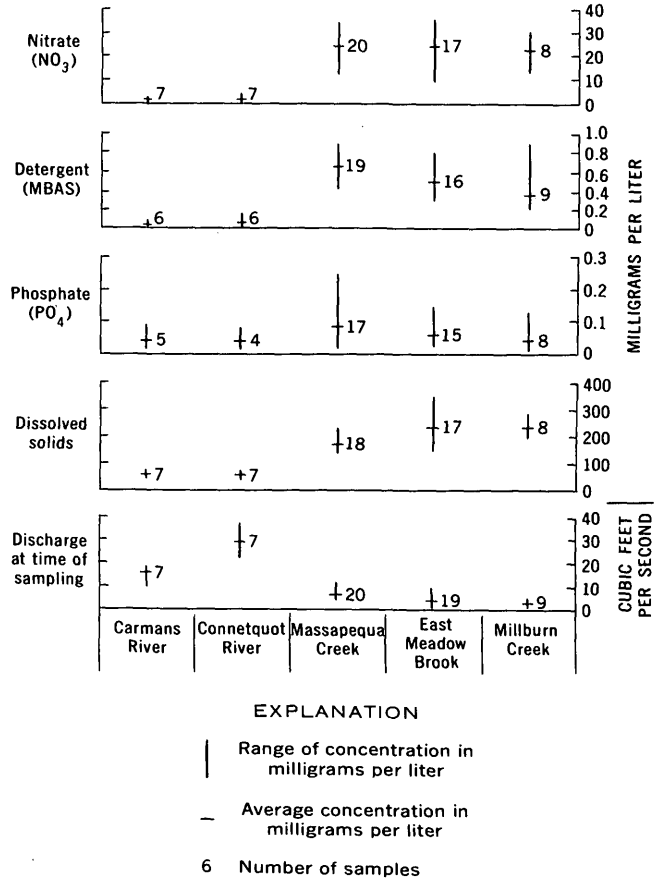

FIGURE 2.—Average values and ranges of concentration of selected constituents in the five study streams, 1966–68.

MBAS content of East Meadow Brook and Massapequa Creek has exceeded the recommended limit for drinking water—0.5 mg/l (U.S. Public Health Service, 1962). The large amount of nitrate and MBAS in the Nassau streams, compared with the amount in the two index streams in Suffolk County, is probably caused by the numerous cesspools and septic tanks in the drainage basins of the streams in Nassau County.

Local public health officials are concerned about the load of dissolved solids in the streams. Load is the product of two variables, discharge and dissolved-solids content. The average annual discharge of all streams in southern Nassau County was about 25 cubic feet per second in water years 1966–68 (U.S. Geol. Survey, 1967, 1968; and A. G. Spinello, oral commun., 1969). The estimated average dissolved-solids and nitrate content (weighted with respect to average discharge) for these streams during the same period was about 215 mg/l and 22 mg/l, respectively. Therefore, the corresponding load was about 14 tons per day of dissolved solids and about 1.5 tons per day of nitrate. The load for the southern Nassau County streams under natural conditions, calculated by using the weighted average concentration of dissolved solids and nitrate obtained from the two Suffolk County index streams, and the average annual discharge of all the southern Nassau County streams, is 3.5 tons per day dissolved solids, and 0.1 ton per day nitrates. Consequently, the difference between the estimated loads of these streams under the assumed natural conditions and under present developed conditions is about 10.5 tons per day of dissolved solids and 1.4 tons per day of nitrate.

CONCLUSIONS

The chemical quality of streams in urbanized southern Nassau County is considerably different from the quality of streams that are under virtually natural conditions in parts of Suffolk County. The concentration of certain chemical constituents in the streams in Nassau County has increased as a result of man's activities. Probably the major cause of this increase is the release of waste from hundreds of thousands of septic tanks and cesspools into the shallow ground-water reservoir from which the water discharges into the streams.

REFERENCES

Nassau and Suffolk Regional Planning Board, 1969, Population—Current population and projections for Nassau and Suffolk Counties 1965–69: Hauppauge, N.Y., Nassau-Suffolk Regional Planning Board Comprehensive Plan Ser., 30 p.

Perlmutter, N. M., Lieber, Maxim, and Frauenthal, H. L., 1963, Movement of waterborne cadmium and hexavalent chromium wastes in South Farmingdale, Nassau County, Long Island, New York: Art. 105 *in* U.S. Geol. Survey Prof. Paper 475–C, p. C179–C184.

———1964, Contamination of ground water by detergents in a suburban environment—South Farmingdale area, Long Island, New York: *in* Geological Survey Research 1964: U.S. Geol. Survey Prof. Paper 501–C, p. C170–C175.

Pluhowski, E. J., and Kantrowitz, I. H., 1964, Hydrology of the Babylon-Islip area, Suffolk County, Long Island, New York: U.S. Geol. Survey Water Supply Paper 1768, 119 p.

U.S. Geological Survey, 1967, Water resources data for New York, 1966—Part 1. Surface water records: U.S. Geol. Survey, New York District Office, 363 p.

———1968, Water resources data for New York, 1967—Part 1. Surface water records: U.S. Geol. Survey, New York District Office, 376 p.

U.S. Public Health Service, 1962, Drinking water standards: U.S. Public Health Service Pub. No. 956, 61 p.

USE OF CHANNEL SLOPE AND DISCHARGE TO DETERMINE REAERATION COEFFICIENTS FOR THE ELKHORN RIVER IN NEBRASKA

By K. A. Mac KICHAN, NEIL G. STUTHMANN,
and RAY BENTALL, Lincoln, Nebr.

Abstract.—Earlier workers have shown that the reaeration coefficient, k_2, of a stream at a given point can be computed from an empirical formula expressing k_2 in terms of mean velocity and mean depth. As both velocity and depth vary with discharge and channel slope, k_2 for a given stream obviously can be expressed equally well in terms of discharge and slope. An equation is presented whereby k_2 for any point along the Elkhorn River in Nebraska can be computed, using channel-slope data, for minimum 7-day discharges having different recurrence intervals.

The ability of a stream to assimilate organic wastes is governed by the amount of oxygen dissolved in the water. If it were not for the capacity of flowing water to absorb oxygen from the atmosphere, thereby replacing the dissolved oxygen consumed in the waste-assimilation process, streams would be relatively ineffective as disposers of organic pollutants. Streeter and Phelps (1925) described the combined action of deoxygenation and reoxygenation by the differential equation

$$\frac{dD}{dt}=K_1L-K_2D,$$

where L is the biochemical oxygen demand, D is the oxygen deficit, and K_1 and K_2 are the deoxygenation and reaeration coefficients (logarithmic to base e), respectively. Therefore, K_2 expresses the effect of the hydraulic properties of a stream on its ability to absorb oxygen from the atmosphere.

Several investigators, among them O'Connor and Dobbins (1958) and Churchill, Elmore, and Buckingham (1964), have measured the reaeration coefficient and have indicated a relation between it and mean velocity, V, and mean depth, H. Plotting values of reaeration coefficients obtained by earlier investigators against $V/H^{1.33}$, Langbein and Durum (1967) expressed the relation of the reaeration coefficient to mean velocity and mean depth as $k_2=3.3\ V/H^{1.33}$, where k_2 is the proportion per day in common logarithmic units.

In their report on the hydraulic geometry of stream channels, Leopold and Maddock (1953, p. 1) state:

> In the data studied it appeared that when discharges are of equal frequency at different points along a river, that is, equalled or exceeded the same percent of time, the velocity, as well as the width and depth of flow, increases with discharge downstream. This increase of velocity downstream results from the fact that the increase in depth overcompensates for the decrease in slope.

As width, depth, and velocity can be expressed in terms of discharge and slope, it follows that k_2 can be calculated from discharge and slope. The remainder of this article describes formulation of an equation whereby k_2 for any point on the Elkhorn River in Nebraska can be computed for minimum 7-day discharges having different recurrence intervals by using slope data obtained from 7½-minute topographic maps.

The Elkhorn River rises in Rock County, Nebr., on a sand plain adjoining the Sand Hills region of north-central Nebraska (fig. 1). On leaving the sand plain the river flows first through an area of loess plains, then through an area of loess-mantled till. In its lowest reach it flows in the valley of the Platte River to which it becomes tributary in Sarpy County. Throughout its generally east-southeastward course, the Elkhorn River has a sandy bed that adjusts readily to changes in discharge. Unlike the many streams whose slope decreases progressively in a downstream direction, the Elkhorn River is steeper in its middle reach than in either its upper reach or lower reach. As may be computed from figure 2, the average gradient of the river from its head to the mouth of the South Fork is 3.1 feet per mile, from the South Fork to the town of West Point is 4.5 feet per mile, and below West Point is 2.8 feet per mile.

U.S. GEOL. SURVEY PROF. PAPER 700-C, PAGES C193-C197

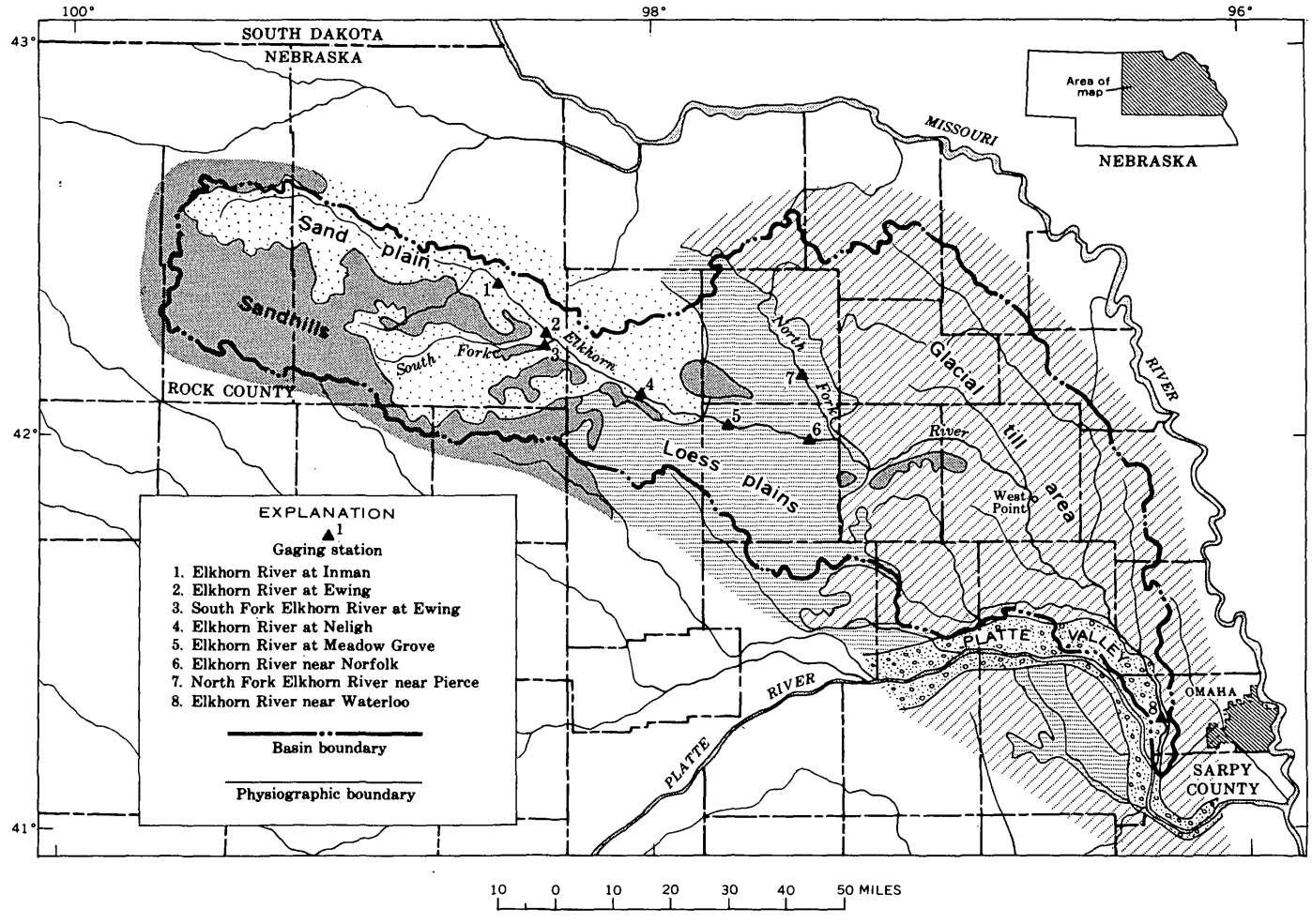

FIGURE 1.—Physiographic areas and locations of stream-gaging stations in the Elkhorn River basin, Nebraska

As a first step in formulating the equation expressing k_2 for the Elkhorn River in terms of discharge and slope, reaeration coefficients for minimum 7-day flows having recurrence intervals of 10, 5, 2.5, 2, 1.5, and 1.1 years at 8 gaging stations in the Elkhorn River basin were computed from the formula $k_2=3.3\ V/H^{1.33}$ (table 1). Mean velocities and mean depths used in the computations were taken from discharge-measurement notes and are regarded as typical of a considerable reach of stream because the sand bed of the Elkhorn River and its tributaries adjusts so readily to changes in discharge. The next step was to determine channel slope at each of the eight gaging stations (table 1). The computed values of k_2 then were plotted against channel slope, as shown in figure 3.

The final step was to use a graphic method[1] of correlation to account for the effect of differences in discharge (fig. 4). The reaeration coefficients plotted against slope in figure 4*A* are the computed k_2 values that have been adjusted according to a method described by Linsley, Kohler, and Paulhus (1949, p. 643–655). Figure 4*B* gives the correction factor for various rates of discharge at a given point on the river as measured by the recurrence intervals of the minimum 7-day discharge, and figure 4*C* gives the correction factor for variation of flow along the stream when the minimum 7-day discharge having a recurrence interval of 2.5 years is used as the indicator.

The relation of k_2 to slope and discharge, as shown in figure 4, is expressed by the equation

$$k_2=1.91\,I^{0.305}Q_{2.5}^{-0.155}S^{1.12},$$

where I is the recurrence interval, in years, of the minimum 7-day discharge for which k_2 is calculated; $Q_{2.5}$ is the minimum 7-day discharge in cubic feet per second, having a recurrence interval of 2.5 years; and S is the channel slope, in feet per mile. The standard error of estimate of k_2 is 0.91 and is much smaller than that of the unadjusted coefficients shown in figure 3.

[1] The equation could have been derived equally well and probably with less effort by using the data in table 1 and a multiple regression analysis.

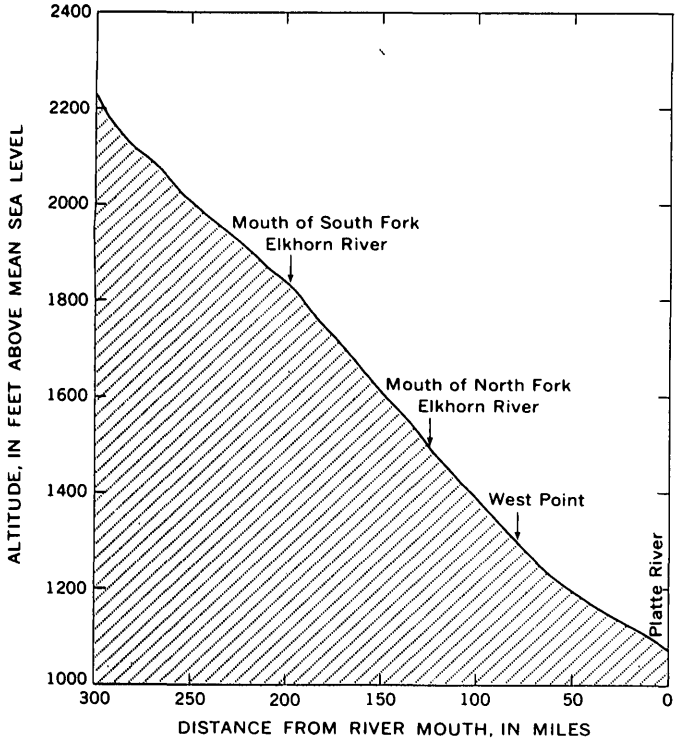

FIGURE 2.—Profile of the Elkhorn River in Nebraska.

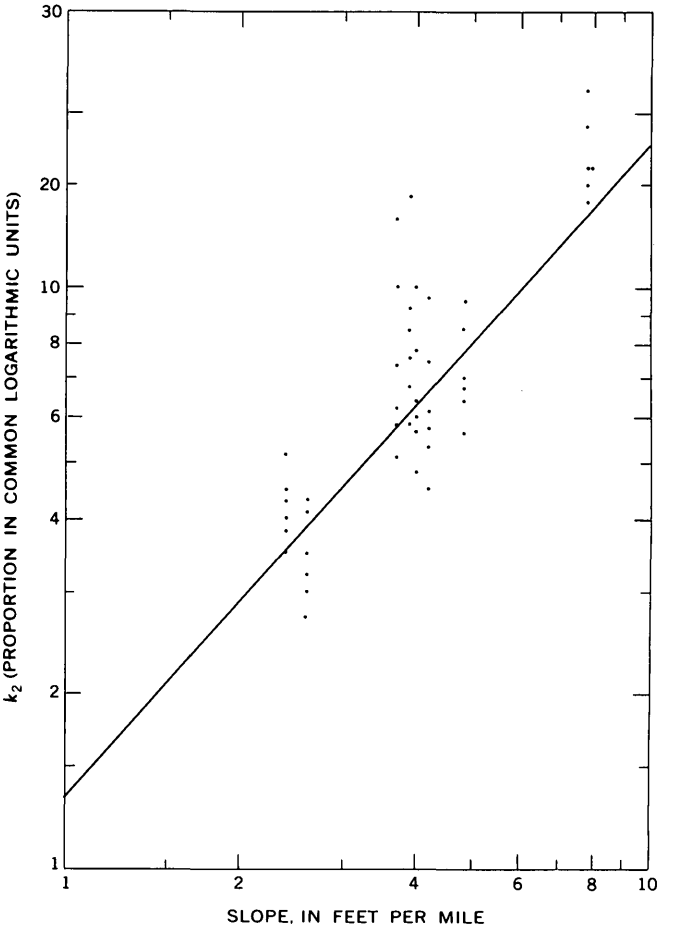

FIGURE 3.—Computed reaeration coefficient at eight stream-gaging stations plotted against average slope of river at respective station sites.

As channel slopes are easily determined and minimum 7-day flows can be estimated to the required accuracy, reaeration coefficients can be computed for minimum 7-day flows at any site along the Elkhorn River even though velocity and depth measurements have not been made at the site. The following example illustrates two methods—one graphic and the other by appropriate substitution in the equation—of computing k_2 from channel-slope and discharge data. As computed from figure 2, the channel slope of the Elkhorn River just below West Point is 3.7 feet per mile; and, from discharge data obtained at the nearest gaging stations in the basin, the minimum 7-day flow having a 2.5-year recurrence interval is estimated at 177 cubic feet per second. From figure 4*A*, the k_2 proportion in common log units for a channel slope of 3.7 feet per mile is found to be 5.90; from figure 4*B*, the correction factor corresponding to a 10-year recurrence interval is 1.62; and

TABLE 1.—*Reaeration coefficients* (k_2, *in days* $^{-1}$) *at the minimum 7-day flow* (Q, *in cubic feet per second*) *for indicated recurrence intervals*

Site [1]	Channel slope (feet per mile)	Recurrence intervals											
		10 years		5 years		2.5 years		2 years		1.5 years		1.1 years	
		Q	k_2	Q	k_2	Q	k_2	Q	k_2	Q	k_2	Q	k_2
Elkhorn River at Inman (*1*)	3.9	3.1	14.5	6.7	9.2	12.0	8.4	17	7.6	22	6.7	32	5.8
Elkhorn River at Ewing (*2*)	3.7	4.0	13	8.2	10	17.5	7.3	26	6.2	31	5.8	43	5.1
South Fork Elkhorn River at Ewing (*3*)	7.9	9.4	22	13.7	19	18.5	17	20	16	23	15	29	14
Elkhorn River at Neligh (*4*)	4.0	22	10	41	7.8	66	6.4	75	6.0	92	5.6	137	4.8
Elkhorn River at Meadow Grove (*5*)	4.2	25	9.6	49	7.5	81	6.1	97	5.7	120	5.3	170	4.5
Elkhorn River near Norfolk (*6*)	4.8	50	9.5	74	8.5	115	7.0	130	6.7	150	6.4	210	5.6
North Fork Elkhorn River near Pierce (*7*)	2.4	13.5	5.2	20	4.5	24	4.3	27	4.0	30	3.8	35	3.5
Elkhorn River near Waterloo (*8*)	2.6	125	4.3	137	4.1	230	3.4	260	3.2	305	3.0	410	2.7

[1] Number refers to location on figure 1.

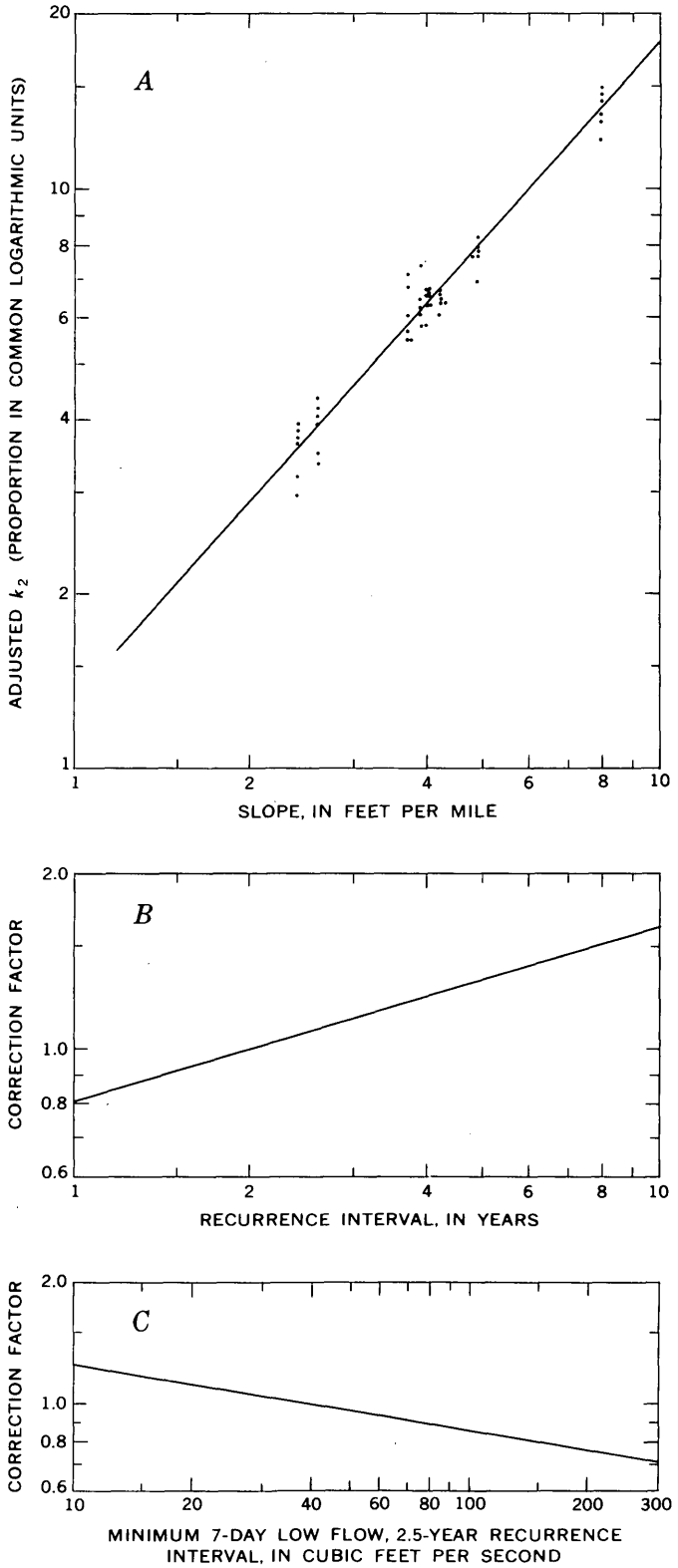

FIGURE 4.—*A*, Adjusted reaeration coefficient at eight stream-gaging stations plotted against average slope of river at respective station sites; *B*, correction factor for various rates of discharge at a given point on river as measured by recurrence intervals of minimum 7-day discharge; and *C*, correction factor for variation of flow along stream when minimum 7-day discharge with recurrence interval of 2.5 years is used as indicator.

from figure 4*C*, the correction factor corresponding to a minimum 7-day flow of 177 cubic feet per second (2.5-year recurrence interval) is 0.79. Multiplication of the three values thus determined gives $k_2=7.5$. As shown below, appropriate substitutions in the equation give the same value:

$$k_2=1.91\times10^{0.305}\times177^{-0.155}\times3.7^{1.12}=7.5.$$

REFERENCES

Churchill, M. A., Elmore, H. L., and Buckingham, R. A., 1964, Prediction of stream reaeration rates: Am. Soc. Civil Engineers Trans., v. 129, p. 24–26.

Langbein, W. B., and Durum, W. H., 1967, The aeration capacity of streams: U.S. Geol. Survey Circ. 542, 6 p.

Leopold, L. B., and Maddock, Thomas, Jr., 1953. The hydraulic geometry of stream channels and some physiographic implications: U.S. Geol. Survey Prof. Paper 252, 57 p.

Linsley, R. K., Jr., Kohler, M. A., and Paulhus, J. L., 1949, Applied hydrology: New York, McGraw-Hill Book Co., Inc., p. 643–655.

O'Connor, D. J., and Dobbins, W. E., 1958, The mechanism of reaeration in natural streams: Am. Soc. Civil Engineers Trans., v. 123, p. 641–684.

Streeter, H. W., and Phelps, E. B., 1925, A study of the pollution and natural purification of the Ohio River: U.S. Public Health Service Public Health Bull. 146, 75 p.

ROCK MOVEMENT TRIGGERED BY A WATER-LEVEL CHANGE IN THE BRUNSWICK AREA, GEORGIA

By DEAN O. GREGG, Brunswick, Ga.

Prepared in cooperation with the Georgia Department of Mines, Mining, and Geology; the city of Brunswick; and Glynn County

Abstract.—Anomalous water-level fluctuations attributed to rock movement were recorded simultaneously in three wells tapping the principal artesian aquifer in Glynn County, Ga. During the time of the fluctuations, water levels in the area were rising after an industrial shutdown for the 1964 Christmas holidays and a massive reduction in ground-water withdrawals. It is postulated that the rapidly changing pressures superimposed on older unresolved stress conditions may have triggered subsidence or movement along a suspected fault zone.

In December 1964, an anomalous water-level fluctuation, similar to that caused by an earthquake, was recorded in three wells penetrating the principal artesian aquifer in Glynn County, Ga. This paper presents one logical, though hypothetical, cause for this anomalous fluctuation. The paper is based on information collected by the U.S. Geological Survey in cooperation with the city of Brunswick, Glynn County, and the Georgia Department of Mines, Mining, and Geology as part of the salt-water encroachment study, Brunswick, Ga.

The principal artesian aquifer in Glynn County, Ga., is made up mainly of Oligocene and Eocene limestone and is characterized by numerous solution channels and openings. The aquifer is divided into an upper and a lower water-bearing zone by a soft, relatively impermeable, fossiliferous limestone. Wells tapping this highly productive aquifer yield abundant supplies of water. The geology and hydrology are described by Wait (1965), and by Wait and Gregg (1967).

The aquifer is the source of water for all the industries in the area. One industry, Brunswick Pulp and Paper Co., withdraws about 62 mgd (million gallons per day) from eight wells. These wells are cased to about 550 feet and uncased from there to almost 1,000 feet. The wells tap both water-bearing zones of the principal artesian aquifer.

WATER-LEVEL FLUCTUATIONS AND INSTRUMENTATION

In December 1964, Brunswick Pulp and Paper Co. shut down production operations for the Christmas holidays and reduced its rate of pumping from about 62 mgd to about 14 mgd. This reduction in pumping was followed by a rapid rise in the ground-water level. The hydrographs from three selected observation wells and the records of pumping for this period are shown in figure 1. The hydrographs show oscillations caused by the ocean tides; Gregg (1966) explained the mechanics and described the magnitude of the influence of ocean tides on the water levels in the wells.

At about 6:30 a.m. (EST), December 26, 1964, the water levels in U.S. Geological Survey test wells 3 (33H127) and 6 (33H133), and the Massey well (33G3) showed an anomalous fluctuation identical with that caused by an earthquake. The double amplitudes of the water-level fluctuations in the three wells were 0.3 foot, 1.6 feet, and (approximately) 48 feet, respectively. The water level in well 33G3 probably did not actually fluctuate over a range of 48 feet; part of this recorded fluctuation is attributed to the mechanics of the recorder and the momentum of the oscillating pen. No hydrologic inference is made as to the difference in the double amplitudes of the fluctuations in the three wells because of the type of instrumentation. All three wells were equipped with pressure recorders having 8-day time gears, a range of 0 to 40 feet of water, and a sensitivity of about 0.1 foot of water.

U.S. GEOL. SURVEY PROF. PAPER 700-C, PAGES C198-C201

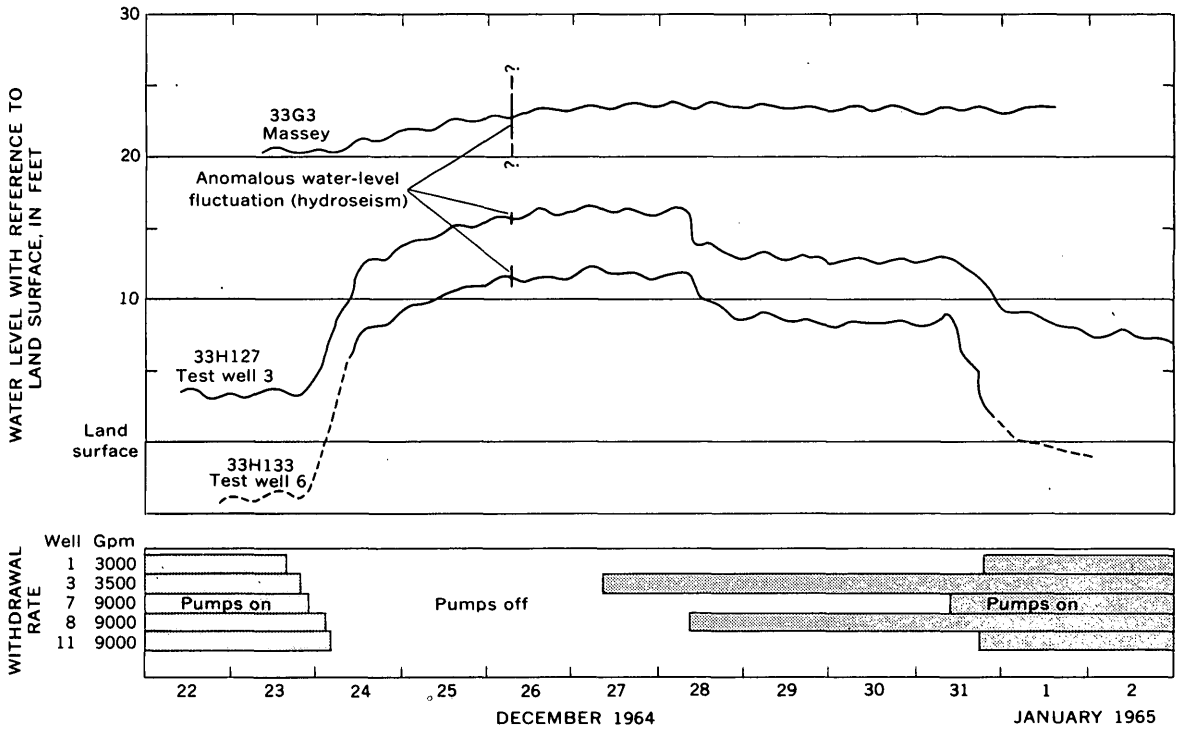

FIGURE 1.—Water levels in three selected wells responding to changes in pumping at Brunswick Pulp and Paper Co., Brunswick, Ga.

WELL CONSTRUCTION

Well 33H127 is 952 feet deep, is cased to 823 feet, and taps the lower water-bearing zone of the principal artesian aquifer. Well 33H133 is 790 feet deep, is cased to 520 feet, and taps the upper water-bearing zone of the principal artesian aquifer. Well 33G3 taps the interval from 610 to 921 feet, or most of both water-bearing zones of the principal artesian aquifer.

Wells 33H127 and 33H133 are within about 15 feet of each other and are about 5,000 feet east of the center of pumping at Brunswick Pulp and Paper Co. (fig. 2).

Well 33G3 is about 21,000 feet south of this center of pumping. The three wells recording the fluctuation are all to the west of the Brunswick peninsula and west of a suspected north-south fault zone (fig. 2). This fault zone is suspected because of a change in slope of the limestone surface and a change in the quality of water contained in the rocks across the zone. All other monitored observation wells except 33H131 are east of the suspected fault zone, and none recorded the fluctuation. Well 33H131 is about 31,000 feet northwest of the center of pumping. Because the fluctuation was much less at wells 33H127 and 33H133 than at well 33G3 to the south, it may have been completely damped out before reaching well 33H131.

STRUCTURAL RESPONSE

A check by Robert C. Vorhis, U.S. Geological Survey (oral commun., January 1965), with the Georgia Institute of Technology's seismology station in Atlanta, Ga., revealed that its seismograph did not record any seismic activity on the morning of December 26, 1964. According to Dr. M. W. Major, of the Geophysics Department, Colorado School of Mines (oral commun., April 1968), the sensitivity of the Georgia Tech instruments might well preclude recording of a low-magnitude disturbance 250 miles from Atlanta (the distance from Brunswick to Atlanta). It is concluded that the source of the water-level fluuctuations was local seismic activity of low magnitude.

The rapid rise of water levels after the reduction in pumping may have triggered some small amount of movement along the suspected fault zone. Davis, Small, and Counts (1963) have shown that as much as 4 inches of subsidence of the land surface near the center of pumping in Savannah, Ga., has occurred as a result of withdrawals from the principal artesian aquifer in that area. Poland and Davis (1969) discussed the theory and case histories of land subsidence due to withdrawal of fluids at Savannah and elsewhere. Brunswick Pulp and Paper Co. increased its average rate of withdrawals by 36.7 mgd in December 1962 and deepened and shifted the

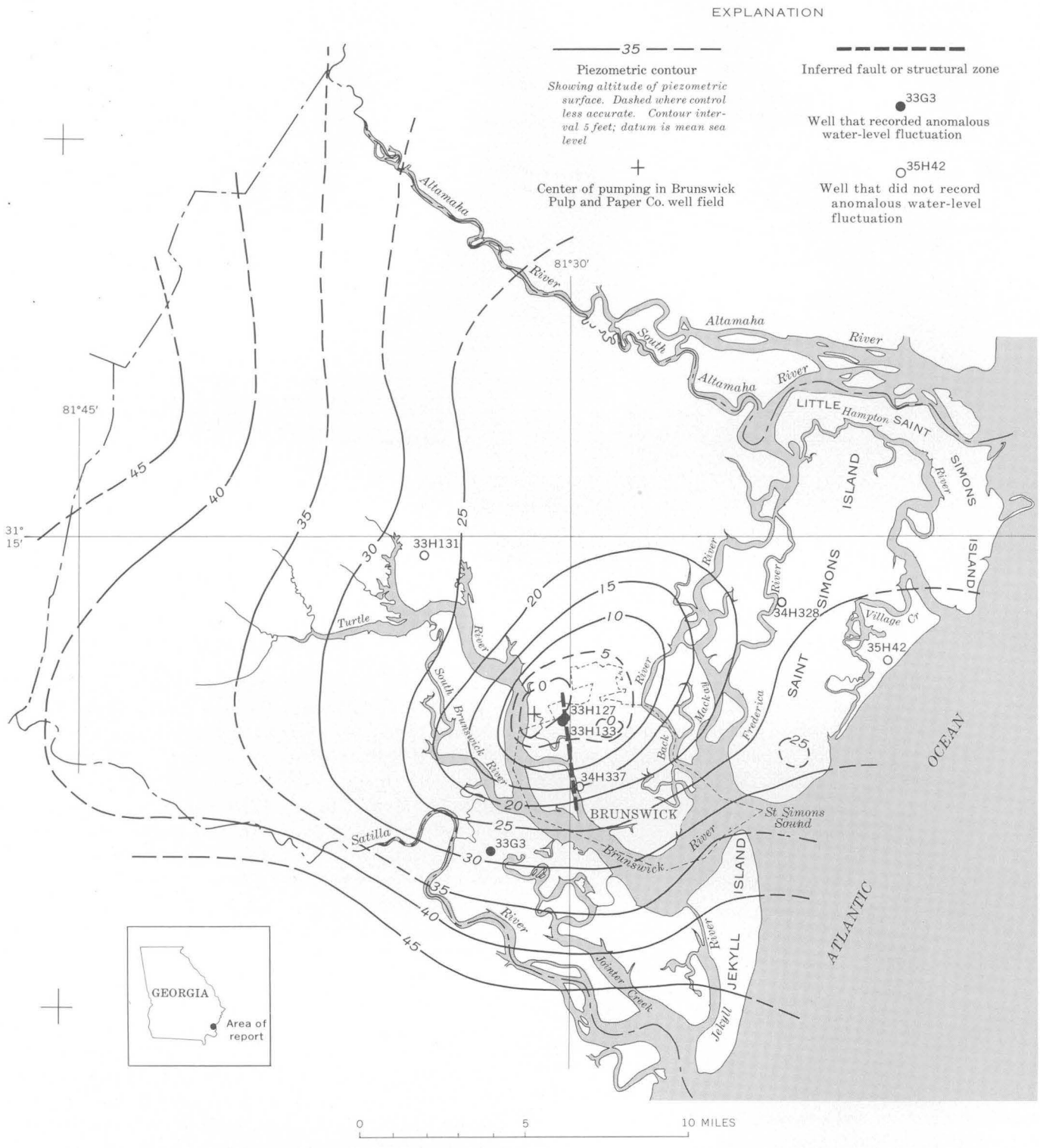

FIGURE 2.—Potentiometric map showing location of wells, a suspected fault zone, and the center of pumping at Brunswick Pulp and Paper Co., Brunswick, Ga. (After Wait and Gregg, 1967.)

main cone of depression away from the well field at Hercules, Inc. Some minor subsidence or structural adjustment should have accompanied the water-level decline in the Brunswick area. There has been, however, no subsequent first-order leveling in the area to determine if subsidence has occurred.

Possibly, subsidence in the Brunswick area was not uniform and did not coincide with water-level decline. Thus the aquifer and the overlying sand and clay may have been subjected to unresolved stress conditons due mainly to the December 1962 increase in pumping. The sudden rise in water levels at the time of the Christmas 1964 shutdown may have triggered a small "earthquake," allowing the aquifer and the overlying materials to adjust to the stress. This adjustment probably took place along a line of weakness, perhaps the suspected fault zone.

REFERENCES

Davis, G. H., Small, J. B., and Counts, H. B., 1963, Land subsidence related to decline of artesian pressure in the Ocala Limestone at Savannah, Georgia: Geol. Soc. America, Eng. Geology Case Histories, no. 4, p. 1–8.

Gregg, D. O., 1966, An analysis of ground-water fluctuations caused by ocean tides in Glynn County, Georgia: Ground Water, v. 4, no. 3, p. 24–32.

Poland, J. F., and Davis, G. H., 1969, Land subsidence due to withdrawal of fluids, *in* D. J. Varnes and George Kiersch, eds., Reviews in engineering geology, v. 2: Boulder, Colo., Geol. Soc. America, p. 187–269.

Wait, R. L., 1965, Geology and occurrence of fresh and brackish ground water in Glynn County, Georgia: U.S. Geol. Survey Water-Supply Paper 1613–E, 94 p., 4 pls., 29 figs.

Wait, R. L., and Gregg, D. O., 1967, Hydrology and chloride contamination of the principal artesian aquifer in Glynn County, Georgia: U.S. Geol. Survey open-file report, 214 p., 40 figs.

NOTES ON THE POSITION OF A PHOSPHATE ZONE AND ITS RELATION TO GROUND WATER IN COASTAL GEORGIA

By ROBERT L. WAIT, Richmond, Va.

Prepared in cooperation with the Georgia Water Quality Control Board and the Georgia Department of Mines, Mining, and Geology

Abstract.—Four inflection points occur on gamma-radiation logs from the coastal area of Georgia. Three of the inflection points are radiation peaks marking phosphate zones. Points A and B occur in the middle and lower Miocene, undifferentiated. Point A occurs in a sand at the base of the silty clay confining bed that lies above and protects the principal artesian aquifer from sea-water intrusion. Inflection point D occurs at the contact of the Oligocene and upper Eocene limestones. Mining of the phosphate zone marked by point A would breach the silty clay confining bed above the principal artesian aquifer and would allow intrusion of sea water into it. Such sea-water intrusion would destroy the ground water resources over a wide area of one of the Nation's largest artesian aquifers and would have dire economic consequences for this area.

During ground-water investigations in Glynn County (Wait, 1962) and Chatham County (McCollum and Counts, 1964), correlations were found to exist between several stratigraphic and lithologic boundaries and four inflection points on gamma-radiation logs. The four inflection points were defined on logs made in Glynn County (Wait, 1962, p. 7). Three of them, *A*, *B*, and *C*, are radiation peaks and mark phosphate concentrations. The fourth inflection point, *D*, occurs at the boundary of the phosphatic sandy Oligocene limestone and the clean biogenic Ocala Limestone. Points *A* and *B* were described as "thin phosphatic sand beds in the Hawthorn Formation." Point *A* has been defined further (Wait and Gregg, 1967, fig. 2) and occurs at the position of a medium- to coarse-grained phosphatic quartz sand immediately beneath the greenish-gray clayey silt identified as middle and lower Miocene, undifferentiated, by Herrick (oral commun., 1966). At places the sand is cemented with calcium carbonate. The phosphate is brown and black, has highly polished, rounded grains, and ranges in size from fine to very coarse. Examination of drill cuttings indicated an increase in phosphate near the base of the clayey silt, but the maximum concentration of phosphate is in the sand beneath it. Gamma-radiation logs show a peak, point *A*, at the position of the sand.

Inflection point *D* is established at the contact of the sandy abundantly phosphatic Oligocene limestone and the clean biogenic Ocala Limestone of late Eocene age. The gamma radiation decreases from a peak in the beds above, to a very low value in the Ocala, and the log becomes nearly featureless to a depth of 1,000 feet or more. The Oligocene limestone generally consists of yellow-gray weathered sandy phosphatic limestone and hard, dense bluish-gray limestone. The bluish-gray material appears to be a secondary deposit, filling cavities in the limestone and may be phosphatic at places. The Ocala Limestone consists of Bryozoa, Foraminifera tests, and pelecypods recemented at places and with large pore spaces where pelecypod fragments have been dissolved.

Figure 1 shows the position of the points *A* through *D* on electric and gamma-radiation logs from test well 3 (33H127) in Brunswick, Glynn County, Ga. (Wait and Gregg, 1967). The configuration as shown by the log of test well 3 remains nearly consistent from Hilton Head Island, S.C., southward along the Georgia coast as far as the middle of Camden County, immediately south of Glynn County. Point *D*, although not as outstanding in figure 1, as in some other gamma-radiation logs, is an easily identifiable feature on nearly all logs made in coastal Georgia.

The thickest section of radioactive materials as indicated by the gamma-radiation logs (see figure 1) occurs

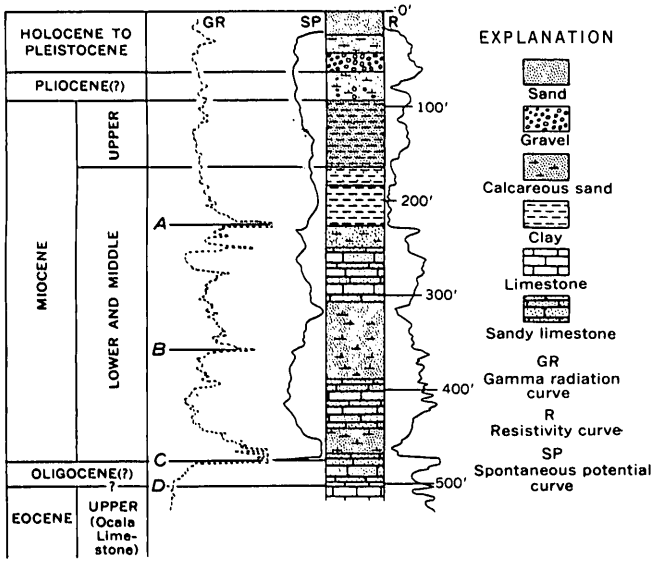

FIGURE 1.—Geology, gamma-radiation and electric logs of test well 3 (33H127), Brunswick, Ga., showing position of inflection points *A* through *D*.

just above point *C* and includes the basal part of the Miocene sediments and the Oligocene limestone. The basal Miocene material in this zone is a much weathered phosphatic sandy limestone, with some phosphatic silt near the base, and light-bluish-gray limestone filling in the solution cavities of the Oligocene limestone.

To date there has been little or no exploration of the Miocene-Oligocene contact in the outcrop area of these sediments. Core drilling and gamma-radiation logging of the core holes, in the outcrop area and in the area immediately downdip, are needed to prove the presence of phosphate there.

Gamma-radiation logs made in the Riceboro area in about 30 water wells in Bryan, Liberty, Long, and McIntosh Counties, show that the inflection points *A* through *D* that were defined in Glynn County, and noted in Chatham County, exist on nearly all the gamma-radiation logs. Some minor variations were noted, especially in the northern part of Bryan County where some of the logs show a zone of radiation above point *A*.

Figure 2 is a structure contour map of the phosphate zone marked by point *A* in parts of Bryan, Liberty, Long, and Glynn Counties and all of McIntosh County. The contour map shows that the phosphatic sand dips gently southwestward throughout the area. A nose trends southwest along U.S. Route 17 in western Bryan County, and a trough trends southeast from Hinesville to an area about 8 miles southeast of Riceboro. The deepest part of the trough is southeast of Riceboro. From Riceboro southward the zone becomes deeper. In the southern part of McIntosh County there is a syncline whose axis is slightly south of east. Because few data are presently available from the area, the position of the syncline is necessarily generalized. The Altamaha River lies on the south limb of the syncline. Although not shown, the Brunswick River at the south boundary of Glynn County also lies in a syncline (Wait, 1965).

The coastal area is one of very low relief, lying mostly between sea level and about 20 feet above sea level with a few small areas as high as 40 feet. Thus, the approximate depth to the phosphatic zone can be determined by adding 20 feet to depth as indicated by the contours. The depth ranges from about 220 to 370 feet below land surface, a depth believed to be beyond economic limits of mining at the present time.

Mining phosphate from the zone represented by point *A*, just beneath the very impermeable clayey silt of the Hawthorn Formation, would be detrimental to the ground-water resources of coastal Georgia. If the clayey silt bed were breached in a mining operation, sea water would be in direct contact with sand above the principal artesian aquifer, and would contaminate fresh ground-water supplies in the sand and the underlying limestone. The sea water would move inland (westward) down the hydraulic gradient to the center of a nearby cone of depression and ruin the aquifer as a fresh-water supply. In the Savannah area where water levels in the principal artesian aquifer are below sea level, sea-water contamination could be expected to proceed at a rapid rate.

If the confining bed where deeply cut but not breached, sea water would penetrate the now weakened confining layer and enter the aquifer nevertheless. This would be especially true where the piezometric surface is below sea level and the gradient across the clayey silt confining bed would cause movement of sea water into the aquifer.

Salt-water contamination has occurred in the coastal area of North Carolina, where fresh-water aquifers have been dewatered in a phosphate mining operation in Beaufort County. A large cone of depression has been created along the coast and extends eastward beneath Pamlico Sound. The ground-water gradient has been reversed, and downward movement of the salty water from the Sound has contaminated fresh-water aquifers (Peek, 1969 p. 12–20).

Whether the confining bed is deeply cut or breached, salt-water contamination would occur, and the resulting deterioration of the fresh ground-water supply would have dire economic consequences in the coastal area where use of ground water amounts to more than 180 million gallons per day.

380-189 O - 70 - 14

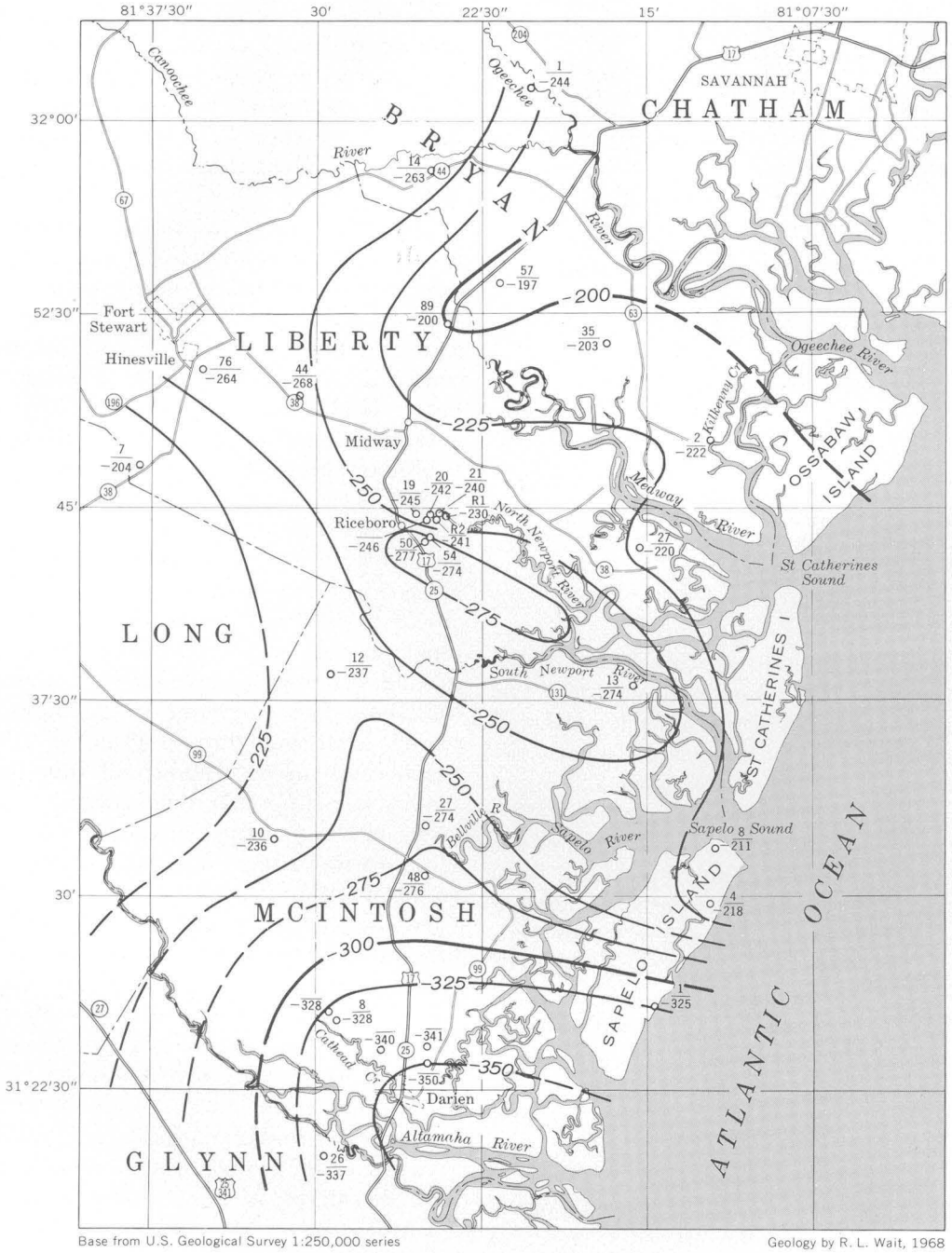

FIGURE 2.—Structure contour map of the phosphate zone indicated by inflection point *A*.

REFERENCES

McCollum, M. J., and Counts, H. B., 1964, Relation of salt-water encroachment to the major aquifer zones, Savannah area, Georgia and South Carolina: U.S. Geol. Survey Water-Supply Paper 1613–D, 26 p.

Peek, H. M., 1969, Effects of large-scale mining withdrawals of ground water: Ground Water, v. 7, no. 4, p. 12–20.

Wait, R. L., 1962, Interim report on test drilling and water sampling in the Brunswick area, Glynn County, Ga.: Georgia Geol. Survey, Inf. Circ. 23, 46 p.

——— 1965, Geology and occurrence of fresh and brackish ground water in Glynn County, Georgia: U.S. Geol. Survey Water-Supply Paper 1613–E, 94 p.

Wait, R. L. and Gregg, D. O., 1967, Hydrology and chloride contamination of the principal artesian aquifer in Glynn County, Georgia; U.S. Geol. Survey open-file report, 214 p.

NONSTEADY INFLOW TO A CHAMBER WITHIN A THICK AQUITARD

By W. W. DUDLEY, JR., Denver, Colo.

Work done in cooperation with the U.S. Atomic Energy Commission

Abstract.—Nuclear devices for underground testing must often be kept dry in chambers excavated in rocks of low permeability thousands of feet beneath the water table. For calculating the time-variable discharge to such a chamber, the chamber interval is arbitrarily treated as an aquifer, although the entire zone actually is an aquitard. Those parts of the aquitard above and below the chamber interval are treated as leaky confining beds. Combining the upper and lower recharge systems into a hydraulically equivalent system with only one recharge source allows the application of a type-curve method developed by Hantush for the constant-drawdown, leaky artesian inflow to a well.

The construction of large cylindrical chambers for nuclear devices in rocks of low permeability, sometimes under hydraulic heads of thousands of feet, has made necessary the prediction of the inflow of water that must be removed to keep such chambers dry. Mining zones are chosen in the least permeable rocks, on the basis of hydraulic testing of exploratory holes, at approximately the desired depth of detonation. Hydraulically, the problem is to compute the gradually declining discharge at constant drawdown to a large-diameter opening in the interior of an aquitard, which is bounded above and below by recharge boundaries.

HYDRAULIC TESTING TECHNIQUES

Hydraulic testing by the U.S. Geological Survey at the Nevada Test Site on behalf of the U.S. Atomic Energy Commission has been described by Blankennagel (1967, 1968). The most applicable tests are conducted in deep exploratory holes at intervals which are isolated by inflatable packers. Packers are lowered on tubing through which water is added to, or withdrawn from, the isolated interval. In the injection test the tubing is filled and purged of air before the ports between the packers are opened. This test closely meets the specifications for an instantaneous slug-injection test. As a check on the injection test, or as a primary technique where the static water level is near the surface, water is withdrawn from the tubing with one or more swabs, and the recovery is measured.

Until recently, analysis of these slug tests has been restricted to determining the specific capacity for the 3- to 4-minute interval after the beginning of recovery (relative specific capacity). To predict nonsteady inflow, however, the test data must be solved for the transmissivity and storage coefficient of the tested interval. A method of analyzing slug tests by type curves has been presented by Cooper, Bredehoeft, and Papadopulos (1967) and has been used successfully for tests at the Nevada Test Site (V. R. Baker, written commun., 1969) and in central Nevada (G. A. Dinwiddie, written commun., 1968).

To determine the positions of recharge boundaries above and below proposed chambering intervals, information gained from hydraulic tests is compared to geophysical logs to pinpoint the depths of permeable zones. Resistivity, caliper, and radioactive-tracer logs are the most useful for this purpose.

SCHEME OF ANALYSIS

No direct analytical method is presently available to the field hydrologist faced with predicting chamber inflow, but, through a series of transformations, a relatively simple type-curve method can be employed.

A chamber located in the central part of a hydrologic unit is analogous to a large-diameter well partly penetrating the unit. Hantush (1961) has shown that the behavior of a well that partly penetrates its source is similar to that of a well tapping a leaky aquifer. This suggests carrying the analogy one step further and arbitrarily considering the chamber interval as a leaky "aquifer" enclosed above and below by aquitards. Figure 1 compares schematically the flow nets for the actual

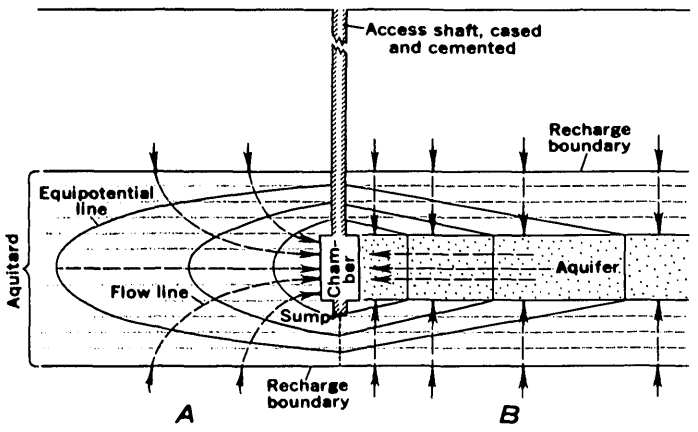

FIGURE 1.—Schematic diagram comparing flow nets for: *A*, actual conditions for part penetration of an aquitard; *B*, hypothetical conditions for a leaky aquifer.

and hypothetical conditions. Similarity is enhanced if the actual horizontal permeability is greater than the vertical permeability.

Hantush (1959) has also provided equations for evaluating constant-drawdown tests of infinite leaky aquifers having but a single aquitard and recharge boundary. To make use of this method, the hypothetical two-aquitard model must be modified to a hydraulically equivalent system which is receiving recharge from only one source. This change or transformation is treated in the section, "Development of model."

In computing discharge to a large-diameter chamber by means of well formulas, the inflow through the top and bottom is neglected. Where the chamber geometry is such that the exposed ends constitute a significant part of the total surface area of the chamber, the neglect of inflow through the ends may cause a serious error. Therefore, an adjustment must be made in the geometry of the model.

ASSUMPTIONS

In addition to the approximations in geometry, certain assumptions are required to solve analytically the constant-drawdown, nonsteady discharge to a well supplied by a leaky aquifer. These assumptions are as follows:

1. The "aquifer" is isotropic, and its transmissivity and storage coefficient are constant in both space and time.
2. The "aquifer" is of sufficient areal extent to encompass the entire cone of depression when steady-state flow is achieved. When no leakage is present, strict adherence to theory requires that the aquifer be of infinite areal extent.
3. Leakage through the confining beds is vertical and proportional to drawdown.
4. Water is released from storage in the "aquifer" instantaneously with a decline in head.
5. Storage in the confining beds is neglected.
6. Drawdown at the chamber radius, r_w, occurs instantaneously and is held constant.

The last assumption is necessary for purposes of computation, although certainly the chamber dimensions increase gradually through the construction period. The effect of this assumption on inflow is considered in a later section.

An assumption that the chamber is of infinitesimal diameter, which is common in constant-discharge analyses, is not required in constant-drawdown analyses, for there is no change in storage in the chamber.

DEVELOPMENT OF MODEL

Figure 2*A* shows the idealized system and the data required to analyze it. The input data are

b_c, b_a, b_b = thicknesses of the chambering zone, the confining bed above, and the confining bed below,

h_c, h_a, h_b = heads in the chambering zone and at the recharge boundaries above and below,

s_c, s_a, s_b = drawdowns with respect to the cavity center for the chambering zone and the recharge boundaries above and below,

k_{va}, k_{vb} = vertical hydraulic conductivities of the confining beds above and below,

k_c = hydraulic conductivity of the chambering zone,

S = storage coefficient of the chambering zone,

r_w = radius of cylindrical chamber, and

r_{sa}, r_{sb} = radii on top and bottom of chamber which are sealed to inflow by construction method.

At the instant that drawdown occurs and inflow begins, the potential gradient at the chamber walls is infinite but begins to decline rapidly as water is released from storage. Equipotential surfaces migrate away from the chamber walls, remaining approximately parallel to them. Consequently, the inflow during the early stages is proportional to the surface area of the chamber, and inflow to the ends can be precisely accounted for by assuming that the ends are sealed and by adding sufficient height to the cylinder to keep the total area constant (fig. 2*B*):

$$A_w = A_c + A_a + A_b,$$

$$2\pi r_w b_w = 2\pi r_w b_c + \pi(r_w^2 - r_{sa}^2) + \pi(r_w^2 - r_{sb}^2), \text{ and}$$

$$b_w = b_c + \frac{2r_w^2 - r_{sa}^2 - r_{sb}^2}{2r_w}, \quad (1)$$

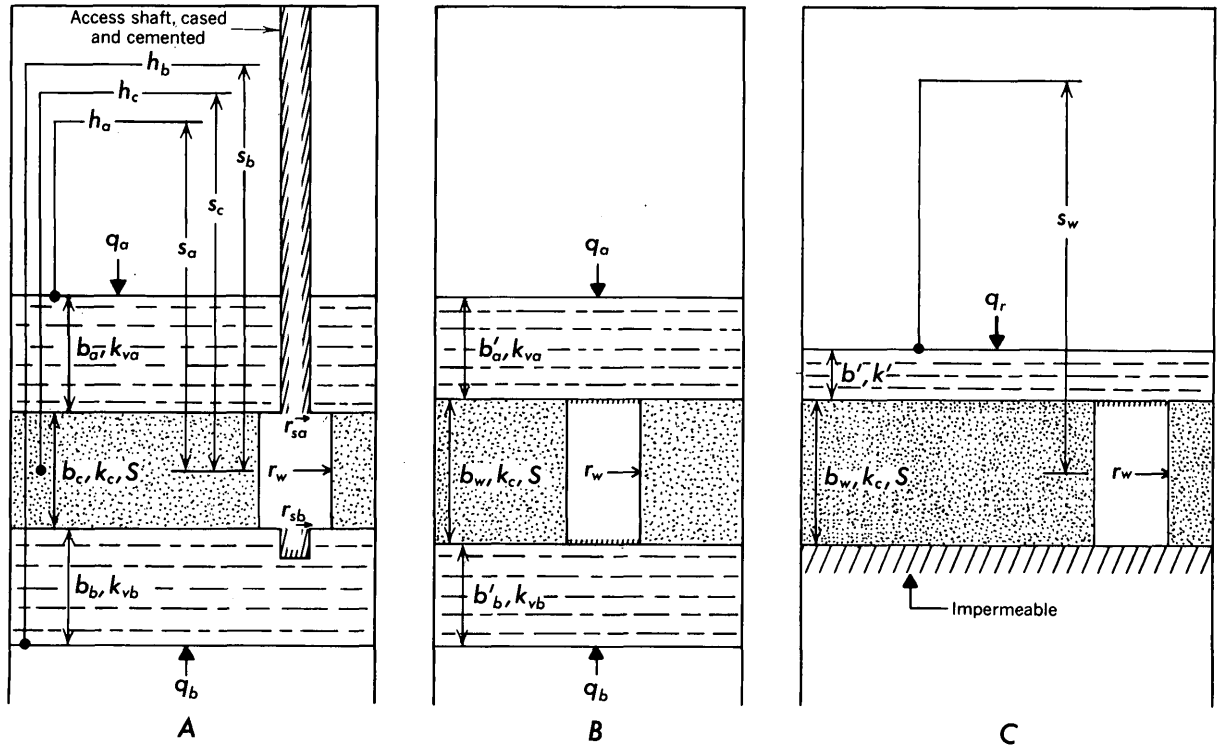

FIGURE 2.—Schematic diagrams showing transformations to account for seepage through the ends of chambers and to produce a single-confining-bed model. *A*, idealized system; *B*, systems wherein ends of chamber are assumed to be sealed; and *C*, single-confining-bed model.

where

A_w=total area of exposed chamber surfaces,
A_c=area of cylindrical surface,
A_a=surface area open to seepage at top of chamber,
A_b=surface area open to seepage at bottom of chamber, and
b_w=enhanced height of chamber.

By this conversion the thickness of the model aquifer is increased to b_w, increasing both its transmissivity, $T=k_c b_w$, and the potential leakage through the confining beds. The resulting adjustment in inflow is approximately correct for early stages but too high for later stages. The thickness of the upper confining bed becomes

$$b_a'=b_a-\frac{(r_w^2-r_{sa}^2)}{2r_w}, \tag{2}$$

whereas that of the lower is

$$b_b'=b_b-\frac{(r_w^2-r_{sb}^2)}{2r_w}. \tag{3}$$

The recharge rate per unit area of aquifer in the single-confining-bed model (fig. 2*C*), q_r, must be equal to the sum of the components from above and below, q_a and q_b:

$$q_r=q_a+q_b,$$

$$s_w k'/b'=s_a k_{va}/b_a'+s_b k_{vb}/b_b', \text{ and}$$

$$s_w=\frac{s_a k_{va}/b_a'+s_b k_{vb}/b_b'}{k'/b'} \tag{4}$$

where

s_w=drawdown with respect to the single recharge boundary,
k'=transformed hydraulic conductivity in the single-confining-bed model, and
b'=transformed thickness of the single confining bed.

Equation 4 contains two unknowns (s_w and k'/b'), but, by analogy with electrical conductors in parallel, the model leakance may be defined as

$$k'/b'=k_{va}/b_a'+k_{vb}/b_b'. \tag{5}$$

Equations 1 through 5 provide the transformed input data for the model depicted in figure 2*C*.

The model drawdown, s_w, computed from equation 4 should be the same as that (s_c in fig. 2*A*) determined from a preconstruction head measurement in the chambering zone. However, in applying this method of generalizing the hydraulic system to analysis of a true aquifer, differences in the computed and measured

drawdowns may occur. This indicates that natural flow is not unidirectional, but rather that the aquifer is either a drain ($s_w > s_c$) or a recharge source ($s_w < s_c$) for the local hydraulic system. In such aquifers, the prediction of early inflow should be obtained using s_c, whereas the sustained inflow, when well yield is supplied entirely from leakage, is best estimated using s_w.

ANALYSIS OF MODEL

Hantush (1959) has shown that the time-variable inflow at constant drawdown is described with consistent units by

$$Q = 2\pi T s_w G(\lambda, r_w/B), \tag{6}$$

where

$$\lambda = \frac{Tt}{r_w^2 S}, \text{ and} \tag{7}$$

$$r_w/B = r_w \sqrt{\frac{1}{T} \cdot k'/b'}. \tag{8}$$

$G(\lambda, r_w/B)$ is the well function for leaky artesian aquifers at constant drawdown and is given by

$$G(\lambda, r_w/B) = (r_w/B)[K_1(r_w/B)/K_0(r_w/B)] + (4/\pi^2) \exp[-\lambda(r_w/B)^2] \int_0^\infty \frac{u \exp(-\lambda u^2)}{J_0^2(u) + Y_0^2(u)} \cdot \frac{du}{u^2 + (r_w/B)^2},$$

where

$$u = r_w \sqrt{1/[\exp(i\pi) B^2]},$$

$K_1(r_w/B)$ = first-order modified Bessel function of the second kind,

$K_0(r_w/B)$ = zero-order modified Bessel function of the second kind,

$J_o(u)$ = zero-order Bessel function of the first kind, and

$y_o(u)$ = zero-order Bessel function of the second kind.

If units are expressed in common field nomenclature (table 1), the discharge equation is (Walton, 1962)

where

$$Q = \frac{Ts_w}{229} G(\lambda, r_w/B), \tag{6a}$$

$$\lambda = 9.29 \times 10^{-5} \frac{Tt}{r_w^2 S}, \text{ and} \tag{7a}$$

$$r_w/B = r_w \sqrt{\frac{1}{T} \cdot k'/b'}. \tag{8a}$$

TABLE 1.—*Units and definitions for inflow equations*

[Abbreviations: gpm, gallons per minute; gpd, gallons per day]

	Consistent units	Field units	Definition
Q	L^3/T	gpm	Discharge.
T	L^2/T	gpd per ft	Transmissivity of chambering zone.
s_w	L	ft	Drawdown.
t	T	min	Time.
r_w	L	ft	Radius of chamber.
S			Storage coefficient.
k'	L/T	gpd per ft^2	Vertical hydraulic conductivity of aquitard.
b'	L	ft	Thickness of aquitard.

Hantush (1959) gives values of $G(\lambda, r_w/B)$ for the ranges of λ and r_w/B that are practical for aquifer analysis. A set of type curves at a convenient scale is published by Walton (1962). Many attempts at solutions in the current study revealed that application of the method to aquitard analysis often requires higher leakage factors. A computer program was written by D. B. Grove, U.S. Geological Survey (written commun., 1968), to extend the curves from $r_w/B = 1 \times 10^{-2}$ to $r_w/B = 1 \times 10^{0}$. Figure 3 shows the type curves; table 2 gives the $G(\lambda, r_w/B)$ values needed to extend Hantush's (1959) data.

The graphical solution of equation 6 can be found as follows:

1. Compute r_w/B.
2. At an arbitrary time, t, compute λ_t.
3. Enter type curves or table with r_w/B and λ to find the well function $G(\lambda, r_w/B)_t$.
4. Compute Q_t.
5. Plot the arbitrarily chosen t (abscissa) and the computed Q_t (ordinate) on a logarithmic overlay of the same scale as the type curves.
6. Place the overlay on the type curves, keeping the axes parallel, and superimpose the point (t, Q_t) on $[\lambda_t, r_w/B\ G(\lambda, r_w/B)_t]$.
7. Trace the proper r_w/B curve to give the variation of discharge with time.

SIGNIFICANCE OF RESULTS

Inherent errors in field data and restrictive assumptions necessary for computations compromise the accuracy of the type-curve solution. The major sources of error are discussed in the following paragraphs.

Quite obviously the assumption of the instantaneous appearance of a full-sized chamber is not met. Accordingly, the calculated inflow during early stages will be higher than that actually found. However, since the gradual construction of the chamber retards early inflow, the dissipation of gradient is also retarded and

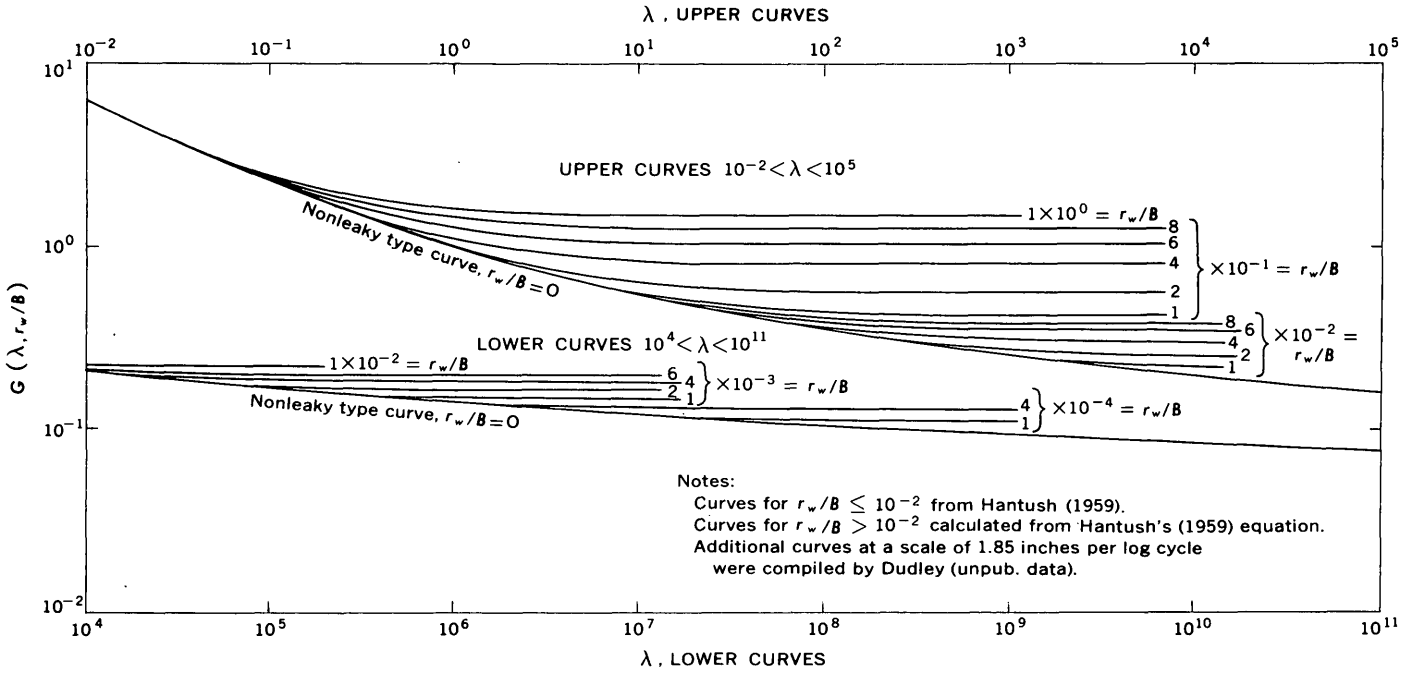

FIGURE 3.—Type curves for nonsteady-state leaky-artesian constant-drawdown discharge to a large-diameter chamber.

TABLE 2.—*Values of the function* $G(\lambda, r_w/B)$

[Data from D. B. Grove, written commun., 1968]

λ \ r_w/B	0	1×10^{-2}	2×10^{-2}	4×10^{-2}	6×10^{-2}	8×10^{-2}	1×10^{-1}	2×10^{-1}	4×10^{-1}	6×10^{-1}	8×10^{-1}	1×10^{0}
1×10^{-1}	2. 24	2. 24	2. 25	2. 25	2. 25	2. 25	2. 25	2. 26	2. 28	2. 31	2. 36	2. 43
2	1. 71	1. 71	1. 71	1. 72	1. 72	1. 72	1. 72	1. 73	1. 76	1. 81	1. 87	1. 96
5	1. 23	1. 23	1. 23	1. 23	1. 23	1. 24	1. 24	1. 25	1. 30	1. 38	1. 48	1. 61
1×10^{0}	. 983	. 983	. 984	. 985	. 986	. 987	. 990	1. 01	1. 07	1. 18	1. 32	1. 49
2	. 800	. 800	. 801	. 802	. 804	. 806	. 809	. 834	. 929	1. 07	1. 25	1. 44
5	. 628	. 628	. 629	. 630	. 633	. 637	. 642	. 682	. 824	1. 01	1. 22	1. 43
1×10^{1}	. 534	. 534	. 535	. 537	. 541	. 547	. 554	. 611	. 793	1. 01	1. 22	1. 43
2	. 461	. 461	. 462	. 466	. 472	. 481	. 491	. 569	. 785			
5	. 389	. 389	. 390	. 397	. 407	. 421	. 438	. 548	. 784			
1×10^{2}	. 346	. 346	. 349	. 359	. 374	. 394	. 417	. 545	. 784			
2	. 311	. 312	. 316	. 331	. 353	. 380	. 408	. 545				
5	. 274	. 276	. 284	. 309	. 341	. 374	. 406					
1×10^{3}	. 251	. 255	. 266	. 301	. 339	. 374	. 406					
2	. 232	. 238	. 255	. 299	. 339							
5	. 210	. 222	. 249	. 299								
1×10^{4}	. 196	. 216	. 248									
2	. 185	. 213	. 248									
5	. 170	. 212										
1×10^{5}	. 161	. 212										
2	. 152											
5	. 143											
1×10^{6}	. 136											

the inflow calculated for later times will be somewhat less than the actual inflow (fig. 4).

The upper and lower limits of discharge can be defined very simply for times after the end of construction. The minimum discharge is obtained by computing the discharge on the assumption that the chamber was formed instantaneously at the beginning of the construction period. Curve *A* on figure 4 is based on this assumption. Curve *B*, on the other hand, gives the theoretical inflow if the chamber had been constructed suddenly on day 8, at the end of the construction period. It was prepared by plotting at day 9 the inflow occurring at day 1 on curve *A*; the inflow at day 10 on curve *B* is the same as that at day 2 on curve *A*. This procedure merely shifts the inflow curve to the right by a constant time increment, which is the length of the construction period. The inflow to be expected in reality falls between these extremes after the chamber is mined to its full size. As figure 4

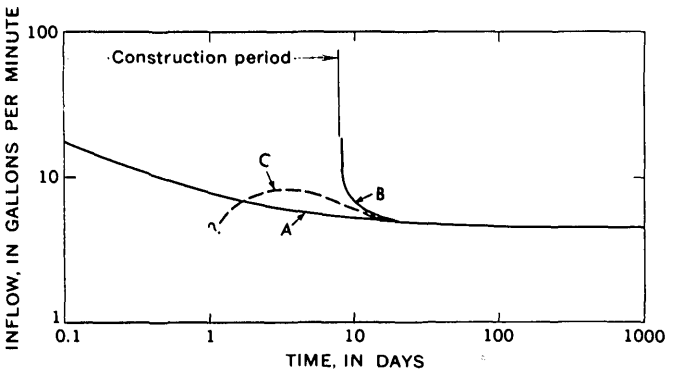

FIGURE 4.—Anticipated discharge to a chamber constructed during an 8-day period. Curve *A* shows the theoretical inflow if the chamber had been constructed instantaneously at the beginning of the construction period, whereas curve *B* gives the inflow if the chamber had been constructed at the end of this period. The actual inflow (curve *C*) falls between these two extremes when the chamber is completed.

shows, the error introduced by assuming that the chamber is formed instantaneously early in the mining stage is very slight by the time full enlargement is reached. For engineering purposes it is suggested that only curve *A* be used. The inflow at a time of 0.1 day provides a safe basis for design of construction-phase pumping systems, while the postconstruction seepage to the chamber can be read directly from the curve.

Reliable results cannot be obtained if the data used in the calculations are subject to error. The inflow is directly proportional to errors in s_w, as can be seen from equation 6. The computed inflow is less sensitive to error in k'/b', although this error does persist throughout the discharge history. As can be seen in equation 7, an incorrect storage coefficient affects the discharge curve by shifting it along the λ-axis. The major effect on predicted inflow will be at early stages, where the type curve is steep, but the error disappears as steady-state flow is approached. Errors in T, although affecting Q directly in equation 6, are partly compensated through its effect on r_w/B and $G\ (\lambda, r_w/B)$.

REFERENCES

Blankennagel, R. K., 1967, Hydraulic testing techniques of deep drill holes at Pahute Mesa, Nevada Test Site: U.S. Geol. Survey open-file rept., 50 p.

——— 1968, Geophysical logging and hydraulic testing, Pahute Mesa, Nevada Test Site: Ground Water, v. 6, no. 4, p. 24–31.

Cooper, H. H., Jr., Bredehoeft, J. D., and Papadopulos, I. S., 1967. Response of a finite-diameter well to an instantaneous charge of water: Water Resources Research, v. 3, no. 1, p. 263–269.

Hantush, M. S., 1959, Nonsteady flow to flowing wells in leaky aquifers: Jour. Geophys. Research, v. 64, no. 8, p. 1043–1052.

——— 1961, Drawdown around a partially penetrating well: Am. Soc. Civil Engineers Proc., Jour. Hydraulics Div., v. 87 (HY4), p. 83–98.

Walton, W. D., 1962, Selected analytical methods for well and aquifer evaluation: Illinois Water Survey Bull. 49, 81 p.

DETERMINING TRANSMISSIVITY FROM WATER-LEVEL RECOVERY OF A STEP-DRAWDOWN TEST

By J. R. HARRILL, Carson City, Nev.

Abstract.—A modified form of the Theis recovery formula provides a means of computing transmissivity from the water-level recovery of a step-drawdown test. This variation of the recovery-test technique is designed primarily for use where no observation wells are available and where it is not feasible to schedule a separate recovery test in addition to a step-drawdown test.

Step-drawdown tests provide information helpful in evaluating the performance of a well and in selecting the optimum pumping rate. A modified form of the Theis recovery formula provides a means of computing transmissivity from water-level recoveries after such a test. Values thus computed provide fairly independent checks of results computed from drawdowns during the pumping period and, if no observation well is available, may provide the best basis for determining transmissivity of the aquifer.

If a well is pumped at a constant rate for a known period of time and then shut down and allowed to recover, the residual drawdown at any instant will be the same as if the discharge of the well had been continued but a recharge well with the same rate of flow had been introduced at the same point at the instant the discharge stopped. The residual drawdown is the difference between the drawdown caused by the pumped well and the recovery represented by water hypothetically injected into the aquifer through the hypothetical recharge well. This relation (Theis, 1935) has been expressed as

$$s'=\frac{264Q}{T}\log t/t',$$

where

s' is the residual drawdown, in feet,
Q is the well discharge, in gallons per minute,
T is the transmissivity of the aquifer, in gallons per day per foot,
t is the elapsed time since the pump was turned on, and
t' is the elapsed time since the pump was turned off.

If discharge is incrementally increased at various times during the pumping period, the resulting drawdown is the same as if pumping of the well were continued at the original rate and an additional well, discharging at a rate equal to the increase in discharge, were introduced at the same point at each instant the discharge is increased. Thus, after a number of increases in discharge, drawdown in the well is equal to the sum of drawdowns from several hypothetical wells which have been pumped at different but constant rates for different periods of time. After the pump on the well is turned off, the residual drawdown at any instant is equal to the sum of the residual drawdowns in each of the hypothetical wells.

For example, assume that a well has been pumped at increments of increased discharge during a step-drawdown test where

$t_1, t_2 \ldots t_n$ are elapsed times since the pump was turned on or discharge increased,
t' is the elapsed time since the pump was turned off,
$Q_1, Q_2 \ldots Q_n$ are well discharge rates, and
$\Delta Q_1, \Delta Q_2 \ldots \Delta Q_n$ are the incremental increases in discharge.

The residual drawdown may be expressed as

$$s'=\frac{264\Delta Q_1}{T}\left(\log\frac{t_1}{t'}\right)+\frac{264\Delta Q_2}{T}\left(\log\frac{t_2}{t'}\right)+\ldots\frac{264\Delta Q_n}{T}\left(\log\frac{t_n}{t'}\right).$$

Further simplification results in

$$T=\frac{264}{s'}\log\frac{t_1^{\Delta Q_1}t_2^{\Delta Q_2}\ldots t_n^{\Delta Q_n}}{t'(\Delta Q_1+\Delta Q_2+\Delta Q_n)}.$$

The exponents, ΔQ, will result in large numbers for the terms, t, which may be cumbersome to work with;

however, because $\Delta Q_1+\Delta Q_2+ \ldots \Delta Q_n=Q_n$ the preceding equation may be rewritten as

$$T=\frac{264Q_n}{s'}\log\frac{t_1^{(\Delta Q_1/Q_n)}t_2^{(\Delta Q_2/Q_n)}\ldots t_n^{(\Delta Q_n/Q_n)}}{t'}. \quad (1)$$

This form of the equation is similar to that developed by Brown (1963, p. 326) to express drawdowns resulting from cyclic intervals of discharge. In the present example, however, the expression is modified to allow for changes in discharge and nonequal periods of pumping at the individual specified rates.

Formula 1 is applied in the same manner as the Theis recovery formula. The residual drawdown, s', is plotted against

$$\frac{t_1^{(\Delta Q_1/Q_n)}t_2^{\Delta Q_2/Q_n)}\ldots t_n^{(\Delta Q_n/Q_n)}}{t'}$$ on semilogarithmic paper, s' being plotted on the arithmetic scale. After the value of t' becomes sufficiently large, the observed data should fall on a straight line. The slope of this line gives the value of the quantity log

$$\frac{t_1^{(\Delta Q_1/Q_n)}t_2^{(\Delta Q_2/Q_n)}\ldots t_n^{(\Delta Q_n/Q_n)}}{t'}\Big/ s'.$$ If the value of

$$\frac{t_1^{(\Delta Q_1/Q_n)}t_2^{(\Delta Q_2/Q_n)}\ldots t_n^{(\Delta Q_n/Q_n)}}{t'}$$ is chosen over one log cycle, its logarithm is unity and equation 1 reduces to

$$T=\frac{264Q_n}{\Delta s'},$$

where $\Delta s'$ is the change in residual drawdown in feet per log cycle of time. Application of this expression is subject to the same limitations as the Theis recovery formula.

REFERENCES

Brown, R. H., 1963, Drawdown resulting from cyclic intervals of discharge: U.S. Geol. Survey Water-Supply Paper 1536–I, p. 324–330.

Theis, C. V., 1935, The relation between the lowering of the piezometric surface and the rate and duration of discharge of a well using ground-water storage: Am. Geophys. Union Trans. pt. 2, p. 517–524.

A SEMIQUANTITATIVE METHOD FOR DETERMINING THE SOURCE OF SPRINGFLOW IN THE MISSOURI OZARKS

By G. L. FEDER, Rolla, Mo.

Work done in cooperation with the Missouri Geological Survey and Water Resources

Abstract.—Springflow-recession curves in conjunction with data on carbonate saturation can be used to make semiquantitative determinations of the source of springflow in the terranes of carbonate rock of the Missouri Ozarks. The recession curve having the maximum slope represents rapid local drainage through nearby sinkholes, losing streams, cave networks, and flow from the regional artesian aquifer. The curve also represents periods of maximum regional flow from the aquifer. As the local drainage is depleted, the springflow-recession curve slowly approaches the minimum slope and primarily represents flow from the aquifer. During periods when the springflow-recession curve approaches the maximum slope, the saturation of the water with respect to dolomite is low, reflecting the short residence time of the local drainage. As the minimum slope of the recession curve is approached, the saturation with respect to dolomite increases and reflects the greater distance traveled and the longer residence time of the regional artesian water.

The determination of the source of water discharged by large springs of the Missouri Ozarks has intrigued many investigators since the springs were first discovered. The problem of source is still not completely resolved, and an understanding of the drainage area from which the water comes has important implications for present-day prevention of pollution and for the proper development of springs.

The purpose of this paper is to present a method for analyzing springflow records to determine whether the springflow is derived from local precipitation, from the regional artesian aquifers, or both. The method used is the analysis of springflow-recession curves. Measurements of carbonate saturation are also used to support the findings. To illustrate the method of analysis, Greer Spring, near Greer, Mo., was chosen because this spring is one of the largest in the State and has the longest continuous discharge records (1921–67). In addition, Greer Spring is the only large spring in Missouri that is not subject to inundation by the river into which it flows.

LOCATION AND GENERAL DESCRIPTION OF AREA

The Missouri Ozarks include most of southern Missouri south of the Missouri River (fig. 1). The area is maturely dissected and is mostly underlain by carbonate rocks. In the eastern part of the area, Precambrian igneous rocks crop out; elsewhere, the Precambrian is mostly 1,200–2,000 feet below the surface. A generalized stratigraphic section of southeastern Missouri is shown in figure 2. Throughout most of the Ozarks large quan-

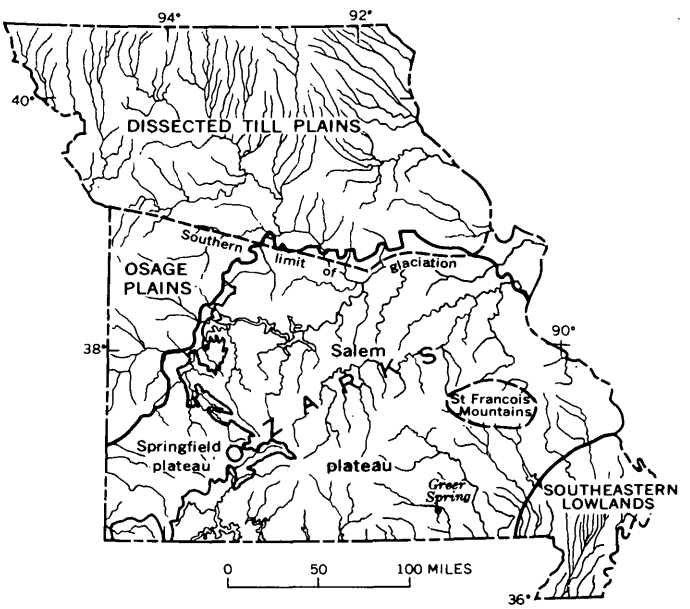

FIGURE 1.—Map showing the physiographic division of Missouri, and the location of Greer Spring, southeastern Missouri.

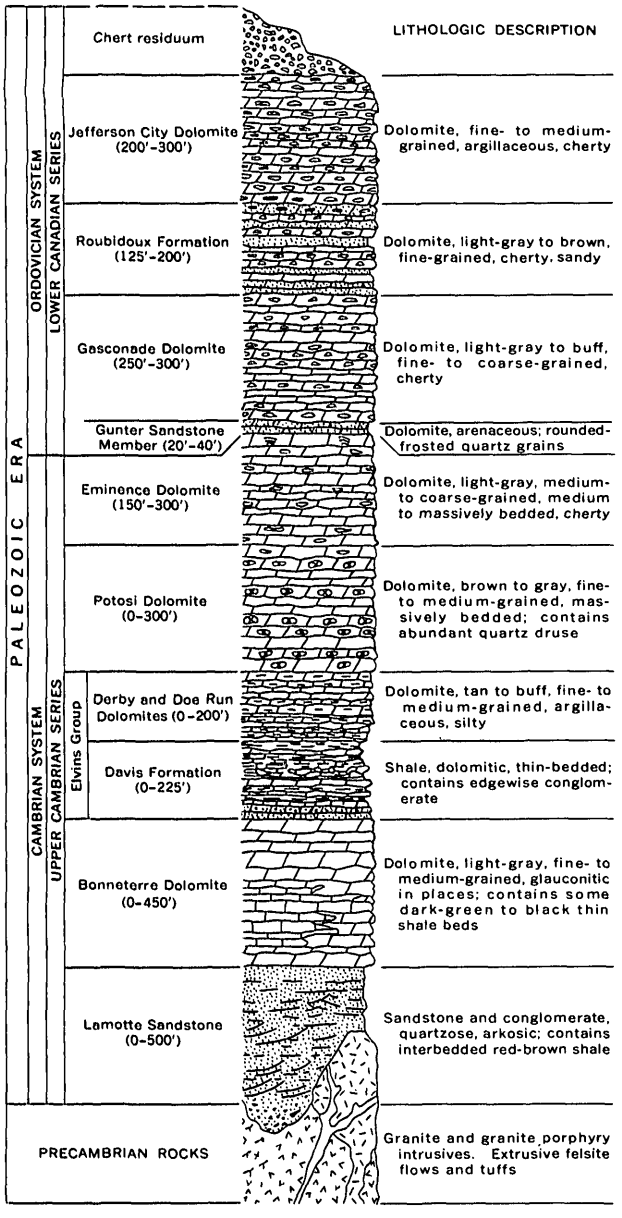

FIGURE 2.—Generalized stratigraphic section of southeastern Missouri (adapted from Hayes, 1961).

tities of fresh artesian water circulate at depth in carbonate-rock aquifers. This is shown by the large yields and the low dissolved-solids content of most wells drilled more than 1,000 feet deep. Deep wells (more than 1,000 feet) in the area generally yield between 50 and 500 gpm (gallons per minute) (Robertson, 1962), and the water has a dissolved-solids content below 300 mg/l (milligrams per liter). The major outlets for this artesian water are the numerous springs in the area.

The region contains some of the largest springs in the United States. There are nine springs with an average discharge greater than 100 cfs (cubic feet per second) (Beckman and Hinchey, 1944). Near most springs are numerous sinkholes and cave systems that connect with the springs. During periods of heavy percipitation, water rapidly drains through the sinkholes and caves and is discharged through the springs. The supply of water from local drainage is depleted rapidly, and flow from the regional artesian aquifers becomes the major source of springflow during dry periods.

Most of the ground-water movement in the Ozarks is through enlarged solution openings. The area has most of the features of typical karst terrane. In many parts of the area all drainage moves underground, except during periods of intense or protracted rainfall. The average annual precipitation ranges from 39 inches in the northwest to 45 inches in the southeast. The average annual runoff from drainage areas greater than 100 square miles ranges from less than 3 inches to more than 17 inches. Some springs in the area exhibit a rapid increase in discharge after precipitation, whereas others show little change even after heavy precipitation.

PREPARATION OF RECESSION CURVES

The maximum and minimum 5-day recession curves for Greer Spring were drawn according to methods outlined by Riggs (1964). To eliminate the effects of surface runoff from a 2.97-square mile drainage area above the spring, the first 5 days after a hydrograph peak were not used in the computation. As the starting point for the recession curves, 600 cfs was chosen. The minimum flow for the period of record was 104 cfs. The resulting recession curves are shown in figure 3.

CARBONATE SATURATION

Data from wells and springs in the Missouri Ozarks indicate that the percentages of saturation of ground water and spring water, with respect to both calcite and dolomite, increase with the length of time the water is

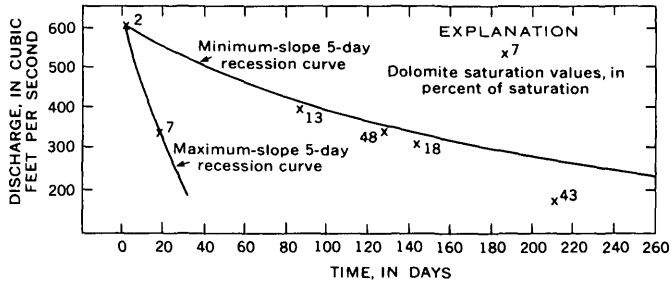

FIGURE 3.—Graph showing maximum and minimum 5-day recession curves and plot of dolomite saturation values for Greer Spring, Mo.

in contact with the aquifer. Figure 4, which is a graph of the percentage of saturation of calcite versus dolomite for samples of well and spring water collected in the region, shows that at first the saturation with respect to calcite is higher than the saturation with respect to dolomite. At about 60 percent of saturation both values are almost equal. Above a value of 60 percent, saturation with respect to dolomite increases more rapidly than that of calcite. Saturation values with respect to dolomite were chosen for comparison with the springflow-recession curves because the greater range in values permits more accurate analysis within the limits of sampling accuracy.

Owing to the complexity of the hydrologic system, various factors may cause dilution of spring water. Water in the regional artesian aquifer may be diluted to various degrees by precipitation. Variations in the carbon dioxide content of the soil can further complicate the effects of dilution resulting from precipitation. For example, if the carbon dioxide content of the soil were high, water infiltrating through the soil would pick up a large amount of carbon dioxide. If this water then mixed with ground water containing little carbon dioxide and saturated with respect to dolomite, it would lower the degree of saturation of the ground water more than the same quantity of water which had infiltrated through the soil when it contained little carbon dioxide. Another source of low carbon dioxide waters is from rapid recharge through sinkholes. The effects of these processes result in wide fluctuations in percentage of dolomite saturation in some deep wells in the region.

Saturation values with respect to dolomite for spring water are affected both by hydrochemical changes in the regional artesian aquifer and by rapid dilution resulting from local drainage. The effects of dilution result in saturation values that cannot be used to interpret the relative age of the water. However, the data can be used to support interpretation of springflow-recession data by indicating when dilution is occurring, and whether the dilution is occurring within the regional artesian aquifer or from local drainage.

Saturation values with respect to dolomite at Greer Spring were calculated according to methods outlined by Back (1961). The values were plotted with respect to the springflow-recession curves (fig. 3) by the following procedure:

1. The spring discharge on the day of sampling was obtained, and the discharge 5 days before sampling was determined from the discharge record.
2. The number of days separating the recession curves having the maximum and minimum slopes at the discharge value on the day of sampling was determined from figure 3.

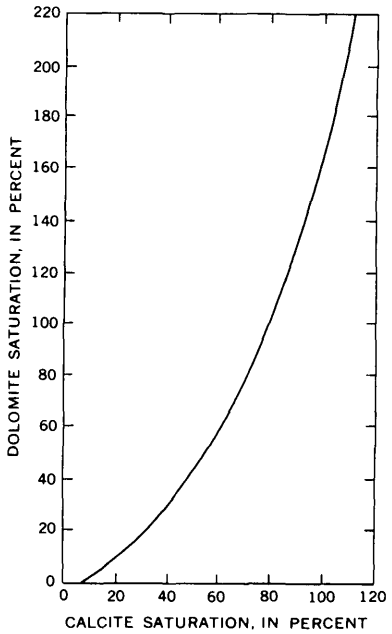

FIGURE 4.—Graph showing the general relation between the percentage of saturation with respect to calcite and dolomite for samples of well and spring water collected in the Missouri Ozarks.

3. The location of the value of the dolomite saturation (point X) with respect to the recession curves having the maximum and minimum slopes was computed by use of the formula

$$X=D\frac{S-L}{M-L},$$

where

X=length measured in terms of days from the recession curve of minimum slope at the spring discharge on the day of sampling,

D=length measured in terms of days between the recession curves having the minimum and maximum slopes at the spring discharge on the day of sampling,

S=difference (in cfs) between the measured spring discharge on the day of sampling and the discharge 5 days before, and

L=difference (in cfs) between (1) the measured spring-discharge value on the day of sampling plotted on the recession curve having the minimum slope and (2) the discharge on that curve 5 days before.

ANALYSIS

The two recession curves obtained in figure 3 are a result of variations in the source of water to the spring. Large perennial springs in Missouri obtain water from local drainage and regional artesian aqui-

fers. The local drainage may extend for a few tens-of-miles around the spring and may include sinkholes, losing streams, and extensive cave networks connected to the surface. The local drainage is quite sensitive to local precipitation, and water from this source drains rapidly to the spring. Owing to the short time of travel to the spring, and the relatively small surface area exposed to solution in large openings, the percentage of dolomite saturation of this water is low.

The maximum 5-day recession curve is a result of predominantly rapid local drainage to the spring in addition to drainage of regional artesian ground water. The dolomite-saturation values (fig. 3), which are lower at similar discharge rates as the values approach the maximum recession curve, indicate that most of the springflow is from nearby sources.

The maximum 5-day recession curve cannot be used to predict flows for more than 5 days. After 5 days the slope of an actual springflow-recession curve would diminish, and eventually the slope will approximate the minimum 5-day recession curve.

The minimum 5-day recession curve (fig. 3) characterizes the springflow when the supply of water from the regional artesian aquifers is at a maximum. The regional water generally travels a long distance through diverse openings before reaching the spring. There is also much more ground-water storage available in the regional aquifer than in the local system of solution openings. These factors result in better sustained springflow and higher dolomite saturation.

CONCLUSIONS

Springflow-recession curves and saturation data with respect to dolomite or calcite can be used to estimate the relative quantities of local drainage and regional artesian-aquifer drainage to a spring at a particular time. Variations in dilution of water in the regional aquifer does not always permit comparison of carbonate-saturation data for different recessions. In other words, a given point on the minimum-sloped-recession curve (fig. 3) may have different carbonate-saturation values for different events.

The minimum 5-day recession curve represents the most well-sustained periods of flow resulting from a maximum amount of regional artesian ground water discharging to the spring at a given rate. The maximum 5-day recession curve represents flow after precipitation, and represents a maximum amount of local drainage and storage, which are rapidly depleted. Both curves (fig. 3) represent the extremes for the period of record.

In addition to providing an insight into the character of springflow, recession curves can be used to determine causes and sources of changes in springflow regimen or quality, and to predict the effects of manmade changes on the spring system.

REFERENCES

Back, William, 1961, Calcium carbonate saturation in ground water, from routine analyses: U.S. Geol. Survey Water-Supply Paper 1535–D, 14 p.

Beckman, H. C., Hinchey, N. S., 1944, The large springs of Missouri: Missouri Div. Geol. Survey and Water Resources, v. 29, ser. 2, 141 p.

Hayes, W. C., 1961, Physiographic features of the St. Francois Mountains, *in* Guidebook to the geology of the St. Francois Mountain area, Association of Missouri Geologists, 8th annual field trip, 1961: Missouri Div. Geol. Survey and Water Resources Rept. Inv. 26, p. 115–118.

Riggs, H. C., 1964, The base-flow recession curve as an indicator of ground water, *in* Symposium—Surface Waters, Gen. Assembly of Berkeley of Internat. Union Geodesy and Geophysics, 1963: Internat. Assoc. Sci. Hydrology, Pub. 63, p. 352–363.

Robertson, C. E., 1962, Water well yield map of Missouri: Missouri Div. Geol. Survey and Water Resources, scale 1 inch = 12 miles.

OPTIMIZATION OF CONJUNCTIVE USE OF WATER IN A STREAM-AQUIFER SYSTEM, USING LINEAR PROGRAMING

By O. JAMES TAYLOR, Denver, Colo.

Work done in cooperation with the Colorado Water Conservation Board and the Southeastern Colorado Water Conservancy District.

Abstract.—A linear program was used to show how conjunctive use of ground water and surface water in a stream-aquifer system can be manipulated to minimize depletion of the stream. The program was designed to achieve the objective by satisfying the demand for irrigation water, using ground water and surface water selectively during a 2-month period.

In irrigated river basins, water is commonly obtained from canals, which divert water from a stream, and from large-capacity irrigation wells, which obtain water from an alluvial aquifer which is in hydraulic connection with the stream. The effect of irrigation practices on streamflow and the aquifer is dependent on the spatial and temporal patterns of conjunctive use.

In many river basins in the Western United States, surface water is abundant enough to satisfy demands during the spring and early summer when the principal yearly runoff occurs. In late summer, when streamflow is low, much less water is available for canal diversion and ground-water withdrawals may have a marked effect on streamflow.

This paper discusses a scheme for conjunctive use in the late summer which minimizes the effect of irrigation practices on depletion of the stream.

REACH-CELL STRUCTURE

The Arkansas River valley is an intensively irrigated area in southeastern Colorado. Between Pueblo, Colo., and the Kansas State line, irrigation water is supplied by 23 canals and more than 1,300 irrigation wells. To facilitate simulation studies of the hydrologic system, the valley has been divided into reaches between canal diversion points and gaging stations (fig. 1). Thus, the reach boundaries represent locations where streamflow records are available or where diversions for downstream areas can be specified.

The aquifer in each reach has been subdivided into cells which are roughly parallel to the stream (Moulder and Jenkins, 1969). Three cells on one side of the stream are shown in figure 1. In wide reaches of the river valley, as many as 10 cells on each side of the stream were used to subdivide the reach. The subdivision of the aquifer into cells was devised to facilitate handling of large amounts of hydrologic data and numerous response curves relating aquifer stress at various locations to streamflow effect. The use of this scheme requires the assumption that the positive stresses (recharge) or negative stresses (discharge) are uniform over the cell. The *sdf*—stream depletion factor—values (Jenkins,

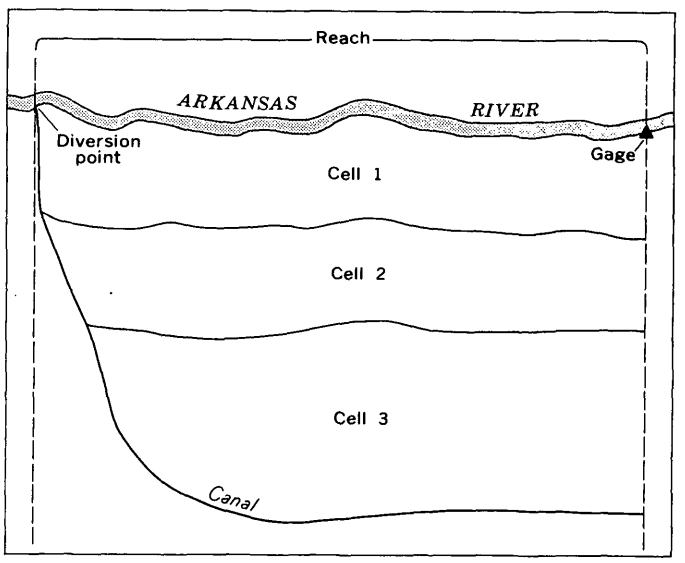

FIGURE 1.—Example of a three-cell subdivision of a reach of the Arkansas River valley.

1968a, 1968b) of cells 1, 2, and 3 are 1, 16, and 65 days, respectively. The relation between a cell stress of 1-month duration in each cell and the effect on the stream is shown in figure 2. The response curves shown were derived using the techniques and assumptions of Jenkins (1968a, 1968b). The nonlinear response curves shown in figure 2 were partitioned into volumetric effects for time units of 1 month for use in a linear program.

LINEAR PROGRAMING

A linear program [1] was devised to supply irrigation water to the three-cell reach shown in figure 1. The objective was to minimize stream depletion during July and August subject to certain specified constraints. The data necessary for the program are:

1. Area and ground-water storage of each cell,
2. Allowable pumpage in each cell,
3. Demand for water in each month, and
4. Response coefficients for each month and cell.

Properties of the cells and hydrologic demands and constraints are shown in table 1. The area and ground-water storage of each cell were calculated from field measurements. The allowable pumpage in each cell was arbitrarily specified as a portion of the total storage in that cell. The demand data were computed by prorating estimated monthly demands for the reach on the basis of cell area. The last two columns of table 1 represent the time-partitioned coefficients of v/Qt, where v is the cumulative volumetric streamflow effect and Qt represents the monthly stress volume. The coefficients are those due to a stress for only 1 month.

The linear program matrix is shown in table 2. The following assumptions were made:

1. Eighty percent of all applied water is consumed,
2. All water diverted by the canal is applied uniformly over the entire reach,
3. All water withdrawn from wells is applied in the same cell from which it was withdrawn, and
4. The initial hydraulic gradient between the aquifer and stream was zero.

[1] A solution was obtained using International Business Machines Corp. mathematical programing system/360 (360A–CO–14X) linear and separable programing.

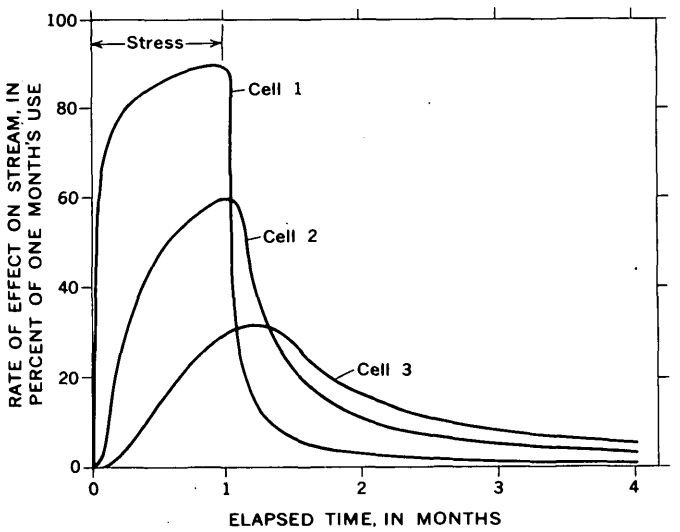

FIGURE 2.—Effect of cell stress for 1 month on streamflow in a reach of the Arkansas River bordered by a three-cell subdivision. Stress is either positive (recharge) or negative (discharge).

The objective equation, DEPLETE, shows the effect of all possible actions on streamflow in the 2-month period. D_1 and D_2 represent canal diversions in acre-feet in July and August, respectively. Diversions during the second month deplete the streamflow more than diversions the first month because of the different durations of return flow in the simulation period. The variable P_{ij} represents pumpage in acre-feet, where i is the serial number of the month and j is the number of the cell. The effect of pumpage on streamflow decreases with increasing distance from the stream and with elapsed time because of the relations shown in figure 2.

The coefficients in the objective equation were derived using values of v/Qt shown in table 1 and considering:

1. Diversion from the stream by the canal,
2. Consumption of canal water,
3. Return flow from applied canal water,
4. Effect of ground-water withdrawals on streamflow,
5. Consumption of ground-water withdrawals, and
6. Return flow from applied ground water.

The three constraining equations CELSTOR$_j$ represent pumpage restraints in the cell j which were speci-

TABLE 1.—*Cell statistics used to design linear program*

Cell No.	Area (acres)	Percentage of total area	Ground-water storage (acre-feet)	Allowable pumpage (acre-feet)	Demand (acre-feet)		Month 1 v/Qt	Month 2 v/Qt
					July	August		
1	570	29	3, 640	730	536	508	0. 81	0. 10
2	500	25	1, 500	375	463	438	. 41	. 26
3	910	46	2, 550	760	851	804	. 14	. 25
Total	1, 980	100	7, 690	1, 865	1, 850	1, 750		

380-189 O - 70 - 15

TABLE 2.—*Matrix for linear program*

Objective equation														
DEPLETE=	$0.88D_1$		$+0.92D_2$		$+0.73P_{11}$		$+0.65P_{21}$		$+0.54P_{12}$		$+0.33P_{22}$		$+0.31P_{13}$	$+0.11P_{23}$
Constraining equations														
$CELSTOR_1$=					P_{11}	+	P_{21}							≤ 730
$CELSTOR_2$=									P_{12}	+	P_{22}			≤ 375
$CELSTOR_3$													P_{13} +	$P_{23} \leq 760$
DEM_{11}=	$0.29D_1$			+	P_{11}									=536
DEM_{21}=			$0.29D_2$			+	P_{21}							=508
DEM_{12}=	$0.25D_1$							+	P_{12}					=463
DEM_{22}=			$0.25D_2$							+	P_{22}			=438
DEM_{13}=	$0.46D_1$											+	P_{13}	=851
DEM_{23}=			$0.46D_2$										+	P_{23}=804

fied in table 1. The six constraining equations DEM_{ij} express the demand in the month i and cell j.

The problem was solved on an IBM 360 computer, model 65. The total computation time in the central processing unit was 1.00 second. Values used in the optimal solution are shown in table 3.

TABLE 3.—*Values used in optimal solution of linear program*

Month	Cell		
	1	2	3
Surface-water diversions, in acre-feet			
1	536	462	850
2	74	64	118
Ground-water withdrawals, in acre-feet			
1	0	1	1
2	434	374	686

The computed minimum for stream depletion, DEPLETE, in the 2-month period was 2,344 acre-feet. Thus, about 65 percent of all applied water was depleted from the stream during the 2-month simulation. The stream depletion in the absence of irrigation wells would have been 3,238 acre-feet, which was computed from the objective equation in table 2.

The optimal solution suggests that the effect of irrigation practices on streamflow can be minimized by using canal water in the first month and using pumped ground water in the second month. Thus, the system benefits from (1) return flow the second month owing to canal diversions the first month, and (2) the smaller effect on the stream of pumpage the second month compared to pumpage the first month. The maximum amount of allowable pumpage was realized only in cell 2.

A sensitivity analysis accompanies the solution of the linear program and is partly shown in table 4. The analysis shows the effect of limited unit adjustments in variables and constants on stream depletion. The analysis shows the critical effect of the relatively small allowable pumpage in cell 2. (See table 1.) In general, the effects of irrigation in cell 1 are more critical than in cell 3 because of the proximity to the stream.

TABLE 4.—*Sensitivity analysis of linear program*

Variable	Change (acre-feet)	Limit (acre-feet)	Decrease in DEPLETE (acre-feet)
DEM_{12}	−1.0	462.0	2.94
DEM_{22}	−1.0	398.4	2.72
$CELSTOR_2$	+1.0	414.6	2.39
P_{11}	−1.0	−.5	.72
DEM_{21}	−1.0	74.2	.65
DEM_{13}	−1.0	850.2	.31
DEM_{23}	−1.0	117.6	.11

It seems unlikely that lowering the demand for water by 1 acre-foot to a limit of 462 acre-feet in the first month and the second cell would cause the stream depletion to decrease by 2.94 acre-feet, as shown in table 4. The large effect is due to a radical change in the diversion and ground-water withdrawal pattern as documented in table 5. The lower demand allows a smaller diversion the second month with corresponding adjustments in pumpage.

The sensitivity analysis may also suggest a number of previously ignored options to the analyst, such as artificial recharge, modification of crop type, and so forth. In summary, the analysis indicates the most sensitive variables in the program and gives information useful for improving the specified objective.

TABLE 5.—*Effect of lowering DEM_{12} by 1 acre-foot*

Variable	Change (acre-feet)	Effect on DEPLETE (acre-feet)
P_{12}	−1.00	−0.54
P_{22}	+1.00	+.33
D_2	−4.00	−3.68
P_{23}	+1.84	+.20
P_{21}	+1.16	+.75
Net change		−2.94

Most large computer systems with linear programing options are capable of handling a much larger matrix than presented here. Therefore, the analyst could easily investigate a system involving a greater number of cells, time periods, and constraints. For a longer simulation period the amount of allowable stream depletion in intervening months could be constrained. Additional pumpage could be allowed owing to recharge from applied canal water. Also, it would be beneficial to investigate the result of pumping ground water distant from the stream and applying the water near the stream, thus delaying the effect of pumpage on the stream and accelerating the return flow to the stream from applied water. If the best pattern of conjunctive use in each reach of a river basin is found, the results can be combined into a management scheme for the entire irrigation system.

CONCLUSIONS

If the irrigation system of a river basin can be reduced to a series of linear equations of tolerable errors, a great deal of insight is provided by the solution and sensitivity analysis of a linear program. The results of the program are highly dependent on the specified constraints which should be based on field measurements.

REFERENCES

Jenkins, C. T., 1968a, Techniques for computing rate and volume of stream depletion by wells: Ground Water, v. 6, no. 2, p. 37–46.

——— 1968b, Electric-analog and digital-computer analysis of stream depletion by wells: Ground Water, v. 6, no. 6, p. 27–34.

Moulder, E. A., and Jenkins, C. T., 1969, Analog-digital models of stream-aquifer systems: Ground Water, v. 7, no. 5, p. 19–24.

380-189 O - 70 - 16

THE USE OF AUTOMATED TITRIMETRY FOR ANALYSES OF NATURAL WATER

By MARVIN J. FISHMAN and RALPH F. PASCOE,
Denver, Colo., Oklahoma City, Okla.

Abstract.—Automated titrimetric analysis has been applied to the determination of alkalinity, chloride, and sulfate in fresh water. Replicate analyses and comparison of results with those obtained by similar manual titration methods show that automated titrimetric methods are accurate and reproducible, and provide a rapid means for the determination of these substances in water.

Automation of routine chemical analyses, using flame photometers, atomic absorption spectrophotometers, colorimeters, and titrimeters, has assumed major proportions in the field of analytical chemistry. Although originally used almost exclusively for clinical analysis, automation now finds widespread application in water analysis. This paper describes automated titrimetric procedures for determining alkalinity, chloride, and sulfate in water. Presently used manual procedures by Rainwater and Thatcher (1960, p. 281) and Clarke (1950) were adapted to a Fisher Titralyzer equipped with potentiometric and photometric accessories.

REAGENTS

Alkalinity

Sulfuric acid, 0.01639*N*, 1.00 ml≎1.00 mg HCO_3^{-1}: Add 0.5 ml concentrated H_2SO_4 to 950 ml demineralized water. Standardize the solution after it has been thoroughly mixed.

Chloride

Mercuric nitrate standard solution, 1.00≎0.50 mg Cl^{-1}: Dissolve 2.4160 g $Hg(NO_3)_2H_2O$ in demineralized water, add 0.25 ml concentrated HNO_3, and dilute to 1,000 ml with demineralized water.

Mixed-indicator solution: Dissolve 0.5 g *s*-diphenylcarbazone and 0.05 g bromphenol blue in 100 ml ethanol. Store in a dark bottle. The reagent is stable for approximately 6 months.

Nitric acid, 0.05*N*: Dilute approximately 3 ml concentrated HNO_3 to 1 liter with demineralized water.

Chloride standard solution, 1.00 ml≎1.00 mg Cl^{-1}: Dissolve 1.648 g of primary standard NaCl crystals in demineralized water and dilute to 1,000 ml.

Sulfate

Barium chloride standard solution, 1.00 ml≎0.20 mg SO_4^{-2}: Dissolve 0.434 g anhydrous $BaCl_2$, dried for 1 hr at 180°C, in demineralized water and dilute to 1 liter.

Solvent-indicator solution: Dissolve 0.025 g thorin (K & K Labs, Inc., No. 5983 has been found to be satisfactory) and 0.5 g anhydrous sodium acetate completely in 10 ml water. Heat on steam bath if necessary. Add the solution to 1,000 ml 95-percent ethanol (SDA–3A is satisfactory) and mix. Add 12 ml glacial acetic acid and mix. Larger quantities may be prepared because the solution is stable.

Sulfate standard solution, 1.00 ml≎1.00 mg SO_4^{-2}: Dissolve 1.47 g Na_2SO_4, dried for 2 hrs at 180°C, in demineralized water and dilute to 1,000 ml.

Ion-exchange columns, charged with Amberlite IR–120 (hydrogen form).

PROCEDURE

The titralyzer is set up according to the directions given in the instruction manual. The potentiometric head is used for the alkalinity determination, and the photometric head is used for the chloride and sulfate determinations. The procedures used in this study are discussed below.

Alkalinity

Pipet a volume of sample containing less than 30 mg alkalinity as bicarbonate (50.0 ml maximum) into a 200-ml Berzelius beaker. Do not use a volume less than 25.0 ml because inconsistent results will occur. If a sample contains more than 1,200 mg bicarbonate per liter, use a stronger titrant.

Set the bicarbonate end point to pH 4.5 with a standard pH-4 buffer. Follow the instructions provided with the instrument. Place the samples in position in the turntable and activate the automatic potentiometric titration, using 0.01639*N* sulfuric acid as titrant (1.00 ml≏1.00 mg HCO_3^{-1}). Set the ACID-BASE switch in the BASE position. If the samples contain carbonate, indicated by a pH greater than 8.3, first set the end point to pH 8.3. After titrating the carbonate, set the pH to 4.5 and titrate the bicarbonate. If a set contains both carbonate-bicarbonate and bicarbonate samples, first titrate all the samples to pH 8.3, because the titralyzer will print 0.00 ml for the bicarbonate samples. Samples will then remain in the same sequence for the bicarbonate titration.

Chloride

Pipet a volume of sample containing less than 12.5 mg chloride (100.0 ml maximum) into a 200-ml Berzelius beaker and adjust the volume to 100 ml with demineralized water. Prepare three standards (5 mg chloride) and two demineralized-water blanks and adjust the volume of each to 100 ml with demineralized water. Add 0.2 ml mixed-indicator solution to each sample, standard, and blank. If a blue, blue-violet, or red color develops, add 0.05*N* nitric acid, dropwise, until the color changes to pale yellow. Then add an additional 2 ml of 0.05*N* nitric acid. If the sample is yellow after adding the indicator, add 1*N* sodium hydroxide, dropwise, until the color changes to blue, and then proceed with the nitric acid.

Visually titrate one of the standard chloride samples with standard mercuric nitrate solution to a faint purple end point. Place the titrated standard into a light shield, lower the photometric assembly into the beaker, and set the end point according to directions given in the instruction manual. The mixed indicator is not stable, and this end point is set each time samples are analyzed. The indicator should be discarded after 6 months.

Place the samples, standards, and demineralized-water blanks into the light shields in the turntable and activate the automatic photometric titration. Because absorbance increases during the titration, the ACID-BASE switch is set to the ACID position.

Sulfate

Rinse the ion-exchange columns with 30 to 40 ml of sample and discard the rinse. Pass an additional volume of sample through the exchanger to provide a 25-ml effluent for the determination. Pipet a volume of sample containing less than 5.0 mg SO_4 (25.0 ml maximum) into a 200-ml Berzelius beaker and adjust the volume to 25.0 ml. Prepare two standards (1.0 and 5.0 mg SO_4) and two demineralized-water blanks and adjust the volume of each to 25.0 ml with demineralized water. Add 100 ml solvent-indicator solution to each sample, standard, and blank. Place a standard into a light shield, lower the photometric head, and balance the potential. Then set the potential 10 to 12 mv (millivolts) lower. For example, if the initial balance is at 175 mv, the end point is set at about 165 mv. With this technique, the blank titration is approximately 0.35 ml. Alternatively, the end point can be set by adding 0.35 ml titrant manually to the blank, balancing the potential, and titrating automatically three or four additional blanks, while making minor adjustments in the balance to give a blank titration of 0.45 to 0.50 ml. The solvent indicator is stable; however it is advisable to reset the balance each time a set of samples is analyzed.

Place the samples, standards, and blanks into the light shields in the turntable and activate the automatic photometric titration. Because absorbance increases during the titration, the ACID-BASE switch is set to the ACID position.

CALCULATIONS

Alkalinity

$$CO_3^{-2} \text{ in mg/l} = \frac{1{,}000}{\text{ml sample}} \times \text{ml titrant to pH 8.2} \times 0.9835.$$

$$HCO_3^{-1} \text{ in mg/l} = \frac{1{,}000}{\text{ml sample}} \times [(\text{ml titrant pH 8.2 to 4.5}) - (\text{ml titrant to pH 8.2})].$$

Chloride

$$Cl^{-1} \text{ in mg/l} = \frac{1{,}000}{\text{ml sample}} \times (\text{ml titrant} - \text{ml blank}) \times f_1,$$

where f_1 = mg Cl^{-1}≏1.00 ml standard mercuric nitrate solution.

Sulfate

$$SO_4^{-2} \text{ in mg/l} = \frac{1{,}000}{\text{ml sample}} \times (\text{ml titrant} - \text{ml blank}) \times f_2,$$

where f_2 = mg SO_4≏1.00 ml standard barium chloride solution.

Calculate f_1 and f_2 each time a set of samples is analyzed.

DISCUSSION OF RESULTS

Figures 1 and 2 show the spectra obtained for chloride and sulfate samples before and after titration. The operating wavelength is normally selected as the point where the differential of the curves is greatest in an area of relatively small horizontal change. For chloride, this occurs at about 518 nm (nanometers).

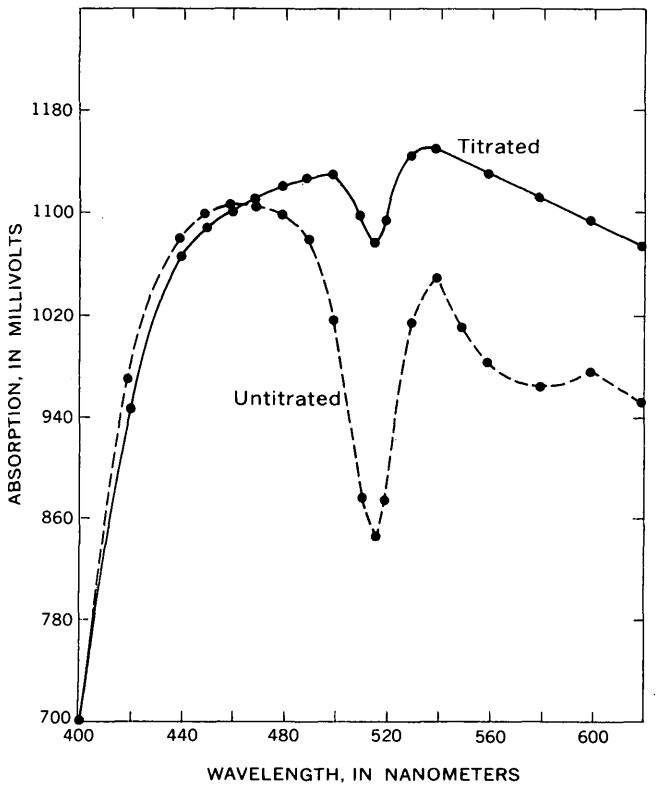

FIGURE 1.—Comparison of absorption spectra of a chloride standard solution before and after titration.

Reproducible results were found anywhere from 515 to 530 nm. The optimum point for sulfate lies between 520 and 530 nm. To simplify operation, a wavelength of 520 nm was selected for both the chloride and sulfate determinations.

Titration curves for the chloride and sulfate determinations are shown in figures 3 and 4. One can see that it is extremely difficult to determine the inflection point for both determinations and, in turn, set the automated end points. Even if a better inflection point occurred, it is still time consuming to run a titration curve each time a set of samples is analyzed and then set the end point. However, for chloride, one can rapidly titrate a standard visually and then set the end point as described under the procedure. It is necessary, each time a set of samples is analyzed, to titrate a standard visually and then set the end point since the mixed chloride indicator is not stable. A different end point is obtained each time.

In contrast, visually titrating the sulfate is very difficult. However, the titration curve indicates that the inflection occurs about 10 to 12 mv lower than the potential of an untitrated sample. It has been observed that the end point of the automated titration can be set by noting the initial balanced potential of a standard

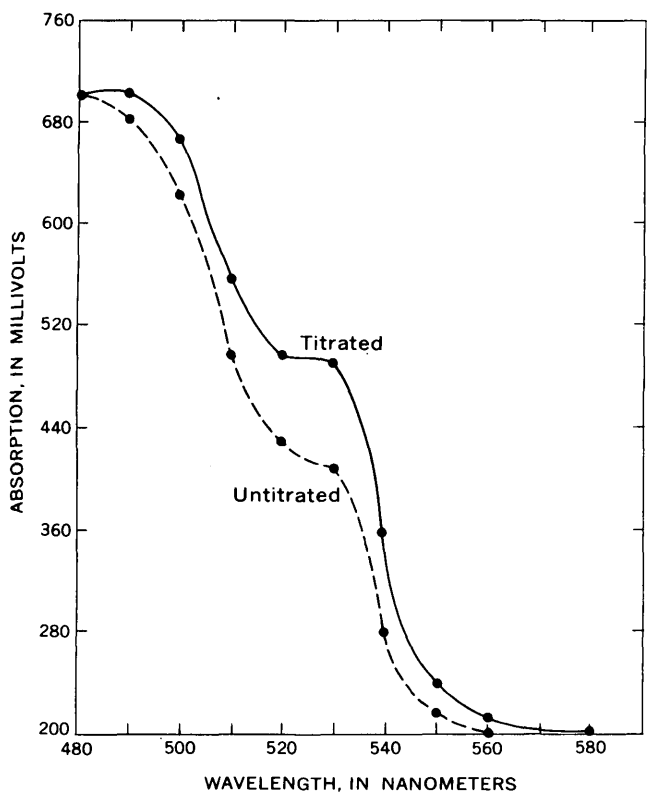

FIGURE 2.—Comparison of absorption spectra of a sulfate standard solution before and after titration.

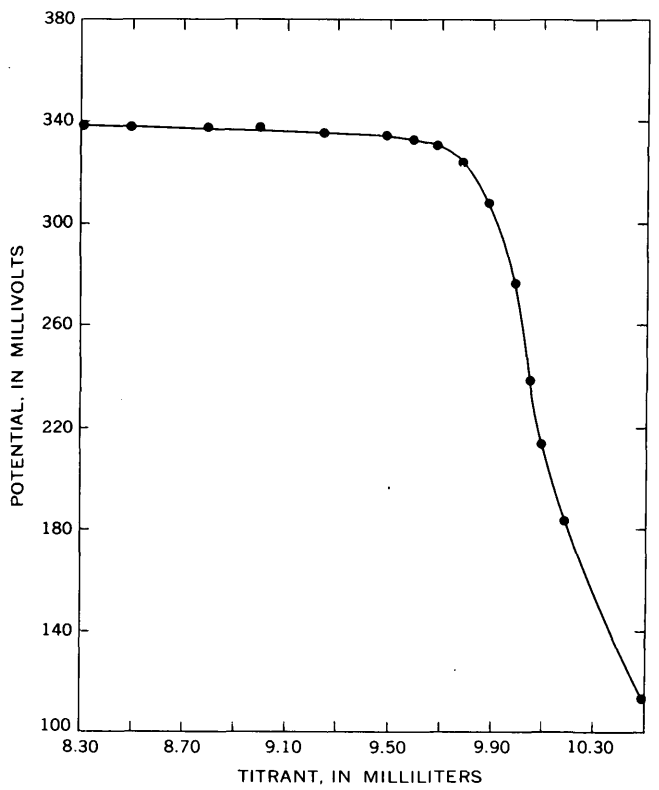

FIGURE 3.—Spectrophotometric titration of chloride with mercuric nitrate, using diphenylcarbazone indicator.

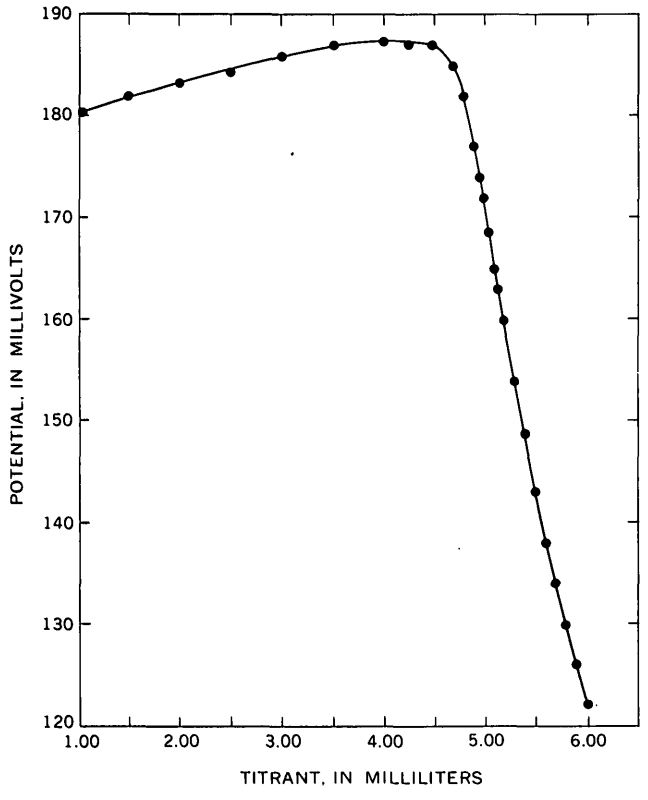

FIGURE 4.—Spectrophotometric titration of sulfate with barium chloride, using thorin indicator.

prior to titration and then reset the potential 10 to 12 mv lower.

The alkalinity determination is an acid-base reaction, and there are no problems in setting the end point.

In table 1, results of replicate analyses for bicarbonate, chloride, and sulfate are shown. The mean, standard deviation, and number of replicate analyses are given. The concentrations of bicarbonate, chloride, and sulfate used in this study represent, fairly well, the concentration ranges that are found in many natural waters. The reproducibility is good for all concentration levels. Table 2 shows the bicarbonate, chloride, and sulfate concentrations found in some fresh water by automated and manual procedures. The instruments used are noted at the end of the table. Methods are similar. The results obtained by the two techniques are in good agreement.

CONCLUSIONS

The three constituents discussed can be determined rapidly by automated titrimetric procedures. Accuracy is as good as that of the manual techniques. Automated titrimetric procedures should become one of the more useful techniques for the determination of alkalinity, chloride, and sulfate in water-quality laboratories.

TABLE 1.—*Results of replicate titrimetric analyses, in milligrams per liter, for chloride, bicarbonate, and sulfate in water samples*

Constituents	Mean	Standard deviation	Number of analyses
Chloride	0. 97	0. 07	9
	26. 2	. 19	9
	43. 7	. 22	9
Bicarbonate	35. 3	. 55	16
	74. 0	. 35	14
Sulfate	21. 7	. 15	7
	29. 4	. 23	7
	388. 9	. 69	7
	[1] 178. 1	3. 70	12

[1] Four different aliquot volumes of sample used.

TABLE 2.—*Comparison of titrimetric methods for bicarbonate, chloride, and sulfate*

[Results in milligrams per liter]

HCO_3^{-1}		Cl^{-1}		SO_4^{-2}	
Titralyzer	Manual [1]	Titralyzer	Manual [2]	Titralyzer	Manual [2]
35	35	0. 3	0. 7	21	21
112	112	1. 0	1. 0	30	29
160	158	5. 8	6. 3	35	34
199	199	11	11	92	93
217	217	21	21	132	130
237	236	22	21	153	152
252	252	27	26	214	214
273	272	29	28	254	256
276	278	44	43	389	394
283	284	117	116	472	475
813	810			841	850

[1] Potentiometric titration.
[2] Spectrophotometric titration.

REFERENCES

Clarke, F. E., 1950, Determination of chloride in water: Anal. Chemistry, v. 22, p. 553–555, 1458.

Rainwater, F. H., and Thatcher, L. L., 1960, Methods for collection and analysis of water samples: U.S. Geol. Survey Water-Supply Paper 1454, 301 p.

AUTOMATED POTENTIOMETRIC DETERMINATION OF CHLORIDE IN WATER

By MARVIN J. FISHMAN and OLIVER J. FEIST, JR.,
Denver, Colo.

Abstract.—Chloride is determined with standard silver nitrate solution by automated potentiometric titration using chloride ion-selective and reference electrodes. Replicate analyses and comparison of results with those obtained by other automated methods show that the automated potentiometric method is as accurate and reproducible as other methods, and provides a rapid means for the determination of chloride in water.

In the past few years, automation has found widespread application in water analysis. Recently, a Fisher Titralyzer equipped with a photometric titration assembly was tested to determine chloride mercurimetrically (Fishman and Pascoe, 1970) (p. C222–C225, this chapter). A disadvantage of this automated method is the interference of sample color, which causes low chloride recovery. In extremely colored samples, no titration is possible.

The Technicon AutoAnalyzer is also being used in our laboratory to determine chloride. The method used is based on the manual thiocyanate method described by Zall, Fisher, and Garner (1956). Chloride reacts with mercuric thiocyanate and releases thiocyanate. In the presence of ferric ion, thiocyanate forms a red ferric thiocyanate complex which is then measured colorimetrically. Original sample color does not seem to interfere; however, filtration of the samples is necessary prior to analysis if sediment is present.

Chloride can also be determined by potentiometric titration, with silver nitrate solution, using a glass reference and silver-silver chloride indicator electrode system (American Public Health Association and others, 1965 p. 372). This method has not found widespread application in water analysis but should lend itself well to automation because color and sediment will not cause interference.

This report describes an automated potentiometric method using a Fisher Titralyzer for determining chloride. Chloride is titrated with standard silver nitrate solution and the end point detected potentiometrically using chloride ion-selective and reference electrodes. The equivalence point is determined by manually titrating a standard chloride solution and then preparing a titration curve (fig. 1). An equivalence point of +315 mv (millivolt) is obtained (pH-mv dial 3.85). The instrument is then adjusted to this setting. There is no need to prepare a titration curve with each set of samples.

The delivery tube on the Titralyzer must be modified so that the titrant is delivered against the indicating surface of the chloride ion-selective electrode to achieve the proper end point anticipation. (See fig. 2.)

A nonionic surfactant (detergent) must be added to prevent fouling of the electrodes. In the absence of the

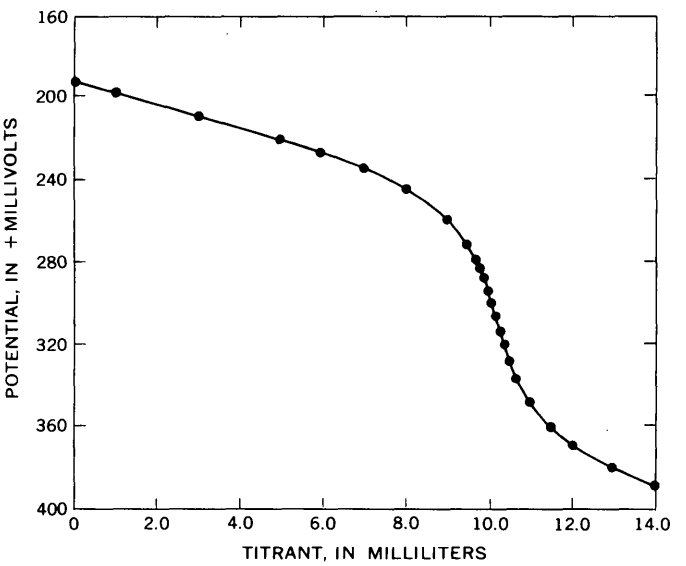

FIGURE 1.—Potentiometric titration of chloride with silver nitrate.

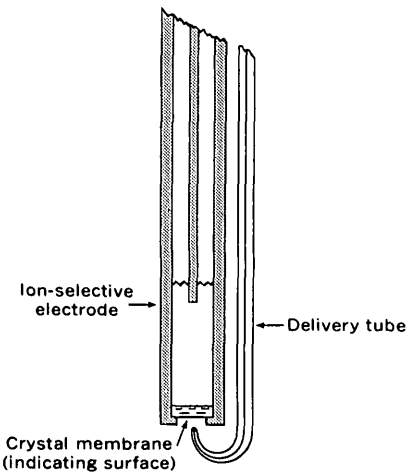

FIGURE 2.—Modification of titrant delivery tube for use with the chloride ion-selective electrode.

surfactant, precipitated silver chloride tends to coat the electrodes and cause a loss in both sensitivity and response. Shiner and Smith (1956) also state that the detergent coats each microscopic particle of the silver halide almost instantaneously upon formation, and prevents any coagulation of the precipitate. Equilibrium between the precipitate and solution is then achieved rapidly. Without the detergent, erratic results are obtained.

APPARATUS

Fisher Titralyzer.

Chloride ion-selective electrode (Orion No. 94–17, or equivalent).

Combination pH-reference electrode (Fisher No. 13–639–90, or equivalent).

REAGENTS

Chloride standard solution, 100 ml≏1.00mg Cl^{-1}: Dissolve 1.648 g NaCl crystals in demineralized water and dilute to 1,000 ml.

Detergent, Cutscum, nonionic surfactant (Fisher No. C–54, or equivalent).

Nitric acid, conc.

Silver standard solution I, 1.00 ml≏5.00 mg Cl^{-1}: Pulverize approximately 30 g $AgNO_3$ crystals in a clean mortar and dry at 150°–120°C. Discoloration of the crystals indicates decomposition caused by excessive drying temperature or impurities. Dissolve 23.96 g dried $AgNO_3$ in demineralized water and dilute to 950 ml. Store in an amber bottle.

Silver standard solution II, 1.00 ml≏0.50 mg Cl^{-1}: Dilute 100 ml silver standard solution I with demineralized water to 1,000 ml. Larger volumes may be prepared. Store in an amber bottle. Standardize the solution each time a set of samples is analyzed by taking 10.0 ml of chloride standard solution (10.0 mg Cl^{-1}) and treating it like the samples.

PROCEDURE

1. Pipet a volume of sample containing less than 15 mg Cl^{-1} (100 ml max) into a 200-ml Berzelius beaker and adjust volume to approximately 100 ml.
2. Prepare 2 standards (10.0 mg Cl^{-1}) and 2 demineralized-water blanks and adjust the volume of each to 100 ml.
3. Add 2.0 ml conc HNO_3 and mix.
4. Add 5 drops of the nonionic surfactant and mix.
5. Set the chloride end point by following the instructions provided with the instrument. Place the samples, standards, and blanks in the turntable and activate the automatic potentiometric titration, using silver standard solution II (1.00 ml≏0.50 mg Cl^{-1}). Set the ACID-BASE switch in the BASE position.

CALCULATIONS

$$Cl^{-1} \text{ in mg/l} = \frac{1{,}000}{\text{ml sample}} \times (\text{ml titrant} - \text{ml blank}) \times (\text{mg } Cl^{-1} \text{ per ml titrant}).$$

DISCUSSION OF RESULTS

In table 1, results of replicate analyses for chloride by the automated potentiometric method are shown. The number of replicate analyses, mean, standard deviation, and range are given. The concentrations of chloride in the samples used in this study represent the concentration ranges in many natural waters. For samples containing more than 150 mg chloride per liter, a smaller aliquot of sample is required. The reproducibility is good for all concentration levels. The results for sample C could possibly be improved if a double-junction reference electrode were used in place of the saturated KCl electrode because small traces of chloride from the electrode come in contact with the sample. Table 2 shows the chloride found in samples of natural water by three automated procedures. The results obtained by the three techniques are in good agreement for colorless samples. Samples 11 through 16 were colored water. Good agreement was obtained for samples 11 through 13 by using the potentiometric and AutoAnalyzer methods, whereas there was no agreement between the mercurimetric and potentiometric methods for samples Nos. 14 through 16. As was mentioned before, low values are obtained on colored water by the mercurimetric method. Tests indicate that the automated potentiometric method determines chloride rapidly, eliminates color interference, and is as accurate as other automated techniques.

TABLE 1.—*Precision of automated potentiometric method for the determination of chloride, in milligrams per liter*

Sample No.	Number of analyses	Mean	Standard deviation	Range
A	20	26. 4	±0. 28	25. 8 –27. 0
B	20	42. 9	. 33	42. 2 –43. 7
C	20	1. 13	. 34	. 39– 2. 04
D	20	95. 1	. 47	93. 9 –95. 9

TABLE 2.—*Comparison of automated methods used in the determination of chloride in water, in milligrams per liter*

Sample No.	Mercurimetric titration	Potentiometric titration	AutoAnalyzer
1	1.8	1.9	1.8
2	5.1	4.8	4.6
3	9.8	10	10
4	11	11	12
5	5.0	6.0	6.2
6	20	20	21
7	13	13	13
8	21	22	22
9	38	44	43
10	29	29	29
11 [1]	(2)	13	14
12 [1]	(2)	23	24
13 [1]	(2)	33	33
14 [1]	0	29	(2)
15 [1]	9	37	(2)
16 [1]	15	47	(2)
17	27	25	27
18	44	42	43
19	1.2	1.5	1.4
20	96	95	96

[1] Colored water.
[2] Samples not analyzed by this method.

REFERENCES

American Public Health Association and others, 1965, Standard methods for the examination of water and wastewater, 12th ed.: New York, Am. Public Health Assoc., Inc., 769 p.

Fishman, M. J., and Pascoe, R. F., 1970, The use of automated titrimetry for analyses of natural water, *in* Geological Survey Research, 1970: U.S. Geological Survey Prof. Paper 700–C, p. C222–C225.

Shiner, V. J., Jr., and Smith, M. L., 1956, Rapid argentimetric determination of halides by direct potentiometric titration: Anal. Chemistry, v. 28, p. 1043.

Zall, D. M., Fisher, Donald, and Garner, M. D., 1956, Photometric determination of chlorides in water: Anal. Chemistry, v. 28, p. 1665.

CHANNEL-SCARP FORMATION IN WESTERN NORTH DAKOTA

By THOMAS M. HAMILTON, Grand Forks, N. Dak.

Work supported in part by the North Dakota Water Resources Institute with funds provided by the U.S. Department of the Interior, Office of Water Resources Research, under P.L. 88-379

Abstract.—A reconnaissance of the present gully system and valley surfaces of small drainage basins in western North Dakota indicates that channel-scarp formation may most often be the result of one of three general conditions. These conditions are: (1) cutoff of the downvalley toe of alluvial fill in tributaries by encroachment of a migrating main channel; (2) cutting on a local reach of steeper gradient as a result of (a) an extreme flood, (b) a shift toward greater precipitation causing channel degradation on the steeper reach, or (c) short time-separation between two storms; and (3) piping collapse.

The maintenance of a stable alluvial river channel has been shown to be related to the quantity of water and the quantity and type of sediment moving through the system (Schumm, 1969). A river system in a semiarid region is subject to at least two great extremes—high-magnitude runoff from a storm and (or) a large influx of sediment from the tributary system. The stability of the trunk stream depends on the conditions existing in its tributaries. If the tributary system alters, on a large scale, from a state of aggradation to degradation, the change will affect the trunk stream. Therefore, any evaluation or prediction of river stability must involve an examination of the tributary system.

In western North Dakota many drainage channels incised into valley fill are characterized by steep unvegetated walls, and by the occurrence in several such channels of actively eroding channel scarps. The rapid erosion associated with these channels occurs primarily as upstream migration of a channel scarp and slumping and soilfall of the vertical walls downstream from the scarp.

The bedrock in the area of study (fig. 1) is predominantly poorly consolidated Tertiary sand, silt, and clay. Dominant vegetation is short prairie grass and sagebrush on the valley flat, short prairie grass on the gentle to moderate slopes, and predominantly shrubs on the most rugged hillslopes. Sediment yield from the bedrock slopes and consequently the sediment concentration of runoff is strongly affected by the type and amount of vegetation. The concentration of sediment in runoff reaching the valley floor determines whether the stream aggrades or degrades; a high sediment concentration, a high proportion of stream load to available discharge, results in aggradation.

An understanding of the formation of channel scarps with which massive sediment removal is associated,

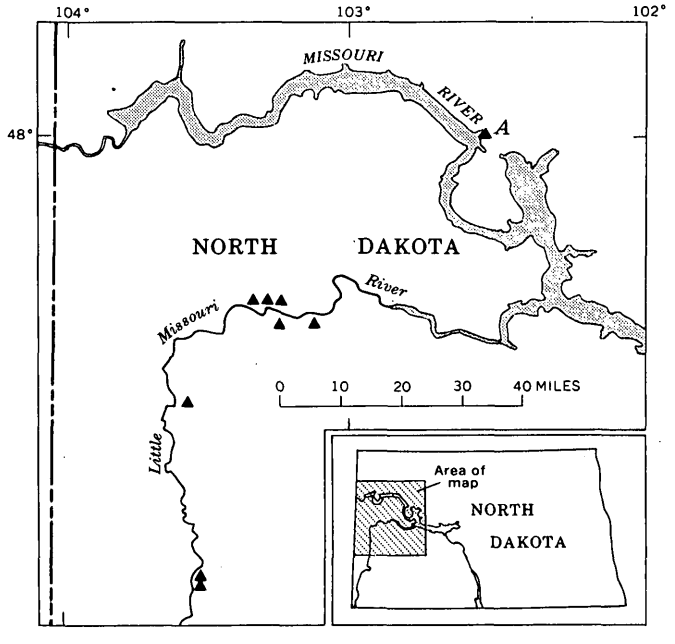

FIGURE 1.—Approximate location of drainage basins (triangles) studied.

should be prerequisite to an estimation of sediment movement through the tributary system. Scarp formation has not been directly observed in western North Dakota; therefore, the determination of the causes of formation becomes a matter of reconstruction of the paleohydrologic controls of sedimentation and erosion in that area.

Prior to valley trenching, a tributary stream is in a state of either alluviation or relative stability; stable periods in western North Dakota are marked by soil development on the valley floors. The result of alluviation is an increase in the gradient at the downstream end of the valley and (or) a gradient increase downstream from some point of deposition in the channel. Longitudinal profiles indicate the presence of locally steepened reaches in large (a few square miles) drainage basins (fig. 2) or steepening at the toe of the fill in small (a few acres) basins. A tributary may be graded to a trunk stream or to a terrace or surface associated with the trunk stream. The profiles indicate a range in slope of from 1° to 3° or more (on steepened reaches), depending on valley size and geometry.

The chronology of late Holocene alluvial events in western North Dakota (Hamilton, 1967) indicates tributary aggradation during periods of subnormal precipitation lasting a few years to a few tens of years. Normal annual precipitation averages about 14 inches.

The following discussion pertains only to channel-scarp formation and not scarp migration, which is controlled by additional factors. The order of presentation does not imply the relative importance of these causes of channel-scarp formation.

MAJOR CAUSES OF CHANNEL-SCARP FORMATION

Channel migration of a trunk stream

One of the more important processes of channel-scarp formation, particularly in the formation of downvalley scarps in the larger tributary valleys, is the encroachment of a laterally migrating river channel. Migration may occur during an extreme hydrologic event (a 50- or 100-year flood) when extensive widening of the river channel can occur, or during the normal course of meander migration. The result is a cutoff or steepening of the downvalley toe of the tributary channel fill, thus forming a scarp. Migration away from the tributary most probably leads to downvalley alluviation of the tributary.

Steepening of reaches of the valley flat

A second mode of formation can be observed on a steepened reach of a valley. This type of scarp formation is probably most important in the middle or headward regions of ungullied alluvial fill and in the inset fill of an existing gully. Schumm and Hadley (1957) have shown the association of channel scarps with steepened reaches of alluvial fill in Wyoming and New Mexico.

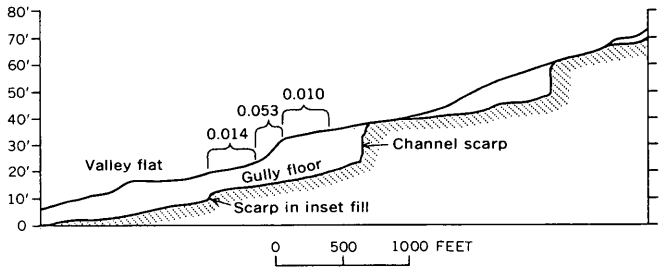

FIGURE 2.—Segment of the gully and valley flat in basin *A* (shown in figure 1). Numbers above the braces indicate the slope of that reach, in foot per foot.

Schumm and Hadley (1957, p. 170) attribute the increased gradient of steepened reaches to deposition at stream junctions, with alluviation above the plugged region. In western North Dakota some steepened reaches appear downstream from the channel junction and resemble migrating fans. The occurrence of steepened reaches may not be wholly the result of damming in the main channel by formation of a fan at the tributary mouth. Flow conditions in the main channel and antecedent moisture conditions in the basin may play important roles in the position of the steepened reach. This problem is presently not entirely resolved.

The formation of a scarp on a steepened reach may be an entirely random event or may be related to one of three more specific events:

(1) Formation of scarps on a steepened reach may be related to the occurrence of a hydrologic event of large magnitude. Schumm and Hadley (1957, p. 169) explain that for a given discharge, scour on the steepened reach may not occur until continued deposition increases the gradient to a point where rapid erosion does occur (a "critical" slope), the corollary being that an increased discharge might initiate scour on a given slope.

(2) Scarp formation on a steepened reach may be associated with a shift toward more rainfall, which increases hillslope vegetational cover. This cover, in turn, reduces the sediment concentration of the water reaching a stream. The result is a stream with a steep gradient receiving overland runoff with a lower sediment concentration than the stream is capable of transporting. The sediment load of a stream that is not carrying its full load is supplemented, to an extent dictated by the hydraulic conditions, by scouring of the streambed. It is reasonable to assume that the most rapid scouring would occur on those reaches of steepest gradient, thereby increasing the probability of channel-scarp formation at those locations.

(3) The distribution of precipitation in time may be important in scarp formation. The discussion here requires a consideration of ground-water conditions in a hypothetical basin. During periods of below-normal precipitation, the water table in the basin is lowered below the valley floor in all areas, with the possible exception of the downstream toe of the valley fan. The lowered water table provides an opportunity for recharge to the valley fill, and some surface flow infiltrates. The quantity of infiltration may be considerable if the permeability is sufficient or if the distance traveled is great.

The concept of negative seepage (infiltration through the channel bed) as opposed to positive seepage (upward seepage through the bed) allows for some interesting possibilities in connection with scour and deposition. Harrison (1968), during laboratory studies using a controlled seepage flume, observed the formation of a mud seal on the channel bottom during negative seepage as a result of mud particles clogging the pore spaces of the bottom sediment. He states (p. 48) "The net effect of the mud seal . . . was to increase the compressive strength of the channel bottom and to eliminate erosion of bottom sediment . . ." This process may be important in holding the surface intact on the steepened reach during a given storm.

Observations on rivers in western North Dakota indicate that sandbars provide sufficient topographic relief for the establishment of a measurable ground-water flow system. The upstream end of the bar is very firm, is resistant to scraping of the surface (erosion resistant?), and supports the weight of a man with little or no compaction. Abundant fine sediment occurs on the bar surface. The existence of negative seepage was verified by measurements obtained from nests of small-diameter piezometers and by trenching exposed portions of the bar. Near the downstream end of the bar, positive seepage becomes evident. The surface is soft, sediment is easily sloughed off, and the surface sediment appears coarser than on the upstream end.

A microflow system could be established through the steepened reach of valley fill during a period of more frequent rainfall. If a condition of near-surface saturation is assumed present, a rainstorm may furnish recharge to the valley fill and establish a flow system through the steepened reach. Positive seepage has been found to be the key element in the formation and migration of erosional scarplets on hillslopes in the semiarid Great Plains (Hadley and Rolfe, 1956). The scarplets are developed in the surficial mantle overlying a fine-grained, weathered bedrock, where subsurface water reaches the surface and saturates the soil, making it readily susceptible to erosion by surface flow. This same process can be imagined occurring on the steepened reach of the alluvial fill during successive periods of runoff with negative seepage in the upstream part of the reach and positive seepage at the downstream end.

Piping

Another observable erosion phenomenon that contributes to the formation of channel scarps in western North Dakota is piping. Piping is a process of subsurface erosion that occurs when surface runoff enters a drainable crack or other opening in the sediment with a hydraulic gradient that is sufficient to allow erosion along the walls of the opening. The mechanics of piping are discussed by Parker and Jenne.[1] The channel scarp results from the collapse of a pipe.

Many presently ungullied alluvial valleys in western North Dakota contain abundant evidence of piping in the form of sinkholes which at depth become integrated with the subterranean tunnels. After extensive piping, the sediment is susceptible to collapse down into the pipe network resulting in a vertical walled gully. A channel scarp occurs in the alluvium where collapse terminates.

Figure 3 shows the early stages of collapse in ungullied alluvial fill. Much of this small basin is affected by piping. The main pipe in the axis of the valley is on the average 8 feet high and 5 feet wide. The two sinkholes visible in the photograph are approximately 15 feet in diameter, 15 feet deep, and 60 feet apart. The photograph was taken during the summer of 1969. In 1968 there was no surficial evidence of piping in this

[1] Parker, G. G., and Jenne, E. A., 1967, Structural failure of western United States highways caused by piping: U.S. Geol. Survey, Water Resources Division, paper prepared for presentation at the 46th annual meeting of the Highway Research Board, 27 p.

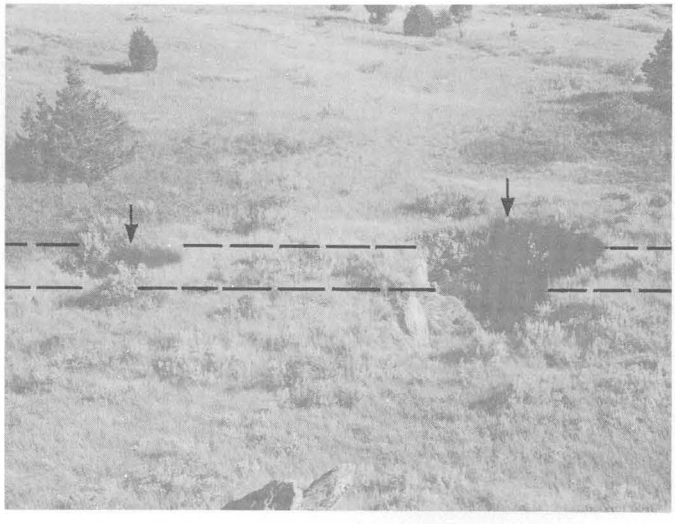

FIGURE 3.—Collapsed pipe in ungullied alluvium. The dashed lines indicate the trend of the pipe, which coincides with the axis of the valley. See text for full description.

tributary, although pipes undoubtedly existed at that time. The remaining bridged areas are very unstable and will probably collapse during the coming runoff period, resulting in a gully some 15 feet deep. This example indicates the rapidity with which an active gully and channel scarp can appear in a previously ungullied basin as a result of piping.

OTHER CAUSES OF SCARP FORMATION

The formation of a channel scarp by other than the means previously discussed has a certain indeterminancy. The occurrence of an unsodded area in an otherwise well-vegetated valley flat, the presence of wagonwheel ruts and animal trails, and the occurrence of prairie fires undoubtedly play a role in the formation of some channel scarps, but they lack predictability. A change in rainfall intensity (Leopold, 1951) is another possibility; however, usable information pertaining to this aspect of meteorologic variation is not available in weather records for western North Dakota.

REFERENCES

Hadley, R. F., and Rolfe, B. N., 1956, Development and significance of seepage steps in slope erosion: Am. Geophys. Union Trans., v. 36, no. 5, p. 792–804.

Hamilton, T. M., 1967, Late-Recent alluvium in western North Dakota: North Dakota Geol. Survey Misc. Ser. 30, p. 151–158.

Harrison, S. S., 1968, The effects of ground-water seepage on stream regimen—a laboratory study: Unpub. Ph. D. dissert., Univ. North Dakota, Grand Forks, 57 p.

Leopold, L. B., 1951, Rainfall frequency: An aspect of climate variation: Am. Geophys. Union Trans., v. 32, p. 347–357.

Schumm, S. A., 1969, River metamorphosis: Am. Soc. Civil Engineers Proc., Jour. Hydraulics Div. HY 1, p. 255–273.

Schumm, S. A., and Hadley, R. F, 1957, Arroyos and the semiarid cycle of erosion: Am Jour. Sci., v. 255, p. 161–174.

A METHOD OF ESTIMATING ANNUAL SUSPENDED-SEDIMENT DISCHARGE

By LEONARD M. NELSON, Tacoma, Wash.

Abstract.—A simple method is proposed for estimating annual suspended-sediment discharge during years for which streamflow records are available but for which sediment records are not available. Readily accessible information on the parameters of annual peak and annual mean water discharges is used with the available sediment records to estimate the average annual suspended-sediment discharge. The relation between the two parameters and the annual suspended-sediment discharge is well defined for many streams. This relation does not fit all streams, however, and a thorough understanding of a basin's geologic and hydrologic characteristics is needed for application of the method proposed.

The periods of record of daily suspended-sediment discharge by most streams in the State of Washington are relatively short in comparison to the periods covered by daily streamflow records. Thus, quantities of sediment transported during years of extremely high flow and during years of extremely low flow generally are not defined, although they differ markedly from those occurring during years of normal streamflow.

At some gaging stations in basins having specific characteristics and where the annual peak and annual mean water discharges, in cubic feet per second, are defined, it has been found that by multiplying together these two readily accessible parameters and then multiplying the product by a factor of 10^{-6}, an independent variable, k_n, is formed. This variable can be used with available daily suspended-sediment discharge data to provide a curve from which the annual suspended-sediment discharge can be estimated for stations having as few as 5 years of daily sediment record. In general, the procedure is as follows: (1) the variable, k_n, and the annual suspended-sediment discharge are plotted on log-log paper for those years for which sediment and streamflow records are concurrent; (2) a curve is drawn through the plotted points by the least-squares method; and (3) the annual suspended-sediment discharge is then estimated from the curve for those years for which the sediment records are not available.

The amount of sediment transported annually is dependent upon the magnitude of the water discharge. In many streams a large part of the annual suspended-sediment discharge is transported during a day in which the peak water discharge has occurred. Because of these two factors, the annual suspended-sediment discharge and k_n are related closely for many streams.

To demonstrate this relation and the application of the method to estimating the suspended-sediment discharge of streams of differing basin characteristics and periods of record, data were used from the Green, Chehalis, Skykomish, and Tucannon Rivers in Washington (table 1). The Green, Chehalis, and Skykomish Rivers are located in areas of high precipitation and high runoff; the Tucannon River is in an area whose climate is semiarid but where runoff is intense at times. The drainage patterns of the Green, Chehalis, and Tucannon Rivers, and the precipitation pattern over their drainage areas are shown in figure 1.

APPLICATION OF THE METHOD TO VARIOUS TYPES OF STREAMS

The quantity of suspended sediment transported by a small stream from its upper reaches in which many small subbasins have similar sediment-transport characteristics would be expected to be closely related to k_n. This relationship has been found to be true, as for example for the Green River near Palmer, station 12–1065. The maximum (1960) and minimum (1941) prob-

TABLE 1.—*Streamflow and sediment data for the Green, Chehalis, Tucannon, and Skykomish Rivers, Wash.*

Station name and number	Length of streamflow records (years)	Length of daily sediment records (years)	Drainage area (sq mi)	Average discharge for period of record (cfs)
Green River near Palmer, 12–1065	31	7	230	1,095
Chehalis River at Porter, 12–310	15	6	1,294	4,218
Tucannon River near Starbuck, 13–3445	15	5	431	164
Skykomish River near Gold Bar, 12–1345	39	0	535	3,892

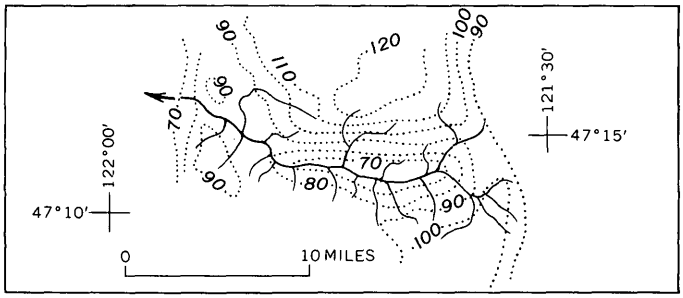

GREEN RIVER ABOVE GAGING STATION (12-1065) NEAR PALMER

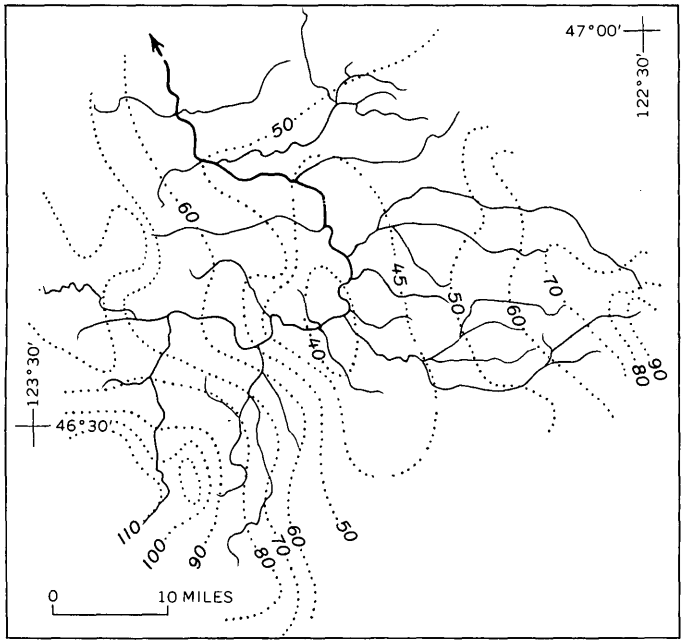

CHEHALIS RIVER ABOVE GAGING STATION (12-0310) AT PORTER

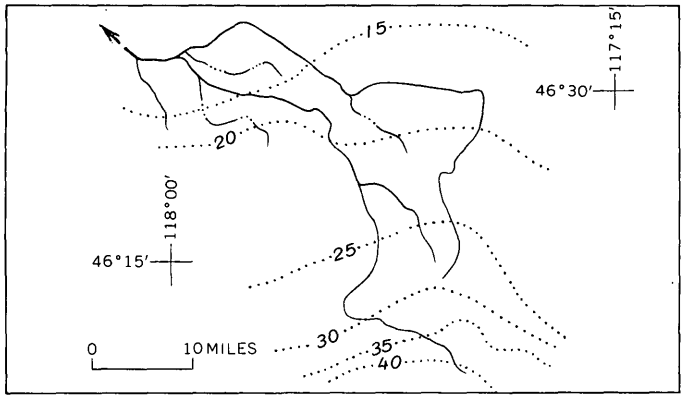

TUCANNON RIVER ABOVE GAGING STATION (13-3445) NEAR STARBUCK

FIGURE 1.—Partial drainage patterns of the Green, Chehalis, and Tucannon Rivers, Wash., and average annual precipitation, in inches (dotted lines), over the drainage areas. From Phillips (1966, p. 10–11).

able suspended-sediment discharges occurring during the period of streamflow records can be extrapolated from the curve for this river (fig. 2).

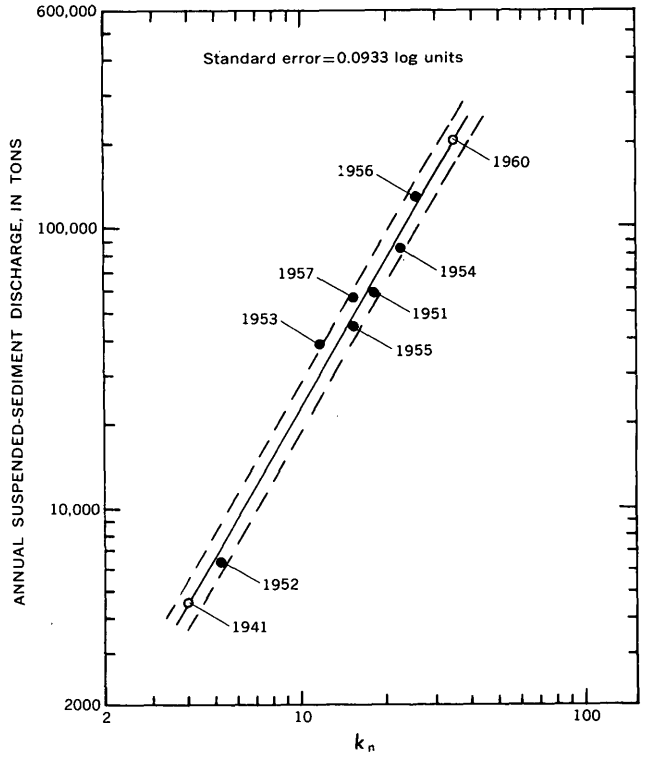

FIGURE 2.—Relation of annual suspended-sediment discharge to k_n, Green River near Palmer, Wash., station 12–1065. Standard error indicated by dashed lines.

The suspended sediment discharged by a stream from a drainage area characterized by a diversity of geology, slope, vegetative cover, and land use would not ordinarily be expected to be closely related to k_n. The Chehalis River has a drainage area in this category. However, because of the widespread distribution of the precipitation from most storms that move over its basin there appears to be a fairly close relationship between k_n and suspended-sediment discharge, as indicated in figure 3. Thus, widespread distribution of precipitation over a basin apparently is also an important factor in determining the applicability of k_n, regardless of the diversities in the basin's other characteristics. To show the accuracy of an estimated sediment discharge in this drainage area, a curve similar to that shown in figure 3 was drawn to include only the data from 1962 to 1966. As extrapolated from this curve, the suspended-sediment discharge estimated for 1967 was only 7 percent less than that measured during 1967.

Good correlation of k_n with suspended-sediment transport has also been noted under conditions of both widespread distribution of precipitation over a basin, as in the Chehalis River basin, and where much of the annual suspended-sediment discharge is transported during a single short storm. Such a situation has been noted on the Tucannon River near Starbuck, station 13–3445 (fig. 4).

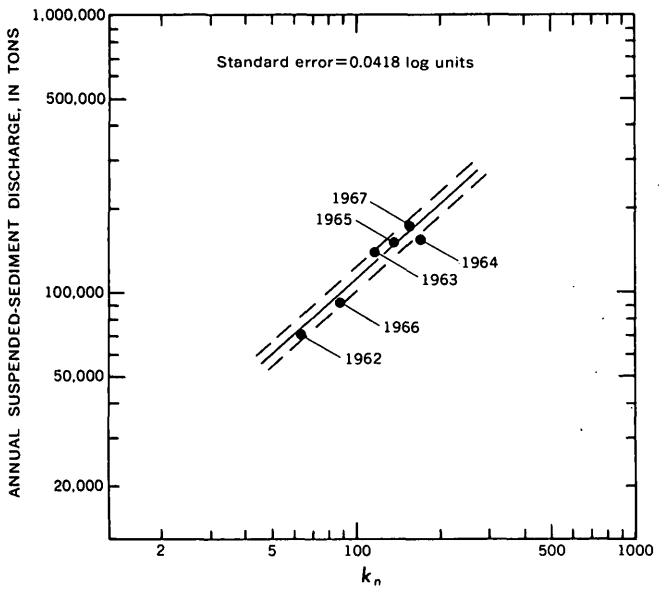

FIGURE 3.—Relation of annual suspended-sediment discharge to k_n, Chehalis River at Porter, Wash., station 12–310. Standard error indicated by dashed lines.

The direct application of suspended-sediment discharge data obtained during only short periods of record to predictions of long-term average suspended-sediment discharges can be highly misleading. Therefore, the relation between suspended-sediment discharge and k_n is used to extend the data over a longer period of time and to more accurately estimate the average suspended-sediment discharge. For example, for the Tucannon River near Starbuck, an erroneously large average annual suspended-sediment discharge of 770,000 tons would be obtained if one estimated the suspended-sediment discharges by averaging the measured discharges. A more accurate figure of 450,000 tons would be derived by using values from the curves for the 15 years of streamflow record.

In reconnaissance studies, when daily sediment records are not available, and in establishing the relation between a stream's suspended-sediment discharge and k_n, the method of estimating annual suspended-sediment discharge described in this paper can be applied by using (1) sediment-transport curves which are prepared from periodic sediment-discharge measurements and (2) prior streamflow records. On the basis of unpublished data for the Snohomish River basin, annual suspended-sediment discharges of the Skykomish River

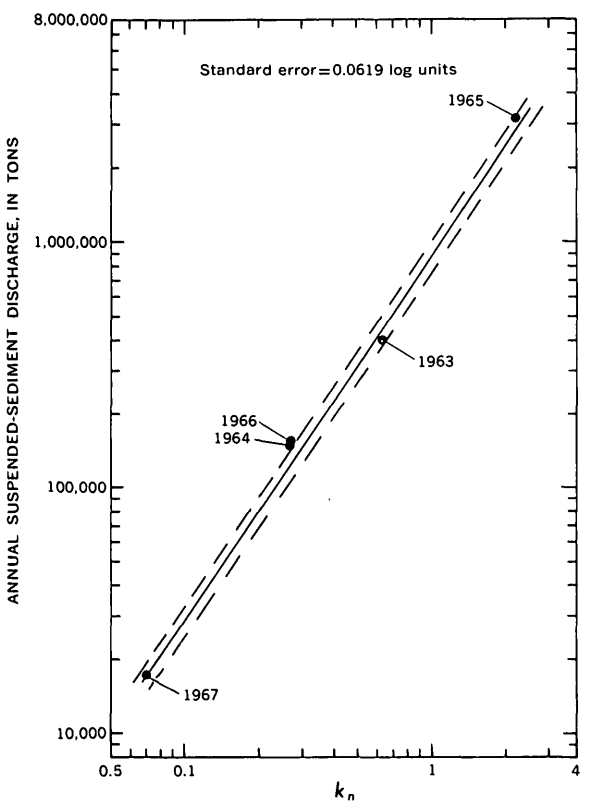

FIGURE 4.—Relation of annual suspended-sediment discharge to k_n, Tucannon River near Starbuck, Wash., station 13–3445. Standard error indicated by dashed lines.

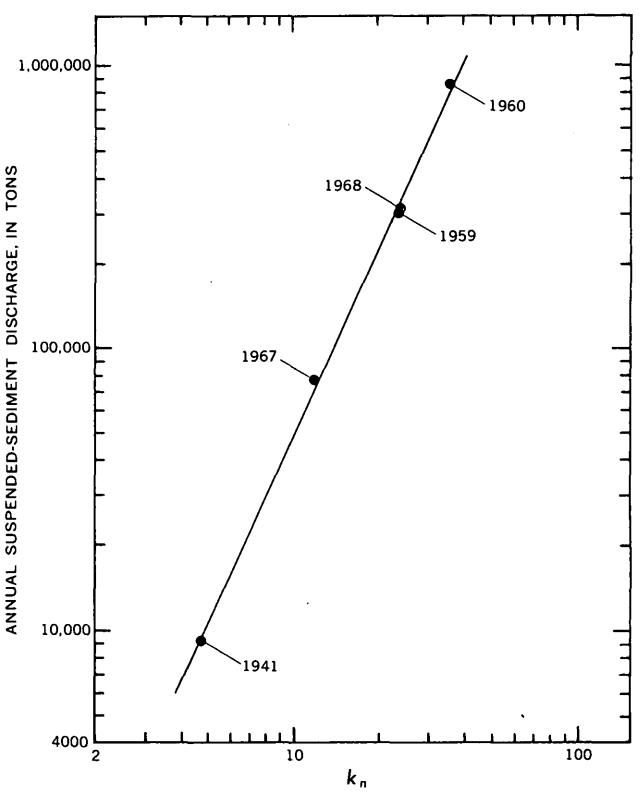

FIGURE 5.—Relation of estimated annual suspended-sediment discharge to k_n. Skykomish River near Gold Bar, Wash., station 12–1345.

near Gold Bar, station 12–1345, for 1941, 1959, and 1960 were estimated from a sediment-transport curve representing the instantaneous sediment loads measured during 1967–69. (The sediment-transport characteristics in the drainage basin were assumed to be largely unchanged during the period of streamflow record.) As shown in figure 5, the estimated sediment discharges then were plotted against the independent variable k_n, on log-log paper and a curve was drawn through the points representing 1941, 1959, and 1960. The discharges for 1967 and 1968 were estimated from the sediment-transport curve and plotted. Because deviations from the curve are small, the average annual suspended-sediment discharge was estimated from the curve by averaging the discharges obtained, using k_n for each of the 39 years of streamflow records.

LIMITATIONS OF THE METHOD

The application of this method to obtain realistic estimates of annual suspended-sediment discharge in a given drainage basin is subject to certain limitations. For example, this method can be used particularly for estimating suspended-sediment discharge by small streams in drainage areas where the geology and soils, slope, vegetative cover, and land use are similar throughout the drainage. It has been found that, except in basins where the precipitation is generally widespread, the method is not applicable to streams draining areas characterized by a large diversity in geology, slope, vegetative cover, and land use.

REFERENCE

Phillips, E. L., 1966, Washington climate: Washington State Univ. Coop. Ext. Service, Pullman, 64 p.

EVALUATION OF INSTALLATION METHODS FOR NEUTRON-METER ACCESS TUBES

By W. E. TEASDALE and A. I. JOHNSON,
Idaho Falls, Idaho, Denver, Colo.

Work done in cooperation with the California Department of Water Resources

Abstract.—A detailed study was started in 1960 to evaluate various methods for installing access tubes for a depth-type neutron-meter probe. At a small test site, soil-moisture content was determined by laboratory analysis of undisturbed volumetric samples as well as by means of a neutron-meter probe. Installation of thin-walled aluminum tubes of approximately the same diameter as that of the probe, in a hole small enough for tight contact between tube and soil, yielded the most favorable results. However, the research also showed that other less complicated and more economical methods of installing access tubes could be used with reasonable accuracy, if neutron-meter measurements made at the installation were calibrated against volumetric sampling at the site. Because of the depths involved in ground-water studies one of the simpler, more economical installation methods is more practical than the skintight-fit method and at the same time provides a reasonable degree of accuracy in the measurement of change in the moisture content of soils.

The changing water content that results from drainage of saturated sediments after a lowering of the water table is important to hydrologic studies of groundwater systems. As one phase of extensive research on the specific yield of water-bearing materials, the U.S. Geological Survey, in cooperation with the California Department of Water Resources, has been evaluating various field methods for measuring the moisture content of soils. As part of this evaluation, the neutron meter has been studied in considerable detail. The neutron meter used was a Nuclear Chicago Model P19 depth moisture probe and a Model 2800 portable scaler. In theory, fast neutrons are emitted from a 5-millicurie radium-beryllium source. Upon collision with hydrogen nuclei, they become slow, or thermal neutrons. The density of the slow neutron flux returned to the detection part of the probe is a function of the hydrogen concentration of the surrounding media.

The paper discusses only a small part of the data collected for the evaluation of the neutron meter, concentrating on the research phase which evaluated various methods of installing access tubes for the probes of depth-type neutron soil-moisture meters.

The determination of the moisture content of soils by the use of neutron meters has been described in detail by Johnson (1962). An extensive bibliography of publications on radiation methods is available in that publication and also is appended to the extensive study reported by Smith, Johnson, Fisher, and Womack (1968). Previous studies by Holmes and Jenkinson (1959) and by Stolzy and Cahoon (1957) indicated a few effects resulting from several types of access-tube installations. Most of the past work indicated that the neutron meter offered considerable promise whenever a measurement of the in situ moisture content of soils under changing conditions was desired. The neutron-meter method does not require continuing sampling, with resulting disturbance of a study area. Therefore, the method is considered desirable for following the gradual change in moisture content resulting from the slow drainage taking place over a period of weeks to years following lowering of a water table.

In the past, access tubes have been installed most frequently as small-diameter, thin-walled tubing in close contact with the sides of the test hole. Because most of the past work with the neutron meter has been done at depths of 20 feet or less, such installation has not presented insurmountable problems. Ground-water

U.S. GEOL. SURVEY PROF. PAPER 700-C, PAGES C237-C241

380-189 O - 70 - 17

studies, however, commonly require investigation of water content to depths of several hundred feet, and a more efficient method for installation of access tubes is required. The optimum installation method would permit measurements that are either quite accurate in themselves or that can be corrected to show the actual moisture content of the soil studied. The study discussed in this paper was designed to evaluate those characteristics of access tubes, and their installation, that would affect moisture-content measurement with the neutron meter, and to determine the relative amount of the effects. For ease of installation, a depth of 10.5 feet was used as an installation depth for the access tubes; however, the conclusions reached by the study can be applied to installations of any depth.

Acknowledgments.—This study was completed with the assistance of D. A. Morris, R. C. Prill, and W. K. Kulp, all of the U.S. Geological Survey.

CHARACTERISTICS OF TEST SITE

The evaluation study was made at a test site established within the grounds of radio station KHIQ at Sacramento, Calif. The site consists of natural-levee alluvial deposits forming a terrace of the American River. The sediments are composed primarily of very fine to fine sands, silts, and clays (fig. 1) and are classified texturally as silty sands, sandy silts, silts, and clay-silts (fig. 2).

Figure 3 shows the generalized lithology across the test site, approximately west to east. To a depth of approximately 1.5 feet the sediments are predominantly silty sands, and from 1.5 to 4 feet they are sandy silts. Silts predominate from 4 to 6.5 feet, clay-silts from 6.5 to 7.5 feet, clays from 7.5 to 8.5 feet, and silts from 8.5 feet to the bottom of the test holes at 10.5 feet.

A sand-point observation well was installed at the site at the time of its establishment in October 1960. The water level at that time was 20.6 feet below land surface.

INSTALLATION OF ACCESS TUBES

Figure 4 is the plan of the test plot and shows relative location of test holes and access tubes. Test holes *a* through *g*, and *x*, *y*, and *z* were made with a hand auger. Volumetric samples were collected at approximate 6-inch intervals, with a 2-inch Pomona core barrel (Johnson, 1962). The access tubes, designated in figure 4 by capital letters *B* through *J*, consisted of plastic (polyvinyl chloride), aluminum, or steel tubing and were installed by a variety of methods. Moisture samples usually were collected from the access-tube holes as the pilot holes were produced. The moisture-content samples were obtained just previous to moisture readings made with a neutron meter.

Access hole *A* was an observation well, of 1.25-inch steel pipe with a sand point, installed to a depth of 22.75 feet in a hole drilled with a hand auger.

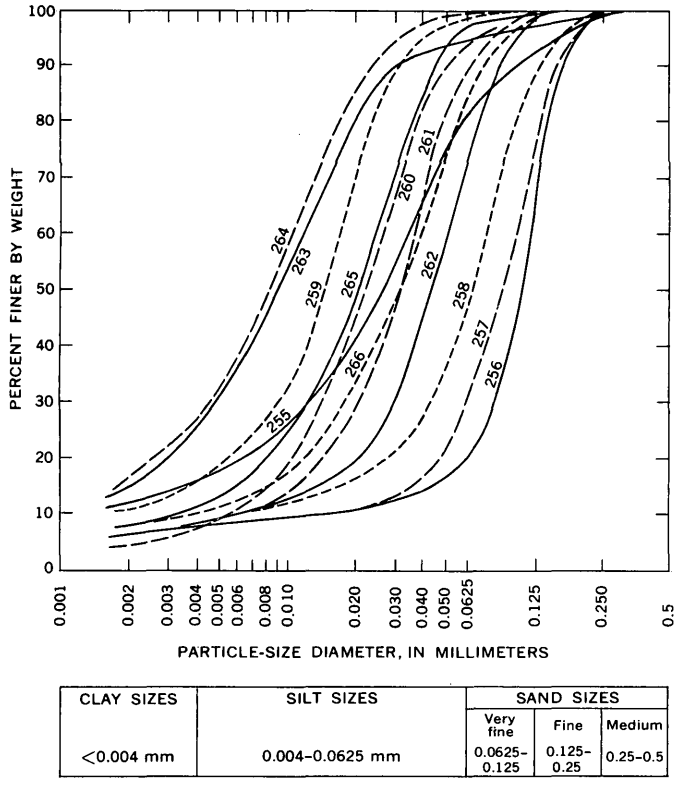

CLAY SIZES	SILT SIZES	SAND SIZES		
		Very fine	Fine	Medium
<0.004 mm	0.004–0.0625 mm	0.0625–0.125	0.125–0.25	0.25–0.5

FIGURE 1.—Particle-size distribution curves for samples from test hole *h*, Sacramento test site (samples 60CAL255–266).

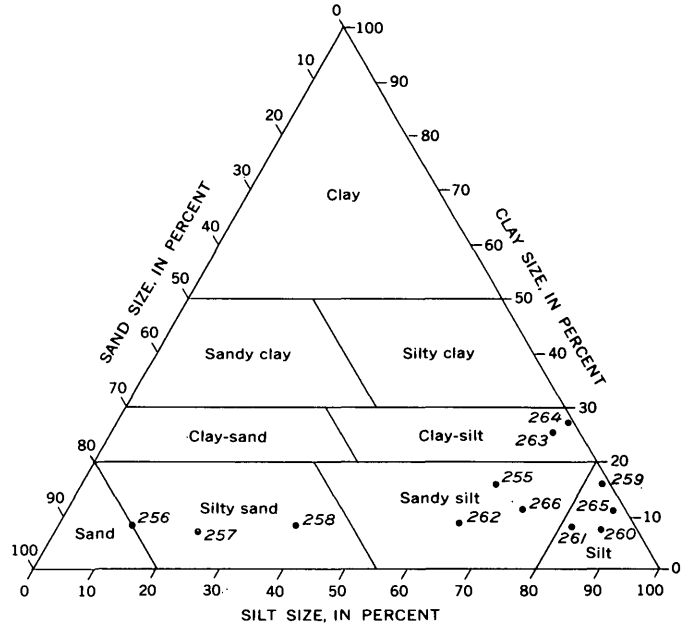

FIGURE 2.—Textural classification of samples from test hole *h*, Sacramento test site (samples 60CAL255–266).

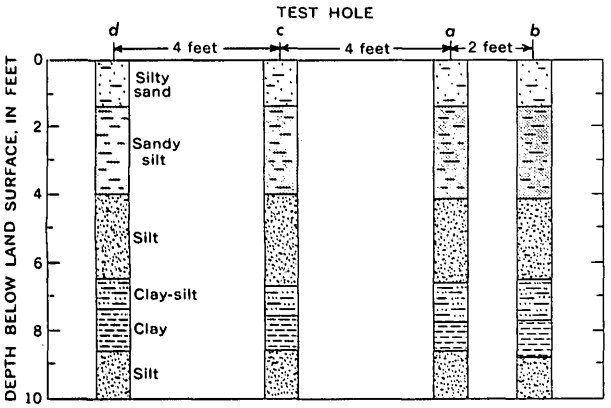

FIGURE 3.—Lithologic logs of test holes at Sacramento test site.

Access tubes *B* and *C* were installed by forcing the access tube into a hole created by driving into the soil an open-end tube of the same diameter. This provided a very tight contact between the access tube and the soil. Moisture samples were collected from the open-end tube.

Access tubes *D*, *E*, *H*, and *I* were installed, centered, in holes made with a 4.5-inch-diameter power auger. The annular space around the access tubing was backfilled with a commercially available fine gravel. The gravel was moistened slightly to diminish the moisture movement from the soil into the gravel, and thereby to cause only a minimum change in moisture content of the wall material.

Access tubes *F* and *G* were installed and centered with board collars placed around the top of the casing in holes made with a 4.5-inch-diameter power-auger, but the annular space was left as air space. The top of the hole was covered to minimize changes in the humidity in the well caused by atmospheric fluctuation.

Access tube *J* was backfilled with the same soil, in relatively the same lithologic sequence, that was removed from the hole with a hand auger. The tube was centered in the 3.5-inch auger hole, and the soil was rammed into the annular space to approximately the original density of each soil type.

As can be seen in figure 4, the access tubes and test holes were arranged close enough together that reasonably similar conditions of lithology, moisture content, and density could be expected, and yet spaced far enough apart that neutron-meter readings at any particular location would not be influenced by the close proximity of other access tubes or test holes. The neutron-meter probe was 1.5 inches in diameter with a 5-millicurie radium-beryllium source, so a 2-foot spacing between access tubes was considered adequate shielding.

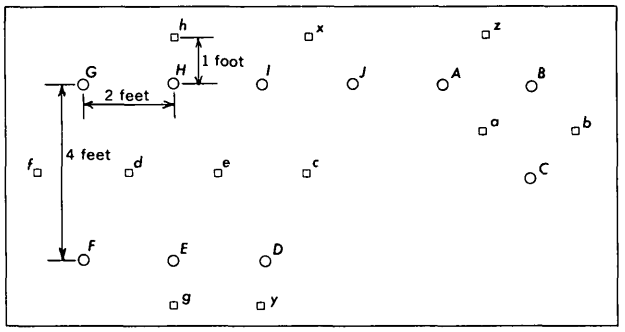

FIGURE 4.—Location plan and description of neutron-meter access tubes, Sacramento test site.
A, 1.25-inch OD steel casing; hand-augered observation well with sand point; depth, 22.75 feet.
B, 1.58-inch OD, 1.55-inch ID, aluminum casing; skintight driven hole.
C, 2.0-inch OD, 1.78-inch ID, stainless steel casing; skintight driven hole.
D, 2.0-inch OD, 1.75-inch ID, aluminum casing; gravel-packed 4.5-inch power-augered hole.
E, 1.58-inch OD, 1.55-inch ID, aluminum casing; gravel-packed 4.5-inch power-augered hole.
F, 1.58-inch OD, 1.55-inch ID, aluminum casing; centered in 4.5-inch power-augered hole.
G, 2.0-inch OD, 1.78-inch ID, stainless steel casing; centered in 4.5-inch power-augered open hole.
H, 1.90-inch OD, 1.74-inch ID, polyvinyl chloride plastic casing; gravel-packed 4.5-inch power-augered hole.
I, 2.0-inch OD, 1.78-inch ID, stainless steel casing; gravel-packed 4.5-inch power-augered hole.
J, 2.0-inch OD, 1.78-inch ID, stainless steel casing; backfilled in original lithologic sequence; in a hole made with a 3.5-inch orchard hand auger. (See Johnson, 1962.)
All access tubes bottom at 10.5 feet below land surface.
Test holes *a* through *g*, and *x*, *y*, and *z*, 3.5-inch holes made with orchard auger.

USE OF NEUTRON MOISTURE METER

Prior to installation of the access tubes at the test site, a calibration curve was obtained for each tube using the neutron moisture meter that had been reserved for exclusive use at the test site. Figure 5 shows the calibration curves of actual moisture content against neutron count ratio for 2 plastic and 4 aluminum tubes of different diameters. The count ratio is the count rate measured by the neutron-meter probe in the soil divided by the count rate measured by the probe while located in the standard shield sitting 3 feet above land surface. Original calibration of the probe at a variety of moisture contents is obtained by taking meter readings while the access tubes are immersed one at a time in a tank containing 40 liters of boric acid solution whose concentration is varied. Although published later, this method of calibration was developed by Van Bavel, Nielsen, and Davidson (1961) and used by the California Department of Water Resources shortly before the authors established the test site in 1960.

Although figure 5 includes data for access tubes other than those described in this paper, the figure does

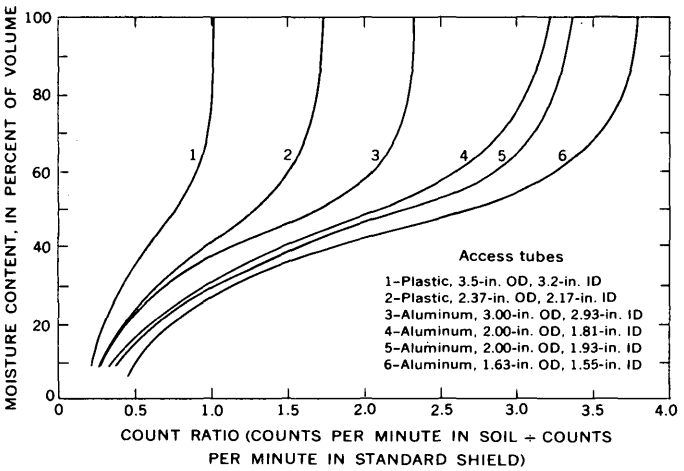

FIGURE 5.—Neutron-meter calibration curves for aluminum and plastic (polyvinyl chloride) access tubes of different dimensions for the probe used in this paper.

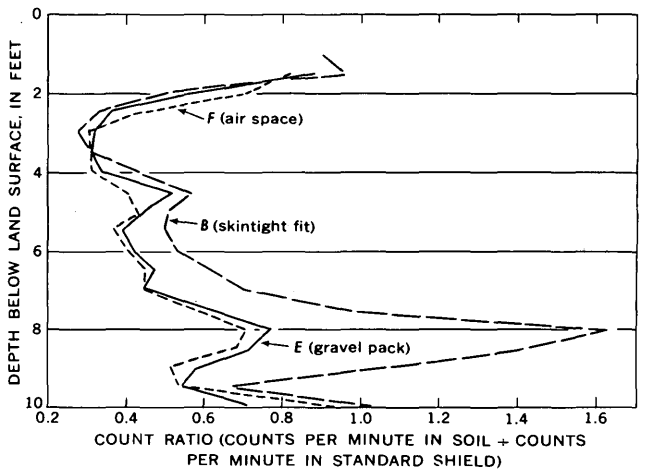

FIGURE 6.—Comparison of neutron-meter count ratio of 2-inch aluminum access tubes, using a variety of installation techniques.

demonstrate that, in general, the moisture content increases as the neutron count ratio increases. However, the moisture-content measurement is seen to have poor precision when the moisture content is high owing to the near-vertical nature of the calibration curves in that moisture range. The figure also shows that there is a considerable dampening effect on the count ratio owing to neutron capture and that there is a decrease in accuracy of moisture measurements as the tube diameter or wall thickness increases, or if plastic rather than aluminum is used for the access tube.

MOISTURE-CONTENT MEASUREMENTS

Readings, in counts per minute, were taken with a neutron moisture meter in each access tube over the period of years following the original installation in 1960. Samples, for moisture-content analysis in the laboratory, were collected from nearby test holes (*a* through *g*, and *x*, *y*, and *z*) each time neutron-meter readings were made at the site.

Figure 6 shows three of the moisture-content logs obtained by the neutron meter in 2-inch-diameter aluminum access tubes. The lines do not represent the continuous distribution of moisture content, but merely connect data points collected at intervals of approximately 6 inches. Although this figure represents only a very small percentage of the data, it does present some of the more obvious conclusions reached by the study. The data show that a much higher apparent moisture content is indicated, especially at approximately 8 feet below land surface, in the installation having a skintight fit between access tube and soil (installation *B*), than in installation *E*, having the gravel pack, or installation *F*, having only air space surrounding the access tube. The actual moisture content of the soil was similar to that indicated by the neutron-meter measurements made in access tube *B*.

The neutron-meter moisture measurements made in access tube *J*, which a 2-inch-diameter stainless steel tube installed with the sediments from the hole replaced around the tube in their original sequence and compacted to near their original density, showed good correlation with the actual moisture measurements made in the laboratory. Although the measurements from this tube may have been as accurate as the measurements from the gravel-packed tubes *D*, *E*, *H*, and *I*, the installation of a uniform gravel pack is much easier than replacing the sediments in their original order and hand ramming them to their original density. (Further investigation of the installation method used at *J*, especially with a power auger, might be useful.)

The measurements shown in figure 6 cannot be converted directly to moisture-content measurements of the soil, except for installation *B*, because the calibration curves (fig. 5) do not represent the effect of air space or gravel pack around the access tube but are directly indicative of conditions only where the soil is in close contact with the tube. However, figure 7 presents one of the correlation graphs developed to permit use of other types of access-tube installations—here, the gravel-packed hole. The correlation curve was developed by using moisture-content values determined from samples collected nearby at the same time that apparent moisture contents were measured with the neutron meter in various access tubes installed with a gravel packing. The trend line represents the median for an actual moisture-content spread of about 5 percent.

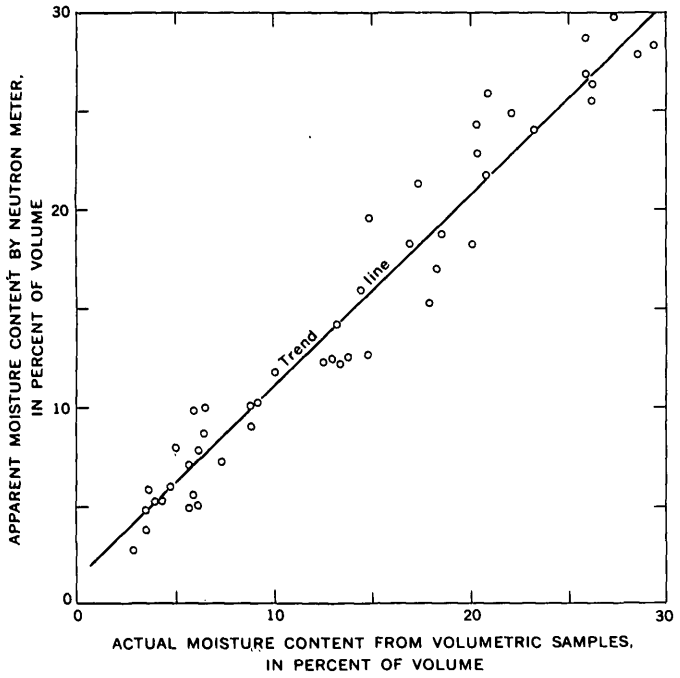

FIGURE 7.—Correlation of apparent moisture content in gravel-packed installations determined by neutron meter with actual moisture content determined from volumetric soil samples.

CONCLUSIONS

The research indicated that installation of thin-walled aluminum tubes of a diameter approximately the same as that of the probe, in a hole small enough to cause tight contact between tube and soil, yields results closest to results obtained by the volumetric sampling procedure. Because it is very difficult to reliably or economically install a thin-walled tube in a tight-fitting hole to depths much greater than 20 feet, this method cannot be used for many ground-water studies. However, the research also showed that a reasonable degree of accuracy in measurements could be obtained by the neutron meter when used in less complicated and more economical installations, such as with gravel-packed access tubes, provided that the neutron-meter measurements are corrected by correlation with moisture content determined from volumetric sampling at the site.

The study emphasized that neutron meters must be calibrated in tubing of identical composition, diameter, and wall thickness as that used in the field installation. The research also indicated that aluminum tubing is the most efficient material for access tubes because of its less dampening effect.

REFERENCES

Holmes, J. W., and Jenkinson, A. F., 1959, Techniques for using the neutron moisture meter: Jour. Agr. Eng. Research, v. 4, no. 2, p. 100–109.

Johnson, A. I., 1962. Methods of measuring soil moisture in the field: U.S. Geol. Survey Water Supply Paper 1619–U, 25 p.

Smith, P. C., Johnson, A. I., Fisher, C. P., and Womack, L. M., 1968, The use of nuclear meters in soils investigations—A summary of worldwide research and practice: Philadelphia, Pa., Am. Soc. Testing and Materials Spec. Tech. Pub. 412, 142 p.

Stolzy, L. H., and Cahoon, G. A., 1957, A field-calibrated portable neutron rate meter for measuring soil moisture in citrus orchards: Soil Sci. Soc. America Proc., v. 21, no. 6, p. 571–575.

Van Bavel, C. H. M., Nielsen, D. R., and Davidson, J. M., 1961, Calibration and characteristics of two neutron moisture probes: Soil Sci. Soc. America Proc., v. 25, no. 5, p. 329–334.

ANALYSIS OF ICE MOVEMENT AT THE POLE STATION, ANTARCTICA

By WILLIAM H. CHAPMAN and WILLIAM J. JONES,
Washington, D.C.

Abstract.—The 12 astronomic positions that have been observed at the Pole Station during the last 12 years were analyzed to determine the rate and direction of ice movement. The positions were reduced to the mean pole and to a common location and then fitted, by a least-squares method, to linear movement equations. Four positions were rejected from the analysis, and the fitting of the remaining eight positions gave satisfactory results. The computed average movement is 19 meters/year in a direction parallel to the 37° W. meridian. The projected position of the Pole Station for January 1, 1970, is latitude 89°59'29.7'' S. and longitude 27.2° W.

The Pole Station was built at the beginning of the International Geophysical Year, in December 1956, and since then has been continuously manned by United States scientists and Navy personnel. The station is located roughly 1 kilometer from the South Geographical Pole, on an extensive sheet of ice about 3 kilometers thick. It was known that the ice sheet flows slowly toward the coastline, but the rate and direction of movement were not known.

From December 1956 to February 1969, 12 groups of astronomic observations were obtained to determined the position of points at the Pole Station. These observations have been analyzed and compared to determine the magnitude and direction of ice movement.

ASTRONOMIC OBSERVATIONS

Figure 1 is a plan diagram of the Pole Station which may be used to identify the sites of observation. The fieldwork of the observations is described by group in chronological order, as follows:

1. During construction of the Pole Station, Lt. Richard Bowers, USN, observed the altitude of the sun 60 times with a T–3 theodolite. All altitudes were observed with the telescope direct, and a previously determined vertical collimation correction was applied. The instrument was set up at the south end of a temporary Jamesway hut. Mean date of observation: December 25, 1956.

2. During the first winter, Dr. Paul A. Siple observed the altitude of Canopus 273 times with a T–3 theodolite in directions well distributed around the horizon. Each altitude measurement consisted of several pointings with telescope direct and reversed. The instrument was mounted on a wooden stand under an aluminum pibal dome in a corner of the inflation shelter. Abnormal star images were frequently noted and can be explained by the extreme temperature difference between the instrument and the exterior of the dome. In a distance of 4 feet, the temperature dropped 60°–80° F. Mean date of observation: May 30, 1957.

3. During the same season, Lt. Jack Tuck, USN, observed the altitude of Canopus 67 times, and the altitude of Al Nair 59 times, using the same instrument and setup.

4. During the second winter season, Palle Mogenson observed the altitude of Canopus 88 times with a DKM–2 theodolite. The instrument was set up on the same stand used by Siple and Tuck the previous year. Because

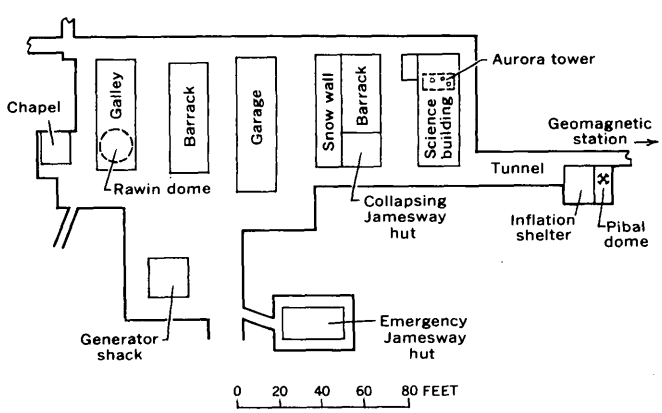

FIGURE 1.—Plan of the Pole Station, Antarctica, derived from a large-scale plan of the base dated about 1959 and compiled by the Bureau of Yards and Docks, U.S. Navy.

the instrument froze on upwind sights, almost all altitudes were observed in the two downwind quadrants. Mean date of observation: June 21, 1958.

5. Three summer seasons later, Robert D. Martin, U.S. Geological Survey (USGS), made 7 paired altitude observations on Hadar and Achernar with a T–3 theodolite. Each observation consisted of 6 altitude measurements (telescope direct) on one star, and then another 6 measurements on the other star (telescope still direct), which was situated nearly 180° in azimuth from the original star. Collimation and refraction errors were approximately canceled by taking the mean of the two lines of position obtained from each pair. The observations were well distributed around the horizon. The instrument was set up on a standard tripod in the open, and a distance-and-direction tie was made to a corner of the inflation shelter. Mean date of observation: December 28, 1961. Martin also made 9 other star-altitude observations, consisting of 3 pointings with telescope direct and 3 pointings with telescope reversed.

6. Concurrently with the altitude observations, Martin also made 24 azimuth observations on various stars, which determined a position independent of the one obtained from the altitude observations.

7. Two years later, a USGS party consisting of Peter F. Bermel, Donald C. Barnett, Kenneth S. McLean, and Ezekiel R. Soza made 19 altitude measurements with a DKM–3 theodolite on high stars well distributed around the horizon. Each observation consisted of several pointings with telescope direct and an equal number with telescope reversed. The instrument was set up on a standard tripod near the entrance to the galley, and a distance-and-direction tie was made to the aurora tower. The observation point was marked with a USGS tablet welded to the top of a pipe embedded 10 feet in the ice. Mean date of observation: February 4, 1963.

8. Concurrent with the altitude observations, the Bermel party made 18 azimuth observations for a position determination independent of Group 7.

9. Five years later, a USGS party consisting of Merle E. Southern, William F. Marshall, David E. Reed, and Bruce L. Schwartz made 25 altitude measurements on various high stars in the four cardinal directions with a DKM–3A theodolite. Each observation consisted of 3 pointings with telescope direct and 3 with telescope reversed. The instrument was set up on a 4- by 4-inch timber embedded in the ice, and a distance-and-direction tie was made to a corner of the inflation shelter. The marker established by the Bermel party could not be recovered because the pipe had been disturbed and the USGS tablet removed by a souvenir hunter. Mean date of observation: January 21, 1968.

10. Southern's party also made 27 azimuth observations for an independent determination of position. Each observation consisted of the mean time and direction of the star's crossing a 5-wire-reticle field, with telescope direct and reversed. Times of crossing were recorded on a chronograph.

11. In 1969, a USGS party consisting of Karlheinz Eissinger, Frederick S. Brownworth, and Charles E. Morrison reoccupied the point established by Southern's party and made 16 altitude observations on selected stars in the 4 cardinal directions with a DKM–3A theodolite. Each observation consisted of 3 pointings with telescope direct and 3 with telescope reversed. A chronograph was used to record times of pointing. Mean date of observation: February 12, 1969.

12. Concurrently, Eissinger's party also made 25 azimuth observations by the 5-wire method on stars selected for balance in the cardinal directions.

COMPUTATION OF POSITIONS

The 12 mean astronomic positions obtained from the groups of observations are listed in table 1. The computations were divided into three major steps: (1) reduction of the observations to an astronomic position, based on the instantaneous Pole, for the instrument setup; (2) correction of the coordinates and azimuths to refer them to the Conventional International Pole; and (3) correction of the positions to refer them to a common ground point.

For reduction to an instrument position, the standard formulas of spherical astronomy were used. Star data were taken from "Apparent Places of Fundamental Stars, 1957–1969" (International Astronomical Union, 1956–1966), sun data were taken from "the American Ephemeris and Nautical Almanac, 1956" (U.S. Naval Observatory, 1954), and refraction corrections were taken from tables V, VI, and VII of Special Publication 237 of the U.S. Coast and Geodetic Survey (Hoskinson and Duerksen, 1952). The position obtained from each group of observations is the result of a least-squares adjustment. All observations were computed by the U.S. Geological Survey, except Mogenson's, which were computed by the U.S. Coast and Geodetic Survey. Generally, a standard deviation of about 30 meters on the ground was obtained in the group adjustments.

Instrument positions were referred to the Conventional International Pole by means of tables supplied by the U.S. Naval Observatory and formulas developed for high latitudes.

The pibal dome of the inflation shelter (fig. 1) was selected as the fiducial ground point for all positions, and positions obtained for other points were corrected accordingly. Distance-and-direction ties from instru-

TABLE 1.—*Summary of information for each observed astronomic position at the Pole Station*

Position No.	Observer or party chief	Date [1]	Method of observation [2]	Instrument (theodolite)	ϕ [3] 89°59′ S.	λ [3]	X	Y
1	Bowers	1956. 984	Sun-LOP	T–3	48. 6″ S.	45°46′ W.	126. 933	328. 960
2	Siple	1957. 415	Canopus-LOP	T–3	38. 0″	24°10′	−5. 982	682. 461
3	Tuck	1957. 415	Al Nair-LOP	T–3	31. 5″	25°15′	8. 940	883. 502
4	Mogensen	1958. 471	Canopus-LOP	DKM–2	43. 6″	24°48′	1. 184	508. 792
5	Martin	1961. 992	Stars-LOP	T–3	27. 9″	29°08′	77. 736	994. 073
6	do	1961. 992	Stars-Az	T–3	35. 2″	23°43′	−12. 663	769. 509
7	Bermel	1963. 096	Stars-LOP	DKM–3	33. 5″	28°26′	53. 894	819. 038
8	do	1963. 096	Stars-Az	DKM–3	31. 5″	25°06′	6. 741	884. 452
9	Southern	1968. 058	Stars-LOP	DKM–3A	31. 5″	24°25′	−3. 897	882. 421
10	do	1968. 058	Stars-Az	DKM–3A	32. 5″	25°28′	11. 963	852. 559
11	Eissinger	1969. 118	Stars-LOP	DKM–3A	31. 0″	27°51′	49. 903	897. 426
12	do	1969. 118	Stars-Az	DKM–3A	28. 4″	28°57′	73. 282	978. 171

[1] Dates are calculated to the nearest one-thousandth of a year.
[2] LOP, line of position; Az, azimuth.
[3] All astronomic positions are for the pibal dome except position 1, which could not be properly reduced.

ment setups to structures at the Pole Station were combined with distances and directions scaled from the large-scale (1:240) plan of the station compiled by the Bureau of Yards and Docks, U.S. Navy. (Figure 1 is derived from this plan.)

The instrument setup used by Lt. Bowers could not be accurately identified. The position listed in table 1 was computed on the assumption that his "temporary Jamesway" was the same as the "collapsing Jamesway" shown in figure 1. However, Dr. Siple states that the Jamesway used by Bowers was removed after the Station had been constructed. Therefore, the position obtained from Bowers' observations was not used in this analysis.

COORDINATE SYSTEM

The formulas relating horizontal position and linear movement are much simpler if the positions are expressed in a rectangular system. Therefore, the coordinate system shown in figure 2 was adopted. The meridian adopted as the Y axis, 24°40′ W., is the mean of all observed longitudes. In this system, the Y coordinate is mainly a function of latitude, and the X coordinate is mainly a function of longitude.

FORMULAS FOR LINEAR MOVEMENT

Two formulas are used to relate positions to linear movement parameters:

$$X_i = X_o + (T_i - T_o)R_x, \text{ and} \quad (1)$$
$$Y_i = Y_o + (T_i - T_o)R_y, \quad (2)$$

where

X_i and Y_i = coordinates at time i,
X_o and Y_o = coordinates at selected time origin,
R_x = rate of movement in X,
R_y = rate of movement in Y, and
$T_i - T_o$ = time interval, in years.

The amount and direction of movement is

$$S = (R_x^2 + R_y^2)^{1/2} \text{ and} \quad (3)$$
$$\alpha = \arctan (R_x/R_y). \quad (4)$$

The observation equations for a least-squares adjustment are

$$V_i(x) = X_o + (T_i - T_o)R_x + (X_a - X_i) \text{ and} \quad (5)$$
$$V_i(y) = Y_o + (T_i - T_o)R_y + (Y_a - Y_i), \quad (6)$$

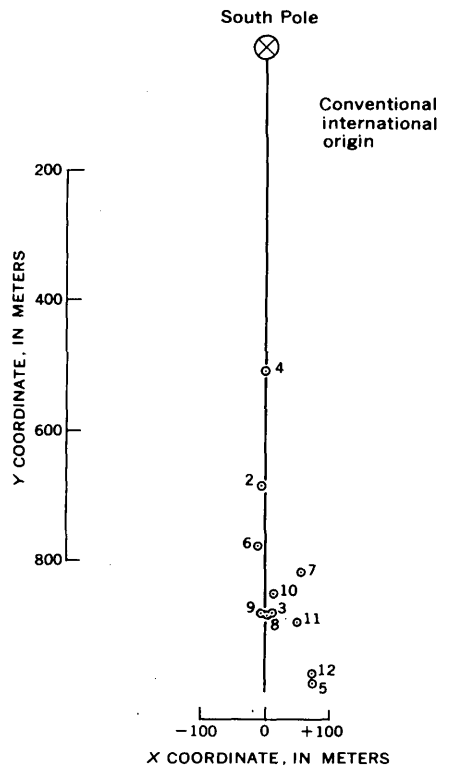

FIGURE 2.—Local rectangular coordinate system developed for the ice-movement analysis, showing the observed astronomic positions at the Pole Station. The origin is the mean pole, and the Y axis is the 20°40′ W. meridian.

where

$V_i(x)$ and $V_i(y)$ = residuals,
X_o and Y_o = corrections to coordinates of assumed origin,
$T_i - T_o$ = time interval (years),
R_x and R_y = corrections to assumed rates,
X_a and Y_a = coordinates at T_i based on assumed rates and origin, and
X_i and Y_i = observed coordinates (from astronomic observations).

The standard deviations of the direction and amount of movement are computed from the standard deviations of the X and Y rates obtained from the least-squares adjustment. From equations 3 and 4

$$m^2_S = (R_x/S)^2 m^2_{R_x} + (R_y/S)^2 m^2_{R_y} \text{ and} \quad (7)$$

$$m^2_\alpha = C^2(R_x/S^2)^2 m^2_{R_x} + C^2(R_y/S^2)^2 m^2_{R_y}, \quad (8)$$

where

m^2_S = variance of rate of movement,
m^2_α = variance of direction of movement,
$m^2_{R_x}$ = variance of rate of movement in X,
$m^2_{R_y}$ = variance of rate of movement in Y, and
C = conversion constant, radians to degrees.

COMPUTATION OF LINEAR MOVEMENT

The computational sequence for determining linear movement is as follows:

1. Select a time origin.
2. Estimate X and Y values for the selected time origin.
3. Estimate rates of movement in X and Y.
4. Using these values of the origin and rates, compute X and Y at the time of each observed position (equations 1 and 2).
5. Form equations 5 and 6 for each observed position.
6. Form the normal equations and solve for the corrections to the estimated coordinates and rates. Also, compute standard deviations for the estimated coordinates and rates.
7. Substitute adjusted rate values in equations 3 and 4 to obtain the rate and direction of movement.
8. Compute variance of the rate and direction of movement (equations 7 and 8).

In the first pass through this computational sequence, using all positions except position 1, the origin time was selected as the mean of all dates of observation, and the initial coordinates were estimated as the means of all the X's and Y's. Both movement rates were estimated as zero. The observation equations in X and Y were formed, normalized, and solved. Each position was given unit weight. The corrections were substituted back into the observation equations to obtain residuals, which were checked for outliers. Three positions (3, 4, and 5) had residuals greater than 100 meters in Y and were rejected from further computations.

In the second pass, the origin was selected as January 1, 1970, and the same estimates of initial coordinates and rates were used. A least-squares solution in X and Y was computed for the remaining eight positions. All the residuals were well within the 100-meter limit (see figs. 3 and 4), and the results of the adjustment appear to be sound.

RESULTS

The second least-squares solution, containing only the eight acceptable positions as input, gave the following results:

$X_o = 41.493 \pm 17.1$ meters,
$R_x = 3.962 \pm 2.67$ meters/year,
$Y_o = 938.250 \pm 31.6$ meters, and
$R_y = 18.475 \pm 4.16$ meters/year.

Substituting these values in equations 3, 4, 7, and 8 gives

$S = 18.9 \pm 4.1$ meters/year, and
$\alpha = 167.9° \pm 12.5°$.

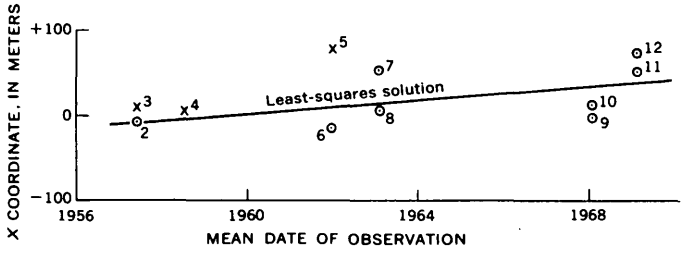

FIGURE 3.—X coordinate of the Pole Station astronomic positions plotted against the mean date of observation. The line is the least-squares solution for linear ice movement in the X component. Rejected values are indicated by an "x".

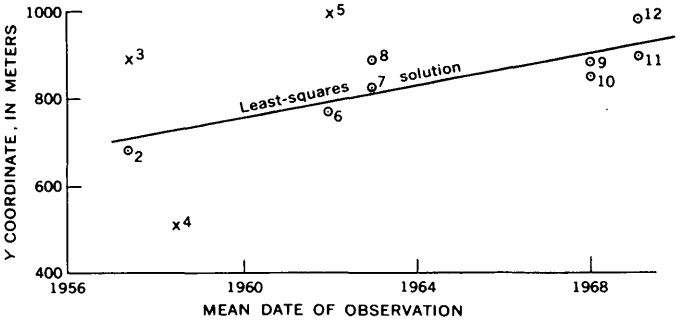

FIGURE 4.—Y coordinate of the Pole Station astronomic positions plotted against the mean date of observation. The line is the least-squares solution for linear ice movement in the Y component. Rejected values are indicated by an "x".

With alpha converted into a geographical direction, the direction of movement is parallel to the meridian of 36.8° W. When X_o and Y_o are transformed to geographic coordinates, the projected position of the pibal dome for January 1, 1970, is

$\phi = 89°59'29.7''$ S. $\pm 1''$ and
$\lambda = 27.2°$ W. $\pm 1°$.

REFERENCES

Hoskinson, A. J., and Duerksen, J. A., 1952, Manual of geodetic astronomy: U.S. Coast and Geodetic Survey Spec. Pub. 237. 205 p.

International Astronomical Union, 1956–66, Apparent places of fundamental stars 1957–1969: Heidelberg, Astronomisches Rechen-Institut.

U.S. Naval Observatory, 1954, The American ephemeris and nautical almanac for the year 1956; Washington, U.S. Government Printing Office.

SUBJECT INDEX

[For major headings such as "Economic geology," "Geochemistry," "Ground water," see under State names or refer to table of contents]

AUTHOR INDEX

U.S. GOVERNMENT PRINTING OFFICE: 1970 O—380-189